

Development of Photocatalysts towards the Visible-Light driven C-Terminal Bioconjugation of Peptides and Proteins

Présentée le 12 novembre 2020

à la Faculté des sciences de base
Laboratoire de catalyse et synthèse organique
Programme doctoral en chimie et génie chimique

pour l'obtention du grade de Docteur ès Sciences

par

Marion Marie-Agnès GARREAU

Acceptée sur proposition du jury

Prof. J. Zhu, président du jury
Prof. J. Waser, directeur de thèse
Dr L. Malins, rapporteuse
Prof. T. Noël, rapporteur
Prof. C. Heinis, rapporteur

Pour mes proches,

Merci,

*« Ce n'est pas ce que nous sommes qui nous empêche de réaliser nos rêves,
c'est ce que nous croyons que nous ne sommes pas »*

Paul-Emile Victor

Acknowledgements

First, I would like to say thank you to you Jérôme. I am very happy of those 4 years within the group, which were full of learning. I am glad you offered to me to work on this interdisciplinary project, which tremendously broadened my interest in chemistry. Your vision of science and how you are implicated to transmit your knowledge is truly inspiring. I am grateful for your support and involvement, especially in the difficult moments of my PhD. I also acknowledge your important efforts to render the exchange possible. This made a great difference to me. That time enhanced my passion for biomolecule functionalization and inspired me for the next chapter. Merci

I also want to warmly thank Gonçalo Bernardes for hosting me in his lab during the exchange. I am happy to had the opportunity to come in your fascinating group, even for such a short time. Discussing science with you is always motivating thanks to your strong enthusiasm and ambition to envision larger applications. I am very grateful for all group members for their nice welcome and support.

I would like to express my gratitude to Dr. Lara Malins and Professors Jieping Zhu, Christian Heinis and Timothy Noël for accepting to read this manuscript and assist to my defense.

I have been lucky to be very well surrounded during those for years at the LCSO. A huge thank to all the past and present group members! You have made this time working in such a positive atmosphere, inside and outside the lab. First, among the old generation, I am especially thankful for Durga, Johannes, Sebastien and the Italian team, Paola and Dani. Javier, I think the bio team was lost before you arrived! I have learnt so much through all our discussions and I am very thankful for this time you took. All the best with the small family! Lots of good mood from Guillaume, Eljia, Ming-Ming, Mikus and Vincent, thank you guys.

Au tour des labmates du 4409/1410. Stef, tu as été d'un soutien précieux. Merci pour ces discussions et ce temps que tu as toujours à offrir. Un immense merci à toi Romain pour tout ce que tu m'as transmis entre deux batailles musicales. Je te dois beaucoup. Julien, quel plaisir de t'avoir eu comme labmate ! Juste encore un peu de travail sur ton goût pour le fromage. Et le labmate, Bastian. Juste merci ! Ça n'aurait pas été pareil sans toi, la gomina, les lundis matin difficiles, les sciences manip et les 6 mois de Warhaus/Balthazar. On la créera cette start-up d'estérification !

Eliott je suis toujours aussi impressionnée par ces mails à 7h. Je te souhaite un avenir plein de bières belges ! Un immense merci pour ces mois à travailler ensemble, c'était un grand plaisir. J'espère que tu surmonteras le traumatisme des peptides ! Luca, I still can't believe we fished you with those drinks! So happy to hunt for food with you, but not to close as we hate people. I wish you to get to this food paradise you dream of. Stéphanie, petit caribou, si contente d'avoir fait ces années ensemble entre ta folie rafraichissante et tes histoires sans queue ni tête qui t'appartiennent qu'à toi. Merci. Nina, mon petit

éléphant, un immense merci. Pour être là, toujours, ton sourire et toutes ces histoires de cailloux aux temps des mammoths !

Franck, le champion. Pour te paraphraser, un merci pour TOUT et d'avoir joué un rôle spécial ! De m'avoir transmis autant sur la photoredox même si je n'avais pas des gros bras, d'avoir cherché Nessie sur le lac en toba. Et surtout d'avoir lancé le concept des deux PhD en parallèle !

The other teams from the BCH (LCSA, LSPN) are great neighbors, thanks a lot guys for the nice moments on campus, by the lake or in the city! Special thanks to Alexandre, Dina, Bastien and Balázs. I am also grateful for the support services at EPFL, especially the MS with Daniel and Francesco who were always there with a big smile to help, and Aurélien from the NMR. I would also like to thank all the people I had the chance to work with outside of the lab, in particular Ophélie Planes.

Anto, un grand merci pour cette ambiance à la coloc et les balades initiatiques au No Name. Coralie, petit Puccino, tu as joué un rôle particulier dans ma thèse, en étant là, en allant grimper. Simplement merci. Jack, the resident DJ from 4404 club, I'm so glad of those crazy adventures together. Not many people would go skiing in May in a Smart, happy to have met one to found the blue monsters team. Parce que la team des Vikings s'est agrandie, merci Pierre pour l'aide dans mon PhD montagne et l'établissement de ces records de CKT ! Une pensée pour les copains montagne du CAS, Charly, Nelson, Sylvain et Corinne, merci pour ces aventures toutes plus incroyables (et longues). Pour finir avec la vie Lausannoise, grand merci aux colocs de La Lucerna !

A mon petit Nico, j'ai si hâte de commencer le nouveau chapitre de nos aventures suédoises ! Ma Gatoune, cette thèse n'aurait pas été la même sans nos appels intemporels. Ma Fanouille, merci de m'avoir fait aimer l'eau liquide et de me donner toujours envie de réaliser des rêves plus fous. A huge thank to the Blueberries team. Jan, bonjou, bonjour, the Scandinavian adventure is only getting started! Enfin, Paul, merci d'avoir cru en moi et de m'avoir soutenu dans mes rêves.

To my previous supervisors who inspired me and transmitted their passion for chemistry, Giovanni, Alec, Maud and Bernard, thank you.

Je ne remercierais jamais assez ma famille pour leur soutien et inspiration. Damien, je suis fière de t'avoir comme grand frère. Quel plaisir qu'on partage cette passion de la montagne. Oui je vais continuer à être ton guide et je t'écis ici oui tu peux avoir mon matos ! Merci. A mes parents, un merci sincère de m'avoir transmis la curiosité de toujours apprendre et la passion pour les montagnes. Maman, il est temps d'admettre que j'ai fait toute cette thèse juste pour te faire changer d'avis sur les produits chimiques.

Lausanne, septembre 2020

Abstract

If small molecules have led to tremendous progress in curing diseases, new therapeutic agents such as peptides or antibody-drugs conjugates have emerged as a highly promising next generation of pharmaceuticals. Some native biomolecules already possess strong activities. However, as for small molecules, their derivatization is often the key to custom activity or physicochemical properties. Peptide and protein modification methods are thus in important demand. Despite impressive achievements, the need of more efficient and diverse strategies remains present. Single-site selective chemical modification of native proteins is currently intensively explored. This is however particularly challenging as it requires physiological conditions, as well as excellent chemoselectivities. Mild activation techniques are thus under special attention.

For that purpose, photoredox catalysis stands as a mild strategy to generate radicals selectively, in comparison to UV light. Visible-light is thus attractive for biomolecule functionalization and impressive reports have been disclosed in the last years, even if the field is still at an early stage. Another mild strategy towards protein functionalization is the use of hypervalent iodine reagents as an electrophilic alkyne source. This has been successful for biomolecule bioconjugation on several residues. Gratifyingly, those two concepts could be combined and a decarboxylative alkynylation of α -amino acids using photoredox catalysis and hypervalent iodine reagents was previously released.

The goal of my PhD was to contribute to the field of biomolecules site-selective chemical modification by providing a novel labeling of carboxylic acids. To this end, it was envisioned to extend the existing photoredox-catalyzed decarboxylative alkynylation, from simple carboxylic acids to peptides, and later proteins. Among the diverse possible positions for protein bioconjugation, the C-terminal extremity is extremely attractive as it allows for a single-site selectivity. Available methodologies remain however scarce and are not general.

Our investigations started with the development of novel fine-tuned organic dyes from the carbazolyldicyanobenzene family. A rational design allowed us to report organophotocatalysts filling existing gaps in redox properties. At the time of this project the concept of fine-tuning the redox properties of organic dyes was only emerging. Those fluorophores were notably crucial to achieve high efficiencies in a decarboxylative-fragmentation-alkynylation cascade. The following extensions of this concept and the use of this library to unlock novel reactivities demonstrated the impact of this contribution.

Those organophotocatalysts were precious in the success of our peptide decarboxylative alkynylation. This metal-free reaction was found to proceed with an excellent regio and chemoselectivity towards the C-terminal position. Native peptides up to hexamers were suitable substrates and the potential of our approach was confirmed by the introduction of bioorthogonal functional groups. This was the first report of such transformation on native peptides bearing multiple functional groups.

Unfortunately, larger native peptides could not be modified under those conditions, leading us to design a novel strategy. We envisioned that a covalent linkage of an organophotocatalyst on proteins would allow an alkynylation at the C-terminus through a proximity-induced photoredox-catalyzed decarboxylation. For this unprecedented concept, 4CzIPN derivatives were thus designed to be introduced on a single-site on peptides. Ongoing work aims to assess the success of this approach. A high potential towards site-selective protein modification is envisioned.

Finally, another direction explored during this thesis was a decarboxylative oxidation of peptides towards the formation of *N,O*-acetals. They were employed as a platform for derivatization. Through Friedel-Crafts arylations, phenols and indoles could be successfully introduced. This strategy was further extended towards the cross-linking of peptides, providing a novel scaffold of unnatural tetramers of potential interest for drug discovery. This project is also still under study in order to modify more complex peptides.

Keywords: photoredox catalysis, radical chemistry, bioconjugation, peptides, proteins, organic dyes, decarboxylation, alkynylation, hypervalent iodine reagents, proximity, late-stage functionalization.

Résumé

Si les molécules organiques ont permis des avancées spectaculaires dans le traitement des maladies, une nouvelle génération très prometteuse d'agents thérapeutiques a émergé avec notamment les peptides ou les conjugués anticorps-médicament. Les molécules biologiques naturelles possèdent déjà des activités importantes. Cependant, de même que pour les plus petites molécules, leur modification est souvent la clé de l'optimisation de leur activité ou propriétés physico-chimiques. Les méthodes pour fonctionnaliser les peptides et les protéines sont donc très demandées. En dépit des impressionnants progrès réalisés, des stratégies toujours plus diverses et efficaces sont requises. La modification de protéines natives de façon sélective à une seule position est actuellement le sujet d'intenses explorations. Ceci est particulièrement difficile car des conditions physiologiques sont requises, en même temps qu'une excellente chimiosélectivité. Des techniques d'activation en conditions douces sont donc requises.

Dans ce contexte, la catalyse en photorédox permet de générer des radicaux de façon sélective en conditions douces par rapport aux UV. La lumière visible est donc très attractive pour la fonctionnalisation de molécules biologiques et des impressionnants travaux ont été reportés ces dernières années. Une autre méthode pour fonctionnaliser les molécules biologiques de façon douce est l'utilisation de réactifs d'iode hypervalent comme source d'alcyne électrophile. Ceci s'est révélé fructueux pour des réactions de bioconjugaison sur plusieurs résidus. Finalement, ces deux concepts peuvent être réunis et une réaction de décarboxylation suivie d'alcynylation d'acides-aminés utilisant la catalyse en photorédox et les réactifs d'iode hypervalent a été précédemment développée.

Le but de ma thèse était de contribuer à ce domaine de modification de molécules biologiques de façon sélective à une seule position, en apportant une nouvelle méthode spécifique aux acides carboxyliques. Pour ce fait, il a été envisagé d'étendre l'alcynylation catalysée par photorédox existante, des acides carboxyliques simples à des peptides, puis plus tard à des protéines. Parmi les diverses positions possibles pour modifier une protéine, la position C-terminale est particulièrement attirante car elle permet d'accéder à une sélectivité à un site unique. Les méthodes existantes dans ce but sont cependant rares et non générales.

Nos investigations ont commencé avec le développement de nouveaux photocatalyseurs organiques. En se basant sur design rationnel de l'électronique du groupement donneur, nous avons pu reporter des nouveaux catalyseurs qui comblaient un écart important dans les

propriétés oxydantes. Le concept de modifier les propriétés des photocatalyseurs était seulement à son début à l'époque de ce projet. Ces fluorophores ont été notamment cruciaux pour l'obtention d'une cascade efficace de décarboxylation suivie de fragmentation puis d'alcynylation. L'extension de ce concept et l'utilisation de cette librairie de composés qui a été faite par la suite montre l'impact de cette contribution.

Ces photocatalyseurs ont été précieux pour le succès de notre réaction de décarboxylation suivie d'alcynylation sur des peptides. Cette dernière modifie la position C-terminale avec une excellente regio- et chimiosélectivité, sans métal. Des peptides natifs jusqu'à des hexamères étaient compatibles et le potentiel de notre approche a été confirmé par l'introduction de groupements fonctionnels bio-orthogonaux. Ceci est la première occurrence d'une telle transformation sur des peptides natifs comportant plusieurs groupements fonctionnels.

Malheureusement, des peptides natifs de plus grande taille n'ont pas pu être modifiés dans ces conditions. Cela nous a poussé à concevoir une nouvelle stratégie. Nous avons envisagé qu'un photocatalyseur organique, lié de façon covalente aux protéines, permettrait une alcynylation en position C-terminale, par une réaction de proximité. Pour permettre ce concept novateur, des dérivés de 4CzIPN ont été modifiés pour être introduits à une seule position sur des protéines. Cette approche est encore à l'étude pour pouvoir évaluer son succès. Un fort potentiel est envisagé pour la modification de protéines en une seule position.

Finalement, une autre direction qui a été explorée pendant cette thèse est une décarboxylation oxydante de peptides pour former des *N,O*-acétals. Ceux-ci ont été utilisés comme une plateforme de diversité. Grâce à des arylations de Friedel-Crafts, des indoles et phénols ont pu être introduits. Un nouveau squelette de tétramères non naturel est donc proposé et pourrait être intéressant pour la recherche médicale. Ce projet est aussi encore en cours, avec le but de modifier des peptides plus complexes.

Mots clés : catalyse photorédox, chimie radicalaire, bioconjugaison, peptides, protéines, photocatalyseur organique, décarboxylation, alcynylation, iode hypervalent, proximité.

Table of contents

Acknowledgements	7
Abstract	11
Résumé	13
Table of contents	16
List of abbreviations	20
1 Introduction	27
2 Background and Significance	31
2.1 Functionalization of peptides and proteins	31
2.1.1 Significance of peptide functionalization	31
2.1.2 Significance of site-selective protein modification	33
2.1.3 Overview of chemical site-selective modification methods	36
2.1.4 C-terminal bioconjugation	37
2.2 Hypervalent iodine reagents for alkynylation of peptides and proteins	42
2.2.1 Structure and general reactivity	42
2.2.2 Alkynylation with EBX reagents	44
2.2.3 Functionalization of peptides and proteins with hypervalent iodine reagents	46
2.3 Photoredox chemistry for decarboxylation on peptides and proteins	50
2.3.1 Principle	50
2.3.2 Photoredox catalysts: design and overview	52
2.3.3 Decarboxylative alkynylation reactions using photoredox chemistry	59
2.3.4 Photocatalytic transformations on peptides and proteins	66
2.3.5 Photoinduced bioconjugation on carboxylic acids residues	68
3 Goal of the thesis	79
4 Towards a decarboxylative alkynylation in aqueous media	83
4.1 Preliminary work	83
4.1.1 Proof of concept and choice of model substrate	83
4.1.2 Optimization in buffers	87
4.1.3 Optimization of other parameters	88
4.2 Synthesis and screening with water-soluble catalysts	90
4.2.1 Design and synthesis of catalysts	90
4.2.2 Screening of water-soluble catalysts	93
4.2.3 Water-soluble EBX	94

4.3	Conclusion	95
5	Development of novel fine-tuned organic dyes for photoredox catalysis	99
5.1	Synthesis and characterization of 4XCzIPN derivatives	99
5.1.1	Significance and design	99
5.1.2	Synthesis.....	101
5.1.3	Characterization of 4XCzIPN derivatives	103
5.2	Application of 4XCzIPN derivatives in a fragmentation cascade.....	107
5.3	Synthesis of 4XDPAIPN derivatives	110
5.3.1	Significance and design	110
5.3.2	Synthesis.....	111
5.3.3	Characterization of 4XDPAIPN derivatives	113
5.4	Conclusion	114
6	Photoredox-catalyzed decarboxylative alkynylation of peptides in organic solvent.....	119
6.1	Optimization	119
6.1.1	From Iridium catalyst to organic dyes	119
6.1.2	Preliminary scope investigation	122
6.1.3	Optimization on Cbz-Ala-Ala	123
6.1.4	Control experiments.....	125
6.2	Towards C-terminal selectivity	126
6.3	Reagents and dipeptides scope.....	127
6.3.1	Scope of hypervalent iodine reagents.....	127
6.3.2	Scope of dipeptides	131
6.3.3	Robustness test	132
6.4	Tetramer peptides scope.....	133
6.4.1	Optimization	133
6.4.2	Functional group tolerance	135
6.4.3	C-terminal variation.....	136
6.4.4	Selectivity between carboxylic acids.....	137
6.5	Labeling of GRGDNP	138
6.6	Towards the labeling of larger peptides.....	138
6.7	Screening of organic dyes.....	141
6.8	Conclusion	142
7	Towards a proximity-induced protein C-terminal decarboxylative alkynylation.....	147
7.1	Background and significance	147
7.1.1	Significance.....	147
7.1.2	Proximity-induced photoredox transformations on proteins	148

7.2	Design and synthesis of dyes.....	152
7.2.1	Design of dyes.....	152
7.2.2	Synthesis of the first generation dye.....	154
7.3	Preliminary results.....	160
7.3.1	Proof of concept on peptides.....	160
7.3.2	Towards a proximity-induced decarboxylative alkynylation on proteins	163
7.4	Second generation of dyes.....	165
7.4.1	Synthesis.....	166
7.4.2	Preliminary investigations	170
7.5	Conclusion and outlook.....	174
8	Photoredox-catalyzed sequential decarboxylative-oxidation-arylation of peptide C-terminus.	179
8.1	Background and significance	179
8.1.1	Significance	179
8.1.2	Hofer–Moest reaction	181
8.1.3	Decarboxylative oxidation and dehydrogenative strategies in photoredox catalysis	183
8.1.4	Decarboxylative hydroxylation with other activation methods.....	184
8.2	Optimization.....	186
8.3	Robustness tests.....	192
8.4	Dipeptides and nucleophiles scope.....	197
8.4.1	Scope of alcohols.....	197
8.4.2	Scope of phenols	197
8.4.3	Scope of dipeptides	198
8.5	Possible mechanism	199
8.6	Conclusion and outlook.....	201
9	General conclusion	207
10	Outlook.....	213
10.1	Staple and cross-linked peptides.....	213
10.2	Optimization in aqueous media	214
10.3	Design of novel organophotocatalysts.....	215
11	References	217
12	Experimental part.....	229
12.1	General methods.....	229
12.2	Synthesis of peptides.....	232
12.3	Development of novel fine-tuned organic dyes for photoredox catalysis.....	233
12.3.1	Synthesis of 4CzIPN and 4DPAIPN derivatives	233
12.3.2	Physical measurements of 4CzIPN derivatives 5.3 to 5.5	243

12.3.3	Physical measurements of 4CzIPN and 4DPAIPN derivatives 5.25 to 5.28	250
12.3.4	Crystal structures.....	261
12.4	Decarboxylative alkynylation of peptides	262
12.4.1	Preparation of reagents.....	262
12.4.2	Preparation of water-soluble iridium catalysts	277
12.4.3	Optimization	286
12.4.4	Robustness experiments	288
12.4.5	Reagents and dipeptide scope	290
12.4.6	Peptide tetramers scope	303
12.4.7	Scope on Gly-Arg-Gly-Asp-Asn-Pro-OH	332
12.5	Towards a proximity-induced proteins C-terminal decarboxylative alkynylation	341
12.5.1	Preparation of catalysts.....	341
12.5.2	Scope on peptides	354
12.6	Photoredox-catalyzed sequential decarboxylative-oxidation-arylation of peptides C-terminus	367
12.6.1	Preparation of reagents and catalysts.....	367
12.6.2	Optimization	368
12.6.3	Robustness experiments	369
12.6.4	Scope on dipeptides	371
13	Annexes	378
13.1	NMR spectra	378
13.2	List of publications.....	379
13.3	Curriculum Vitae.....	380

List of abbreviations

3c-4e	3-Center-4-electron
Å	Angstrom
ABX	Azidobenziodoxolone
Ac	Acetyl
AcOH	Acetic acid
ACN	Acetonitrile
Ala	Alanine
Aq.	Aqueous
Ant	Anthracene
Asn	Asparagine
Asp	Aspartic acid
Ar	Aryl
Arg	Arginine
atm	atmosphere
9-BBN	9-Borabicyclo[3.3.1]nonane
BF ₃ .Et ₂ O	Boron trifluoride etherate
BHT	butylhydroxytoluene
Bn	Benzyl
Boc	<i>Tert</i> -butoxycarbonyl
Bu	Butyl
BuLi	Butyllithium
Bz	Benzoyl
° C	Degrees centigrade
Calcd	Calculated
Cat.	Catalytic
Cbz	Carboxybenzyl
CBX	Cyanobenziodoxolone
<i>m</i> CPBA	<i>Meta</i> -chloroperbenzoic acid
CuAAC	Copper-catalyzed azide-alkyne cycloaddition
Cy	Cyclohexyl
Cys	Cysteine
4CzIPN	2,4,5,6-Tetra(9 <i>H</i> -carbazol-9-yl)isophthalonitrile
δ	NMR chemical shift in ppm

d	Doublet
DABCO	1,4-diazabicyclo[2.2.2]octane
dba	Dibenzylideneacetone
DBU	1,8-diazabicycloundec-7-ene
DCE	dichloroethane
DCM	dichloromethane
DFT	Density functional theory
DIPEA	diisopropylethylamine
DMAP	4-dimethylamino pyridine
DMF	N,N-dimethylformamide
DMSO	dimethyl sulfoxide
d.r.	diastereomeric ratio
EBX	ethynyl benziodoxolone
EDG	electron donating group
ee	enantiomeric excess
EI	electron impact ionization
eq.	equation
equiv	equivalent(s)
ESI	electrospray ionization
Et	ethyl
Et ₂ O	Diethyl ether
EtOAc	ethyl acetate
EtOH	Ethanol
EPPS	4-(2-Hydroxyethyl)-1-piperazinepropanesulfonic acid
EWG	electron withdrawing group
Fmoc	Fluorenylmethyloxycarbonyl
g	gram
GC	gas chromatography
Gln	Glutamine
Glu	Glutamic acid
Gly	Glycine
GSH	Glutathione
h	Hours
HEPES	4-(2-Hydroxyethyl)-1-piperazineethanesulfonic acid
His	Histidine

HMBC	Heteronuclear multiple bond correlation spectroscopy
HPLC	High pressure liquid chromatography
HRMS	High resolution mass spectroscopy
HSQC	Heteronuclear single-quantum correlation spectroscopy
Hz	Hertz
IBA	iodosylbenzoic acid
IBX	2-Iodoxybenzoic acid
Ile	Iso-leucine
J	Coupling constant
kcal	kilocalories
L	Ligand
LED	Light-emitting diode
Leu	Leucine
LHMDS	Lithium bis(trimethylsilyl)amide
Lys	Lysine
m	Multiplet
<i>m</i>	Meta
M	mol/L
Me	methyl
Mes	mesityl
mg	milligram
min	minute(s)
mixt.	mixture
mL	milliliter
μL	microliter
mmol	millimol
M.p.	melting point
MS	mass spectrometry
ν	frequency (cm ⁻¹)
N	normality
<i>nBuLi</i>	<i>n-butyllithium</i>
NMR	nuclear magnetic resonance
n.r.	no reaction
Nu	Nucleophile
<i>o</i>	ortho

<i>p</i>	para
PB	Phosphate buffer
PBS	Phosphate buffered saline
PCET	Proton Coupled Electron Transfer
PEG	Polyethylene glycol
PG	protecting group
PIDA	phenyliodide diacetate
PIFA	phenyliodide ditrifluoroacetate
pH	Hydrogen potential
Ph	phenyl
Ph-EBX	1-[phenylethynyl]-1,2-benziodoxol-3(1 <i>H</i>)-one
ppm	parts per million
Pr	propyl
PTM	Post-translational modification
q	quartet
quint.	quintet
quant.	quantitative
R _f	retention factor
RP-HPLC	Reversed-Phase High performance liquid chromatography
RT	room temperature
RuAAC	Ruthenium-catalyzed azide-alkyne cycloadditions
s	singlet
sat.	saturated
SCE	Saturated calomel electrode
Ser	Serine
SET	single electron transfer
SiO ₂	Silica gel
sol.	solution
t	triplet
T	temperature
TBAF	tetra- <i>n</i> -butylammonium fluoride
TBHP	tertbutylhydroperoxide
<i>t</i> Bu	tertbutyl
<i>t</i> Bu-EBX	1-[tert-butylethynyl]-1,2-benziodoxol-3(1 <i>H</i>)-one
TBS	tertbutyldimethylsilyl

TES	triethylsilyl
Tf	triflate
TFA	trifluoroacetic acid
TFE	trifluoroethanol
THF	tetrahydrofuran
Thr	Threonine
TIPS	triisopropylsilyl
TIPS-EBX	1-[(triisopropylsilyl)ethynyl]-1,2-benziodoxol-3(1H)-one
TLC	thin layer chromatography
TMS	trimethylsilyl
TMS-EBX	1-[(trimethylsilyl)ethynyl]-1,2-benziodoxol-3(1H)-one
TMS-OTf	Trimethylsilyl trifluoromethanesulfonate
Tos	tosyl
Tris	2-Amino-2-(hydroxymethyl)propane-1,3-diol
Trp	Tryptophan
V	Volt
VBX	Vinylbenziodoxolone

Introduction

1

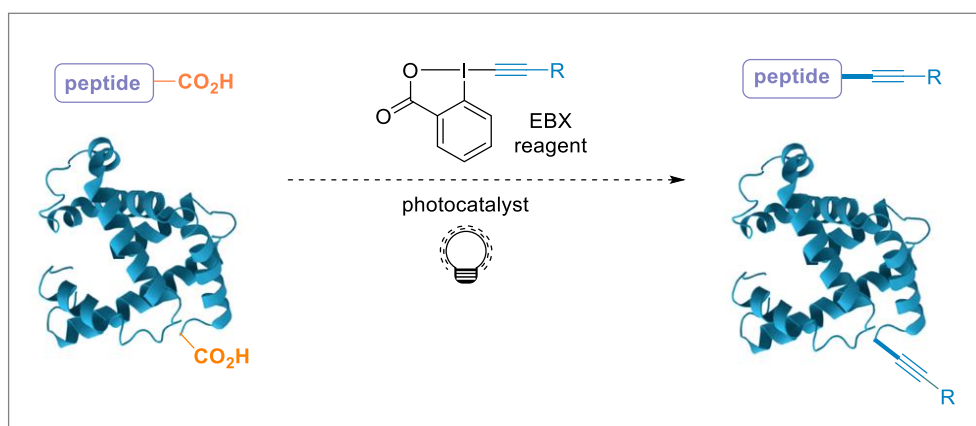
1 Introduction

Curing diseases, such as cancer, strongly relies on the study and the understanding of biological processes to afford more insight for the design of medicines.^[1] However, the study of biomolecules in their native environment is very challenging due to the complexity of cellular systems. The chemical modification of biomolecules has emerged as a powerful tool for the study of their structure and function. There is thus an urgent need for biomolecules functionalization methods. Due to the limited stability of proteins, classical conditions of organic chemistry cannot be applied, such as some organic solvents or high temperature. Physiological conditions are thus required and there has been a growing interest towards the development of biomolecule compatible methodologies.^[2]

One of the main interest of biomolecule functionalization is the incorporation of a bioorthogonal functional group, which can be later derivatized with chromophores for instance. Alkynes are very attractive as cycloadditions of an alkyne and an azide have demonstrated their efficiency in biomolecule labeling.^[1,3] Our group has gained expertise in the alkynylation of different functional groups.^[4,5] Especially, late stage alkynylation of peptides and proteins has been implemented.^[6,7] Our strategy towards alkynylation is to use Umpolung to reverse the reactivity of functional groups and allow new disconnections. To this end, EBX hypervalent iodine reagents have been extensively studied. They are very attractive as they combine the reactivity of transition metal reagents together with low toxicity and price.

In the search for mild conditions to generate reactive intermediates, photoredox catalysis has gained recently tremendous interest from the scientific community. It indeed allows a chemo-selective generation of radicals under very mild conditions, using light as an inexpensive and renewable energy source.^[8,9] The potential for the highly valuable functionalization of peptides and protein has started to be exploited.^[10] This field was still at an early stage at the beginning of this thesis.

Gratifyingly, photoredox catalysis and hypervalent iodine reagents can be combined to perform alkynylation under mild conditions. Carboxylic acids have been described as a traceless activating group, which is prone to decarboxylation with photoredox catalysis.^[11,12] A decarboxylative alkynylation of amino acids using photoredox catalysis and hypervalent iodine reagents has been previously achieved in our group.^[13] The purpose of my PhD was to contribute to the field of biomolecules site-selective chemical modification by providing a novel carboxylic acids residues bioconjugation tool on peptides first, then to proteins (Equation 1).



Equation 1: Visible-light catalyzed decarboxylative alkynylation of peptides and proteins

In this thesis, the first chapter will consist of a background description. The principle of biomolecule functionalization and the most frequent methods will first be presented. A description of hypervalent iodine chemistry and how it has been applied to peptides and proteins bioconjugation will then be disclosed. Photoredox catalysis, with application together with hypervalent iodine reagents and biomolecule compatible transformations, will later be described. Those three concepts will be detailed with a focus on C-terminal bioconjugation on proteins. This will conclude this literature chapter and be followed by the goal of this thesis (Chapter 3). Results and discussion chapters will then begin with the preliminary results towards a decarboxylative alkynylation in aqueous media (Chapter 4). An overview of our efforts on the development of novel organophotoredox catalysts will follow (Chapter 5). Results on the peptide decarboxylative alkynylation in organic solvent will then be presented and discussed (Chapter 6). Further extension of this methodology to proteins with the concept of proximity-induced photoredox catalysis will be the topic of the next chapter (Chapter 7). Finally, the optimization of a sequential decarboxylative-oxidation-arylation of peptides will conclude this results part (Chapter 8). A general conclusion of the work achieved during this thesis together with the proposed outlook will be proposed. The last chapter will consist of experimental and characterization data.

Background and Significance



2 Background and Significance

2.1 Functionalization of peptides and proteins

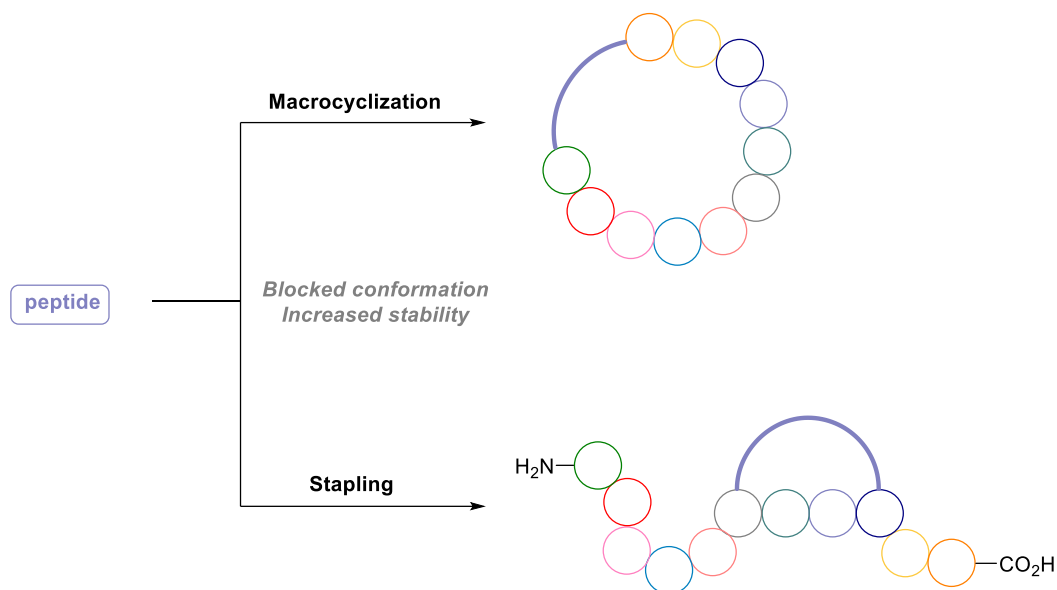
In this part, the significance of peptide and protein modification will first be described. As both the applications and the requirements can be quite different, distinct sections will cover those topics. Some methodologies are compatible with both classes of substrates, but adapted reaction conditions are most often encountered.

2.1.1 Significance of peptide functionalization

Bioactive peptides have emerged as key therapeutic agents to either activate receptors or disturb protein–protein interactions.^[14–19] They stand in between biologics and small molecules in terms of size. This results in an increased potency in comparison to small molecules, together with better target selectivity. The cell permeability is however better than those of larger biologics such as antibody-drug conjugates (ADCs). They also often present lower toxicity profiles due to their biodegradability. The synthesis and handling of peptides is also less tedious and expensive than those of biologics such as ADCs. Thanks to the developments of high-throughput screening and phage-display technologies, peptide screening is relatively easy.^[20–23] As a result, there were 140 compounds in clinical trials in 2015.^[16,19] Applications can be found in antimicrobial,^[24] cell-penetrating,^[25] amyloid, structural or antioxidant peptides for instance.^[14,16,26] In this context, the ability to selectively modify and introduce novel functionality on peptides is highly promising for the design of novel drugs. Functionalization strategies can be classified into either generation of peptide-conjugates (with glycosides,^[27–31] small-molecules,^[32] fluorophores^[33]...) or structural modifications towards novel scaffolds.

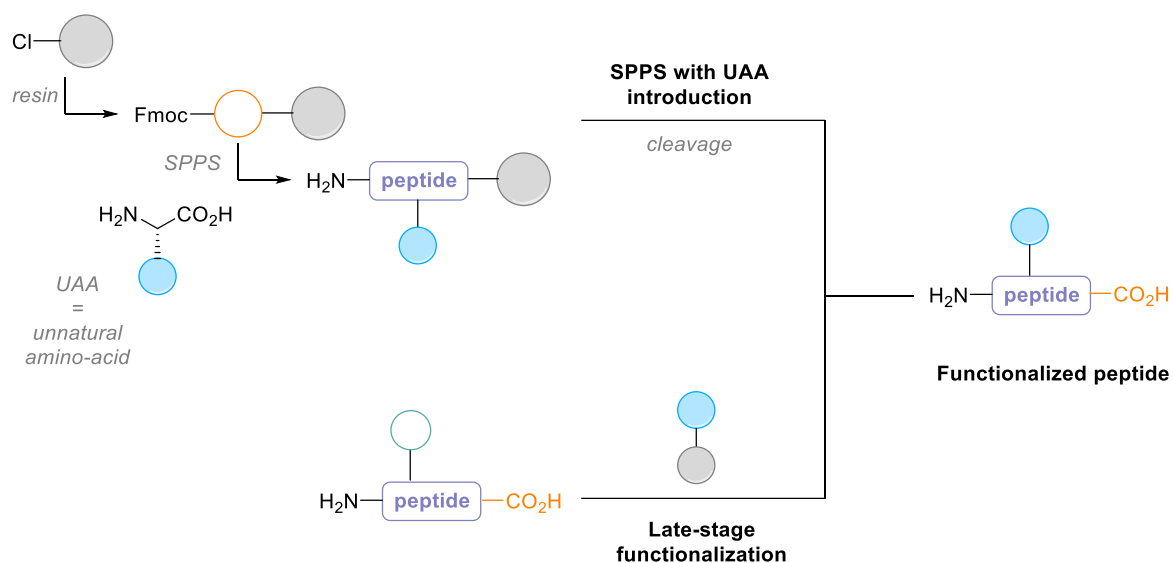
The sub-class of peptides macrocycles has grown exponentially recently, with continuous search for novel cyclization methods in order to access novel scaffolds (Scheme 1).^[34–41] Interestingly, even tetrapeptides can be efficiently cyclized.^[42,43] Stapled peptides, which consist of peptides where two amino acids are bonded by a linker, are another source of possible drugs, with various design of complexes bridges.^[44–46] Both macrocycles and staple peptides present the main advantages to possess a locked conformation and be more stable towards metabolism. Rigidity in the structure results in a better target affinity. Stability in the human body is indeed the main limitation of peptides drugs at the moment.^[17] Proteolysis

results in very short half-times and peptides are degraded within hours, if not minutes, in living organisms.



Scheme 1: Peptide stapling and macrocyclization

As peptides are most often synthesized by solid-phase peptide synthesis techniques (SPPS) with known sequences, the use of unnatural amino acids is a method of choice for introduction of a desired moiety, especially bioorthogonal functional groups (Scheme 2). However, this requires that the targeted group is stable under SPPS conditions and unnatural amino acids synthesis can turn out to be quite tedious. The late-stage functionalization of native peptides is thus highly attractive as it allows a more general approach. Mild conditions such as in the case of proteins together with excellent chemoselectivity are of paramount importance. Specific methodologies will be described in the next section.



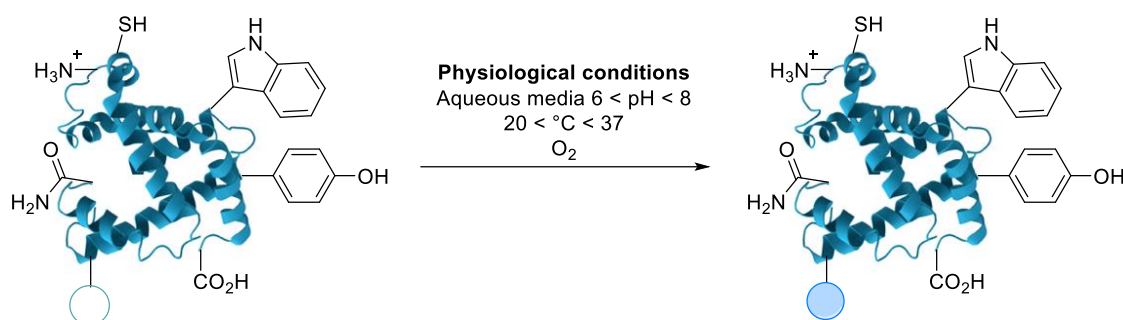
Scheme 2: General concept of peptide functionalization: SPPS with unnatural amino-acids vs. late-stage

2.1.2 Significance of site-selective protein modification

The advent of selective functionalization of one residue in proteins had a tremendous impact in the field of chemical biology. One of the major applications of the functionalization of biomolecules such as proteins is the elucidation of cellular processes.^[3] Cellular events can be monitored *in vivo*, for instance using fluorescent probes. This knowledge can possibly lead to a design of inhibitors for new therapies.^[33,47–49] Post-translational protein modifications (PTMs) have a major role in proteins activity by regulating their structure and physicochemical properties.^[50] The access to such transformations, or the exploration of novel directions, can be achieved by chemical methods. Therapeutic agents mixing biologics and chemicals, such as antibody-drug conjugates (ADCs) have been also an intensive field of research.^[51,52] They indeed combine the specificity of antibodies with the possible variety of small molecules to create targeted drugs. However, the development of successful ADCs rely on efficient and selective biomolecule functionalization methods. Other bioconjugates of proteins, such as glycosides are also highly valuable.^[27–30]

In chemoselective protein functionalization, one residue is targeted among all present functional groups. Challenges are encountered to achieve conditions compatible with biomolecules.^[3,53–55] The reason for that stands in the inherent nature of proteins, with the sensitivity of secondary structures for instance. The transformation has thus to be performed under physiological conditions, meaning: an aqueous media of neutral pH (6-8), moderate

temperature (20-37 °C), atmospheric pressure and in the presence of air (Equation 2). Regarding the selectivity, it is of paramount importance to achieve excellent regio- and chemo-selectivity, with the numerous naturally occurring functional groups tolerated. Purification is indeed quite tedious, or even not applicable in living cells. The reaction kinetics has also to be fast. Biomolecules solubility indeed requires a low concentration, together with the large molecular weight which decreasing molarity. Nevertheless, as biomolecules are highly precious, it is not an issue to employ a large excess of reagents for functionalization.



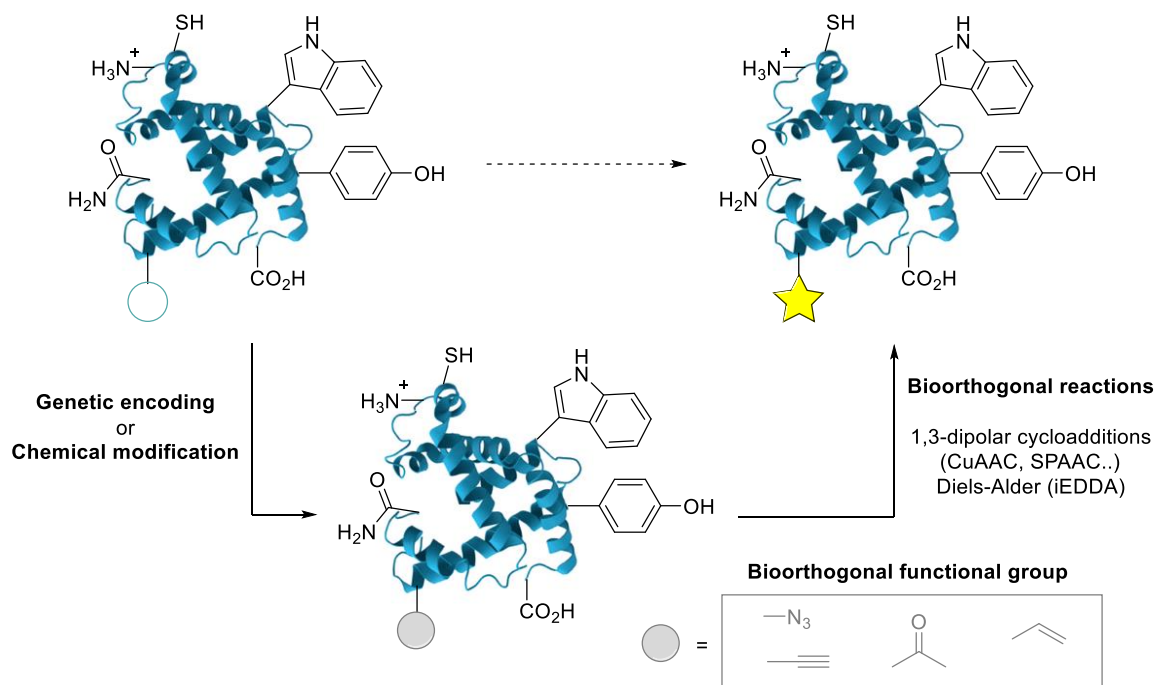
Equation 2: General concept of bioconjugation under physiological conditions

Protein modification methodologies can either be employed to insert directly the desired moiety, or very often serve to introduce a bioorthogonal functional group which can be employed as a platform for further derivatization (Scheme 3). The advantage of relying on that sequential approach is that only a few bioorthogonal functional groups need to be compatible with the functionalization methodology. In a second step, diverse targeted molecules can be linked with bioorthogonal reactions from a common intermediate.

Regarding protein modification, two main approaches are available: genetic encoding or chemical modification. For the former, some bioorthogonal functional groups can be incorporated into proteins by replacement of amino acids by their unnatural counter-part in the cell media.^[55] The work from the Schultz group allowed key advances in this field.^[56,57] However, this requires prior knowledge of the targeted protein sequence and engineering. An unknown protein sequence can thus not be modified and identified with this strategy. Despite those impressive advances, this methodology still lacks generality as not all functional groups possess their unnatural amino acid counterpart. Chemical labeling is thus highly attractive as it allows the study of native proteins in their environment. The next section will be dedicated to this concept.

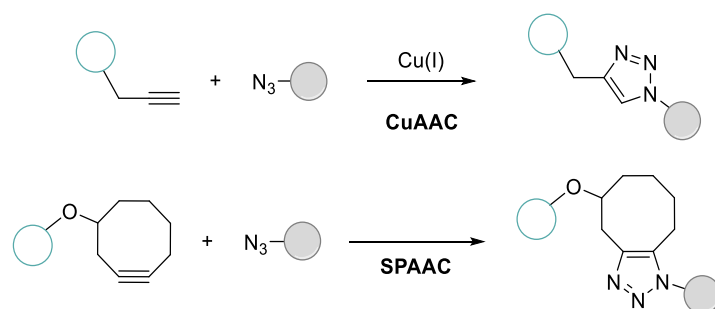
When designing bioorthogonal functional groups, they first have to be stable in aqueous media and inert regarding other functional groups present on the biomolecule.^[1,3,47,53,58,59] A

compromise has thus to be found between reactivity and stability under physiological conditions. In order to alter the structure and thus the activity as little as possible, it is preferable to employ small groups. Only a limited number of moieties match those criteria, with terminal alkynes and azides as the historically most important ones.



Scheme 3: Protein labeling using bioorthogonal functional groups

Various chemical reactions have been developed for bioorthogonal chemistry (Scheme 4).^[54,55,60,61] The most widely used bioorthogonal reactions are the cycloadditions,^[47,53,62] such as the Cu-catalyzed azide-alkyne cycloaddition (CuAAC), the strain-promoted azide-alkyne-cycloaddition (SPAAC),^[63] the Inverse electron demand Diels-Alder reaction (iEDDA),^[64,65] or the Ruthenium-catalyzed azide-thioalkyne cycloadditions (RuAtAC).^[66] Recent developments also include light-induced Click reactions,^[67] or the use of cyclopropenes as a novel bioorthogonal functional group.^[68]

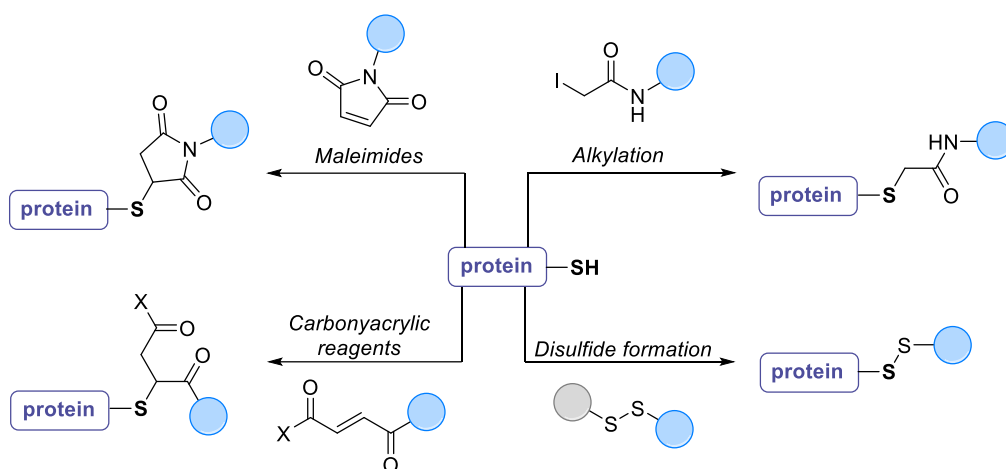


Scheme 4: Examples of bioorthogonal reactions, CuAAC and SPAAC

2.1.3 Overview of chemical site-selective modification methods

Chemical methods have led to very efficient direct modifications of peptides and native proteins. Major advances have already been reviewed and will not be described in details.^[2,47,69–75] The field of selective chemical biomolecule modification has evolved rapidly in the last two decades, starting from few reactions exploiting the nucleophilicity of cysteines and lysines, to a broad scope of methods that can even be run *in vivo*. Examples based on hypervalent iodine reagents or photoredox catalysis will be described in the dedicated sections (sections 2.2.3 and 2.3.4).

Among the modification of natural amino acids, cysteine stands as the most intensively studied with numerous reports on selective reactions thanks to its low abundance (<2%) and its strong nucleophile character (Scheme 5).^[47] This rare amino acid has been intensively targeted using site-directed mutagenesis. Mutants bearing a single cysteine can then be subjected to the following methodologies.^[2] The thiol moiety can undergo additions to Michael acceptors and maleimides are widely employed. However, the resulting adducts often lack stability, with retro-Michael or thiol-exchange reactions. To overcome this limitation, irreversible addition of carbonylacrylic derivatives has been described.^[76,77] Alkylation with alkyl halides (α -halocarbonyls and iodoacetamide especially) has also been reported.^[78,79] Mixed disulfides can be obtained by disulfide exchange.^[3] Radical reactions are emerging methods and are described in section 2.3.4.

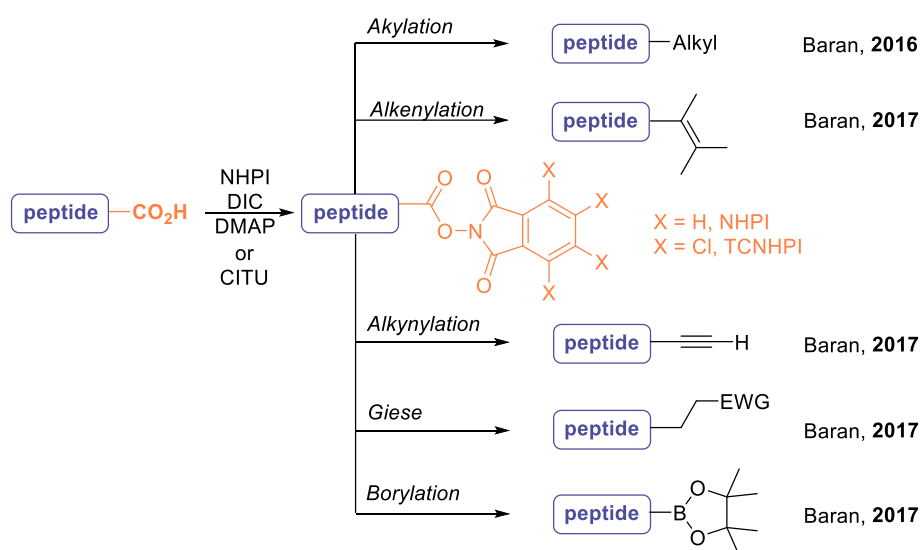


Scheme 5: Selected examples of site-selective modification of cysteines

Lysine is also an attractive target thanks to the numerous methods known for primary amine functionalization and its nucleophilicity. However, the amount of lysines in proteins (around 6%) renders single-site modifications challenging and heterogeneous mixtures are often obtained. Interesting advances were made based on the tertiary structure to target the most reactive residue.^[2] Popular reagents are activated esters, aldehydes, sulfonyl chlorides and isocyanates.^[3] If labeling of tyrosine and tryptophan has not been widely studied, single-site modification can be envisioned due to the rarity of those amino acids. There are examples of electrophilic aromatic substitution on the phenol moiety,^[80] as well as oxidative coupling of two phenol groups using transition-metal catalysis,^[81] or electrochemistry,^[82] Ene-type reaction,^[83] and O-glycosylation.^[31] The N-terminus is an attractive site because of a pKa difference with other lysines, which can be employed for site-selectivity.^[84] Transamination is an efficient technique for selective modification at the N-terminus, although specific residues at the N-terminus are often required to afford good yields. In the case of N-terminal cysteine residues, native chemical ligation has emerged since its discovery in 1994 by Kent and co-workers as a very selective and efficient method for protein synthesis.^[85,86] Following the equilibration between a C-terminal thioester and the cysteine residue, an irreversible S-N acyl transfer affords a native peptide bond.

2.1.4 C-terminal bioconjugation

Carboxylic acid residues have been investigated as target in both peptide and protein late-stage functionalization. Relevant works on peptides will first be described. A successful approach relies on the pre-functionalization of the carboxylic acid to a redox-active ester (RAE), followed by single electron reduction, decarboxylation and subsequent radical addition.^[87] RAE are made in a single step, can be isolated and are stable in aqueous media (Scheme 6). Key advances were made by the Baran group using this strategy including alkylation,^[88,89] alkenylation,^[90] alkynylation,^[91] Giese coupling,^[92,93] and borylation.^[94] The general principle relied on a nickel-catalyzed decarboxylation followed by reaction with zinc reagents. By a judicious choice of orthogonal groups during the Fmoc-SPPS, on-resin reactions on protected peptides were achieved, later extended to unprotected peptides with the use of unnatural amino acids. This approach was also extended to access DNA-encoded libraries. In that case, the Michael acceptor was located on DNA. It is important to note that in most of those cases, the decarboxylation was occurring on the side-chains and not at the C-terminal position. As the carboxylic acid needs to be pre-functionalized, this prevents any selectivity between positions. Photocatalytic pathways for carboxylic acids functionalization are described in a dedicated section (2.3.5).

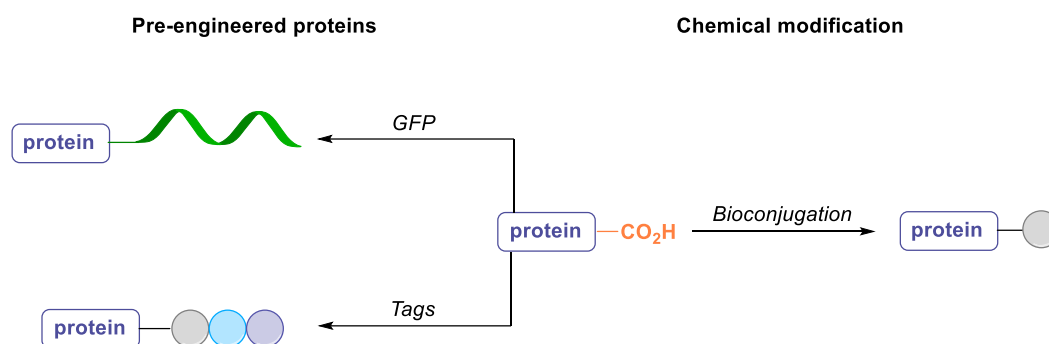


Scheme 6: Decarboxylative reactions on peptides using RAEs described by the Baran group

The C-terminal position is highly attractive site for selective protein modification. As for the N-terminus, abundance is a key factor. Chemoselectivity between all canonical amino acids is already very important, but site specificity as well among all occurrences of the same amino acid. The abundance of other residues with carboxylic acids on the side-chains, aspartic and glutamic acids is respectively of 5.3 and 6.3%.^[84] Regioselectivity is thus challenging. It is interesting to note that extremities of proteins are usually accessible and poses quite distinct chemical environments in comparison to the rest.^[2] Functionalization has been explored both from pre-engineered proteins and chemical approaches on native proteins.

Fusion with tag-proteins has demonstrated its efficiency since the first breakthrough with the genetically encoded fluorescent proteins (GFP),^[95–97] which led to unprecedented imaging of living systems (Scheme 7). This discovery was awarded the 2008 Nobel Prize in Chemistry. However, this method only stands for proteins and requires prior knowledge of the sequence for the expression process. No labeling of a native protein can be achieved. The size of the tag which is protein on its own of around 200 residues also consists of a drawback. Possible loss of structure and activity can occur. Finally, applications of GFP insertion are limited to imaging, no bioconjugation with valuable molecules can be envisioned. Labeling with smaller functional groups is thus highly desirable. An engineered combination of natural amino acids can also induce a selective labeling at a specific site, by introducing a single cysteine for example.^[98] This sequence can be genetically encoded for incorporation into a protein. Different sites have been described, among them the C-terminus.^{[99][73]} Tsien and co-workers

demonstrated for instance that the tetracysteine motif CCXXCC can react selectively with biarsenical-functionalized dyes.^[3] More recently, the HALO-, SNAP-, CLIP-tags were developed.^[98,100–102] Once the tag is covalently linked to the protein of interest, further functionalization can be performed. Despite valuable applications, those tags still require engineering of the desired protein with drawbacks of a tedious synthesis, possible loss of function and lack of variety of the introduced moiety.

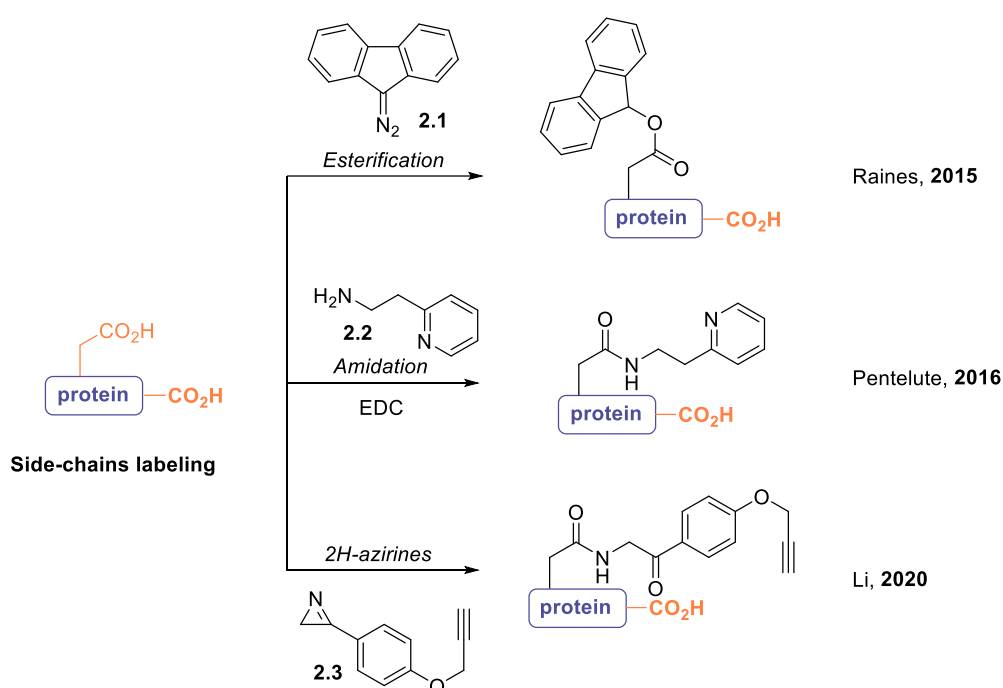


Scheme 7: C-terminal modification approaches

There are only few reports about C-terminal extremity or glutamate and aspartate residues chemical labeling due to the challenging selectivity between those positions (Scheme 8).^[103] A seminal work was disclosed in the 1960s using diazo compounds towards esterification.^[104–106] Single addition on the most reactive side-chain residue on the active site of the protein was then observed by the authors. However, large excess of the diazo reagent was required, together with careful control of the pH. This strategy was later extended by the Raines group towards protein prodrugs development.^[107] Depending on the diazo compound employed, several residues were esterified, including the C-terminal in one case. The pattern likely also depends on the reactivity and accessibility of each carboxylic acid. The esterified proteins were later subjected to esterases to provide a bioreversible modification. The reactivity of diazo compounds **2.1** in regard to proteins was further studied by the same group.^[108]

Using carbodiimides such as EDC, amide-bond formation with amines **2.2** has also been reported. Building on early works,^[109,110] the Pentelute group disclosed a bioconjugation using N-hydroxysulfosuccinimides (NHS) together with EDC.^[111] An intensive study of the possible side-products, from other residues as well as from the reagents themselves, was performed. This lack of understanding was indeed preventing the use of this transformation by the community. However, study on a model protein highlighted that several acid residues, but also other side-chains were labeled. This limits potential applications.

Recent progress was made with the successful reaction of 2H-azirines **2.3**.^[112] This novel bioconjugation method presented an excellent chemoselectivity towards aspartic and glutamic residues. Although an increase in labeling of glutamic residues was detected, no site-specificity was observed and several residues were functionalized in each substrate. Most modifications occurred in proteins binding sites. Several native proteins were studied, demonstrating the generality of this method and its high potential. Especially, the introduced moiety is small and modular as it is substituted with a free alkyne, which was used in the study for Click reactions and imaging. Very interestingly, labeling can even be performed in living cells, which is the first occurrence of such an achievement on carboxyl residues.



Scheme 8: Chemical modification of proteins on carboxylic acid residues

Some strategies are employing the inherent activity or structure of targeted proteins. Although conceptually interesting and useful for the targeted substrates, broad applications remain limited. An early work from the Bertozzi group achieved the labeling of glycosidases in cells lysates with azide-substituted glycosides.^[113] Selective addition was obtained by using the reactivity of glycosidases, leading to addition of a carboxylate from the active site on the probe. The Waldmann group also reported a glutamic acid bioconjugation method.^[114] An inhibitor of the target protein was modified to achieve a selective labeling at one glutamic residue inside the binding pocket, through a tether strategy. This elegant method however required engineering and lacks generality in terms of protein targets at the moment.

Single-site protein modification remains difficult despite recently disclosed impressive achievements. Different methods are showing complementarity and even when targeting the same residue, different conditions can result in an interesting change of selectivity. An attractive site for a selective labeling is the C-terminus but only limited methods have been developed so far. Introduction of an alkyne moiety would afford a versatile platform for further derivatization using bioorthogonal reactions to label with fluorophores or create a peptide linkage for instance. Although some methods have been developed, late-stage introduction of alkynes on peptides and proteins remains a challenging task, which would require mild conditions for alkynylation. We have thus envisioned to use hypervalent iodine reagents as the alkyne source. Their reactivity will be described in the next section.

2.2 Hypervalent iodine reagents for alkynylation of peptides and proteins

2.2.1 Structure and general reactivity

Hypervalent iodine compounds exist with oxidation state of iodine of III, V or VII. Depending on the ligands on the iodine atom, they are named λ^3 -iodanes (one carbon ligand), λ^3 -iodoniums (two carbon ligands) or λ^5 -iodanes (Figure 1).^[115–118] When iodine(III) is substituted only with carbon ligands, the compounds are unstable.

Hypervalent iodine reagents are attractive thanks to their ability to react like metal reagents, while being less toxic and expensive. This reactivity results from the hypervalent bond. This a three-atom four-electron bond involving non-hybridized 5p orbitals, which is weaker and longer than usual covalent bonds. This linear hypervalent bond induces a T-shaped geometry at the iodine atom, which has been observed by X-Ray analysis. This observation is in accordance with the Martin-Arduengo designation 10-I-3 for λ^3 -iodanes. In this N-X-L notation, N represents the number of valence electrons, X the central atom, and L gives the number of ligands. λ^3 -iodanes present a pseudo-trigonal bipyramidal geometry with the most electronegative ligands located in the apical (axial) positions.

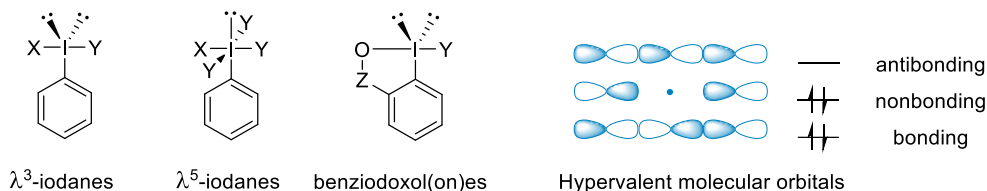


Figure 1: Structure of hypervalent iodine compounds

λ^5 -iodanes, such as Dess-Martin periodinane (**2.1**) or 2-iodoxybenzoic acid (IBX, **2.2**) (Figure 2), possess oxidizing properties and have been extensively studied for mild oxidation, for instance of alcohol to carbonyls. As they are not suitable for group transfer, only hypervalent (III) reagents will be further detailed.

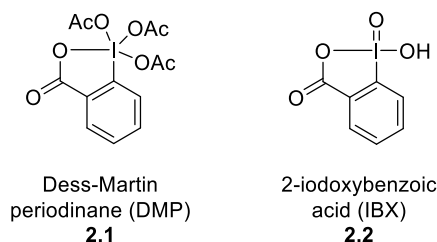


Figure 2: Classic λ^5 -iodanes reagents

Among the λ^3 -iodanes, one class has been widely studied in the last decade, the benziodoxoles, where the iodine atom belongs to a 5-membered ring (Figure 3). More precisely, when this oxygen atom is part of a carboxylate, the derivatives are called benziodoxolones. Cyclic hypervalent iodine reagents are more stable, as a better overlap of orbitals between the iodine atom and the benzene ring is possible. The destabilizing *trans*-effect in the hypervalent iodine bond is then compensated. Work from the group of Schaefer highlighted that the cyclic structure also prevents reductive elimination to occur.^[119] This results in compounds stable to air and moisture, hence more convenient for use. Variation of the substituents on the aromatic ring or in Z position has an impact on the properties. Ethynyl benziodoxolones (EBX) were first synthesized by Ochiai et al.,^[120] then by Zhdankin and co-workers^[121] and studied in details by our group, especially TIPS-EBX (**2.4**) and Ph-EBX (**2.5**).^[4,5,115] Other important benziodoxolones are hydroxybenziodoxole (BI-OH, **2.6**), cyanobenziodoxolone (CBX, **2.7**), Togni's reagent (**2.8**) and azidobenziodoxolone (ABX, **2.9**).

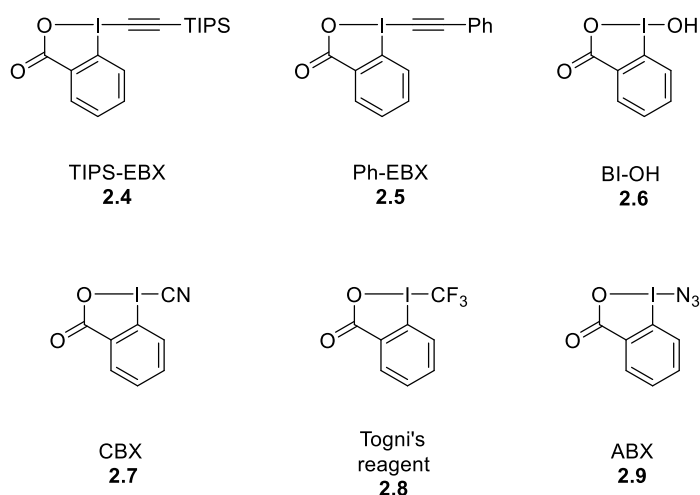
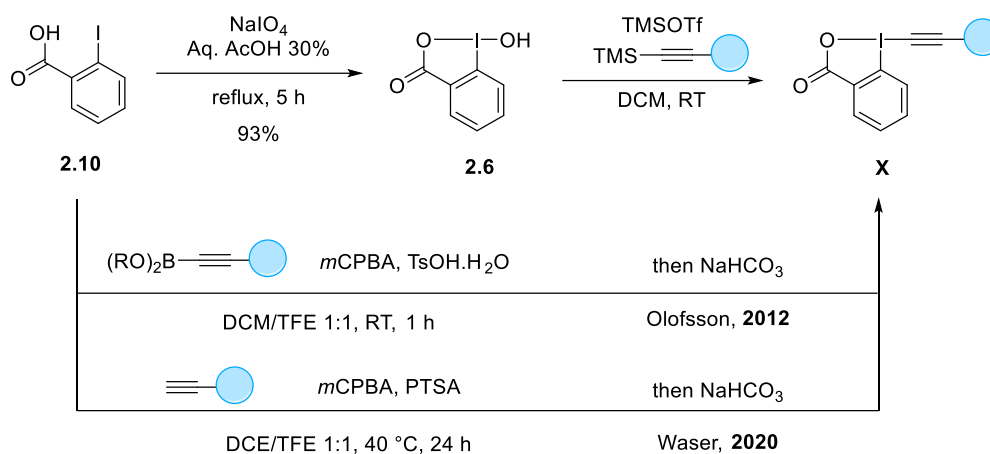


Figure 3: Examples of hypervalent-iodine group-transfer reagents

EBX reagents are readily available from 2-iodobenzoic acid (**9**) and the synthesis is depicted in Scheme 9.^[115] The first step consists of an oxidation towards hydroxybenziodoxole (BI-OH, **2.6**), which is then converted to the desired EBX reagents upon addition of TMS-alkynes. In order to increase the accessibility of synthesis, novel protocols have been reported. A major contribution from the Olofsson group describes a fast, one-pot procedure.^[122] However, practicability remained limited as ethynylboron precursors are expensive, if they are commercially available, and difficult to synthesize. Our group further optimized this approach and reported terminal alkynes as suitable starting materials.^[123] Not all EBX reagents are

nevertheless compatible with those conditions, such as the ones bearing electron rich alkynes. Care in the choice of the procedure is thus the key to high synthetic efficiency.

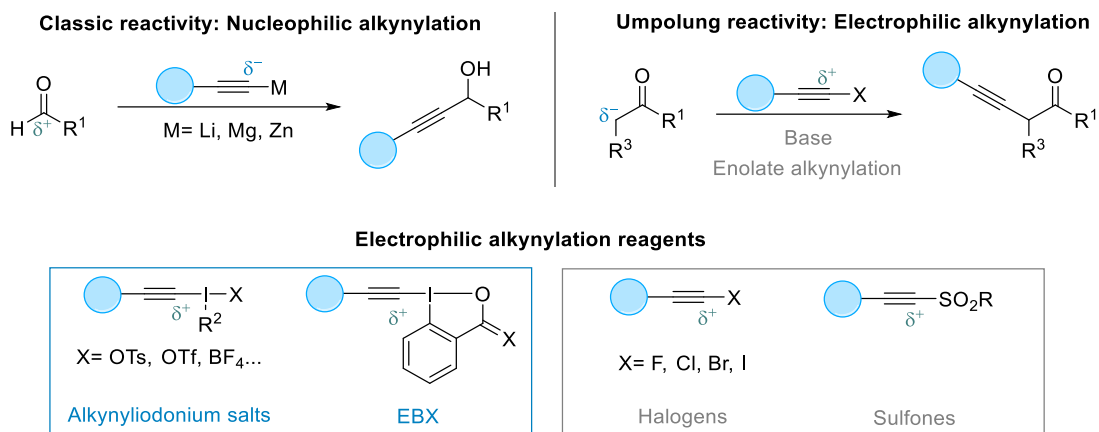


Scheme 9: Synthesis of EBX reagents

λ^3 -iodanes are weak oxidants but the strong electrophilicity of the iodine introduces a great potential as electrophilic group-transfer reagents. Extensive work on alkynylation, cyanation, azidation and trifluoromethylation has been performed.^[115–117,124,125] This report will focus on electrophilic alkynylation reagents.

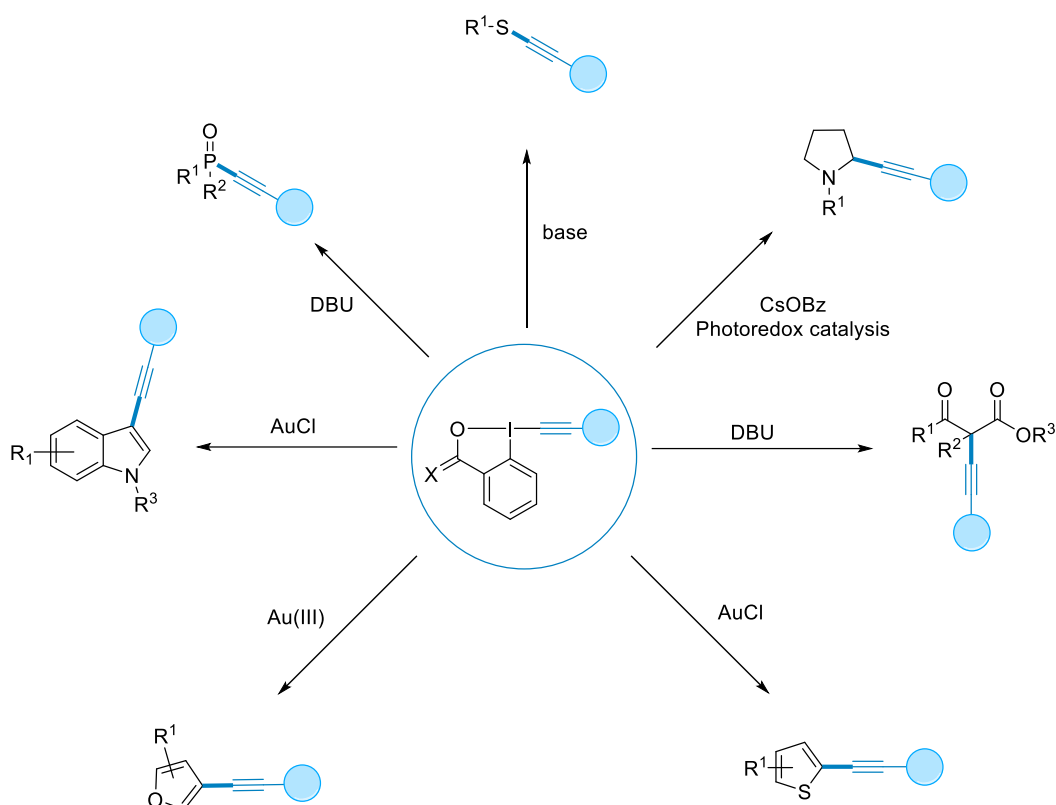
2.2.2 Alkynylation with EBX reagents

Alkynes synthesis by nucleophilic alkynylation has been intensively described (Scheme 10). The high acidity of the terminal C-H bond renders access to acetylide anions straightforward. The terminal alkyne addition to a carbonyl under basic conditions or the Sonogashira cross-coupling allow a reliable access to substituted alkynes.^[116] The opposite approach, addition of alkynes to nucleophiles requires inversion of polarity, an Umpolung, which is more challenging.^[115] If alkynyl halides or sulfones are suitable electrophilic alkynylation reagents, hypervalent iodine reagents are most often preferred for their increased reactivity. First results were obtained using alkynyliodonium salts but the better stability and selectivity of cyclic reagents have led to their extensive use.^[4,115]



Scheme 10: From nucleophilic alkynylation to electrophilic alkynylation

Application of this strategy have led to successful methods for alkynylation of C-H, C-C and C-heteroatoms (N, S and P) bonds. Our group has investigated electrophilic alkynylation reactions in α -position of carbonyls,^[126] olefins,^[127] thiols,^[128,129] heterocycles (anilines,^[130] pyrroles,^[131] indoles,^[132] thiophenes,^[133] furans^[134] and benzofurans^[135]) and β -ketoesters.^[136] A selection of the state of the art of electrophilic alkynylation is presented on Scheme 11.^[4,115] Alkynylation of biomolecules will be described in section 2.2.3.

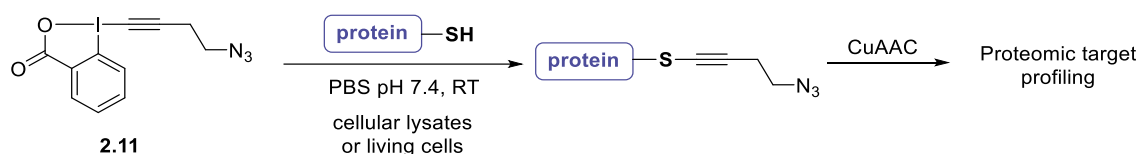


Scheme 11: A selection of electrophilic alkynylation reactions with hypervalent iodine reagents

2.2.3 Functionalization of peptides and proteins with hypervalent iodine reagents

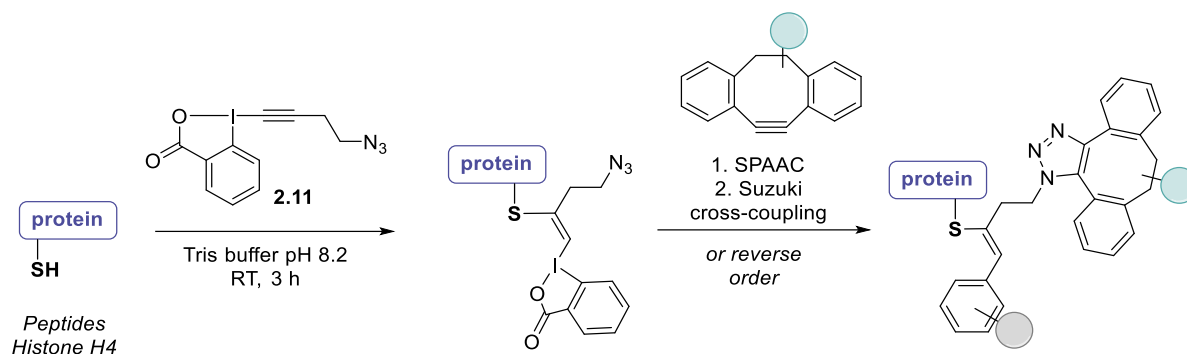
Thanks to their stability and relative non-toxicity, hypervalent iodine reagents are attractive candidates for biomolecule modification. This section will be dedicated to reactions involving hypervalent iodine compounds as group transfer reagents towards C-C bond formation. Only reports involving peptides and proteins as starting materials will be covered. Works on amino acids, or towards their synthesis, will not be disclosed here. Methodologies can be distinguished depending on the introduced functional group and arylation, alkynylation, difluoromethylation and diazo group addition have been reported. Reports involving photoredox catalysis will be described in the dedicated section 2.3.4. Oxidative properties of IBX reagents were also used, notably by the group of Kanai in an elegant Asn-selective peptide bond cleavage.^[137] Upon oxidation with PIDA, an Hofmann rearrangement takes place to afford two peptide fragments after hydrolysis.

Knowing the ability of hypervalent iodine reagents to perform electrophilic alkynylation under mild conditions on non-activated substrates, the introduction of an alkyne as a bioorthogonal functional group can be envisioned. The thiol-alkynylation reported by our group in 2013 tolerated a broad range of functional groups on the EBX reagent, as well as substrates.^[128,129] The extraordinary rate of this transformation together with the high chemoselectivity allowed its use for biomolecule labeling. Within a collaboration with the Adibekian group, a cysteine alkynylation in biomolecules was achieved (Scheme 12).^[6] Higher efficiency and selectivity than alkylating reagents were obtained. Starting from an azide-substituted EBX **2.11**, the obtained thioalkynes were further functionalized by CuAAC. This efficient method was even performed in living cells. The major drawback of this thiol-alkynylation is the limitation to highly reactive positions. Cysteine-active enzymes are specific targets. Thiol-alkynylation using this azide-substituted EBX was further extended by the group of Matile to cell-penetrating poly(disulfide)s (CPDs).^[138] CPDs were synthesized by ring-opening disulfide-exchange polymerization, with EBX as the terminator. Our group recently reported the formation of thiol-alkynes on peptides, proteins and antibodies using hypervalent iodine reagents.^[139]



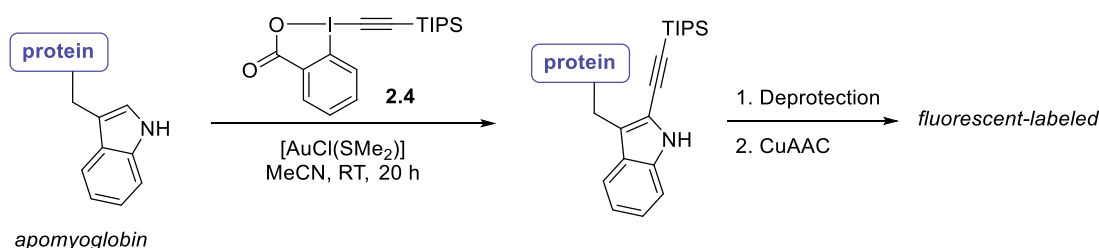
Scheme 12: Thiol-alkynylation in living cells

When investigating this thiol-alkynylation in aqueous media, a different outcome was obtained. Novel vinyl benziodoxolone reagents, formed by addition of cysteines on EBX reagents such as **2.11**, allowed a doubly-orthogonal labeling of proteins (Scheme 13).^[7] Indeed, two distinct functional groups are introduced on proteins in this selective bioconjugation. The azide group can be further employed in a Click reaction with cyclooctynes and the hypervalent iodine can be engaged in a Suzuki-Miyaura cross-coupling. The successful labeling from small-molecules to proteins such as Histones was possible thanks to the physiological conditions.



Scheme 13: Doubly-orthogonal bioconjugation on cysteines

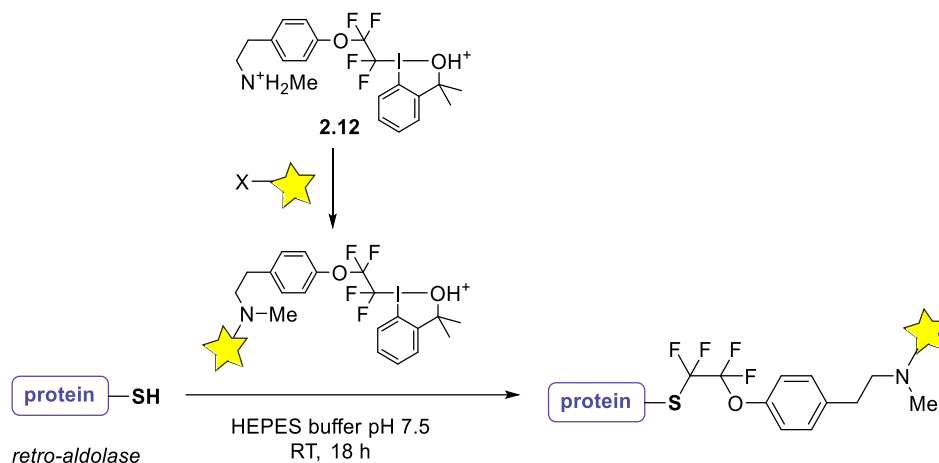
Other residues have also been studied. Our group built on results of a gold(I) indole alkynylation towards tryptophan-containing dipeptides.^[132] This methodology was extended to an ethynylation of tryptophans in peptides and in a protein with TIPS-EBX (**2.4**) under gold(I) catalysis by Hansen *et al.* (Equation 3).^[140] This chemo- and regioselective ethynylation in C2-position of indoles could be further followed by CuAAC after deprotection. However this reaction required acetonitrile as a solvent, limiting applications on sensitive proteins.



Equation 3: Ethynylation of Trp residues with TIPS-EBX

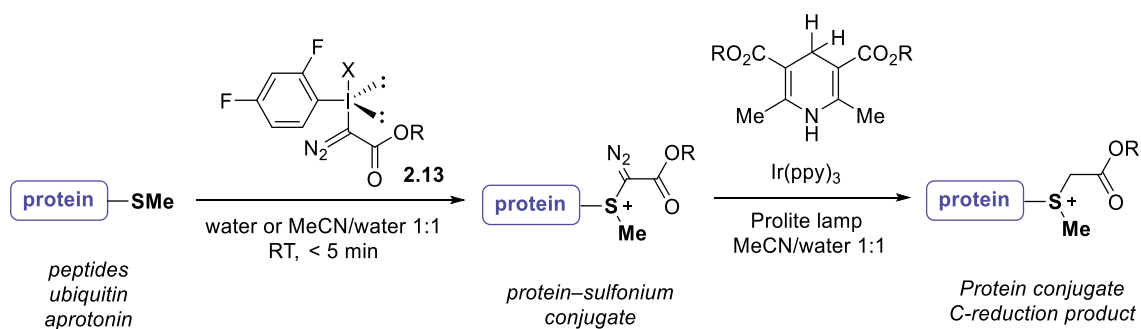
Hypervalent iodine reagents have also been employed for other group-transfer reactions than alkynylation. Electrophilic fluorination has been the subject of recent studies on peptides and proteins due to the importance of fluorine substitution in drug discovery. Difluoromethylation of protected cysteines was described by the Togni group with novel tetrafluoroethyl substituted hypervalent-iodine reagents.^[141] Recently, the same group developed a cysteine-selective labeling using novel hypervalent iodine fluoroalkylation reagents (Equation 4).^[142] The approach was interesting, with the synthesis of an amine substituted reagent **2.12** which allowed easy diversification afterwards. Better solubility of the reagent was achieved by protonation of a tertiary amine group. A synthetic retro-aldolase was irreversibly labeled with fluorophores, with full selectivity for cysteine compared to lysine. This is in contrast with established methods using maleimide or iodoacetamide reagents leading to

non-selective, and for maleimide reversible, labeling. Trifluoromethylthiolation with hypervalent iodine has also been reported on dipeptides.^[143] Efficient labeling of cysteines in dipeptides was achieved in HFIP with a good functional group tolerance.



Equation 4: Cysteine-selective protein difluoromethylation

Selective bioconjugation at methionine residues on proteins was described recently by Gaunt and co-workers (Equation 5).^[144] Through the use of a iodonium salt **2.13**, protein-sulfonium conjugates were obtained on various proteins. This electrophilic addition of a diazo group was fast, efficient even in very diluted conditions and in aqueous media.



Equation 5: Methionine bioconjugation using hypervalent iodine reagents

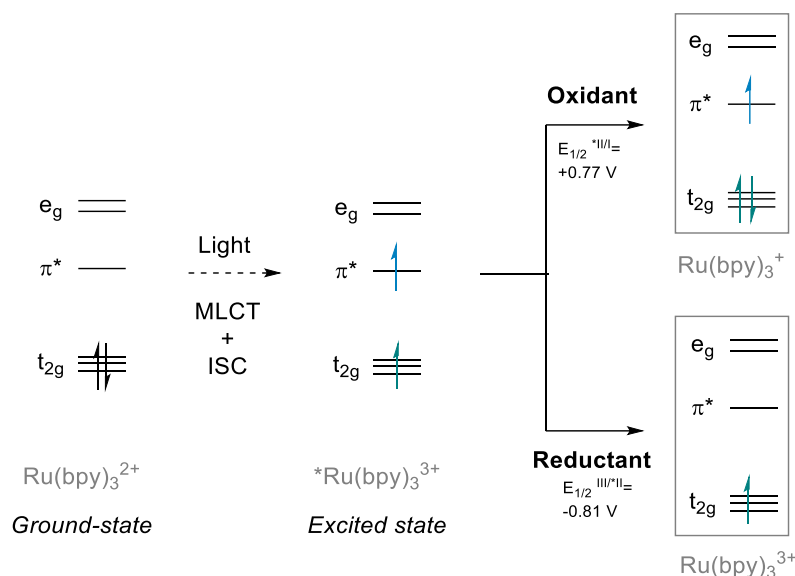
Despite a limited number of examples on the functionalization of proteins using hypervalent iodine reagents, existing reports are very promising and highlighted the potential of those reagents for selective labeling under physiological conditions. We thus envisioned to target a different residue. The C-terminal extremity of peptides has never been functionalized using hypervalent iodine reagents towards C-C bond formation to the best of our knowledge.

2.3 Photoredox chemistry for decarboxylation on peptides and proteins

2.3.1 Principle

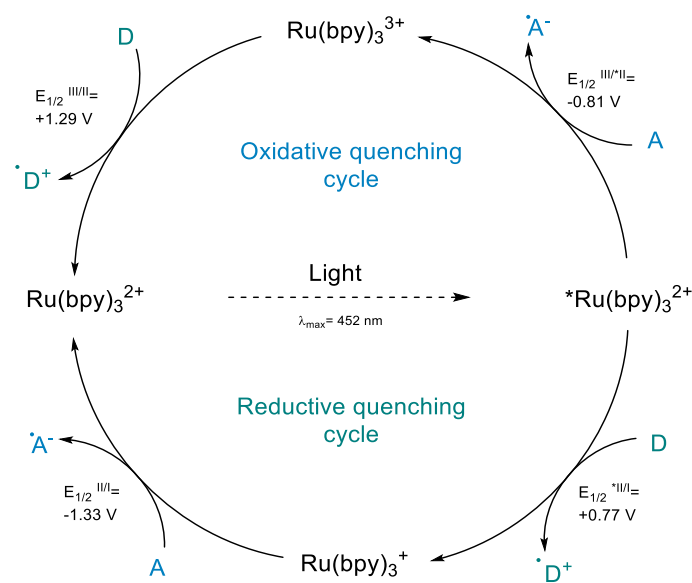
Using light as an energy source is very attractive as sunlight is costless and renewable. Generation of radicals using UV light has been known for decades but suffers from the need of specific glassware as well as the high energy of UV light, leading to side-reactions. For that reason, visible-light catalysis has gained interest and has been an extensively studied field in the last decade. If plenty of applications for solar cell materials had been previously developed, it is only recently that this field gained interest from an organic chemistry point of view.^[8] Photoredox catalysis allows novel reactivity and unprecedented transformations can now be performed under mild conditions. This is due to the photoredox catalysts (PC) characteristic to be both oxidants and reductants.

In the case of metal-based catalysts, the PC absorbs a photon upon light-irradiation and generates an excited state PC* by a metal to ligand charge transfer (MLCT).^[8,9,145] During this process, one electron from a metal-centered orbital is excited to a ligand-centered π^* -orbital. Commonly used transition-metal PC absorb in higher energy visible-light (400-475 nm) in order to prevent undesired direct excitation of organic molecules. Then a fast intersystem crossing to the lowest-energy triplet excited state can take place, which has a longer life time and can thus be engaged in single-electron transfers. Return to the ground-state is spin-forbidden and this increases the life time. The key for exceptional reactivity in photoredox catalysis is that the excited catalyst is both more oxidizing and more reducing than the ground-state. The explanation lies in a molecular orbital diagram: the excited electron is in a higher energy orbital, together with a lower-energy hole (Scheme 14).

Scheme 14: Molecular orbital and photoactivation of Ru(bpy)_3

Once the photocatalyst has reached the excited state, several activation modes have been explored. Photoinduced electron transfer (PET) has been widely explored using the exceptional oxidative and reductive properties of photocatalysts. Energy transfer (EnT), affording an excited substrate, has emerged more recently and will not be discussed in details in this report. Atom transfer is also possible. Two different mechanisms are possible in PET: either by oxidative quenching or reductive quenching (Scheme 15). The scheme presents the photoredox properties of Ru(bpy)_3 as it is maybe the most extensively employed catalyst.^[8,9,145] If the first step of the mechanism is reduction of the substrate via a single electron transfer, the latter is defined as an oxidative quencher of the photocatalyst and the catalytic cycle named an oxidative quenching. Similarly, if the substrate is first oxidized, the process is occurring through a reductive quenching. Further oxidation or reduction of the PC regenerates the ground-state. Each step proceeds with either a donor or an acceptor molecule which can be either the substrate, a sacrificial electron donor/acceptor, or a reactive intermediate. The oxidant and reductant strength of photocatalysts can be estimated by the half reduction and oxidation potentials. Comparison between values from the reactants and the photocatalyst allows prediction of reactivity. This indeed indicates whether the elementary step is thermodynamically feasible. Fluorescence quenching techniques can be used to confirm this experimentally. Stern-Volmer analysis consists of the measure of the quantity of emitted photons in presence or absence of a quencher. Those results indicate if the excited catalyst is quenched by the studied compound and thus if a PET occurs. Different intensities of quenching indicates the most likely reactive species. Processes can be distinguished depending on the presence or not of a radical chain. In the case of a chain, it is a light-induced transformation.

Experimental techniques for this determination include on/off measurements. If there is no propagation, the reaction is photoredox-catalyzed.



Scheme 15: Oxidative and reductive quenching cycles of $\text{Ru}(\text{bpy})_3$

The field of photoredox-catalysis has grown rapidly in the last decade with tremendous achievements.^[8,9,146] Current topics include the merge with transition-metal catalysis,^[147] organocatalysis,^[148,149] electrochemistry,^[150,151] biocatalysis^[152–154] or flow chemistry for industrial applications.^[155] As the basis for any photoredox transformation is the photocatalyst, this will be discussed in the next section. Application of photoredox catalysis for biomolecule functionalization will be presented later in section 2.3.4.

2.3.2 Photoredox catalysts: design and overview

Transition-metal photocatalysts

The advent of photoredox catalysis relied on the use of transition-metal based catalysts. They were first employed in solar energy conversion before being the basis of the seminal works. Extensive studies have been performed regarding the modulation of their redox properties by variation of either the metal or the ligands, resulting in a large variety of polypyridyl complexes (Figure 4).^[8,9] Substitution of the metal with two different ligands, leading to heterolyptic complexes, allows an easy rational design. Indeed, the LUMO and HOMO of the catalyst are in that case spatially separated and this allows selective tuning of one of the

redox potentials, either oxidation or reduction. Regarding the choice of metal between Ru(II) and Ir(III), the main difference is the ability of Ir of supporting orthometalated phenylpyridine (ppy) ligands. It is good to keep in mind that those anionic LX ligands necessitate electron-withdrawing groups for stabilization, hence the recurrent presence of fluorine atoms. In addition, Ir(III) is less electron rich than Ru(II) which makes it harder to oxidize. Those effects explain the larger redox window of iridium complexes. A rational ligand design is possible because excited electrons are promoted from a HOMO with both metal d and ligand π character to a ligand π^* orbital.^[156,157] As a result electron-donating substituents on the ligands increase the reducing character of the catalyst. The opposite effect with electron-withdrawing groups (EWG) on ligands is observed. An EWG will indeed lower the energy of the π^* -orbital of the ligand and as consequence, the energy level of the excited state. It is noteworthy that electrochemical properties are environment dependent. Variation depending on the solvent and pH for instance are important and have to be taken into account. The most widely used photocatalysts are Ru(bpy)₃Cl₂ (**2.14**) and [Ir{dF(CF₃)ppy}₂(dtbpy)]PF₆ (**2.15**). Tremendous work has been achieved in the study of their reactivity, allowing novel transformations design. However, their synthesis in several steps from precious transition-metals and the resulting high prices have become an important drawback.

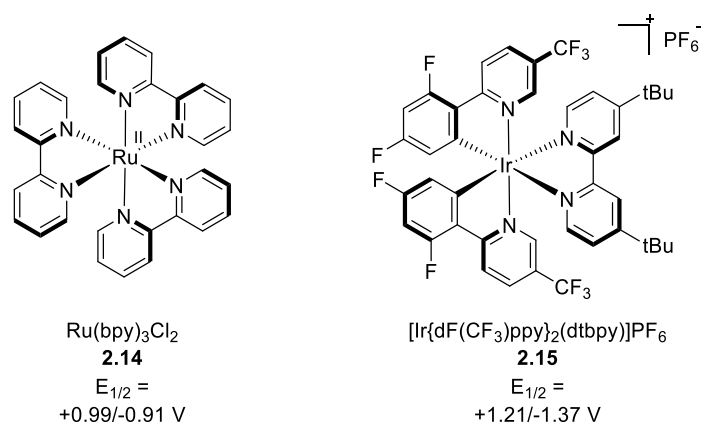


Figure 4: Common transition-metal photocatalysts

Organic dyes

A large variety of organic dyes, also possess the ability to participate in photoinduced electron transfer (PET) processes.^[158] Those alternatives do not only allow metal-free transformations, but thanks to the diversity of dyes, also provide photocatalysts with very diverse redox properties. Highly oxidizing or reducing dyes have been reported, with values beyond the window of metal-based catalysts. Among the most widely used (Figure 5) are the

Xanthenes family (Fluorescein (**2.16**), Eosin Y (**2.17**) and Rhodamine 6G (**2.18**)), diaryl ketones (benzophenone (**2.19**)), cyanoarenes (DCA (**2.20**) and DCB (**2.21**)), flavins ((-)-riboflavin (**2.24**)), acridiniums (Fukuzumi dye (**2.25**)) and thiazines (PHTH (**2.26**)). If at first the lack of stability of several dyes limited their use, important efforts towards the optimization of the structures paid off. Both modification of existing scaffolds together with the design of novel families have been explored. Rational design allowed the improvement of catalytic activities through a better understanding of the relation between the structure and the physicochemical and redox properties. Especially, extensive work has been achieved on the cyanoarene family. A major breakthrough was done by Luo and Zhang in 2016 and their use of donor acceptors cyanoarenes fluorophores in photoredox.^[159] The dyes had been described before by Adachi and coworkers for OLED applications but not in catalysis.^[160] The most interesting dyes, which processes similar redox windows from classical metal photoredox catalysis and good stability for organic dyes, were 4DPAIPN (**2.22**)¹ and 4CzIPN (**2.23**). Acridinium salts have been intensively studied as well. Important contributions from the Nicewicz^[161] and Sparr^[162,163] groups among others have led to the developments of numerous dyes which present both an increased stability and various redox properties.^[164] The difference in terms of cost is enormous: $[\text{Ir}\{\text{dF}(\text{CF}_3)\text{ppy}\}_2(\text{dtbpy})]\text{PF}_6$ can be purchased for 954 CHF/100 mg from Sigma-Aldrich, whereas DCA costs only 182 CHF/1 g. The development and use of organophotocatalysts have become recently a quite intense field and the important advances have been the subject of reviews.^[148,158,164–170]

¹ The structure was first miss assigned, further discussion can be found in section 5.3.

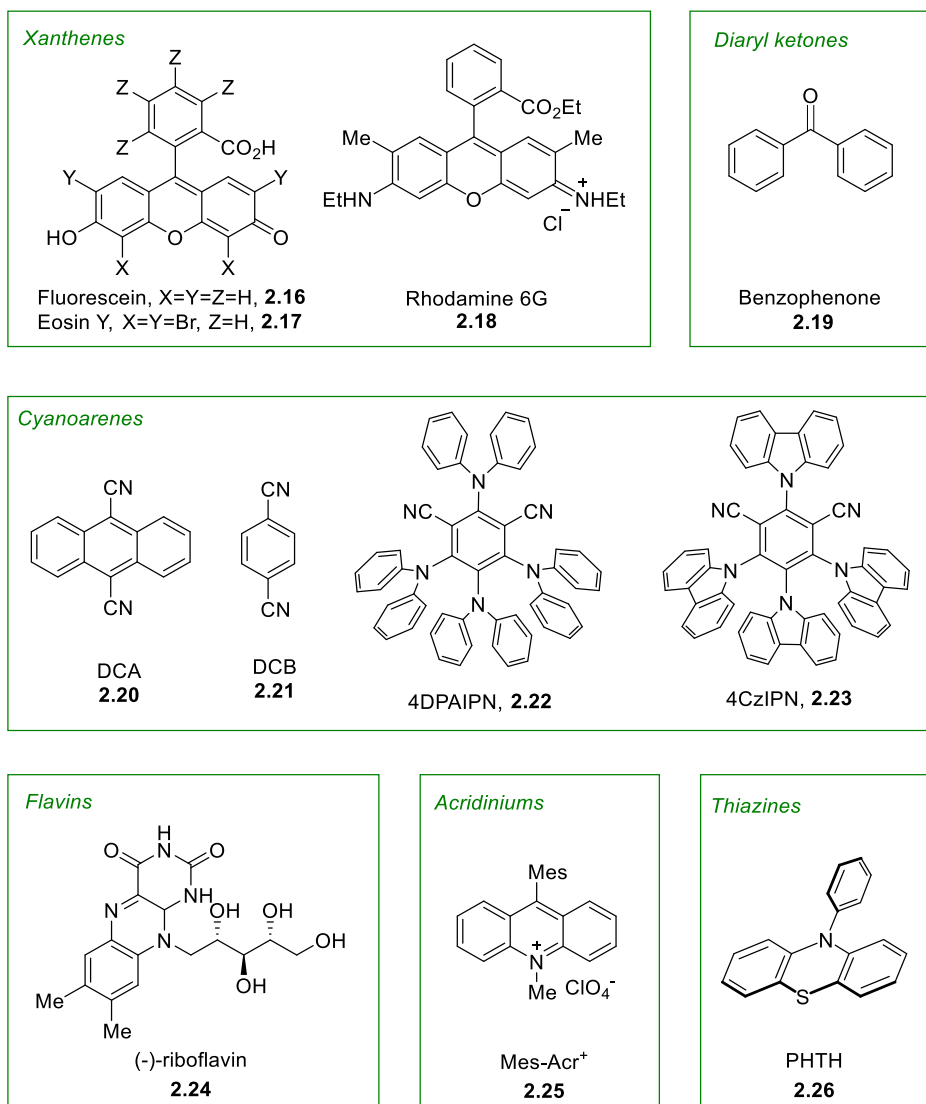


Figure 5: Examples of common organic dyes

DCA: 9,10-dicyanoanthracene (**2.20**), 4DPAIPN: 1,3-dicyano-2,4,5,6-tetrakis(*N,N*-diphenylamino)benzene (**2.22**), 4CzIPN: 1,2,3,5-tetrakis(carbazol-9-yl)-4,6-dicyanobenzene (**2.23**), Mes-Acr⁺: 9-mesityl-10-methylacridinium (**2.25**), PHTH: 10-phenylphenothiazine (**2.26**).

Photocatalysts properties

Important properties in the design and in the choice of a catalyst for a specific transformations are the following.^[157,158] $\lambda_{\text{max}}^{\text{abs}}$ is the maximum of absorption and determines the source of irradiation. It should be different from other species in the media. Most catalysts are usually excited with blue or green LEDs. τ_f stands for the lifetime of fluorescence, typical values are between 6 μs to 300 ns. Φ_f represents the quantum yield of fluorescence. The closer it gets from 1 the more likely the catalyst is susceptible to undergo a PET. The quantum yield of intersystem crossing is given by Φ_{isc} and indicates the population of the triplet state T_1 .

This is particularly important for organic dyes where most molecules react at the singlet state. Finally, E_{ox} and E_{red} correspond to the redox potentials and are probably the most commonly discussed values when comparing catalysts. Values at the excited state cannot be measured and are calculated from those at the ground-state. A more detailed discussion on redox potential determination can be found in section 5.1.3.

Tuning of carbazolydicyanobenzene family

In their seminal work, Adachi and co-workers described 4CzIPN (**2.23**) and several derivatives as thermally activated delayed fluorescence (TADF) dyes.^[160] A donor-acceptor system with carbazoles as the donor groups and nitriles as acceptors was designed (Figure 6). The interest of this scaffold stands in the spatial separation of the HOMO and the LUMO, allowing tuning of the redox properties. The structure is indeed distorted by steric hindrance of the carbazoles and a dihedral angle of around 60° can be measured. As a result, the HOMO is delocalized over the donor groups, the carbazoles, while the LUMO involves the acceptors, meaning the dicyanobenzene core. The cyano group is a highly valuable acceptor as it limits the non-radiative deactivation. It indeed diminishes changes in the geometries of the singlet and triplet states. The energy gap between singlet S_1 and triplet T_1 has been designed to be quite low. An efficient reverse intersystem crossing (ISC) can thus take place and S_1 is the most populated state. It is interesting to note that those dyes possess relatively small Stokes shifts, which is indicating high efficiency in the excitation to the singlet state.

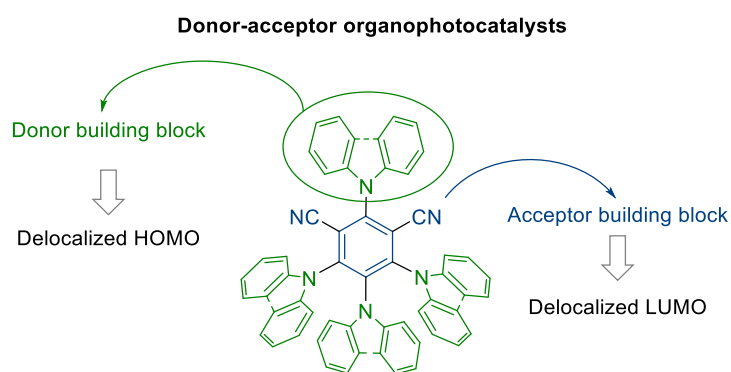


Figure 6: General structure and electronics of carbazolydicyanobenzene family

A first study about the influence on the number and position of the donor and acceptor groups was disclosed in the seminal works of Adachi and Zhang.^[159,160] A selection is presented on Figure 7 (**2.27** to **2.31**). Measurement of the redox properties highlighted that dyes based on this carbazolydicyanobenzene scaffold behave both as strong oxidants (+1.10

$< E_{1/2}(*P/P^-) < +1.41$ V) and reductants ($-1.41 < E_{1/2}(P^+/*P) < -0.99$ V). Especially, 4CzIPN (**2.23**) ($E_{1/2}(*P/P^-) = 1.35$ V and $E_{1/2}(P^+/*P) = -1.21$ V) is comparable to the classic $[Ir\{dF(CF_3)ppy\}_2(dtbbpy)]PF_6$ (**2.15**) ($E_{1/2}^{*III/II} = +1.21$ V and $E_{1/2}^{II/III} = -1.37$ V). This is why this family has received considerable attention. More precisely, increasing the number of carbazoles, hence of donor groups, from 2 to 4 renders the photocatalyst less oxidizing but more reducing. The same effect was observed when diphenylamine was used as a donor. Stability was also studied, both from a thermal point of view,^[160] and by analyzing the residual catalyst at the end of the reaction.^[159] 4CzIPN (**2.23**) and 4DPAIPN (**2.22**) demonstrated high stability. For all others, either complete degradation or traces only were detected, preventing those catalysts from broad applications in organophotocatalysis.

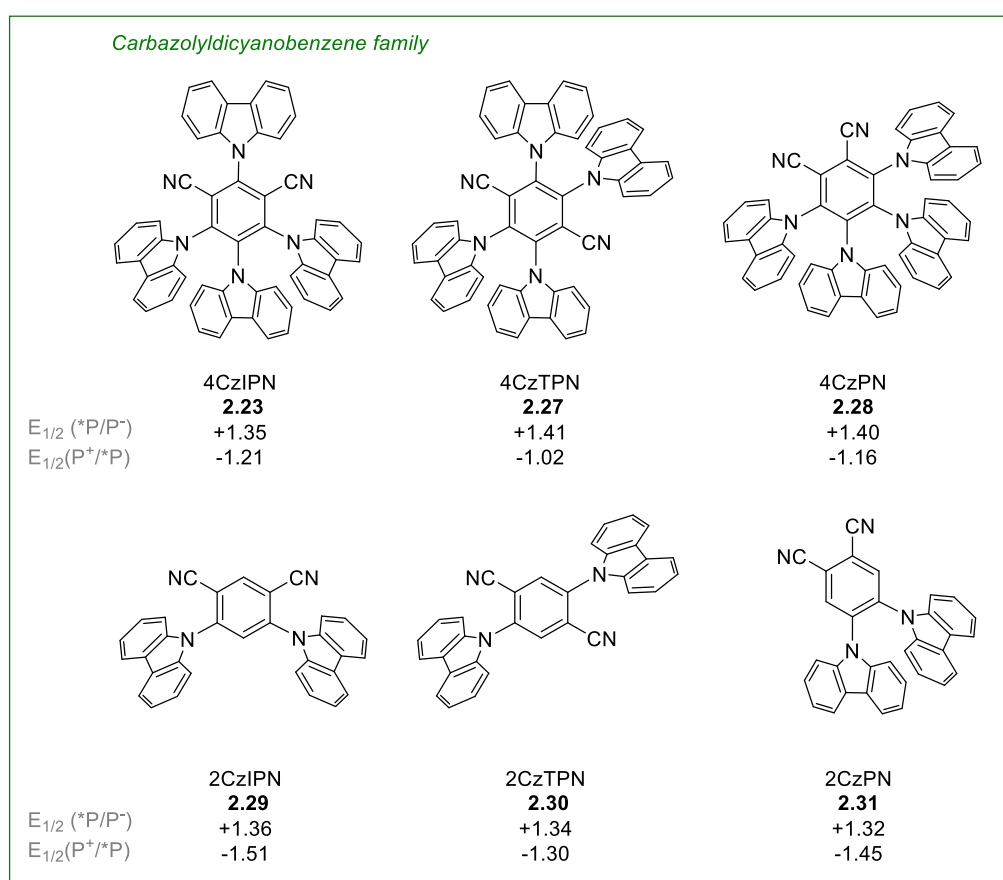


Figure 7: A selection of carbazolyldicyanobenzene family organophotocatalysts

Water-soluble transition-metal photocatalysts

As part of our work aims for photoredox catalyzed reactions in aqueous media, we will now focus on water-soluble catalysts. At the time of this study, organic dyes were only emerging as modular photoredox catalysis. Our study was thus focused on transition-metal photocatalysts. One common way to increase the solubility in water is to introduce sulfonates, carboxylates, ammonium or phosphonates groups on the molecule of interest. An extensive work concerning substituted bipyridine ligands bearing those functional groups has been carried out on ruthenium,^[171–174] providing a first insight of their effect on the redox properties and the water-solubility of the resulting catalysts. A study on solubility of classic ruthenium and iridium photocatalysts was performed recently.^[175]

Regarding iridium based catalysts, **2.32** to **2.40** were known at the beginning of this study (Figure 8). Introduction of an ester on the bipyridine ligand led to an easier reduction, in agreement to previously described ligand effect.^[176] Except **2.34**, the following catalysts are water-soluble before counter-ion exchange between Cl^- and PF_6^- . Paul and co-workers highlighted that an ester group on the cyclometalated ligand increase the oxidation potential by reducing the energy gap between the HOMO and the LUMO, which was confirmed by Liu and co-workers.^[177] The reported potentials (in V vs SCE) were measured for the ground-state.

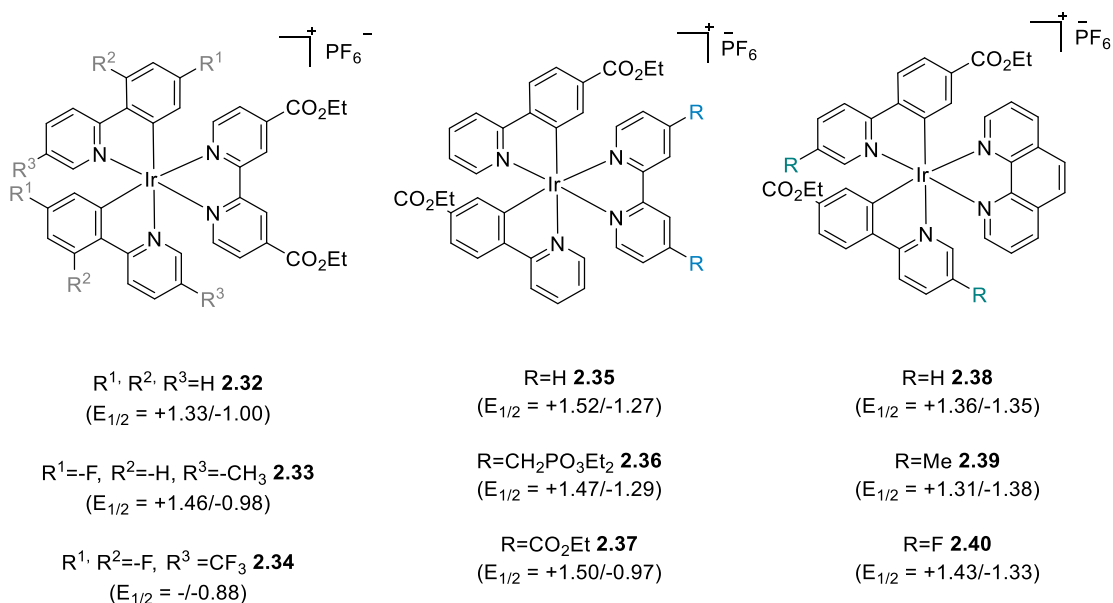
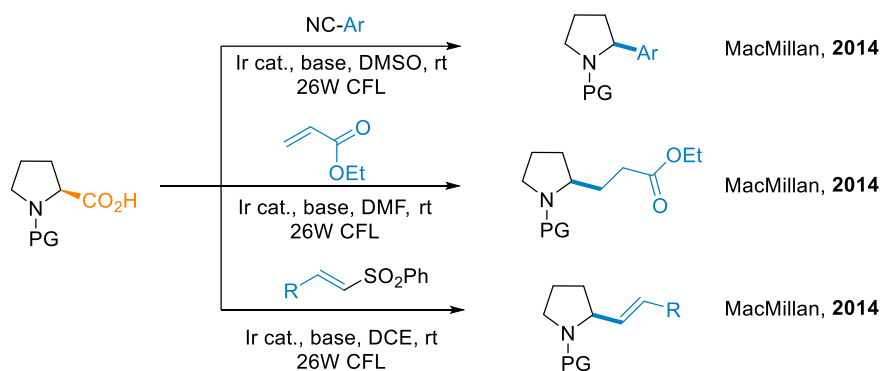


Figure 8: A selection of known iridium photocatalysts

2.3.3 Decarboxylative alkynylation reactions using photoredox chemistry

Carboxylic acids are very attractive starting materials as they are readily available and inexpensive. From a synthetic point of view, they provide chemoselectivity and carbon dioxide is the only waste generated in a decarboxylative reaction. This has led to a growing interest in the last years. Due to the numerous reports, only the ones released prior to our study and with high relevance will be presented. This includes seminal results, aqueous conditions or when hypervalent iodine was the alkyne source. Early work has been performed by Li and co-workers with the first decarboxylative alkynylation using hypervalent iodine reagents.^[178] Free alkyl carboxylic acids were successfully alkynylated under aqueous conditions (DMF or acetone/water 1:1). However, a stoichiometric amount of potassium persulfate was required as an oxidant, in addition of catalytic silver nitrate.

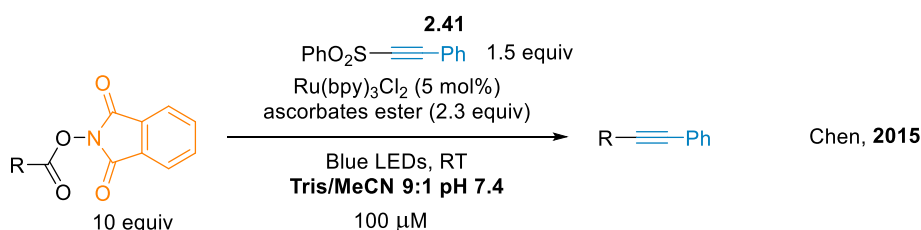
The group of MacMillan released in 2014 a series of decarboxylative transformations under photoredox catalysis (Scheme 16). Upon deprotonation, the carboxylates can be oxidized by the excited photocatalyst, leading to the corresponding carbon radicals after decarboxylation. Decarboxylation was followed by arylation,^[11] Giese coupling^[12] and vinylation.^[179] Racemic mixtures are obtained in all cases, resulting from a radical pathway. If only proline is represented on Scheme 16, the scope of carboxylic acids was broad, with for instance aliphatic acids in the case of alkylation. Regarding the protecting groups, both Boc and Cbz were suitable. Those first results led to the observation of the “Cesium effect”,^[180] as cesium salts often afforded better results.



Scheme 16: Early works on proline decarboxylation

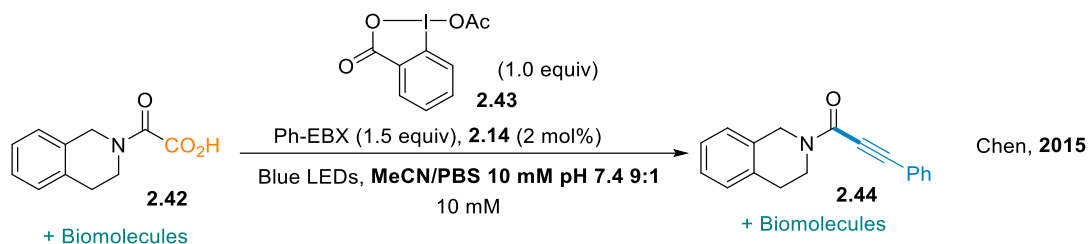
The group of Chen developed in 2015 a decarboxylative alkynylation of N-hydroxy phthalimide esters with alkynyl sulfones **2.41** under photoredox catalysis (Equation 6).^[181] The scope is broad and this chemoselective transformation can also be performed under biomolecule compatible conditions: in an aqueous acetonitrile Tris buffer at pH 7.4. If EBX

reagents were also studied, they afforded lower yields than sulfones. The main drawback stands in the synthesis of the precursors as it adds one step. The interest of those redox-active esters (RAEs) is that they are activated by SET reduction. A different mechanism in comparison to the free carboxylic acids is thus occurring. This allows reaction with other partners as oxidation is required to close the catalytic cycle. However, in that case the transformation was not redox neutral and a stoichiometric reductant was employed.



Equation 6: Decarboxylative alkynylation of phthalimide-esters

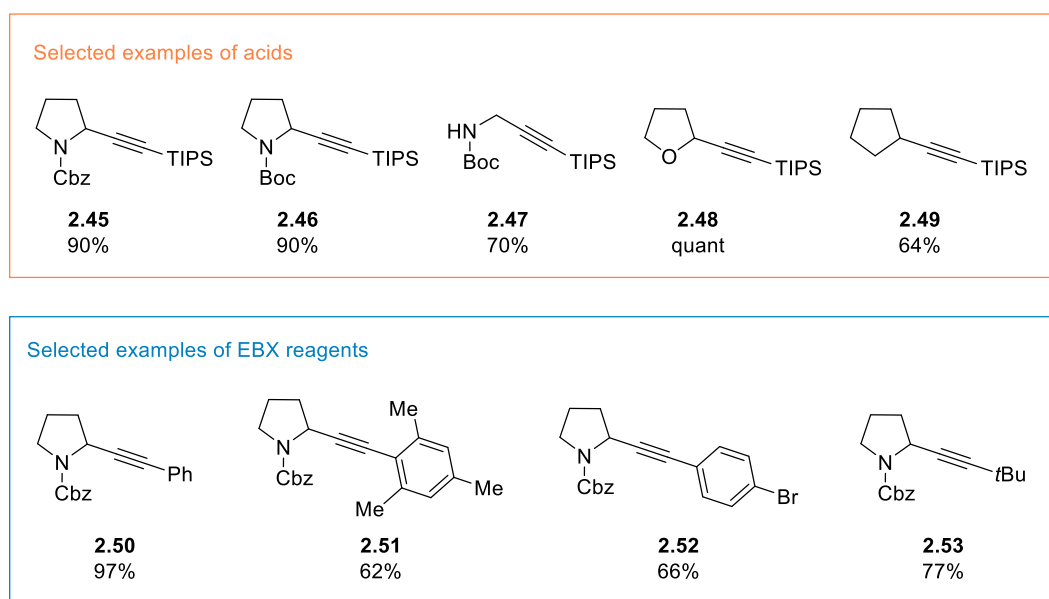
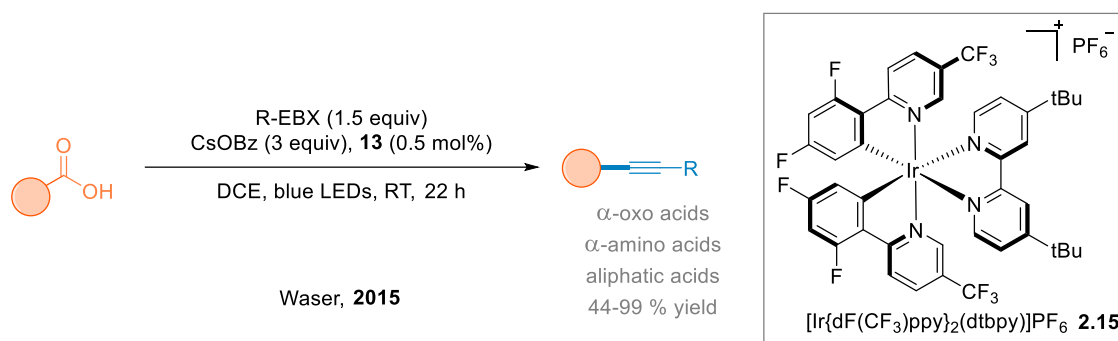
Another work from the group of Chen focused on a decarboxylative ynoneylation under a dual hypervalent iodine and photoredox catalysis (Equation 7).^[182] Acyl radicals were obtained from α -ketoacids **2.42** in presence of BI-OAc (**2.43**), and underwent addition on EBX reagents **2.5**. This methodology was applied under neutral aqueous conditions with success. The presence of biomolecules did not interfere with the outcome of the reaction and **2.44** was still obtained in good yields.



Equation 7: Decarboxylative ynoneylation under biomolecule compatible conditions

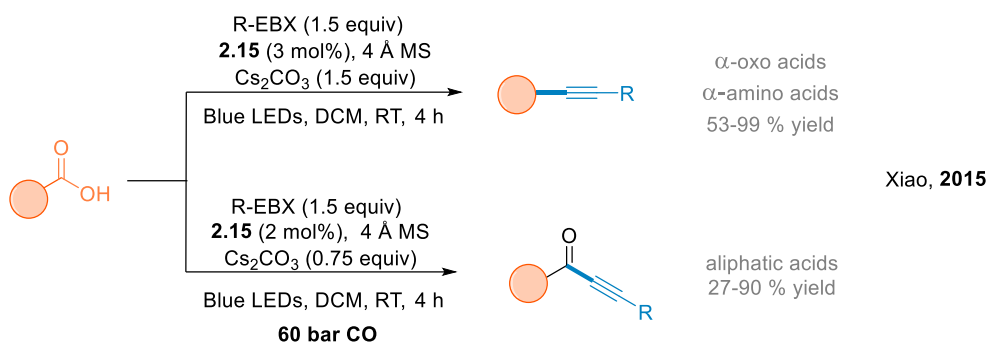
Building on those works, decarboxylative alkynylation methods using photoredox catalysis and hypervalent iodine reagents were developed simultaneously within our group and Xiao's group in 2015.^[13,183] In our group, decarboxylative alkynylation of free carboxylic acids was achieved using visible-light catalysis and EBX reagents (Scheme 17).^[13] Good to excellent yields were obtained with a broad scope of both acids (α -amino, α -oxo and aliphatic acids **2.45** to **49**), and alkynes (silyl-, aryl- and alkyl- substituted **2.50** to **2.53**). The alkynes products could be further functionalized, especially by Click chemistry, and a successful sun-light experiment was carried out. One important point was the lower reactivity of silylated EBX reagents

observed in the study. Milder bases are required to prevent undesired deprotection. The catalyst loading could be decreased to only 0.5 mol%.



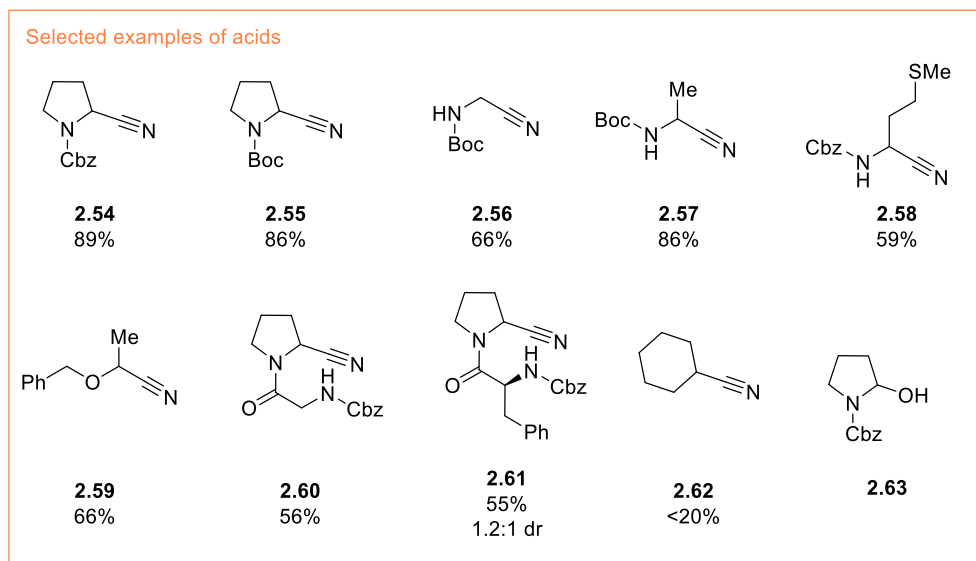
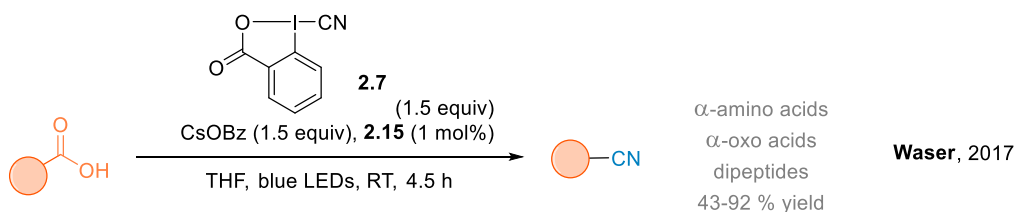
Scheme 17: Decarboxylative alkynylation developed within the group

Very similar conditions and substrate scope were developed in the group of Xiao (Scheme 18),^[183] although the catalyst loading was higher (3 mol%) and cesium carbonate was used as a base. The same observation about lower reactivity of TIPS-EBX was made, but their optimization was carried out with Ph-EBX which tolerates well cesium carbonate on the contrary to silylated EBX. Interestingly, they also reported a decarboxylative carbonylative alkynylation under high pressure of CO (60 bars of CO), leading to ynones in good to excellent yields. Only aliphatic acids were tolerated in that transformation.



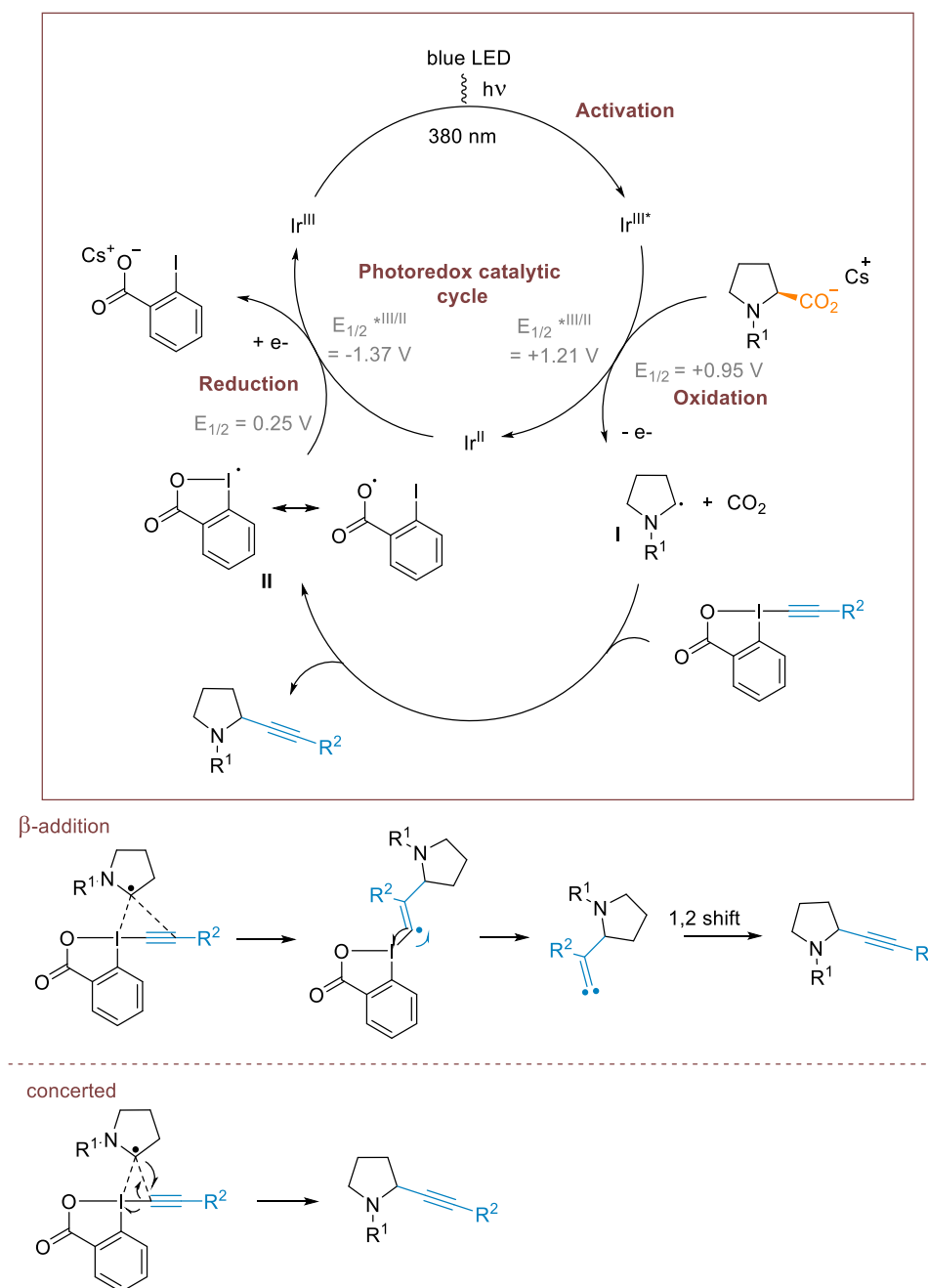
Scheme 18: Decarboxylative alkynylation and ynonylation of Xiao group

Mechanistic studies about this transformation were carried out in our group in the context of the development of a decarboxylative cyanation (Scheme 19).^[184] In that project, α -amino and α -oxo acids were suitable substrates (**2.54** to **2.59**). Interesting features for our present study are both the excellent yields obtained in THF and the successful cyanation of two dipeptides (**2.60** and **2.61**). The difference in scope (aliphatic acids were not tolerated **2.62**) and the observation of water addition side products **2.63** indicated a probable difference in mechanism. More details about the mechanism will be given in the next paragraph.



Scheme 19: Decarboxylative cyanation developed within the group

Under visible-light excitation, the iridium catalyst $[\text{Ir}\{\text{dF}(\text{CF}_3)\text{ppy}\}_2(\text{dtbpy})]\text{PF}_6$ (**2.15**) generates the excited state which is strongly oxidizing ($E_{1/2}^{*\text{III/II}} = +1.21 \text{ V vs. SCE}$) and undergoes a single-electron-transfer (SET) with the *in-situ* generated cesium carboxylate (Scheme 20).^[184] The formed carboxy radical decarboxylates fast to generate a nucleophilic radical **I**. Reaction with the hypervalent iodine reagent would afford radical **II** which oxidizes the catalyst back to the ground-state. Unknown parameters at the time of the study were the mechanism of the alkynylation/cyanation step as well as the reduction potential of radical **II**. Radical clock experiment demonstrated the radical character of the mechanism in the case of alkynylation, but not for cyanation. Computations from the group of Chen proposed a resonance structure for **II**, with an iodine and an oxygen radicals.^[185] Computations from our group gave a reduction potential of 0.25 V, which shows this step as thermodynamically feasible when considering the reduction potential of the catalyst ($E_{1/2}^{\text{II/III}} = -1.37 \text{ V vs. SCE}$). Concerning the key alkynylation step, several pathways would be possible: α -addition, β -addition, SET or a concerted mechanism. If α -addition followed by β -elimination had been proposed before,^[178] density functional theory (DFT) computations demonstrated that it is not the favored pathway. Alkynylation occurs most likely through a radical mechanism, either by a concerted mechanism, or by β -addition, the two of them being close in energy. Cyanation however is most likely to occur through a single electron transfer to form an iminium intermediate followed by cyanide addition. For clarity, only the alkynylation mechanism is represented in the following scheme.



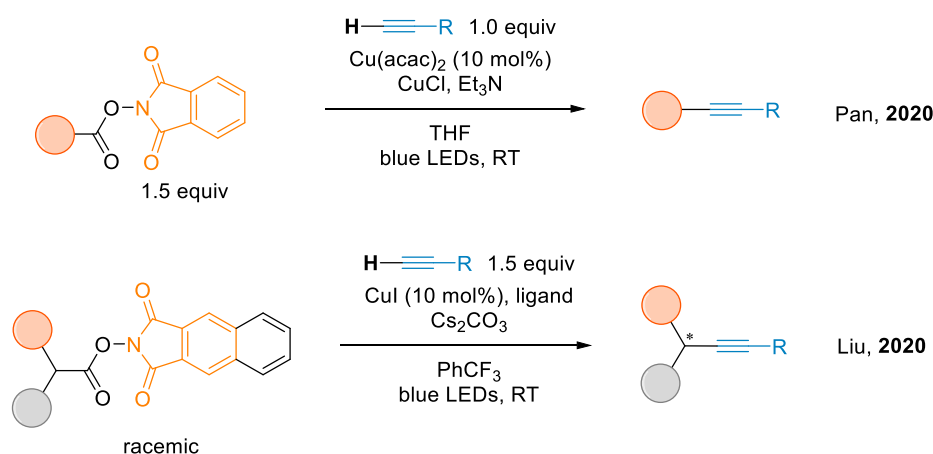
Scheme 20: Proposed mechanism of the decarboxylative alkynylation

The potential of this decarboxylative alkynylation strategy can be fully understood upon the analysis of the number of publications since those first reports. A first review from Xiao was released in 2015,^[183] a more recent one was already published in 2017 by Jin and Fu.^[186] Decarboxylative strategies with or without light were also the subject of a comparison from König.^[187] Alkynylation reactions in photoredox catalysis were reviewed by our group.^[188]

One very interesting improvement is the replacement of the transition-metal catalyst by organic dyes. Cheng *et al.* described the first organophotocatalytic decarboxylative

alkynylation.^[189] Commercially available DCA was used as the catalyst and a broad scope of α -amino-acids, α -oxo acids and α -keto acids was described. More recently, the group of König proposed an organocatalyzed version of the decarboxylative alkynylation developed by Chen in 2015 and described before (Equation 6).^[190] The use of the Eosin Y is possible in this case because of the pre-functionalization of carboxylic acids by esterification to RAEs.

Recent developments since the beginning of this work include a dual photoredox/transition-metal catalysis which was applied towards a copper mediated decarboxylative alkynylation of RAEs with terminal alkynes (Scheme 21).^[191–193] The main drawback of a radical decarboxylative coupling remains the racemic nature of the products. An enantioselective decarboxylative alkynylation using a dual photoredox/copper catalysis was recently disclosed starting from RAEs.^[194] This methodology is however limited to aliphatic acids. Starting from free carboxylic acids has not been reported in neither of the last two concepts and would be highly valuable.



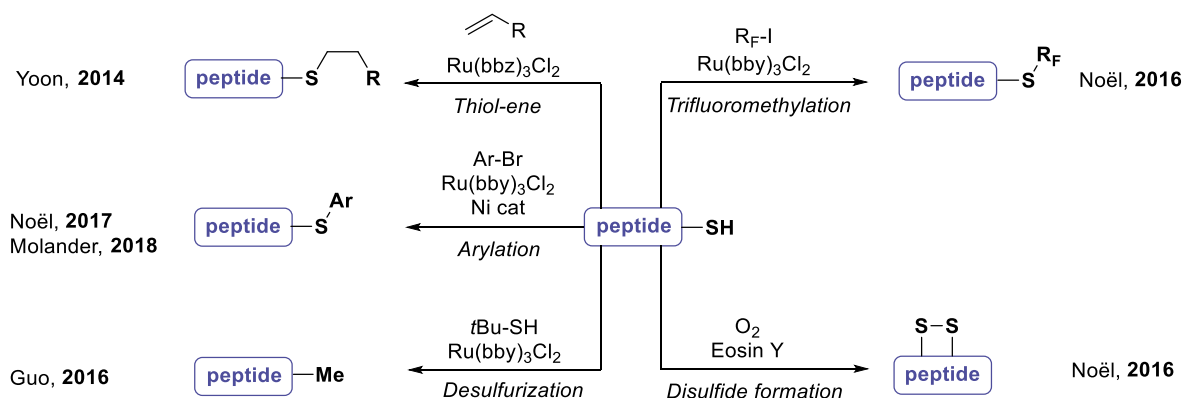
Scheme 21: Decarboxylative alkynylation from RAEs and free alkynes

Those highly valuable advances and the efficiency of the developed transformations were quite promising towards the extension of such strategies on more complex substrates. Literature precedents on the use of visible-light for peptides and proteins modification would give us highly valuable information for the design of conditions. This will be presented in the next section.

2.3.4 Photocatalytic transformations on peptides and proteins

Using light as the energy source to generate radicals under mild conditions on biomolecules such as peptides and proteins is highly attractive. The phototoxicity of UV light is thus avoided, as well as the possible distortion of the conformation of proteins under UV irradiation. In addition, photoredox transformations are usually performed at RT or slightly above, which is ideal for proteins. Finally, as most reactions require light to be induced, they are terminated by the end of illumination. This is quite desirable as it avoids the use of quenchers, which could potentially denature the substrates. As a result, visible-light mediated reactions have been investigated both for bioconjugation methods, recently reviewed by Bottecchia and Noël,^[10] as well as bioorthogonal transformations.^[195] Photoactivable probes are also an intense field but this will not be covered here.^[196,197] Synthesis and modification of amino acid derivatives in radical chemistry was also reviewed.^[198]

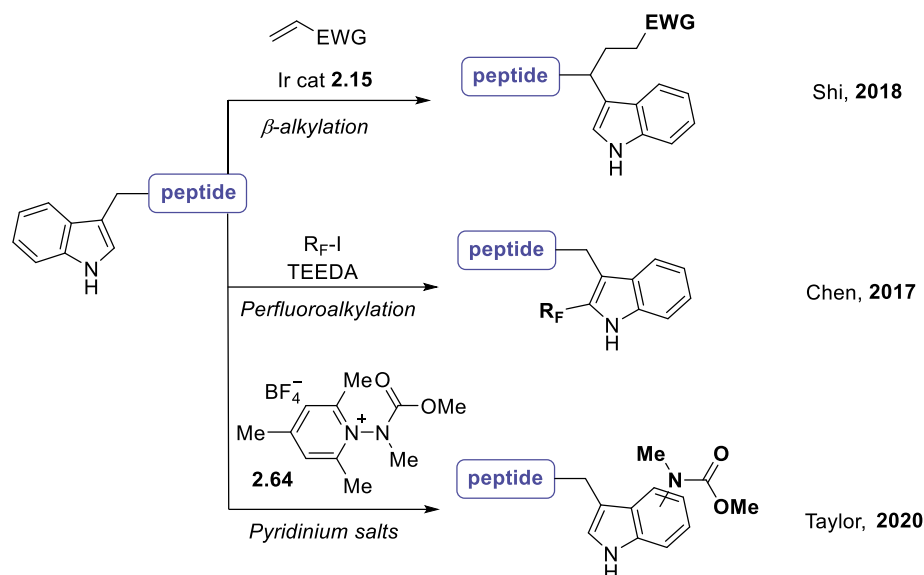
As in non-photocatalytic methods, cysteines have been the most widely studied residues, with thiol-ene reactions by the Yoon group in aqueous media,^[199] arylation by Noël^[200] and Molander,^[201] desulfurization by Guo,^[202] trifluoromethylation by Noël^[203] and disulfide formation by Noël (Scheme 22).^[204,205]



Scheme 22: Examples of photoinduced reactions on cysteines

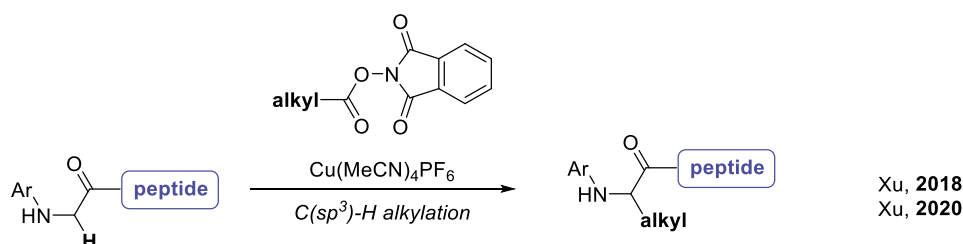
Tryptophan represents an interesting target due to its very low abundance, as it would allow a site-selective bioconjugation. β -alkylation through an oxidation of the indole moiety followed by deprotonation and addition to a Michael acceptor has been reported.^[206] Despite some side-reactions with other residues (Lys and His in particular), the good chemoselectivity allowed applications on large peptides. Perfluoroalkylation was explored by Chen using perfluoroalkyl iodides and tertiary amines such as N,N,N',N'-tetraethyl- ethylenediamine

(TEEDA).^[207] More recently, an elegant bioconjugation of tryptophan in proteins was disclosed using pyridinium salts **2.64** as the electrophile source under UV light irradiation.^[208] The reaction is likely mediated by electron-transfer between the pyridinium salt and tryptophan.



Scheme 23: Examples of photoinduced reactions on tryptophan

A site-specific alkylation of glycine residues was developed by Wang et al. (Equation 8).^[209] Combining oxidation of the glycine moiety and decarboxylation of a redox-active ester, C(sp³)-H alkylation of glycine was achieved on tetramers. This approach was later extended to alkylation with Katritzky salts.^[210]



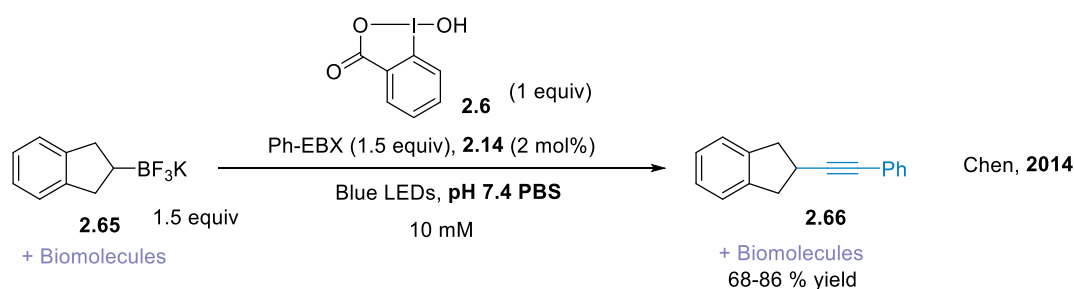
Equation 8: C(sp³)-H alkylation of glycine residues

A recent advance has been disclosed on histidine bioconjugation with a selective C-H alkylation using C₄-alkyl-1,4-dihydropyridine (DHP) reagents which could even be applied to insulin.^[211] Some reports about tyrosine, methionine or dehydroalanine functionalization can also be found.^[10] The main advantage of tyrosine targeting is the difference of reactivity in correlation with the media pH, allowing selectivity between sites. Methionine however is a very

challenging amino acid because of its lower nucleophilicity and high hydrophobicity in comparison to other residues. Serine was targeted recently in a macrocyclization strategy.^[212]

Other examples of reactions induced by visible-light under biomolecule-compatible conditions have been developed, including azide reduction,^[213] and are summarized in a review written by Chen and co-workers.^[214] Some interesting features can be noted, such as the compatibility of PBS, Tris, MES and HEPES buffers with photoredox catalysis, but also that Ru(II) catalyst **2.14** was used for most of the studies, most likely due to its solubility in water.

As a last example, which was not conducted on peptides but in presence of biomolecules. The Chen group developed in 2014 a deboronative alkynylation (Equation 9).^[215] This transformation was highly chemoselective with a large variety of functional groups tolerated. The main drawback is the need of trifluoroborates **2.65** as precursors from alkynes **2.66**. Nevertheless, this work is of high interest for us as it was the evidence for the compatibility of alkynylation with EBX reagents with aqueous conditions. The reaction could indeed be run under biomolecule compatible conditions: a phosphate saline buffer (PBS) pH 7.4 in presence of biomolecules.

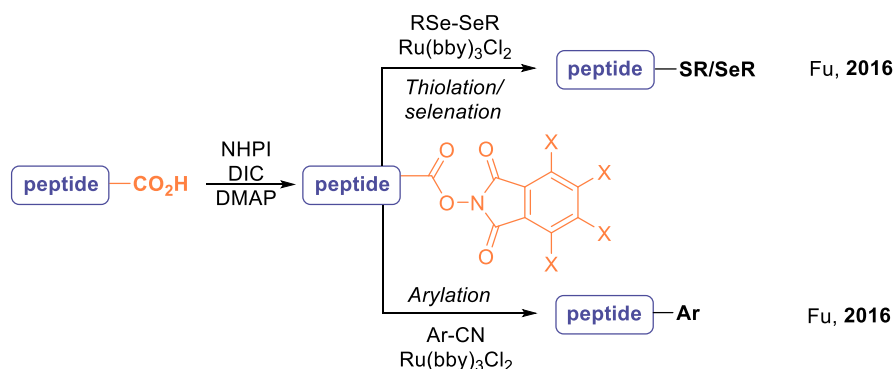


Equation 9: Deboronative alkynylation in presence of biomolecules

2.3.5 Photoinduced bioconjugation on carboxylic acids residues

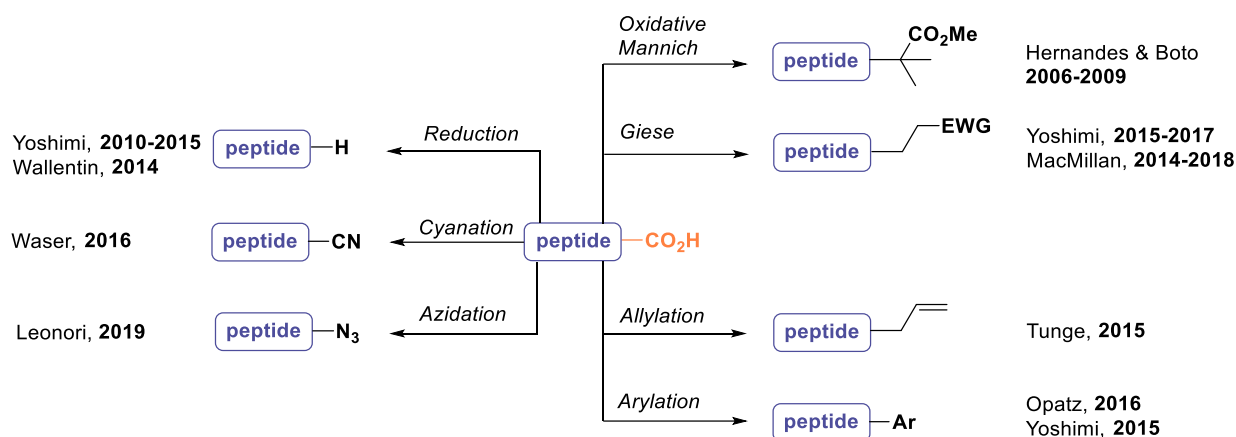
The extension of the numerous methods available on carboxylic acids to peptides is very seductive. The resulting methods could contribute to expand this underexplored area (Section 2.1.4). Tremendous work has been achieved in the last years based on decarboxylative strategies, which were reviewed by Malins.^[87] Building on the results on small molecules, two different approaches were selected. Either employing redox-active esters (RAEs) or starting from the free carboxylic acids.

Regarding RAEs, key advances were made with the development of arylation^[216–218] and thiolation/selenation^[219,220] reactions (Scheme 24). The first step of the catalytic cycle is then a SET reduction of the RAE. Alkylation, alkenylation, alkynylation and Giese coupling were reported under non-photocatalytic pathways and were discussed before (Section 2.1.4). The main drawback of those methods is the need of prefunctionalization of the carboxylic acid. Selectivity between acids would then require to be achieved during the activation step, which has not been reported to date. The same approach was employed to generate DNA-encoded libraries, with the Michael acceptor located on DNA.^[221] Similarly, decarboxylation of redox-active esters followed by addition of the formed radical to dehydroalanine has been investigated on peptides.^[222,223]



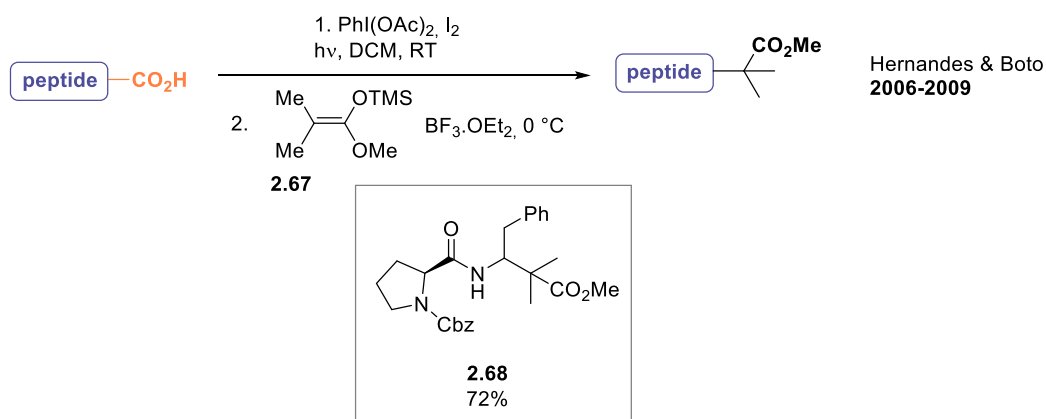
Scheme 24: Light-mediated decarboxylative couplings from RAEs

To overcome this limitation, direct decarboxylative strategies starting from free carboxylic acids have been studied. Applications on native peptides and proteins can then be envisioned. In this case, the same mechanism as described in the previous section (section 2.3.3) takes place, with first oxidation of the carboxylate followed by decarboxylation and radical trapping. An overview of the available methods is presented on Scheme 25, including oxidative Mannich,^[224,225] Giese coupling,^[12,37,226,227] allylation,^[228] arylation,^[227,229] reduction,^[227,230,231] cyanation (section 2.3.3),^[184] and azidation.^[232] It is important to note that among all those examples, only the decarboxylative Giese coupling was performed on larger and more complex substrates than protected tripeptides.



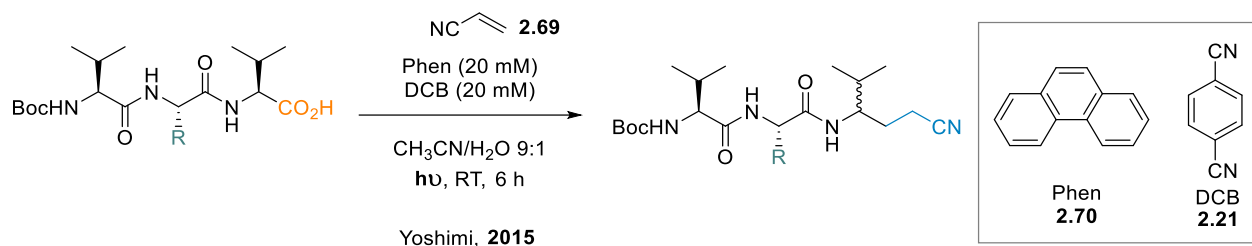
Scheme 25: Overview of light-mediated decarboxylative couplings from free carboxylic acids

Early work was disclosed by Hernandez and Boto with a decarboxylative oxidative Mannich reaction starting from free carboxylic acids (Scheme 26).^[224,225] In the presence of hypervalent iodine and under visible-light irradiation, N,O-acetals were obtained, which were further engaged with silyl ketene acetal **2.67** under Lewis acid catalysis. Good yields were obtained on protected dipeptides, for example **2.68**, starting from Cbz-Pro-Phe.



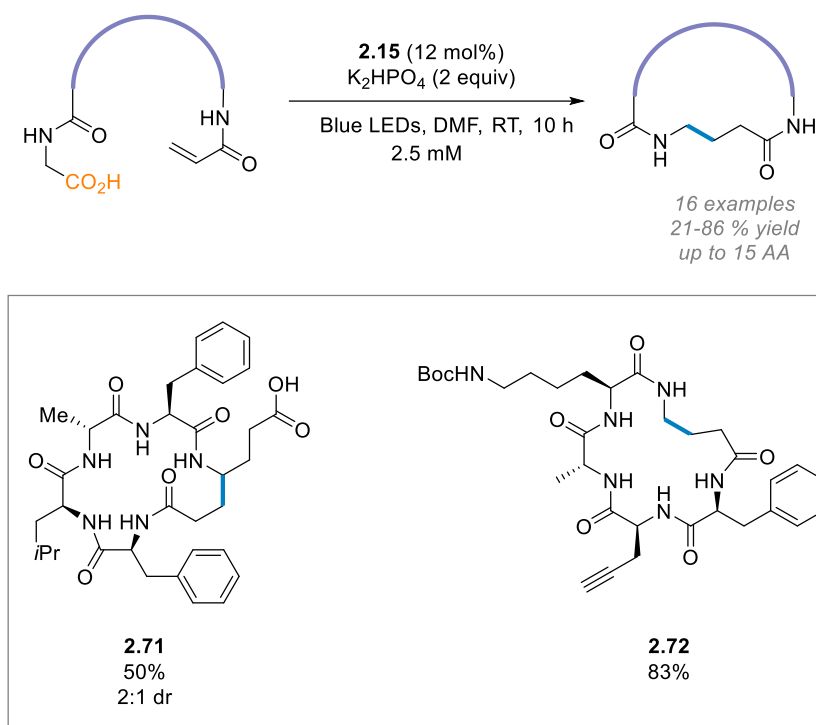
Scheme 26: Light-mediated decarboxylative oxidative Mannich reaction on peptides

The group of Yoshimi performed a valuable study on the influence of the amino acids side-chain in photoinduced decarboxylative radical reactions.^[227] A phenanthrene (Phen **2.70**) / 1,4-dicyanobenzene (DCB **2.21**) system was employed to decarboxylate tripeptides, followed by addition on an electron-deficient alkene **2.69**. Side-chains containing thioethers, hydroxy and amide were well-tolerated but phenols and indole moieties needed to be protected. Electron-rich arenes are acting as quenchers in their system. If the reaction tolerated 10% of water, the main-solvent remained acetonitrile.



Equation 10: Decarboxylative radical addition on electron-poor olefins from tripeptides

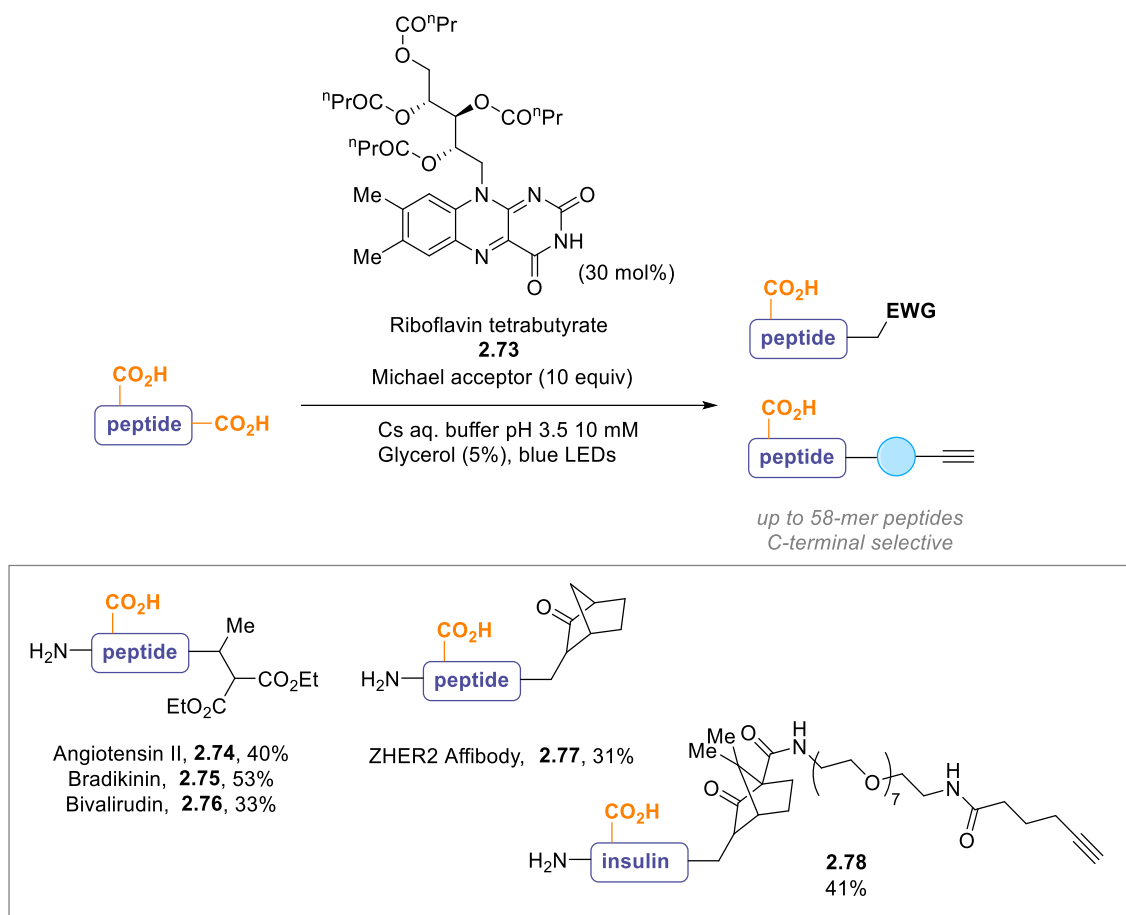
Following an intermolecular decarboxylative conjugate addition released in 2014 on α -amino acids,^[12] the MacMillan group applied the same methodology towards a peptide macrocyclization (Equation 11).^[37] The transformation was tolerant to functionalities found in amino acids and linear peptides with up to 15 amino acids were efficiently cyclized (**2.71** and **2.72**). Protected peptides were employed in this case.



Equation 11: Photoredox-catalyzed decarboxylative peptide macrocyclization

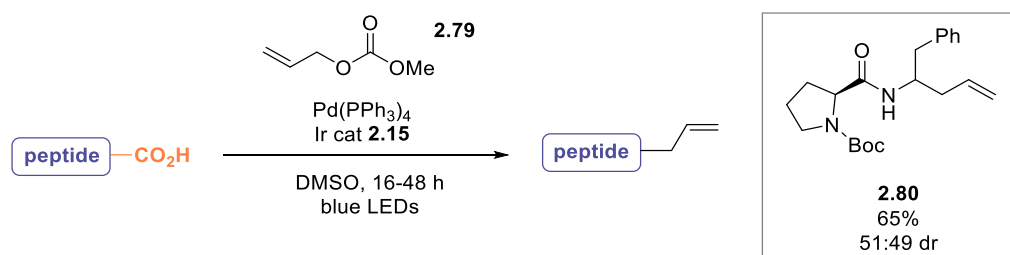
In an impressive further extension, the MacMillan group released a decarboxylative Giese reaction on native peptides in aqueous buffer (Scheme 27).^[226] Thanks to the development of novel Flavin water-soluble catalyst **2.73**, efficient and C-terminal selective labeling of numerous bioactive peptides (**2.74** to **2.77**) and human insulin was achieved (**2.78**). The functional group tolerance was quite broad in a phosphate buffer at pH 7, although the presence of Lys, Tyr and His led to lower yields. Lowering the pH to 3.5 in a cesium buffer was

found to improve the tolerance. In the Tyr case, changing to a less oxidizing dye was also beneficial. No alkylation of the carboxylic acids side-chains was reported. Finally, Cys and Trp were not compatible with this transformation. This is the first report of a photoredox-catalyzed proteins C-terminal bioconjugation.



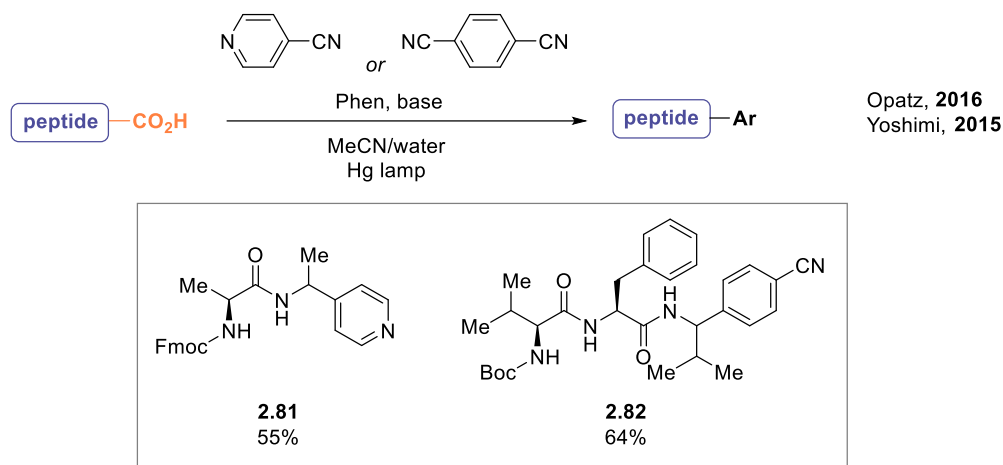
Scheme 27: Photoredox-catalyzed decarboxylative Giese coupling on native peptides

A decarboxylative allylation strategy has been reported by Tunge and co-workers using a palladium/visible-light dual catalysis system (Equation 12).^[228] Allyl groups were introduced from allyl methyl carbonate **2.79** on the C-terminal position of dipeptides such as **2.80**.



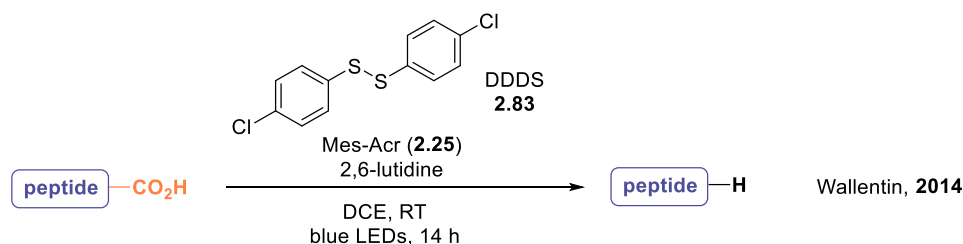
Equation 12: Dual photoredox and palladium catalysis for a decarboxylative allylation on peptides

The last transformation using this decarboxylative approach towards C-C bond formation on peptides is arylation (Scheme 28). The same catalytic system which was developed by Yoshimi and co-workers in their Giese coupling (Equation 10) was extended towards arylation C-terminal carboxylic acids of tripeptides (**2.82**).^[227] Similar conditions were later reported by Opatz (**2.81**).^[229]



Scheme 28: Light-mediated decarboxylative arylation on peptides

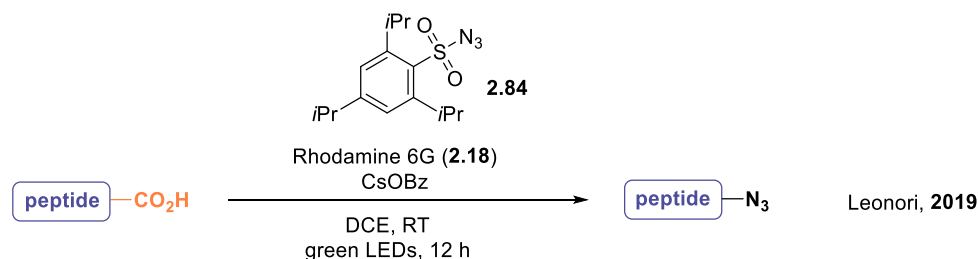
The α -amino radical formed after decarboxylation can also perform hydrogen atom abstractions, on thiols for instance, to afford reduced products. The dual phen/DCB catalytic system from Yoshimi was also suitable for this purpose on peptides.^[227,230] More recently, the Wallentin group reported photoredox conditions for this transformation, using Mes-Acr (**2.25**) as photocatalyst (Equation 13).^[231]



Equation 13: Light-mediated decarboxylative reduction on peptides

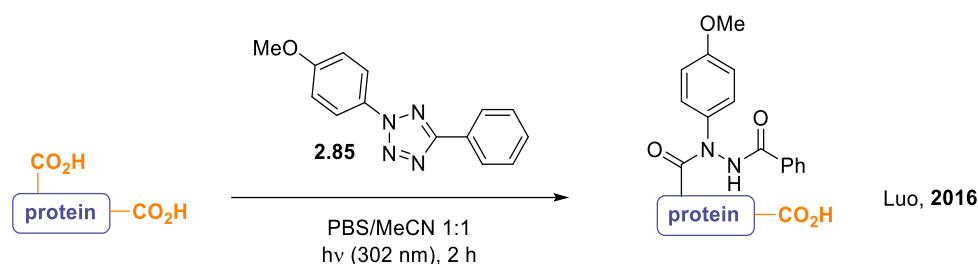
Azides are highly valuable functional groups for biomolecule functionalization. A decarboxylative azidation strategy on peptides was thus highly desirable. The Leonori group has filled that gap recently (Equation 14).^[233] Under green light irradiation, azidation occurs

smoothly with aryl sulfonyl azides **2.84**. Those conditions are however limited to cyclic α -amino acids and only C-terminal proline could be modified.



Equation 14: Light-mediated decarboxylative azidation on peptides

As mentioned, the reports described so far were limited to peptides smaller than tripeptides at the exception of the Giese coupling. Regarding proteins, in addition of the MacMillan results on insulin, an interesting work was released by Luo and co-workers, which targeted glutamic acid residues (Scheme 29).^[234] Under UV light irradiation, tetrazoles **2.85** react with proteins to form diacylhydrazine products. They extended the concept of photoclick chemistry by trapping of one of the intermediate with carboxylic acids. A robustness study was performed and almost all natural amino acids were very well tolerated, at the exception of Tyr, Lys or Cys which slightly decreased the yield. This encouraged the authors to explore protein bioconjugation. The target protein was myoglobin, which led to several sites of modification. But they were all on glutamic residues which were on surface and accessible. This strategy was further extended to photo-affinity labelling both in cell lysates and living cells.



Scheme 29: Light-mediated tetrazine bioconjugation on proteins

Impressive progress towards the development of light-mediated carboxylic acids residues labeling in peptides and proteins has been achieved. Notably, an increasing in substrate complexity, with excellent functional group tolerance in some cases, has been reported. Aqueous conditions have been investigated and the introduction of valuable moieties such as

bioorthogonal functional groups was successful. However, the field is still quite young and no general method for photoredox catalyzed protein bioconjugation has been disclosed so far. The challenge of the difficult chemoselectivity under physiological conditions has limited advances.

Goal of the thesis



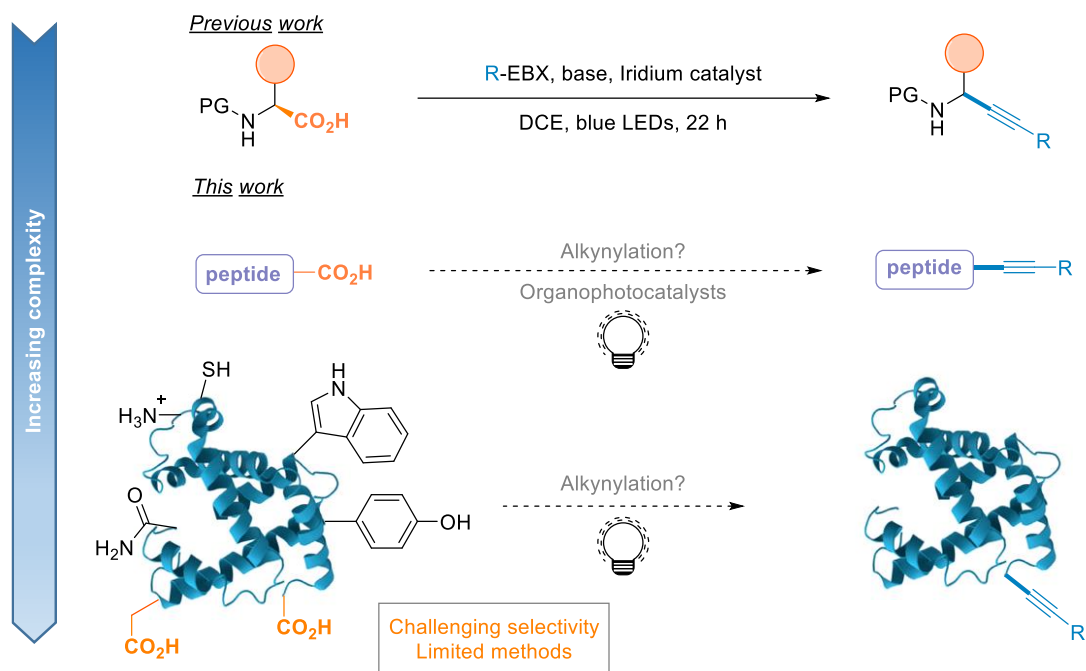
3 Goal of the thesis

Peptides have emerged as major therapeutic agents, and it is thus highly important to discover novel late-stage functionalization strategies.^[16–18] Bioconjugation tools are indeed needed to access new scaffolds for drug discovery, as well as improving physicochemical properties. Regarding proteins, despite numerous methods available for selective chemical modification, efficient C-terminal labeling remains challenging.^[2,73] This position is however interesting as it provides diversity in the modification site in comparison to existing methods, but also selectivity for single-site labeling. C-terminal modification is also less likely to disturb the protein structure and function. Introduction of a bioorthogonal functional group, such as an alkyne, is especially very attractive in regards to the demonstrated efficiency of Click reactions in bioorthogonal chemistry.^[63,67,235]

If photoredox-catalyzed alkynylation of the peptides C-terminus has been achieved before, pre-functionalization of the carboxylic acid was required and those strategies cannot be employed for direct modification of complex biomolecules.^[37,214,236] Direct decarboxylation from free carboxylic acids under biomolecule-compatible conditions has not been achieved yet and would overcome those limitations.

I aimed in this thesis to develop a novel methodology for carboxylic acids residues labeling in biomolecules. Previous work within the group had led to the development of an efficient decarboxylative alkynylation of free α -amino acids using photoredox catalysis and hypervalent iodine reagents (Scheme 30).^[13] The extension of this decarboxylative alkynylation to more complex substrates was thus envisioned.

In order to extend the methodology, the first step would be to demonstrate that the presence of water is compatible, and that peptides are suitable substrates. After optimization, a complete study of functional group tolerance on the peptides and on the EBX reagent would provide insight about the potential applications. The development of novel fine-tuned organic dyes would at that stage be highly valuable to achieve regio- and chemo-selectivity. The study of peptides of medium size would be highly valuable both from a synthetic point of view and to better understand the reactivity prior to investigate proteins. The next step of the project would then consist of designing an approach for protein decarboxylative alkynylation. The final efforts were dedicated to assess whether our C-terminal decarboxylative strategy could be further extended towards introduction of other functional groups onto peptides.



Scheme 30: Goal of the thesis

Towards a decarboxylative alkynylation in aqueous media



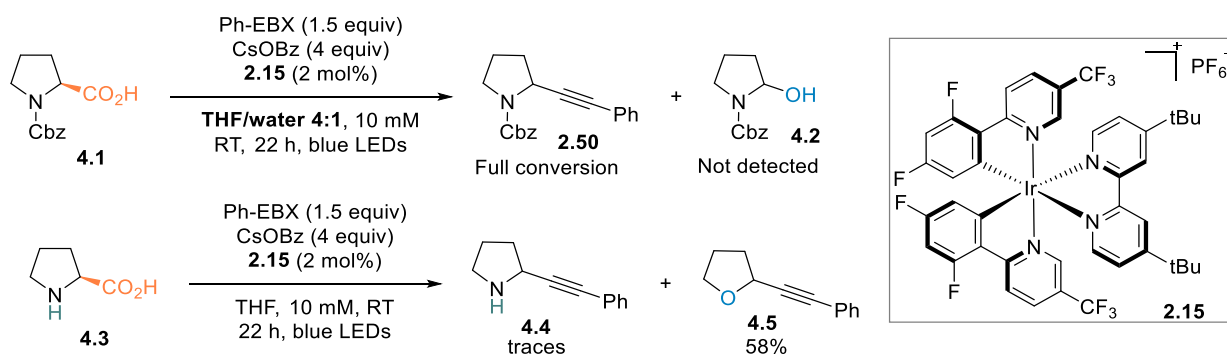
4 Towards a decarboxylative alkynylation in aqueous media

Within our efforts to develop an efficient decarboxylative alkynylation on peptides, we began our investigations by the development of conditions in aqueous media. This chapter will be dedicated to the results obtained in this direction.

4.1 Preliminary work

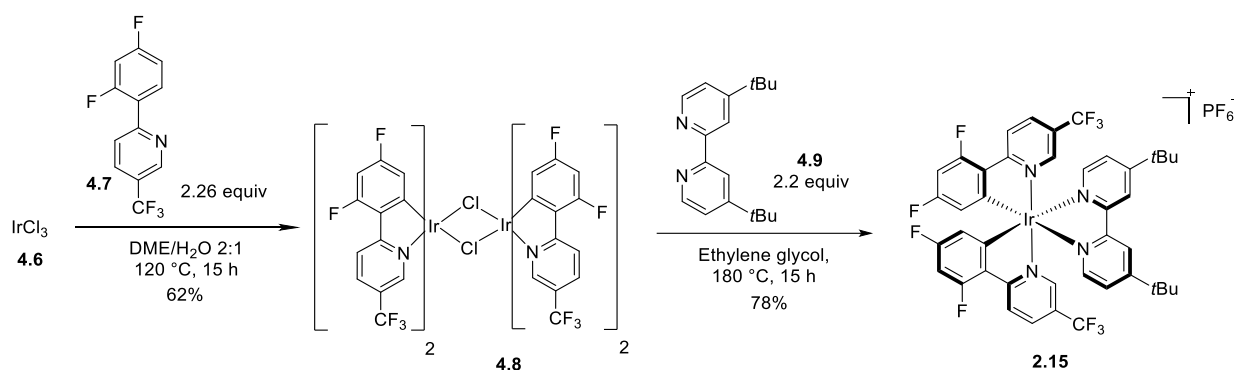
4.1.1 Proof of concept and choice of model substrate

With the long-term goal of expanding the visible-light decarboxylative alkynylation to biomolecules under aqueous conditions, the first step was to demonstrate the water compatibility. Tetrahydrofuran had been described as a suitable solvent for the reaction and was thus used due to its water miscibility. A first attempt was carried out in the conditions of Scheme 31, which were designed according to previous results (section 2.3.3).^[13] The molarity was diminished from 0.2 M to 10 mM and THF/water 4:1 was chosen as a solvent. Diluted conditions are indeed required for future work with larger peptides. Cbz-Pro (**4.1**) was chosen for this first attempt due to its excellent reactivity. To our delight, the desired product **2.50** was obtained with full conversion, with no traces of by-product **4.2**. This transformation is thus compatible with the presence of water, on the contrary to the decarboxylative cyanation.^[184] Conditions in aqueous media could then be envisioned. With this first result in hand, attempts on non-protected proline (**4.3**) led to the conclusion that the protecting group was required. Indeed, only traces of product **4.4** were detected and alkynylation of THF (**4.5**) was the major product (Scheme 11). With Ph-EBX considered as the limiting substrate, **4.5** could be isolated in 58% yield.



Scheme 31: Water-compatibility and protecting group requirement

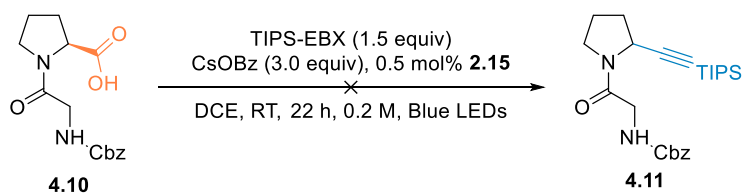
The study was started with iridium catalyst $[\text{Ir}\{\text{dF}(\text{CF}_3)\text{ppy}\}_2(\text{dtbpy})]\text{PF}_6$ (**2.15**) as it afforded the best results in previous work from the group. The synthesis is described in Scheme 32. Following a reported procedure, starting from iridium trichloride **4.6** a first double complexation of C-N fluoro ligand **4.7** affords a dichloro-bridged iridium dimer **4.8** at high temperature.^[156] Heating further this dimer allows complexation with a di-*tert*-butylbipyridine ligand **4.9**, affording monomeric catalyst **2.15** in 78% yield after recrystallization.



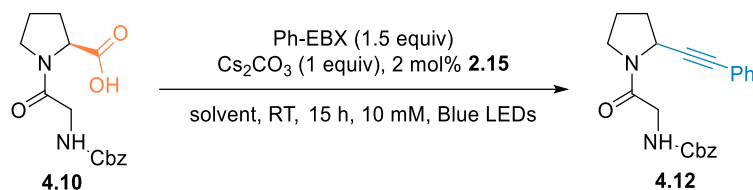
Scheme 32: Synthesis of $[\text{Ir}\{\text{dF}(\text{CF}_3)\text{ppy}\}_2(\text{dtbbpy})]\text{PF}_6$

Further work was thus carried out on N-terminal protected substrates. The Cbz group was preferred to the Boc group for practical reasons as it afforded UV-active compounds. Cbz-Gly-Pro (**4.10**) was then chosen as a model-substrate for a study on dipeptides. Proline has been described as an excellent substrate for decarboxylation due to its rigid structure and the alkyl groups substituting the nitrogen atom are making the nitrogen atom more electron rich, resulting in a more nucleophilic radical after decarboxylation.^[12] As the simplest dipeptide bearing a proline at the C-terminal, Cbz-Gly-Pro (**4.10**) would allow to evaluate if peptides are suitable substrates. After decarboxylation, the radical would indeed be generated in α -position to a nitrogen belonging to an amide bond, not to a carbamate as in the previous study.

Attempts within the group starting from dipeptides in the conditions of Equation 15 (TIPS-EBX (**2.4**) as a reagent, cesium benzoate as a base in DCE) had led to complex mixtures.^[13] TIPS-EBX presents a lower reactivity towards radical addition, as well as a lower stability under basic conditions compared to Ph-EBX (**2.5**). Ph-EBX was thus the model reagent for the proof of concept and the optimization in aqueous media.

Equation 15: Previous attempt of decarboxylative alkynylation on Cbz-Gly-Pro (**4.10**)

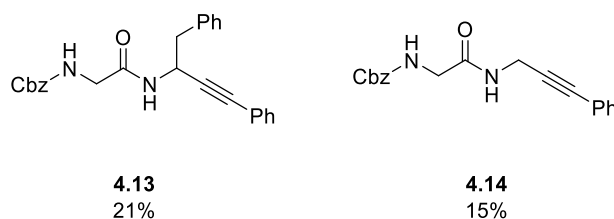
Our investigations on Cbz-Gly-Pro (**4.10**) started with a change of base to cesium carbonate and increasing the catalyst loading to 2 mol% (Table 1). Using this stronger base was possible in this study with Ph-EBX (**2.5**), which is less sensitive than TIPS-EBX (**2.4**). As a stronger base, cesium carbonate should ensure complete deprotonation, together with the counter-ion effect, namely “cesium-effect”.^[180] This beneficial effect in photoredox decarboxylation which had been observed experimentally was confirmed by the group of Leonori in oxidation potential measurements.^[237] On their oxime model substrate, the cesium carboxylate has an oxidation potential of +1.62 V compared to +1.68 V for potassium. The molarity of 10 mM, employed in the preliminary results, was kept. This system in THF afforded the desired alkynylated dipeptide **4.12** in 66% isolated yield (entry 1). A screening of biomolecule-compatible solvents was then carried out. Surprisingly, **4.12** could be obtained in 55% yield in acetonitrile (entry 2). No reactivity had been observed on Cbz-Pro (**4.1**).^[13] This result is likely due to a dilution effect, which led to a better solubility of Ph-EBX. Using DMSO as a solvent led to only traces of the product together with decomposition (entry 3), which was in line with previous results. Further work was carried out to determine the influence of the proportion of water. Running the reaction in THF/water 9:1 afforded **4.12** in 71% yield (entry 4). However, in acetonitrile/water 9:1, the yield dropped to 11% (entry 5). This is likely due to solubility reasons as Ph-EBX is neither soluble in acetonitrile, nor in water. The main drawback in the choice of THF is that THF alkynylation occurs as the main side-reaction. Nevertheless, further work was conducted with THF as the aim was to diminish the amount of co-solvent during the study. Changing to dioxane led to similar result and alkynylation of dioxane was observed. Variation of the THF/water ratio highlighted a drop of yield when water was the main solvent (entries 6-8). A 1:1 ratio of THF/water led to 48% of yield, despite a homogeneous mixture. Below 30% of THF as solvent, solubility issues were encountered and the yield dropped to 35% (entry 7) and to 10% when using only 20% of THF (entry 8). Those results highlighted that no less than 20% of THF as a co-solvent should be employed for solubility reasons, but also that solubility was not the only origin for the observed low reactivity.

Table 1: Solvent screening of the decarboxylative alkynylation on Cbz-Gly-Pro (**4.10**)

Entry	Co-solvent	Co-solvent/water	Yield (%)
1	THF	10:0	66 ^a
2	CH ₃ CN	10:0	55 ^a
3	DMSO	10:0	traces
4	THF	9:1	71 ^a
5	CH ₃ CN	9:1	11 ^a
6	THF	1:1	48 ^b
7	THF	3:7	35 ^b
8	THF	2:8	10 ^b

^a isolated yield, ^b HPLC yield. The screening was performed on a 0.05 mmol scale.

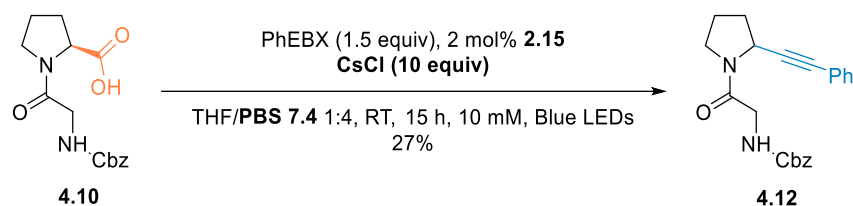
In order to have a first insight of the scope and evaluate the reactivity of substrates leading to a less stabilized radical after decarboxylation, 2 dipeptides were tested on 0.1 mmol scale in the conditions from Table 1, entry 4 (modified to THF/water 4:1). To our delight, Cbz-Gly-Phe and even Cbz-Gly-Gly were suitable substrates for this decarboxylative alkynylation (Scheme 33). Nevertheless, very low yields of **4.13** and **4.14** were obtained and alkynylation of THF (**39**) was the major product. Future work will be carried out on Cbz-Gly-Pro (**4.10**) as this excellent substrate.



Scheme 33: First scope of dipeptides in the of the decarboxylative alkynylation

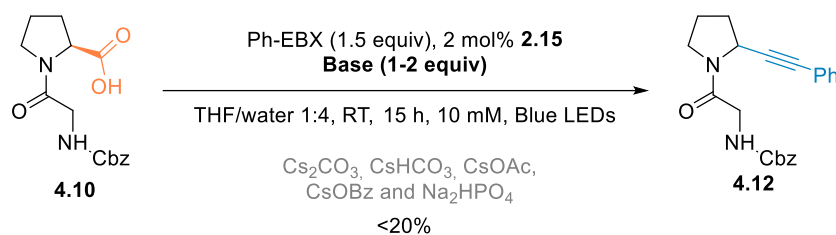
4.1.2 Optimization in buffers

Encouraged by those promising results, attempts in aqueous neutral conditions using buffers were carried out. Following previous reports, PBS (phosphate saline buffer) and Tris buffer were described as the most common buffers for photoredox catalyzed reactions in aqueous media.^[214] A pH of 7.4 was chosen as a reference for a buffer screening as it is the physiological pH. A pH range of 6-8 was then screened. A first attempt was carried out using commercial PBS (pH 7.4 at 10 mM). CsCl was introduced as a source of cesium ions, in order to facilitate the decarboxylation according to the previously described cesium effect.^[180] Gratifyingly, the product could be obtained, although in low yield and conversion: 27% isolated yield of **4.12** on 0.1 mmol scale (Equation 16). Similar solubility issues than in Table 1 were observed. Lowering the proportion of THF led not surprisingly to a decrease in yield: 18% for 10% THF and 12% for 5%. An amount of 20% was thus selected, as a compromise between reactivity and the proportion of co-solvent.



Equation 16: Buffer screening on Cbz-Gly-Pro (**4.10**)

A screening of pH within the 6-8 range was performed with PBS under the conditions of Equation 16, as well as attempts in Tris buffer and PB buffer at pH 7.4. The latter having the same composition as the PBS but without NaCl, likely affording a better solubility. No real influence of the pH and the nature of the buffer can be observed. In all cases, heterogeneous mixtures were obtained with low conversion and no yield higher than 19%. In order to confirm whether the limiting parameter was the use of water as the major solvent or the use of buffers, a screening of base using water/THF 4:1 was thus performed (Cs_2CO_3 , CsHCO_3 , CsOAc , CsOBz and Na_2HPO_4). No significant changes were observed (Equation 17), although a slight increase of yield was measured with sodium phosphate (19%), indicating that neither the base nor the counter-ion were the limiting factor in those conditions.



Equation 17: Base screening in THF/water 1:4

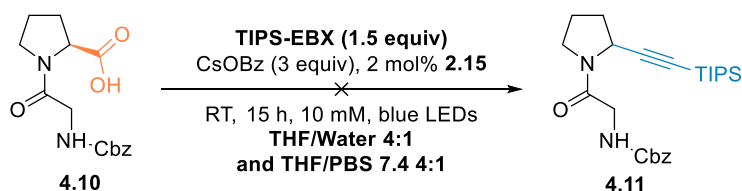
4.1.3 Optimization of other parameters

The previous screening of parameters (buffer, base and co-solvent) have not afforded successful conditions in aqueous media. Further attempts were carried out to get a better insight of the limiting parameters in the transformation. Conditions from Equation 17, with cesium carbonate as a base and water as a solvent, were used.

Developing a metal-free transformation would be of high interest in the context of biomolecule functionalization. Moreover, the large variety of organic dyes provides a large redox windows. DCA (**2.20**) is known to be a suitable catalyst for this reaction, as demonstrated in previous work from Cheng.^[189] Its high oxidation potential ($E_{1/2}(*\text{P}/\text{P}^-) = +2.06 \text{ V}$) would favor the decarboxylation, although possible side-reactions could occur. 4CzIPN (**2.23**) was first synthesized by Uoyama *et al.* and was presented as an alternative to commercial DCA.^[160] Its redox potential window (+1.37/-1.21 V) matches with the one of $[\text{Ir}\{\text{dF}(\text{CF}_3)\text{ppy}\}_2(\text{dtbpy})]\text{PF}_6$ (**2.15**) (+1.21/-1.37 V) employed so far in our study. It has already been employed for a Photoredox/Ni-catalyzed decarboxylative cross-coupling of α -amino-acids and aryl halides.^[159] Among the several donor-acceptor fluorophores screened in the work from Luo, 4CzIPN (**2.23**) appeared to be suitable for our transformation. Both catalysts afforded the desired product (Equation 18), although low yields comparable with previous experiments with the iridium catalyst **2.15** were obtained.



(**4.11**) could not be obtained despite several attempts (Equation 20). Mixture of unknown products were obtained. Although the desired product was detected by MS, no isolation and characterization could be achieved. TIPS-EBX has been previously demonstrated to be less reactive towards radical addition, as well as less stable under basic conditions.^[13] Further work was conducted and is described in section 6.3.1.



Equation 20: TIPS-EBX as a reagent

With those results in hand, solubility appeared to be a major issue. It was thus decided to focus on water-soluble reagents and catalysts for this study.

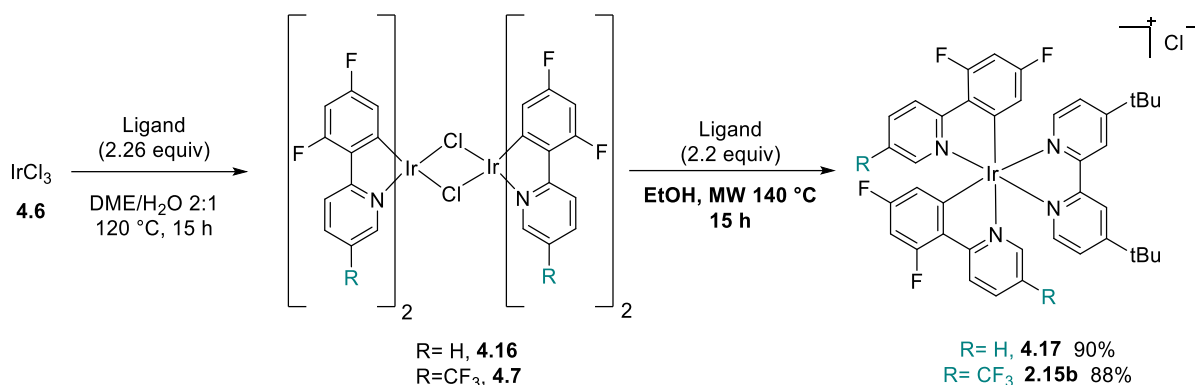
4.2 Synthesis and screening with water-soluble catalysts

4.2.1 Design and synthesis of catalysts

As none of the catalysts used in the previous section were soluble in water, one direction for improvement was the synthesis of water-soluble catalysts. It was decided to modulate the structure from the catalysts already employed in order to maintain similar redox properties. Despite the interesting redox properties of the known iridium catalysts described in section 2.3.2, either they were not water-soluble or their redox properties would not match the requirements of our transformation. They were thus not synthesized but analysis of their structures and synthetic pathways were used as a base for modifications.^[176,177,238]

First, changing the counter-ion to Cl^- should improve the water-solubility of the known catalyst **2.15**.^[157] This synthesis would require the use of a solvent with a lower boiling point than ethylene glycol in order to recover easily the catalyst. Indeed, in this case no precipitation after anion metathesis by addition of NH_4PF_6 would occur.^[156] Concentrating under vacuum prior to recrystallization would likely be an efficient purification method. Work of the Bernhard group showed that iridium catalyst **2.34** can be synthesized in refluxing ethanol in 24 h.^[176] Adapting those conditions, by replacing ethylene glycol with ethanol and heating in a microwave reactor at 140 °C for 15 h, was successful (Scheme 34). High temperature is

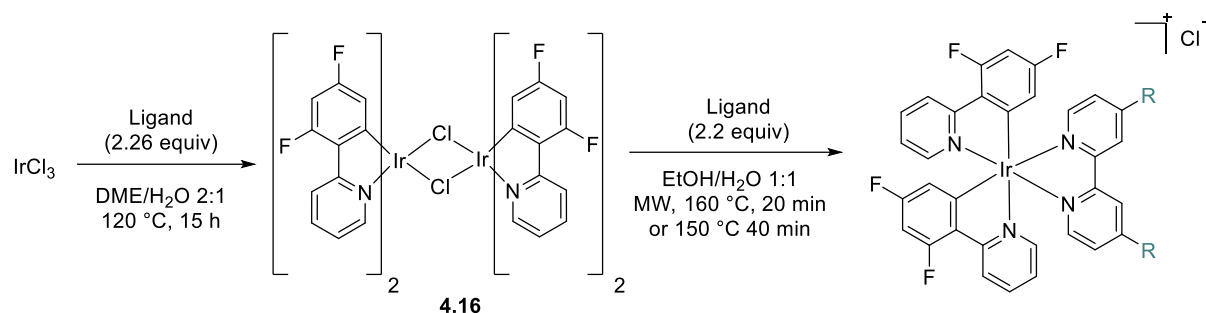
required in the synthesis of **2.15** to afford the desired *fac* stereoisomer.^[156] The desired catalyst **2.15b** was obtained in 88% yield after recrystallization in acetone/hexane. Further work on dimer **4.16** showed that only 10 h was required for the ligand exchange and the desired catalyst **4.17** was obtained in 90% yield after recrystallization. The reaction time could likely be reduced for further work. Those catalysts were not water-soluble hence a variation of ligand was envisaged.



Scheme 34: Synthesis of water-soluble iridium catalysts, first scaffold

A first study was carried out on the difluoro-substituted dimer **4.16**. In comparison to the scaffold of the Iridium catalyst used in the precedent part, the phenylpyridine ligand was not substituted with a CF₃ group in order to increase the water-solubility. It was decided to synthesize the catalysts described in Table 2, with electron withdrawing groups (CO₂Et, CO₂H, PO(OEt)₂ and PO(OH)₂) and one weak electron-donating group (CH₂PO(OEt)₂). Those substituted bipyridine ligands have demonstrated their ability to induce water-solubility in iridium catalysts (section 2.3.2). The different ligands were synthesized using reported procedures.^[239–241] Following the work of Ashford *et al.*,^[173] the dimer **4.16** was heated in presence of ligand in EtOH/water in a microwave reactor to afford the desired catalysts **4.18** to **4.22** (Table 2). After concentration under vacuum, the different catalysts were recrystallized in acetone/ether and obtained in good yields. In our study, phosphonic acid substituted bipyridine ligand was hydrolyzed prior to complexation but Norris *et al.* have reported that this hydrolysis can be performed directly on the catalyst, although the catalyst synthesis is more efficient with phosphonic acid substituted bipyridines.^[174] The catalysts water-solubility was evaluated by placing 1 mg in 1 mL of water. To our delight, all catalyst except **4.18** were soluble. To the best of our knowledge, those catalysts were not reported at the time of this study.

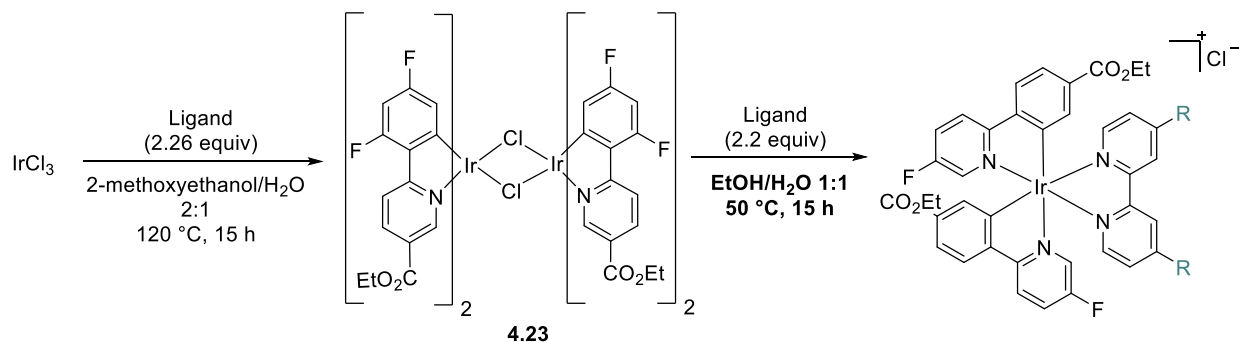
Table 2: Synthesis of water-soluble iridium catalysts, second scaffold



Entry	R=	Temperature	Time	Yield (%)	Water-soluble at 1 mg/mL
1	CO ₂ Et, 4.18	160 °C,	20 min	56	No
2	CO ₂ H, 4.19	160 °C	20 min	71	Yes
3	PO(OH) ₂ , 4.20	150 °C	40 min	77	Yes
4	PO(OEt) ₂ , 4.21	150 °C	40 min	73	Yes
5	CH ₂ PO(OEt) ₂ , 4.22	160 °C	20 min	67	Yes

Following the work from Liu *et al.*,^[177] an ester-substituted cyclometalated ligand has also been studied. Building on their procedure and our previous work (Scheme 34), the solvent was changed from CH₂Cl₂/MeOH 2:1 mixture to EtOH/water 1:1 (Table 2). Heating the dimer **4.23** at only 50 °C was sufficient to obtain the catalysts **4.24** and **4.25** in excellent yields (Table 3). Only catalysts bearing electron-donating groups on the bipyridine ligands were synthesized. The screening of **4.24** and **4.25** did not improve the outcome of our decarboxylation alkynylation, hence no further work using this cyclometalated ligand was carried out. To the best of our knowledge, those catalysts have not been reported before. The characterization of their redox properties, such as the oxidation and reduction potentials were not determined at that stage and are envisioned to be measured in case of success.

Table 3: Synthesis of water-soluble iridium catalysts, third scaffold

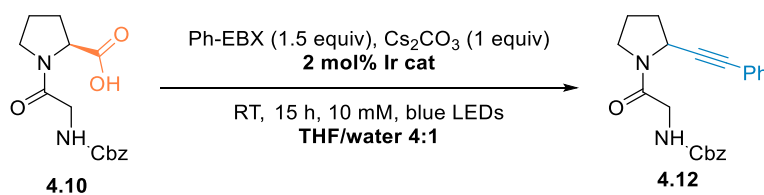


Entry	R=	Yield (%)	Water-soluble at 1 mg/mL
1	<i>t</i> Bu 4.24	quant	No
2	CH ₂ PO(OEt) ₂ 4.25	92	Yes

4.2.2 Screening of water-soluble catalysts

With this library of catalysts in hand, a screening of catalyst was carried out both in a THF/water 4:1 mixture (Table 4) and then in a PBS/THF 4:1 mixture (phosphate buffer saline at pH 7.4). The first screening provided a comparison in organic solvent and validated their catalytic efficiency. The second screening allowed to conclude whether using a water-soluble catalyst had a positive impact on the formation of the alkynylated peptide (Equation 21). To our delight, all the catalysts afforded full conversion and good yield in organic solvent (Table 4). As a reference, [Ir{dF(CF₃)ppy}₂(dtbpy)]PF₆ **2.15** afforded an excellent yield (92%, entry 1). Changing the counter-ion of **2.15** to Cl⁻ resulted in a lower yield (69%, entry 2). Excellent yield was obtained using **4.17** (entry 3). Among the water-soluble ones, the best results were obtained with phosphonate-substituted catalyst **4.21** and **4.22**, carboxylic acid-substituted catalyst **4.19** and ester-substituted catalyst **4.18** (entries 4-7). As evoked in the previous section, the ester substituted cyclometalated ligand afforded lower yields (entries 8-9) and less clean reactions and no further work was conducted with those catalysts.

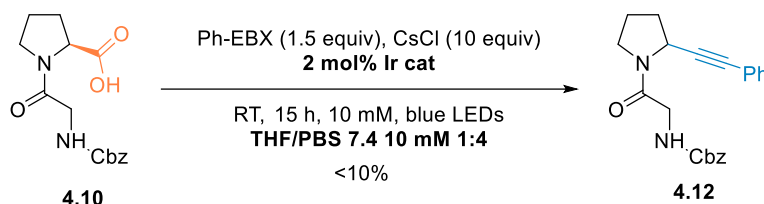
Table 4: Screening of water-soluble catalysts in THF/water 4:1 as a solvent



Entry	Catalyst	Yield (%) ^a
1	2.15	92
2	2.15b	69 (50)
3	4.17	79
4	4.21	74 (77)
5	4.22	66 (44)
6	4.19	59
7	4.18	95
8	4.24	39 (48)
9	4.25	49 (44)

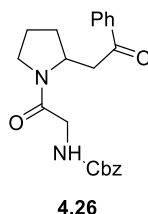
^a HPLC yield, (isolated yield). The screening was performed on a 0.05 mmol scale.

All the catalysts were also screened under aqueous conditions (Equation 21). Unfortunately, no yield was higher than 10%. The solubility of the catalyst was thus not the limiting parameter in the transformation. The next section will thus focus on the last reactant which was not water-soluble: Ph-EBX.



Equation 21: Screening of water-soluble catalysts in aqueous media

It is noteworthy to mention that during this screening of catalysts, the side-product **4.26** was isolated. Indeed, traces of **4.26** can be found in most of the experiments, but not in quantities sufficient to be able to isolate and characterize this compound. **4.26** is likely formed by hydration of the alkyne.



4.2.3 Water-soluble EBX

Water-soluble EBX reagents have been under study in the group. The most successful ones are bearing a sulfonate group in *para* position of the hypervalent iodine.² Only a limited amount of reagent was available for those attempts hence only two experiments were performed, both in aqueous PB (phosphate buffer) (Table 5). We indeed wondered if the large concentration of salts in the PBS buffer was detrimental. First, a control experiment, using catalyst **2.15**, allowed a comparison of reactivity with the normal Ph-EBX (entry 1). However, EBX reagent **4.27** was not compatible with those conditions and only 13% of **4.12** was obtained. Then, using the water-soluble catalyst **4.22**, which had demonstrated good activity

² Romain Tessier, *unpublished results*.

(Section 0), provided a system where all components were water-soluble but without a better result (entry 2). If the water-soluble EBX **4.27** was stable when using catalyst **2.15**, degradation was observed with catalyst **4.22**. The first experiment was reproduced and the yield measured after 6 h and 24 h. No significant increase of yield was obtained, with the starting peptide remaining the major component. The sulfonate group is likely oxidized by the excited state of the photocatalyst, leading to degradation. No further work was conducted with those reagents. Another class of water-soluble EBX reagents would need to be designed in order to be compatible with those photoredox conditions.

Table 5: Attempts using water-soluble EBX in the decarboxylative alkynylation

Reaction scheme: Peptide **4.10** (a 5-membered lactam with a carboxylic acid and a Cbz-protected amine) reacts with EBX **4.27** (a phenyl-substituted sulfonate) in the presence of CsCl (10 equiv), 4 mol% Ir catalyst, THF/PB 7.4 1:4, at room temperature for 15 h, 10 mM, under blue LEDs. The product **4.12** is the corresponding alkynylated peptide where the carboxylic acid has been replaced by a phenylethynyl group.

Entry	Catalyst	Ratio SM/P ^a	Yield (%) ^b
1	2.15	85:15	13
2	4.22	85:15	14

^a Ratio of product compared to remaining starting material by HPLC analysis, ^b HPLC yield

The screening was performed on a 0.025 mmol scale.

4.3 Conclusion

Within our goal to develop a decarboxylative alkynylation on peptides and proteins, attempts towards optimization under aqueous conditions were carried out. If the first results suggested that solubility was the main issue in this transformation, results on water-soluble reagents highlighted that it was maybe not the only limiting parameter. Indeed, neither novel water-soluble iridium-based photocatalysts, nor water-soluble EBX reagents, led to an increase of conversion. Possible explanations could be found in a solvent effect on the reactivity of the radical, or an increase in the oxidation potential of the carboxylic acid. With those results in hand, it was decided to focus first on peptide alkynylation which does not

require aqueous conditions. The development of aqueous conditions for more complex biomolecules will be resumed once that first methodology will be implemented.

Development of novel fine-tuned organic dyes for photoredox catalysis



5 Development of novel fine-tuned organic dyes for photoredox catalysis

5.1 Synthesis and characterization of 4XCzIPN derivatives³

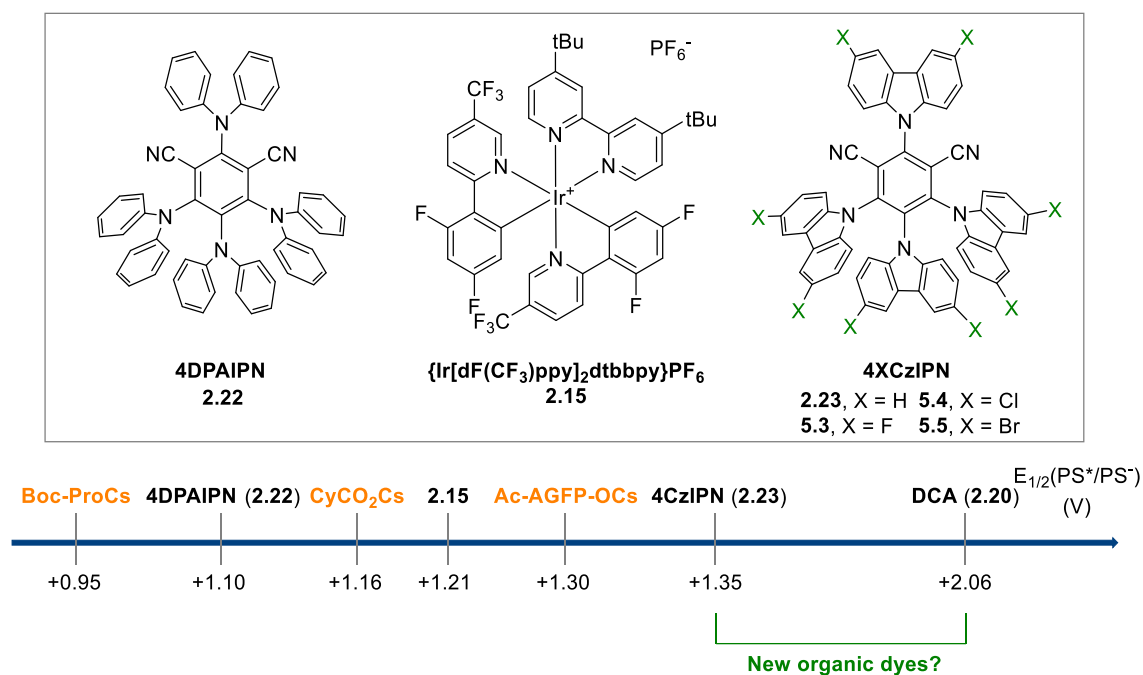
5.1.1 Significance and design

During the previous works from our group on the photoredox-catalyzed decarboxylative alkynylation and cyanation, we understood that the reactivity of each carboxylic acid can be rationalized from the structure.^[13,184] The presence, or absence, of an heteroatom in α -position has a paramount role on the stabilization of the generated radical, as well as its substitution (from primary to tertiary). The environment, such as the solvent or the counter-ion, are also key parameters to take into account. The potentials of each substrate can be measured by cyclic voltammetry. This allows a rational design when knowing the redox properties of the catalysts in hand. Substrates such as aliphatic acids have higher reduction potentials and were thus leading to a decrease of yield when using $\text{Ir}[\text{dF}(\text{CF}_3)\text{ppy}]_2\text{dtbbpy}.\text{PF}_6$ (**2.15**). It is important to note that the oxidation potential of peptides carboxylates in water is higher than in organic solvent (+1.30 V for Ac-AGFP-OCs (**5.1**) in comparison to +0.95 V for Boc-Pro-OCs (**5.2**)).^[11,226] We thus wondered whether it would be possible to employ different catalysts to target a broader class of substrates. At the time of the study, a rise of interest occurred towards metal-free approaches, in order to be more environmentally friendly with a lower cost than with transition-metals. We thus envisioned to provide an organic dye which would be an efficient catalyst for this transformation and potentially novel ones. Indeed, if DCA (**2.20**) was shown to be a suitable catalyst, its strong oxidizing properties renders degradation and poor substrate tolerance likely. Hence modulation of the redox properties of organophotocatalysts was highly desirable. Ideally, a valuable contribution would consist of presenting a platform with possible adaption depending on the required properties.

Among the numerous scaffolds (Section 2.3.2),^[158] we decided to focus on 4CzIPN (**2.23**). The reason for that is the similar oxidation and reduction potentials at the excited state ($E_{1/2}(\text{P}^+/\text{P}^-) = +1.35$ V and $E_{1/2}(\text{P}^+/\text{P}^*) = -1.21$ V) in comparison to $[\text{Ir}\{\text{dF}(\text{CF}_3)\text{ppy}\}_2(\text{dtbpy})]\text{PF}_6$ (**2.15**) ($E_{1/2}^{*\text{III/II}} = +1.21$ V and $E_{1/2}^{\text{II/III}} = -1.37$ V).^[159,160] As a consequence, **2.23** was employed

³ This work was performed together with Franck Le Vaillant and Dr. Stefano Nicolai, who are sincerely thanked. “” The text in between is a direct quotation from our publication: F. Le Vaillant, M. Garreau, S. Nicolai, G. Gryn'Ova, C. Corminboeuf, J. Waser, *Chem. Sci.* **2018**, 9, 5883–5889. Dr Ganna Gryn'ova from the group of Prof Corminboeuf performed all the DFT calculations and is acknowledged.

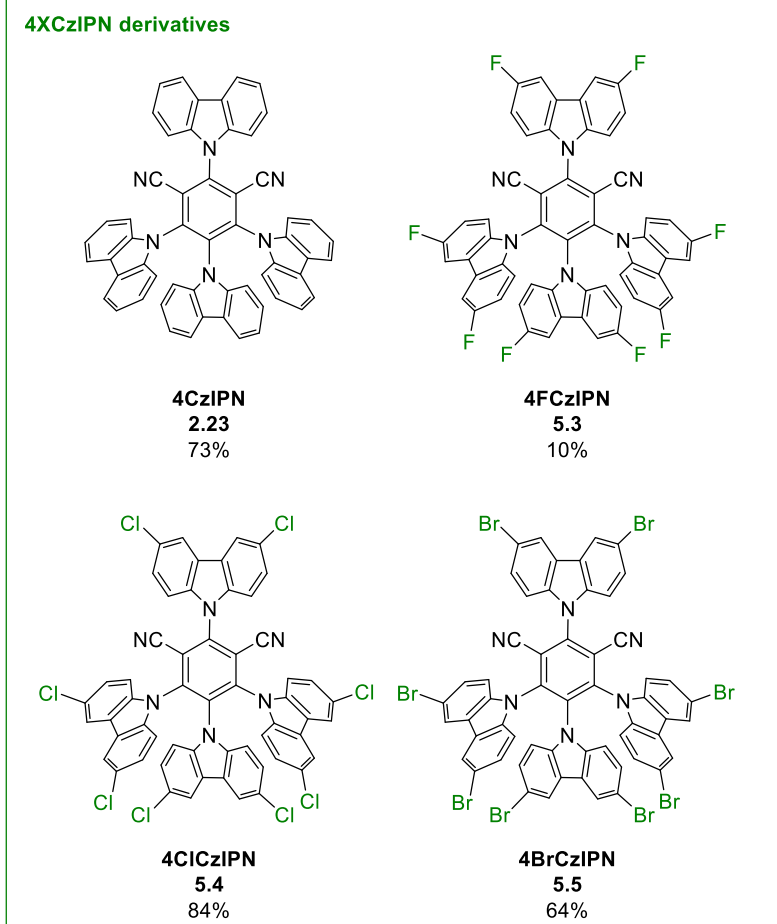
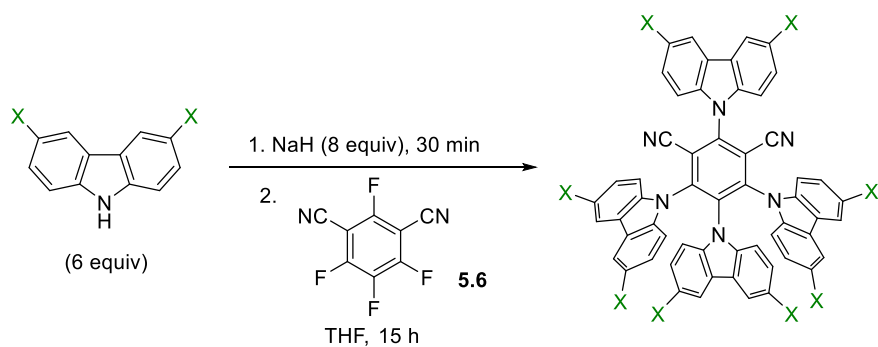
in a decarboxylative Giese transformation, highlighting its potential as a valuable alternative to Ir[dF(CF₃)ppy]₂dtbbpy.PF₆ (**2.15**). Another important feature is that it can be easily accessed in one-step from inexpensive starting materials. Furthermore, investigations on the influence of the number and position of carbazoles and cyano groups had already been explored by Zhang.^[159] This was quite promising for our desired modulation of the redox properties of this donor-acceptor dye. An overview of the knowledge about the carbazolyldicyanobenzene family is presented in Section 2.3.2. Upon analysis of the available organophotocatalysts, a gap was existing between 4CzIPN (**2.23**) and the strong oxidants DCA (**2.20**) and Fukuzumi dye (**2.25**) (Scheme 35). The aim of this project was thus to provide novel organic dyes as alternatives in this underexplored region. The basis for our design was the observation that 4DPAIPN (**2.22**) was less oxidizing than 4CzIPN (**2.23**). The carbazoles, and diphenyl amines, indeed have the role of donor on this scaffold and the presence of more electron-poor carbazoles renders the dye more oxidant. Building on that observation, we wondered whether the addition of electron-withdrawing groups on the carbazoles would have a similar effect. Carbazoles substituted with halogen atoms in *para* position of the nitrogen were thus targeted. Those commercially available starting material would be a good starting point to test our hypothesis. It is worth mentioning that mechanistic investigations demonstrated the importance of the reductive properties of the catalyst to close the catalytic cycle when employing EBX reagents.^[184] When modulating the redox properties of this scaffold, the reductive character has to be conserved if we want to employ them with EBX reagents.

Scheme 35: Scale of redox potentials of carboxylates and common photocatalysts⁴

5.1.2 Synthesis

The standard procedure described for the synthesis of 4CzIPN (**2.23**) was employed, with a slight increase in equivalents of sodium hydride and carbazoles (Scheme 36).^[159,160] Starting from 2,4,5,6-tetrafluorophthalonitrile (**5.6**), nucleophilic aromatic substitution with the corresponding carbazoles afforded the desired dyes **2.23** and **5.3** to **5.5**. Gram scale synthesis were performed and excellent yields were obtained, with the exception of **5.3**, where polymerization was observed, probably by substitution of the fluorine atom on the carbazole. The procedure is simple and the dyes are efficiently purified by recrystallisation followed by column chromatography. If 4ClCzIPN (**5.4**) and 4BrCzIPN (**5.5**) had already been described as Thermally Activated Delayed Fluorescence Materials (TADF),^[242] they had never been reported as photoredox catalysts. Their redox properties had thus not been measured.

⁴ Value for 4DPAIPN (**2.22**) reported by Zhang, further discussion in Section 5.3.



Scheme 36: Synthesis of novel 4XCzIPN derivatives

5.1.3 Characterization of 4XCzIPN derivatives

With those dyes in hand, the next step was the characterization of their redox properties to test our hypothesis. We determined the oxidation and reduction potentials, both at the ground and excited state (Table 6). Cyclic voltammetry experiments were carried out first to determine the redox potentials at the ground state. The conditions were chosen identical as the ones from the work on 4CzIPN derivatives in order to have comparable values.^[243,244] The redox potentials at the excited state can be estimated from the values at the ground state by the Rehm-Weller equation: $E_{1/2}(P^+/P^*) = E_{1/2}(P^+/P) - E_{0-0}$ and $E_{1/2}(P^*/P^-) = E_{0-0} + E_{1/2}(P/P^-)$.^[158] The excitation energy E_{0-0} was estimated by the point of intersection of the normalized absorbance and emission signals for each dye.

“Ground state reduction and oxidation potentials of -1.21 V and +1.52 V for catalyst **2.23** in acetonitrile have been reported based on cyclic voltammetry. Estimation of the potentials in the excited state was: +1.35 V and -1.04 V for reduction and oxidation, respectively (entry 1). In our hand, slightly different values were obtained (entry 2). In particular, a higher reduction potential of +1.59 V was observed in the excited state. We then turned to halogenated dyes. With catalyst **5.4**, both the cathodic and anodic shifts were measured, with reduction and oxidation potentials of -0.97 V and +2.05 V (entry 3). This resulted in an increased reduction potential of +1.71 V of the photoexcited dye. Unfortunately, the cyclic voltammograms of dyes **5.3** and **5.4** could not be determined in acetonitrile due to their limited solubility. Only the absorption/emission spectra of dye **5.5** could be measured. We therefore turned to theory to have a more reproducible and expended access to redox potential values. At the PCM-UAKS/PBE0-D3BJ/def2-SVP level, the ground state reduction potentials decrease and the oxidation potentials increase in the order of **2.23**, **5.3**, **5.4**, **5.5** (entries 4-7).⁵ This leads to a higher reduction potential in the excited state for catalyst **5.4** and **5.5** compared to **2.23** (+1.58 V and +1.82 V respectively compared to +1.35 V). Therefore, both measurement and computation confirmed the increased potential for **5.4**. The same trends but with lower reduction potentials were obtained in dichloromethane as solvent (entries 8-11). In this case, absorption and emission spectra could be measured for all dyes, but no good quality cyclic voltammograms could be acquired. Values in the ground state were therefore again obtained by computation.”

⁵ See SI for a more detailed discussion.

Table 6: Literature (lit), measured (mes) and computed (comp) values for reduction potentials of dyes **2.23** and **5.3-5.5**.^[a]

Entry	Catalyst	Solvent	$E_{1/2}(P/P^-)$	$E_{1/2}(P^+/P)$	E_{0-0}	$E_{1/2}(P^*/P^-)$	$E_{1/2}(P^+/P^*)$
1	2.23 (lit)	CH ₃ CN	-1.21	+1.52	2.56	+1.35	-1.04
2	2.23 (mes)	CH ₃ CN	-1.05	+1.68	2.64	+1.59	-0.96
3	5.4 (mes)	CH ₃ CN	-0.97	+2.05	2.68	+1.71	-0.63
4	2.23 (comp)	CH ₃ CN	-1.29	+1.56	2.64 ^b	+1.35	-1.08
5	5.3 (comp)	CH ₃ CN	-1.18	+1.67	-	-	-
6	5.4 (comp)	CH ₃ CN	-1.10	+1.76	2.68 ^b	+1.58	-0.92
7	5.5 (comp)	CH ₃ CN	-0.83	+1.89	2.65 ^b	+1.82	-0.76
8	2.23 (comp)	CH ₂ Cl ₂	-1.29	+1.67	2.59 ^b	+1.30	-0.92
9	5.3 (comp)	CH ₂ Cl ₂	-1.18	+1.79	2.60 ^b	+1.42	-0.81
10	5.4 (comp)	CH ₂ Cl ₂	-1.10	+1.87	2.59 ^b	+1.49	-0.72
11	5.5 (comp)	CH ₂ Cl ₂	-0.85	+1.98	2.58 ^b	+1.73	-0.60

^[a] Potentials in V vs SCE. The excitation energy E_{0-0} was estimated by the point of intersection of the normalized absorbance and emission signals. $E_{1/2}(P^+/P^*) = E_{1/2}(P^+/P) - E_{0-0}$ and $E_{1/2}(P^*/P^-) = E_{0-0} + E_{1/2}(P/P^-)$. See SI for details.

^[b] Experimental values of E_{0-0} were used.

“The trend in reduction potentials increasing in the order of **2.23**<**5.3**<**5.4**<**5.5** (substituents on catalyst **2.23**: H<F<Cl<Br) can be rationalized as follows. Upon reduction, an electron is added to the lowest unoccupied molecular orbital (LUMO), located mostly on the central isophthalonitrile ring (Figure 9). However, the LUMO also involves the carbazole moieties in the 4 and 6 positions of the isophthalonitrile ring and is potentially stabilized by them to a greater extent in the case of Cl and Br substituents (resonance donors) compared to H and F (Figure 10).”

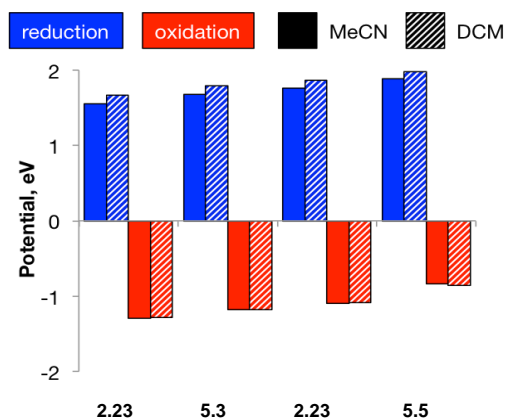


Figure 9: Influence of the substitution on the redox potentials of the 4XCzIPN

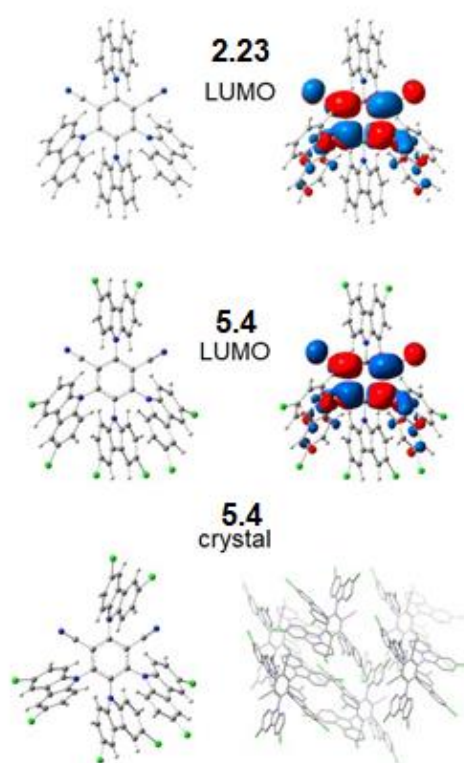


Figure 10: Optimized structures and LUMO plots (isovalue 0.02) of the dyes **2.23** and **5.4** at the PBE0/def2-SVP level, as well as the crystal structure of **5.4**.⁶

“We also note that while molecules **2.23** and **5.3** are fairly symmetric, systems **5.4** and **5.5** feature noticeable distortion of the 4-carbazole (Figure 11). This peculiar geometrical feature, observed both in the gas-phase optimized geometries, obtained at several dispersion-corrected DFT levels, and experimental crystal structures,⁷ Geometries of all species were optimized using several different DFT methods and dispersion corrections. All methods give comparable results indicating that, compared to rather symmetric species **2.23** and **5.3**, molecules **5.4** and **5.5** feature noticeable distortion of the carbazole moiety in the 4th position of the central ring. This distortion is equally observed in the gas-phase optimized geometries and in the experimental crystal structures. The likely cause of this feature is the halogen...halogen bonding between the halogen atoms of the neighbor carbazole moieties, absent/insignificant in **2.23** and **5.3** but increasingly pronounced in **5.4** and **5.5**, as exemplified by the corresponding interatomic distances. Similar intermolecular interaction also causes distortion of the 1-carbazole ring in the crystal of **5.4**. This hypothesis is supported by the fact

⁶ This picture was prepared by Dr Ganna Gryn'ova from Prof. Corninboeuf group.

⁷ (a) Crystal structure of **2.23** is available at CCDC under number 1052646 (YUGDOV), see S. Wang, Y. Zhang, W. Chen, J. Wei, Y. Liu and Y. Wang, *Chem. Commun.* **2015**, 51, 11972. (b) Crystal structure of **5.4** is available at CCDC under number 1838186.

(i) that distortion is almost entirely lifted in solution and (ii) is absent in the optimized structures of dyes, analogous to **5.4** and **5.5**, but with halogens selectively removed from the carbazole moieties in either the 4th and or the 3rd and 5th positions of the central ring.”

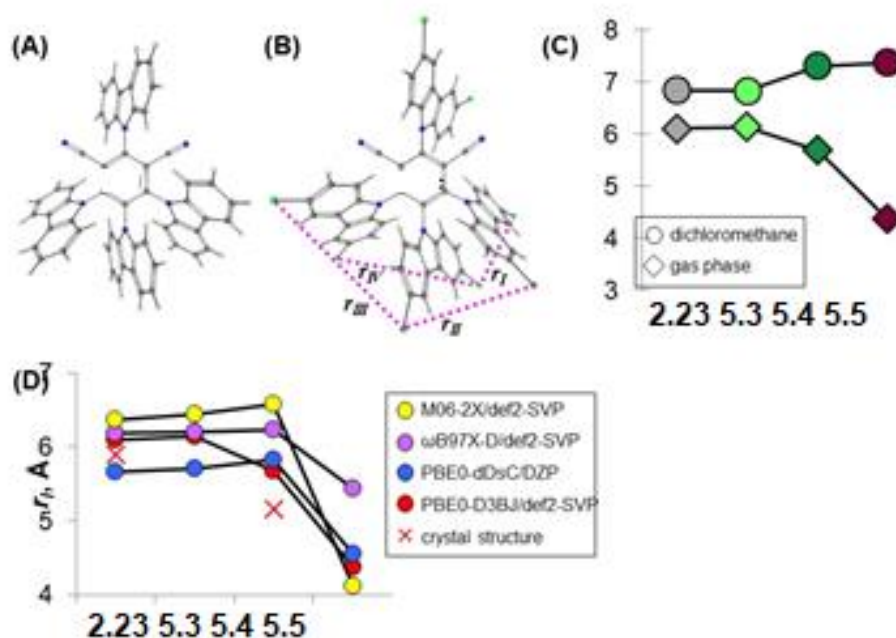


Figure 11: X-ray structures of dyes **2.23** (A) and **5.4** (B). Interhalogen distances in **5.4** are labelled as r_I - r_{IV} (dotted pink lines). (C) Interhalogen distance r_I in the optimized geometries of the studied dyes in the gas phase (PBE0-D3BJ/def2-SVP) and dichloromethane solution (PCM-UAKS/PBE0/6-31G(d)). (D) Shortest interhalogen distances r_I in the optimized geometries for several different dispersion-corrected DFT methods and experimental crystal structures.⁸

Our rational design was successful and this library now provides a range of organophotocatalysts between +1.35 V to +1.82 V at the excited state (Figure 12). A combination of experiments and computations was employed to determine the redox properties of the dyes.

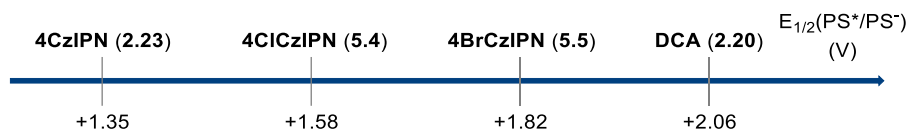
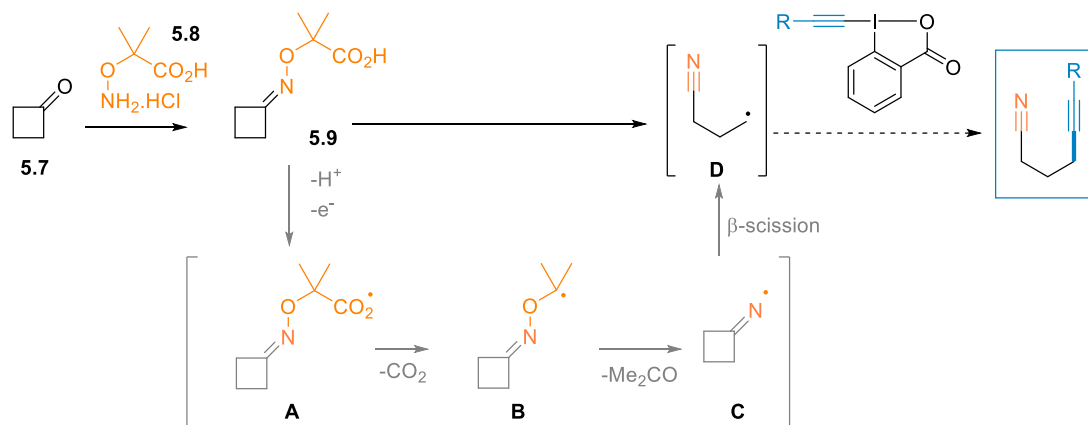


Figure 12: Scale of measured redox potentials of novel 4XCzIPN derivatives

⁸ This picture was prepared by Dr Ganna Gryn'ova from Prof. Corninboeuf group.

5.2 Application of 4XCzIPN derivatives in a fragmentation cascade⁹

Those novel dyes render the oxidation of other classes of substrates accessible. Among them, the cyclic oximes ethers **5.9** were targeted. They have been recently described as a novel mode of activation to generate iminyl radicals.^[245–247] In particular, the groups of Leonori and Studer reported elegant iminyl radical driven cascades.^[237,248,249] Those works set the path for our design of a fragmentation cascade starting from oximes **5.9** and EBX reagents (Scheme 37). First, upon deprotonation of **5.9**, oxidation can take place to **A**, triggering decarboxylation towards **B** and loss of acetone, forming the radical intermediate **C**. Strain release would then drive β -scission to generate a nitrile together with an alkyl radical on **D**. The last step of this process would be the addition of EBX reagents onto this radical to generate products containing both an alkyne and a nitrile moieties. From the catalyst point of view, the excited state is first reduced, and then the catalytic cycle is closed by reduction to form iodobenzoic acid, similarly as for the decarboxylative alkynylation (2.3.3). In the previous work from Leonori, several electrophilic radical trapping reagents have been used, but no C-C bond formation was achieved.^[250] The oximes ethers **5.9** can be prepared in one-step from the corresponding ketones **5.7** by condensation with hydroxylamine **5.8**.



Scheme 37: Proposed strategy for a photoredox-catalyzed fragmentation cascade on cyclic oximes ethers

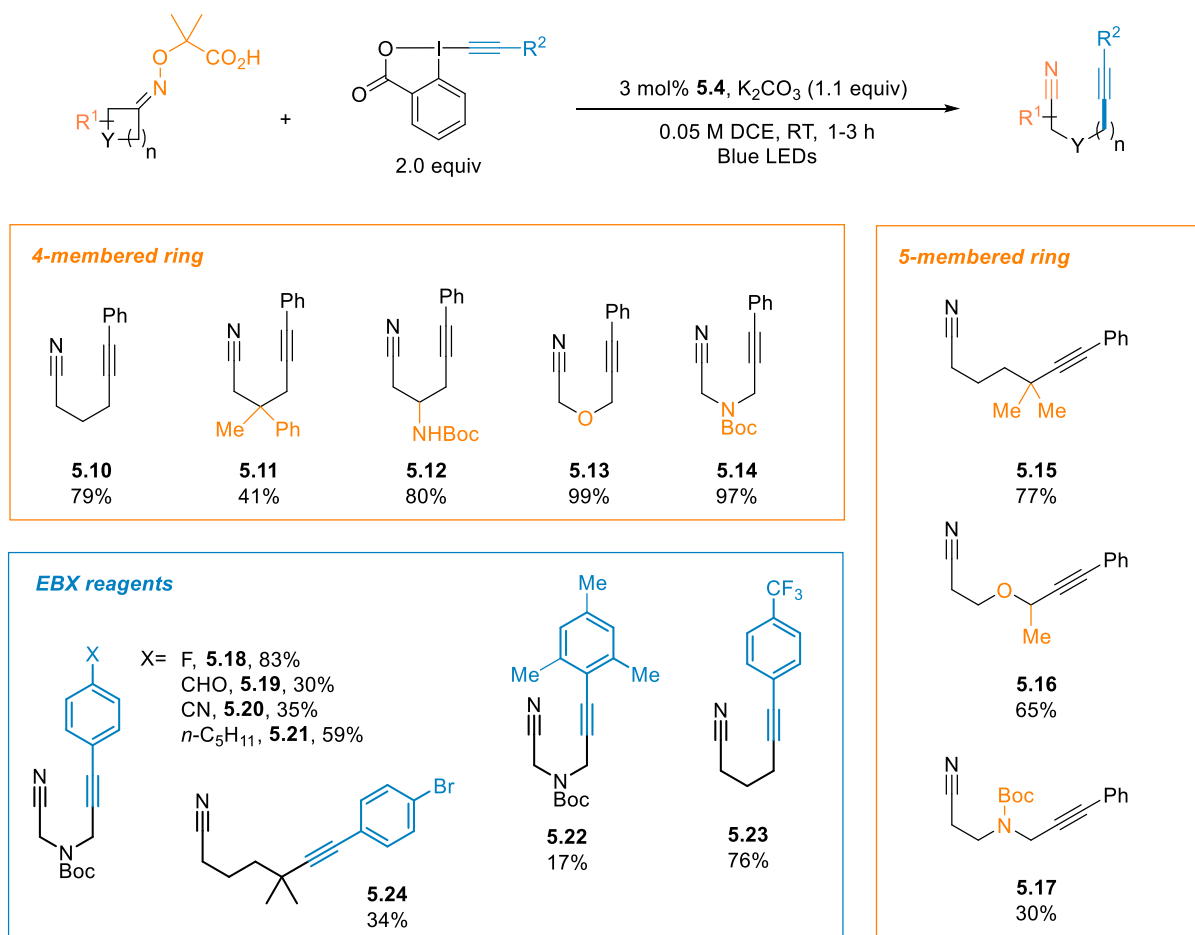
The novel dyes were key for the development of this transformation, as the reported 4CzIPN (**2.23**) afforded only 50% yield. The rational of this limitation stands in the oxidation

⁹ Only an overview is depicted here as this project was not the main topic of this thesis. A complete description can be found in the thesis of Franck Le Vaillant (number 9212) and in the publication F. Le Vaillant, M. Garreau, S. Nicolai, G. Gryn'Ova, C. Corminboeuf, J. Waser, *Chem. Sci.* **2018**, 9, 5883–5889. Characterization of the scope products will not be included in the SI and can be found in the original publication. My main contribution was in the synthesis and experimental characterization of the organic dyes, together with substrates synthesis.

potential of oximes **5.9**, which are higher than previously studied α -amino acids (between +1.48 and 1.59 V). Those values were measured by cyclic voltammetry. With the optimized conditions in hand, with 4ClCzIPN (**5.4**) as the best catalyst, the scope of this transformation was explored. Selected examples are presented in Scheme 38.

“Oxime **5.9** afforded **5.10** in 79% isolated yield. Phenyl, alkyl and protected amines were tolerated at the β -position (**5.11** and **5.12**, 41-80% yield). Oxetanone and azetidinones oximes ethers were also excellent substrates (**5.13** and **5.14**). Cyclopentanones derivatives were also successful. Using a *gem*-dimethyl substituent for the generation of a δ -tertiary alkyl nitrile radical allowed the isolation of **5.15** in 77% yield. An α -heteroatom was exploited to promote ring opening. With an oxygen linker, product **5.16** was obtained in 65% yield, whereas a nitrogen group led to a modest yield (30%) of **5.17**.”

“We then turned our attention to the scope of the reagents. The conversion of azetidinone oxime ether into α - α' -cyanoalkynylamines was achieved in good yields, tolerating electron-withdrawing groups (**5.18-20**) and electron-donating groups (**5.21**) in *para* position of the benzene ring. Using Mesityl-EBX, only 17% isolated yield of product **5.22** was isolated. Cyclobutanone oxime **5.9** could also be used with fluorinated arene substituents on the EBX (**5.23**). Product **5.24** bearing a bromine at the *para*-position was obtained in moderate yield from cyclopentanone oxime.”



Scheme 38: Scope of the fragmentation cascade from cyclic oxime ethers

5.3 Synthesis of 4XDPAIPN derivatives

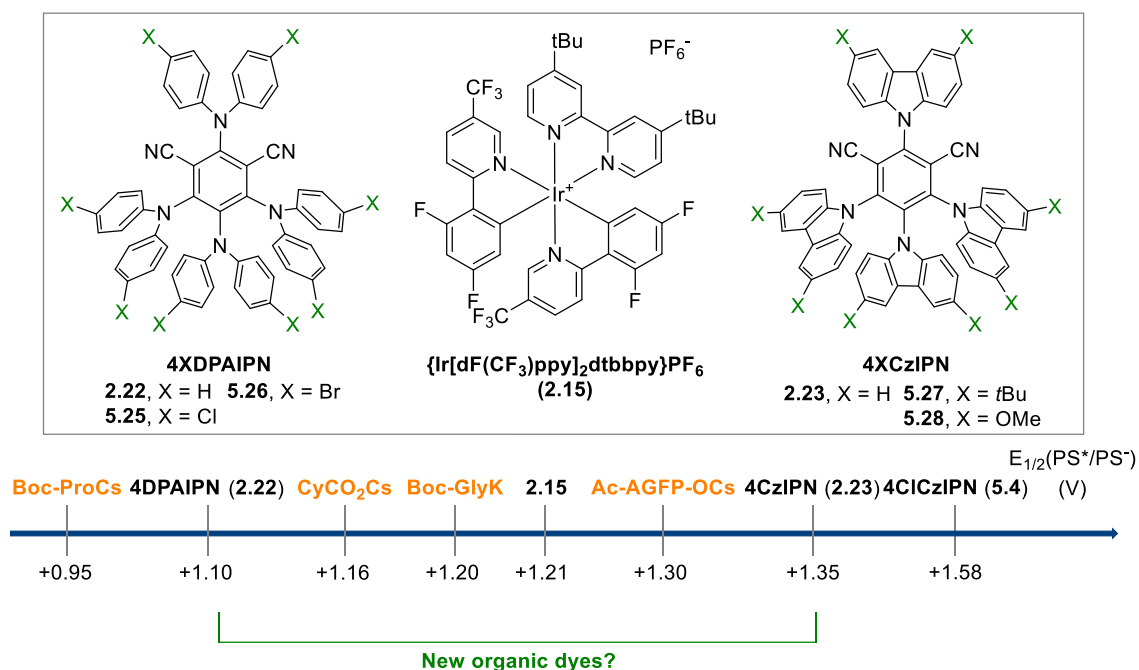
5.3.1 Significance and design

Our previous work on the development of strongly oxidative organophotocatalysts based on 4XCzIPN derivatives demonstrated the strong potential of the tuning of photocatalysts to access high efficiency in novel transformations. We thus envisioned to build on this knowledge in our targeted decarboxylative alkynylation of peptides.

In the Giese coupling developed by the MacMillan group,^[226] selectivity was achieved based on the redox potentials of the carboxylic acids (Section 2.3.5). We thus wondered if a similar approach would afford the same selectivity in our decarboxylative alkynylation. The redox potentials of different carboxylates have been described previously. If a proline carboxylate has a potential of +0.95 V vs SCE,^[11] a glycine carboxylate¹⁰ is at +1.20 V vs SCE,^[37] a secondary aliphatic acid such as CyCO₂Cs is at +1.16 V vs SCE,^[11] and primary amino acids such as the one encountered on the side-chains can be as high as +1.45 V. vs SCE (Scheme 39).^[251] With this measured gap, C-terminal selectivity can be envisioned with an appropriate catalyst choice. In addition, when studying peptides, easy to oxidize side-chains have also to be taken into account. Tyrosine (+1.1-1.27 V vs SCE) and tryptophan (+0.77-1.16 V vs SCE) will be challenging residues as they can lead to side reactivity.^[252–256] A less oxidizing dye than 4CzIPN would thus be of high interest to achieve this selectivity. A sufficiently reducing dye is also required in order to close the catalytic cycle.^[184] As no organic dye was available at the time of the study, we wanted to close the gap between 4CzIPN (**2.23**) and 4DPAIPN (**2.22**), to be in a similar range as the previously used [Ir{dF(CF₃)ppy}₂(dtbpy)]PF₆ (**2.15**) ($E_{1/2}^{*III/II} = +1.21$ V and $E_{1/2}^{II/III} = -1.37$ V).^[159,160]

Two different directions were explored. First, the reverse approach from Section 5.1, meaning adding electron-donating groups on the carbazole moieties of 4CzIPN (**2.23**), was studied to generate less oxidizing dyes than 4CzIPN (**2.23**). We also envisioned to follow the strategy of placing electron-deficient diphenyl amines on the scaffold of DPAIPN (**2.22**). By analogy with results on the introduction of electron-withdrawing groups on the carbazole moieties, those novel dyes were expected to possess the targeted properties.

¹⁰ It is important to note when comparing potentials that the counter-ion and solvent have a strong effect.

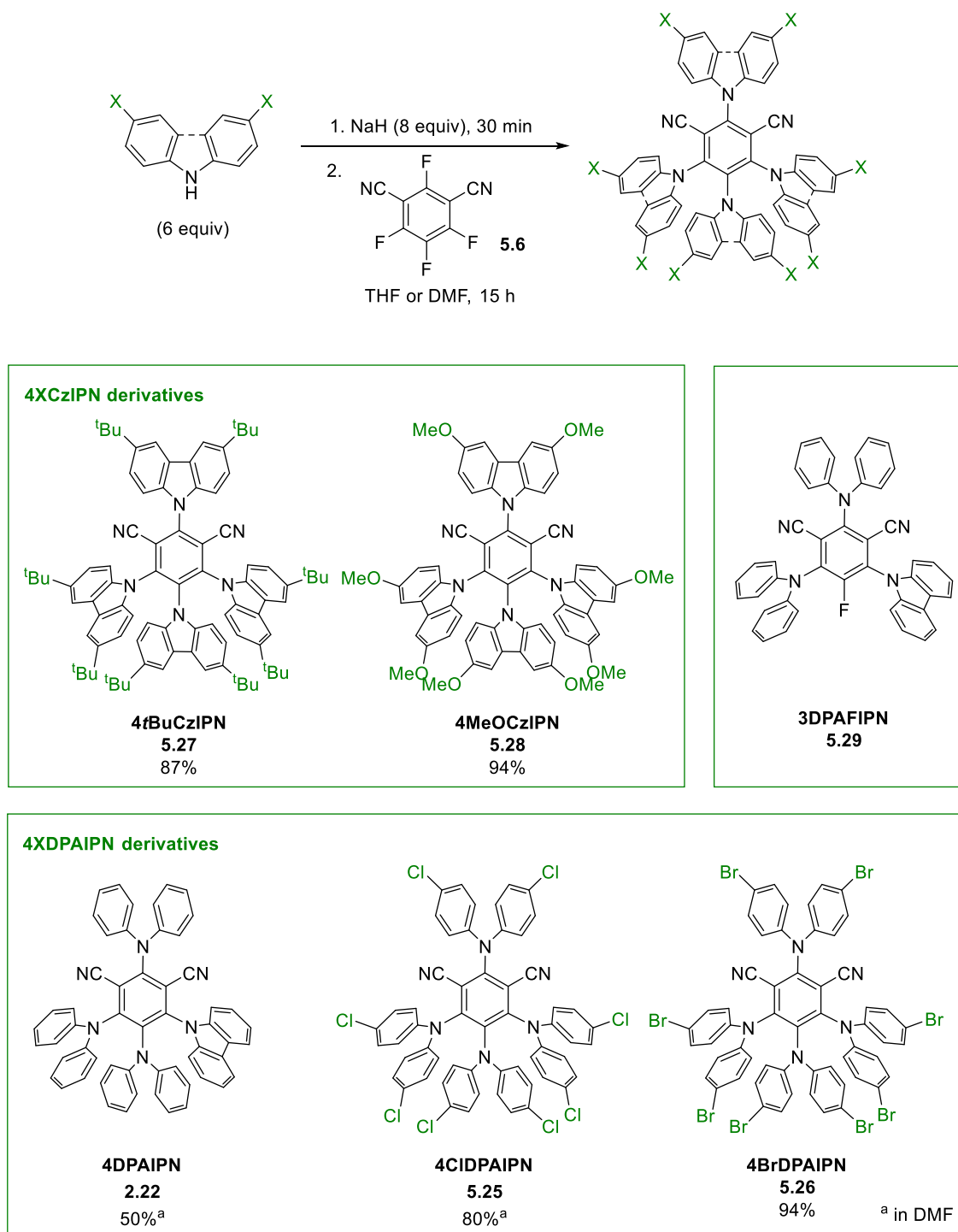
Scheme 39: Selected redox potentials of reported catalysts and amino acids carboxylates¹¹

5.3.2 Synthesis

First, the dyes 4*t*BuCzIPN (**5.27**) and 4MeOCzIPN (**5.28**) were obtained from 4CzIPN (**2a**) by the introduction of electron-donating groups in *para* position on the carbazoles (Scheme 40). The former had been reported for uses in material science but not for catalysis.^[257,258] The latter was reported simultaneously to this work by the group of Zeitler.^[259] The derivatives of 4DPAIPN (**2.22**) were investigated next. We started by the synthesis of 4DPAIPN (**2.22**), however the work from Zhang could not be reproduced and only traces of the dye were obtained.^[159] The dye with only three diphenyl amine units (**5.29**) was the major product. The same observation was made by Zeitler.^[259] This catalyst has thus be miss-assigned. Switching the reaction solvent from THF to DMF was key to the synthesis of the desired dye **2.22**. The structure was confirmed by X-rays analysis.¹² Heating during deprotonation was also found to improve the yield of **2.22**. Substitution with electron-withdrawing groups afforded the dyes 4CIDPAIPN (**5.25**) and 4BrDPAIPN (**5.26**) in excellent yields.

¹¹ Value for 4DPAIPN (**2.22**) reported by Zhang, further discussion in next section.

¹² See supporting information.



Scheme 40: Synthesis of 4XDPAIPN and 4XCzIPN derivatives

5.3.3 Characterization of 4XDPAIPN derivatives¹³

The redox properties of the dyes were then measured. “Cyclic voltammetry experiments were carried out first to determine the redox potentials at the ground state. The conditions were chosen identical as the ones from the work on 4CzIPN derivatives in order to have comparable values.^[159,244,260] For 4CzIPN derivatives, irreversible waves were observed in the anodic scan. As reported by Ishimatsu et al.^[244] they correspond to the oxidation of the carbazole moieties leading to polymerization.^[261] They also described that this polymerization could be avoided by the introduction of *t*Bu groups.^[258] Reversibility was evaluated through plots of the intensity of the peaks related to the square root of the scan rate.^[262] Reversible waves were observed in the cathodic scans in all cases. They correspond to the reduction of the dicyanobenzene group.^[258] For 4BrDPAIPN (**5.26**), higher scan rates gave non exploitable curves for the reduction, hence the reversibility could not be determined by this method. With a peak to peak separation of 60 mV, this process can be described as quasi-reversible. As described in section 0, the redox potentials at the excited state can be estimated from the values at the ground state by the Rehm-Weller equation.^[158] The excitation energy E_{0-0} was estimated by the point of intersection of the normalized absorbance and emission signals for each dye.¹⁴ The measured and calculated values are reported in the following table (Table 7). In the conditions of this study, the expected anodic and cathodic shifts upon substitution effect were measured. The trend in reduction potentials of 4DPAIPN derivatives (**2.22**<**5.26**<**5.25**) followed the electronegativity of the substituents (H<Br<Cl). By the reverse effect (section 2.3.2), 4*t*BuCzIPN (**5.27**) and 4OMeCzIPN (**5.28**) were less oxidant than 4CzIPN (**2.23**) by destabilization of the LUMO. It is important to note that the actual 4DPAIPN (**2.22**) was less oxidizing in the exciting state than the dye having only three diphenylamine units **5.29** (+0.90 V vs +1.10 V).^[19] In this study no solubility problems were encountered and the experimental values were thus exploited with no need to perform DFT calculations.”

Table 7: Electrochemical properties of 4CzIPN and DPAIPN derivatives^a

Entry	Photocatalyst	E_{0-0} (eV)	$E_{1/2}(P/P^-)$	$E_{1/2}(P^*/P^-)$	$E_{1/2}(P^+/P)$	$E_{1/2}(P^+/P^*)$
1	4CzIPN (2.23) ^[159]	2.53	-1.21	+1.35	+1.52	-1.04
2	4CzIPN (2.23)	2.64	-1.32	+1.32	+1.39	-1.25
3	4 <i>t</i> BuCzIPN (5.27)	2.53	-1.32	+1.21	+1.22	-1.31

¹³ “” The text in between is a partial quotation from our publication: M. Garreau; F. Le Vaillant; J. Waser *Angew. Chemie Int. Ed.* **2019**, 58, 8182–8186.

¹⁴ See Supporting information for spectra.

4	4OMeCzIPN (5.28)	2.61 ^[259]	-1.38	+1.23	+1.05	-1.56
5	4OMeCzIPN (5.28) ^[259]	2.61	-1.50	+1.27	+1.11	-1.34
6	4ClDPAIPN (5.25)	2.53	-1.44	+1.09	+1.23	-1.30
7	4BrDPAIPN (5.26)	2.53	-1.55	+0.98	+1.12	-1.41
8	"4DPAIPN" (2.22) ^[159]	2.62	-1.52	+1.10	+1.34	-1.28
9	4DPAIPN (2.22)	2.55	-1.65	+0.90	+1.03	-1.52

^aPotentials in V vs SCE, wavelength in nanometers.

This library now provides a range of organophotocatalysts with reduction potentials between +0.90 V to +1.35 V at the excited state (Figure 13).

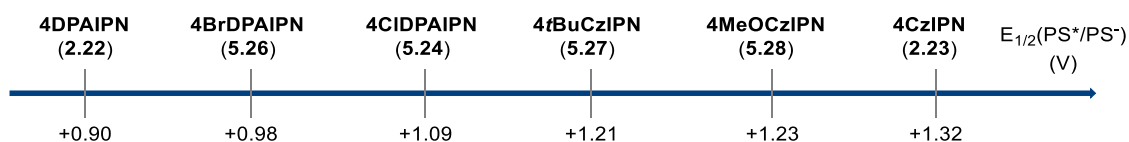


Figure 13: Scale of novel 4XCzIPN and 4DPAIPN derivatives

5.4 Conclusion

We have reported novel organophotocatalysts based on the scaffolds of donor-acceptors 4CzIPN (**2.23**) and 4DPAIPN (**2.22**). Both experimental measurements and computations confirmed our rational design through the electronics of the donor moiety. Electron poor donors, such as carbazoles bearing electron-withdrawing groups in *para* position are increasing the oxidizing character of the dyes. On the contrary, more electron-rich donors such as carbazoles bearing electron-donating groups in *para* position or diphenyl amines are decreasing the oxidizing character. This is the first report of exploiting substitution on the donor groups towards fine-tuning of the properties. As a consequence from our work, organic dyes possessing a reduction potential at the excited state from +0.90 to +1.82 V vs SCE are now available. This is filling a gap in the redox properties of the available catalysts, which prevented many transformations to be performed in a metal-free fashion, or even not optimized at all. This library has already allowed the development of novel reactivity. First, an efficient oxidation of cyclic oxime ethers **5.9** in a fragmentation cascade where 4ClCzIPN (**5.4**) demonstrated to be the key for high efficiency. DPAIPN (**2.22**) also played an important role in another project from

the group lead by Bastian Muriel, who disclosed a annulation of cyclopropenes with aminocyclopropanes.^[263]

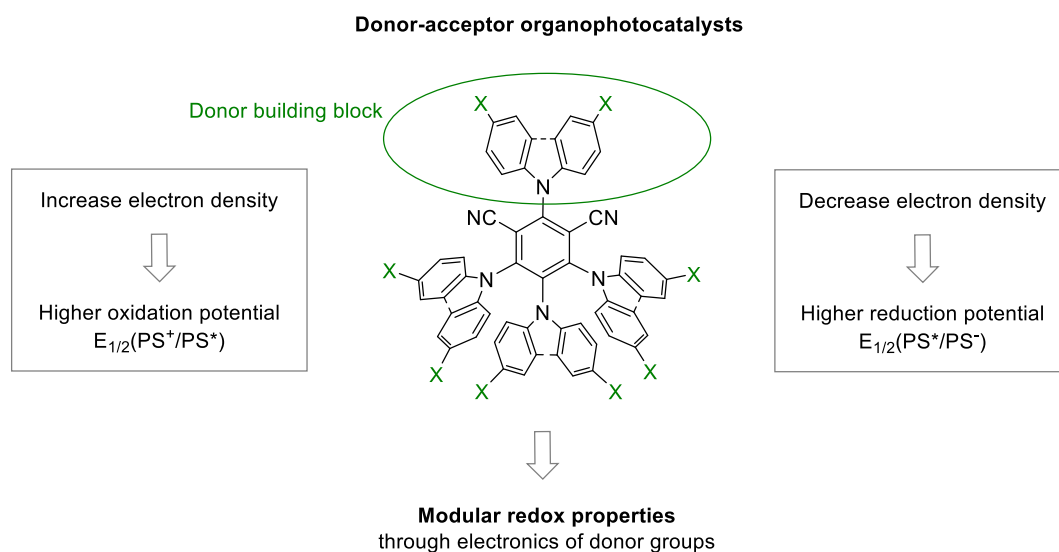


Figure 14: Influence of donor groups in the fine-tuning of 4CzIPN and 4DPAIPN derivatives

If at the early stage of those projects, the field of fine-tuning the redox properties of organophotocatalysts was only emerging, it is now evolving fast due to the high demand. Shortly before the second part of this work on 4DPAIPN derivatives, Zeitler and coworkers reported a study on 4CzIPN scaffold where they also investigated the influence of the acceptor part.^[259] Different combination with variation of both acceptor and donor groups provided a large library of derivatives as well as valuable information on the tuning of the properties. Especially, replacing one donor by an halogen furnished more oxidizing dyes, which can then be modulated with the electronics of the remaining donors. Further work would be the development of water-soluble catalysts. This will be discussed in the outlook (section 10).

Photoredox-catalyzed decarboxylative alkynylation of peptides in organic solvent

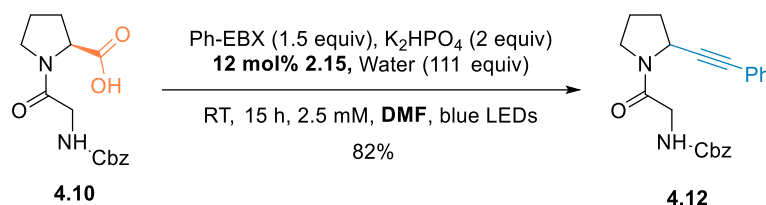


6 Photoredox-catalyzed decarboxylative alkynylation of peptides in organic solvent

6.1 Optimization

6.1.1 From Iridium catalyst to organic dyes

In order to develop a peptide decarboxylative alkynylation, the work from the group of MacMillan on a decarboxylative macrocyclization caught our interest (Section 2.3.5).^[37] It indeed consisted of the first example of a photoredox catalyzed bioconjugation on large peptides C-terminus. We thus wondered if EBX reagents were compatible with those conditions. A first attempt on 0.025 mmol scale, afforded **4.12** in 82 % yield (Equation 22).



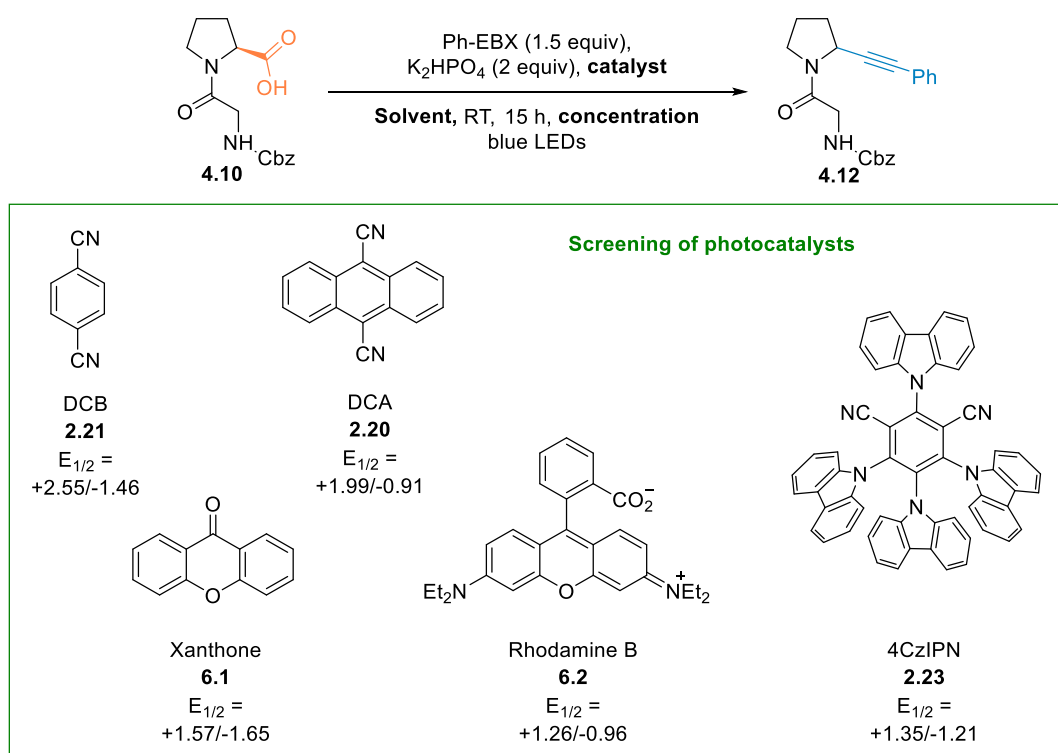
Equation 22: First attempt under conditions developed by MacMillan and co-workers

Encouraged by this excellent result, work was conducted to evaluate the influence of the proportion of co-solvent. An attempt using DMF/water 1:1 as the solvent led to very low conversion (10%) and 8% yield. No increase of yield was observed between 15 h and 24 h and the mixture turned brown, indicating a probable degradation. Further work will thus be carried out with reaction time of maximum 15 h. Despite homogeneous mixtures in all cases, the yield dropped as soon as more water was introduced. When increasing the water proportion to 80%, less than 10% conversion was obtained. Those results show that if water is tolerated, reactivity drops as soon as it is the main solvent. Further work was conducted with DMF.

A scale-up of the reaction to 0.1 mmol scale was performed in order to isolate the desired alkynylation product and validate the conditions. 88% isolated yield was obtained when repeating the reaction from Equation 22 (Table 8, entry 1). Decreasing the amount of catalyst to 6 mol%, together with increasing the concentration to 5 mM led to a comparable result (entry 2). Further work will be performed at 5 mM using 6 mol% of catalyst for convenience and cost. In the aim of developing a metal-free transformation, several organic dyes were screened

(Table 8). DCA (**2.20**) and 4CzIPN (**2.23**) had already demonstrated their suitability for this transformation (Section 4.1). To our delight, excellent yield was obtained with 4CzIPN (**2.23**) (entry 3). If DCA (**2.20**) also afforded good conversion, only average yield was obtained (entry 4). Previous work from Luo *et al.* have highlighted the lower activity of DCA in DMF, due to decomposition.^[159] The reaction was thus carried out both in THF/water 4:1 to compare with our previous results and in chloroform, following the work from Yang *et al.*^[189] In both cases, either the conversion was lower, or by-products were observed together with a lower yield (entries 5 and 6). Experiments both in THF and dioxane (entries 7 and 8) afforded alkynylation of solvents as major side-reactions. Those solvents were thus abandoned. DCB (**2.21**), irradiated under UV light, afforded 78% conversion and 33% yield in a 6 h reaction (entry 9). However, due to the toxicity of UV light towards biomolecules and the several observed byproducts, it will not be further optimized. Rhodamine B (**6.2**) was tested under green LEDs irradiation and led to only traces of product (entry 10). Xanthone (**6.1**) (entry 11) afforded only traces of the desired product and a mixture of unknown compounds. A control experiment was run with 4CzIPN (**2.23**) in DCE and no reaction was observed (entry 12), which is in line with previous results of the group.^[13]

Table 8: Screening of photoredox catalysts



Entry	Solvent	Catalyst (mol%)	C (mM)	Ratio SM/P ^a	Yield (%) ^b
1	DMF	2.15 (12)	2.5	>5:95	88
2	DMF	2.15 (6)	5	>5:95	86
3	DMF	4CzIPN (6)	5	>5:95	86
4	DMF	DCA (6)	5	24:76	33
5	THF/water 8:2	DCA (6)	10	48:52	43
6	CHCl ₃	DCA (5)	5	9:91	48
7	THF/water 8:2	4CzIPN (6)	10	16:84	80
8	Dioxane/water 8:2	2.15 (6)	10	15:85	75
9	DMF	DCB (12) ^d	5	22:78	33
10	DMF	Rhodamine B (12) ^e	5	>95:5	-
11	DMF	Xanthone (12)	5	>10:90	39
12	DCE ^c	4CzIPN (6)	5	>90:10	-

^a Ratio of product compared to remaining starting material by HPLC analysis, ^b HPLC yield, ^c Anhydrous conditions, ^d UV irradiation in Rayonet reactor, 6 h reaction, ^e green LEDs irradiation. The screening was performed on a 0.1 mmol scale.

As the most promising catalyst was 4CzIPN (**2.23**), variation of the amount of water was studied with that catalyst (Table 9). Conditions from Table 8, entry 3 were reproduced on scope scale (0.3 mmol). To our delight, 62% of **4.12** was obtained in only 1 h 30 of reaction (entry 1). Both running the reaction in anhydrous conditions (entry 3) and increasing the amount of water to 20% (entry 2) afforded excellent yields. The reaction is not sensitive to the presence of water as long as DMF remains the main solvent. 4CzIPN (**2.23**) was chosen as the photocatalyst for the rest of the project.

Table 9: Variation of water amount with 4CzIPN

Entry	Solvent	Catalyst (mol%)	C (mM)	Ratio SM/P ^a	Yield (%) ^b
1	DMF ^c	4CzIPN (6)	5	>5:95	84 (62)
2	DMF ^d	4CzIPN (6)	5	>5:95	>95
3	DMF/water 8:2	4CzIPN (6)	5	>5:95	>95

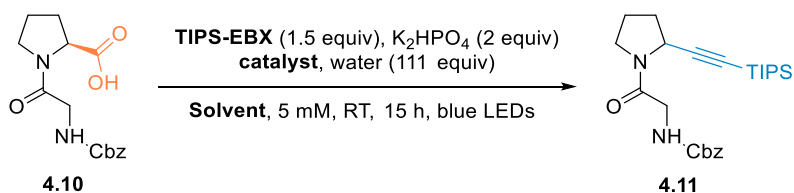
^a Ratio of product compared to remaining starting material by HPLC analysis, ^b HPLC yield, ^c 0.3 mmol,

^d Anhydrous conditions. The screening was performed on a 0.1 mmol scale.

6.1.2 Preliminary scope investigation

Results from previous section confirmed that Cbz-Gly-Pro (**4.10**) and Ph-EBX (**2.5**) were excellent substrates for this transformation. Unfortunately, when TIPS-EBX (**2.4**) was subjected to the reaction conditions, no desired product was obtained (Table 10, entry 1). Employing a milder base and cesium as a counter-ion did not lead to a better result (entry 2). Cesium benzoate had demonstrated high efficiency for the decarboxylative alkynylation of proline using TIPS-EBX.^[13] We hypothesized that degradation in DMF was occurring and an attempt was performed in chloroform, following the work from Yang *et al.*^[264] Although no starting material was recovered, only traces of the desired product were observed by HPLC analysis together with side-products which could not be isolated for characterization (entry 3). Changing the photocatalyst back to iridium **2.15** did not afford more than traces of the product (entry 4).

Table 10: Attempts of decarboxylative alkynylation with TIPS-EBX



Entry	Solvent	Catalyst (mol%)	Base (equiv)	HPLC yield (%)
1	DMF	4CzIPN (6)	K ₂ HPO ₄ (2)	-
2	DMF	4CzIPN (6)	CsOBz (4)	-
3	CHCl ₃	4CzIPN (6)	CsOBz (2)	traces
4	DMF	Ir cat 2.15 (2)	CsOBz (2)	traces

The screening was performed on a 0.1 mmol scale.

Similarly, when starting from an aliphatic-substituted EBX reagent (*t*Bu-EBX), less than 10% of conversion was detected by HPLC and no isolation was performed (Table 11). Further work with an alkyl chain (C₁₄-EBX) was later conducted on optimized conditions to be able to conclude whether this lack of reactivity arose from a bulky substituent or from electronics. When the challenging Cbz-Gly-Gly (**6.3**) was employed as a starting material together with Ph-EBX, no complete conversion was reached and only 18% yield of isolated product **4.14** could be obtained (entry 2). Despite this low yield, this result is promising as glycine is the only amino acid leading to a primary radical after decarboxylation. Achieving high efficiencies in glycine decarboxylation is thus much more challenging. Cbz-Ala-Ala (**6.4**) and Cbz-Gly-Phe (**6.5**)

afforded complete conversion to **6.7** and **4.13** although isolated yields were significantly lower, highlighting that further optimization was required.

Table 11: Preliminary scope of dipeptide alkynylation

Entry	Peptide	R	Ratio SM/P ^a	Product, yield (%) ^b
1	Cbz-Gly-Pro (4.10)	<i>t</i> Bu	>90:10	6.6 , -
2	Cbz-Gly-Gly (6.3)	Ph	52:48	4.14 , 18 ^c
3	Cbz-Ala-Ala (6.4)	Ph	>5:95	6.7 , 55
4	Cbz-Gly-Phe (6.5)	Ph	>5:95	4.13 , 45

^a Ratio of product compared to remaining starting material by HPLC analysis, ^b isolated yield, ^c 0.1 mmol scale. Reactions performed on a 0.3 mmol scale.

6.1.3 Optimization on Cbz-Ala-Ala

As lower yields were obtained with more challenging substrates, an optimization was carried out with Cbz-Ala-Ala (**6.4**) as a model substrate. The radical formed after decarboxylation is secondary and less nucleophilic than on proline, which is more representative of the general reactivity of amino acids.

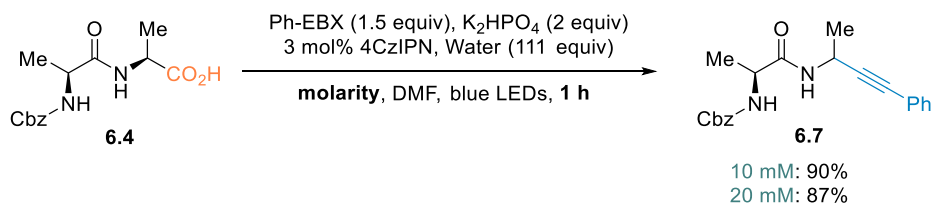
The first parameter under study was the source of light (Table 12). The maximum of absorption of 4CzIPN (**2.23**) being 435 nm, previous work has been conducted with either blue LEDs or white CFL (compact fluorescence) household bulbs.^[159] A first experiment was set up using a Rayonet photoreactor equipped with blue LEDs absorbing at 420 nm. The desired product was obtained in 87% yield in only 2 h 30 of reaction (entry 1). Encouraged by this shorter reaction time, blue LEDs were used again and full conversion and 83% HPLC yield was obtained in 2 h (entry 2). CFL household bulbs led to only 27% yield in 2 h and no improvement overnight (entry 3). This is likely due to the broader emission spectra of those bulbs, with presence of UV light. Degradation was thus possible. Further work was conducted using blue LEDs as it is a more widely used set-up.

Table 12: Optimization of light source on Cbz-Ala-Ala (6.4)

Entry	Light source	Time	Ratio SM/P ^a	Yield (%) ^b
1	Rayonet	2 h 30	12:87	87
2	LEDs	2 h	>5:95	83
3	CFL	2 h	25:74	27

^a Ratio of product compared to remaining starting material by HPLC analysis, ^b HPLC yield. Reactions performed on a 0.1 mmol scale.

Concentrating the reaction mixture to 10 mM simultaneously to a decrease of catalyst loading to 3 mol% was very interesting. The reaction was complete within one hour and 90% yield could be obtained (Equation 23). The reaction was clean and no degradation was observed when irradiation was continued overnight. When increasing the molarity to 20 mM, excellent yield was also obtained (87%), although the mixture became less homogeneous. No further concentration of the mixture was attempted and further work was conducted with a molarity of 10 mM, which is a good compromise between the dilution required for peptide modification and convenience of work.



Equation 23: Reaction molarity optimization on Cbz-Ala-Ala (6.4)

Variation of the catalyst loading from 0.5 to 6 mol% did not have any significant impact on the yield (Table 13). When adding either 0.5 or 1 mol% of catalyst, 64-65% yield was obtained, with no further evolution over time. Similar results were obtained either with 3 or 6 mol%. To our delight, in all cases complete conversion was obtained within 30 min. A catalyst loading of 3 mol% was thus used for further work.

Table 13: Variation of catalyst loading, yield according to time on Cbz-Ala-Ala (**6.4**)

Entry	Time	X= 0.5	X= 1	X= 3	X= 6
1	30 min	65	64	77	71
2	1 h	65	64	77	77
3	2 h	65	-	77	72

HPLC yield, Reactions performed on a 0.1 mmol scale.

6.1.4 Control experiments

First attempts at scope scale (0.3 mmol) led to lower yields in comparison to 0.1 mmol scale: 72% HPLC yield for Cbz-Ala-Ala (**6.4**) and 88% HPLC yield for Cbz-Gly-Pro (**4.10**). This drop of yield could arise either from the difference of flask as a schlenk with thicker glass and less surface of irradiation was employed, or because of an inefficient degassing method. A control experiment without degassing neither DMF nor water afforded 71% yield of **6.7** (Table 14, entry 1). Bubbling nitrogen during 30 min prior to use, which was the preferred degassing method so far, led to 77% yield. Degassing both DMF and water by Freeze-Pump-Thaw method afforded better results with 86% yield (entry 3). Further work was thus conducted using this degassing method. The good yield obtained in non-degassed conditions is very relevant for future work on complex biomolecules.

Table 14: Variation of degassing methods Cbz-Ala-Ala (**6.4**)

Entry	Degassing method	Yield (%)
1	Non	71
2	Nitrogen bubbling	77
3	Freeze-Pump-Thaw	86

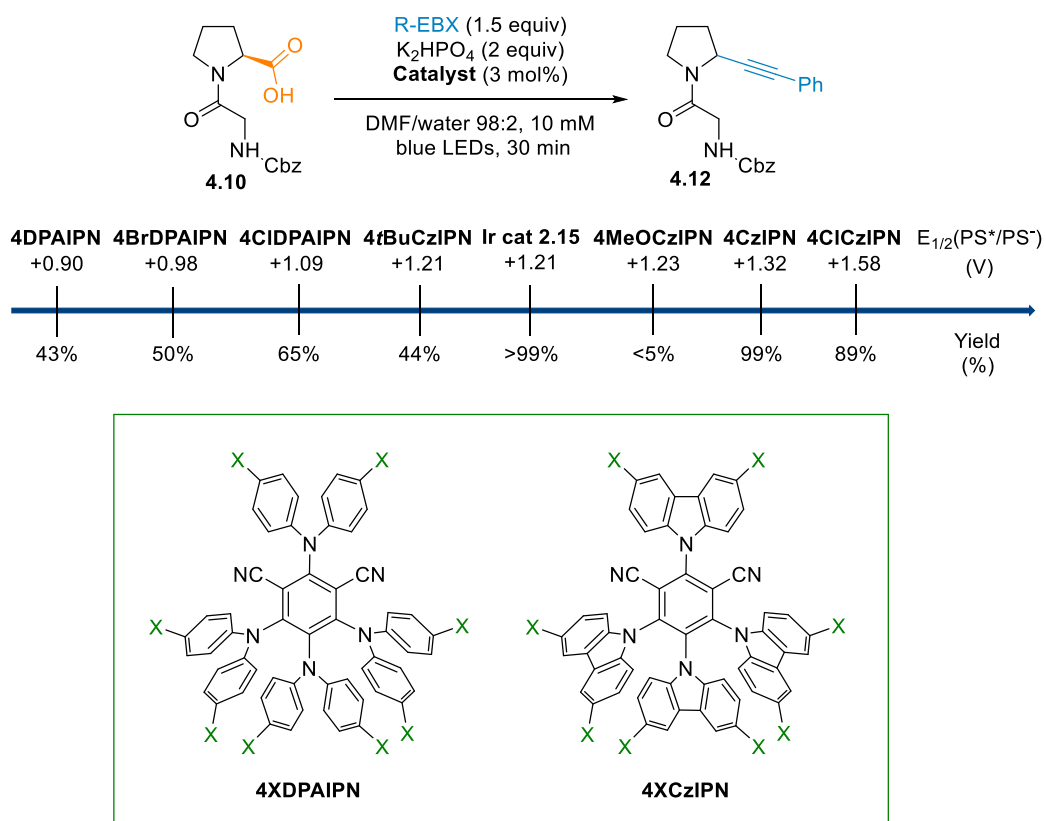
HPLC yield, Reactions performed on a 0.1 mmol scale.

Control experiments were then performed. Carrying the reaction in absence of light or catalyst led to only traces of the product. Interestingly, the presence of a base is not required for the transformation as 24% yield was still obtained without addition of dipotassium phosphate.

We then wondered whether a possible selective decarboxylation could occur between carboxylic acids either at the C-terminal position or on the side-chains. This would indeed be of high interest for labeling studies as it would allow a selective site functionalization (Section 2.1.4). For that purpose we studied organic dyes. The design and synthesis of novel fine-tuned organophotocatalysts is described in Section 5.

6.2 Towards C-terminal selectivity

The novel dyes were evaluated under the optimized conditions for the decarboxylative alkynylation of Cbz-Gly-Pro (**4.10**). In that case, a clean and quantitative reaction towards **4.12** was obtained with 4CzIPN (**2.23**) in only 30 minutes. The use of a stronger oxidant, 4ClCzIPN (**5.4**), led to 89% yield (Scheme 41). 4MeOCzIPN (**5.28**) and 4*t*BuCzIPN (**5.27**) afforded lower yields. The former was similarly inefficient in the study from the Zeitler group. They hypothesized that a fast intramolecular (back) electron transfer from the excited state was occurring, leading to a non-productive cycle.^[259] Regarding the latter, 4*t*BuCzIPN (**5.27**), a stability problem was noted as no catalyst could be detected at the end of the reaction. Indeed, by increasing the catalyst loading to 5 mol% an increase to 57% yield was measured. For comparison, the iridium catalyst **4**, was screened as well as it has a similar reductive properties than 4*t*BuCzIPN (**5.27**). This confirmed the preliminary results and quantitative yield was measured under those optimized conditions. The dyes based on the scaffold of 4DPAIPN were then evaluated. A general trend was observed which can be rationalized through the reduction potentials of the dyes. The least powerful oxidant, namely 4DPAIPN (**2.22**) with the corrected structure, afforded 43% yield. Its derivatives with substitution of electron-withdrawing groups demonstrated more efficient behaviour, respectively 50 and 65% for 4BrDPAIPN (**2.26**) and 4ClDPAIPN (**2.25**). Except 4MeOCzIPN (**2.28**), all the novel organic dyes demonstrated good catalytic activity for this model system. 4CzIPN (**2.23**) was selected for further work as it should demonstrate better functional group tolerance than 4ClCzIPN (**5.4**). However, it is important to keep in mind that less powerful oxidants can be selected for more sensitive substrates, when selectivity can be an issue. In those optimized conditions, it is worth to note that degassing was not of paramount importance anymore as 87% yield was measured without.

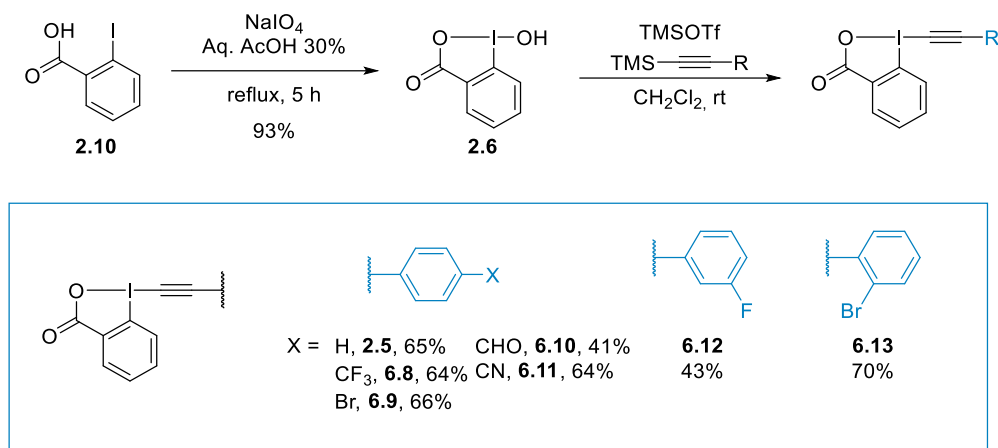


Scheme 41: Screening of novel organic dyes

6.3 Reagents and dipeptides scope

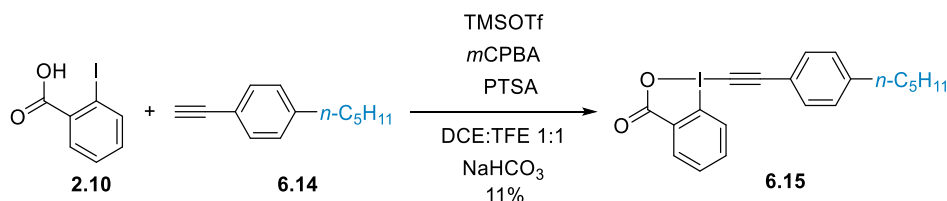
6.3.1 Scope of hypervalent iodine reagents

The aromatic substituted EBX reagents were prepared by first an oxidative cyclization of 2-iodobenzoic acid (**2.10**) using $NaIO_4$ in acidic media under reflux to afford BI-OH (**2.6**) (Scheme 42).^[13] Then, substitution on BI-OH (**2.6**) using TMS protected alkynes in presence of trimethylsilyltriflate led to the different EBX reagents (**2.5** and **6.8-6.13**) in good yields. Alkynes precursors were purchased or synthesized by a Sonogashira coupling.^[265]



Scheme 42: Synthesis of aryl substituted EBX reagents

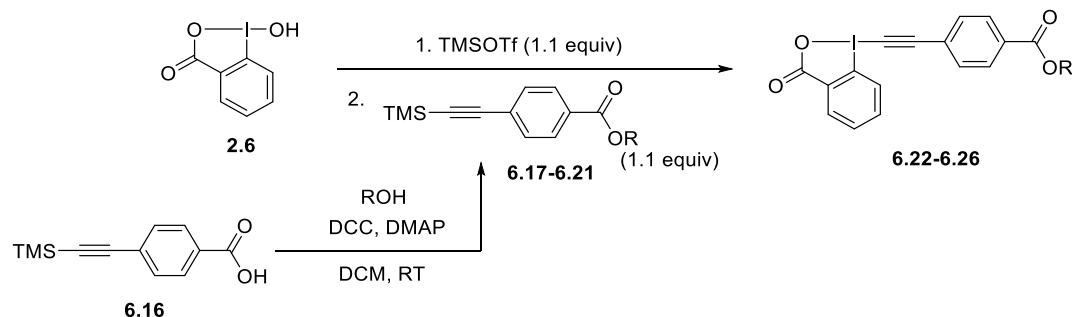
The synthesis of the novel reagent *n*C₅H₁₁-Ph-EBX (**6.15**) was achieved following the work of Olofsson.^[266] Starting from iodobenzoic acid (**2.10**) and the aryl alkyne **6.14**, the desired EBX can be obtained in a one-pot procedure although with a very low yield (Equation 24).

Equation 24: Synthesis of *n*C₅H₁₁-Ph-EBX (**6.15**)

The efficient introduction of bioorthogonal functional groups on the peptides was key to the project as it would allow very straightforward further derivatization together with paving the way for *in situ* labeling. As TIPS-EBX (**2.4**) could not be successfully employed, there was the need for a source of free alkyne. After several unfruitful attempts to access a reagent bearing a free-alkyne directly on the aryl ring, a linker was considered. An ester was selected as we envisioned a straightforward synthetic path. Reagent **6.22** was obtained in two steps although in very low yield due to purification issues (Table 15, Entry 1). Encouraged by this result, the same approach was employed for the synthesis of **6.23**, bearing an azide (Entry 2). The same difficulties were indeed encountered when attempting the synthesis of EBX reagents with the azide moiety directly on the aryl ring linked to the alkyne. The diphenyl diazene moiety was considered due to its ability to isomerize upon irradiation, either in UV or visible-light. Its introduction on peptides would be highly interesting for conformation changes. Gratifyingly, both the ester **6.19** and the EBX **6.24** were obtained in good yields (Entry 3). A norbornene and cyclooctyne derivatives were also considered but despite quantitative yields for the TMS-

Alkynes formation **6.20** and **6.21** (Entries 4 and 5), only complex mixtures of **6.25** and **6.26** were obtained in the EBX synthesis step. No further attempts were carried out.

Table 15: Synthesis of EBX substituted with bioorthogonal functional groups

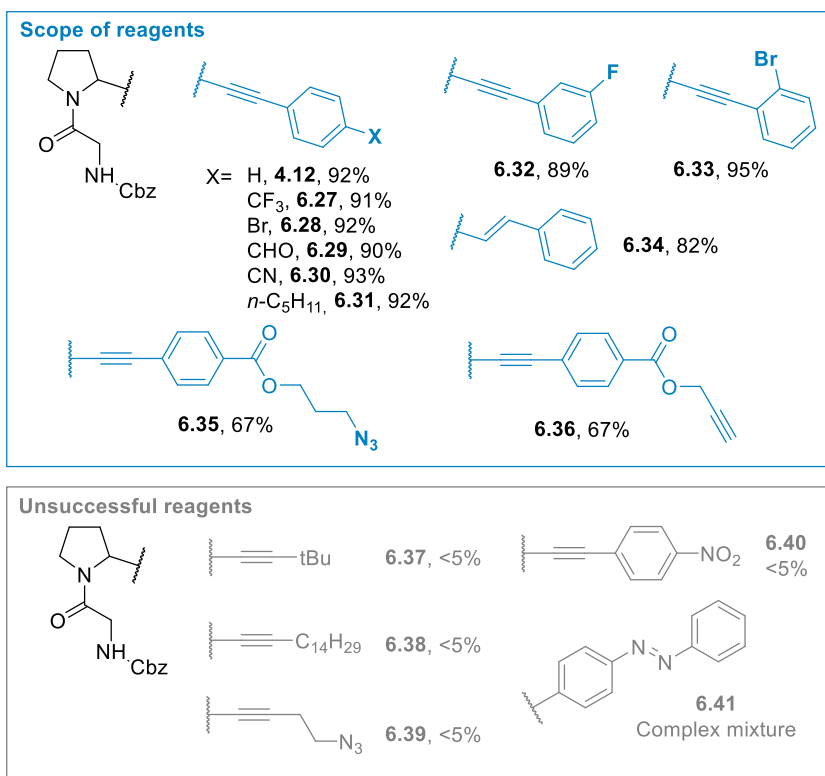
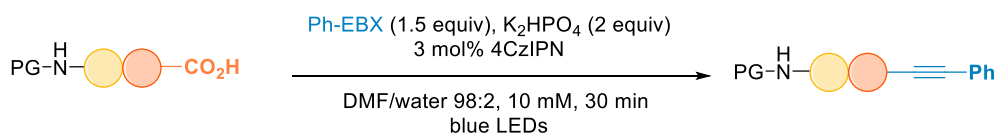


Entry	R=	Compound	Yield esterification	Yield EBX
1		6.17, 6.22	80%	8%
2		6.18, 6.23	82% (61) ^a	53%
3		6.19, 6.24	44%	70%
4		6.20, 6.25	99%	Complex mixture
5		6.21, 6.26	99%	Complex mixture

^a performed on bromo-alkyl substrate, ^b Azidation reaction

The scope of alkynes in regard to Cbz-Gly-Pro (**4.10**) was investigated on a synthetically useful scale (0.30 mmol). Starting with Ph-EBX (**2.5**) led to the model substrate **4.12** in 92% yield (Scheme 43). Electron-poor aryl substituents on EBX reagents were successfully introduced, with CF₃, bromine, aldehyde or cyanide substituents (**6.27-6.30**). The EBX reagent bearing a weak electron-donating pentyl chain was a suitable substrate as well (**6.31**). Variation of position was possible with both *meta*- and *ortho*-substitution tolerated (**6.32** and **6.33** in 89 and 95% yield respectively) similarly to the outcome on amino acids.^[13] Those

derivatives could be further engaged into cross-coupling reactions and led to more complex peptides. The novel reagents designed for the introduction of bioorthogonal functional groups were then engaged. To our delight, they were compatible and good yields were obtained for the highly interesting **6.35** and **6.36**. Without modification of the conditions, a vinylbenziodoxolone (VBX) reagent could be employed in this methodology and afforded **6.34**.^[266] The described compounds were all obtained as a mixture of rotamers. As already described in the preliminary scope investigations (Section 6.1.2), alkyl-substituted EBX were not suitable reagents (**6.37** to **6.39**, neither *t*Bu-EBX nor *n*C₁₄-EBX and the azide-substituted EBX (**2.11**)). A nitro group in *para* position on the aryl ring led to decomposition of the reagent and no **6.40** formation. Unfortunately, a complex mixture was obtained with the diphenyl diazene substituted EBX reagent **6.24**. and **6.41** could not be isolated. Isomerization of the diazene under those conditions can be expected.

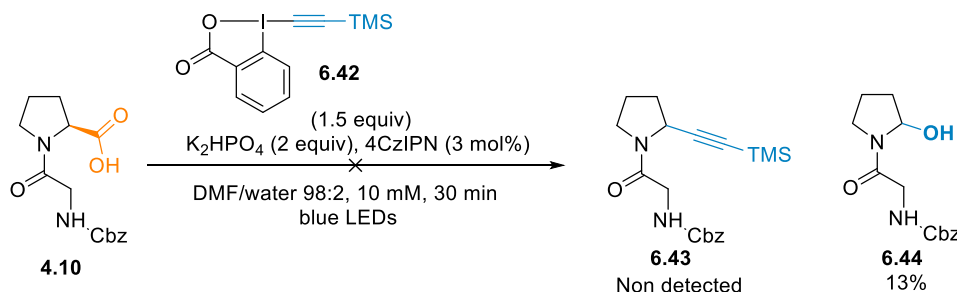


Reactions performed on a 0.3 mmol scale, isolated yields.

Scheme 43: Scope of EBX reagents on Cbz-Gly-Pro (**4.10**)

Interestingly, when attempting to overcome the lack of reactivity of TIPS-EBX (**2.4**), using TMS-EBX (**6.42**) gave another outcome (Scheme 44). No desired alkynylation product -

6.43 was observed. Instead, over-oxidation of the α -amino radical followed by water addition formed the hemiaminal **6.44**, together with degradation products. Optimization of this result towards C-terminal functionalization will be discussed in the section 8.

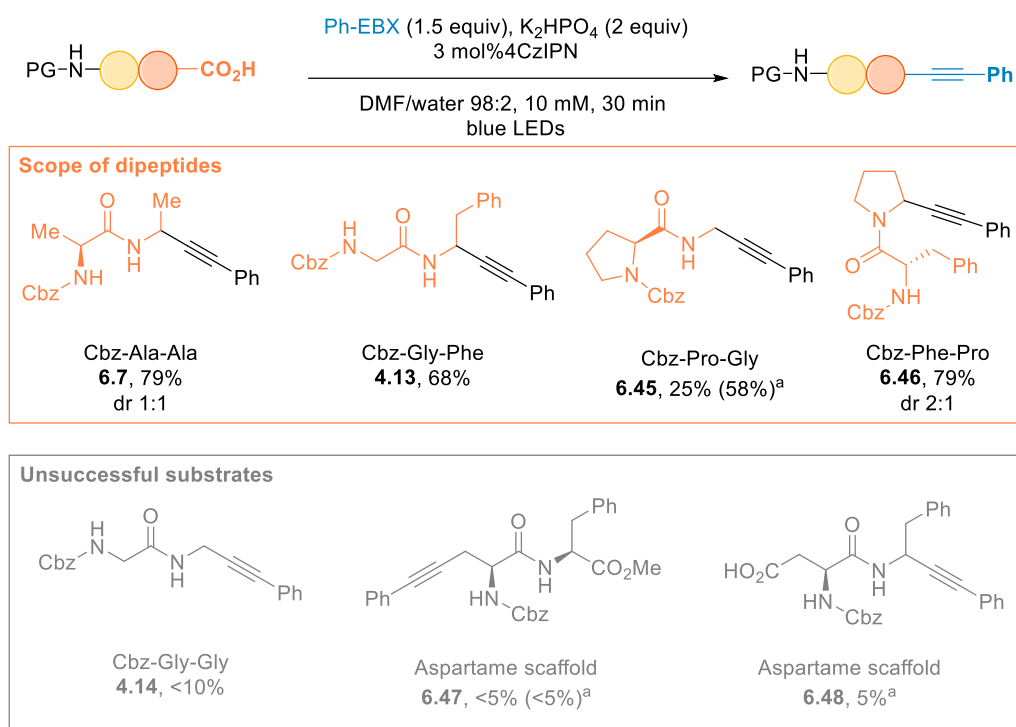


Scheme 44: Attempt with TMS-EBX (**6.42**) as reagent for the decarboxylative alkynylation

6.3.2 Scope of dipeptides

A first insight of the reactivity of different acids at the C-terminus was explored in a dipeptide scope. The excellent reactivity of proline towards decarboxylative reaction could lead to significant decrease of yield when switching to more challenging substrates. Gratifyingly, when alanine was located at the C-terminal position, the desired alkynylated product **6.7** could be obtained in 79% yield as a mixture of 1:1 diastereoisomers (Scheme 45). Phenylalanine also afforded **4.13** in excellent yield. Changing the second amino acid had little influence and starting from Cbz-Phe-Pro, a 1:1 mixture of diastereoisomers of **6.46** was isolated in 79 % yield. For the more challenging glycine, leading to a primary α -amino radical, only partial conversion was observed starting from Cbz-Gly-Gly. The particular structure of this simple dipeptide was probably the origin of the lack of reactivity.^[267] Indeed, variation of the second amino acid to proline was key and 25% isolated yield were obtained from Cbz-Pro-Gly. However the conversion was not complete. We hypothesized that the higher oxidation potential of glycine was the origin of this lower reactivity ($E_{1/2}^{red}(\text{Boc-Gly-CO}_2\text{K}) = +1.2 \text{ V}$, $E_{1/2}^{red}(\text{Boc-Pro-CO}_2\text{Cs}) = +0.95 \text{ V}$)^[11,37]. Indeed, switching to the more oxidizing dye 4CICzIPN (**5.4**) improved the yield of **6.45** to 58%. All the substrates of this scope were commercially available and used directly without prior purification. The reactivity of glutamic and aspartic side-chains in this transformation was an important question to answer. As a very common additive, Aspartame raised our interest. After protection of the N-terminal extremity with a Cbz protecting group,^[268,269] Cbz-Asp-Phe was submitted to the reaction conditions. To our delight, no reaction on the side-chain of aspartic acid was observed. Only traces product **6.47** were detected by HRMS. This result was very promising for further work on larger peptides with a probable selectivity for the C-terminal position. However, with the hydrolyzed substrate, only traces of

the desired alkynylation at the C-terminal (**6.48**) was observed and the starting material was recovered.



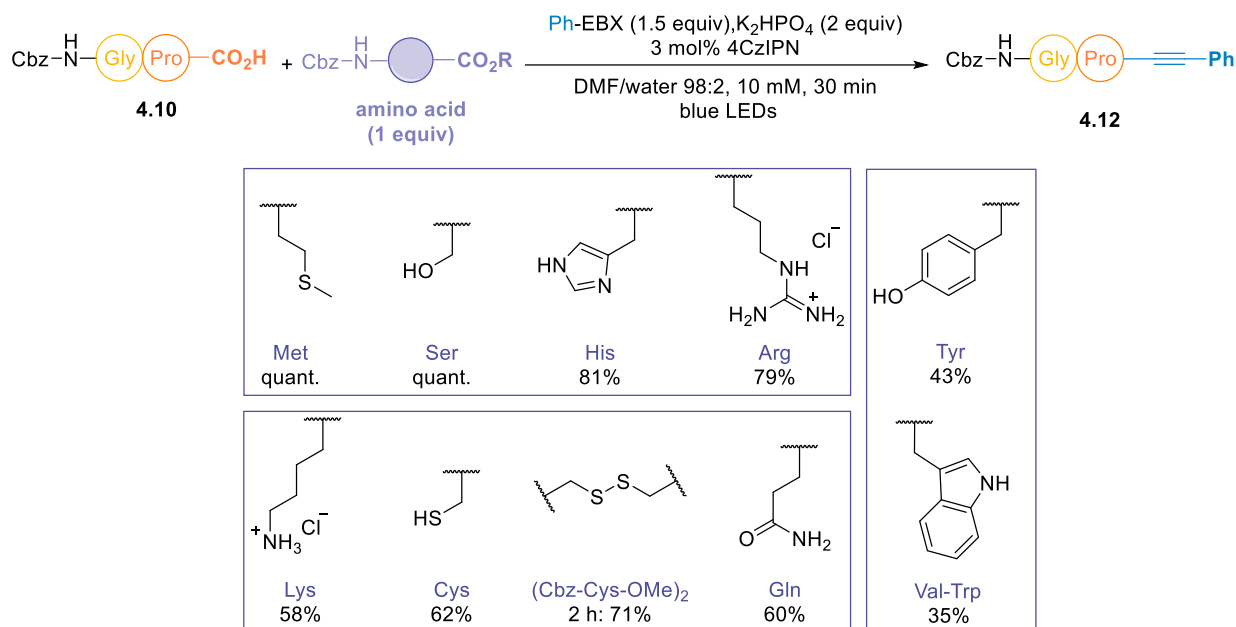
Reactions performed on a 0.3 mmol scale, isolated yields. ^a With 4CICzIPN as catalyst.

Scheme 45: Scope of dipeptides in the decarboxylative alkynylation

6.3.3 Robustness test

As described by Glorius, a fast and efficient technique to access the functional group tolerance of a reaction is a robustness test.^[270] Quenching experiments were performed to evaluate the tolerance towards the functional groups of the amino acids side-chains. Under the optimized conditions set-up with Z-Gly-Pro (**4.10**) as the starting material, one equivalent of C- and N-terminal protected amino acid was added (Scheme 46). Neither methionine nor serine have influence on the rate of the transformation, which is in line with previous results.^[184,227] Gratifyingly, histidine and arginine led to only a small decrease in the conversion. However, tyrosine, tryptophan, glutamine and lysine residues lower the yield, tryptophan being the most effective quencher. It is important to note that good reactivity is still obtained in all cases, with no complete shutdown unlike in the work of Maeda et al.^[227] Tyrosine (+1.1-1.27 V vs SCE) and tryptophan (+0.77-1.16 V vs SCE) quench the excited state of 4CzIPN (**x**), preventing the SET to the carboxylate..^[252-256] Increasing the reaction time to 15 h did not lead to an increase of conversion in the case of tyrosine. Interestingly, the oxidized form of cysteine led to 50% yield within 30 min and increasing the reaction time to 2 h led to 71% yield. As most

of cysteines are present as disulfide bonds in large peptides, this result is promising regarding the need of protecting group. Addition of free cysteine still afforded alkynylation of Cbz-Gly-Pro (**x**) in 62% yield together with thiol-alkynylation which likely takes place first, acting as a protective group of the thiol group. This is interesting for the future work on larger peptides.



Reactions performed on a 0.1 mmol scale, HPLC yield.

Scheme 46: Side-chain functional groups tolerance

6.4 Tetramer peptides scope

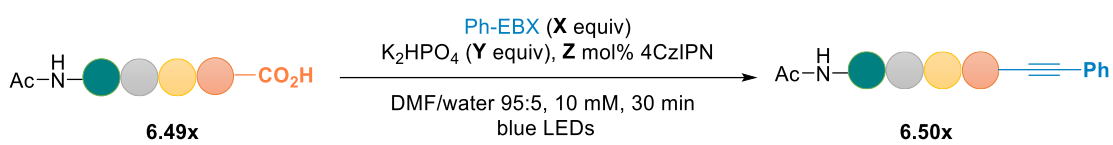
6.4.1 Optimization

Encouraged by the results of the robustness test, an extensive study was performed on tetramers. Two scaffolds were designed, first with a C-terminal proline and variation at the N-terminal to explore the functional group tolerance. Changing the C-terminal amino acid was investigated later. For the model substrates, glycine and alanine residues were chosen not to have any influence on the outcome of the reaction. A phenylalanine residue was added for ease of analysis in UV. N-terminal acetylation was carried out in order to study only the influence of the side-chains. The peptides were synthesized by solid phase peptide synthesis (SPPS).¹⁵ Preliminary tests highlighted that optimization was required. Indeed, submitting Ac-AFGA (**6.49a**) to 1.5 equiv of Ph-EBX (**2.5**), 10 equiv of K₂HPO₄ and 10 mol% of 4CzIPN (**2.23**)

¹⁵ See SI for more information.

led to only 64% conversion to **6.50a** (Table 16, Entry 1). At the time of this study, problems in the peptide synthesis led to substrate availability issues, the optimization was thus performed on different scaffolds. Increasing the catalyst loading was beneficial and full conversion was observed on Ac-RFGP (**6.49b**) (Entry 2). The base loading was also important as no full conversion was obtained with Ac-AFGP (**6.49c**) when only 3 equivalents were added (Entry 3). When turning to the more challenging Ac-KFGP (**6.49f**), no full conversion of **6.50f** was obtained under those conditions. The presence of the primary amine had already showed detrimental impact on the reactivity in the robustness experiments (Section 6.3.3). However, the desired product overlapped with hypervalent iodine peaks in HPLC, preventing the exact determination of the conversion. A catalyst loading of 50 mol% did not improve the outcome and degradation started to occur (Entry 7). Increasing the equivalents of EBX to 3 was key to improve the conversion (Entry 8).

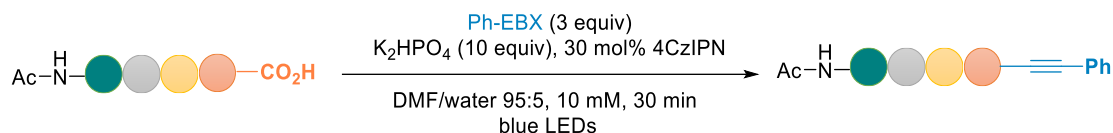
Table 16: Optimization of the decarboxylative alkynylation on tetramers

						
Entry	Peptide	X	Y	Z	Product	Conversion (%)
1	Ac-AFGA (6.49a)	1.5	10	10	6.50a	64
2	Ac-RFGP (6.49b)	1.5	10	30	6.50b	>95
3	Ac-AFGP (6.49c)	1.5	3	30	6.50c	46
4	Ac-AFGG (6.49d)	1.5	10	30	6.50d	81
5	Ac-DFGP (6.49e)	1.5	10	30	6.50e	55
6	Ac-KFGP (6.49f)	1.5	10	30	6.50f	Not full ^a
7	Ac-KFGP (6.49f)	1.5	10	50	6.50f	Not full ^a
8	Ac-KFGP (6.49f)	3	10	30	6.50f	Not full ^a

^a The product was overlapping with hypervalent iodine peaks in HPLC. Reactions performed on a 1 μ mol scale, HPLC yield.

The conditions of Equation 25 were thus employed for the rest of the work on tetramers. All following results are reported as an average of a minimum of 3 independent trials on 1 μ mol. The yields were determined by RP-HPLC-MS. In all reactions, iodobenzoic acid (**2.10**),

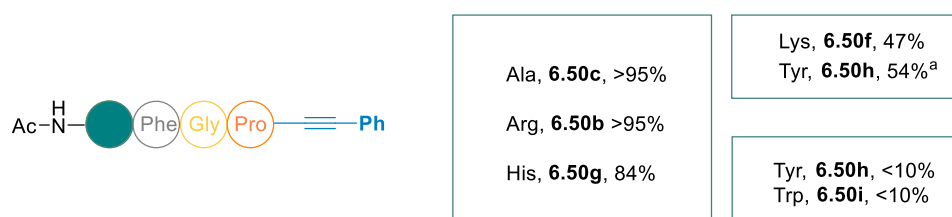
Ph-EBX (**2.5**) and the catalyst (**2.23**) were present, together with side products, among which the alkyne dimer and alkynylated DMF were identified by NMR. The latter is likely formed by HAT.



Equation 25: Optimized conditions on tetramers

6.4.2 Functional group tolerance

The functional group tolerance was investigated on the first scaffold. The model substrate, Ac-Ala-Phe-Gly-Pro-OH (**6.49c**) afforded full and clean conversion under those optimized conditions (Figure 15). Similar excellent reactivity was observed with arginine to **6.50b**. The introduction of basic side-chains, either from histidine or lysine had a deleterious impact to 84% and 47% (**6.50g** and **6.50f**). The main exceptions being tyrosine and tryptophan where no product could be detected under those conditions (**6.50h** and **6.50i**). As described in section 5.3.1, easy to oxidize phenols and indoles are the origin of this lack of reactivity. To our delight, changing the catalyst to $[\text{Ir}(\text{dF}(\text{CF}_3)\text{ppy})_2\text{dtbbpy}]\text{PF}_6$ (**2.15**) ($E_{1/2}^{*\text{III/II}} = +1.21 \text{ V}$) improved the tyrosine containing peptide **6.50h** formation to 54%. This result is in line with a previous report from the MacMillan group, describing this improvement upon the use of a milder oxidant.^[226] The novel organic dyes were also tested. Despite similar redox properties, 4*t*BuCzIPN (**5.27**) afforded only 20% yield. More side-products formation was observed in that case. However, 4DPAIPN (**2.22**) and its derivatives 4BrDPAIPN (**5.26**) and 4CIDPAIPN (**5.25**) afforded only traces of the desired product. The novel fine-tuned organic dyes were thus not useful to overcome selectivity issues in this case, and the transition-metal based catalyst **2.15** remained the most efficient one. In the presence of tryptophan, switching to $[\text{Ir}(\text{dF}(\text{CF}_3)\text{ppy})_2\text{dtbbpy}]\text{PF}_6$ (**2.15**) did not improve the formation of **6.50i**.



^a **2.15** as catalyst. Reactions performed on a 1 μmol scale, HPLC yield.

Figure 15: Functional group tolerance at N-terminal position

Although it is one of the rarest amino acid in proteins, the cysteine case was very interesting. As mentioned in the section 2.2.3, the reaction between thiols and hypervalent iodine EBX reagents is very fast and efficient. Thiols are known to be excellent hydrogen atom sources through Hydrogen Atom Transfer (HAT) cycles.^[271] They were thus very unlikely to be tolerated in the transformation. We wondered whether we could take advantage of the thiol-alkynylation developed by our group to act as a protective group for the thiols.^[128] To our delight, submitting the cysteine containing tetramer to the reaction conditions of Equation 25 afforded full and clean formation of the double-alkynylated product **6.50j** (Figure 16). Further work can be envisioned using different EBX reagents in order to functionalize orthogonally the two alkynes. Various methods exist as well for selective thiol bioconjugation to achieve this orthogonal labelling. Most of cysteines are present in peptides and proteins as disulfide bonds. Their compatibility in this transformation would be thus highly desirable. To our delight, the dimer bearing a disulfide bond led to the desired bis-alkynylated peptide **6.50k**. However, the desired product and **6.50j**, coming from the reduction of the disulfide bond followed by double alkynylation were too close in polarity for separation and yield determination.

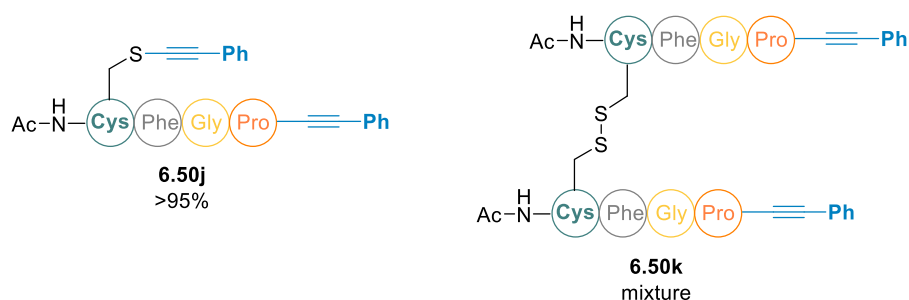


Figure 16: Cysteine derivatives in the decarboxylative alkynylation

6.4.3 C-terminal variation

With those results in hand, variation of amino acids at the C-terminal position was investigated (Figure 17). Alanine, phenylalanine, arginine, serine, methionine, asparagine, and even glycine at the C-terminal position afforded full and clean conversion to alkynylated peptides (**6.50a**, **6.50d** and **6.50l** to **6.50p**). Histidine led to a small decrease of conversion (**6.50q**). The lowest efficiencies were measured for lysine and tyrosine (**6.50r** and **6.50s**). The latter was obtained using $[\text{Ir}(\text{dF}(\text{CF}_3)\text{ppy})_2\text{dtbbpy}]\text{PF}_6$ (**2.15**) as a catalyst.



Ala, **6.50a**, >95%
 Phe, **6.50l**, >95%
 Arg, **6.50m**, >95%
 Ser, **6.50n**, >95%
 Met, **6.50o**, >95%
 Asn, **6.50p**, >95%
 Gly, **6.50d**, >95%

His, **6.50q**, 76%

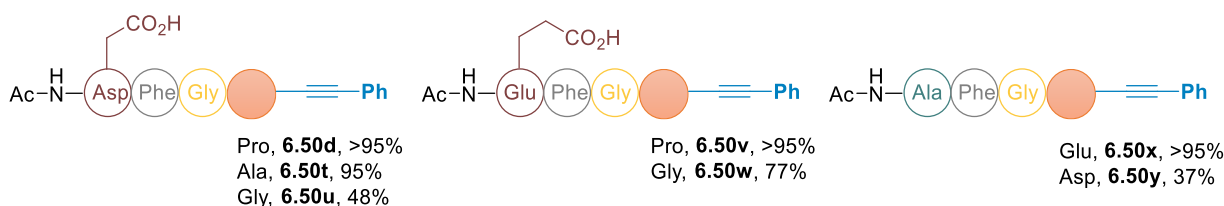
Lys, **6.50r**, 17%
 Tyr, **6.50s**, 29%^[a]

[a] With **2.15** as catalyst. Reactions performed on a 1 μ mol scale, HPLC yield.

Figure 17: Functional group tolerance at C-terminal position

6.4.4 Selectivity between carboxylic acids

The last important question was the selectivity between carboxylic acids, either at the C-terminal position or on the side-chains. Achieving the selective C-terminal functionalization would be highly valuable as detailed in section 2.1.4. Selectivity was evaluated both with an aspartic or glutamic acid at the N-terminal and variation at the C-terminal position (Figure 18). With an aspartic acid, efficient selective C-terminal alkynylation was observed when either a proline or an alanine were located at the C-terminal (**6.50d** and **6.50t**). However, in the case of a C-terminal glycine, a lower but still clean conversion was measured (**6.50u**). If alkynylation of the side-chains could be detected, it was never in more than 5% compared to the major product. For all products, the reactive site was confirmed by MS-MS analysis. A similar outcome was observed in the presence of a glutamic acid with selective alkynylation at the C-terminal position (**6.50v**). It is noteworthy that in this case the drop of yield for glycine was much less important (**6.50w**). With those encouraging results in hand, the transformation on C-terminal aspartic and glutamic acids was attempted, aiming for a selective alkynylation. To our delight, full and clean conversion was obtained for glutamic acid and still 37% for aspartic acid (**6.50x** and **6.50y**). RP-HPLC indicated single major products, with only one decarboxylative alkynylation. The reactive site could not be determined by MS-MS analysis hence the crude mixture was purified by preparative HPLC. NMR analysis confirmed a selective reaction at the C-terminal position.

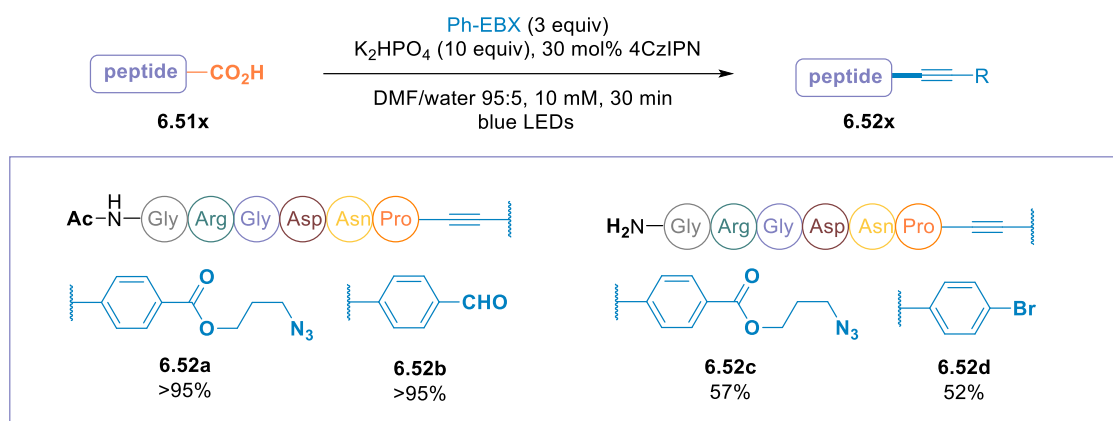


Reactions performed on a 1 μ mol scale, HPLC yield.

Figure 18: C-terminal selectivity of the decarboxylative alkynylation

6.5 Labeling of GRGDNP

The protocol was then extended to larger peptides. The bioactive hexamer GRGDNP, which is a potent inhibitor of cell attachment to fibronectin was first targeted.^[272,273] Without change in the conditions of Equation 25, alkynylation with introduction of an azide and an aldehyde was quantitative to **6.52a** and **6.52b** starting from the N-terminal protected peptide (Scheme 47). The native counterpart with a free N-terminal was alkynylated with more moderate conversions to afford the azide and bromide functionalized peptides **6.52c** and **6.52d**. Those highly valuable products can be employed for further derivatization, either by cross-coupling or by Click reaction. For all products, the reactive site was confirmed by MS-MS analysis.



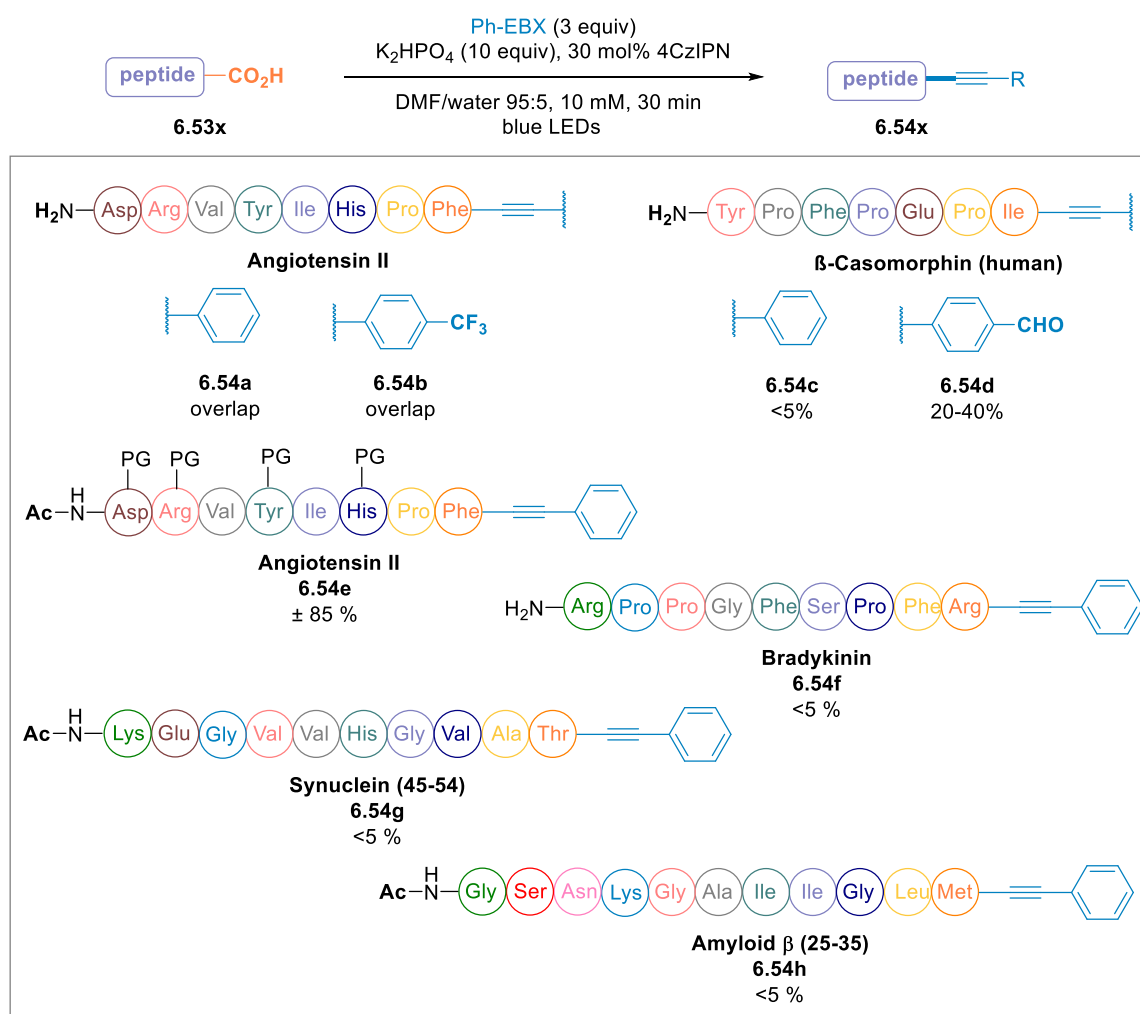
Reactions performed on a 1 μ mol scale, HPLC yield.

Scheme 47: Functionalization of GRGDNP

6.6 Towards the labeling of larger peptides

Larger bioactive peptides were then subjected to the same reaction conditions (Scheme 48). However, none of them was alkynylated in good efficiency. For all tested substrates, poor conversion was the main issue. In the case of Angiotensin II (**6.53a**), the conversion could not be determined with precision as the product (**6.54a**) was overlapping with a side-product. The latter was found in most reactions, although in larger amount when the transformation was not efficient. Attempts to identify it were not successful. It was in too low amount to be isolated and poor ionization prevented a mass determination. Screening of different EBX reagents, in order to vary the retention time of the product was not successful neither (**6.54b**). Control experiments without peptide or with the iridium catalyst **2.15** demonstrated that this side-product was neither peptide nor catalyst based. Acetylation of the N-terminal did not led to an improvement. Changing substrate to β -Casomorphin human (**6.53c**) led to ranges between

20-40% of the desired product (**6.54d**). However, this could not be reproduced and no desired product was detected in other reactions. A last attempt consisted of starting from a fully protected peptide, without cleavage at the end of the synthesis. Even if the desired product **6.54e** was formed in around 85%, cleavage of several protecting groups was observed (trityl for instance), both during purification of the peptide and during the reaction. This approach could be exploitable for further work but would require a fine-tuning of the protecting groups in order to ensure their stability at each step of the process. In all those peptides, a tyrosine residue was present and even if in the work from the MacMillan group reactivity was still good,^[226] this could be the limiting factor. Novel peptides without any tyrosine were thus selected. Bradykinin (**6.53f**), N-terminal protected Ac-Synuclein (45-54) (**6.53g**) and Ac-Amyloid β (25-35) (**6.53h**) unfortunately did not afford a better outcome with the desired product only detected by MS (**6.54f** to **6.54h**). The starting material was the main product in those cases.



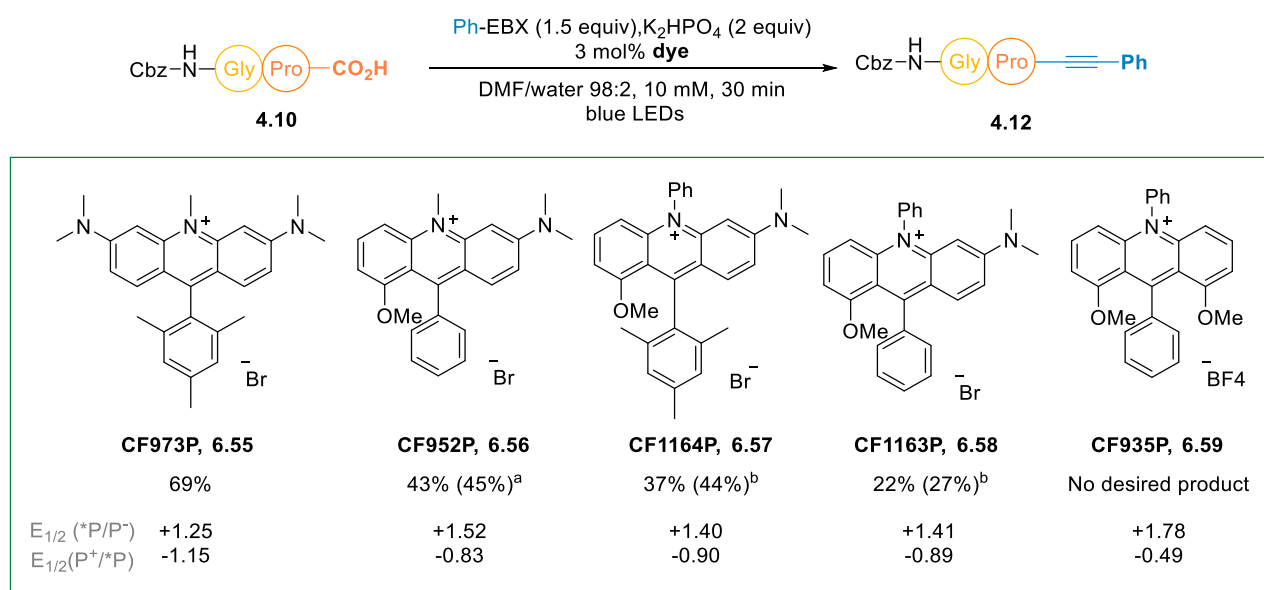
Reactions performed on a 1 μ mol scale, HPLC yield.

Scheme 48: Attempts for the decarboxylative alkynylation of large bioactive peptides

Those results highlighted the need of different conditions in order to alkynylate larger substrates. One approach would be to resume our efforts towards optimization in aqueous media. Control of the pH has indeed been demonstrated to be an efficient strategy to improve the chemoselectivity in the decarboxylative Giese coupling on proteins developed by the MacMillan group (Section 2.3.5).^[274] It indeed allows the selective protonation of functional groups, which has an impact on the redox potentials.^[252–256] Further work will be dedicated to solve those limitations.

6.7 Screening of organic dyes

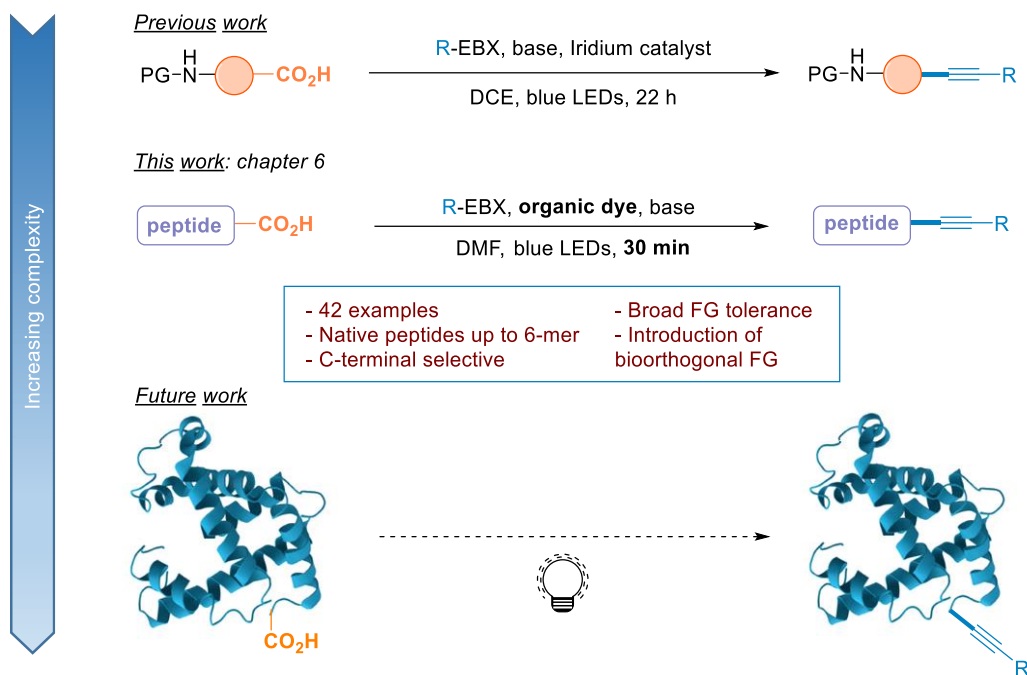
Within a collaboration with the Sparr group, they graciously provided us several Acridinium derivatives **6.55** to **6.59**. Preliminary results for a Giese coupling had demonstrated their potential for decarboxylative reactions.^[162,163] Their water-solubility caught our attention as it would allow the development of a metal-free decarboxylative alkynylation in aqueous media. A first screening was performed on Cbz-Gly-Pro (**4.10**) under the optimized conditions in DMF in order to evaluate their general catalytic efficiency (Scheme 49). Their redox window was comparable with the previously used iridium **2.15** and 4CzIPN (**2.23**), indicating that they could be suitable catalysts. To our delight, CF973P (**6.55**) afforded full conversion and 69% yield within 30 min. CF952P (**6.56**) and CF1164P (**6.57**) led to moderate yields (respectively 43 and 37 %). CF1163P (**6.58**) gave only low yield, and with CF935P (**6.59**) no desired product could be detected. The last result was not surprising, taking into account that **6.97** is likely not a strong enough reductant for this transformation. In some cases, degradation of the dyes was observed and increase of the catalyst loading could have a beneficial effect. Indeed a longer reaction time led to no improvement. The best dye CF973P (**6.55**) was then tested in a DMF/PBS buffer 1:1 mixture. Unfortunately, a significant decrease of reactivity was observed and only traces of the product could be detected. This last result showed that the water-solubility of the photocatalyst did not seem to be the limiting parameter. More stable water-soluble reagents than the ones previously tried would be a direction of investigation, together with highly oxidizing dyes.

Scheme 49: Screening of Acridinium salts in the decarboxylative alkynylation of Cbz-Gly-Pro (**4.10**)

6.8 Conclusion

Efficient methods for peptide C-terminal labeling remain rare and are highly demanded. The purpose of this project was to extend the decarboxylative alkynylation of amino acids developed within the group to peptides and then to proteins. This would furnish a novel path to introduce alkynes on complex biomolecules. Important applications include the synthesis of novel scaffold for drug discovery, or labeling towards imaging in living systems in order to elucidate cellular processes.

Attempts to develop the reaction in aqueous media were unsuccessful despite the encouraging water-compatibility of the transformation and a study was thus performed in organic solvent. A metal-free peptide decarboxylative alkynylation has successfully been implemented using EBX hypervalent iodine reagents and 4CzIPN (**x**) as the photocatalyst, in DMF. This is the first report of such a transformation from free carboxylic acids. The reaction is fast and very tolerant to amino acids side-chains functional groups. Novel fine-tuned organic dyes were reported for that purpose. Selectivity towards the C-terminal position was complete even with a terminal glycine. Native peptides up to hexamers were efficiently functionalized with valuable moieties, including bioorthogonal functional groups. This complexity of the compatible peptides was quite novel as previous works were focusing to small simple peptides. However, unsuccessful attempts towards the labeling of larger peptides highlighted the need of a different approach. Developing a transformation in aqueous media would be one possible strategy.



Scheme 50: Conclusion of chapter 6 on the decarboxylative alkynylation of peptides in organic solvent

Towards a proximity-
induced protein

C-terminal decarboxylative
alkynylation



7 Towards a proximity-induced protein C-terminal decarboxylative alkynylation

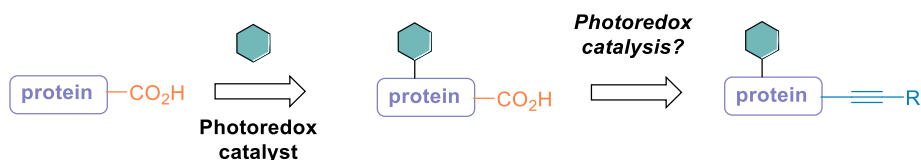
7.1 Background and significance

7.1.1 Significance

The decarboxylative alkynylation on peptides C-terminal position has been described in the previous section (Section 6).^[275] Alkynes are introduced starting from free carboxylic acids in one step using hypervalent iodine reagents and photoredox catalysis. Efficient and fast functionalization of native peptides up to 6-mers with bioorthogonal functional groups was achieved, providing a platform for diversity introduction on peptides. Selectivity towards the C-terminal position together with high functional group tolerance were observed. The promising results obtained on small peptides allowed us to envision further applications of this method in more complex systems.

However, at this stage, our methodology presented two major limitations: First, the reaction could not be implemented in aqueous media (Section 4), and second larger peptides led to poor conversion in DMF, even with few functional groups (Section 6.6). In order to overcome these limitations, a collaboration was developed between our group and the Bernardes Lab in Cambridge University. A 3-month exchange was thus carried out during this PhD thesis in the first half of 2020. Their expertise in handling reactivity and chemoselectivity on more complex biomolecules was essential to progress significantly.

Within the mobility, we decided to focus the work on increasing the efficiency of the decarboxylation for larger peptides. We herein proposed a localization strategy, by designing a methodology for the linkage of the photoredox dyes on peptides and proteins. We believed that this could overcome the peptide size limitation, by having the catalyst in close proximity from the reactive site. To the opposite of previous proximity-induced photoredox transformations on proteins, we aimed for a covalent bond between the photoredox catalyst and the target protein. Taking advantage of existing functionalization strategies, covalent introduction of the dyes at a single reactive-site would be possible. This would provide a robust linkage, together with information on the localization of the catalyst on the protein. No prior knowledge about specific ligands is required with our approach, which aims to be more general and target highly diverse proteins. A reversible linker would regenerate the native protein after the photoredox catalysis step.

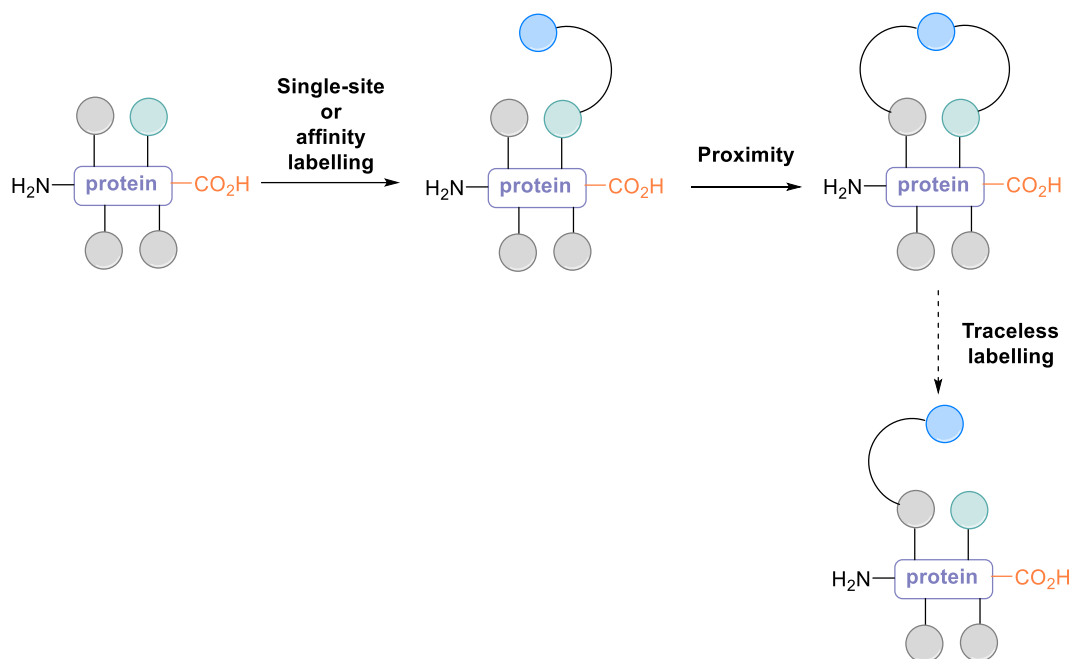


Scheme 51: Proximity-induced decarboxylative alkynylation concept

The design and synthesis of the catalysts were first studied, prior to the evaluation of the reactivity on peptides to provide a proof of concept. Proteins and antibodies were the targeted substrates of this study but could not be tested during this thesis.

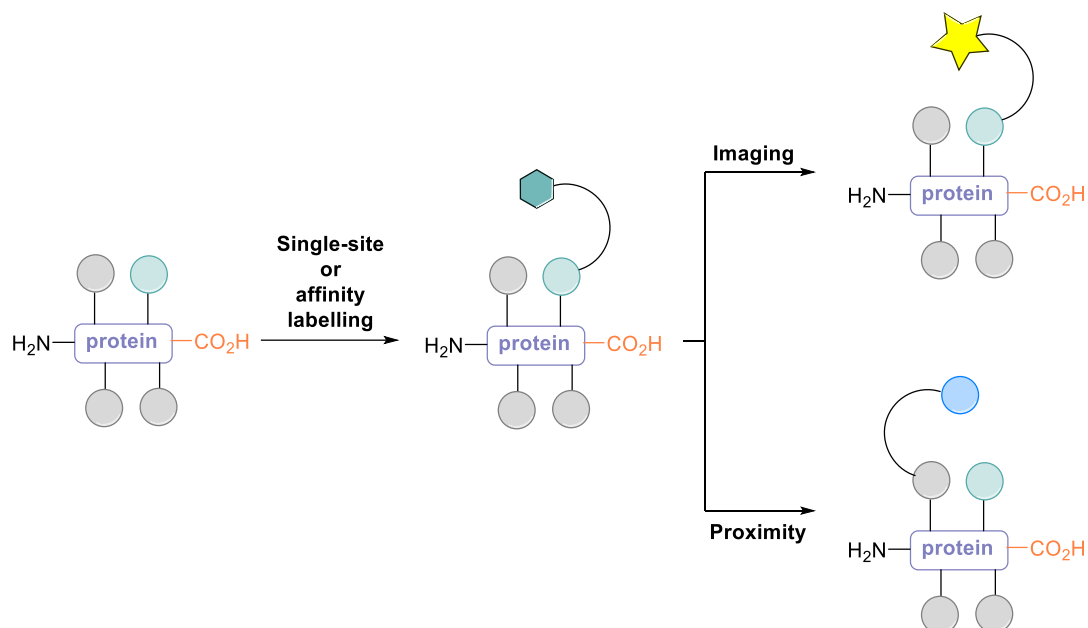
7.1.2 Proximity-induced photoredox transformations on proteins

Proximity-driven reactions have emerged as a powerful tool to achieve regioselectivity in the chemical modification of proteins and were the subject of a recent review.^[276] The general concept is to introduce first a functional group on the protein, later used to carry out directed chemistry. The latter would ideally be efficient only in limited distance, providing selectivity (Scheme 52). This is an elegant way to overcome the inherent challenge of the bioconjugation on very abundant residues. Depending on the method, this labelling can be reversible or not, the goal most often being a traceless activation. One possibility to introduce the desired functional group is affinity labelling, when an enzyme specific ligand is employed, and this has been extensively studied. A general approach, in order to target non-enzymatic proteins as well, or enzyme outside of their active site, has consequently been the subject of studies. The reactive group or catalyst can also be installed either using peptide tags added to the protein, binding to a specific moiety, or the single-site modification with small molecules. The latter is more desirable as the engineering of a protein with a large peptide tag can indeed disturb the activity. The main challenge hence remains to achieve a traceless labelling based on single-site protein modification. Key advances were disclosed recently on the principle of a tethered functional group, which reacts only in close proximity. This thus allows to differentiate residues. Several works took advantage of the unique reactivity of cysteine, for instance for disulfide bond formation, which can be easily reversed, leading to the desired traceless methodology. This attractive field is evolving fast and exciting developments are expected.



Scheme 52: Proximity-induced protein modification concept

The combination of this proximity concept with photoredox catalysis would require the introduction of a photoredox catalyst on the protein as a first step. The applications of the addition of ruthenium and iridium complexes on proteins have already been highlighted and advances in the field have been the subject of recent reviews.^[277,278] One important application consists of the labelling towards imaging by luminescent microscopy (Scheme 53). The field is now more mature and those transition-metal complexes were employed towards the development of the proximity-driven bioconjugation concept.^[71] The principle of this strategy includes the design of a catalyst bond to a moiety allowing protein-binding through molecular recognition. This concept provides an alternative selectivity to the more studied single-site modification based on the difference of reactivity of residues. Photoredox transformations have been described through photolabile groups cleavage but also bond-forming reactions in biological environment.^[277]

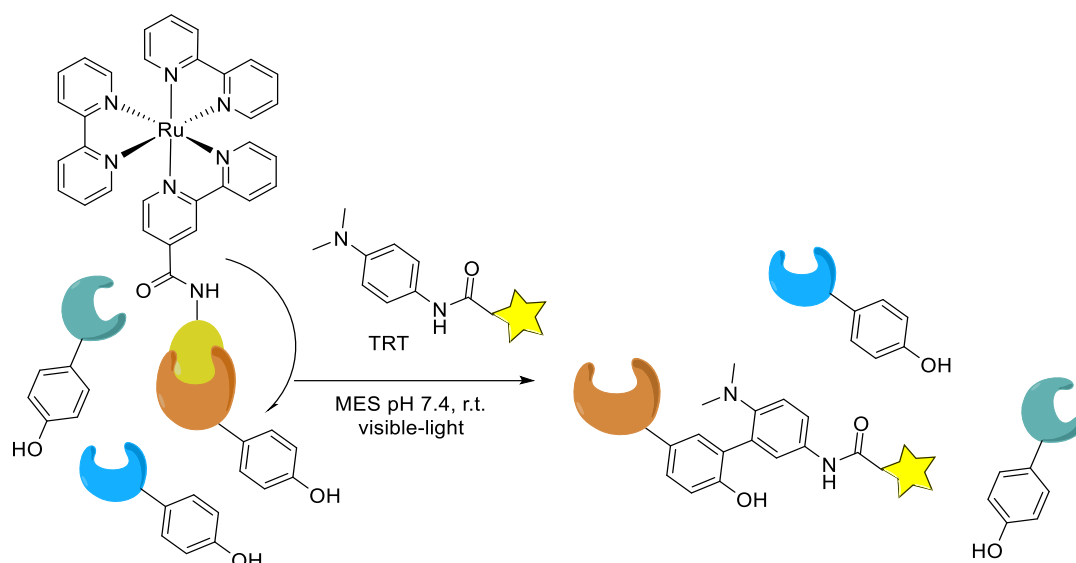


Scheme 53: Protein labelling with fluorophores for imaging or proximity reactions

The knowledge on the attachment of those transition metal complexes is key to ensure an efficient design of the future generation of catalysts. Two main approaches have been described, either by covalent labelling or using non-covalent interactions between the complexes and the proteins. Among covalent bonds, one can note the use of amide bonds formation, aldehydes and isocyanate groups, or Click chemistry.^[277]

The seminal work on proximity-induced photoredox bioconjugation on proteins towards protein modification was disclosed by Sato and Nakamura in 2013 (Equation 26).^[279] A proximity-driven oxidative coupling of tyrosine residues was achieved using a local SET catalyst (LSC). In this work, the photoredox catalyst, Ru(bpy)₃ (**2.14**), was tethered to a ligand of the protein. Tyrosyl radicals can be generated by SET and further react with tyrosyl radical trapping reagents. The selective binding of the ligand with the targeted protein, carbonic anhydrase (CA), allowed a substrate selective transformation. The buffer conditions were compatible with cell lysates as well as living cells. This methodology was later extended to a simultaneous purification and labeling of proteins on magnetic beads,^[280] and protein knockdown.^[281] Screening of the reagents in the radical transformation also allowed to reduce the labeling radius and hence increase the selectivity.^[282] Site-selective labeling of a residue as abundant as tyrosine is very challenging and mixtures are often obtained. In this novel study only one tyrosine could be labeled. A more detailed description of their protocol for distance evaluation will be described in Section 7.3.1. Using covalently linked ruthenium complexes,

templated bond-cleaving reactions were explored intensively by the Winssinger lab, including fluorophore uncaging.^[277]



Equation 26: Local SET catalyst strategy for tyrosine oxidative coupling by Nakamura and co-workers

With the very promising results on tyrosine residues, the extension of this methodology to other residues would be highly valuable in the field of protein modification. Building on this contribution about selective protein modification using ligand-binding, a similar approach could be designed towards carboxylic residues. Although very elegant, this strategy presents the limitation to require the prior knowledge about a specific ligand for the targeted protein. The synthesis has then to be adapted to each protein. A more general approach to target other residues on different classes of proteins would be a significant contribution to the field. For this reason, we envisioned to use a covalent introduction of organophotocatalysts to trigger proximity reactions. This would provide a general access for proteins substituted with photoredox catalysts. If we aim to first assess the potential of this approach on the decarboxylative alkynylation of C-terminus position, this novel concept could have broad applications for site-selective protein modification.

7.2 Design and synthesis of dyes

7.2.1 Design of dyes

The first step of this project was the design of a general structure of the photoredox catalysts for this proximity-induced transformation. According to our previous work, several parameters were identified as of paramount importance. First, the redox properties of the catalyst should remain as close as possible from 4CzIPN (**2.23**), in order to preserve the excellent chemoselectivity observed. The selected scaffold of the organophotocatalyst should thus have been already studied and the structure/activity relationship well understood to allow an efficient rational design. Moreover, a single-site introduction would be highly desirable. Indeed, this should increase the selectivity through proximity as well as by controlling the kinetics of the reaction. In the presence of several equivalents of catalyst per protein, degradation or side-reactivity could occur. Finally, the linker has to be easily and efficiently introduced and stable under the reaction conditions (highly oxidative and reductive). A covalent linker which can be further cleaved after the desired reaction would provide a highly desirable traceless activating method.

Building on the modular nature of 4CzIPN family, novel organic dyes suitable for this localization strategy can be envisioned (Figure 19). It has been demonstrated by that the nature, number and position of donor and acceptor groups is both easily tunable and has important influence on the redox properties of the dyes (Section 5).^[159,259,260,275] We can envision to use variation of one carbazole bearing a functional group designed for further introduction on a biomolecule. Based on our previous studies, anchoring should be either achieved using an electron-withdrawing group in *para*-position on the carbazoles or an electron-donating group in *meta*-position.

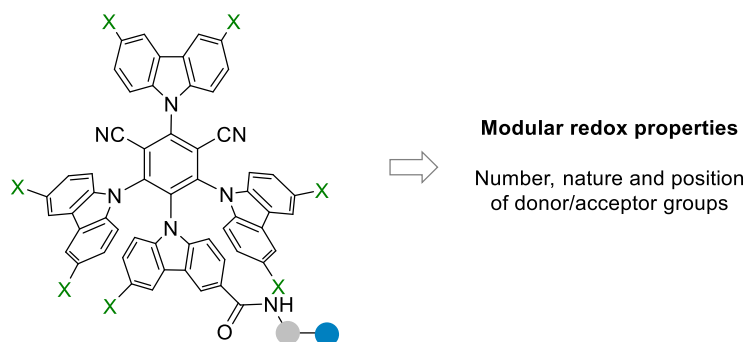


Figure 19: Core structure of the organic dyes for proximity photoredox catalysis

The presence of a linker would diminish the impact on the redox properties together with increasing flexibility of the covalently linked dye. This would also be one important parameter to tune the required distance between the catalyst and the targeted carboxylic acid. In a first approach, we selected a PEG chain in order to provide as well a better water-solubility together with some flexibility (Figure 20).

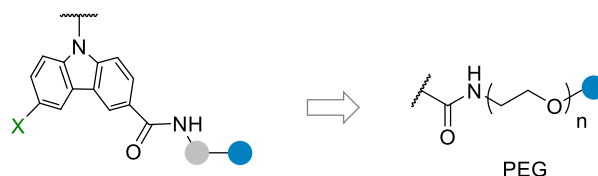
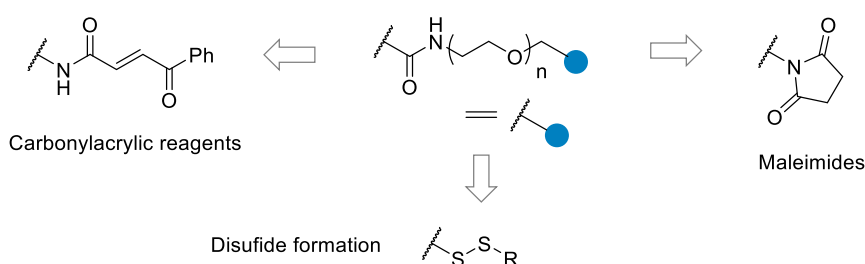


Figure 20: Linker structure of the organic dyes for proximity photoredox catalysis

The linkage method has to be very efficient and selective in order to introduce a single photoredox catalyst on the biomolecule. Cysteines were selected as the target residue due to their low abundance and the numerous existing functionalization methodologies.^[2,283,284] Especially, reaction with carbonylacrylic reagents, maleimides or disulfides have proven their efficiency. This rare amino acid is often either absent in proteins or under disulfide bonds form. Cysteines can then be introduced at a desired position through selective mutation. Among available efficient methodologies, we selected first carbonylacrylic reagents due to the expertise of the Bernardes Lab in this field.^[76,77] They provide an irreversible covalent linkage, which we believe would be valuable for the development of a proof of concept. Stability through the reaction conditions would be very helpful in the optimization of the reaction conditions. Further work can then be performed using other reversible groups to access the targeted traceless methodology.



Scheme 54: Functional group structure of the organic dyes for proximity photoredox catalysis

Taking into account all the previously described elements, the proposed structure of the first generation of dyes is disclosed in Figure 21. Amides bonds were chosen as the link between the three major parts of the dye. This would rend the synthesis easier and match the desired electronics in *para*-position on carbazoles.

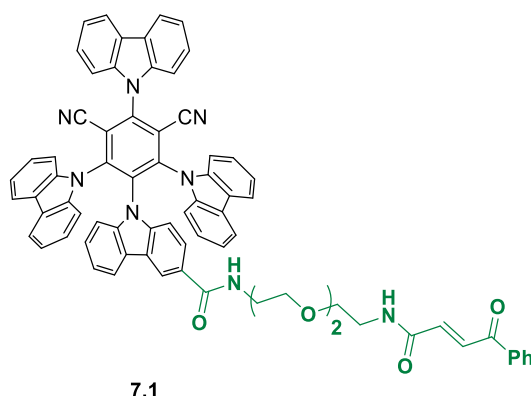
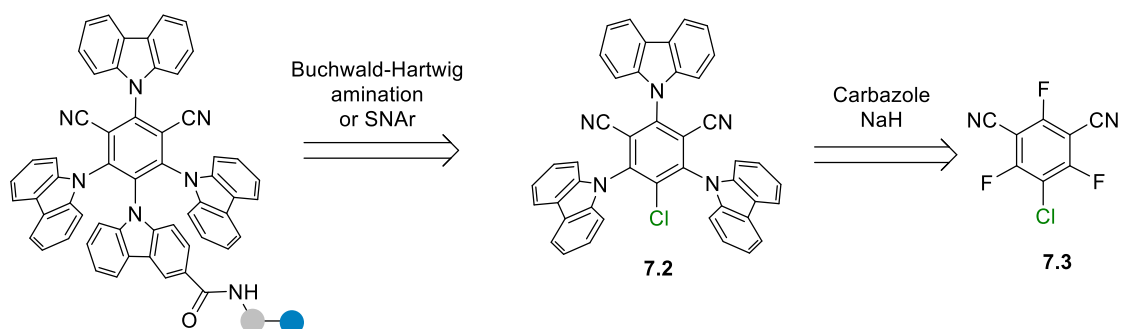


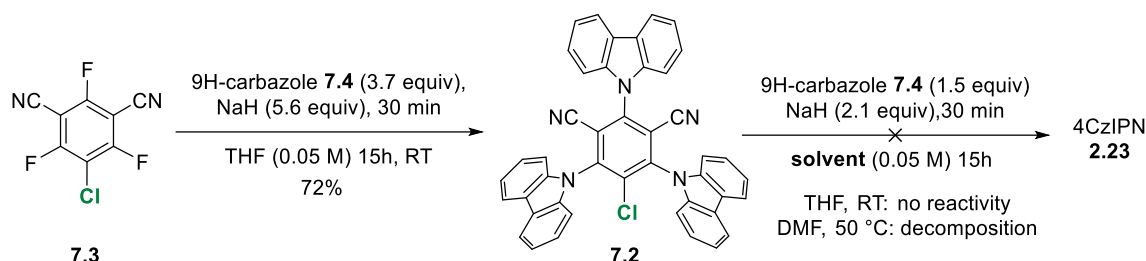
Figure 21: First generation dye for proximity photoredox catalysis

7.2.2 Synthesis of the first generation dye

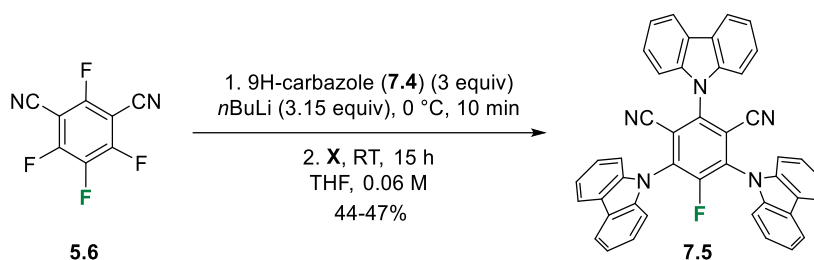
As described in Section 5, dyes of the 4CzIPN (**2.23**) family can be accessed in one step by nucleophilic aromatic substitution, from commercially available 2,4,5,6-tetrafluoroisophthalonitrile (**5.6**) and the corresponding carbazoles.^[159,260] The key in this synthesis was to determine which carbazole should bear the linker for bioconjugation and how to distinguish it from the others. Building on previous reports from Zeitler and Monkman groups, the carbazole located in *meta*-position of the cyano groups appeared to us a realistic target (Scheme 55).^[259,285] Intermediate **7.2** was indeed reported by Zeitler, starting from 5-chloro-2,4,6-trifluoroisophthalonitrile (**7.1**). Further nucleophilic aromatic substitution or Buchwald-Hartwig amination reaction could allow the introduction of the last carbazole. In addition, we aimed to design a modular strategy with a late-stage common intermediate to serve as a platform for further derivatization, **7.2** for instance. A library of dyes with various linkers or functional groups for bioconjugation was highly desirable to ensure the development of an efficient dye or diversity in the possible targets. Furthermore, it is good to keep in mind that all steps should be ideally feasible at gram-scale.

Scheme 55: Retrosynthetic pathway for **7.1**

Following Zeidler procedure, 3CzClIPN (**7.2**) could be obtained in 72% yield starting from 5-chloro-2,4,6-trifluoroisophthalonitrile (**7.3**) and 9H-carbazole (**7.4**) (Scheme 56). In a preliminary approach, all attempts for the introduction of the last carbazole to access 4CzIPN (**2.23**) were unfruitful. Either no reactivity was observed in THF at RT or decomposition was observed in DMF at 50°C. This pathway was thus not continued.

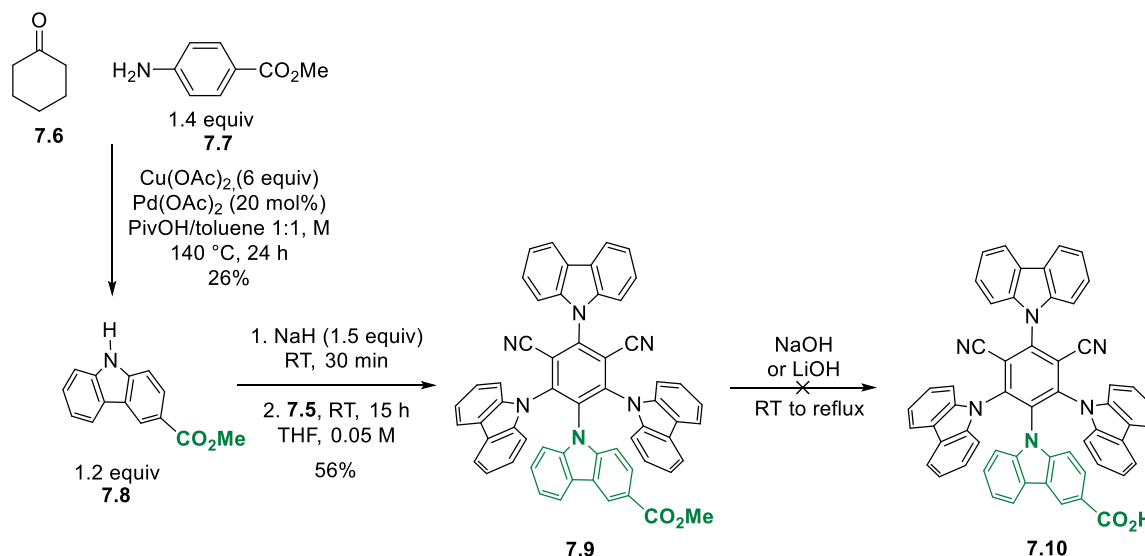
Scheme 56: First synthetic pathway of **7.1**

In a report from 2019, Monkman and coworkers described that the synthesis of 4CzIPN (**2.23**) can be interrupted, providing 3CzFIPN (**7.5**).^[285] In this case, *n*BuLi was employed instead of NaH, affording 3CzFIPN (**7.5**) in 44-47% yield (range of 4 experiments), starting from 2,4,5,6-tetrafluoroisophthalonitrile (**5.6**) and 9H-carbazole (**7.4**) (Equation 27). As the structure is the fluorine counterpart from the previously described Caribou, this dye was named the Faribou.

Equation 27: Synthesis of 3CzFIPN (**7.5**)

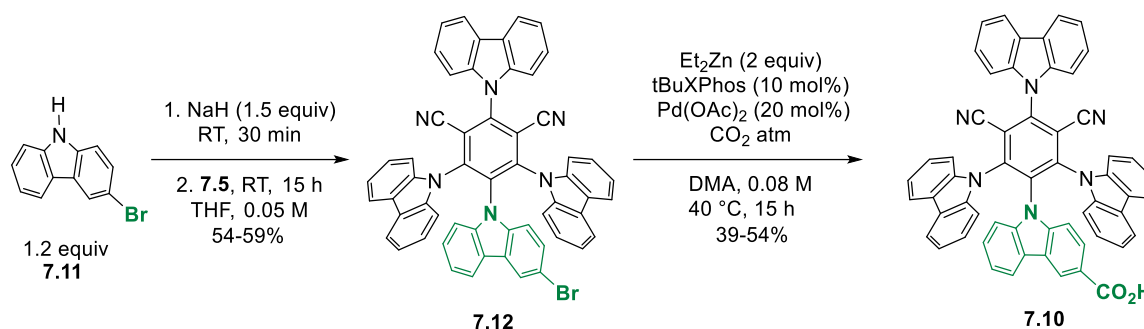
With 3CzFIPN (**7.5**) in hand, we aimed to access the desired dye (**7.1**) through introduction of a carboxylic acid, later subject to amidation with the appropriate PEG chain Scheme 57. The first strategy to access intermediate **7.10** consisted of the introduction of methyl 9H-carbazole-3-carboxylate (**7.8**). After several unsuccessful attempts using classical Chan-Lam coupling, the carbazole **7.8** was synthesized following a dehydrogenative aromatization/C(sp²)-C(sp²) coupling sequence described by Wang and coworkers.^[286] Starting from cyclohexanone (**7.6**) and the corresponding aniline **7.7**, the desired carbazole **7.8** was obtained in low yield, although in a one-step procedure. **7.8** was then submitted to the

standard protocol for 4CzIPN derivatives synthesis and **7.9** was isolated in 56% yield. Unfortunately, all our efforts to convert **7.9** into its hydrolyzed counterpart **7.10** were unfruitful with either no reactivity, or degradation as the outcome of the reaction. Due to the difficult synthesis of **7.10**, this pathway was abandoned, to the benefit of the one on Scheme 58.



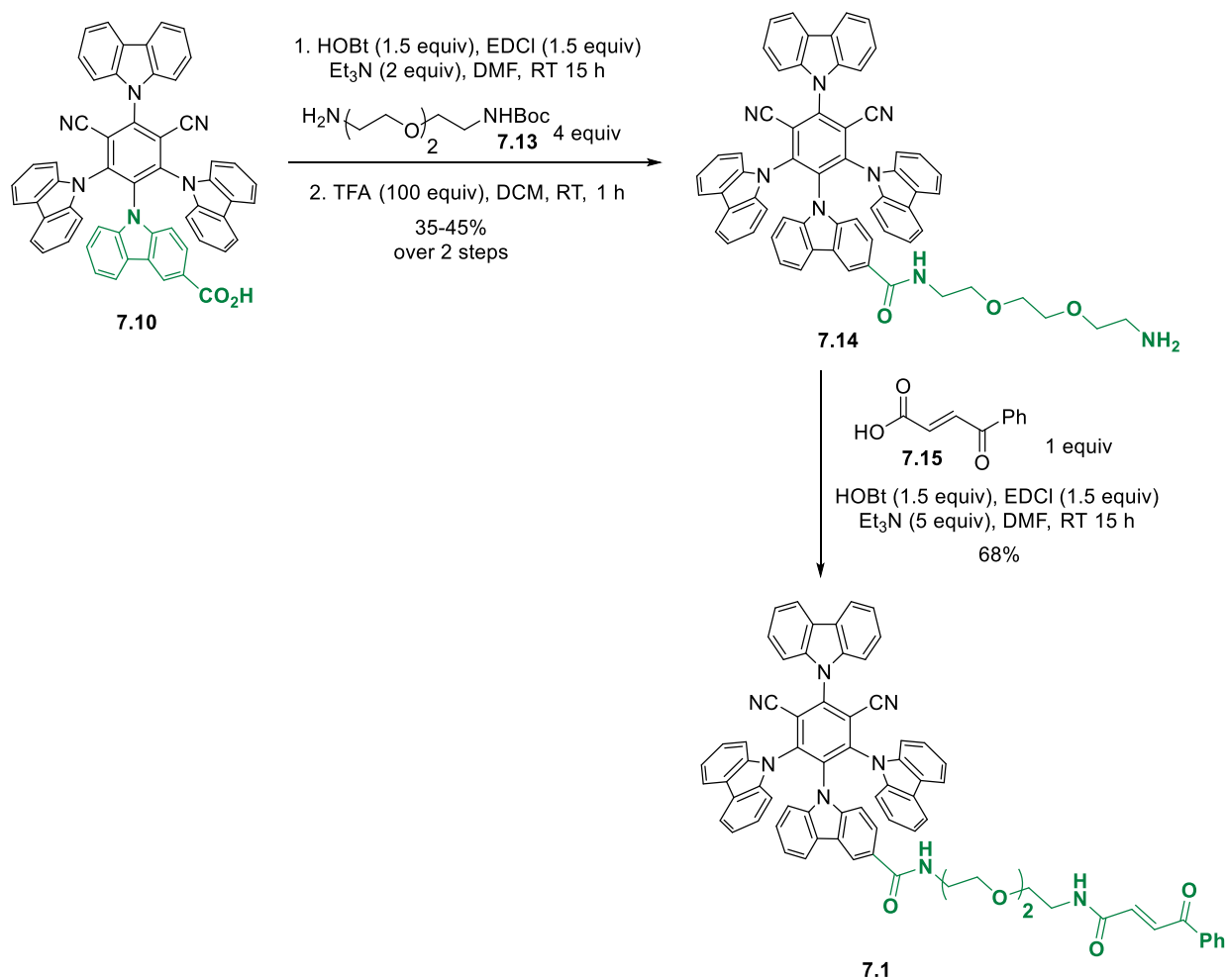
Scheme 57: First pathway towards carboxylic acid substituted dye (**7.10**)

Monkman and coworkers have also described the synthesis of the bromo-substituted dye **7.12**.^[285] Following standard conditions, **7.12** was obtained in 54-59% yield (over 4 times) from **7.5** and 3-bromo-9H-carbazole (**7.11**) (Scheme 58). We envisioned to access our target **7.1** by carboxylation of this known intermediate. Indeed, although carboamination reactions have been described,^[287] this transformation remains challenging and preliminary investigations did not lead to the formation of desired products. However, attempts of lithiation of **7.12** by addition of *n*BuLi followed by carboxylation using a CO₂ balloon only led to complex mixtures.^[288] Even reversing the order of addition as reported in the presence of cyano groups did not improve the outcome of the transformation.^[289] To our delight, when **7.12** was submitted to the palladium-catalyzed carboxylation described by Martin and coworkers,^[290] clean carboxylation took place in moderate albeit reproducible yield to afford the desired intermediate **7.10** in between 39 to 54% yield for 4 batches. As described by the authors, by-products consisted of reduced starting material, 4CzIPN (**2.23**), and a product where the bromine is substituted by an ethyl group. Those two products were easily separated from **7.10**.



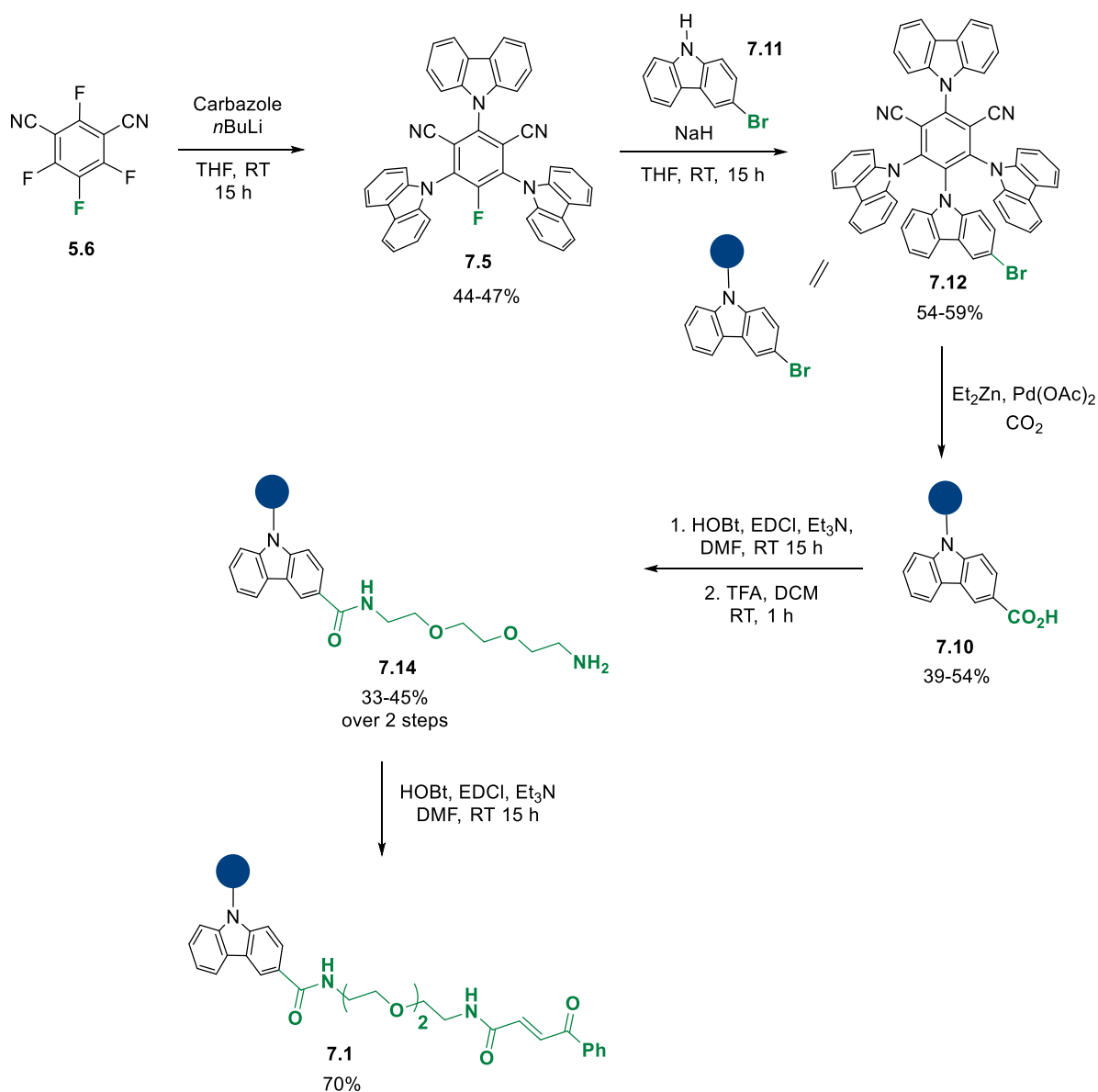
Scheme 58: Synthesis of carboxylic intermediate dye (**7.10**)

With the key intermediate **7.10** in hand, the end-game consisted of attachment of the PEG chain and the carbonylacrylic group (Scheme 59). An amide coupling between **7.10** and the commercially available amine **7.13** under standard conditions followed by Boc deprotection with TFA led to the desired product **7.14**. HOBt and EDCI were chosen as classic coupling reagents without optimization following previous reports.^[76] This step could be optimized. Another amide coupling with (E)-4-oxo-4-phenylbut-2-enoic acid (**7.15**) under the same conditions afforded the desired dye **7.1** in moderate yield. Preliminary observations during the isolation suggested that the dye was not very stable under acidic conditions. Attempts to introduce the amine fragment at once were unsuccessful so far but would be worth investigating once the final dye would be chosen. This dye was named the Narwhal thanks to its long “teeth”.



Scheme 59: End game of dye **7.1** synthesis

The complete synthesis of dye **7.1** is described in Scheme 60. **7.1** was accessed in 6 steps on a 100 mg scale. This modular strategy allows variation of the functional group for bioconjugation at the last step and variation of the linker at the one but last transformation.



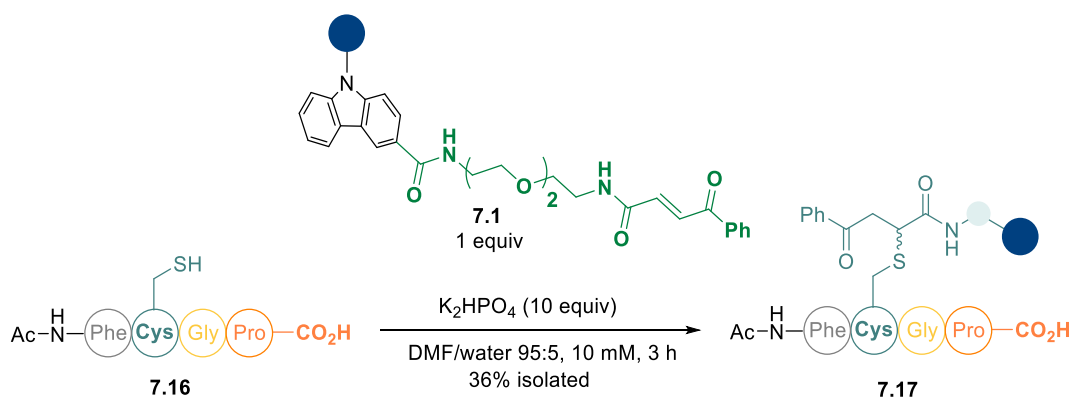
Scheme 60: Overall synthesis of dye **7.1**

7.3 Preliminary results

7.3.1 Proof of concept on peptides

Tetramers

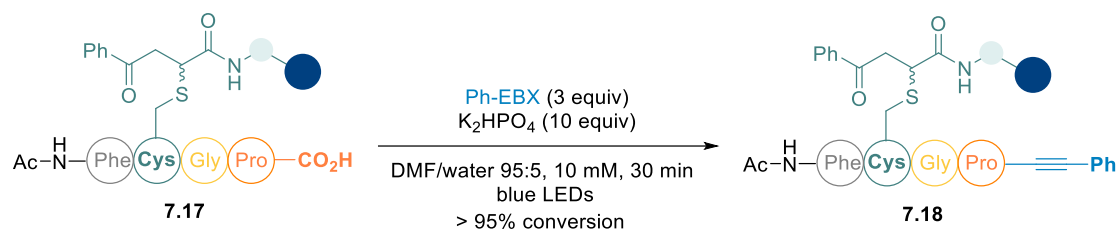
A tetramer was first used to design a proof of principle with dye **7.1**. The reactivity of those substrates was already studied in Section 6.4 and the analysis are more straightforward than for larger substrates. The first parameter to evaluate was the introduction of the dye on the peptide. To this end, Ac-FCGP (**7.16**) was chosen as a model substrate (Equation 28). Proline was kept as the privileged C-terminal amino acid and the cysteine was placed as the third residue. This distance was assumed to be a good starting point in line with previous reports (Section 7.1.2). The tetramer **7.16** was then placed in presence of the dye **7.1** under the same conditions as the following decarboxylative alkynylation, with the long-term goal of achieving a one-pot linkage/photoredox sequence. To our delight, complete conversion towards the desired product **7.17** was obtained in 3 h stirring in the dark. As expected, **7.17** was detected as a mixture of 2 diastereoisomers. A larger scale reaction was performed on 3 μmol scale and after isolation each diastereoisomer was submitted to MS-MS analysis and NMR studies, which confirmed the structure of the product. However, an unknown side-product was detected in the crude reaction mixture and co-eluted with one diastereoisomer, which renders characterization difficult.



Equation 28: Dye introduction on Ac-FCGP (**7.16**)

The purified diastereoisomers were each submitted to the reaction conditions developed in the intermolecular version (Equation 29).^[275] To our delight, the pure diastereoisomer afforded full and clean conversion into its alkynylated counter-part **7.18** as a mixture of diastereoisomers (at the C-terminal position). The structure was confirmed by MS-

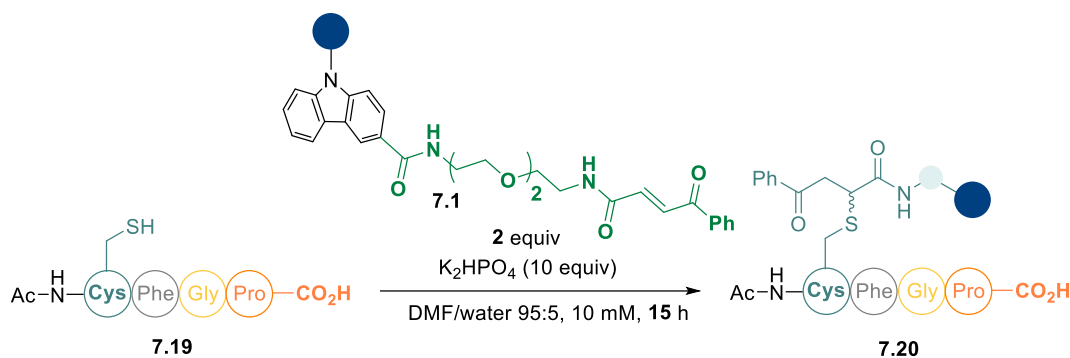
MS analysis. If this results confirms that the dye retained its catalytic activity upon addition of the PEGylated chain and its addition on the peptide, it is however still not possible at this stage to conclude about an intramolecular SET. The very similar peptide Ac-CFGP was indeed an excellent substrate in the previous work after alkynylation of the cysteine (Section 6.4). Further work was thus performed with larger peptides.



Equation 29: Decarboxylative alkynylation on Ac-FCGP substituted with 7.1

With those promising results in hand, the next step of the project took place in the Bernardes Lab in Cambridge University within a 3-month exchange. However, it became rapidly quite clear that the dye stability and thus purity was a main issue. The large scale batch underwent degradation after several weeks. Unfortunately, attempts to purify the dye were not conclusive and showed that **7.1** is unstable in acidic media. Neither carrying out all purification steps in the dark together with storage under inert atmosphere at $-20\text{ }^{\circ}\text{C}$, nor deactivated silica were helpful. Purification and analytics are also complicated due to the very close polarities of all compounds derived from **7.1**. Small pure fractions could nevertheless be obtained to continue the study.

Attempts to reproduce the introduction of the dye **7.1** on Ac-FCGP (**7.16**) were unsuccessful with Ac-CFGP (**7.19**). This change of substrate occurred for availability reasons. Variation of several parameters such as reaction time (increased to 15 h), presence/absence of light, equivalents of dye and base, highlighted that the dye purity was a key factor. Clearer batches afforded cleaner conversions, to the opposite of batches where 3 main products were identified. If one non-identified impurity was not reacting with the tetramer, the second one however led to the side-product already observed in the preliminary results. The best results were obtained with an overnight reaction, without protection from the light and 2 equivalents of the dye, which led to almost full conversion to the desired product **7.20** together with traces of the oxidized dimer from (Equation 30). Attempts in buffers were not conclusive at this stage but need to be resumed once a larger quantity of dye is available.



As attempts of purification did not afford a pure sample, synthesis of a novel batch of **7.1** was carried out. However, purification problems were also encountered with the final step. Upon those results, it was quite clear that a second generation of dyes was needed in order to solve this stability issue. This will be described in Section 7.4.

Decamers

The previous results in Section 6.4 demonstrated that tetramers were already suitable substrates for the decarboxylative alkynylation using 4CzIPN (**x**). Another scaffold was thus required to study this proximity-induced approach. Larger peptides are not compatible with an intermolecular transformation (Section 6.6). They would thus provide key information on whether the decarboxylative alkynylation of peptides substituted with **7.1** is promoted by the proximity effect or not. In addition, a parameter of paramount importance in this project is the required distance between the dye and the reactive site at the C-terminal. In other words, which position of the cysteine on the peptide is optimum, if there is any. The work from the Nakamura group provided key findings.^[282] They have indeed already studied the photocatalyst-proximity dependence in a Ru(bpy)₃ (**2.14**) catalyzed labeling of tyrosines. They described the use of polyproline peptides as molecular rulers due to the rigidity of the structure. It was thus envisioned to employ this approach in the present case. The distance will thus be studied on decamers of proline with one cysteine residue (Figure 22). The influence of the substitution at each position of the cysteine on the outcome will be measured.

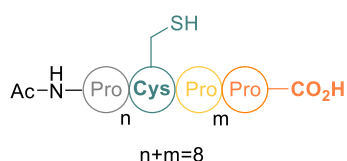
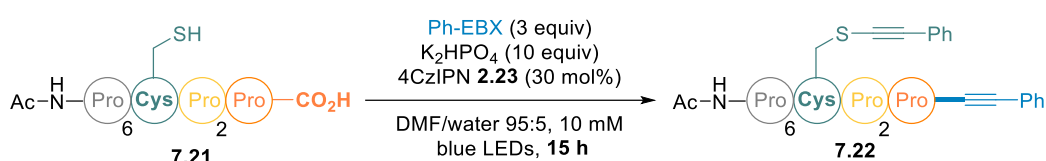


Figure 22: Proline oligomer as molecular ruler

Control experiments were first carried out in order to confirm the absence of reactivity in an intermolecular process. Peptide **7.21**, with the cysteine as the 4th residue, was submitted to the previous reaction conditions (Equation 31). Surprisingly, full and clean conversion towards the alkynylation product **7.22** was observed after 15 h. This results demonstrate that more than the size of the peptides, the number of functional groups was the limiting factor in the previous attempts. Interestingly, upon dilution to 1 mM, only the thiol-alkynylation took place without decarboxylation. Further experiments are needed to confirm this absence of reactivity on those decamers. The goal here is to find the point where no reactivity occurs intermolecularly to optimize the proximity-induced transformation.



Equation 31: Control experiment on proline oligomer

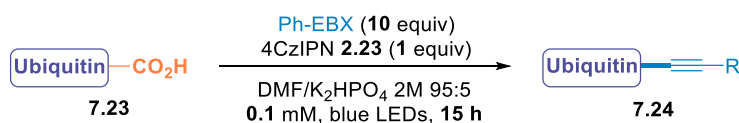
Another peptide scaffold could also be employed. Indeed, peptides such as Angiotensin II, Amyloid β 25-35 or Bradykinin were non compatible with previous conditions. Mutation of one amino acid from their scaffold could afford the proof of principle and a platform to study the distance influence.

7.3.2 Towards a proximity-induced decarboxylative alkynylation on proteins

Appropriate targets to the proof of concept of this strategy are small proteins, with no cysteine in the wild-type. In addition, the expression process, both of the native protein and of any cysteine mutant should already be mastered in order to ensure a relatively fast access to a first substrate to test. Combining those criteria, Histone H3 was proposed by the Bernardes group. A mutant was designed by exchange of the glutamic acid residue at the 3rd position to the C-terminal position (E133) to a cysteine: H3 E133C.¹⁶

¹⁶ The plasmid was generated by Claudia Alfonso who expressed the mutant successfully. Expression was reproduced with the help of Lavinia Dunsmore, who is kindly thanked. Another interesting target is nanobodies due to their relative small size and interesting bioactivity. Mutants with cysteines in various positions are under study by Phil Lindstedt from the Bernardes Lab.

The first step in this next step of the project was to carry out control experiments to rule out any possible intermolecular reactivity. Ubiquitin (**7.23**) was chosen as a model protein as it is commercially available and relatively small (7 kDa). Preliminary tests suggest that no reactivity is occurring neither under the standard nor under stronger conditions (Equation 32). However, the workup of the crude media is under optimization due to the small size of the protein and the presence of a large quantity of DMF. Further work would be required to confirm those observations.



Equation 32: Preliminary experiments on ubiquitin

7.4 Second generation of dyes

As discussed in the previous section, preliminary results highlighted the need for a more stable generation of dyes. Three different parts of the structure can be modified which are expected to have a strong impact on the stability and reactivity: the anchor, the functional group for bioconjugation and the linker (Section 7.2.1). The key in the design is the balance between reactivity and stability. An overview of the targeted dyes (**7.25** to **7.32**) is presented in Figure 23. The rationale of each modification will be discussed together with the synthesis.

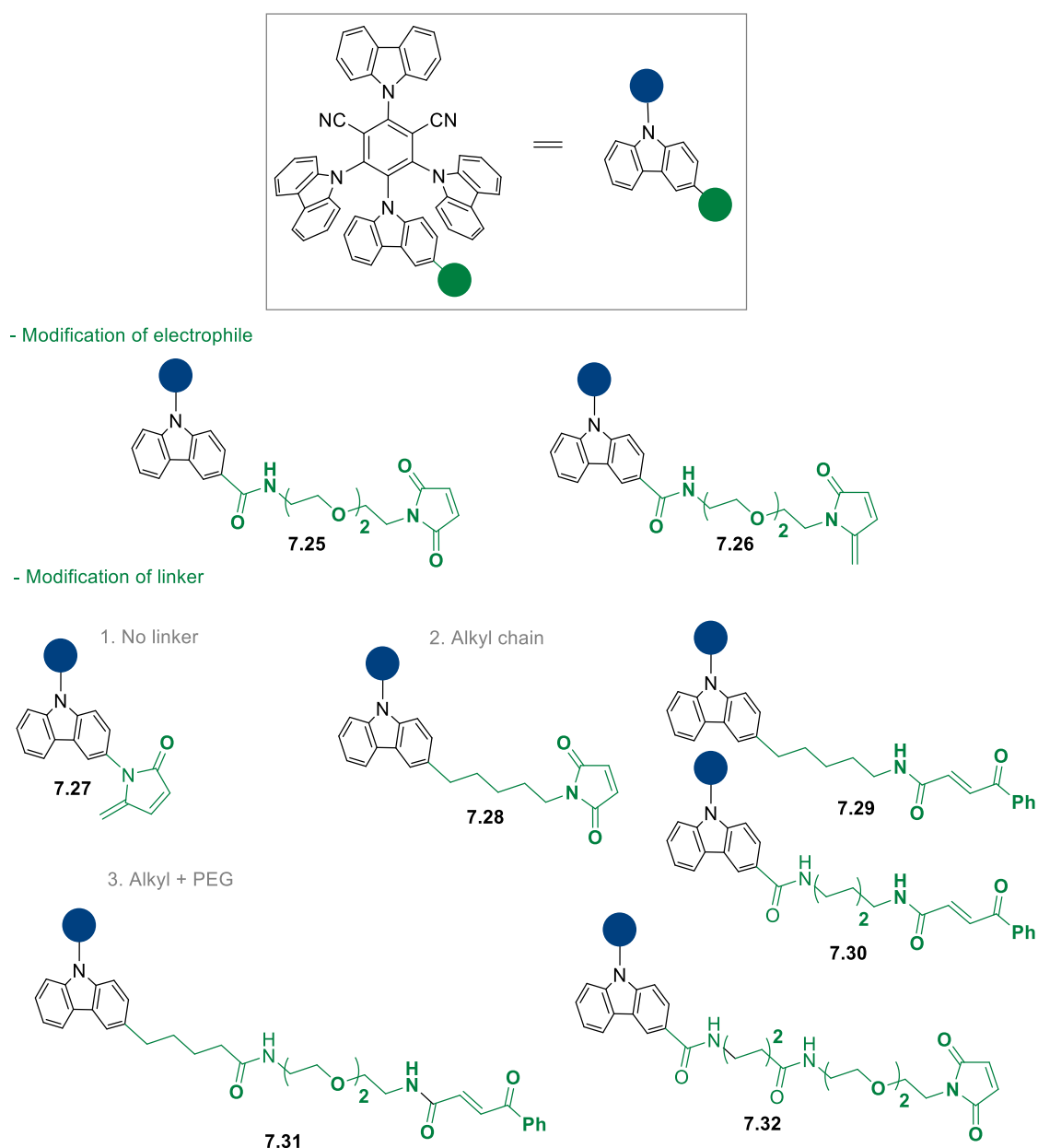
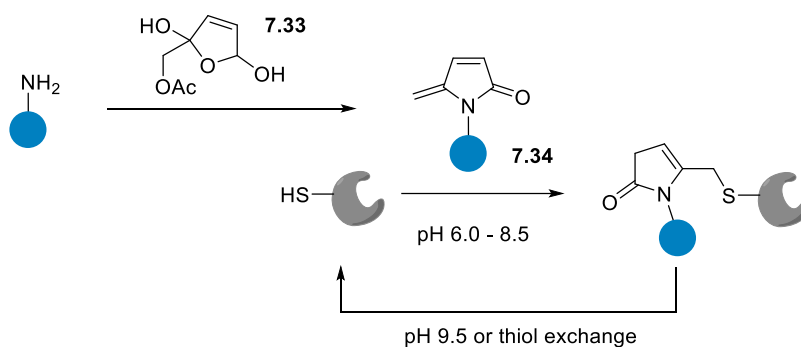


Figure 23: Second generation of dyes

7.4.1 Synthesis

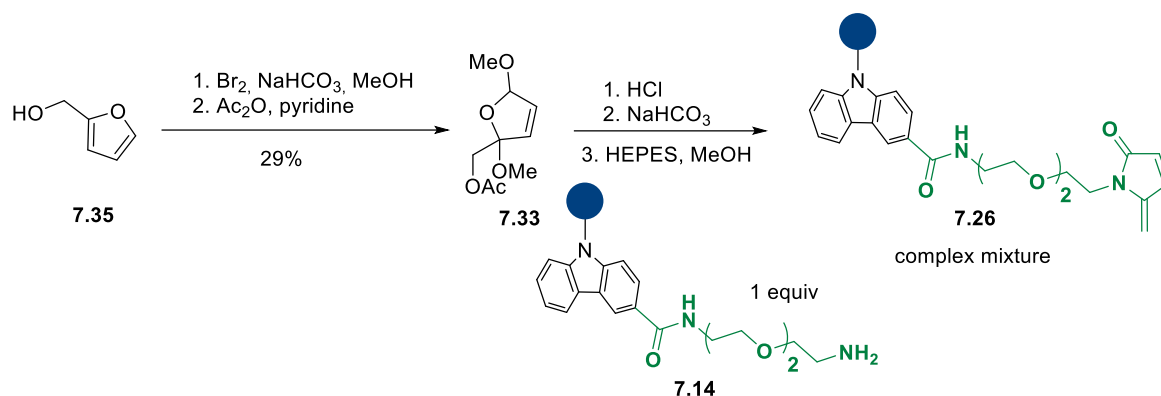
Functional group modification

First, the electrophile could be modified to either a more classic maleimide (**7.25**) or the modified scaffold **7.26**. The latter was described by Zhou and coworkers (Scheme 61).^[291] The efficient synthesis of a variety of 5-Methylene pyrrolones (5MPs, **7.34**) was reported starting from primary amines and **7.33**, including fluorescein or biotin moieties. Bioconjugation on cysteines occurs selectively and rapidly under physiological conditions to generate adducts. The advantage relies in the reversibility of the thiol-addition, which would be of high interest to us. Either under more basic conditions or in the presence of an excess of thiol, a retro-Michael reaction takes place to regenerate the desired protein.



Scheme 61: Cysteine bioconjugation with 5-Methylene pyrrolones

Following the reported procedure, **7.33** was obtained from furfuryl alcohol (**7.35**) in low yield as a mixture of diastereoisomers (Scheme 62). Unfortunately, the addition of the amine **7.14** to form the desired dye **7.26** was unsuccessful and a complex mixture was observed. At this point, attempts of purification of the amine intermediate **7.14** highlighted stability problems at this early stage, suggesting that the PEG chain was the source of the instability. This scaffold was thus abandoned.

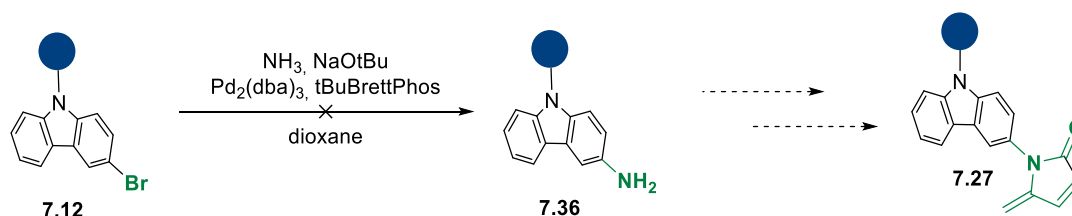


Scheme 62: Synthesis of 5-Methylene pyrrolones substituted dye 7.26

Linker modification

- No linker

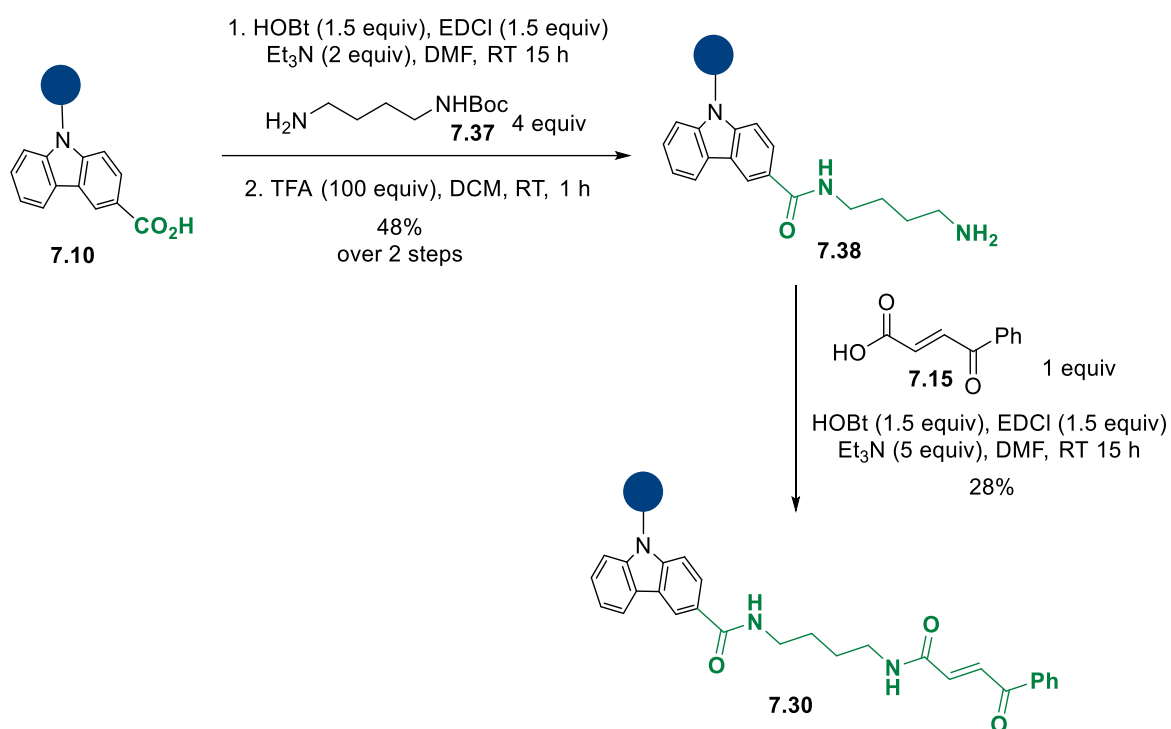
The successful synthesis and application in labelling of a 5-Methylene pyrrolone substituted with Fluorescein without any linker in the report from Zhou made us interested into dye **7.27**. A first attempt of amination starting from **7.12** using a Buchwald coupling did not afford the desired product **7.36** (Scheme 63).^[292] Full conversion was observed but decomposition occurred during purification on silica. No further work was conducted due to the promising results obtained with other scaffolds.



Scheme 63: Attempt towards the synthesis of dye without linker 7.27

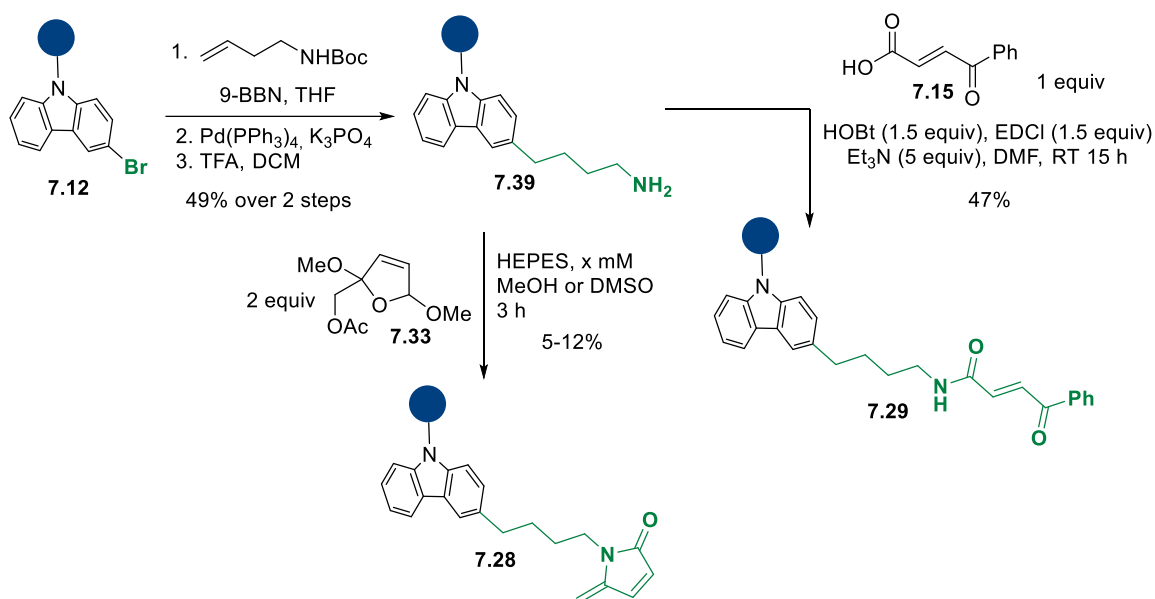
- Alkyl chain with amide anchor

In previous reports (Section 7.1.2) the active catalyst is often spaced from the reactive site with an alkyl chain. Dyes **7.28** to **7.32** would thus have some of the flexibility from **7.1**, together with stability arising from the isolation of the radical carbanion site from the reactive site. One important parameter to determine was whether the instability of dye **7.1** was arising from the PEG chain or from the amide linker. To this end, we synthesized the catalyst **7.30** following the same synthetic route than for **7.1** but with diamine alkyl chain **7.37** (Scheme 64). After amide coupling and Boc deprotection affording the amine **7.38**, a second amidation with carbonylacrylic reagent **7.15** led to the targeted dye **7.30** in moderate yield.

Scheme 64: Second generation dyes, synthesis of **7.30**

- Alkyl chain

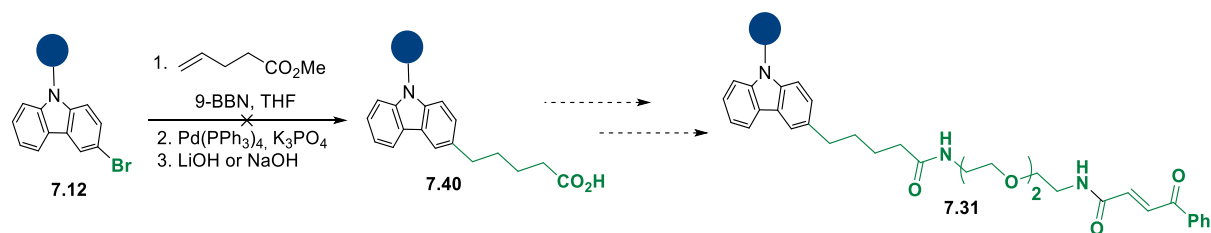
Another prevalent scaffold in fluorescent imaging is the direct linkage of an alkyl chain on the dye, to serve as a spacer between the two reactive parts. Dye **7.29** was thus targeted (Scheme 65). On this scaffold, an electron-donating group is introduced in *para*-position, instead of *meta*. The reason was that was synthesis practicability as bromine intermediate **7.12** was already in hand. Future work could be dedicated to variation of the substitution position on the carbazole. Starting from intermediate **7.12**, a Suzuki coupling followed by Boc deprotection afforded the desired dye **7.39** in good yield.^[293] Final coupling with different functional groups led to dye **7.29** from amidation with **7.15** and dye **7.28** bearing the 5-Methylene pyrrolone moiety. This step afforded a complex mixture with the desired dye as a minor product. Attempts to improve the yield by changing of cosolvent from methanol to DMSO, as it has been reported by Zhou for some substrates, were not promising. No further work was conducted.



Scheme 65: Synthesis of dyes with alkyl chain linker

- Mixed chain

Among possible linkers, a chain composed of both an alkyl part together with a PEG have been described. This would be an interesting scaffold, allowing both spatial separation of the reactive sites, flexibility and solubility. Preliminary investigations towards dye **7.31** were unfruitful (Scheme 66). Indeed, if the Suzuki coupling was successful in the same conditions as for the amine-substituted dye **7.39**, all attempts of hydrolysis led to either no conversion or complex mixtures with hydrolysis of the cyano groups. We envision to solve this issue by starting with a *tert*-butyl ester, as TFA has been shown previously to be compatible with amine **7.14**.

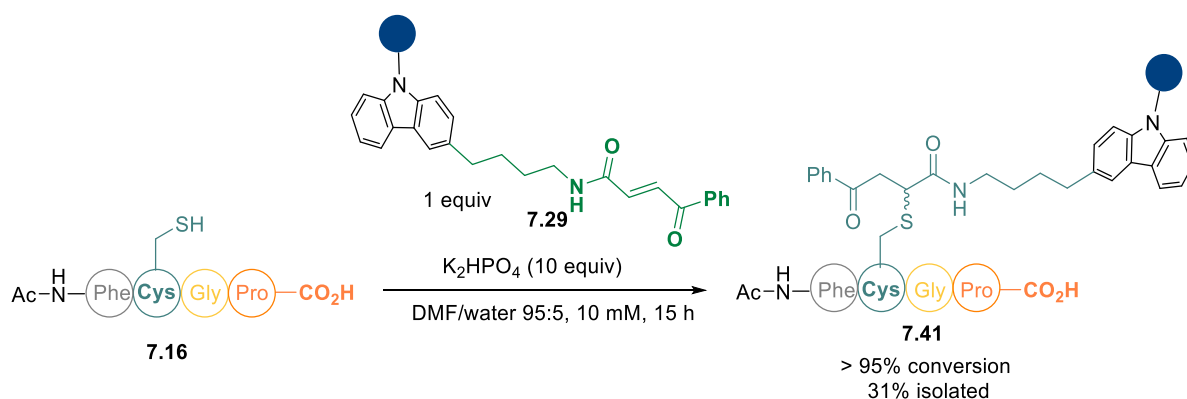


Scheme 66: Attempts towards mixed-linkers on dyes

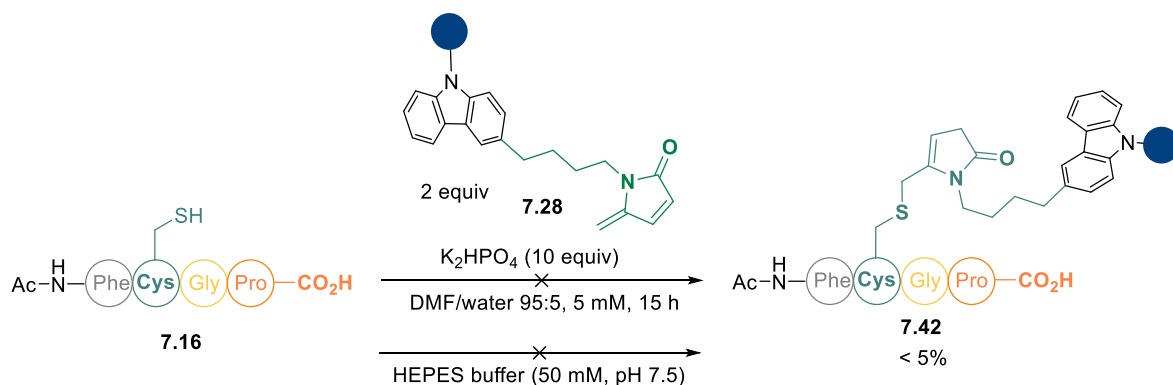
7.4.2 Preliminary investigations

Tetramers

The investigations on the reactivity of dyes **7.29** and **7.28** started with the tetramer Ac-FCGP (**7.16**) as a model substrate as in Section 7.3.1. When **7.16** was submitted to the same conditions as in the first investigations, meaning 1 equivalent of dye for 3 h in DMF, full conversion to **7.41** was obtained only after 15 h of reaction time (Equation 33). This confirmed the reproducibility issues observed with Ac-CFGP (**7.19**). It is good to note that the flask was not protected from the light and that only traces of oxidation to the disulfide dimer were detected. Isolation by preparative RP-HPLC on 3 μ mol scale afforded 31% yield and allowed full characterization of the mixture of diastereoisomers by MS-MS analysis and NMR studies. No decarboxylation was attempted on the intermediate **7.41** as it would not provide any information regarding the existence of a proximity effect.

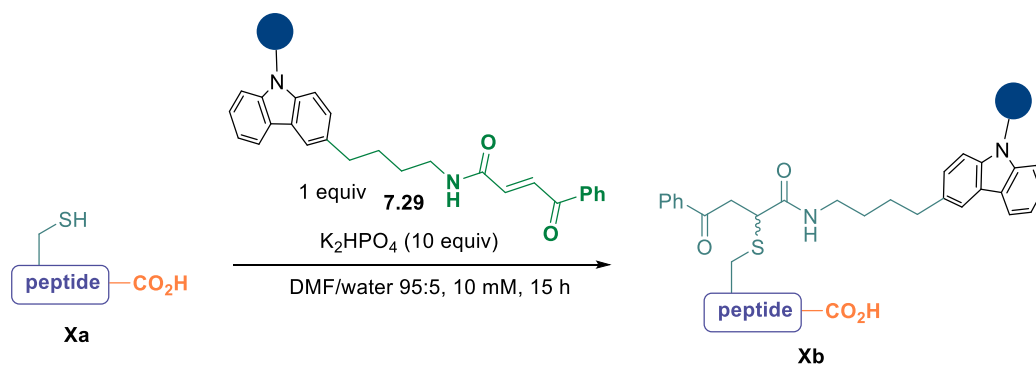
Equation 33: Addition of dye **7.29** on tetramer Ac-FCGP (**7.16**)

Investigations were also carried out with dye **7.28**. Due to the little amount obtained during the synthesis, only few attempts were possible (Scheme 67). No conversion to **7.42** was observed in the same conditions as in Equation 33. Following the report from Zhou and coworkers, the addition was also conducted in aqueous buffer but without a better outcome.

Scheme 67: Attempts for the addition of dye **7.28** on tetramer Ac-FCGP (**7.16**)

Large bioactive peptides

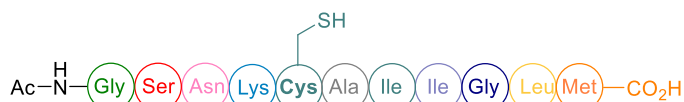
With the good results on tetramers, a strategy was designed to assess the potential of the proximity approach at an intermediate stage before protein investigations. We envisioned to start from peptides which demonstrated no reactivity in the intermolecular decarboxylation, as highlighted in Section 6.6. Our hypothesis was that after mutation of one amino acid to a cysteine and introduction of the dye, reactivity if any would arise from the proximity effect. Two peptides were selected: α -Synuclein (45-54) and Amyloid β (25-35). The first one bearing a glutamic residue to be able to conclude on possible selectivity between carboxylic acid residues. For each peptide two mutations sites were chosen, one at the third position from the C-terminal and one further away. After SSPS and purification, those mutated peptides **7.43a** and **7.44a** were subjected to the dye introduction conditions from the previous section (Scheme 68). To our delight, full and clean conversion was obtained in both cases. Isolation was performed on the products from α -Synuclein (45-54) G3C **7.43b** and G8C **7.43c** on respectively 7.9 and 6.1 μmol to afford 42% and 44% yield. For time reasons, Amyloid β (25-35) derivatives **7.45a** and **7.46a** have not been studied yet.

**Synuclein (45-54)****7.43**

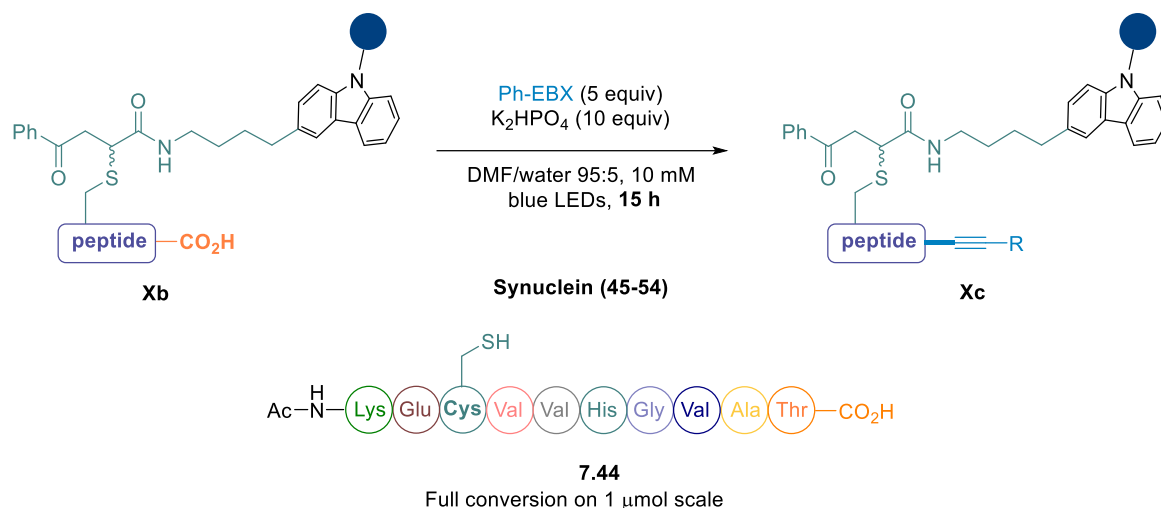
> 95% conversion
 42% isolated on 7.9 μ mol scale

**7.44**

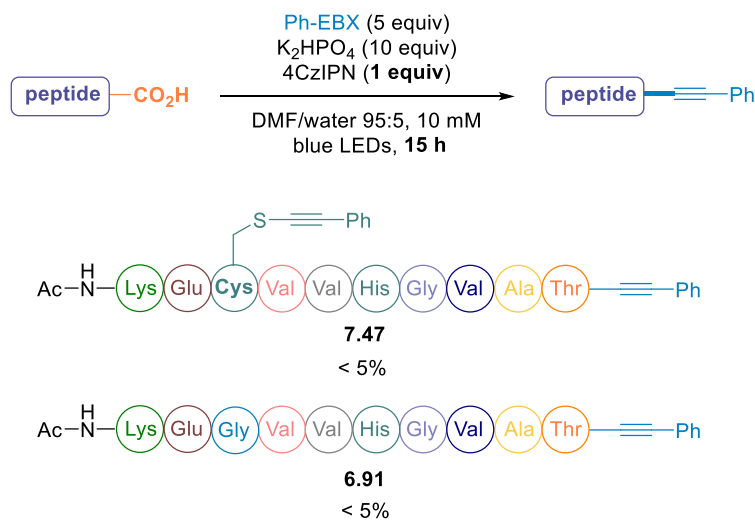
> 95% conversion
 44% isolated on 6.1 μ mol scale

Amyloid β (25-35)**7.45****7.46***Scheme 68: Dye introduction on large peptides*

Only α -Synuclein (45-54) G8C with the tethered dye **7.44b** could be subjected to alkynylation conditions (Scheme 69). If full conversion was observed on 1 μ mol scale and the product detected by HRMS further work on larger scale will be required to confirm the structure of the product and thus the yield. Experiments on other scaffolds are the priority and will be carried out very shortly.

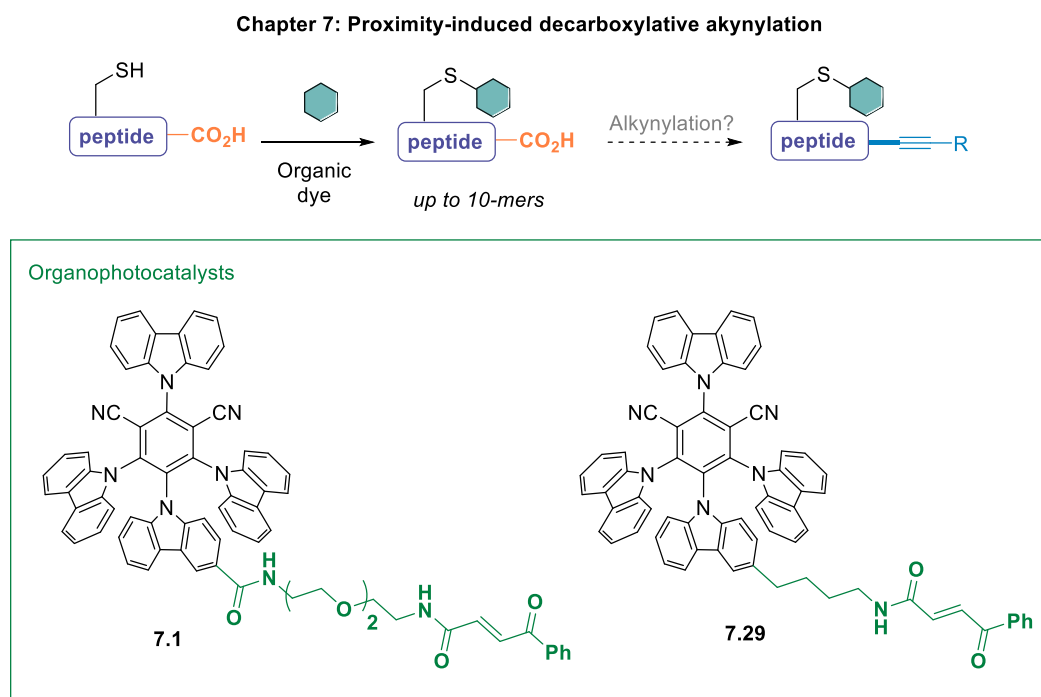
Scheme 69: Proximity-induced decarboxylation on α -Synuclein (45-54)

In parallels, control experiments were carried out under the same conditions, but with 4CzIPN (**2.23**) as the dye (Scheme 70). Only traces of the decarboxylative alkynylation product **6.91** were detected. No increase of conversion was observed on α -Synuclein (45-54) with those harsher conditions. In the case of α -Synuclein (45-54) G3C **7.44a**, the major product resulted from the thiol-alkynylation, with no further decarboxylation to **7.47**.

Scheme 70: Control experiments on α -Synuclein (45-54)

7.5 Conclusion and outlook

A novel approach has been designed towards a C-terminal protein decarboxylative alkynylation and overcome the limits of our previous study. We aimed to develop a proximity-induced photoredox transformation by covalent linkage of an organic dye based on the scaffold of 4CzIPN (**2.23**) on proteins. This strategy had not been explored so far. Building on our expertise on the rational design of 4CzIPN (**2.23**) derivatives, a first generation dye **7.1** has been designed and synthesized (Scheme 71). A proof of concept on a tetramer has then been performed. Substrates for further studies, proteins and nanobodies have been designed and their synthesis was ongoing when writing this thesis. The main limitation encountered in the preliminary studies was the stability of the dye **7.1**, which could not be cleanly isolated. Those mixtures led to by-products and non-reproducible results during the introduction of the catalyst on the peptides. Novel dyes **7.26**, **7.29** and **7.30** have thus been designed and accessed. To our delight, the organocatalyst **7.29** demonstrated better stability and was successfully introduced on decamers with excellent conversions. Model substrates at that stage consisted of bioactive peptides mutated with a single cysteine. Efficient site-selective introduction of the photocatalyst is already an important achievement towards the success of our strategy. Preliminary results suggest that the dye triggered a proximity-induced decarboxylation alkynylation on a decamer. This result awaits confirmation but it would consist of an important intermediate step before proteins. Before this project, the labeling of peptides with 4CzIPN (**2.23**) was unprecedented, even for fluorescence applications. Future results on the optimization of the decarboxylative alkynylation step are of paramount importance as it could not only allow us to overcome the limitation of our methodology, but set the path for other applications of this novel strategy. High potential towards site-selective protein modification is indeed envisioned.



Scheme 71: Conclusion on the chapter 7 about a proximity-induced decarboxylative alkynylation

Future work will consist of the confirmation of this proof of concept on larger peptides and extend the methodology to proteins. With this insight of reactivity on peptides, suitable conditions for proteins will be developed. Proteins such as Histone H3 or Ubiquitin will be first studied in DMF due to their small size. However, in the long-term aqueous conditions should be investigated. To this end, one can think of either developing novel water-soluble hypervalent iodine reagents or changing the radical acceptor. Once the proof of concept achieved on proteins, the work on a reversible dye introduction should be resumed in order to provide a traceless-activating methodology. Applications of this project should be highly valuable in chemical biology as C-terminal modification methods are still very limited. Possible uses can be found either in post-translational modifications such as PEGylation or glycosylation, and in the synthesis of antibody-drug conjugates.

Photoredox-catalyzed
sequential decarboxylative-
oxidation-arylation of
peptide C-terminus

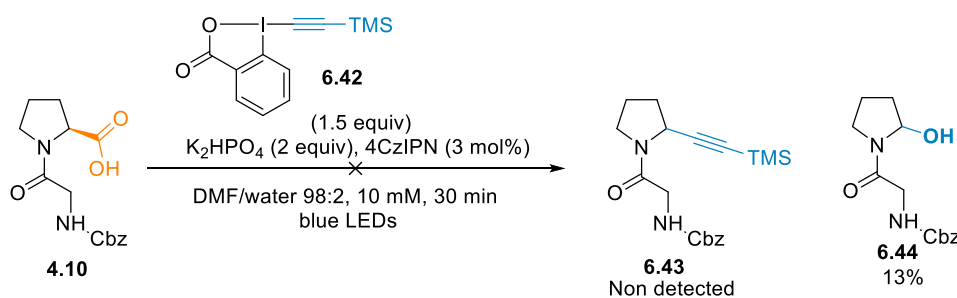


8 Photoredox-catalyzed sequential decarboxylative-oxidation-arylation of peptide C-terminus¹⁷

8.1 Background and significance

8.1.1 Significance

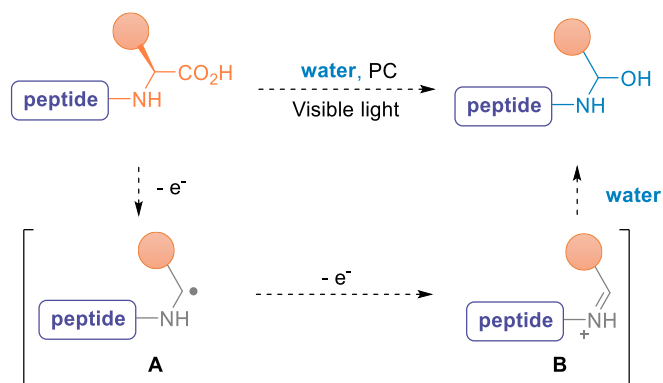
In the course of our previous investigations on the decarboxylative alkylation of peptides (Section 6.3.1), one side-product caught our interest. Indeed, when TMS-EBX (**6.42**) was employed as a reagent together with Cbz-Gly-Pro (**4.10**), no desired alkylation to **6.43** was observed but the hemiaminal **6.44** was formed instead (Scheme 72).



Scheme 72: First isolation of hemiaminals dipeptides from decarboxylative hydroxylation

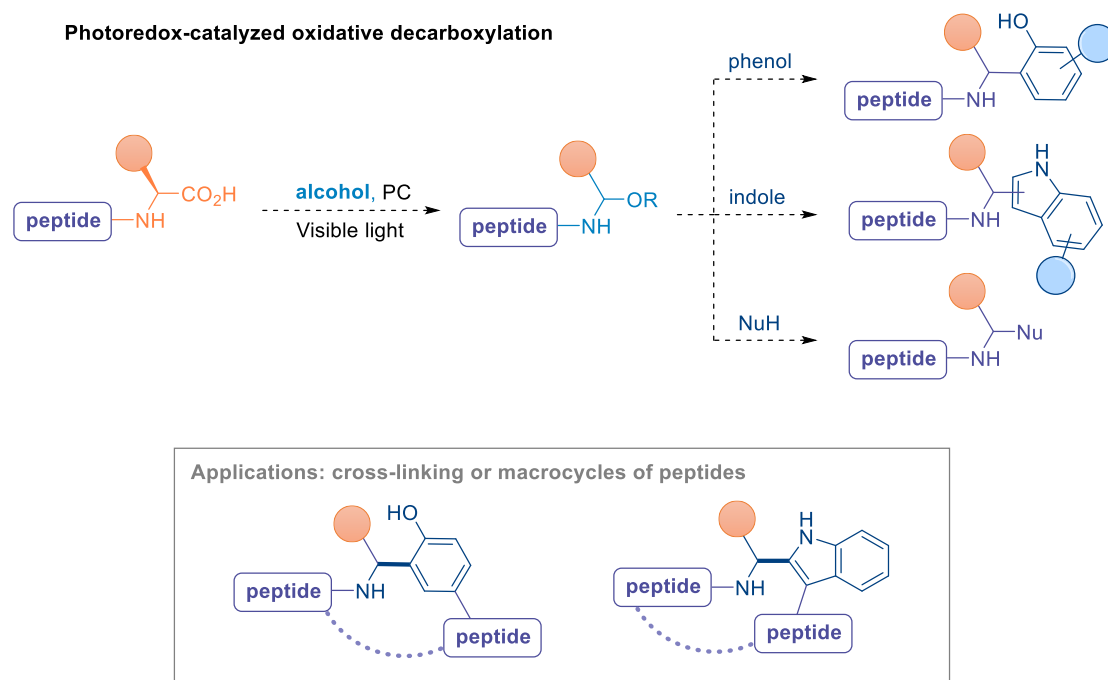
We hypothesized that **6.44** is formed through further oxidation of the α -amino radical **A** towards an intermediate iminium **B**, followed by water addition to **6.44** (Scheme 73). If this mechanism is unlikely in presence of EBX reagents because of their oxidative potential, previous computations carried out by our group demonstrated that in the presence of CBX (**2.7**), such a transformation is feasible (Section 2.3.3).^[184] *N,O*-acetals were indeed observed in the photoredox catalyzed decarboxylative cyanation study from our group, with addition of water. We thus wondered whether this result could be optimized and exploited for a valuable C-terminal peptides functionalization. To the best of our knowledge this approach had not been explored on peptides in photoredox catalysis prior to this study.

¹⁷ This project was carried out as a collaborative work with Elliott Le Du who is sincerely thanked for his precious help by taking over the experimental work at the early stage of the scope. *Manuscript in preparation.*



Scheme 73: General principle of photoredox-catalyzed decarboxylative hydroxylation

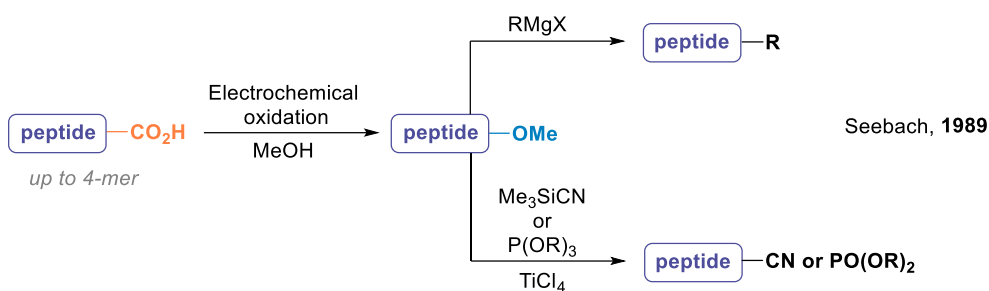
The relevance of C-terminal bioconjugation methods has been described in Section 2.1.4. Introduction of alcohols would be highly valuable as peptides *N,O*-acetals have not been intensively investigated. If some reports have been disclosed on C-C bond formation, C-O bond have only been reported with simple alcohols. This would provide a novel scaffold which can be investigated in drug discovery (Scheme 74). In terms of experimental practicability, using alcohols as reagents is quite convenient as it doesn't require prefunctionalization from either commercially available or easily accessed compounds. In addition, one can envision to use the inherent instability of *N,O*-acetals for pro-drugs development or release of fluorophores, for instance.^[294] Under mild acidic conditions the alcohol counter-part will indeed be released at an equilibrium, which kinetics depends of the substitution and can be engineered.^[295] The formed iminium intermediate could also be trapped with different nucleophiles and form stable adducts by C-C bond formation. This would provide a whole new class of C-terminal functionalized peptides. In particular, the compatibility of phenols and indoles would be highly valuable as possible extension towards the cross-linking of peptides can be envisioned. Those scaffolds have not been reported to date and would consist of a novel platform for peptides drug discovery. Macrocycles synthesis would also be a key application due to the current interest in this field (Section 2.1.1).



Scheme 74: Goal of the project of photoredox-catalyzed decarboxylative oxidation

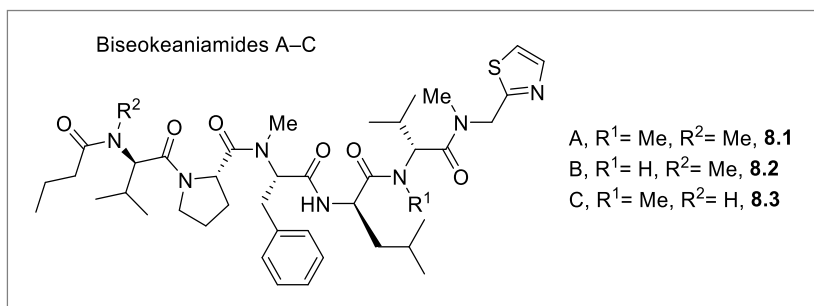
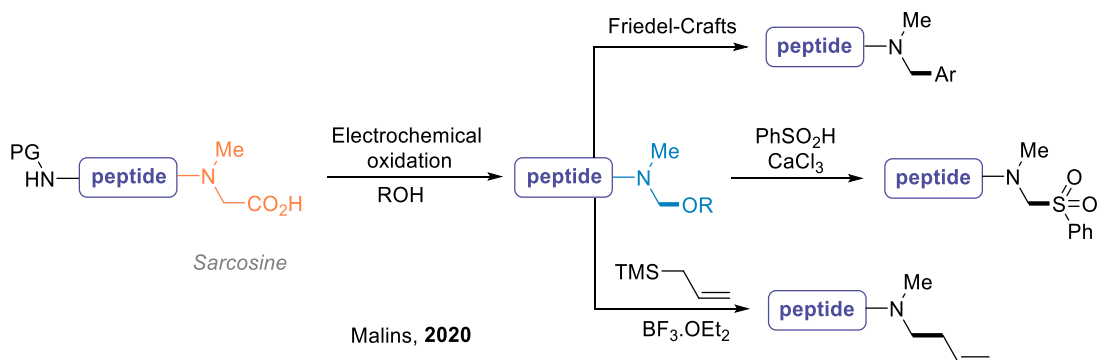
8.1.2 Hofer–Moest reaction

Oxidative decarboxylation has been known and studied since the early days of electrochemistry.^[296] The Kolbe electrolysis describes the electrochemical decarboxylation of carboxylic acids, following the seminal work from Kolbe in 1849.^[297] The main limitation of the strategy is the required high current densities, which diminishes the functional group tolerance. Dimerization is the favored pathway. When further oxidation to form a cation followed by trapping by water occurs, the reaction was called Hofer-Moest. Numerous reports have been disclosed, in particular Seebach and coworkers exploited this strategy on peptides C-terminus in 1989 (Scheme 75).^[298] Starting from N-terminal protected peptides up to tetramers, electrochemical decarboxylation afforded N,O-acetals with methanol. Reactivity of the latter with Grignard reagents as well as in Michaelis-Arbuzov reactions was investigated, providing elegant C_{sp3}-C_{sp3} and C_{sp3}-P bond formation. However, it is good to note that no functional group tolerance was studied on the peptides and that the only non-alkyl residue present in this study was serine. This concept was later exploited towards the synthesis of sulfones and phosphonium salts from α -amino acids.^[299,300]



Scheme 75: Seminal work from Seebach on electrochemical decarboxylation

During the course of our work, the Malins group disclosed a novel study extending this approach to more complex peptides.^[301] The development of an electrochemical oxidative decarboxylation–nucleophilic addition was key towards the access of natural peptides Biseokeaniamides A to C (**8.1** to **8.3**). Starting from native peptides, *N,O*-acetals were first targeted as intermediates. Further reaction with electron-rich aromatics or organometallic reagents afforded the desired and highly valuable C-terminal modified peptides. This strategy was successfully applied to the synthesis of analogs from natural peptides to study the activity. Only C-terminal sarcosine, an *N*-methylated amino acid, derived peptides were studied for this total synthesis oriented study and the functional group tolerance was not disclosed beyond aliphatic and aromatic amino acids. A more general approach would thus still be valuable for complex peptides with natural amino acids at the C-terminal position.

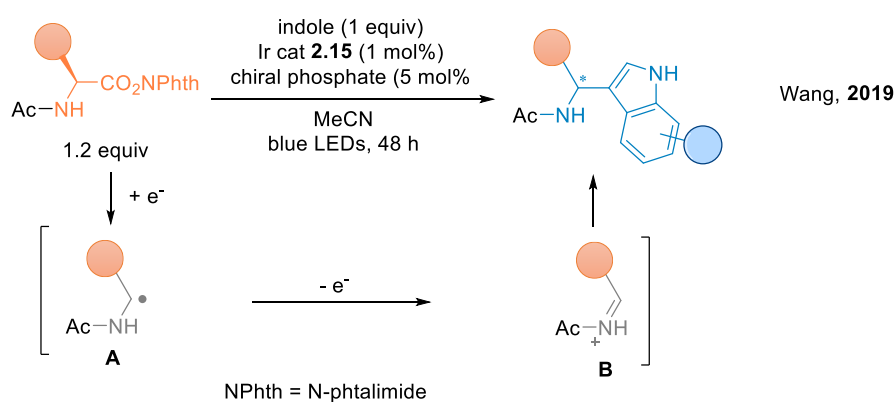


Scheme 76: Electrochemical oxidative decarboxylation from the Malins group

8.1.3 Decarboxylative oxidation and dehydrogenative strategies in photoredox catalysis

Previous reports in photoredox catalysis can be classified into two main categories, either through decarboxylative strategies or dehydrogenative strategies on glycine derivatives. Photoredox-catalyzed decarboxylative reactions on peptides towards C-C bond formation such as arylation or alkylation have already been described in Section 2.3. This section will be dedicated to reports on amino acids or aliphatic acids.

During our investigations, an elegant approach was described by Wang and coworkers (Scheme 77).^[302] Starting from redox-active esters (RAEs) of α -amino acids, photoredox-catalyzed decarboxylation followed by further oxidation afforded iminium intermediates **B**, which efficiently reacted with indoles. Enantioenriched products were obtained through the use of chiral phosphate catalysts in this asymmetric Friedel-Craft. This transformation was not extended to peptides and the need of prefunctionalization of carboxylic acids would render selectivity between acids in native peptides difficult to achieve.

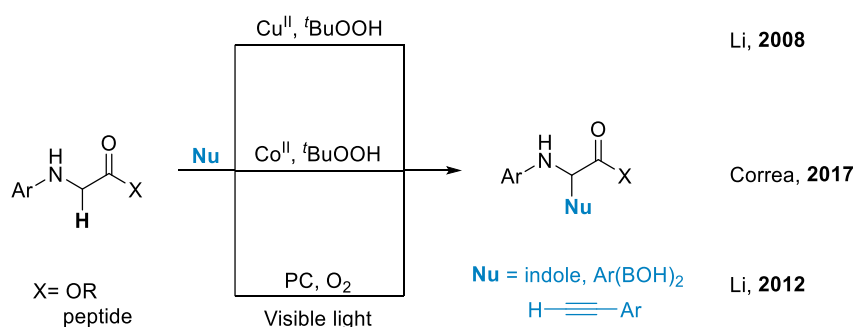


Scheme 77: Photoredox-catalyzed decarboxylative asymmetric Friedel-Crafts from RAEs

Photocatalytic decarboxylative hydroxylation has been described on aliphatic carboxylic acids by Xiao and coworkers.^[303] Interestingly, in that case the intermediate radical was trapped directly by molecular oxygen. Decarboxylative acetoxylation of aliphatic carboxylic acids has been reported by Tunge and coworkers.^[304] The acetate group source was in that case copper (II) acetate.

Literature precedents on the addition of a nucleophile to an iminium, belonging to an amino acid or peptide, mostly focus on the oxidation of glycine derivatives (Scheme 78).^[305]

Seminal work was achieved by Li with a copper-catalyzed cross-dehydrogenative coupling of glycine residues with incorporation of indoles, terminal alkynes and boronic acids.^[306] Similar transformations with cobalt and peroxides were also reported.^[307] With the advent of photoredox catalysis, this methodology was developed under visible-light irradiation by the Li group.^[308] However, all those reports focus on aniline derivatives. This is a major limitation as extension of those methodologies to native peptides would be quite challenging. It is good to note that the dehydrogenative couplings of tetrahydroisoquinolines has been extensively studied in photoredox catalysis.^[158] A large variety of nucleophiles have been studied, as well as various catalysts. Those results would be helpful in the rational design of reaction conditions.

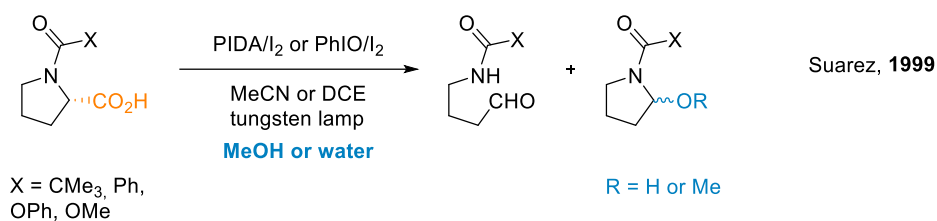


Scheme 78: C-H functionalization of glycine derivatives in radical conditions

At the time of our study, no report had been disclosed on the oxidative decarboxylation on peptides derivatives starting from free carboxylic acids in photoredox catalysis.

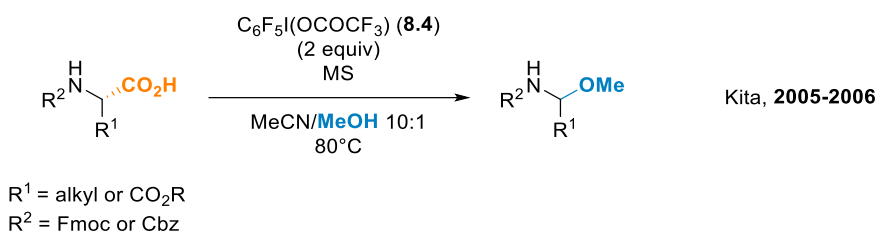
8.1.4 Decarboxylative hydroxylation with other activation methods

Decarboxylative hydroxylation strategies have been implemented using hypervalent iodine to trigger oxidation. Pioneer work was disclosed by Suarez and coworkers (Scheme 79).^[309,310] Proline derivatives were successfully converted into their *N,O*-acetals or aldehydes counterparts with a PIDA/I₂ or PhIO/I₂ system under light irradiation. This strategy was later extended to a decarboxylation-iodination-arylation process.^[311] Arylation was there performed on the corresponding hemiaminals of proline derivatives by addition of BF₃·OEt₂ and aryl reagents such as phenols.



Scheme 79: Hypervalent iodine mediated decarboxylative hydroxylation of Suarez

The oxidative fragmentation of non-cyclic α -amino acids was studied by Kita (Scheme 80).^[312,313] In that report, the activation relied on a combination of the hypervalent iodine reagent $\text{C}_6\text{F}_5\text{I}(\text{OCOCF}_3)$ (**8.4**) and heating. Only simple substrates were subjected to the reaction conditions. Interestingly, when a carboxylic acid was present on the side-chain, intramolecular cyclization occurred on the iminium intermediate.



Scheme 80: Hypervalent iodine mediated decarboxylative hydroxylation from Kita

Other modes of activation have been reported, including a copper-catalyzed decarboxylative coupling of proline derivatives with a variety of nucleophiles.^[314] Mechanistic experiments demonstrated that the reaction proceeds through an iminium intermediate. Such conditions involving strong heating (110 °C) should be avoided with peptides. Neither an extensive functional group tolerance study on the α -amino acids, nor a scope of the possible nucleophiles had been performed in the previous studies. This demonstrates the potential of a general approach to generate *N,O*-acetals under photoredox-catalysis on peptides. Further derivatization of this interesting platform would provide a valuable range of unprecedented peptides bioconjugates.

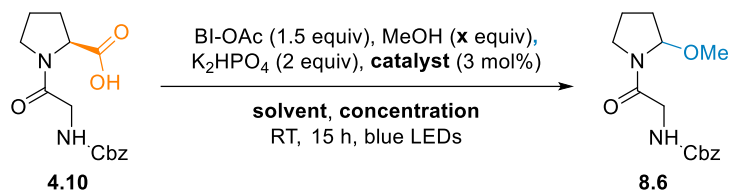
8.2 Optimization

Optimization of the reaction conditions was carried out with Cbz-Gly-Pro (**4.10**) as the model substrate as in our previous study (Section 4.1.1).^[275] Starting from the conditions of Scheme 72, the first step consisted of replacing TMS-EBX (**6.42**) by a more convenient and efficient hypervalent iodine oxidant. Following reports from Chen and Chen,^[182,315] BI-OAc (**8.5**) was screened. To our delight, 40% of the desired hemiaminal **6.44** was observed by NMR (entry 1). BI-OAc was thus a suitable oxidant. Due to the instability of **6.44**, methanol was employed for the next attempts. Under the same conditions, **8.6** could be obtained in 46% HPLC yield and 18% isolated yield (entry 2). Despite an increase of stability, it is important for isolation and analytics of such *N,O*-acetals to deactivate silica and chloroform-*d* to prevent degradation.¹⁸ Following Chen's report on the decarboxylative Minisci reaction of aliphatic carboxylic acids,^[315] we wondered whether a similar mechanism could be possible in our case. Indeed, a iodonium ester formation, followed by SET reduction towards decarboxylation, was proposed. Ru(bpy)₃.Cl₂ (**2.14**) was an efficient photocatalyst under those conditions and was thus screened in this work. To our delight, **2.14** was a suitable catalyst and **8.6** was obtained in 59% yield (entry 3). The next important parameter was the number of equivalents of methanol. For further work on more complex alcohols it would be highly desirable to decrease the required equivalents. Diminishing from 50 to 10 equivalents actually had a beneficial effect on the transformation and allowed the formation of **8.6** in 78% yield (entry 4). Simultaneously, concentrating the reaction mixture was explored for practical reasons. Switching from 10 mM to 50 mM had little influence and more concentrated conditions will be used for the rest of the study (entry 5). Lowering of the methanol amount was continued and full conversion was measured with either 5 or 2 equivalents (entries 6 and 7). For experimental reasons, 5 equivalents were employed for the rest of the optimization to ensure precise measurement. The efficiency of the transformation with as little as 2 equivalents will be valuable for further work on scope scale (section 8.4.1). With those conditions in hand, we screened several organic dyes to achieve a metal-free process. Unfortunately, neither Eosin Y (**2.17**), Rhodamine B (**6.1**) nor Rose Bengal (**8.7**) were suitable and yields from 17 to 35% were obtained with degradation of the dyes (entries 8-10). Despite its similar redox properties, 4DPAIPN (**2.22**) afforded only 45% yield (entry 11). Even if further optimization or fine-tuning of organic dyes could be envisioned, Ru(bpy)₃.Cl₂ (**2.14**) was chosen as the photocatalyst as it is commercially available and widely employed. At this stage, we were curious whether the *N,O*-acetal **8.6** could be further derivatized. Direct addition of 2 equivalents of indole in the

¹⁸ Triethylamine deactivated silica (20% in DCM) and basic alumina filtration of CDCl₃ prior to use.

reactive mixture unfortunately did not afford any desired arylation product. Following a report from our group,^[316] placing the isolated intermediate **8.6** in acetonitrile together with 1.5 equivalents of indole and TFA (1 equiv), afforded the desired product **8.8a** in quantitative conversion. Degradation was however observed during purification, future work was thus conducted using deactivated silica. This result was quite promising for our goal to derivatize *N,O*-acetal **8.6**. Unfortunately, no reaction was observed when changing the solvent to DMF. In order to provide a one-pot protocol, acetonitrile was screened as solvent for the decarboxylative oxidation step. To our delight, full and clean conversion was observed as in DMF (entry 12). As a control experiment, a reaction without the presence of K₂HPO₄ as a base was attempted. The excellent outcome demonstrated that no base was actually required for this transformation (entry 13). Interestingly, DCE can be employed as solvent without any impact on the yield (entry 14). Control experiments were carried out under conditions of entry 13 and only traces of the desired product were observed in the absence of light or catalyst. The need of a photocatalyst is a useful information mechanistically, as this indicates this transformation likely does not proceed through the same pathway as in the work from Gouverneur.^[317] In that proposed mechanism, the first step is an exchange of one acetate group from PIDA with the carboxylic acid starting material. Then, photolysis under blue-light irradiation of this hypervalent iodine intermediate triggered decarboxylation. Finally, it is good to note that 81% yield of **8.6** can still be obtained without degassing solvents (entry 15).

Table 17. Optimization of the oxidative decarboxylation on dipeptides

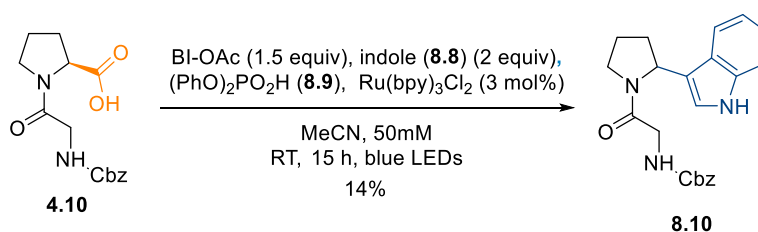


Entry	Solvent	Concentration (mM)	Catalyst	Base (equiv)	<i>x</i>	HPLC yield (%) ^a
1	DMF	10	4CzIPN (2.23)	K ₂ HPO ₄ (2)	Water (50)	40 ^b
2	DMF	10	4CzIPN (2.23)	K ₂ HPO ₄ (2)	50	46 (18) ^c
3	DMF	10	Ru(bpy) ₃ .Cl ₂ (2.14)	K ₂ HPO ₄ (2)	50	59
4	DMF	10	Ru(bpy) ₃ .Cl ₂ (2.14)	K ₂ HPO ₄ (2)	10	78
5	DMF	50	Ru(bpy) ₃ .Cl ₂ (2.14)	K ₂ HPO ₄ (2)	10	82
6	DMF	50	Ru(bpy) ₃ .Cl ₂ (2.14)	K ₂ HPO ₄ (2)	5	>95
7	DMF	50	Ru(bpy) ₃ .Cl ₂ (2.14)	K ₂ HPO ₄ (2)	2	>95
8	DMF	50	Eosin Y (2.17)	K ₂ HPO ₄ (2)	5	17
9 ^d	DMF	50	Rhodamine B (6.1)	K ₂ HPO ₄ (2)	5	27

10 ^d	DMF	50	Rose Bengal (8.7)	K ₂ HPO ₄ (2)	5	35
11	DMF	50	4DPAIPN (2.22)	K ₂ HPO ₄ (2)	5	45
12	MeCN	50	Ru(bpy) ₃ .Cl ₂ (2.14)	K ₂ HPO ₄ (2)	5	>95
13	MeCN	50	Ru(bpy) ₃ .Cl ₂ (2.14)	-	5	>95 (68) ^c
14	DCE	50	Ru(bpy) ₃ .Cl ₂ (2.14)	-	5	>95
15 ^d	MeCN	50	Ru(bpy) ₃ .Cl ₂ (2.14)	-	5	81

^a Ratio of integration at 214 nm by RP-HPLC, ^b NMR yield, ^c isolated yield green LEDs, ^d without degassing. The screening was performed on a 0.1 mmol scale.

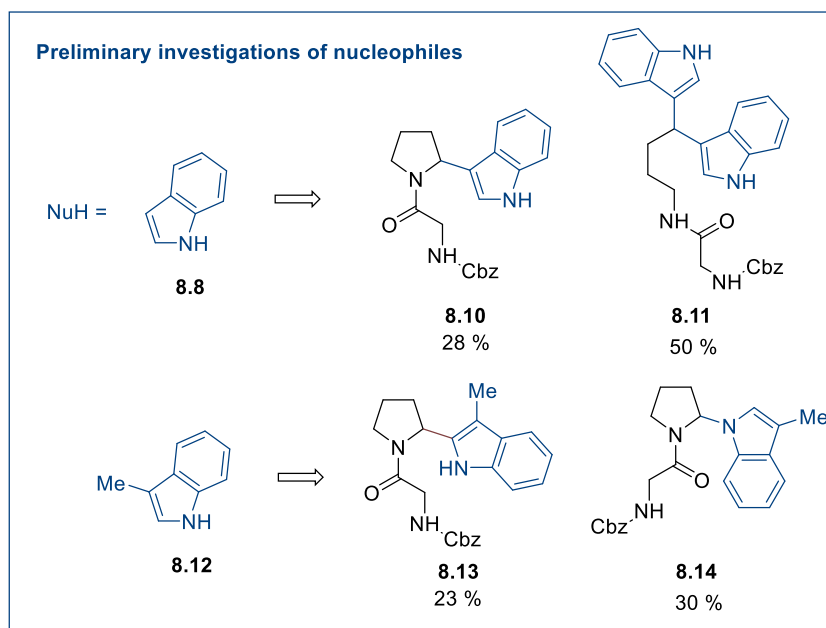
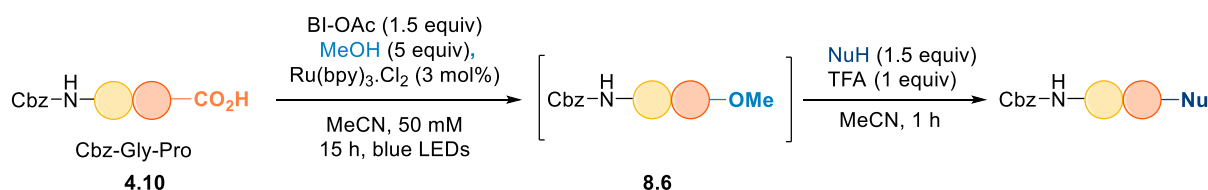
With those optimized conditions, we explored whether other nucleophiles could be suitable for an *in situ* reaction. Replacing methanol by either *p*-cresol, dimethyl malonate, phenylacetylene and CuI, or acetone with pyrrolidine did not led to any formation of the desired products.^[158] In regard of the interesting work from Wang on the decarboxylative indolization of Redox-active esters,^[302] several attempts were also carried out with phosphoric acids (Equation 34). In conditions from Table 17, entry 13, replacing methanol by indole (**8.8**) and adding 10 mol% of (PhO)₂PO₂H (**8.9**), the desired product **8.10** was observed at 14% by NMR. However, all attempts for optimization such as increasing the acid loading or adding water led to degradation. Although this pathway would be promising to develop an enantioselective transformation, those results led to its abandon at that time.



Equation 34: Attempt for indolization following Wang conditions

A sequential approach was thus investigated (Scheme 81). Following conditions reported by our group,^[316] the crude mixture was subjected to an excess of nucleophile and TFA (1 equiv) for 1 h. To our delight, full conversion was observed with indole (**8.8**) and the desired product **8.10** was isolated in 28% yield, together with a product of double addition **8.11** in 50% yield. Addition of 3-Me-indole (**8.12**) was also successful with isolation of **8.13** in 23% yield together with 30% of **8.14**, arising from the nitrogen addition. In both cases degradation was observed during purification and analysis. Further work will require deactivation of both

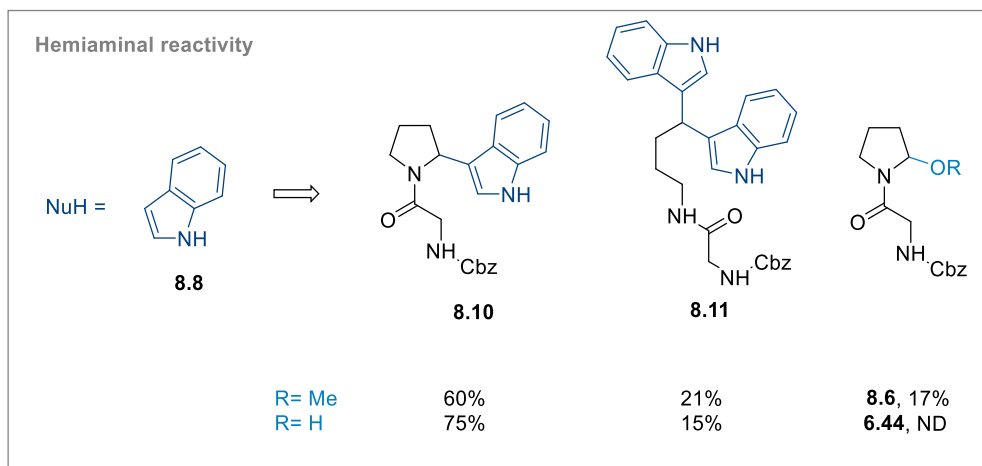
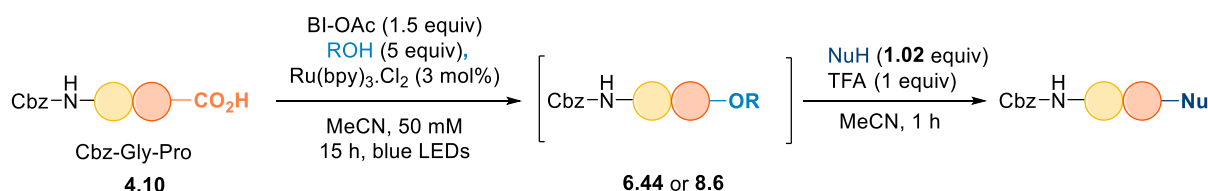
silica and Chloroform-*d*. None of the other attempted nucleophiles led to a positive outcome, especially no addition occurred with *p*-cresol (**8.15**).



The screening was performed on a 0.1 mmol scale.

Scheme 81: Preliminary investigations on a sequential approach for indole addition

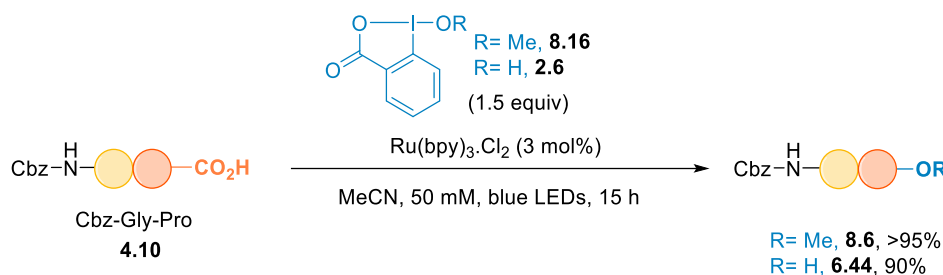
We then investigated shortly the influence of the hemiaminal nature and the acid in the reactivity with indole (**8.8**) (Scheme 82). First, decreasing the equivalents of indole (**8.8**) to only a slight excess (1.02), favored the formation of **8.10** and only 21% of the undesired double addition product **8.11** was observed. 17% of unreacted **8.6** were detected. Gratifyingly, when replacing methanol by water in those conditions, the corresponding hemiaminal **6.44** which is less stable, reacts more efficiently towards **8.10** which was obtained in 75% with no remaining **6.44** at the end of the reaction.



The screening was performed on a 0.1 mmol scale. NMR yields.

Scheme 82: Hemiaminal reactivity

Finally, we wondered whether the desired R group could be directly introduced from the hypervalent iodine reagent. BI-OMe (**8.16**) was thus synthesized following the procedure from Rao and coworkers.^[318] Starting from BI-OAc (**8.5**), simple reflux in methanol afforded BI-OMe (**8.16**) in 76% yield. **8.16** was submitted to the reaction conditions and to our delight, **8.6** was obtained without any drop of yield (Equation 35). Encouraged by this result, BI-OH (**2.6**) was also employed and afforded **6.44** in 90% NMR yield. This provides a more simple protocol for the addition of methanol and will thus be used to study the scope of the transformation. However, in the case of BI-OH (**2.6**), it is important to note that several reactions using this reagent could not be reproduced in the course of our study. This is likely due to the various purity of each batch of this reagent, due to its tendency to polymerize. Further work was thus carried out with either BI-OAc (**8.5**) or BI-OMe (**8.16**).

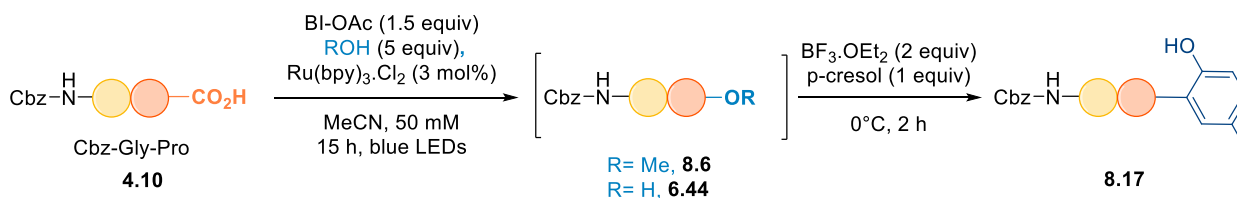


The screening was performed on a 0.1 mmol scale. NMR yields.

Equation 35: Study of BI-OR reagents reactivity in the decarboxylative oxidation

As *in situ* addition of *p*-cresol (**8.15**) was not successful, a sequential procedure was developed. Following the report from White and co-workers, reaction of hemiaminal **6.44** with *p*-cresol (**8.15**) in presence of $\text{BF}_3\cdot\text{OEt}_2$ was assessed to be a good starting point of our investigations.^[319] If a first attempt in acetonitrile led to poor conversion and degradation (Table 18, entry 1), performing the sequence in DCE, as in their report, was the key and the desired product **8.17** was obtained in quantitative yield by HPLC (entry 2). As the *N,O*-acetal with an acetyl group is even more prone to iminium formation, we wondered whether it would be possible not to add any water in the reaction mixture. This hypothesis was confirmed and **8.17** was obtained in quantitative yield (entry 3). A control experiment without addition of $\text{BF}_3\cdot\text{OEt}_2$ demonstrated its role (entry 4). According to previous reports, it is possible to introduce indoles under similar conditions with Lewis acids.^[320,321] In order to provide a unified procedure, both indole (**8.8**) and 3-Me-indole (**8.12**) were subjected to the reaction conditions from entry 3. Unfortunately, both cases led to decomposition and no desired product was obtained. Future work will thus be carried out with different procedure depending on the nature of the aryl group to introduce on the peptides.

Table 18: Optimization for *p*-cresol (x) addition



Entry	Solvent	Alcohol (x)	Other	HPLC yield
1	MeCN	Water (2)	-	Low conversion
2	DCE	Water (2)	-	>95%
3	DCE	No	-	>95%
4	DCE	No	No LA	<5%

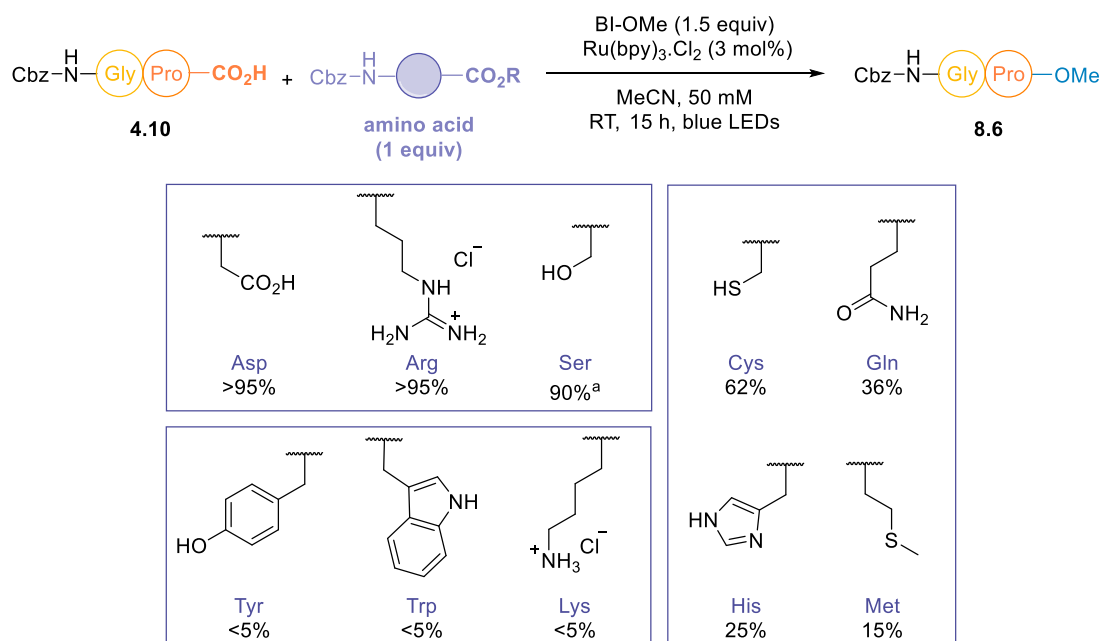
5	DCE	No	Indole	Decomposition
6	DCE	No	3-Me-indole	Decomposition

The screening was performed on a 0.1 mmol scale.

Several optimized conditions have been developed depending on the desired outcome of the transformation. If the decarboxylative hydroxylation can be performed both in acetonitrile and DCE with various hypervalent iodine reagents, the *in situ* arylation reaction requires a judicious choice of conditions. The exploration of the scope was thus performed with different conditions depending of the target products.

8.3 Robustness tests

As in Section 6.3.3, the functional group tolerance was assessed by a robustness test.^[270] Quenching experiments were performed to evaluate the tolerance towards the functional groups of the amino acids side-chains. Under the optimized conditions set-up with Cbz-Gly-Pro (**4.10**) as the starting material, one equivalent of C- and N-terminal protected amino acid was added (Scheme 83). Very interestingly, the presence of aspartic acid had no influence on the reaction outcome and **8.6** was still obtained in quantitative yield. This is an important result regarding the selectivity of this transformation. Gratifyingly, both arginine and serine were very well tolerated. In the case of serine, 10% of serine addition onto Cbz-Gly-Pro (**4.10**) was detected. This was actually employed towards the formation of cross-linking products from peptides (Section 8.4.1). The presence of a cysteine residue still afforded good yield of **8.6**. However, glutamine, histidine and methionine lowered the yield quite significantly. As expected tyrosine, tryptophan and lysine residues are effective quenchers, with complete shutdown. The reactivity of such functional groups in photoredox catalysis has been described in section 6.3.3. Those results are valuable for the future work on larger peptides as they highlight that the functional group tolerance of this transformation is quite poor. We hypothesized at this stage that the development of aqueous conditions should overcome some of those limitations. The redox potentials of several functional groups present on those residues, such as amines are directly correlated to whether they are protonated or not, and thus to the pH.^[252–256]

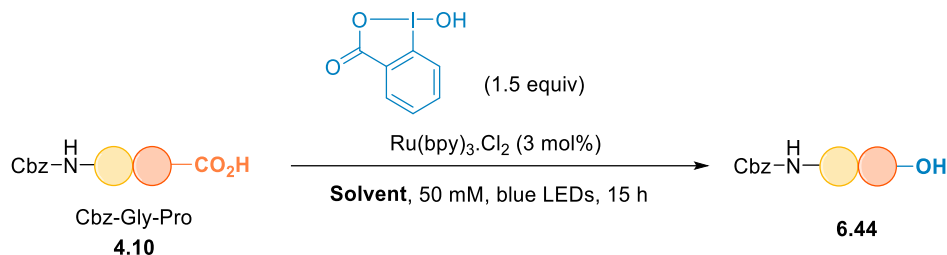


Reactions performed on a 0.1 mmol scale, HPLC yield.

Scheme 83: Side-chain functional groups tolerance

Our investigations towards the development of aqueous conditions began with the evaluation of the optimum proportion of water in the solvent. First, we wondered about the outcome of a transformation in aqueous conditions with BI-OMe (**8.16**) as a reagent. Under conditions from Scheme 83 with MeCN/water 4:1 as a solvent, **8.6** was obtained in 38% NMR yield (Table 19, entry 1). The rest of this study was thus performed with BI-OH (**2.6**) as a reagent on a 0.1 mmol scale and analyzed by NMR yield after workup. Gratifyingly, with MeCN/water 4:1 as a solvent, no difference was observed with pure acetonitrile and quantitative yield was obtained (entry 2). An equimolar ratio of 1:1 led to a slight decrease to 72% with precipitation observed (entry 3). Not surprisingly, no reaction occurs when water is the only solvent (entry 4). Encouraged by those results, buffers were tested. However, neither a cesium formate buffer at pH 3.5, nor a potassium phosphate buffer at pH 7.0, gave promising results (entries 5 and 6). Solubility appeared problematic, together with degradation in the second case. Those buffers were chosen as they were the key to good functional group tolerance in the decarboxylative Giese coupling on proteins reported by the MacMillan group.^[274]

Table 19: Optimization of the decarboxylative hydroxylation under aqueous conditions

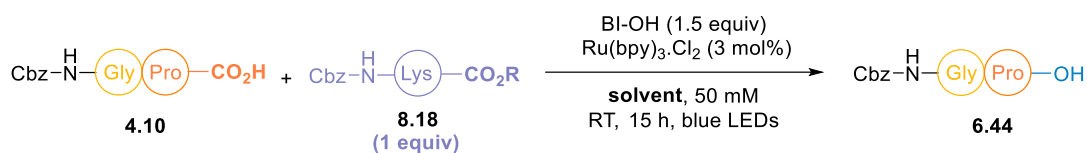


Entry	Solvent	NMR yield (%)
1 ^a	MeCN/water 4:1	38
2	MeCN/water 4:1	>95
3	MeCN/water 1:1	72
4	Water	<5
5	MeCN/Cs formate buffer 3.5, 500 mM 1:1	10
6	MeCN/K phosphate buffer 7.0, 500 mM 1:1	<5

^a With BI-OMe (8.16) as a reagent. The screening was performed on a 0.1 mmol scale.

The tolerance towards lysines was next studied under those conditions (Table 20). First, a control experiment confirmed that no reactivity was observed as well with BI-OH (2.6) as a reagent (entry 1). To our delight, when MeCN/water 4:1 was used as a solvent, **6.44** was obtained in 65% NMR yield (entry 2). Increasing slightly the proportion of water was not beneficial (entry 3). Further attempts with either a higher catalyst loading (entry 4) or with more equivalents of hypervalent iodine (entry 5) did not improve the yield of **6.44** neither. Nevertheless, this dramatic increase for lysine tolerance is very valuable due to its abundance, together with the N-terminal extremity. Unfortunately when tyrosine, tryptophan and histidine were tested under those conditions, no conversion was observed (entries 6 to 8).

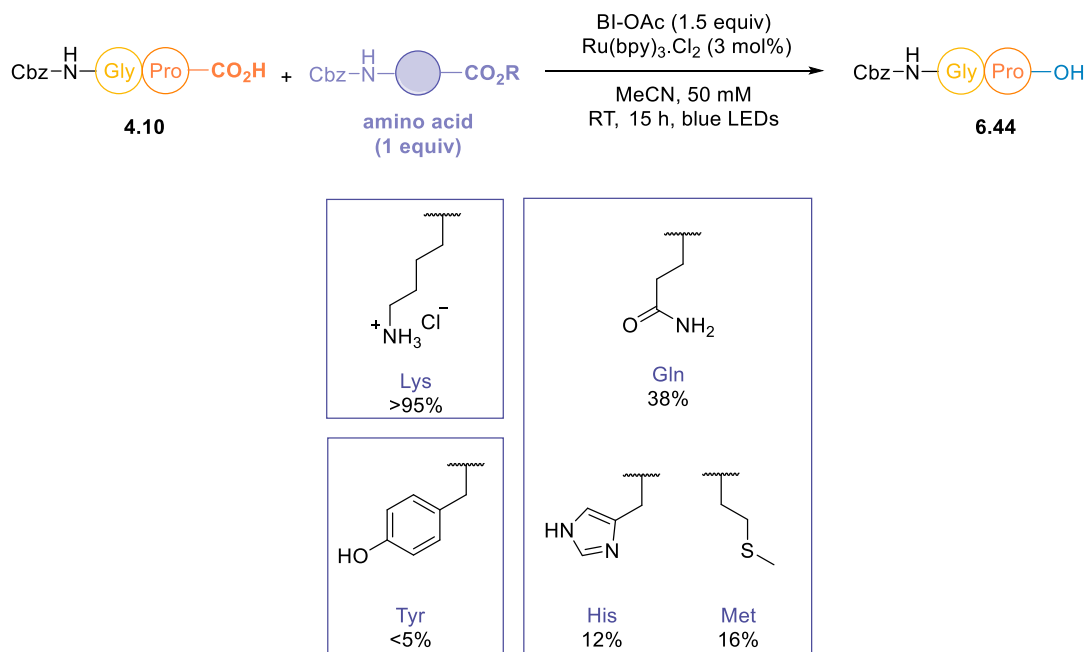
Table 20: Lysine tolerance in aqueous conditions for decarboxylative hydroxylation



Entry	Solvent	Modification	NMR yield (%)
1	MeCN	-	<5
2	MeCN/water 4:1	-	65
3	MeCN/water 2:1	-	54
4	MeCN/water 4:1	5mol% catalyst	70
5	MeCN/water 4:1	2 equiv BI-OH	60
6	MeCN/water 4:1	Cbz-Tyr-OMe	<5
7	MeCN/water 4:1	Cbz-Trp-OMe	<5
8	MeCN/water 4:1	Cbz-His-OMe	<5

The screening was performed on a 0.1 mmol scale.

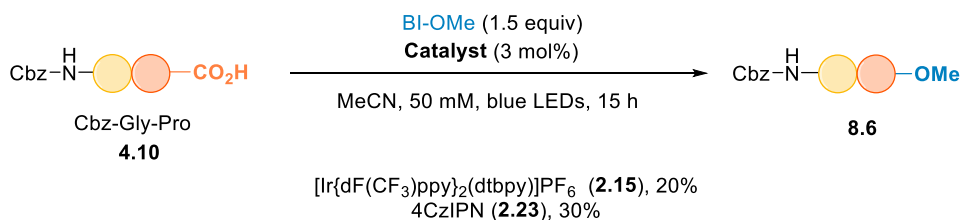
As discussed in section 0, reproducibility problems were encountered when BI-OH (**2.6**) was employed as a reagent. The functional group tolerance in aqueous conditions was thus doubled using BI-OAc (**8.5**), in order to confirm the previous results (Scheme 84). If quantitative yield of **6.44** was obtained in the presence of protected lysine **8.18**, all other residues demonstrated similar behavior that in pure acetonitrile as a solvent.



The screening was performed on a 0.1 mmol scale.

Scheme 84: Functional group tolerance under aqueous conditions with BI-OAc (**8.5**)

Our last hypothesis was to screen different photocatalysts to achieve a better functional group tolerance, as we observed in our previous work on the decarboxylative alkynylation (Section 6.4.2). Unfortunately, neither [Ir{dF(CF₃)ppy}₂(dtbpy)]PF₆ (**2.15**), nor 4CzIPN (**2.23**), were suitable catalysts for this transformation and very low conversion was observed in both cases (Equation 36).



The screening was performed on a 0.1 mmol scale. NMR yields.

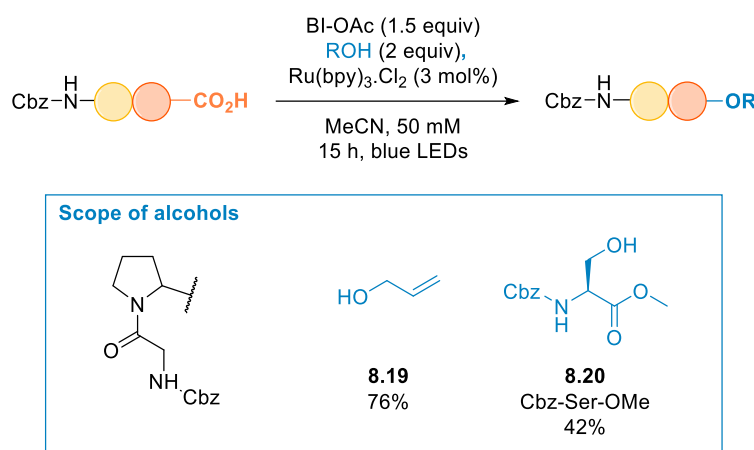
Equation 36: Photocatalyst screening for the synthesis of **8.6**

As a conclusion of those results, it appears that apart from non-functionalized residues, only arginine, aspartic acid, serine and cysteines are well tolerated under the reaction conditions. Aqueous conditions can be employed when lysines are present. Further work will thus be carried out on relatively simple peptides. For complex substrates, a possible approach is to perform this transformation on the protected peptide directly after SPPS. This will be described in section 8.6.

8.4 Dipeptides and nucleophiles scope¹⁹

8.4.1 Scope of alcohols

The scope of alcohols was studied on the model substrate Cbz-Gly-Pro (**4.10**) under conditions from Table 17. Clean and full conversion towards the desired product was observed in the crude reaction mixture by either RP-HPLC or NMR and the lower yields are mostly due to the instability of the products (Scheme 85). Allylic alcohol was a suitable reagent towards **8.19**. Cross-linking of peptides can be achieved with Cbz-Ser-OMe (**8.21**) to the desired product **8.20** in good yield. All compounds were purified on deactivated silica and analyzed in neutralized Chloroform-*d*. We envision that such scaffolds could be tested as prodrugs due to this lack of stability. A large scope of alcohols was thus investigated (Section 8.6).



Reactions performed on a 0.3 mmol scale, isolated yields.

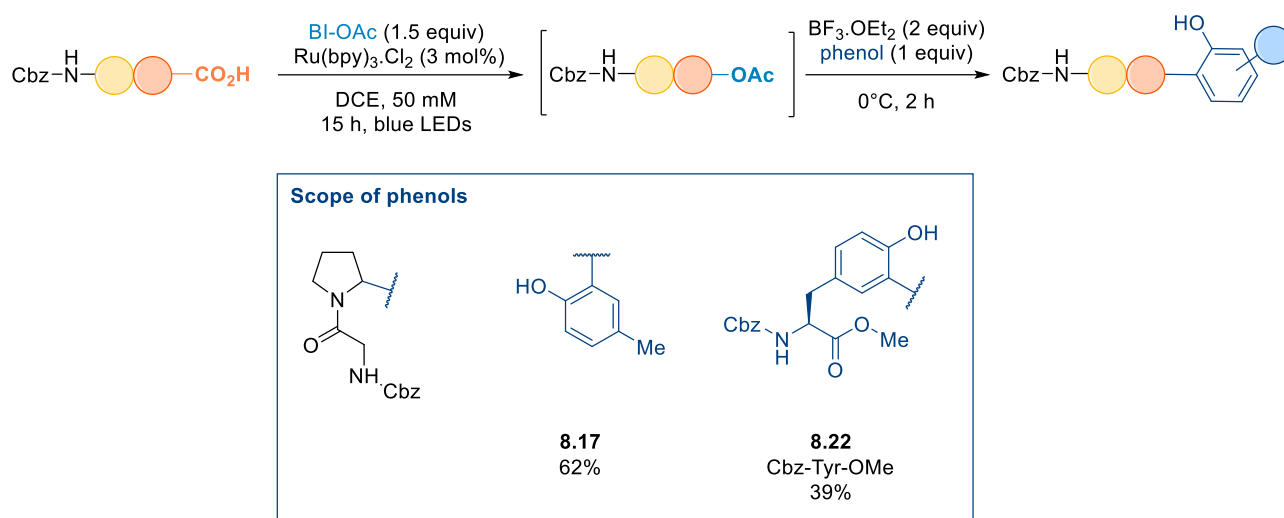
Scheme 85: First part of the scope of alcohols with Cbz-Gly-Pro (**4.10**)

8.4.2 Scope of phenols

The scope of phenols was then explored with Cbz-Gly-Pro (**4.10**) as the model substrate (Scheme 86). An electron-rich phenol such as *p*-cresol was well tolerated (**8.17**). As in the work from the White group, *ortho* selectivity was observed.^[319] Within our aim to generate cross-linking products from peptides, efficient addition of tyrosine residues was quite important. To our delight, reaction with Cbz-Tyr-OMe (**8.23**) afforded **8.22** in 39% yield, establishing a

¹⁹ Only scope entries performed personally are presented. The majority of the scope experimental work was achieved by Elliott Le Du and is summarized in the outlook section.

proof of concept. This good result allowed us to envision future development of this transformation towards cross-linking of peptides.

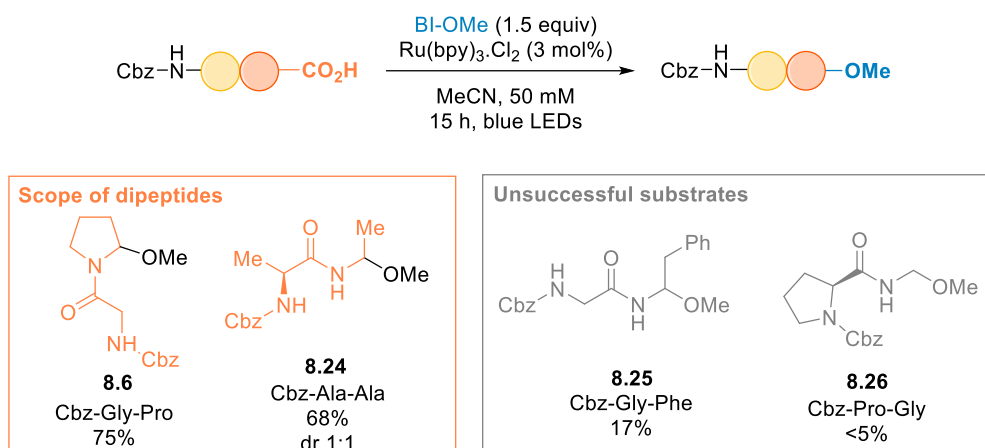


Reactions performed on a 0.3 mmol scale, isolated yields.

Scheme 86: First part of the scope of phenols with Cbz-Gly-Pro (**4.10**)

8.4.3 Scope of dipeptides

The reactivity of various α -amino acids at C-terminal position was evaluated through a short dipeptide scope with conditions from Equation 35 (Scheme 87). Our model dipeptide Cbz-Gly-Pro (**4.10**) demonstrated excellent reactivity and **8.6** was obtained in 75% yield. A similar outcome was obtained starting with Cbz-Ala-Ala (**6.4**) to form **8.24** in 68%. However, when turning to Cbz-Gly-Phe (**6.5**) or Cbz-Pro-Gly (**8.27**), despite excellent conversions measured by RP-HPLC, **8.25** was obtained only in very low yield and **8.26** not isolated at all. Those *N,O*-acetals are probably too unstable. This is why it was decided to perform directly the arylation step with phenols on those unstable intermediates, as discussed in Section 8.6.

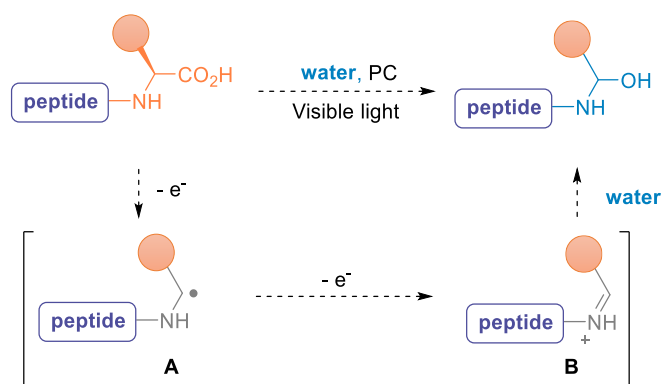


Reactions performed on a 0.3 mmol scale, isolated yields.

Scheme 87: Scope of dipeptides

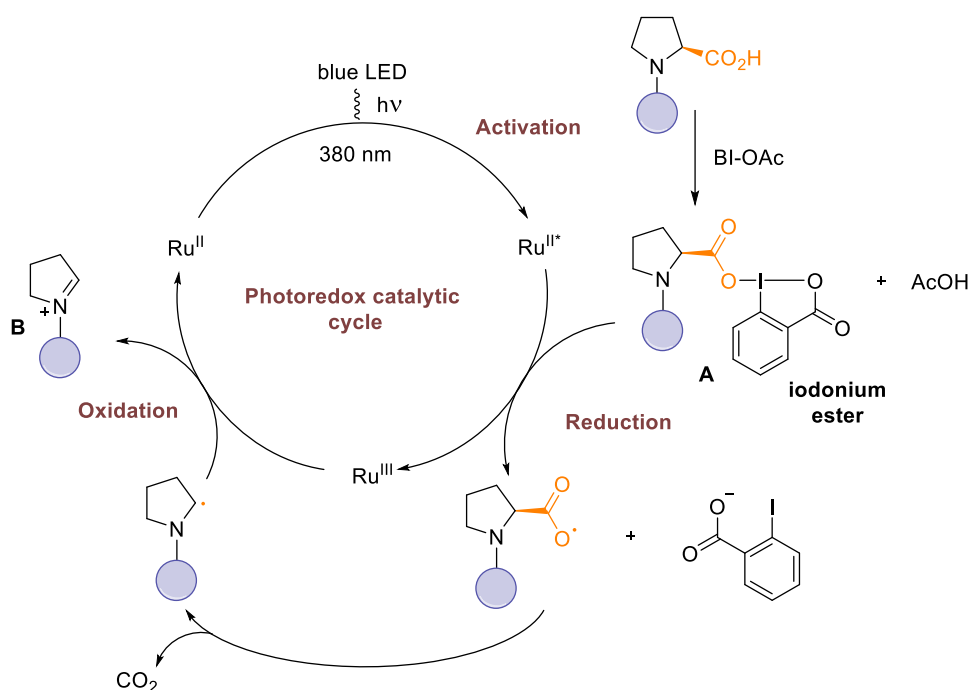
8.5 Possible mechanism

The mechanism of this transformation can seem quite simple at first sight (see Scheme 88 and section 8.1.1): SET from the excited state of the photoredox catalyst to the amino acid carboxylate, triggering decarboxylation towards the α -amino radical **A** as in previous studies.^[275] Further oxidation towards the iminium intermediate **B**, which can be trapped by water or alcohols would afford the observed *N,O*-acetals. However, both experimental observations as well as previous reports highlight that the actual pathway could be quite different with the active oxidant species being unknown.



Scheme 88: General principle of photoredox-catalyzed decarboxylative hydroxylation

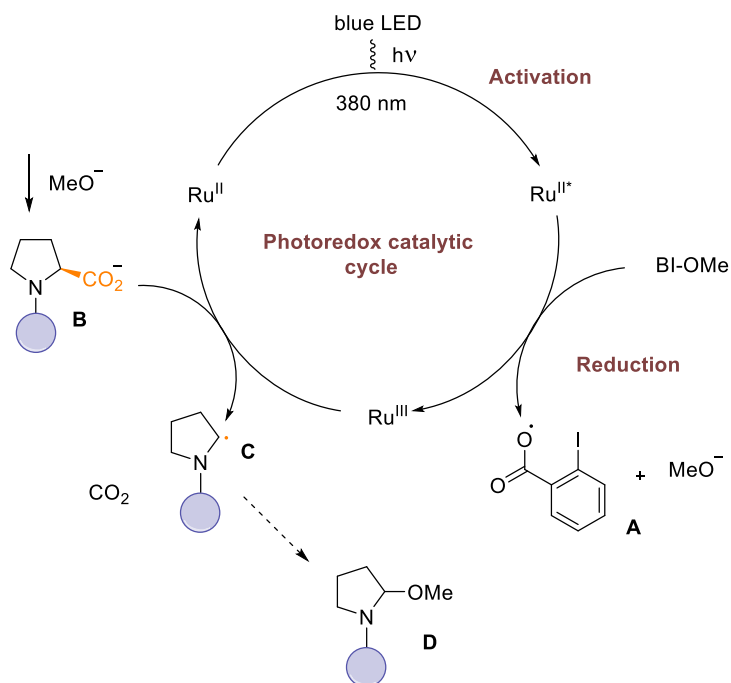
First, according to Chen and Chen works,^[182,315] decarboxylation could arise from SET mediated reduction of a iodonium ester **A** (Scheme 89). This step has been proposed using $\text{Ru}(\text{bpy})_3\text{Cl}_2$ (**2.14**) as a photocatalyst ($E_{1/2} \text{Ru}^{\text{III}}/\text{Ru}^{\text{II}*} = -0.81 \text{ V}$). No redox potentials of iodonium esters has been reported to date, but Chen and coworkers described similar yields starting directly from isolated iodonium esters instead of carboxylic acids.^[315] Unfortunately, our attempts to generate **A** type derivatives were not successful so far. Their isolation and study by cyclic voltammetry and Stern-Volmer analysis would provide key information. In that case, closing of the catalytic cycle would arise from SET from the oxidized catalyst Ru^{III} to generate iminium **B**. Examples have been found in literature on similar substrates.^[322–324] This pathway seems to us as the most likely. However, the selectivity observed between the proline and side-chain aspartic acid, together with the absence of reactivity of serine derivatives is questioning the formation of the iodonium ester intermediate (Sections 8.3 and 8.4.3). Alcohols have indeed been reported to follow a similar pathway.^[325]



Scheme 89: Possible mechanism of the decarboxylative hydroxylation through a iodonium ester intermediate

Many reports also present the reductive activation of BI-OR type reagents.^[315,322] Upon SET, fragmentation occurs to generate **A** together with the corresponding counter-ion. The formed $\text{Ru}(\text{III})$ is then capable of oxidizing the α -amino acids carboxylates, even the one derived from glycine ($E_{1/2} \text{Ru}^{\text{III}}/\text{Ru}^{\text{II}} = 1.29 \text{ V}$). How the final product of the process **D** would be generated from α -amino radical **C** is not fully understood at this stage. One can think of

involvement of another catalytic cycle, with reduction of iodosyl radical **A**, and oxidation of the generated α -amino radical to form the corresponding iminium. The SET reduction of BI-OR reagents can also serve as an activation step occurring catalytically to initiate the actual cycle.



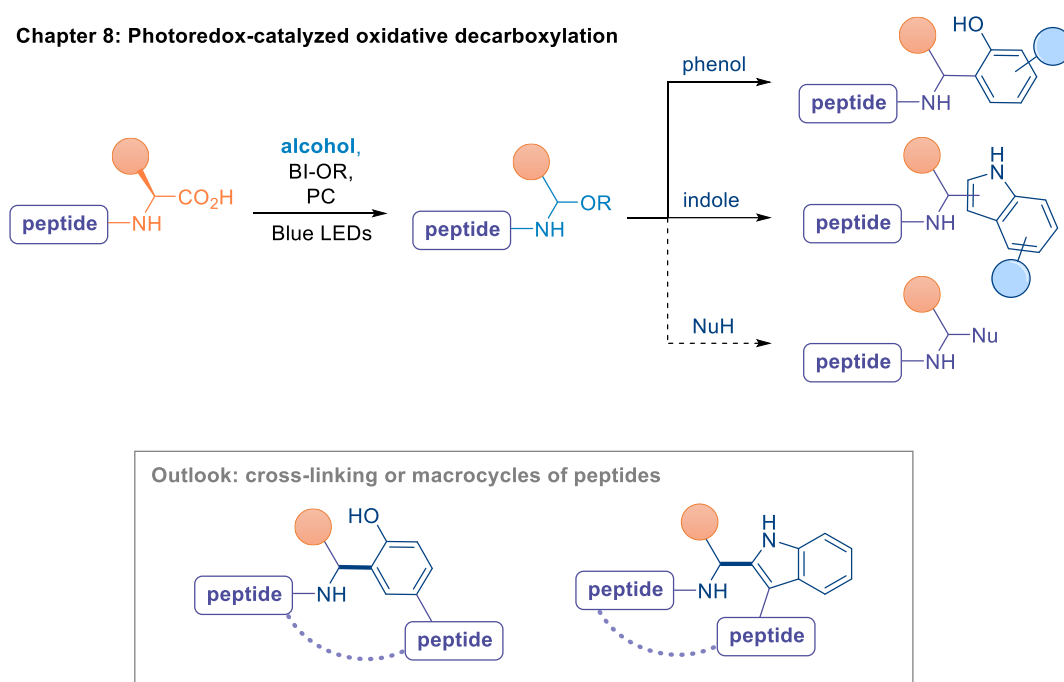
Scheme 90: Possible mechanism through activation of BI-OR reagents

Current investigations have not allowed to conclude on any mechanism. Experiments will be carried out as a future work to better understand this transformation.

8.6 Conclusion and outlook

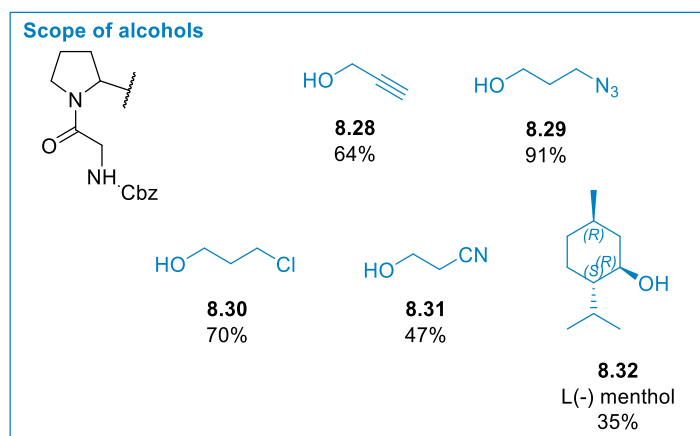
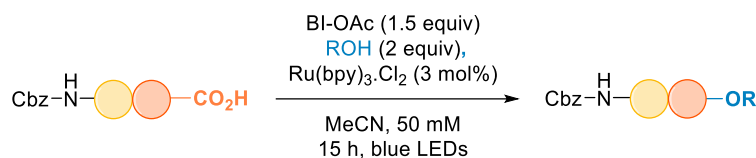
This project took place within the general aim of this thesis to provide novel methods for peptides C-terminal modification. Our photoredox-catalyzed decarboxylative strategy was extended towards the introduction of diverse functional groups on peptides. From isolation of hemiaminal **6.44** as a side-product in our previous photoredox-catalyzed decarboxylative alkynylation on peptides, this reaction was optimized for a novel peptides C-terminal modification methodology (Scheme 91). This transformation proceeds by oxidation of α -amino radicals formed by decarboxylation, further converted into *N,O*-acetals through an iminium formation. The application of this concept on peptides was unprecedented in photoredox catalysis although known in electrochemistry. Under those conditions, functionalization with

valuable alcohols was successful. As an extension, the inherent instability of such *N,O*-acetals could be later investigated for pro-drugs development with controlled release of bioactive alcohols. In this work, *N,O*-acetals were also employed as key intermediates towards arylation reactions with phenols and indoles. Especially, tyrosine and tryptophan derivatives were synthesized. Those results were an important proof of concept for our goal to access a novel class or cross-linked peptides. The moderate functional group tolerance from the side-chains residues suggests that it would be challenging to extend this methodology towards large native peptides. This study was thus more focused on small peptide functionalization, with the generation of bioconjugates with bioactive compounds and with derivatization towards cross-linking and macrocycles.



Scheme 91: Conclusion of the photoredox-catalyzed decarboxylative oxidation in chapter 8

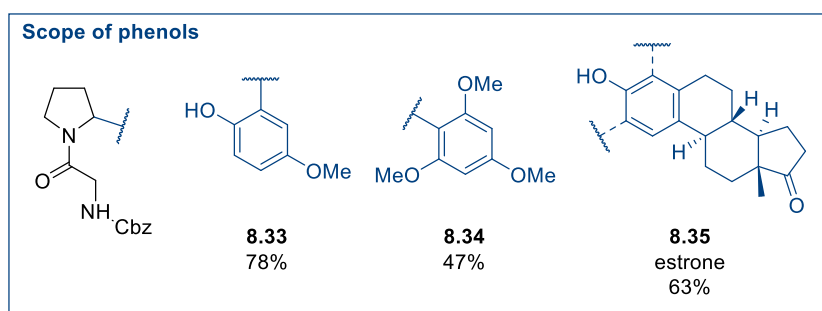
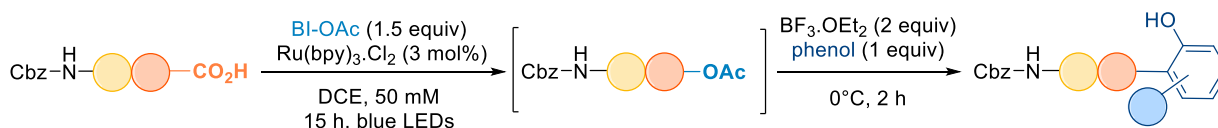
The experimental work on this project was further continued by Elliott Le Du and is still ongoing. An overview of the main important scope results is presented here to have a better vision of the project at the time of this manuscript. Regarding alcohols, bioorthogonal groups such as a free alkyne or an azide can be introduced (**8.28** and **8.29**). A chlorine atom and a cyano group on an alkyl chains were well tolerated as well (**8.30** and **8.31**). Introduction of the valuable L-menthol afforded a lower yield (**8.32**), but this remains an interesting result.



Reactions performed on a 0.3 mmol scale, isolated yields.

Scheme 92: Selection of the scope of alcohols with Cbz-Gly-Pro (**4.10**)

Electron-rich aryls such as *p*-methoxyphenol or 1,3,5-trimethoxybenzene were well tolerated (**8.33** and **8.34**). Interestingly, a complex phenol such as estrone could be introduced in good yield, leading to the interesting bioconjugate **8.35**.

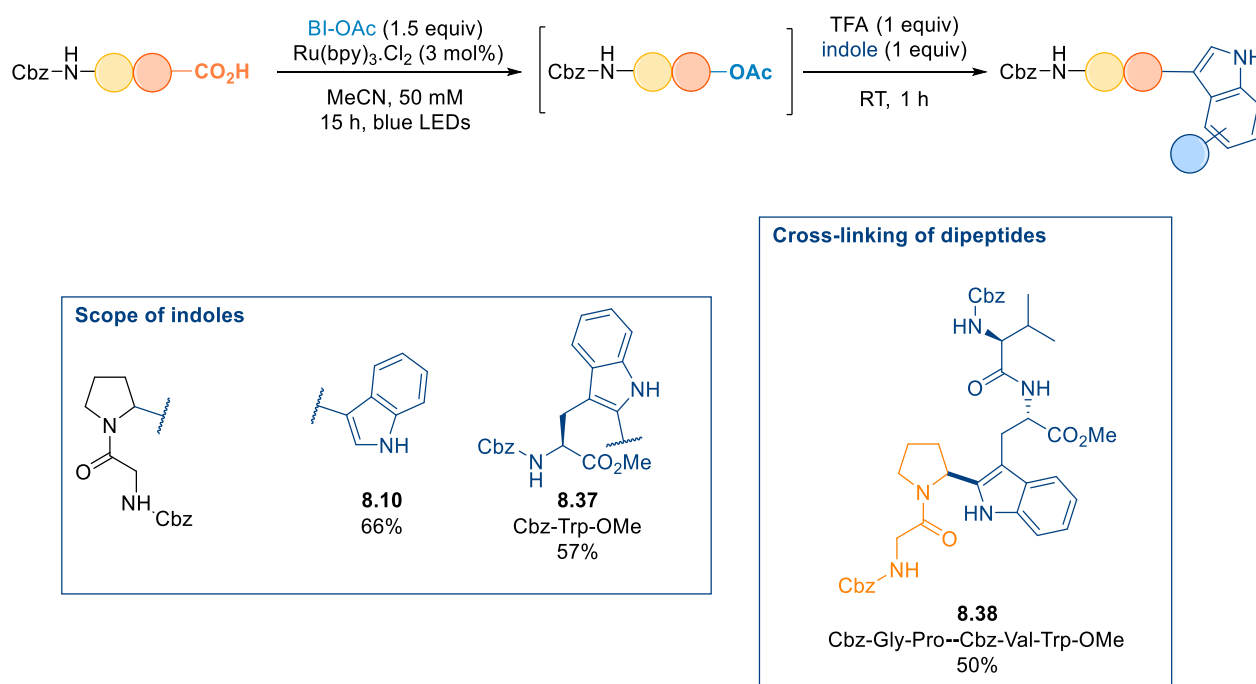


Reactions performed on a 0.3 mmol scale, isolated yields.

Scheme 93: Selection of the scope of phenols with Cbz-Gly-Pro (**4.10**)

The scope of indoles was investigated next (Scheme 94). Under the optimized conditions from Scheme 82, indole derived product **8.10** was isolated in good yield. Another proof of concept towards the cross-linking of peptides was obtained with Cbz-Trp-OMe (**8.36**) which was successfully introduced on Cbz-Gly-Pro (**4.10**) to form **8.37**. To our delight, Cbz-

Val-Trp-OMe could be added on Cbz-Gly-Pro in good yield to form the unnatural tetrapeptide **8.38**.



Reactions performed on a 0.3 mmol scale, isolated yields.

Scheme 94: Selection of the scope of phenols with Cbz-Gly-Pro (**4.10**)

This project is still ongoing and current efforts are focusing on the synthesis of cross-linked peptides. Especially, introduction of tyrosine-based peptides to access a novel unnatural tetrapeptide scaffold. Development of conditions suitable for the decarboxylative-oxidation of tetramers is under study. In addition of providing interesting bioconjugates, this would also allow to exploit this strategy towards macrocyclization of peptides. Future directions include further attempts towards the development of aqueous conditions and fine-tuning of photocatalysts in order to increase the functional group tolerance to render this methodology compatible with larger native peptides.

General conclusion



9 General conclusion

The aim of my thesis was to develop novel methods for the modification of peptides, and later proteins, on the carboxylic acids residues and especially the C-terminal position. Despite its high potential for the site-selective chemical functionalization of proteins, this position has not been explored intensively yet.^[2]

In the course of our investigations, we became interested by the fine-tuning of organophotoredox catalysts (chapter 5). Indeed, metal-free transformations present important advantages for biomolecule transformations. The carbazolyldicyanobenzene family was selected due to its convergent and straightforward synthesis, together with its potential in fine-tuning the redox properties.^[159] Novel derivatives of 4CzIPN (**x**) and 4DPAIPN (**x**), were presented and the measurement of their redox properties confirmed our rational design (Figure 24).^[260] Our strategy employed the variation of the electronics of the donor part of those donor-acceptor molecules. As a result, increasing the donating character of their substituents decreased their oxidation potential. Thanks to this modularity, organophotoredox catalysts are now available with reduction potentials at the excited state from +0.90 to +1.82 V vs SCE. Those catalysts were determinant to achieve high efficiency in a fragmentation cascade starting from cyclic oximes and other interesting developments have already been disclosed. At the time of this project, the field of fine-tuning the redox properties of organic dyes was only emerging and has grown dynamically since. The later extensions of the concept and the use of this library to unlock novel reactivity demonstrated the impact of this contribution.

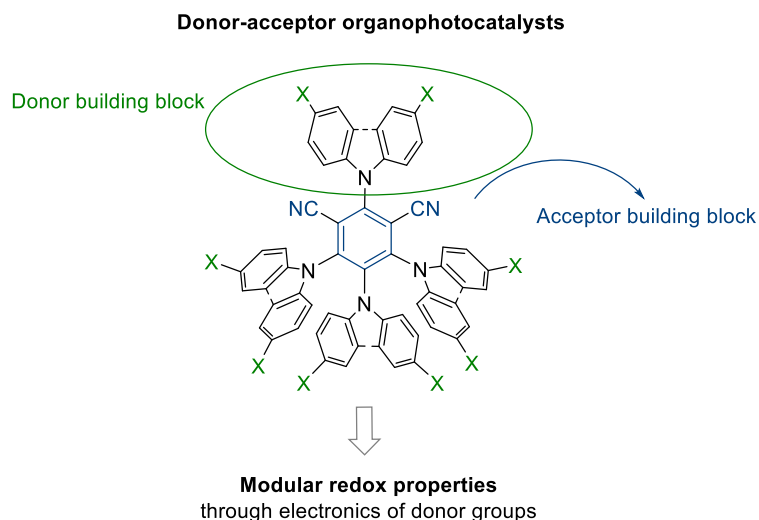


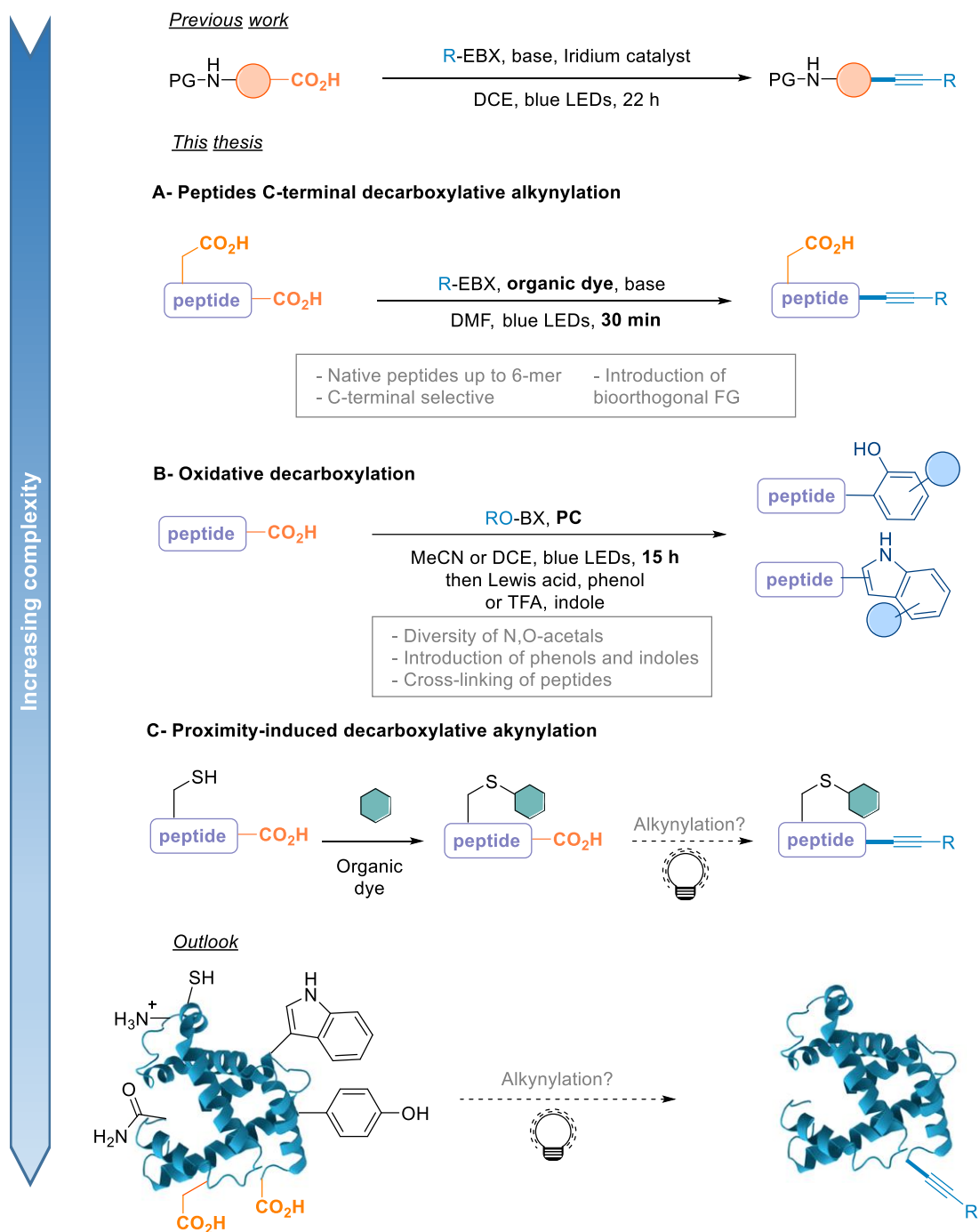
Figure 24: Conclusion on the fine-tuning of carbazolyldicyanobenzene catalysts in the thesis

Regarding our goal to develop a carboxylic acid residues labeling on proteins, our investigations started on peptides. In line with promising precedents in our group, we selected a decarboxylative strategy using photoredox catalysis.^[87] Starting from free carboxylic acids was important to us as it did not require pre-functionalization of the peptides and would consist of an important step towards protein bioconjugation. Thanks to the use of EBX hypervalent iodine reagents, alkynes were successfully introduced on peptides in DMF (Chapter 6 and Scheme 95A).^[275] Through the use of novel organic dyes, C-terminal selectivity and high chemoselectivity could be achieved. Indeed, most of amino acids side-chains were well tolerated. This methodology now provides a site-selective chemical labeling of native peptides up to hexamers. To our delight, bioorthogonal functional groups were compatible with this transformation, opening possibilities for further derivatization. This work was the first report of a decarboxylative alkynylation on complex native peptides. The field of photoredox-mediated bioconjugation was still at an early stage and only few reports had been disclosed about C-terminal functionalization of such substrates.

Unfortunately, native peptides larger than 6 residues were not compatible with the conditions developed in this first study. As attempts to develop the reaction in aqueous media were unsuccessful so far (chapter 4), another approach was envisioned to overcome this limitation. We wondered whether the concept of proximity-induced photoredox catalysis could provide the desired reactivity (Chapter 7 and Scheme 95C). To this end, the 4CzIPN (**x**) scaffold was modified towards its covalent introduction on peptides, with proteins as a longer-term goal. The cysteine residue was selected as single-site introduction position thanks to its low abundance and the availability of numerous labeling methods. This project is still ongoing but preliminary results demonstrated that the designed photoactive structure can be added on

peptides up to decamers and retain its redox properties. Future work will be dedicated to the optimization of the proximity-induced decarboxylative step first on peptides before being extended further to proteins. Such a proximity-induced photoredox-catalyzed transformation using an organophotocatalyst covalently attached on a proteins has not been reported to date. A high potential of this strategy towards site-selective protein modification is envisioned.

The last part of my thesis was dedicated to a decarboxylative-oxidation-arylation sequence (chapter 8). Indeed, after isolation of products coming from the addition of water leading to *N,O*-acetals in the previous decarboxylative alkynylation, I was interested to optimize this transformation. This would indeed provide another platform for C-terminal peptides modification. In addition, *N,O*-acetals are quite versatile compounds which can further react, for instance in Friedel Crafts reactions. Introduction of valuable alcohols was successful, as well as further arylation with phenols and indoles under acidic conditions. This approach was further extended to the cross-linking of peptides. The formed novel unnatural tetramers display a high potential for screening in drug discovery. Ongoing work is dedicated to the development of this transformation on larger peptides, as well as macrocycle synthesis.



Scheme 95: General conclusion of the thesis on the photoredox catalyzed peptides C-terminal decarboxylative strategies

Outlook

10

10 Outlook

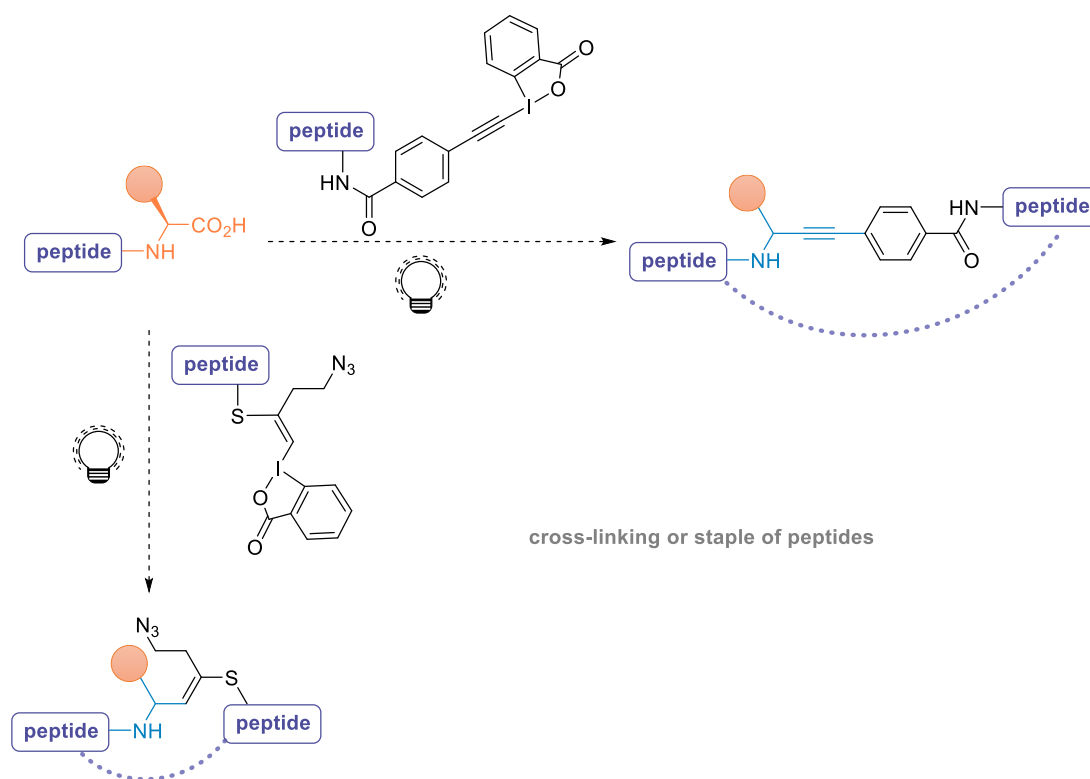
The specific outlook for chapters 7 about proximity-induced decarboxylative strategies and chapter 8 on decarboxylative oxidation have already been disclosed in the dedicated sections.

10.1 Staple and cross-linked peptides

Macrocycles and staple peptides have become highly valuable compounds in drug discovery (section 2.1.1). It can be envisioned to synthesize either staple or macrocycles peptides using the moiety introduced on the C-terminal position to react with another residue (Scheme 96). For instance, starting from either unnatural amino acids or functionalized residues, we can envision cross-coupling reactions,^[326] Glaser couplings,^[327] Click reactions,^[328] C-H activation.^[329–331] In particular, the N-terminal position or cysteines are target of choice due to their ease of site-selective functionalization. Coupling with group's methodologies such as the synthesis of thiol-VBX,^[7] or ongoing work on lysine functionalization²⁰ would afford novel scaffolds of cross-linked or staple peptides. The proposed unprecedented linked would be interesting to test for the modulation of activity and stability of peptides.

²⁰ Unpublished results from Dr Javier de Ceballos Cerrajería and Elija Grinhagena

Applications of photoredox-catalyzed peptides C-terminal decarboxylation



Scheme 96: Proposed outlook of the decarboxylative alkynylation

10.2 Optimization in aqueous media

One priority would be to resume the investigations towards conditions in aqueous media for the decarboxylative alkynylation. Possible directions to investigate are more oxidizing water-soluble photoredox catalysts, in combination with water-soluble hypervalent iodine reagents. The ones tested in this thesis were indeed not stable under the reaction conditions. Investigations towards another alkyne source can also be envisioned. Building on our expertise on the rational design of the carbazolyldicyanobenzene family, this scaffold could be further tuned for this purpose.

10.3 Design of novel organophotocatalysts

Photoredox catalysis using blue LEDs has allowed tremendous achievements. However, for long-term applications in live-cells or tissues, it would be quite important to use catalysts absorbing in longer wavelengths which are less energetic.^[33] It has been demonstrated that only red light can penetrate tissues efficiently.^[332] Red-absorbing fluorophores have been already described for imaging applications, such as Si-Rhodamines by the Johnsson group.^[48,333,334] Modifying the structures of the carbazolyldicyanobenzene family, or another scaffold, to absorb in those regions would thus be highly valuable.^[335]

11 References

- [1] J. A. Prescher, C. R. Bertozzi, *Nat. Chem. Biol.* **2005**, *1*, 13–21.
- [2] E. A. Hoyt, P. M. S. D. Cal, B. L. Oliveira, G. J. L. Bernardes, *Nat. Rev. Chem.* **2019**, *3*, 147–171.
- [3] E. M. Sletten, C. R. Bertozzi, *Angew. Chem. Int. Ed.* **2009**, *48*, 6974–6998.
- [4] D. P. Hari, P. Caramenti, J. Waser, *Acc. Chem. Res.* **2018**, 3112–3225.
- [5] J. Waser, *Synlett* **2016**, *27*, 2761–2773.
- [6] D. Abegg, R. Frei, L. Cerato, D. Prasad hari, C. Wang, J. Waser, A. Adibekian, *Angew. Chem. Int. Ed.* **2015**, *54*, 10852–10857.
- [7] R. Tessier, J. Ceballos, N. Guidotti, R. Simonet-Davin, B. Fierz, J. Waser, *Chem* **2019**, *5*, 2243–2263.
- [8] M. H. Shaw, J. Twilton, D. W. C. MacMillan, *J. Org. Chem.* **2016**, *81*, 6898–6926.
- [9] C. K. Prier, D. A. Rankic, D. W. C. MacMillan, *Chem. Rev.* **2013**, *113*, 5322–5363.
- [10] C. Bottecchia, T. Noël, *Chem. Eur. J.* **2019**, *25*, 26–42.
- [11] Z. Zuo, D. W. C. Macmillan, *J. Am. Chem. Soc.* **2014**, *136*, 5257–5260.
- [12] L. Chu, C. Ohta, Z. Zuo, D. W. C. MacMillan, *J. Am. Chem. Soc.* **2014**, *136*, 10886–10889.
- [13] F. Le Vaillant, T. Courant, J. Waser, *Angew. Chem. Int. Ed.* **2015**, *54*, 11200–11204.
- [14] S. Sharma, S. Rana, S. Sharma, *Int. J. Bioautomation* **2011**, *15*, 223–250.
- [15] H. Korhonen, A. Pihlanto, *Int. Dairy J.* **2006**, *16*, 945–960.
- [16] I. W. Hamley, *Chem. Rev.* **2017**, *117*, 14015–14041.
- [17] A. K. Sato, M. Viswanathan, R. B. Kent, C. R. Wood, *Curr. Opin. Biotechnol.* **2006**, *17*, 638–642.
- [18] A. Henninot, J. C. Collins, J. M. Nuss, *J. Med. Chem.* **2018**, *61*, 1382–1414.
- [19] K. Fosgerau, T. Hoffmann, *Drug Discov. Today* **2015**, *20*, 122–128.
- [20] N. K. Bashiruddin, H. Suga, *Curr. Opin. Chem. Biol.* **2015**, *24*, 131–138.
- [21] W. Liu, X. Wang, P.-H. Chen, J. T. Hampton, J. Tharp, C. Reed, S. Das, D.-S. Wang, H. Hayatshahi, Y. Shen, et al., *Angew. Chem. Int. Ed* **2019**, *58*, 15904–15909.
- [22] S. Bellotto, S. Chen, I. Rentero Rebollo, H. A. Wegner, C. Heinis, *J. Am. Chem. Soc.* **2014**, *136*, 5880–5883.
- [23] G. K. Mothukuri, S. S. Kale, C. L. Stenbratt, A. Zorzi, J. Vesin, J. Bortoli Chapalay, K. Deyle, G. Turcatti, L. Cendron, A. Angelini, et al., *Chem. Sci.* **2020**, *11*, 7858–7863.
- [24] A. A. Bahar, D. Ren, *Pharmaceuticals* **2013**, *6*, 1543–1575.
- [25] L. Peraro, J. A. Kritzer, *Angew. Chem. Int. Ed.* **2018**, *57*, 11868–11881.
- [26] H. Korhonen, A. Pihlanto, *Int. Dairy J.* **2006**, *16*, 945–960.
- [27] S. V. Moradi, W. M. Hussein, P. Varamini, P. Simerska, I. Toth, *Chem. Sci.* **2016**, *7*, 2492–2500.
- [28] U. Westerlind, *Beilstein J. Org. Chem.* **2012**, *8*, 804–818.
- [29] M. R. Pratt, C. R. Bertozzi, *Chem. Soc. Rev.* **2005**, *34*, 58–68.
- [30] O. Seitz, *Angew. Chem. Int. Ed* **2000**, *39*, 214–246.
- [31] T. J. Wadzinski, A. Steinauer, L. Hie, G. Pelletier, A. Schepartz, S. J. Miller, *Nat. Chem.* **2018**, *10*, 644–652.

- [32] D. T. Cohen, C. Zhang, C. M. Fadzen, A. J. Mijalis, L. Hie, K. D. Johnson, Z. Shriver, O. Plante, S. J. Miller, S. L. Buchwald, et al., *Nat. Chem.* **2019**, *11*, 78–85.
- [33] L. D. Lavis, R. T. Raines, *ACS Chem. Biol.* **2008**, *3*, 142–155.
- [34] C. J. White, A. K. Yudin, *Nat. Chem.* **2011**, *3*, 509–524.
- [35] J. R. Frost, Z. Wu, Y. C. Lam, A. E. Owens, R. Fasan, *Org. Biomol. Chem.* **2016**, 5803–5812.
- [36] L. R. Malins, J. N. Degruyter, K. J. Robbins, P. M. Scola, M. D. Eastgate, M. R. Ghadiri, P. S. Baran, *J. Am. Chem. Soc.* **2017**, *139*, 5233–5241.
- [37] S. J. McCarver, J. X. Qiao, J. Carpenter, R. M. Borzilleri, M. A. Poss, M. D. Eastgate, M. M. Miller, D. W. C. MacMillan, *Angew. Chem. Int. Ed.* **2017**, *56*, 728–732.
- [38] J. S. Davies, *J. Pept. Sci.* **2003**, *9*, 471–501.
- [39] T. A. Hill, N. E. Shepherd, F. Diness, D. P. Fairlie, *Angew. Chem. Int. Ed.* **2014**, *53*, 13020–13041.
- [40] A. A. Vinogradov, Y. Yi, H. Suga, *J. Am. Chem. Soc.* **2019**, jacs.8b13178.
- [41] P. G. Dougherty, A. Sahni, D. Pei, *Chem. Rev.* **2019**, *119*, 10241–10287.
- [42] H. N. Hoang, T. A. Hill, G. Ruiz-Gómez, F. Diness, J. M. Mason, C. Wu, G. Abbenante, N. E. Shepherd, D. P. Fairlie, *Chem. Sci.* **2019**, *10*, 10595–10600.
- [43] V. Sarojini, A. J. Cameron, K. G. Varnava, W. A. Denny, G. Sanjayan, *Chem. Rev.* **2019**, *119*, 10318–10359.
- [44] A. F. M. Noisier, J. García, I. A. Ionuț, F. Albericio, *Angew. Chem. Int. Ed.* **2017**, *56*, 314–318.
- [45] Y. Wu, Y. H. Li, X. Li, Y. Zou, H. L. Liao, L. Liu, Y. G. Chen, D. Bierer, H. G. Hu, *Chem. Sci.* **2017**, *8*, 7368–7373.
- [46] Y. H. Lau, P. De Andrade, Y. Wu, D. R. Spring, *Chem. Soc. Rev.* **2015**, *44*, 91–102.
- [47] C. D. Spicer, B. G. Davis, *Nat. Commun.* **2014**, *5*, 4740.
- [48] G. Lukinavičius, K. Umezawa, N. Olivier, A. Honigsmann, G. Yang, T. Plass, V. Mueller, L. Reymond, I. R. Corrêa, Z. G. Luo, et al., *Nat. Chem.* **2013**, *5*, 132–139.
- [49] G. Bassolino, P. Rivera-Fuentes, *Chimia (Aarau)*. **2016**, *70*, 796–799.
- [50] C. T. Walsh, S. Garneau-Tsodikova, G. J. Gatto, *Angew. Chem. Int. Ed.* **2005**, *44*, 7342–7372.
- [51] E. L. Sievers, P. D. Senter, *Annu. Rev. Med.* **2013**, *64*, 15–29.
- [52] P. Agarwal, C. R. Bertozzi, *Bioconjugate Chem.* **2015**, *26*, 176–192.
- [53] T. Carell, M. Vrabel, *Top. Curr. Chem.* **2016**, *374*, 9.
- [54] M. King, A. Wagner, *Bioconjug. Chem.* **2014**, *25*, 825–839.
- [55] K. Lang, J. W. Chin, *Chem. Rev.* **2014**, *114*, 4764–4806.
- [56] W. Liu, A. Brock, S. Chen, S. Chen, P. G. Schultz, *Nat. Methods* **2007**, *4*, 239–244.
- [57] Y. Ryu, P. G. Schultz, *Nat. Methods* **2006**, *3*, 263–265.
- [58] X. Chen, Y.-W. Wu, *Org. Biomol. Chem.* **2016**, *14*, 5417–5439.
- [59] H. C. Hang, C. Yu, D. L. Kato, C. R. Bertozzi, *Proc. Natl. Acad. Sci.* **2003**, *100*, 14846–14851.
- [60] O. Boutureira, G. J. L. Bernardes, *Chem. Rev.* **2015**, *115*, 2174–2195.
- [61] D. M. Patterson, J. A. Prescher, *Curr. Opin. Chem. Biol.* **2015**, *28*, 141–149.
- [62] L. Li, Z. Zhang, *Molecules* **2016**, *21*, 1–22.
- [63] J. C. Jewett, C. R. Bertozzi, *Chem. Soc. Rev.* **2010**, *39*, 1272.

- [64] M. L. Blackman, M. Royzen, J. M. Fox, *J. Am. Chem. Soc.* **2008**, *130*, 13518–13519.
- [65] N. K. Devaraj, R. Weissleder, S. a Hilderbrand, *Communications* **2008**, *19*, 2297–2299.
- [66] P. Destito, J. R. Couceiro, H. Faustino, F. López, J. L. Mascareñas, *Angew. Chem. Int. Ed.* **2017**, *56*, 10766–10770.
- [67] M. A. Tasdelen, Y. Yagci, *Angew. Chem. Int. Ed.* **2013**, *52*, 5930–5938.
- [68] D. M. Patterson, L. A. Nazarova, B. Xie, D. N. Kamber, J. A. Prescher, *J. Am. Chem. Soc.* **2012**, *134*, 18638–18643.
- [69] J. N. DeGruyter, L. R. Malins, P. S. Baran, *Biochemistry* **2017**, *56*, 3863–3873.
- [70] L. R. Malins, *Curr. Opin. Chem. Biol.* **2018**, *46*, 25–32.
- [71] J. Ohata, S. C. Martin, Z. T. Ball, *Angew. Chem. Int. Ed.* **2019**, *58*, 6176–6199.
- [72] J. M. Chalker, G. J. L. Bernardes, B. G. Davis, *Acc. Chem. Res.* **2011**, *44*, 730–741.
- [73] D. G. Rawale, K. Thakur, S. R. Adusumalli, V. Rai, *European J. Org. Chem.* **2019**, *2019*, 6749–6763.
- [74] K. Maruyama, M. Kanai, *Chem. Lett.* **2019**, *48*, 1421–1432.
- [75] P. K. Sasmal, C. N. Streu, E. Meggers, *Chem. Commun.* **2013**, *49*, 1581–1587.
- [76] B. Bernardim, P. M. S. D. Cal, M. J. Matos, B. L. Oliveira, N. Martínez-Saéz, I. S. Albuquerque, E. Perkins, F. Corzana, A. C. B. Burtoloso, G. Jiménez-Osés, et al., *Nat. Commun.* **2016**, *7*, 1–9.
- [77] B. Bernardim, M. J. Matos, X. Ferhati, I. Compañón, A. Guerreiro, P. Akkapeddi, A. C. B. Burtoloso, G. Jiménez-Osés, F. Corzana, G. J. L. Bernardes, *Nat. Protoc.* **2019**, *14*, 86–99.
- [78] M. L. Nielsen, M. Vermeulen, T. Bonaldi, J. Cox, L. Moroder, M. Mann, *Nat. Methods* **2008**, *5*, 459–460.
- [79] H. P. Hemantha, S. N. Bavikar, Y. Herman-Bachinsky, N. Haj-Yahya, S. Bondalapati, A. Ciechanover, A. Brik, *J. Am. Chem. Soc.* **2014**, *136*, 2665–2673.
- [80] A. N. Glazer, *Annu. Rev. Biochem.* **1970**, *39*, 101–130.
- [81] E. S. and M. G. F. Stephane Meunier, *Chem. Biol.* **2004**, *11*, 319–326.
- [82] C. Song, K. Liu, Z. Wang, B. Ding, S. Wang, Y. Weng, C. W. Chiang, A. Lei, *Chem. Sci.* **2019**, *10*, 7982–7987.
- [83] H. Ban, J. Gavriluk, C. F. Barbas, *J. Am. Chem. Soc.* **2010**, *132*, 1523–1525.
- [84] C. B. Rosen, M. B. Francis, *Nat. Chem. Biol.* **2017**, *13*, 697–705.
- [85] A. C. Conibear, E. E. Watson, R. J. Payne, C. F. W. Becker, *Chem. Soc. Rev.* **2018**, *47*, 9046–9068.
- [86] P. Dawson, T. Muir, I. Clark-Lewis, S. Kent, *Science* **1994**, *266*, 776–779.
- [87] L. R. Malins, *Pept. Sci.* **2018**, *110*, e24049.
- [88] T. Qin, J. Cornella, C. Li, L. R. Malins, J. T. Edwards, S. Kawamura, B. D. Maxwell, M. D. Eastgate, P. S. Baran, *Science* **2016**, *352*, 801.
- [89] J. N. Degruyter, L. R. Malins, L. Wimmer, K. J. Clay, J. Lopez-Ogalla, T. Qin, J. Cornella, Z. Liu, G. Che, D. Bao, et al., *Org. Lett.* **2017**, *19*, 6196–6199.
- [90] J. T. Edwards, R. R. Merchant, K. S. McClymont, K. W. Knouse, T. Qin, L. R. Malins, B. Vokits, S. A. Shaw, D.-H. Bao, F.-L. Wei, et al., *Nature* **2017**, *545*, 213–218.

- [91] J. M. Smith, T. Qin, R. R. Merchant, J. T. Edwards, L. R. Malins, Z. Liu, G. Che, Z. Shen, S. A. Shaw, M. D. Eastgate, et al., *Angew. Chem. Int. Ed.* **2017**, *56*, 11906–11910.
- [92] T. Qin, L. R. Malins, J. T. Edwards, R. R. Merchant, A. J. E. Novak, J. Z. Zhong, R. B. Mills, M. Yan, C. Yuan, M. D. Eastgate, et al., *Angew. Chem. Int. Ed.* **2017**, *56*, 260–265.
- [93] J. Wang, H. Lundberg, S. Asai, P. Martín-Acosta, J. S. Chen, S. Brown, W. Farrell, R. G. Dushin, C. J. O'Donnell, A. S. Ratnayake, et al., *Proc. Natl. Acad. Sci.* **2018**, *115*, 6404–6410.
- [94] C. Li, J. Wang, L. M. Barton, S. Yu, M. Tian, D. S. Peters, M. Kumar, A. W. Yu, K. A. Johnson, A. K. Chatterjee, et al., *Science* **2017**, *356*, eaam7355.
- [95] J. Lippincott-Schwartz, *Science* **2003**, *300*, 87–91.
- [96] N. C. Shaner, G. H. Patterson, M. W. Davidson, *J. Cell Sci.* **2007**, *120*, 4247–4260.
- [97] R. Y. Tsien, *Biochemistry* **1998**, *67*, 509–44.
- [98] M. J. Hinner, K. Johnsson, *Curr. Opin. Biotechnol.* **2010**, *21*, 766–776.
- [99] C. Zhang, M. Welborn, T. Zhu, N. J. Yang, M. S. Santos, T. Van Voorhis, B. L. Pentelute, *Nat. Chem.* **2016**, *8*, 120–128.
- [100] G. V. Los, L. P. Encell, M. G. McDougall, D. D. Hartzell, N. Karassina, C. Zimprich, M. G. Wood, R. Learish, R. F. Ohana, M. Urh, et al., *ACS Chem. Biol.* **2008**, *3*, 373–382.
- [101] N. George, H. Pick, H. Vogel, N. Johnsson, K. Johnsson, *J. Am. Chem. Soc.* **2004**, *126*, 8896–8897.
- [102] A. Keppler, S. Gendreizig, T. Gronemeyer, H. Pick, H. Vogel, K. Johnsson, *Nat. Biotechnol.* **2003**, *21*, 86–89.
- [103] E. Baslé, N. Joubert, M. Pucheault, *Chem. Biol.* **2010**, *17*, 213–227.
- [104] T. G. Rajagopalam, W. H. Stein, S. Moore, *J. Biol. Chem.* **1966**, *241*, 4295–4297.
- [105] Delpierre G. R., J. S. Fruton, *Proc. Natl. Acad. Sci.* **1966**, *56*, 1817–1822.
- [106] D. G. R., J. S. Fruton, *Proc. Natl. Acad. Sci.* **1965**, *54*, 1161–1167.
- [107] N. A. McGrath, K. A. Andersen, A. K. F. Davis, J. E. Lomax, R. T. Raines, *Chem. Sci.* **2015**, *6*, 752–755.
- [108] K. A. Mix, R. T. Raines, *Org. Lett.* **2015**, *17*, 2358–2361.
- [109] H. Yamada, T. Imoto, K. Fujita, K. Okazaki, M. Motomura, *Biochemistry* **1981**, *20*, 4836–4842.
- [110] N. Nakajima, Y. Ikada, *Bioconjug. Chem.* **1995**, *6*, 123–130.
- [111] K. A. Totaro, X. Liao, K. Bhattacharya, J. I. Finneman, J. B. Sperry, M. A. Massa, J. Thorn, S. V. Ho, B. L. Pentelute, *Bioconjug. Chem.* **2016**, *27*, 994–1004.
- [112] N. Ma, J. Hu, Z.-M. Zhang, W. Liu, M. Huang, Y. Fan, X. Yin, J. Wang, K. Ding, W. Ye, et al., *J. Am. Chem. Soc.* **2020**, *142*, 6051–6059.
- [113] D. J. Voadlo, C. R. Bertozzi, *Angew. Chem. Int. Ed.* **2004**, *43*, 5338–5342.
- [114] P. Martín-Gago, E. K. Fansa, M. Winzker, S. Murarka, P. Janning, C. Schultz-Fademrecht, M. Baumann, A. Wittinghofer, H. Waldmann, *Cell Chem. Biol.* **2017**, *24*, 589–597.
- [115] Y. Li, D. P. Hari, M. V. Vita, *Angew. Chem. Int. Ed.* **2016**, *55*, 4436–4454.
- [116] A. P. Antonchick, S. Canesi, L. Catalano, G. Cavallo, J. Charpentier, D. Deffieux, T. Dohi, N. Früh, Y. Kita, R. Kumar, et al., *Hypervalent Iodine Chemistry*, **2016**.
- [117] J. P. Brand, D. F. González, S. Nicolai, J. Waser, *Chem. Commun.* **2011**, *47*, 102–115.

- [118] V. V. Zhdankin, *Hypervalent Iodine Chemistry: Preparation, Structure, and Synthetic Applications of Polyvalent Iodine Compounds*, **2013**.
- [119] X. Zhang, H. F. Schaefer, *Chem. Commun.* **2016**, 52, 5371–5374.
- [120] M. Ochiai, Y. Masaki, M. Shiro, *J. Org. Chem.* **1991**, 56, 5511–5513.
- [121] V. V. Zhdankin, A. P. Krasutsky, C. J. Kuehl, A. J. Simonsen, J. K. Woodward, B. Mismash, J. T. Bolz, *J. Am. Chem. Soc.* **1996**, 118, 5192–5197.
- [122] M. J. Bouma, B. Olofsson, *Chem. Eur. J.* **2012**, 18, 14242–14245.
- [123] D. P. Hari, P. Caramenti, L. Schouwey, M. Chang, S. Nicolai, D. Bachert, T. Wright, C. Orella, J. Waser, *Org. Process Res. Dev.* **2020**, 24, 106–110.
- [124] J. Waser, *Synlett* **2016**, 27, 2761–2773.
- [125] A. Yoshimura, V. V. Zhdankin, *Chem. Rev.* **2016**, 116, 3328–3435.
- [126] D. Fernández González, J. P. Brand, R. Mondière, J. Waser, *Adv. Synth. Catal.* **2013**, 355, 1631–1639.
- [127] S. Nicolai, J. Waser, *Org. Lett.* **2011**, 13, 6324–6327.
- [128] R. Frei, J. Waser, *J. Am. Chem. Soc.* **2013**, 135, 9620–9623.
- [129] R. Frei, M. D. Wodrich, D. P. Hari, P. Borin, *J. Am. Chem. Soc.* **2014**, 136, 16563–16573.
- [130] J. P. Brand, J. Waser, *Org. Lett.* **2012**, 14, 744–747.
- [131] J. P. Brand, J. Charpentier, J. Waser, *Angew. Chem. Int. Ed.* **2009**, 48, 9346–9349.
- [132] G. L. Tolnai, J. P. Brand, J. Waser, *Beilstein J. Org. Chem.* **2016**, 12, 745–749.
- [133] J. P. Brand, J. Waser, *Angew. Chem. Int. Ed.* **2010**, 49, 7304–7307.
- [134] Y. Li, J. P. Brand, J. Waser, *Angew. Chem. Int. Ed.* **2013**, 52, 6743–6747.
- [135] Y. Li, J. Waser, *Beilstein J. Org. Chem.* **2013**, 9, 1763–1767.
- [136] M. V. Vita, P. Mieville, J. Waser, *Org. Lett.* **2014**, 16, 5768–5771.
- [137] K. Tanabe, A. Taniguchi, T. Matsumoto, K. Oisaki, Y. Sohma, M. Kanai, *Chem. Sci.* **2014**, 5, 2747.
- [138] P. Morelli, X. Martin-Benlloch, R. Tessier, J. Waser, N. Sakai, S. Matile, *Polym. Chem.* **2016**, 7, 3465–3470.
- [139] R. Tessier, R. K. Nandi, B. G. Dwyer, D. Abegg, C. Sornay, J. Ceballos, S. Erb, S. Cianféroni, A. Wagner, G. Chaubet, et al., *Angew. Chem. Int. Ed.* **2020**, 59, 10961–10970.
- [140] M. B. Hansen, F. Hubálek, T. Skrydstrup, T. Hoeg-Jensen, *Chem. Eur. J.* **2016**, 22, 1572–1576.
- [141] V. Matoušek, J. Václavík, P. Hájek, J. Charpentier, Z. E. Blastik, E. Pietrasiak, A. Budinská, A. Togni, P. Beier, *Chem. Eur. J.* **2016**, 22, 417–424.
- [142] J. Václavík, R. Zschoche, I. Klimankova, V. Matousek, P. Beier, D. Hilvert, A. Togni, *Chem. Eur. J.* **2017**, 23, 6462–6462.
- [143] X. G. Yang, K. Zheng, C. Zhang, *Org. Lett.* **2020**, 22, 2026–2031.
- [144] M. T. Taylor, J. E. Nelson, M. G. Suero, M. J. Gaunt, *Nature* **2018**, 562, 563–568.
- [145] J. W. Tucker, C. R. J. Stephenson, *J. Org. Chem.* **2012**, 77, 1617–1622.
- [146] X. Y. Yu, J. R. Chen, W. J. Xiao, *Chem. Rev.* **2020**, DOI 10.1021/acs.chemrev.0c00030.
- [147] A. Hossain, A. Bhattacharyya, O. Reiser, *Science* **2019**, 364, eaav9713.
- [148] D. Ravelli, M. Fagnoni, A. Albini, *Chem. Soc. Rev.* **2013**, 42, 97–113.

- [149] A. F. Garrido-Castro, M. C. Maestro, J. Alemán, *Tetrahedron Lett.* **2018**, 59, 1286–1294.
- [150] L. Capaldo, L. L. Quadri, D. Ravelli, *Angew. Chem. Int. Ed.* **2019**, 58, 17508–17510.
- [151] Y. Yu, P. Guo, J. S. Zhong, Y. Yuan, K. Y. Ye, *Org. Chem. Front.* **2019**, 7, 131–135.
- [152] K. F. Biegasiewicz, S. J. Cooper, M. A. Emmanuel, D. C. Miller, T. K. Hyster, *Nat. Chem.* **2018**, 10, 770–775.
- [153] K. F. Biegasiewicz, S. J. Cooper, X. Gao, D. G. Oblinsky, J. H. Kim, S. E. Garfinkle, L. A. Joyce, B. A. Sandoval, G. D. Scholes, T. K. Hyster, *Science* **2019**, 364, 1166–1169.
- [154] Z. C. Litman, Y. Wang, H. Zhao, J. F. Hartwig, *Nature* **2018**, 560, 355–359.
- [155] T. Noël, *J. Flow Chem.* **2017**, 7, 87–93.
- [156] A. Singh, K. Teegardin, M. Kelly, K. S. Prasad, S. Krishnan, J. D. Weaver, *J. Organomet. Chem.* **2015**, 776, 51–59.
- [157] D. M. Arias-Rotondo, J. K. McCusker, *Chem. Soc. Rev.* **2016**, 45, 5803–5820.
- [158] N. A. Romero, D. A. Nicewicz, *Chem. Rev.* **2016**, 116, 10075–10166.
- [159] J. Luo, J. Zhang, *ACS Catal.* **2016**, 6, 873–877.
- [160] H. Uoyama, K. Goushi, K. Shizu, H. Nomura, C. Adachi, *Nature* **2012**, 492, 234–238.
- [161] A. Joshi-Pangu, F. Lévesque, H. G. Roth, S. F. Oliver, L. C. Campeau, D. Nicewicz, D. A. DiRocco, *J. Org. Chem.* **2016**, 81, 7244–7249.
- [162] C. Fischer, C. Sparr, *Angew. Chem. Int. Ed.* **2018**, 57, 2436–2440.
- [163] C. Fischer, C. Sparr, *Synlett* **2018**, 29, 2176–2180.
- [164] B. Zilate, C. Fischer, C. Sparr, *Chem. Commun.* **2020**, 56, 1767–1775.
- [165] M. Uygun, O. García Mancheño, *Org. Biomol. Chem.* **2019**, 17, 5475–5489.
- [166] T. Y. Shang, L. H. Lu, Z. Cao, Y. Liu, W. M. He, B. Yu, *Chem. Commun.* **2019**, 55, 5408–5419.
- [167] D. P. Hari, B. König, *Chem. Commun.* **2014**, 50, 6688–6699.
- [168] A. Joshi-Pangu, F. Lévesque, H. G. Roth, S. F. Oliver, L. C. Campeau, D. Nicewicz, D. A. DiRocco, *J. Org. Chem.* **2016**, 81, 7244–7249.
- [169] I. K. Sideri, E. Voutyritsa, C. G. Kokotos, *Org. Biomol. Chem.* **2018**, 16, 4596–4614.
- [170] S. G. E. Amos, M. Garreau, L. Buzzetti, J. Waser, *Beilstein J. Org. Chem.* **2020**, 16, 1163–1187.
- [171] C. M. Elliott, E. J. Hershenhart, *J. Am. Chem. Soc.* **1982**, 104, 7519–7526.
- [172] M. R. Norris, J. J. Concepcion, C. R. K. Glasson, Z. Fang, A. M. Lapidés, D. L. Ashford, J. L. Templeton, T. J. Meyer, *Inorg. Chem.* **2013**, 52, 12492–12501.
- [173] D. L. Ashford, M. K. Brennaman, R. J. Brown, S. Keinan, J. J. Concepcion, J. M. Papanikolas, J. L. Templeton, T. J. Meyer, *Inorg. Chem.* **2015**, 54, 460–469.
- [174] I. Gillaizeau-Gauthier, F. Odobel, M. Alebbi, R. Argazzi, E. Costa, C. A. Bignozzi, P. Qu, G. J. Meyer, *Inorg. Chem.* **2001**, 40, 6073–6079.
- [175] D. Jespersen, B. Keen, J. I. Day, A. Singh, J. Briles, D. Mullins, J. D. Weaver, *Org. Process Res. Dev.* **2019**, 23, 1087–1095.
- [176] D. N. Chirdon, C. E. McCusker, F. N. Castellano, S. Bernhard, *Inorg. Chem.* **2013**, 52, 8795–8804.
- [177] C. Liu, H. Yu, Y. Xing, Z. Gao, Z. Jin, *Dalt. Trans.* **2016**, 45, 734–741.
- [178] X. Liu, Z. Wang, X. Cheng, C. Li, *J. Am. Chem. Soc.* **2012**, 134, 14330–14333.

- [179] A. Noble, D. W. C. MacMillan, *J. Am. Chem. Soc.* **2014**, *136*, 11602–11605.
- [180] G. Dijkstra, W. H. Kruizinga, R. M. Kellogg, *J. Org. Chem.* **1987**, *52*, 4230–4234.
- [181] C. H. and Y. C. Jie Yang, Jing Zhang, Li Qi, *Chem. Commun.* **2015**, *51*, 5275–5278.
- [182] H. Huang, G. Zhang, Y. Chen, *Angew. Chem. Int. Ed.* **2015**, *54*, 7872–7876.
- [183] J. Xuan, Z. G. Zhang, W. J. Xiao, *Angew. Chem. Int. Ed.* **2015**, *54*, 15632–15641.
- [184] F. Le Vaillant, M. D. Wodrich, J. Waser, *Chem. Sci.* **2017**, *8*, 1790–1800.
- [185] G. X. Li, C. A. Morales-Rivera, Y. Wang, F. Gao, G. He, P. Liu, G. Chen, *Chem. Sci.* **2016**, *7*, 6407–6412.
- [186] Y. Jin, H. Fu, *Asian J. Org. Chem.* **2017**, *6*, 368–385.
- [187] J. Schwarz, B. König, *Green Chem.* **2018**, *20*, 323–361.
- [188] F. Le Vaillant, J. Waser, *Chem. Sci.* **2019**, *10*, 8909–8923.
- [189] C. Yang, J. D. Yang, Y. H. Li, X. Li, J. P. Cheng, *J. Org. Chem.* **2016**, *81*, 12357–12363.
- [190] J. Schwarz, B. König, *ChemPhotoChem* **2017**, *1*, 237–242.
- [191] Y. Mao, W. Zhao, S. Lu, L. Yu, Y. Wang, Y. Liang, S. Ni, Y. Pan, *Chem. Sci.* **2020**, *11*, 4939–4947.
- [192] Y. Zhang, D. Zhang, *Org. Biomol. Chem.* **2020**, *18*, 4479–4483.
- [193] H. Zhang, P. Zhang, M. Jiang, H. Yang, H. Fu, *Org. Lett.* **2017**, *19*, 1016–1019.
- [194] H.-D. Xia, Z.-L. Li, Q.-S. Gu, X.-Y. Dong, J.-H. Fang, X.-Y. Du, L.-L. Wang, X.-Y. Liu, *Angew. Chem. Int. Ed* **2020**, DOI 10.1002/anie.202006317.
- [195] C. P. Ramil, Q. Lin, *Curr. Opin. Chem. Biol.* **2014**, *21*, 89–95.
- [196] L. Kowalik, J. K. Chen, *Nat. Chem. Biol.* **2017**, *13*, 587–598.
- [197] J. P. Holland, M. Gut, S. Klingler, R. Fay, A. Guillou, *Chem. Eur. J.* **2020**, *26*, 33–48.
- [198] F. J. A. Troyano, K. Merken, K. Anwar, A. Gómez-Suárez, *Angew. Chem. Int. Ed.* **2020**, DOI 10.1002/anie.202010157.
- [199] E. L. Tyson, Z. L. Niemeyer, T. P. Yoon, *J. Org. Chem.* **2014**, *79*, 1427–1436.
- [200] C. Bottecchia, M. Rubens, S. B. Gunnoo, V. Hessel, A. Madder, T. Noël, *Angew. Chem. Int. Ed.* **2017**, *56*, 12702–12707.
- [201] G. A. Molander, E. J. Petersson, C. R. Walters, S. Bertritt, X. Li, B. A. Vara, *Chem. Sci.* **2017**, *9*, 336–344.
- [202] X. F. Gao, J. J. Du, Z. Liu, J. Guo, *Org. Lett.* **2016**, *18*, 1166–1169.
- [203] C. Bottecchia, X. J. Wei, K. P. L. Kuipers, V. Hessel, T. Noël, *J. Org. Chem.* **2016**, *81*, 7301–7307.
- [204] C. Bottecchia, N. Erdmann, P. M. A. Tijssen, L. G. Milroy, L. Brunsveld, V. Hessel, T. Noël, *ChemSusChem* **2016**, *9*, 1781–1785.
- [205] A. Talla, B. Driessen, N. J. W. Straathof, L. G. Milroy, L. Brunsveld, V. Hessel, T. Noël, *Adv. Synth. Catal.* **2015**, *357*, 2180–2186.
- [206] Y. Yu, L. K. Zhang, A. V. Buevich, G. Li, H. Tang, P. Vachal, S. L. Colletti, Z. C. Shi, *J. Am. Chem. Soc.* **2018**, *140*, 6797–6800.
- [207] Y. Wang, J. Wang, G. X. Li, G. He, G. Chen, *Org. Lett.* **2017**, *19*, 1442–1445.
- [208] S. J. Tower, W. J. Hetcher, T. E. Myers, N. J. Kuehl, M. T. Taylor, *J. Am. Chem. Soc.* **2020**, *142*,

- 9112–9118.
- [209] C. Wang, M. Guo, R. Qi, Q. Shang, Q. Liu, S. Wang, L. Zhao, R. Wang, Z. Xu, *Angew. Chem. Int. Ed.* **2018**, *57*, 15841–15846.
- [210] C. Wang, R. Qi, H. Xue, Y. Shen, M. Chang, Y. Chen, R. Wang, Z. Xu, *Angew. Chem. Int. Ed.* **2020**, 1–7.
- [211] X. Chen, F. Ye, X. Luo, X. Liu, J. Zhao, S. Wang, Q. Zhou, G. Chen, P. Wang, *J. Am. Chem. Soc.* **2019**, *141*, 18230–18237.
- [212] H. Lee, N. C. Boyer, Q. Deng, H. Y. Kim, T. K. Sawyer, N. Sciammetta, *Chem. Sci.* **2019**, *10*, 5073–5078.
- [213] Y. Chen, A. S. Kamlet, J. B. Steinman, D. R. Liu, *Nat. Chem.* **2011**, *3*, 146–153.
- [214] C. Hu, Y. Chen, *Tetrahedron Lett.* **2015**, *56*, 884–888.
- [215] H. Huang, G. Zhang, L. Gong, S. Zhang, Y. Chen, *J. Am. Chem. Soc.* **2014**, *136*, 2280–2283.
- [216] Y. Jin, M. Jiang, H. Wang, H. Fu, *Sci. Rep.* **2016**, *6*, 1–8.
- [217] W. M. Cheng, R. Shang, Y. Fu, *ACS Catal.* **2017**, *7*, 907–911.
- [218] Y. Jin, H. Yang, H. Fu, *Org. Lett.* **2016**, *18*, 6400–6403.
- [219] Y. Jin, H. Yang, H. Fu, *Chem. Commun.* **2016**, 52, 12909–12912.
- [220] M. Jiang, H. Yang, H. Fu, *Org. Lett.* **2016**, *18*, 1968–1971.
- [221] D. K. Kölmel, R. P. Loach, T. Knauber, M. E. Flanagan, *ChemMedChem* **2018**, *13*, 2159–2165.
- [222] T. Brandhofer, O. G. Mancheño, *ChemCatChem* **2019**, *11*, 3797–3801.
- [223] O. Zhang, J. W. Schubert, *J. Org. Chem.* **2020**, *85*, 6225–6232.
- [224] C. J. Saavedra, R. Hernández, A. Boto, E. Álvarez, *Tetrahedron Lett.* **2006**, *47*, 8757–8760.
- [225] C. Saavedra, R. Herna, A. Boto, A. Eleuterio, I. De Cartuja, A. V Ame, **2009**, 4655–4665.
- [226] S. Bloom, C. Liu, D. K. Kölmel, J. X. Qiao, Y. Zhang, M. A. Poss, W. R. Ewing, D. W. C. MacMillan, *Nat. Chem.* **2017**, *10*, 205–211.
- [227] K. Maeda, H. Saito, K. Osaka, K. Nishikawa, M. Sugie, T. Morita, I. Takahashi, Y. Yoshimi, *Tetrahedron* **2015**, *71*, 1117–1123.
- [228] S. B. Lang, K. M. O'Nele, J. T. Douglas, J. A. Tunge, *Chem. Eur. J.* **2015**, *21*, 18589–18593.
- [229] A. Lipp, G. Lahm, T. Opatz, *J. Org. Chem.* **2016**, *81*, 4890–4897.
- [230] T. Itou, Y. Yoshimi, K. Nishikawa, T. Morita, Y. Okada, N. Ichinose, M. Hatanaka, *Chem. Commun.* **2010**, 46, 6177–6179.
- [231] C. Cassani, G. Bergonzini, C. J. Wallentin, *Org. Lett.* **2014**, *16*, 4228–4231.
- [232] D. Leonori, E. Dauncey, D. C. Marcote, A. Ruffoni, J. J. Douglas, R. Street-Jeakings, *Org. Biomol. Chem.* **2018**, *1*, 1839–1842.
- [233] D. C. Marcote, R. Street-Jeakings, E. Dauncey, J. J. Douglas, A. Ruffoni, D. Leonori, *Org. Biomol. Chem.* **2019**, *17*, 1839–1842.
- [234] S. Zhao, J. Dai, M. Hu, C. Liu, R. Meng, X. Liu, C. Wang, T. Luo, *Chem. Commun.* **2016**, 52, 4702–4705.
- [235] L. Liang, D. Astruc, *Coord. Chem. Rev.* **2011**, *255*, 2933–2945.
- [236] H. Huang, K. Jia, Y. Chen, *Angew. Chem. Int. Ed.* **2015**, *54*, 1881–1884.
- [237] J. Davies, N. S. Sheikh, D. Leonori, *Angew. Chem. Int. Ed.* **2017**, *56*, 13361–13365.

- [238] A. Paul, N. Das, Y. Halpin, J. G. Vos, M. T. Pryce, *Dalt. Trans.* **2015**, *44*, 10423–10430.
- [239] J. W. Jurss, J. C. Concepcion, M. R. Norris, J. L. Templeton, T. J. Meyer, *Inorg. Chem.* **2010**, *49*, 3980–3982.
- [240] E.-G. Ha, J.-A. Chang, S.-M. Byun, C. Pac, D.-M. Jang, J. Park, S. O. Kang, *Chem. Commun.* **2014**, *50*, 4462.
- [241] N. M. Shavaleev, F. Monti, R. D. Costa, R. Scopelliti, H. J. Bolink, E. Ortí, G. Accorsi, N. Armaroli, E. Baranoff, M. Grätzel, et al., *Inorg. Chem.* **2012**, *51*, 2263–2271.
- [242] A. Kretzschmar, C. Patze, S. T. Schwaebel, U. H. F. Bunz, *J. Org. Chem.* **2015**, *80*, 9126–9131.
- [243] G. Zhang, L. Zhang, H. Yi, Y. Luo, X. Qi, C. H. Tung, L. Z. Wu, A. Lei, *Chem. Commun.* **2016**, *52*, 10407–10410.
- [244] R. Ishimatsu, S. Matsunami, T. Kasahara, J. Mizuno, T. Edura, C. Adachi, K. Nakano, T. Imato, *Angew. Chem. Int. Ed.* **2014**, *53*, 6993–6996.
- [245] H. Jiang, A. Studer, *CCS Chem.* **2019**, 38–49.
- [246] J. C. Walton, *Molecules* **2016**, *21*, DOI 10.3390/molecules21010063.
- [247] J. Davies, S. P. Morcillo, J. J. Douglas, D. Leonori, *Chem. Eur. J.* **2018**, *24*, 12154–12163.
- [248] J. Davies, S. G. Booth, S. Essafi, R. A. W. Dryfe, D. Leonori, *Angew. Chem. Int. Ed.* **2015**, *54*, 14017–14021.
- [249] H. Jiang, A. Studer, *Angew. Chem. Int. Ed.* **2017**, 201706270, 1–5.
- [250] E. M. Dauncey, S. P. Morcillo, J. J. Douglas, N. S. Sheikh, D. Leonori, *Angew. Chem. Int. Ed.* **2018**, *57*, 744–748.
- [251] H. G. Roth, N. A. Romero, D. A. Nicewicz, *Synlett* **2016**, *27*, 714–723.
- [252] A. Harriman, *J. Phys. Chem.* **1987**, *91*, 6102–6104.
- [253] M. DeFelippis, C. Murthy, *J. Phys. Chem.* **1991**, *8*, 3416–3419.
- [254] D. M. Close, P. Wardman, *J. Phys. Chem. A* **2018**, *122*, 439–445.
- [255] F. Costanzo, M. Sulpizi, R. G. Della Valle, M. Sprik, *J. Chem. Phys.* **2011**, *134*, 244508.
- [256] A. Roy, R. Seidel, G. Kumar, S. E. Bradforth, *J. Phys. Chem. B* **2018**, *122*, 3723–3733.
- [257] Y. J. Cho, K. S. Yook, J. Y. Lee, *Adv. Mater.* **2014**, *26*, 6642–6646.
- [258] R. Ishimatsu, T. Edura, C. Adachi, K. Nakano, T. Imato, *Chem. Eur. J.* **2016**, *22*, 4889–4898.
- [259] E. Speckmeier, T. Fischer, K. Zeitler, *J. Am. Chem. Soc.* **2018**, *140*, 15353–15365.
- [260] F. Le Vaillant, M. Garreau, S. Nicolai, G. Gryn'Ova, C. Corminboeuf, J. Waser, *Chem. Sci.* **2018**, *9*, 5883–5889.
- [261] K. Karon, M. Lapkowski, *J. Solid State Electrochem.* **2015**, *19*, 2601–2610.
- [262] N. Elgrishi, K. J. Rountree, B. D. McCarthy, E. S. Rountree, T. T. Eisenhart, J. L. Dempsey, *J. Chem. Educ.* **2018**, 197–206.
- [263] B. Muriel, A. Gagnebin, J. Waser, *Chem. Sci.* **2019**, *10*, 10716–10722.
- [264] S. Yang, H. Tan, W. Ji, X. Zhang, P. Li, L. Wang, *Adv. Synth. Catal.* **2017**, *359*, 443–453.
- [265] Y. S. Feng, C. Q. Xie, W. L. Qiao, H. J. Xu, *Org. Lett.* **2013**, *15*, 936–939.
- [266] E. Stridfeldt, A. Seemann, M. J. Bouma, C. Dey, A. Ertan, B. Olofsson, *Chem. Eur. J.* **2016**, *22*, 16066–16070.
- [267] C. Cabezas, M. Varela, J. L. Alonso, *Angew. Chem. Int. Ed.* **2017**, *56*, 6420–6425.

- [268] C. Dreyfus, M. Larrouy, F. Cavelier, J. Martinez, D. Pignol, P. Arnoux, *Chem. Commun.* **2011**, 47, 5825–7.
- [269] D. Crich, K. Sasaki, M. Y. Rahaman, A. A. Bowers, *J. Org. Chem.* **2009**, 74, 3886–3893.
- [270] K. D. Collins, F. Glorius, *Nat. Chem.* **2013**, 5, 597–601.
- [271] L. Capaldo, D. Ravelli, *European J. Org. Chem.* **2017**, 2017, 2056–2071.
- [272] V. Sarin, R. D. Gaffin, G. A. Meininger, M. Muthuchamy, *J. Physiol.* **2005**, 564, 603–617.
- [273] A. Sasamoto, M. Nagino, S. Kobayashi, K. Naruse, Y. Nimura, M. Sokabe, *Am. J. Physiol. Physiol.* **2005**, 288, 1012–1022.
- [274] S. Bloom, C. Liu, D. K. Kölmel, J. X. Qiao, Y. Zhang, M. A. Poss, W. R. Ewing, D. W. C. Macmillan, *Nat. Chem.* **2018**, 10, 205–211.
- [275] M. Garreau, F. Le Vaillant, J. Waser, *Angew. Chem. Int. Ed.* **2019**, 58, 8182–8186.
- [276] D. Hymel, F. Liu, *Asian J. Org. Chem.* **2020**, ajoc.202000328.
- [277] S. Angerani, N. Winssinger, *Chem. Eur. J.* **2019**, 25, 6661–6672.
- [278] T. U. Connell, P. S. Donnelly, *Coord. Chem. Rev.* **2018**, 375, 267–284.
- [279] S. Sato, H. Nakamura, *Angew. Chem. Int. Ed.* **2013**, 52, 8681–8684.
- [280] M. Tsushima, S. Sato, H. Nakamura, *Chem. Commun.* **2017**, 53, 4838–4841.
- [281] S. Sato, K. Morita, H. Nakamura, *Bioconjug. Chem.* **2015**, 26, 250–256.
- [282] S. Sato, K. Hatano, M. Tsushima, H. Nakamura, *Chem. Commun.* **2018**, 54, 5871–5874.
- [283] O. Boutureira, G. J. L. Bernardes, *Chem. Rev.* **2015**, 115, 2174–2195.
- [284] J. M. J. M. Ravasco, H. Faustino, A. Trindade, P. M. P. Gois, *Chem. Eur. J.* **2019**, 25, 43–59.
- [285] M. K. Etherington, N. A. Kukhta, H. F. Higginbotham, A. Danos, A. N. Bismillah, D. R. Graves, P. R. McGonigal, N. Haase, A. Morherr, A. S. Batsanov, et al., *J. Phys. Chem. C* **2019**, 123, 11109–11117.
- [286] L. Wen, L. Tang, Y. Yang, Z. Zha, Z. Wang, *Org. Lett.* **2016**, 18, 1278–1281.
- [287] R. Ziesel, A. Steffen, M. Starck, *Tetrahedron Lett.* **2012**, 53, 3713–3716.
- [288] Ł. J. Weseliński, R. Luebke, M. Eddaoudi, *Synthesis* **2014**, 46, 596–599.
- [289] S. Luliński, K. Zajac, *J. Org. Chem.* **2008**, 73, 7785–7788.
- [290] A. Correa, R. Martín, *J. Am. Chem. Soc.* **2009**, 131, 15974–15975.
- [291] Y. Zhang, X. Zhou, Y. Xie, M. M. Greenberg, Z. Xi, C. Zhou, *J. Am. Chem. Soc.* **2017**, 139, 6146–6151.
- [292] C. W. Cheung, D. S. Surry, S. L. Buchwald, *Org. Lett.* **2013**, 15, 3734–3737.
- [293] L. S. Torrie, S. Brand, D. A. Robinson, E. J. Ko, L. Stojanovski, F. R. C. Simeons, S. Wyllie, J. Thomas, L. Ellis, M. Osuna-Cabello, et al., *ACS Infect. Dis.* **2017**, 3, 718–727.
- [294] J. Rautio, N. A. Meanwell, L. Di, M. J. Hageman, *Nat. Rev. Drug Discov.* **2018**, 17, 559–587.
- [295] T. F. Thomas, L. K. Jao, *J. Org. Chem.* **1965**, 30, 1492–1495.
- [296] A. Wiebe, T. Gieshoff, S. Möhle, E. Rodrigo, M. Zirbes, S. R. Waldvogel, *Angew. Chem. Int. Ed.* **2018**, 57, 5594–5619.
- [297] H. Kolbe, **n.d.**
- [298] D. Seebach, R. Charczuk, C. Gerber, P. Renaud, H. Berner, H. Schneider, *Helv. Chim. Acta* **1989**, 72, 401–425.

- [299] R. Mazurkiewicz, J. Adamek, A. Październiak-Holewa, K. Zielińska, W. Simka, A. Gajos, K. Szymura, *J. Org. Chem.* **2012**, *77*, 1952–1960.
- [300] J. Adamek, R. Mazurkiewicz, A. Październiak-Holewa, M. Grymel, A. Kuźnik, K. Zielińska, *J. Org. Chem.* **2014**, *79*, 2765–2770.
- [301] Y. Lin, L. R. Malins, *Chem. Sci.* **2020**, DOI 10.1039/d0sc03701j.
- [302] M.-L. Shen, Y. Shen, P.-S. Wang, *Org. Lett.* **2019**, *21*, 2993–2997.
- [303] H. T. Song, W. Ding, Q. Q. Zhou, J. Liu, L. Q. Lu, W. J. Xiao, *J. Org. Chem.* **2016**, *81*, 7250–7255.
- [304] S. Senaweera, K. C. Cartwright, J. A. Tunge, *J. Org. Chem.* **2019**, DOI 10.1021/acs.joc.9b02092.
- [305] T. Brandhofer, O. García Mancheño, *European J. Org. Chem.* **2018**, 6050–6067.
- [306] L. Zhao, C. J. Li, *Angew. Chem. Int. Ed.* **2008**, *47*, 7075–7078.
- [307] M. S. Segundo, I. Guerrero, A. Correa, *Org. Lett.* **2017**, *19*, 5288–5291.
- [308] Z. Q. Wang, M. Hu, X. C. Huang, L. B. Gong, Y. X. Xie, J. H. Li, *J. Org. Chem.* **2012**, *77*, 8705–8711.
- [309] A. Boto, R. Hernández, E. Suárez, *Tetrahedron Lett.* **1999**, *40*, 5945–5948.
- [310] A. Boto, R. Hernández, E. Suárez, *J. Org. Chem.* **2000**, *65*, 4930–4937.
- [311] V. R. Batchu, I. Romero-Estudillo, A. Boto, J. Miguélez, *Org. Biomol. Chem.* **2014**, *12*, 9547–9556.
- [312] Y. Kita, D. Kamimura, Y. Wada, Y. Harayama, M. Yoshida, *Chem. Eur. J.* **2006**, *12*, 4893–4899.
- [313] Y. Harayama, M. Yoshida, D. Kamimura, Y. Kita, *Chem. Commun.* **2005**, 1764–1766.
- [314] J. Guo, Y. Xie, Q. L. Wu, W. T. Zeng, A. S. C. Chan, J. Weng, G. Lu, *RSC Adv.* **2018**, *8*, 16202–16206.
- [315] G.-X. X. Li, X. Hu, G. He, G. Chen, *ACS Catal.* **2018**, *8*, 11847–11853.
- [316] M. M. Wang, J. Waser, *Angew. Chem. Int. Ed.* **2019**, *58*, 13880–13884.
- [317] C. F. Meyer, S. M. Hell, A. Misale, A. A. Trabanco, V. Gouverneur, *Angew. Chem. Int. Ed.* **2019**, *58*, 8829–8833.
- [318] J. Hu, T. Lan, Y. Sun, H. Chen, J. Yao, Y. Rao, *Chem. Commun.* **2015**, *51*, 14929–14932.
- [319] T. J. Osberger, D. C. Rogness, J. T. Kohrt, A. F. Stepan, M. C. White, *Nature* **2016**, *537*, 214–219.
- [320] A. Yazici, S. G. Pyne, *Org. Lett.* **2013**, *15*, 5878–5881.
- [321] G. M. Ryder, U. Wille, A. C. Willis, S. G. Pyne, *Org. Biomol. Chem.* **2019**, *17*, 7025–7035.
- [322] G. X. Li, C. A. Morales-Rivera, F. Gao, Y. Wang, G. He, P. Liu, G. Chen, *Chem. Sci.* **2017**, *8*, 7180–7185.
- [323] M. Rueping, C. Vila, R. M. Koenigs, K. Poschary, D. C. Fabry, *Chem. Commun.* **2011**, *47*, 2360–2362.
- [324] A. G. Condie, J. C. González-Gómez, C. R. J. Stephenson, *J. Am. Chem. Soc.* **2010**, *132*, 1464–1465.
- [325] G. X. Li, X. Hu, G. He, G. Chen, *Chem. Sci.* **2019**, *10*, 688–693.
- [326] J. M. Chalker, C. S. C. Wood, B. G. Davis, *J. Am. Chem. Soc.* **2009**, *131*, 16346–16347.
- [327] A. P. Silvestri, P. A. Cistrone, P. E. Dawson, *Angew. Chem. Int. Ed.* **2017**, *56*, 10438–10442.

- [328] W. Tang, M. L. Becker, *Chem. Soc. Rev.* **2014**, *43*, 7013–7039.
- [329] W. Wang, M. Lorion, J. Shah, A. R. Kapdi, L. Ackermann, *Angew. Chem. Int. Ed.* **2018**, *57*, 14700–14717.
- [330] Z. Ruan, N. Sauermann, E. Manoni, L. Ackermann, *Angew. Chem. Int. Ed.* **2017**, *56*, 3172–3176.
- [331] W. Wang, M. M. Lorion, O. Martinazzoli, L. Ackermann, *Angew. Chem. Int. Ed.* **2018**, *57*, 10554–10558.
- [332] C. Ash, M. Dubec, K. Donne, T. Bashford, *Lasers Med. Sci.* **2017**, *32*, 1909–1918.
- [333] L. Wang, M. S. Frei, A. Salim, K. Johnsson, *J. Am. Chem. Soc.* **2019**, *141*, 2770–2781.
- [334] Y. Koide, Y. Urano, K. Hanaoka, W. Piao, M. Kusakabe, N. Saito, T. Terai, T. Okabe, T. Nagano, *J. Am. Chem. Soc.* **2012**, *134*, 5029–5031.
- [335] S. Li, J. Zhao, X. Wang, G. Xu, S. Gou, Q. Zhao, **2020**, DOI 10.1021/acs.inorgchem.0c01860.
- [336] K. L. Woon, Z. N. Nadiyah, Z. A. Hasan, A. Ariffin, S. A. Chen, *Dye. Pigment.* **2016**, *132*, 1–6.
- [337] M. L. Louillat, F. W. Patureau, *Org. Lett.* **2013**, *15*, 164–167.
- [338] D. Maiti, B. P. Fors, J. L. Henderson, Y. Nakamura, S. L. Buchwald, *Chem. Sci.* **2011**, *2*, 57–68.
- [339] J. P. Brand, C. Chevalley, R. Scopelliti, J. Waser, *Chem. Eur. J.* **2012**, *18*, 5655–5666.
- [340] C. J. Helal, P. A. Magriotis, E. J. Corey, *J. Am. Chem. Soc.* **1996**, *118*, 10938–10939.
- [341] B. Lu, J. Wu, N. Yoshikai, *J. Am. Chem. Soc.* **2014**, *136*, 11598–11601.
- [342] K. Jia, F. Zhang, H. Huang, Y. Chen, *J. Am. Chem. Soc.* **2016**, *138*, 1514–1517.
- [343] R. J. Rahaim, J. T. Shaw, *J. Org. Chem.* **2008**, *73*, 2912–2915.
- [344] M. Bemquerer, P. Adlercreutz, M. Tominaga, *Int. J. Pept. Protein. Res.* **1994**, *44*, 448–56.
- [345] F. X. Wang, M. H. Chen, X. Y. Hu, R. R. Ye, C. P. Tan, L. N. Ji, Z. W. Mao, *Sci. Rep.* **2016**, *6*, 21–23.
- [346] E. Speckmeier, T. G. Fischer, K. Zeitler, *J. Am. Chem. Soc.* **2018**, *140*, 15353–15365.

12 Experimental part

12.1 General methods

All reactions were carried out in oven dried glassware under an atmosphere of nitrogen, unless stated otherwise. For flash chromatography, distilled technical grade solvents were used. THF, CH₃CN, toluene and DCM were dried by passage over activated alumina under nitrogen atmosphere (H₂O content < 10 ppm, Karl-Fischer titration). The solvents were degassed by Freeze-Pump-Thaw method when mentioned. All chemicals were purchased from Acros, Aldrich, Fluka, VWR, TCI, Merck or Bachem and used as such unless stated otherwise. All dipeptides starting materials and H-GRGDNP-OH were commercially available and used as received. Chromatographic purification was performed as flash chromatography using Macherey-Nagel silica 40-63, 60 Å, using the solvents indicated as eluent with 0.1-0.5 bar pressure. TLC was performed on Merck silica gel 60 F254 TLC aluminum or glass plates and visualized with UV light. ¹H-NMR spectra were recorded on a Bruker DPX-400 400 MHz spectrometer in chloroform-*d*, methanol-*d*₃, DMSO-*d*₆, DMF-*d*₇ or acetone-*d*₆, all signals are reported in ppm with the internal chloroform signal at 7.26 ppm, the internal methanol signal at 3.30 ppm, the internal DMSO signal at 2.50 ppm, the internal DMF signals at 2.75 and 2.92 ppm, or the internal acetone signal at 2.05 ppm as standard. The data is being reported as (s = singlet, d = doublet, t = triplet, q = quadruplet, qi = quintet, m = multiplet or unresolved, br = broad signal, app = apparent, coupling constant(s) in Hz, integration, interpretation). ¹³C-NMR spectra were recorded with ¹H-decoupling on a Bruker DPX-400 100 MHz spectrometer in chloroform-*d*, methanol-*d*₃, DMSO-*d*₆, DMF-*d*₇ or acetone-*d*₆, all signals are reported in ppm with the internal chloroform signal at 77.0 ppm, the internal methanol signal at 49.0 ppm, the internal DMSO signal at 39.5 ppm, the internal DMF signals at 34.89 and 29.76 ppm, or the internal acetone signals at 29.84 and 206.26 ppm as standard. Infrared spectra were recorded on a JASCO FT-IR B4100 spectrophotometer with an ATR PRO410-S and a ZnSe prisma and are reported as cm⁻¹ (w = weak, m = medium, s = strong, br = broad).

High resolution mass spectrometric measurements were performed by the mass spectrometry service of ISIC at the EPFL on a MICROMASS (ESI) Q-TOF Ultima API. MS-MS analyses were performed on a LTQ Orbitrap FTMS instrument (LTQ Orbitrap Elite FTMS, Thermo Scientific, Bremen, Germany) operated in the positive mode coupled with a robotic

chip-based nano-ESI source (TriVersa Nanomate, Advion Biosciences, Ithaca, NY, U.S.A.). A standard data acquisition and instrument control system was utilized (Thermo Scientific) whereas the ion source was controlled by Chipsoft 8.3.1 software (Advion BioScience). Samples were loaded onto a 96-well plate (Eppendorf, Hamburg, Germany) within an injection volume of 5 µl. The experimental conditions for the ionization voltage was +1.4kV and the gas pressure was set at 0.30 psi. The temperature of ion transfer capillary was 275 °C, tube voltages. FTMS spectra were obtained in the 80-1000 *m/z* range in the reduce profile mode with a resolution set to 120,000. In all spectra one microscan was acquired with a maximum injection time value of 1000ms. Typical CID experiments were carried out using Normalized collision energy values of 26-28 and 5 Da of isolation width.

Photoredox catalyzed reactions were performed in test tubes (5 and 10 mL), or Schlenk tubes (50 mL) which were held using a rack for test tubes placed at the center of a crystallization flask. For small scale reactions on peptides, microwave vials of 1 mL were used. For overnight reactions, the latter was filled by water, in order to keep the temperature as constant as possible, in presence of an air flow. On this flask were attached the blue LEDs (RUBAN LED 5MÈTRES - 60LED/M - 3528 BLEU - IP65 with Transformateur pour Ruban LED 24W/2A/12V, bought directly on RubanLED.com). The distance between the LEDs and the test tubes was approximately 2 cm for the test tubes and 5 cm for the Schlenk flasks. Long irradiation resulted in temperature increasing up to 37°C during overnight reactions.

Tetramers peptides were synthesized by solid phase peptide synthesis using a MultiPep RSi Intavis. Crude products were purified by preparative RP-HPLC on an Agilent 1260 HPLC system with a G2260A 1260 Prep ALS Autosampler, a G1361a 1260 Prep Pump, a G1365C 1260 MWD detector and a G1364B 1260 FC-PS collector, coupled with a Waters XBridge semi-preparative C18 column (19 x 150 mm, 5 µm). Water (solvent A) and water:acetonitrile 5:95 (solvent B), each containing 0.1% TFA, were used as the mobile phase at a flow rate of 20 mL.min⁻¹. The following method was used: 100% A to 100% B in 20 minutes.

RP-HPLC-MS measurements were performed on an Agilent 1290 Infinity HPLC system with a G4226a 1290 Autosampler, a G4220A 1290 Bin Pump and a G4212A 1290 DAD detector, connected to a 6130 Quadrupole LC/MS MS, coupled with a Waters XBridge C18 column (250 x 4.6 mm, 5 µm). Water:acetonitrile 95:5 (solvent A) and water:acetonitrile 5:95 (solvent B), each containing 0.1% formic acid, were used as the mobile phase at a flow rate of 0.6 mL/min⁻¹. The gradient was programmed as follows: 100% A to 100% B in 20 minutes then isocratic for 5 minutes (method A). The column temperature was set up to 25 °C. Low resolution mass

spectrometric measurements were acquired using the following parameters: positive electrospray electrospray ionization (ESI), temperature of drying gas = 350 °C, flow rate of drying gas = 12 L. min⁻¹, pressure of nebulizer gas = 60 psi, capillary voltage = 2500 V and fragmentor voltage = 70 V. In few cases, the gradient was programmed as follows: 100% A to 100% B in 40 minutes, in order to resolve peak overlapping (method B). The other parameters were untouched.

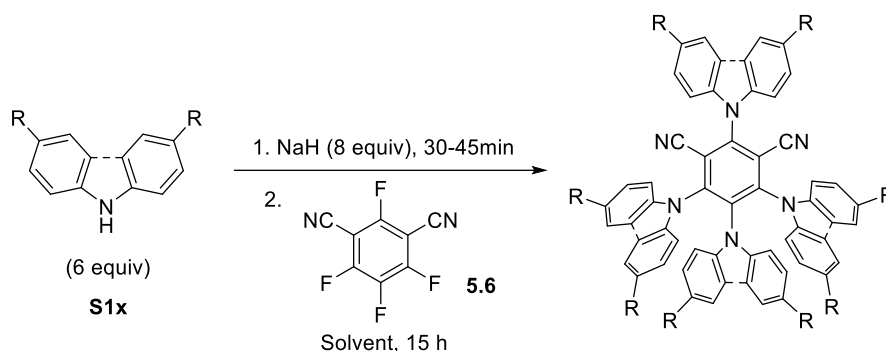
UV/Vis spectroscopy was performed on an Agilent Cary 60 UV-Vis and steady-state luminescence spectroscopy was recorded on a Varian Cary Eclipse spectrophotometer. Cyclic voltammetry experiments were performed on a Biologic SP-150 Potentiostat, with a three-electrode cell configuration: a glassy carbon electrode as the working electrode, Pt wire as a counter electrode and an Ag/AgCl (KCl, 3M) electrode as the reference electrode. Bu₄NPF₆ was employed as the electrolyte (0.1 M).

12.2 Synthesis of peptides

All peptide tetramers were synthesized by solid phase peptide synthesis using a 2-chlorotrityl chloride resin (1.0-1.6 mmol/g, 100-200 mesh). The first amino acid was loaded on the resin by incubation of the Fmoc-protected monomer (3 equiv of the number of active sites on the resin), DIPEA (4 equiv) in dichloromethane for 2 h. A cycle consisted first of the deprotection, achieved by stirring for 20 min with a 20% solution of piperidine in DMF, twice. Then the resin was washed with DMF (7x). Double couplings were performed by adding the Fmoc-protected monomer (4 equiv), HBTU (4 equiv), HOBt (4 equiv), NMM (4 equiv) and stirring for 45 min. Capping was carried out at the end of each cycle, followed by a DMF wash (7x). Acetylation of the N-terminal was achieved by incubating the resin with an Acetic Anhydride/DIPEA/DMF 10/15/75 solution for 30 min, twice. Cleavage of peptides with no protecting groups on the side-chains was performed by stirring the resin in a 20% solution of HFIP in dichloromethane for 30 min. In the presence of protecting groups, a TFA/water/triisopropylsilane 95/2.5/2.5 was used instead and the stirring time increased to 2 h. The cleavage mixture was poured into cold diethyl ether and precipitated peptides were recovered. The crude peptides were purified by preparative RP-HPLC using a gradient water-95% acetonitrile in 20 min. Pure peptides were analyzed by RP-HPLC and HRMS.

12.3 Development of novel fine-tuned organic dyes for photoredox catalysis

12.3.1 Synthesis of 4CzIPN and 4DPAIPN derivatives

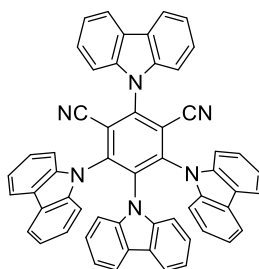


General procedure 1:

Sodium hydride (60% suspension in mineral oil, 8.0 equiv) was added slowly to a stirred solution of substituted-carbazole **S1a-d** (5.0 equiv) in dry THF (0.05 M) under a nitrogen atmosphere at RT. After 30 min, 2,4,5,6-tetrafluoroisophthalonitrile **5.6** (1.0 mmol, 1.0 equiv) was added. After stirring at RT for 15 h, 2 mL water was added to the reaction mixture to quench the excess of NaH. The resulting mixture was then concentrated under reduced pressure. The crude product was purified by recrystallization from hexane/CH₂Cl₂ then filtered. The brown liquid filtrate was concentrated and recrystallized as before. The combined solids were then purified by column chromatography on silica gel with DCM/Hexane.

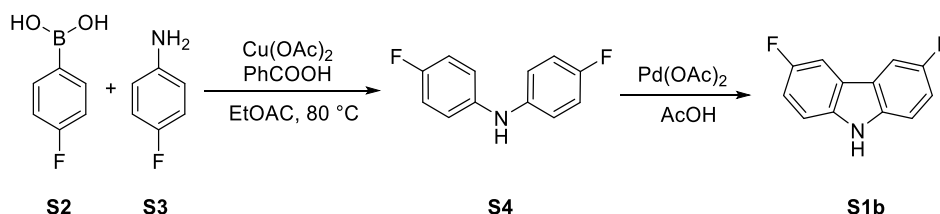
General procedure 2:

Sodium hydride (60% suspension in mineral oil, 8.0 equiv) was added slowly to a stirred solution of substituted-diphenylamine **S1d-f** (6.0 equiv) in dry DMF (0.1 M) under a nitrogen atmosphere at RT. After 45 min - 1 h, 2,4,5,6-tetrafluoroisophthalonitrile **5.6** (1.0 equiv) was added. After stirring at RT for 15 h, water and ice were added to the reaction mixture to quench the excess of NaH. The precipitate was filtered and purified by recrystallization from pentane/CH₂Cl₂ then filtered. The brown liquid filtrate was concentrated and recrystallized as before. The combined solids were then purified by column chromatography on silica gel with DCM/Hexane.

2,4,5,6-Tetra(9*H*-carbazol-9-yl)isophthalonitrile (4CzIPN, 2.23)

Following the general procedure 1 and starting from 9*H*-carbazole **S1a** (1.67 g, 10.0 mmol, 5.00 equiv), sodium hydride (0.60 g, 15 mmol, 7.5 equiv) and 2,4,5,6-tetrafluoroisophthalonitrile **5.6** (0.40 g, 2.0 mmol) in 40 mL of THF. Recrystallization (Hexanes/CH₂Cl₂ (1:1, 90 mL)) afforded the crude product as a yellow powder. Column chromatography afforded 2,4,5,6-tetra(9*H*-carbazol-9-yl)isophthalonitrile (**2.23**) as a bright yellow crystalline solid (1.14 g, 1.45 mmol, 73%).

R_f (Hexane/DCM 1/1) = 0.29. (yellow spot on TLC). ¹H NMR (400 MHz, Chloroform-*d*) δ 8.2 (d, *J* = 7.7 Hz, 2H, Ar*H*), 7.8 – 7.6 (m, 8H, Ar*H*), 7.5 (ddd, *J* = 8.0, 6.6, 1.6 Hz, 2H, Ar*H*), 7.3 (d, *J* = 7.5 Hz, 2H, Ar*H*), 7.2 (dd, *J* = 8.4, 1.5 Hz, 4H, Ar*H*), 7.2 – 7.0 (m, 8H, Ar*H*), 6.8 (t, *J* = 7.8 Hz, 4H, Ar*H*), 6.6 (td, *J* = 7.6, 1.2 Hz, 2H, Ar*H*). ¹³C NMR (101 MHz, Chloroform-*d*) δ 145.2, 144.6, 140.0, 138.2, 136.9, 134.7, 127.0, 125.8, 124.9, 124.7, 124.5, 123.8, 122.4, 121.9, 121.4, 121.0, 120.4, 119.6, 116.3, 111.6, 109.9, 109.5, 109.4. ¹H NMR shift in Chloroform-*d* are consistent with reported data.^[160]

3,6-Difluoro-9*H*-carbazole (S1b)

Following a reported procedure,^[336] a mixture of anhydrous Cu(OAc)₂ (182 mg, 1.00 mmol, 0.2 equiv), benzoic acid (611 mg, 5.00 mmol, 1.0 equiv), 4-fluoroaniline (**S3**) (556 mg, 5.00 mmol, 1.0 equiv), 4-fluorophenylboronic acid (**S2**) (2.10 g, 15.0 mmol, 3.0 equiv) and K₂CO₃ (61 mg, 5.0 mmol, 1.0 equiv) in ethyl acetate (15 mL) was heated at 80 °C for 4 hours. The crude

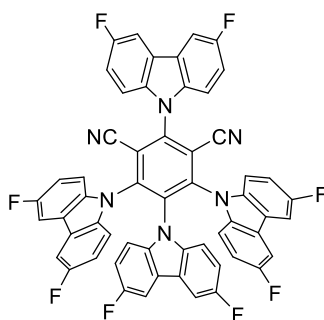
mixture was concentrated under vacuum and purified by column chromatography (pentane/ethyl acetate 1:1) to afford bis(4-fluorophenyl)amine (**S4**) (184 mg, 0.897 mmol, 18%) as a sticky black oil.

^1H NMR (400 MHz, Chloroform-*d*) δ 7.03 – 6.89 (m, 8H, ArH), 5.46 (bs, 1H, NH). ^{13}C NMR (101 MHz, Chloroform-*d*) δ 157.9 (d, J = 239.9 Hz), 139.6, 119.5 (d, J = 7.7 Hz), 116.0 (d, J = 22.4 Hz). NMR matches the literature data.^[336]

A mixture of bis(4-fluorophenyl)amine (**S4**) (159 mg, 0.775 mmol, 1.0 equiv), Pd(OAc)₂ (174 mg, 0.775 mmol, 1.0 equiv) in glacial acetic acid (14 mL) was heated at reflux for 30 minutes. The reaction mixture was filtered through celite, which was subsequently washed with sodium bicarbonate (3 X 40 mL) and ethyl acetate (3 X 40 mL). The filtrate was concentrated under vacuum and purified by column chromatography (pentane/ethyl acetate 5:1) to afford 3,6-difluoro-9H-carbazole (**S1b**) (115 mg, 5.66 mmol, 73%) as a pale brown solid.

^1H NMR (400 MHz, Chloroform-*d*) δ 7.98 (s, 1H, NH), 7.66 (dd, J = 8.9, 2.5 Hz, 2H, ArH), 7.35 (dd, J = 8.8, 4.3 Hz, 2H, ArH), 7.18 (td, J = 9.0, 2.5 Hz, 2H, ArH). ^{13}C NMR (101 MHz, Chloroform-*d*) δ 157.3 (d, J = 235.9 Hz), 136.8, 123.5 (dd, J = 9.5, 4.3 Hz), 114.4 (d, J = 25.7 Hz), 111.5 (d, J = 8.9 Hz), 106.1 (d, J = 23.8 Hz). NMR matches the literature data.^[336]

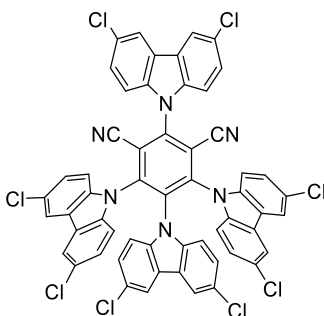
(2*r*,4*s*,5*r*)-2,4,5,6-Tetrakis(3,6-difluoro-9H-carbazol-9-yl)isophthalonitrile (4FCzIPN, **5.3**)



Following the general procedure 1 and starting from 3,6-difluoro-9H-carbazole (**S1b**) (105 mg, 0.517 mmol, 5.0 equiv), sodium hydride (33 mg, 0.83 mmol, 8.0 equiv) and 2,4,5,6-tetrafluoroisophthalonitrile **5.6** (20.7 mg, 0.103 mmol) in 2 mL of THF, (2*r*,4*s*,5*r*)-2,4,5,6-tetrakis(3,6-difluoro-9H-carbazol-9-yl)isophthalonitrile (**5.3**) was obtained as a bright yellow crystalline solid (10 mg, 11 μmol , 10%) after recrystallization in acetone (5 mL) and column chromatography using pure dichloromethane.

R_f (Hexane/DCM 1/1) = 0.23. (yellow spot on TLC). ¹H NMR (400 MHz, DMSO-*d*₆) δ 8.34 – 8.27 (m, 2H, Ar*H*), 8.09 (dd, *J* = 9.0, 4.2 Hz, 2H, Ar*H*), 7.81 (dd, *J* = 9.0, 2.6 Hz, 3H, Ar*H*), 7.72 – 7.61 (m, 6H, Ar*H*), 7.45 (dd, *J* = 8.9, 2.6 Hz, 2H), 7.36 (dd, *J* = 9.1, 4.2 Hz, 2H, Ar*H*), 7.15 – 7.05 (m, 4H, Ar*H*), 6.73 – 6.63 (m, 3H, Ar*H*). ¹³C NMR not enough material for recording a clean spectra. ¹⁹F NMR (376 MHz, DMSO-*d*₆) δ -120.6 (s, 2F), -120.8 (s, 4F), -121.5 (s, 2F). IR (ν_{max}, cm⁻¹) 3670 (w), 2985 (s), 2897 (s), 2367 (w), 2330 (w), 1725 (w), 1464 (m), 1395 (m), 1233 (m), 1183 (m), 1071 (s), 859 (m), 753 (w). HRMS (APPI/LTQ-Orbitrap) *m/z*: [M]⁺ Calcd for C₅₆H₂₄F₈N₆⁺ 932.1929; Found 932.1955.

(2*r*,4*s*,5*r*)-2,4,5,6-Tetrakis(3,6-dichloro-9*H*-carbazol-9-yl)isophthalonitrile (4ClCzIPN, 5.4)

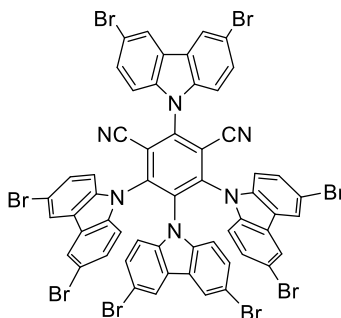


Following the general procedure 1 and starting from 3,6-dichloro-9*H*-carbazole **S1c** (1.96 g, 6.00 mmol, 6.0 equiv), sodium hydride (320 mg, 8.00 mmol, 8.0 equiv) and 2,4,5,6-tetrafluoroisophthalonitrile **5.6** (200 mg, 1.00 mmol) in 20 mL of THF. Recrystallization (Hexanes/CH₂Cl₂ (1:2, 80 mL)) gave 900 mg of yellow powder, then second recrystallization gave 325 mg of brown powder. Column chromatography of the combined solid afforded (2*r*,4*s*,5*r*)-2,4,5,6-tetrakis(3,6-dichloro-9*H*-carbazol-9-yl)isophthalonitrile (**5.4**) as a bright yellow crystalline solid (830 mg, 0.780 mmol, 87%).

R_f (Hexane/DCM 1:1): 0.25. (yellow spot on TLC). ¹H NMR (400 MHz, DMSO-*d*₆) δ 8.60 (d, *J* = 2.1 Hz, 2H, Ar*H*), 8.15 (d, *J* = 2.1 Hz, 4H, Ar*H*), 8.08 (d, *J* = 8.8 Hz, 2H, Ar*H*), 7.87 (dd, *J* = 8.8, 2.1 Hz, 2H, Ar*H*), 7.80 (d, *J* = 2.2 Hz, 2H, Ar*H*), 7.69 (d, *J* = 8.8 Hz, 4H, Ar*H*), 7.46 (d, *J* = 8.8 Hz, 2H, Ar*H*), 7.32 (dd, *J* = 8.8, 2.2 Hz, 4H, Ar*H*), 6.93 (dd, *J* = 8.8, 2.2 Hz, 2H, Ar*H*). ¹³C NMR (101 MHz, DMSO-*d*₆) δ 145.0, 144.5, 138.5, 137.4, 136.5, 135.8, 134.5, 127.8, 127.0, 126.4, 125.7, 125.3, 124.2, 123.8, 123.3, 121.6, 120.9, 120.3, 116.8, 112.6, 112.5, 112.3, 111.7. HRMS (ESI) calcd for C₅₆H₂₄Cl₈N₆ [M⁺] 1059.9565; found 1059.9573.

^1H NMR shift in CDCl_3 are consistent with reported data.^[242] However, for better solubility and better resolution new ^1H and ^{13}C spectra were recorded in $\text{DMSO}-d_6$.

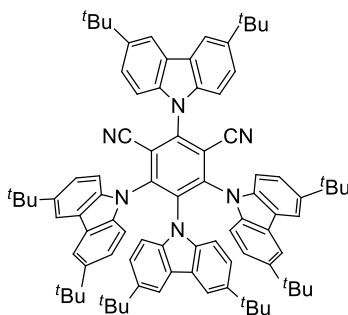
(2r,4s,5r)-2,4,5,6-Tetrakis(3,6-dibromo-9*H*-carbazol-9-yl)isophthalonitrile (4BrCzIPN, 5.5)



Following the general procedure 1 and starting from 3,6-dibromo-9*H*-carbazole **S1d** (1.00 g, 3.08 mmol, 5.0 equiv), sodium hydride (0.197 g, 4.92 mmol, 8.0 equiv) and 2,4,5,6-tetrafluoroisophthalonitrile **5.6** (0.123 g, 0.615 mmol) in 12 mL of THF, (2r,4s,5r)-2,4,5,6-tetrakis(3,6-dibromo-9*H*-carbazol-9-yl)isophthalonitrile (**2.71d**) was obtained as a bright yellow crystalline solid (562 mg, 0.396 mmol, 64%) after recrystallization in acetone (15 mL) and column chromatography using pure dichloromethane.

R_f (Hexane/DCM 1/1) = 0.43. (yellow spot on TLC). ^1H NMR (400 MHz, $\text{DMSO}-d_6$) δ 8.74 (d, $J = 1.8$ Hz, 2H, Ar*H*), 8.30 (d, $J = 2.0$ Hz, 4H, Ar*H*), 8.04 – 7.99 (m, 4H, Ar*H*), 7.96 (dd, $J = 8.6$, 1.9 Hz, 2H, Ar*H*), 7.64 (d, $J = 8.8$ Hz, 4H, Ar*H*), 7.47 – 7.35 (m, 6H, Ar*H*), 7.05 (dd, $J = 8.8$, 2.0 Hz, 2H, Ar*H*). ^{13}C NMR (101 MHz, $\text{DMSO}-d_6$) δ 145.0, 144.5, 138.6, 137.7, 136.8, 135.9, 130.4, 129.1, 128.0, 124.7, 124.2, 123.9, 123.8, 116.8, 115.0, 114.4, 113.6, 112.9, 112.7, 111.7. NMR matches the literature data.^[242,336]

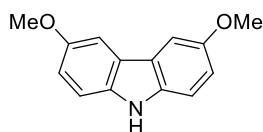
(2r,4s,5r)-2,4,5,6-Tetrakis(3,6-di-*tert*-butyl-9*H*-carbazol-9-yl)isophthalonitrile (4*t*BuCzIPN, 5.27)



Following the general procedure 1 and starting from 3,6-*tert*-butyl-9*H*-carbazole **S1d** (1.22 g, 4.37 mmol, 5.0 equiv), sodium hydride (280 mg, 7.00 mmol, 8.0 equiv) and 2,4,5,6-tetrafluoroisophthalonitrile **5.6** (175 mg, 0.875 mmol) in 17.5 mL of THF, (2*r*,4*s*,5*r*)-2,4,5,6-tetrakis(3,6-di-*tert*-butyl-9*H*-carbazol-9-yl)isophthalonitrile (**5.27**) was obtained as a yellow (light orange) crystalline solid (940 mg, 0.759 mmol, 87%) after recrystallization and column chromatography using dichloromethane:pentane (1:2).

^1H NMR (400 MHz, Acetone- d_6) δ 8.42 (d, J = 1.8 Hz, 2H, Ar*H*), 7.95 (d, J = 8.5 Hz, 2H, Ar*H*), 7.87 (d, J = 1.9 Hz, 4H, Ar*H*), 7.77 (dd, J = 8.6, 2.0 Hz, 2H, Ar*H*), 7.45 (d, J = 8.6 Hz, 4H, Ar*H*), 7.42 (d, J = 1.9 Hz, 2H, Ar*H*), 7.14 (dd, J = 8.7, 2.0 Hz, 4H, Ar*H*), 7.10 (d, J = 8.6 Hz, 2H, Ar*H*), 6.65 (dd, J = 8.7, 2.0 Hz, 2H, Ar*H*), 1.50 (s, 18H, *t*Bu), 1.32 (s, 36H, *t*Bu), 1.24 (s, 18H, *t*Bu). ^{13}C NMR (101 MHz, Acetone- d_6)²¹ δ 146.0, 144.9, 144.6, 144.1, 143.1, 139.0, 137.6, 136.5, 136.2, 124.6, 124.3, 124.2, 122.9, 121.8, 117.3, 116.8, 116.3, 115.3, 112.6, 110.4, 110.2, 109.8, 34.6, 34.3, 34.0, 31.4, 31.2. The characterization data matches the reference.^[258]

3,6-Dimethoxy-9*H*-carbazole (**S1e**)

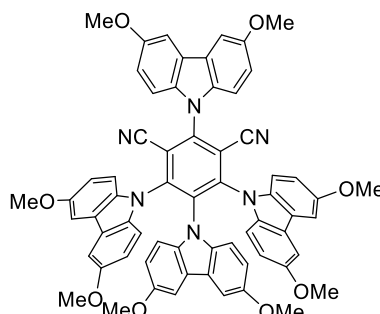


Following a reported procedure,^[337] in a 25 mL microwave tube were placed 3,6-dibromo-9*H*-carbazole (975 mg, 3.00 mmol, 1.0 equiv) and copper(I) iodide (1.14 g, 6.00 mmol, 2.0 equiv) under a nitrogen atmosphere. DMF (6 mL) and a 30% solution of NaOMe in MeOH (4 mL) were added. The tube was sealed and heated at 85 °C for 15 h, then at 105 °C for 5 h. The crude mixture was diluted in ethyl acetate and filtered over a silica pad, then concentrated under vacuum. The crude was purified by column chromatography with pentane/dichloromethane 1:1 to afford 3,6-dimethoxy-9*H*-carbazole (**S1e**) (477 mg, 2.10 mmol, 70%) as a white solid.

R_f (pentane/DCM 1:1): 0.6. ^1H NMR (400 MHz, Chloroform- d) δ 7.74 (bs, 1H, NH), 7.51 (d, J = 2.5 Hz, 2H, Ar*H*), 7.29 (d, J = 8.8 Hz, 2H, Ar*H*), 7.06 (dd, J = 8.8, 2.5 Hz, 2H, Ar*H*), 3.94 (s, 6H, OMe). ^{13}C NMR (101 MHz, Chloroform- d) δ 153.6, 135.2, 123.7, 115.2, 111.5, 102.8, 56.0. Consistent with reported data.^[337]

²¹ The signals were not fully resolved.

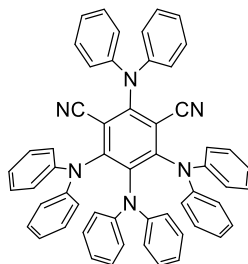
(2r,4s,5r)-2,4,5,6-Tetrakis(3,6-dimethoxy-9*H*-carbazol-9-yl)isophthalonitrile
(4MeOCzIPN, 5.28)



Following the general procedure 1 and starting from 3,6-dimethoxy-9*H*-carbazole **S1e** (443 mg, 1.95 mmol, 6.0 equiv), sodium hydride (104 mg, 2.60 mmol, 8 equiv) and 2,4,5,6-tetrafluoroisophthalonitrile **5.6** (65.0 mg, 0.325 mmol) in 6.5 mL of THF. Recrystallization and column chromatography in pure dichloromethane afforded (2r,4s,5r)-2,4,5,6-Tetrakis(3,6-dimethoxy-9*H*-carbazol-9-yl)isophthalonitrile (**5.28**) as a red crystalline solid (321 mg, 0.312 mmol, 94%).

^1H NMR (400 MHz, Chloroform-*d*) δ 7.48 (d, J = 2.5 Hz, 2H, Ar*H*), 7.41 (d, J = 8.8 Hz, 2H, Ar*H*), 7.18 – 7.15 (m, 2H, Ar*H*), 7.04 (d, J = 2.5 Hz, 4H, Ar*H*), 6.93 (d, J = 8.9 Hz, 4H, Ar*H*), 6.71 (d, J = 2.5 Hz, 2H, Ar*H*), 6.64 – 6.53 (m, 6H, Ar*H*), 6.19 (dd, J = 8.9, 2.5 Hz, 2H, Ar*H*), 3.87 (s, 6H, OMe), 3.67 (s, 12H, OMe), 3.57 (s, 6H, OMe). ^{13}C NMR (101 MHz, Chloroform-*d*) δ 155.6, 155.1, 154.3, 145.0, 144.5, 135.3, 133.7, 133.5, 132.4, 125.6, 125.2, 124.5, 115.7, 114.9, 114.4, 113.6, 112.0, 110.8, 110.5, 110.1, 104.0, 103.4, 102.8, 56.0, 55.8, 55.7. The characterization data matches the reference.^[259]

2,4,5,6-Tetrakis(diphenylamino)isophthalonitrile (4DPAIPN, 2.22)

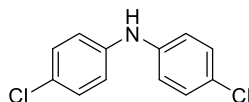


Following the general procedure 2 and starting from diphenylamine **S1f** (1.01 g, 6.00 mmol, 6.0 equiv), sodium hydride (320 mg, 8.00 mmol, 8.0 equiv) and 2,4,5,6-tetrafluoroisophthalonitrile **5.6** (200 mg, 1.00 mmol) in 10 mL of DMF. The deprotonation was performed at 50°C for 1 h, followed by stirring at the same temperature for 4 h. Recrystallization (CH₂Cl₂/pentane (1:2)) gave 2,4,5,6-tetrakis(diphenylamino)isophthalonitrile (**2.22**) as a yellow-orange crystalline solid (400 mg, 0.502 mmol, 50%).

R_f (pentane/DCM 1:1): 0.3. (yellow spot on TLC). ¹H NMR (400 MHz, Chloroform-*d*) δ 7.32 – 7.22 (m, 4H, *ArH*), 7.12 – 7.05 (m, 12H, *ArH*), 7.07 – 6.98 (m, 2H, *ArH*), 6.96 – 6.84 (m, 8H, *ArH*), 6.73 – 6.63 (m, 10H, *ArH*), 6.56 (d, *J* = 7.4 Hz, 4H, *ArH*). ¹³C NMR (101 MHz, Chloroform-*d*) δ 154.2, 151.7, 145.5, 144.6, 143.1, 140.3, 129.4, 128.6, 127.5, 124.2, 123.9, 122.9, 122.6, 122.6, 121.1, 113.1, 113.0. IR (ν_{max}, cm⁻¹) 3065 (w), 3040 (w), 2361 (w), 1586 (m), 1535 (m), 1497 (s), 1415 (s), 1275 (m), 1244 (m), 1028 (w), 907 (m), 742 (s), 698 (s). HRMS (ESI/QTOF) *m/z*: [M + H]⁺ Calcd for C₅₆H₄₄N₆⁺ 797.3387; Found 797.3375.

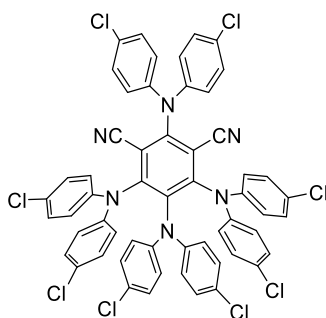
The data were not in alignment with the reported values,^[159] a crystal structure confirmed the structure (see section 12.3.4).

Bis(4-chlorophenyl)amine (**S5**)



Following a reported procedure,^[338] in a 25 mL dry microwave vial was placed Pd₂dba₃ (27.5 mg, 0.0300 mmol, 1 mol%), BrettPhos (48.3 mg, 0.0900 mmol, 3 mol%), 1-chloro-4-iodobenzene (715 mg, 3.00 mmol, 1 equiv), 4-chloroaniline (459 mg, 3.60 mmol, 1.2 equiv), Cs₂CO₃ (2.34 g, 7.20 mmol, 2.4 equiv). The vial was placed under an argon atmosphere and toluene (6 mL) was added. The reaction mixture was stirred at 70 °C overnight and then at 95 °C for 4 h. The mixture was diluted with ethyl acetate, filtered over a celite pad and concentrated under vacuum. The crude was purified by column chromatography pentane/ethyl acetate 100:0 to 95:5 to afford bis(4-chlorophenyl)amine (**S5**) (595 mg, 2.50 mmol, 83%) as a yellow-brown solid.

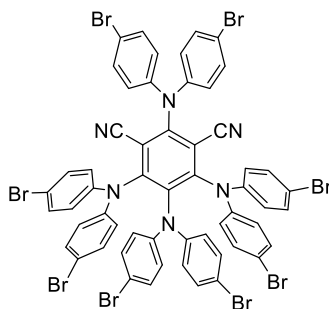
R_f (pentane/ethyl acetate 95:5): 0.45. ¹H NMR (400 MHz, Chloroform-*d*) δ 7.25 – 7.17 (m, 4H, *ArH*), 7.01 – 6.95 (m, 4H, *ArH*), 5.71 (s, 1H, *NH*). ¹³C NMR (101 MHz, Chloroform-*d*) δ 141.3, 129.4, 126.2, 119.2. Consistent with reported data.^[338]

2,4,5,6-Tetrakis(bis(4-chlorophenyl)amino)isophthalonitrile (4CIDPAIPN, 5.25)

Following the general procedure 2, and starting from bis(4-chlorophenyl)amine **S5** (550 mg, 2.31 mmol, 6.0 equiv), sodium hydride (123 mg, 3.08 mmol, 8.0 equiv) and 2,4,5,6-tetrafluoroisophthalonitrile **5.6** (77.0 mg, 0.385 mmol) in 4 mL of DMF. Recrystallization (Hexanes/CH₂Cl₂ (1:1)) followed by column chromatography afforded 2,4,5,6-tetrakis(bis(4-chlorophenyl)amino)isophthalonitrile (**5.25**) as a bright yellow crystalline solid (332 mg, 0.310 mmol, 80%).

R_f (pentane/DCM 1:1): 0.57. (yellow spot on TLC). ¹H NMR (400 MHz, Chloroform-*d*) δ 7.28 – 7.23 (m, 4H, ArH), 7.13 – 7.07 (m, 8H, ArH), 6.98 – 6.91 (m, 8H, ArH), 6.59 – 6.54 (m, 8H, ArH), 6.46 – 6.40 (m, 4H, ArH). ¹³C NMR (101 MHz, Chloroform-*d*)²² δ 153.2, 143.5, 142.8, 141.3, 138.8, 130.5, 130.2, 129.9, 129.2, 128.6, 128.3, 124.2, 123.6, 121.9, 112.5, 112.4. IR (ν_{max}, cm⁻¹) 2367 (w), 1586 (w), 1535 (w), 1485 (s), 1409 (w), 1282 (m), 1098 (m), 1015 (w), 913 (w), 825 (m), 729 (m), 660 (w). HRMS (APPI/LTQ-Orbitrap) m/z: [M+H]⁺ Calcd for C₅₆H₃₃Cl₈N₆⁺ 1069.0269; Found 1069.0277. A crystal structure confirmed the structure (see section 12.3.4).

²² One carbon is not resolved.

2,4,5,6-Tetrakis(bis(4-bromophenyl)amino)isophthalonitrile (4BrDPAIPN, 5.26)

Following the general procedure 1 and starting from bis(4-bromophenyl)amine **S1g** (1.10 g, 4.47 mmol, 5.00 equiv), sodium hydride (0.286 g, 7.16 mmol, 8.00 equiv) and 2,4,5,6-tetrafluoroisophthalonitrile **5.6** (0.179 g, 0.895 mmol) in 18 mL of THF. Before recrystallization, water (5 mL) was added and the mixture was sonicated for 5 min before being filtered. Two recrystallization (pentane/CH₂Cl₂ 2:1) afforded 2,4,5,6-tetrakis(bis(4-bromophenyl)amino)isophthalonitrile (**5.26**) as a bright yellow crystalline solid (1.34 g, 0.938 mmol, 94%).

R_f (pentane/DCM 1:1): 0.6. (yellow spot on TLC). ¹H NMR (400 MHz, Chloroform-*d*) δ 7.45 – 7.37 (m, 4H, ArH), 7.26 – 7.22 (m, 8H, ArH), 7.13 – 7.05 (m, 4H, ArH), 6.93 – 6.82 (m, 4H, ArH), 6.58 – 6.45 (m, 8H, ArH), 6.42 – 6.33 (m, 4H, ArH). ¹³C NMR (101 MHz, Chloroform-*d*) δ 153.1, 151.4, 143.9, 143.2, 141.7, 138.7, 132.9, 132.3, 131.3, 124.6, 124.0, 122.2, 118.3, 118.0, 116.2, 112.6, 112.5. IR (ν_{max}, cm⁻¹) 2367 (w), 1777 (w), 1586 (w), 1523 (w), 1485 (s), 1421 (m), 1389 (m), 1307 (m), 1282 (m), 1231 (w), 1072 (m), 1009 (m), 818 (m), 710 (w). HRMS (ESI/QTOF) *m/z*: [M + K]⁺ Calcd for C₅₆H₃₂Br₈KN₆⁺ 1458.5787; Found 1458.5812.

12.3.2 Physical measurements of 4CzIPN derivatives **5.3** to **5.5**

Spectroscopic characterization

4CzIPN derivatives **2.23** and **5.3** to **5.5** were studied at $10\ \mu\text{mol.L}^{-1}$ in acetonitrile and dichloromethane. Absorbance was recorded between 200 and 800 nm. The excitation wavelength for fluorescence was 360 nm.

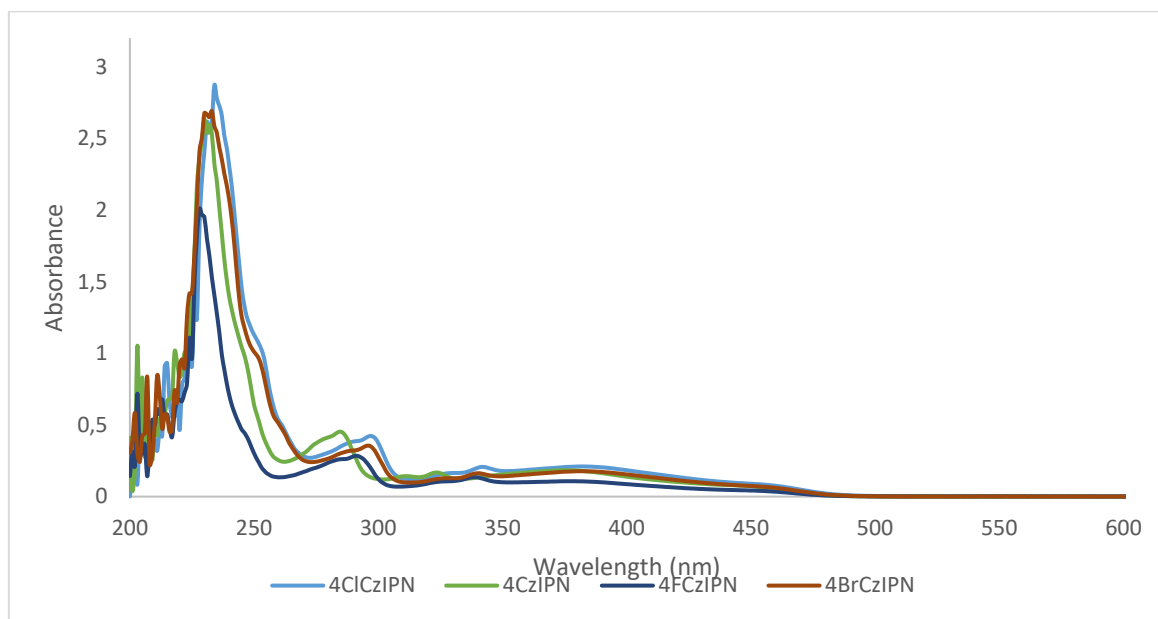


Figure 25: UV-Vis spectra of 4CzIPN derivatives **2.23** and **5.3** to **5.5** in DCM.

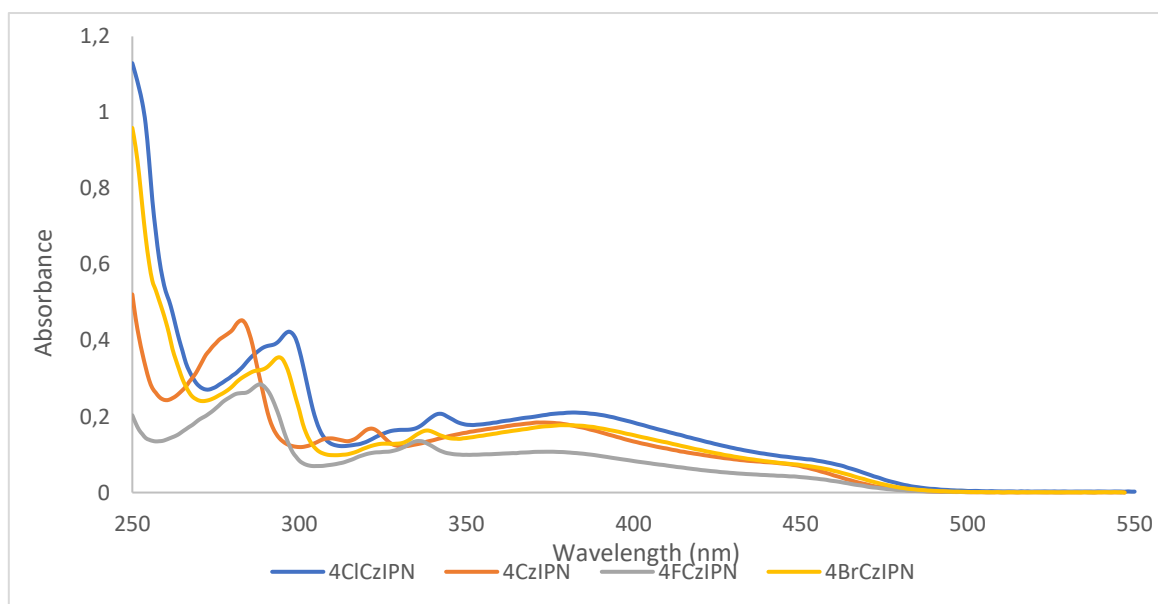


Figure 26: Zoom on the 250-550 nm region of the UV-Vis spectra of 4CzIPN derivatives **2.23** and **5.3** to **5.5** in DCM.

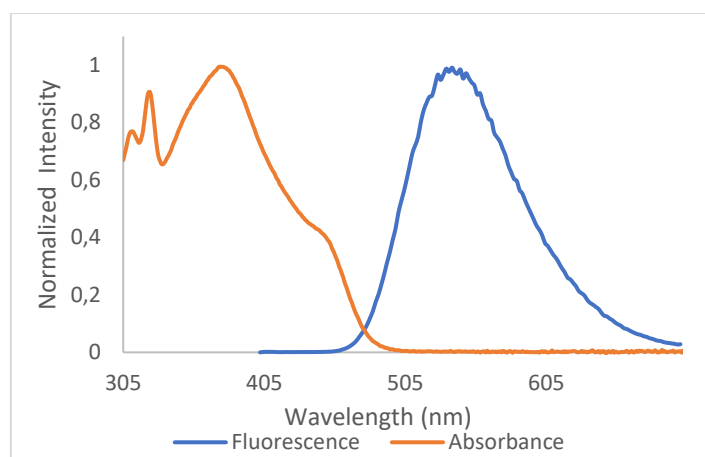


Figure 27: Absorbance and emission of 4CzIPN (**2.23**) at $10\ \mu\text{mol.L}^{-1}$ in DCM.

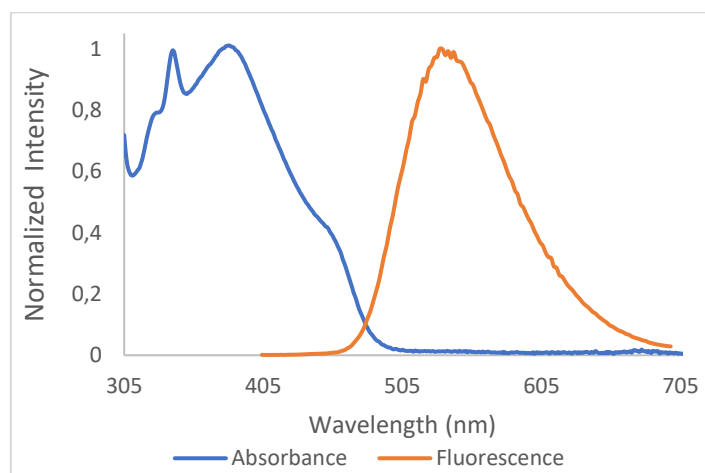


Figure 28: Absorbance and emission of 4ClCzIPN (**5.4**) at $10\ \mu\text{mol.L}^{-1}$ in DCM.

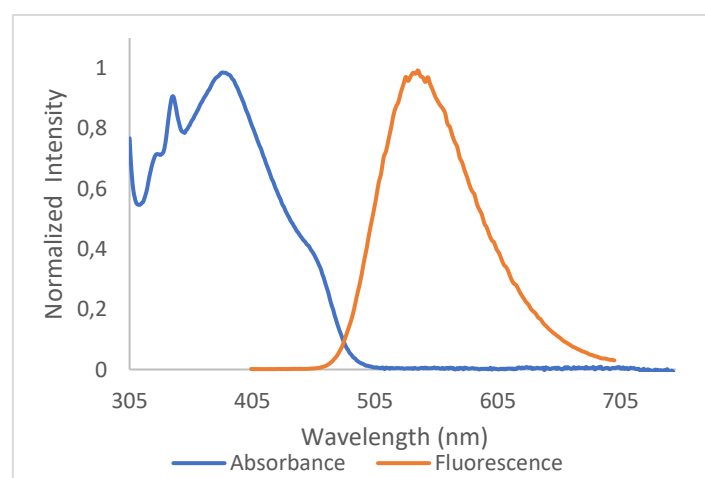


Figure 29: Absorbance and emission of 4BrCzIPN (**5.5**) at $10\ \mu\text{mol.L}^{-1}$ in DCM.

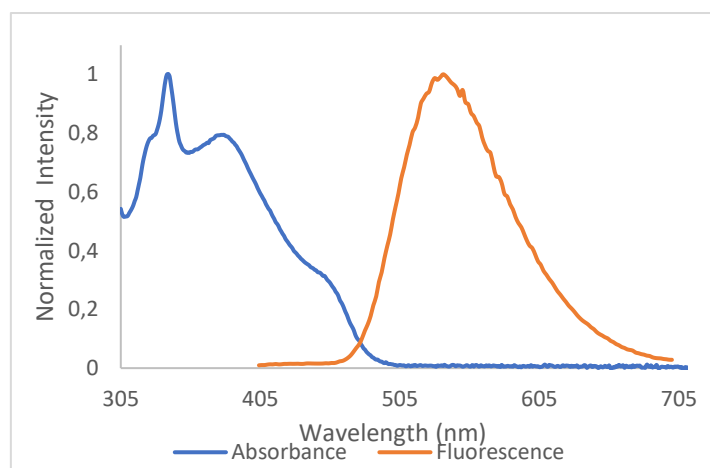


Figure 30: Absorbance and emission of 4FCzIPN (**5.3**) at $10 \mu\text{mol.L}^{-1}$ in DCM.

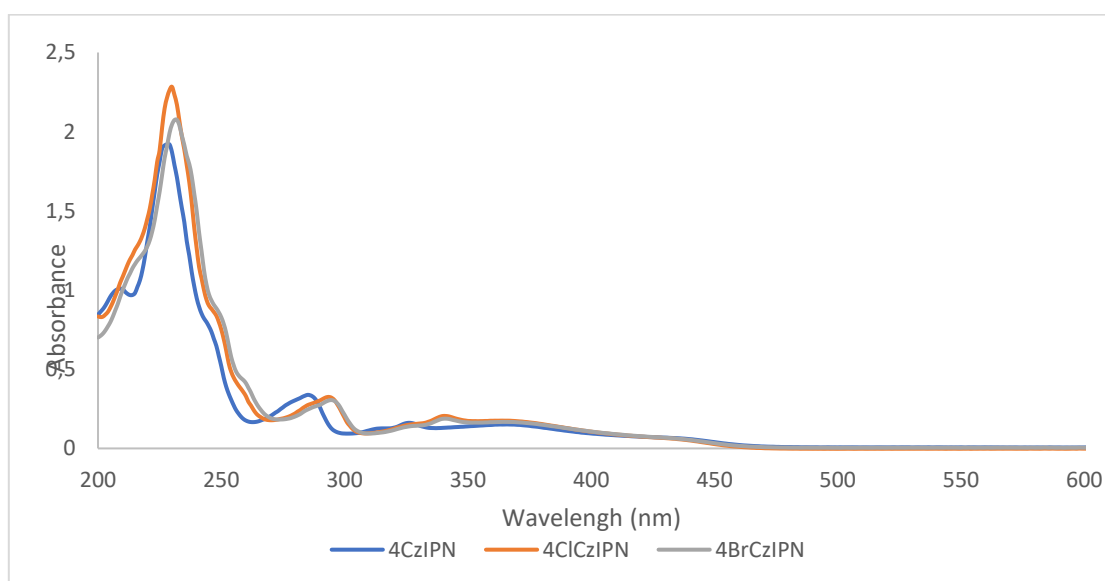


Figure 31: UV-Vis spectra of 4CzIPN derivatives **2.23** and **5.3** to **5.5** in acetonitrile.

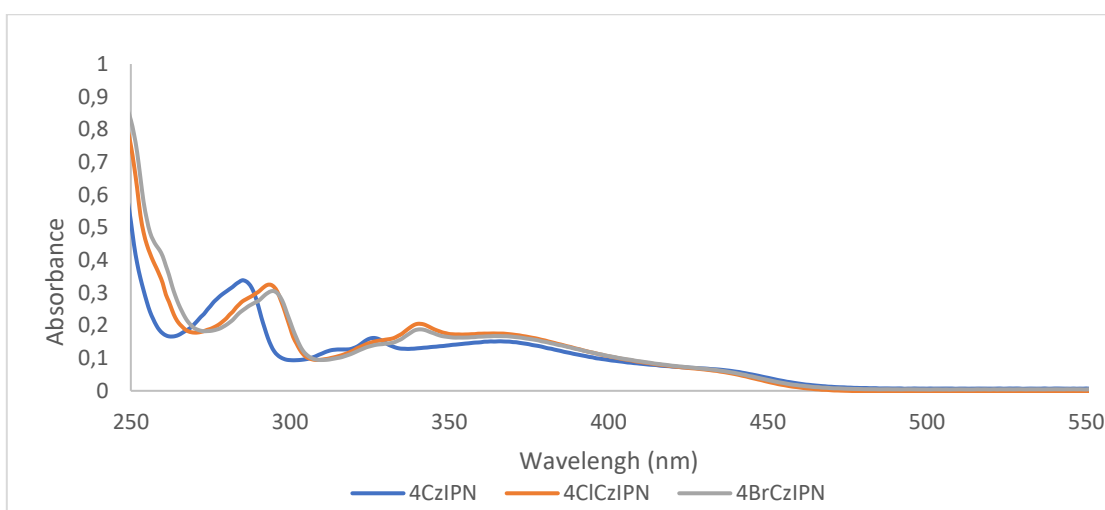


Figure 32: Zoom on the 250-550 nm region of the UV-Vis spectra of 4CzIPN derivatives **2.23** and **5.3** to **5.5** in acetonitrile.

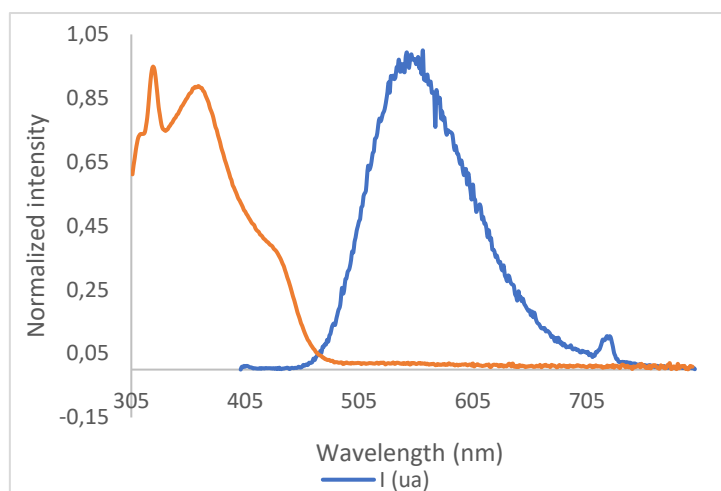


Figure 33: Absorbance and emission of 4CzIPN (**2.23**) at $10 \mu\text{mol.L}^{-1}$ in acetonitrile.

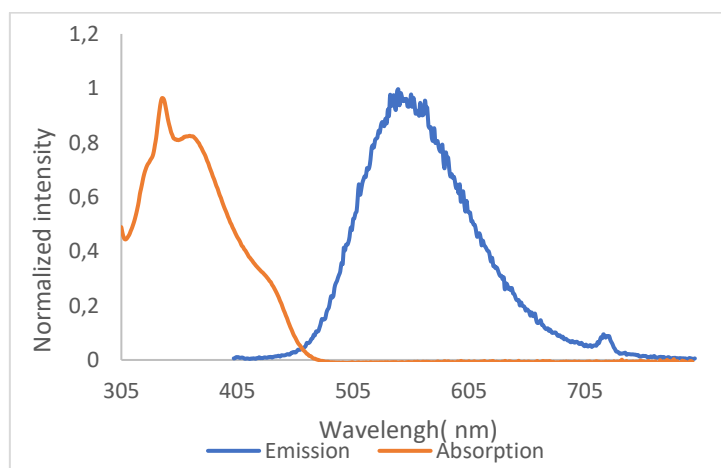


Figure 34: Absorbance and emission of 4ClCzIPN (**5.4**) at $10 \mu\text{mol.L}^{-1}$ in acetonitrile.

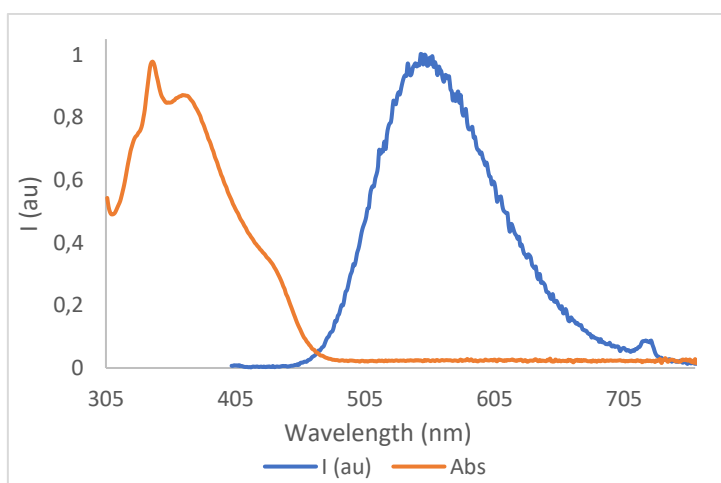


Figure 35: Absorbance and emission of 4BrCzIPN (**5.5**) at $10 \mu\text{mol.L}^{-1}$ in acetonitrile.

Electrochemical measurements

Cyclic Voltammetry (CV) was performed using an Autolab Potentiostat, with a three-electrode cell configuration: a glassy carbon electrode as the working electrode, Pt wire as a counter electrode and an Ag/AgCl (KCl, 3M) electrode as the reference electrode. Bu_4NPF_6 was employed as the electrolyte (0.1 M) and ferrocene was added as the internal standard.

For comparison, 4ClCzIPN (**5.4**) was studied in the same conditions as previous reports on 4CzIPN, at 1mM in degassed acetonitrile.^[159,244] All 4CzIPN derivatives were studied in 1 mM solutions in degassed DCM at a scan rate of 0.1 V/s, to ensure solubility. Measures on 4FCzIPN were performed on a 0.5 mM solution due to the quantity of available material.

Table 21: Redox potentials of 4CzIPN derivatives in acetonitrile^a

Photocatalyst	$E_{1/2}(\text{P}/\text{P}^-)$	$E_{1/2}(\text{P}^+/\text{P})$	E_{0-0}	$E_{1/2}(\text{P}^+/\text{P}^*)$	$E_{1/2}(\text{P}^*/\text{P}^-)$
4CzIPN ^[159]	-1.21	+1.52	2.56	-1.04	+1.35
4CzIPN _{exp}	-1.05	+1.68	2.64	-0.96	+1.59
4ClCzIPN	-0.97	+2.05	2.68	-0.63	+1.71

Table 22: Redox potentials of 4CzIPN derivatives in DCM^a

Photocatalyst	$E_{1/2}(\text{P}/\text{P}^-)$	$E_{1/2}(\text{P}^+/\text{P})$	E_{0-0}	$E_{1/2}(\text{P}^+/\text{P}^*)$	$E_{1/2}(\text{P}^*/\text{P}^-)$
4CzIPN	-1.16	+1.61	2.59	-0.98	+1.43
4ClCzIPN	-1.11	+1.73	2.59	-0.86	+1.48
4BrCzIPN	-1.06	+1.76	2.58	-0.82	+1.52
4FCzIPN	-1.08	+1.45	2.60	-1.15	+1.52

^aPotentials in V vs SCE, wavelength in nanometers. The excitation energy E_{0-0} was estimated by the point of intersection of the normalized absorbance and emission signals. $E_{1/2}(\text{P}^+/\text{P}^*) = E_{1/2}(\text{P}^+/\text{P}) - E_{0-0}$ and $E_{1/2}(\text{P}^*/\text{P}^-) = E_{0-0} + E_{1/2}(\text{P}/\text{P}^-)$.

It worth to be noted that measured values were significantly different from previous reports, both in cyclic voltammetry and in the estimation of E_{0-0} , likely due to difference of approximation methods (Table 1). However, in the conditions of this study, an anodic and cathodic shift were measured for 4ClCzIPN in acetonitrile in comparison to 4CzIPN. This confirmed our hypothesis regarding the influence of electron-withdrawing substituents on the carbazole moieties. Results

in DCM were in alignment, with anodic and cathodic shifts measured for 4BrCzIPN and 4FCzIPN.

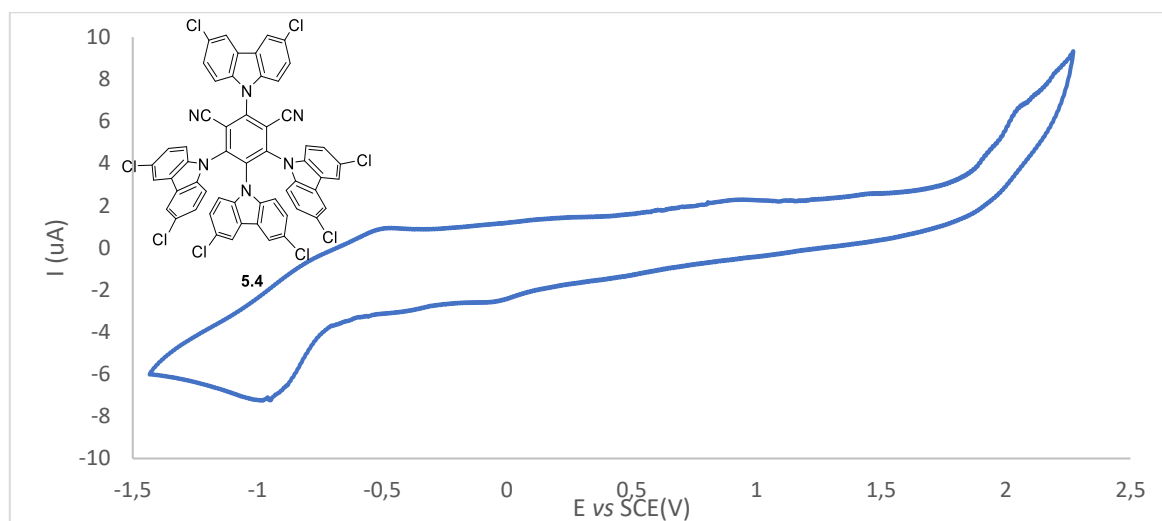


Figure 36: Cyclic Voltammetry of 4ClCzIPN (**5.4**) in acetonitrile.

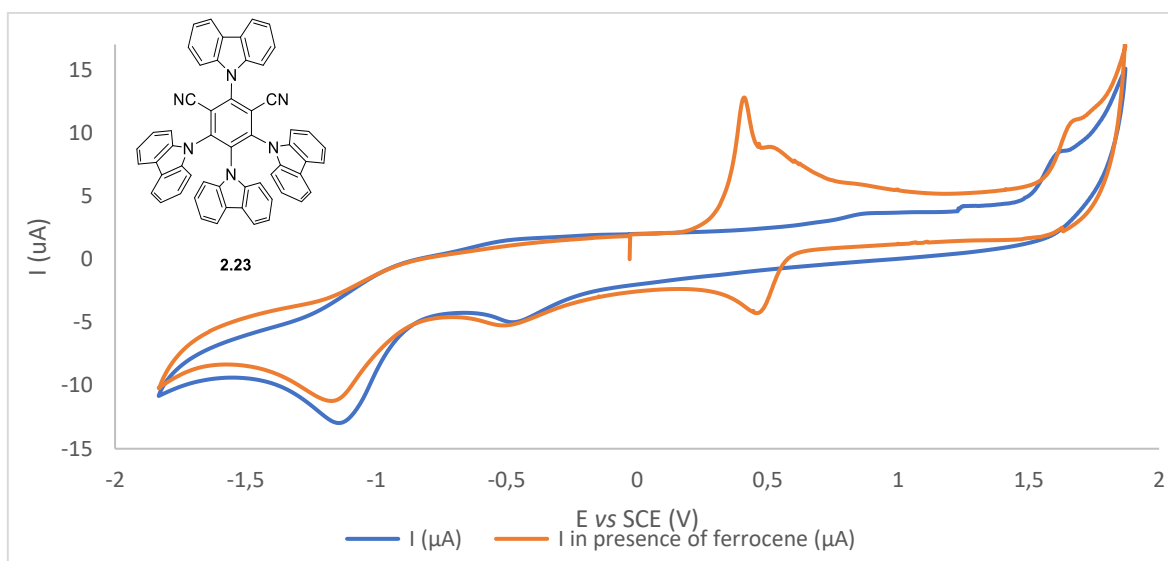


Figure 37: Cyclic Voltammetry of 4CzIPN (**2.23**) in DCM.

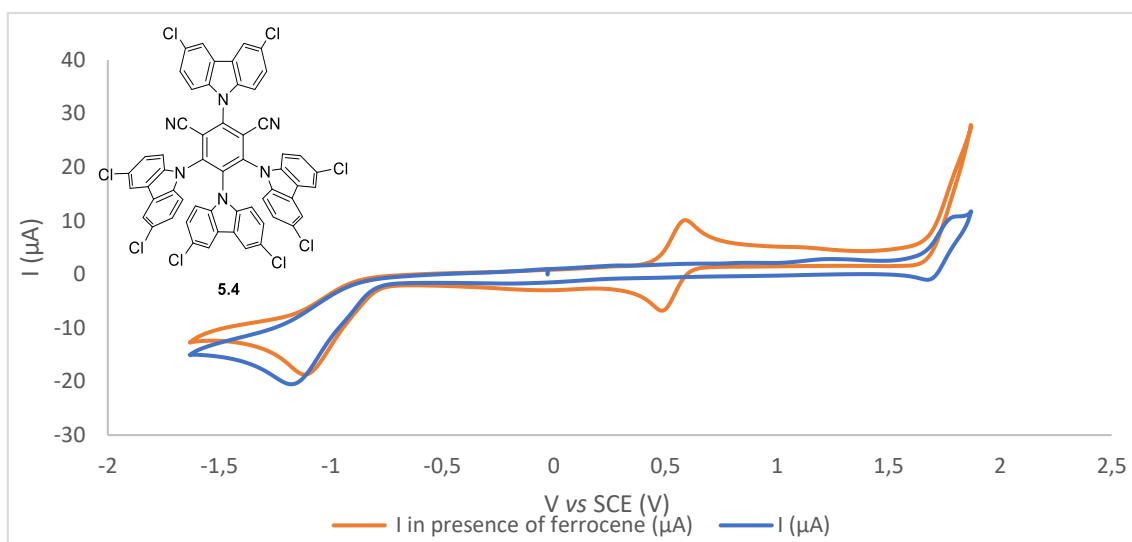


Figure 38: Cyclic Voltammetry of 4ClCzIPN (**5.4**) in DCM.

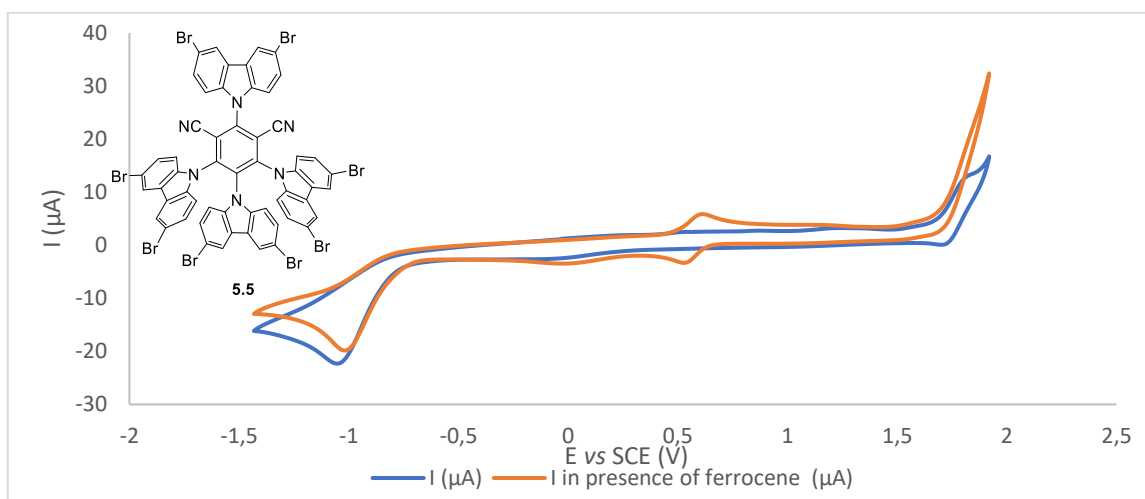


Figure 39: Cyclic Voltammetry of 4BrCzIPN (**5.5**) in DCM.

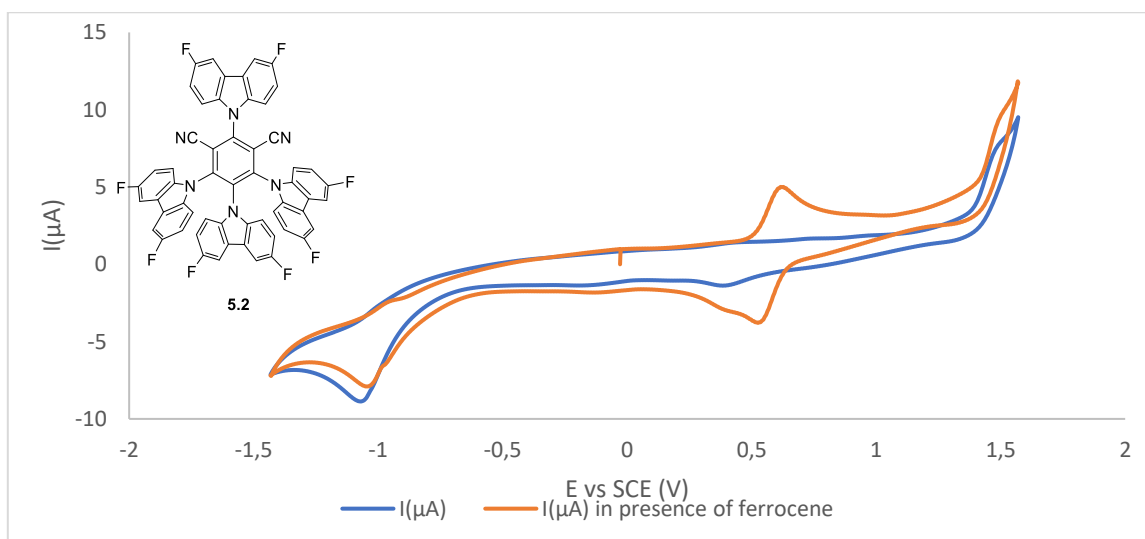


Figure 40: Cyclic Voltammetry of 4FCzIPN (**5.2**) in DCM.

12.3.3 Physical measurements of 4CzIPN and 4DPAIPN derivatives **5.25** to **5.28**

Spectroscopic characterization

4CZIPN and 4DPAIPN derivatives **5.25** to **5.28** were studied at $10\ \mu\text{mol.L}^{-1}$ in acetonitrile. Absorbance was recorded between 200 and 800 nm. The excitation wavelength for fluorescence was 360 nm.

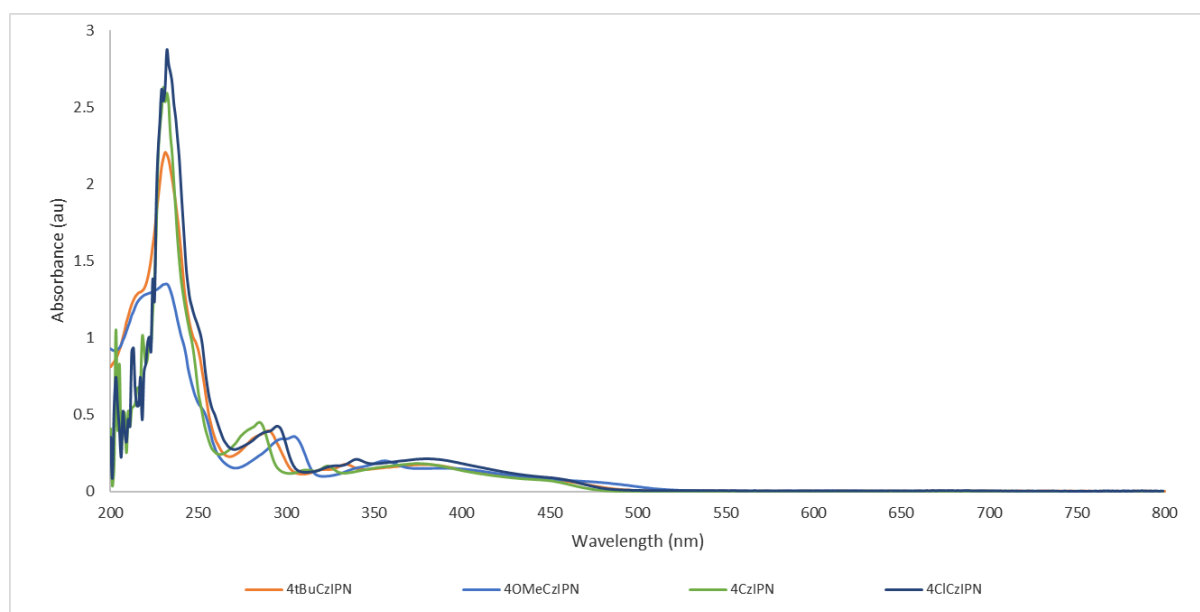


Figure 41: UV-Vis spectra of 4CzIPN derivatives in acetonitrile

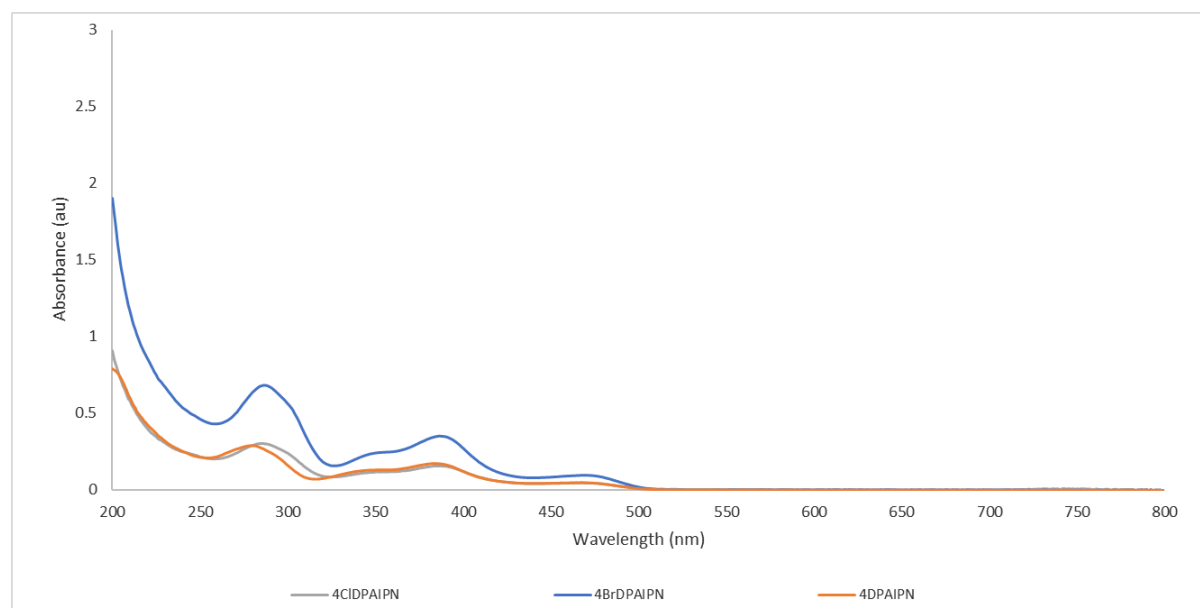


Figure 42: UV-Vis spectra of 4DPAIPN derivatives **5.25** to **5.28** in acetonitrile

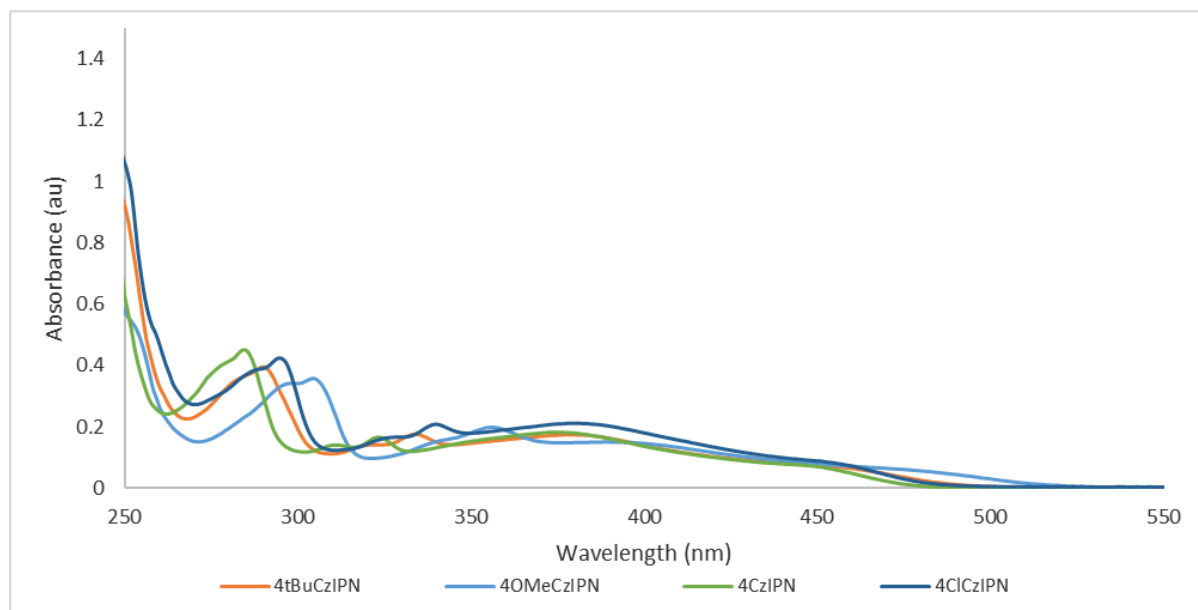


Figure 43: Zoom on the 250-550 nm of the UV-Vis spectra of 4CzIPN derivatives in acetonitrile

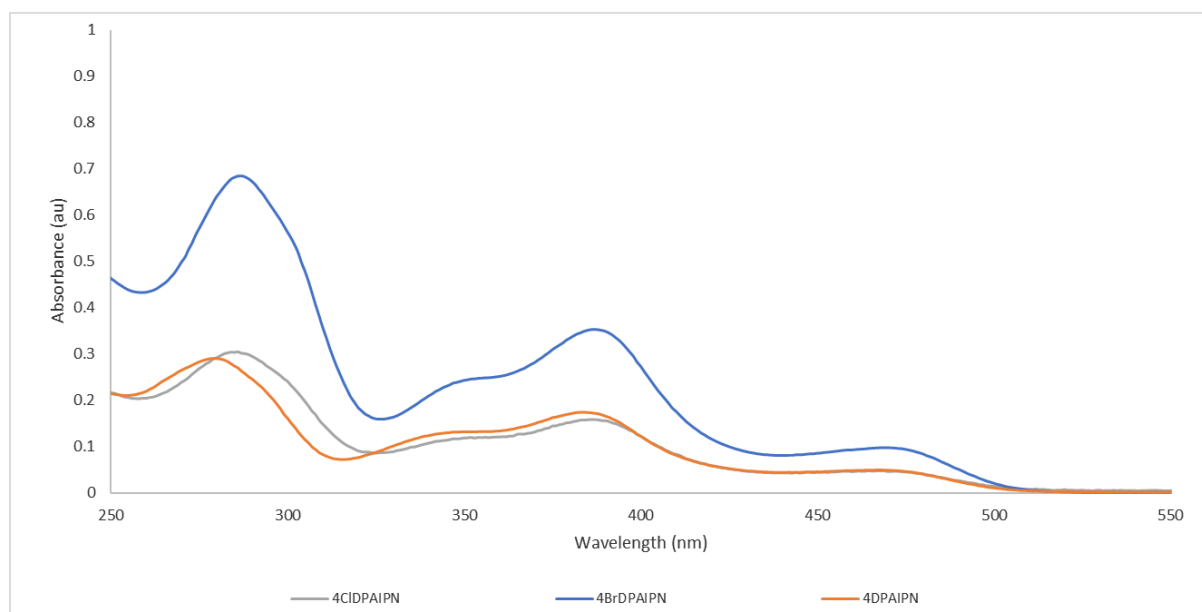


Figure 44: Zoom on the 250-550 nm of the UV-Vis spectra of 4DPAIPN derivatives **5.25** to **5.28** in acetonitrile

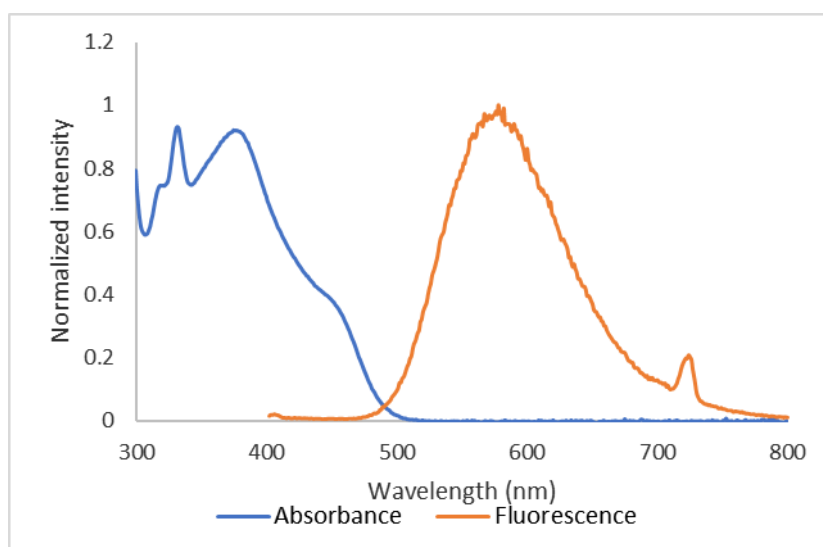


Figure 45 : Absorbance and emission of 4tBuCzIPN (**5.27**) at 10 $\mu\text{mol.L}^{-1}$ in acetonitrile

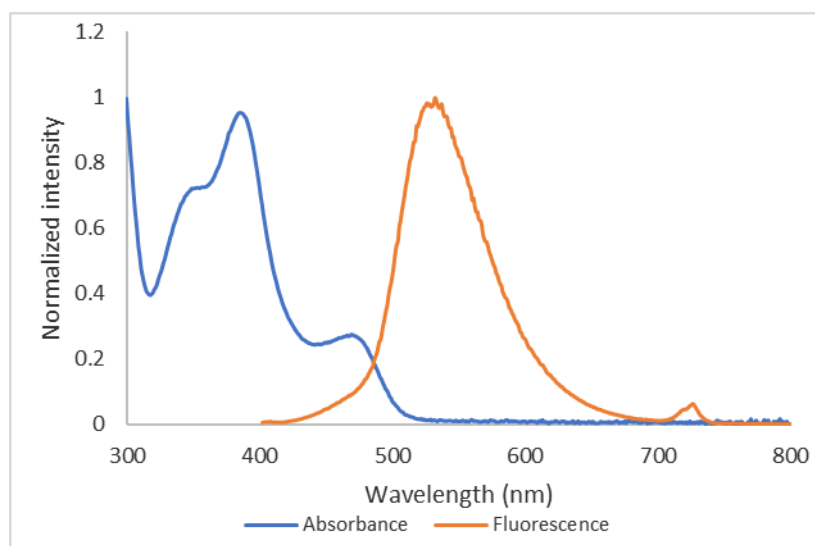


Figure 46 : Absorbance and emission of 4DPAIPN (**2.22**) at 10 $\mu\text{mol.L}^{-1}$ in acetonitrile

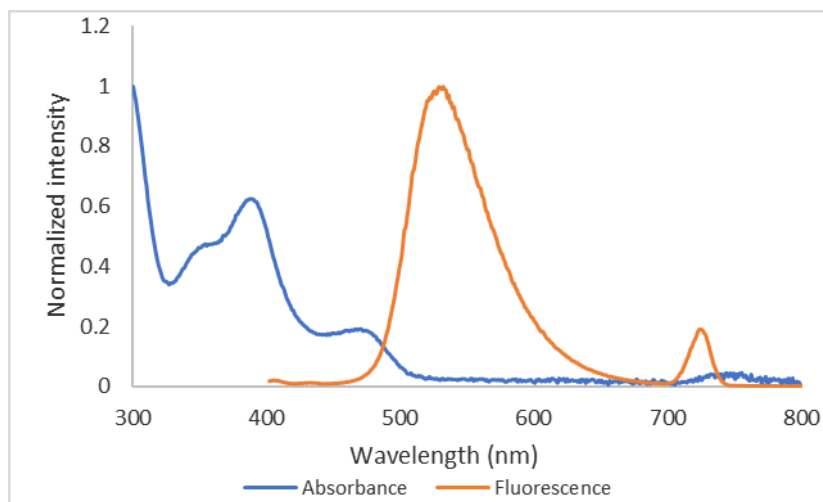


Figure 47 : Absorbance and emission of 4CIDPAIPN (**5.25**) at 10 $\mu\text{mol.L}^{-1}$ in acetonitrile

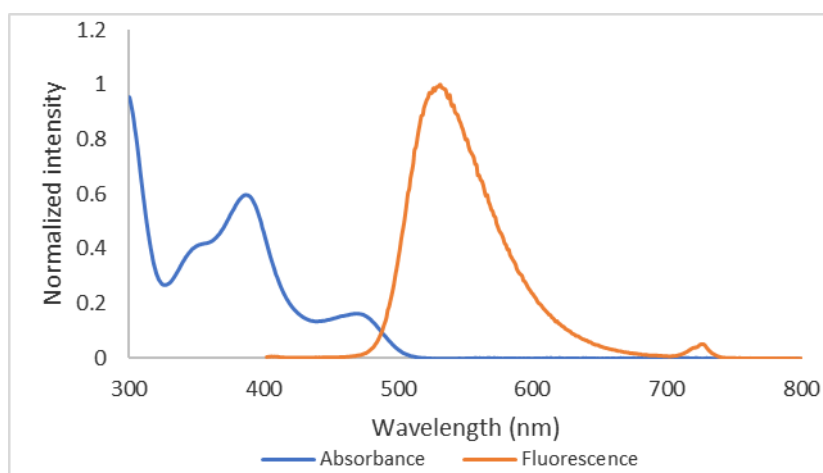


Figure 48: Absorbance and emission of 4BrDPAIPN (**5.26**) at 10 $\mu\text{mol.L}^{-1}$ in acetonitrile

Electrochemical measurements

The cyclic voltammetry of the organic dyes were performed. For comparison, the organic dyes were studied in the same conditions as previous reports on 4CzIPN, at 1mM in degassed acetonitrile at scan rates of 0.1, 0.5 and 1 V/s.^[159,244,260] For clarity, curves are presented at 0.1 V/s as well as a superposition.

In the case of 4CzIPN derivatives, irreversible waves were observed in the anodic scan and correspond to the oxidation of the carbazole moieties, as reported by Ishimatsu et al.^[244] The same group described that the introduction of *t*Bu groups prevents this polymerization.^[258] Reversibility was evaluated through plots of the intensity of the peaks related to the square root of the scan rate.^[262] Reversible waves were observed in the cathodic scans in all cases. They correspond to the reduction of the dicyanobenzene group.^[258] For 4BrDPAIPN (**2.22**), higher scan rates gave surprising curves for the reduction, hence the reversibility could not be determined by this method. With a peak to peak separation of 60 mV, this process in quasi-reversible.

In the conditions of this study, the expected anodic and cathodic shifts upon substitution effect were measured (Table 23). The trend in reduction potentials of 4DPAIPN derivatives (**2.22**<**5.26**<**5.25**) follows the electronegativity of the substituents ($\text{H}<\text{Br}<\text{Cl}$). This can be rationalized by a greater stabilization of the lowest unoccupied molecular orbital (LUMO) with substitution.^[260] Similarly, 4*t*BuCzIPN (**2.27**) and 4OMeCzIPN (**2.28**) were less oxidant than 4CzIPN (**2.23**) by destabilization of the LUMO.

The excitation energy E_{0-0} was estimated by the point of intersection of the normalized absorbance and emission signals (Section 12.3.3). $E_{1/2}(P^+/P^*) = E_{1/2}(P^+/P) - E_{0-0}$ and $E_{1/2}(P^*/P^-) = E_{0-0} + E_{1/2}(P/P^-)$.^[158]

Table 23: Electrochemical properties of 4CzIPN and DPAIPN derivatives^a

Photocatalyst	E_{0-0} (eV)	$E_{1/2}(P/P^-)$	$E_{1/2}(P^*/P^-)$	$E_{1/2}(P^+/P)$	$E_{1/2}(P^+/P^*)$
4CzIPN (2.23) ^[159]	2.53	-1.21	+1.35	+1.52	-1.04
4CzIPN (2.23)	2.64	-1.32	+1.32	+1.39	-1.25
4tBuCzIPN (2.27)	2.53	-1.32	+1.21	+1.22	-1.31
4OMeCzIPN (2.28)	2.61 ^[259]	-1.38	+1.23	+1.05	-1.56
4OMeCzIPN (2.28) ^[259]	2.61	-1.50	+1.27	+1.11	-1.34
4CIDPAIPN (5.25)	2.53	-1.44	+1.09	+1.23	-1.30
4BrDPAIPN (5.26)	2.53	-1.55	+0.98	+1.12	-1.41
"4DPAIPN" (2.22) ^[159]	2.62	-1.52	+1.10	+1.34	-1.28
4DPAIPN (2.22)	2.55	-1.65	+0.90	+1.03	-1.52

^aPotentials in V vs SCE, wavelength in nanometers.

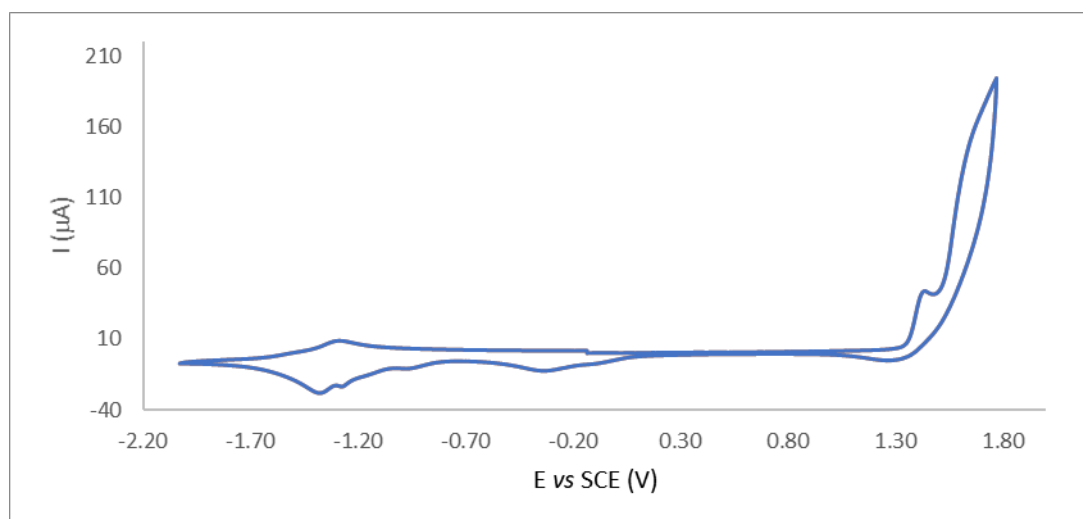


Figure 49: Cyclic voltammetry of 4CzIPN (**2.23**) in acetonitrile at 0.1 V/S

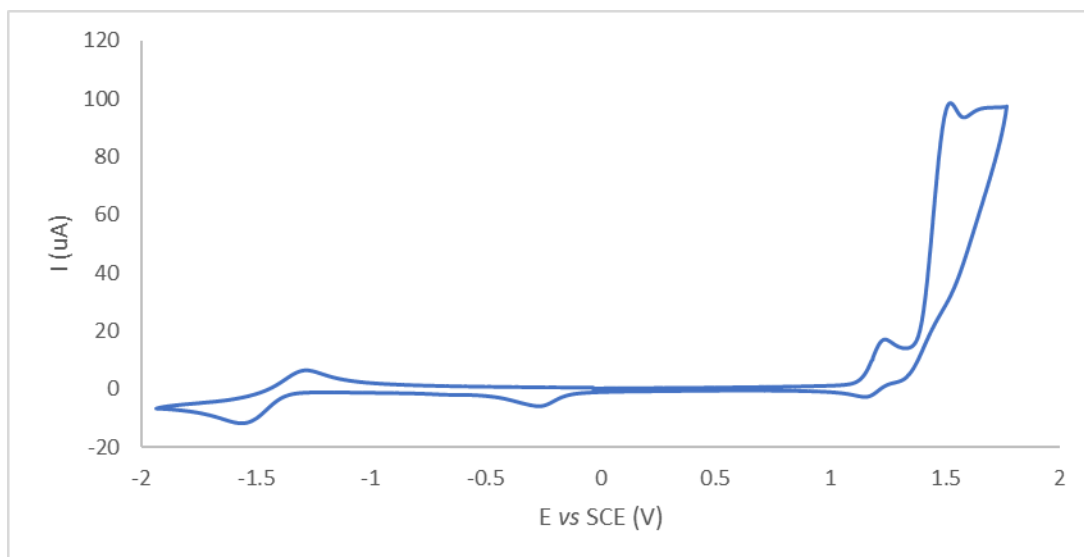


Figure 50 : Cyclic voltammetry of 4tBuCzIPN (**5.27**) in acetonitrile 0.1 V/S

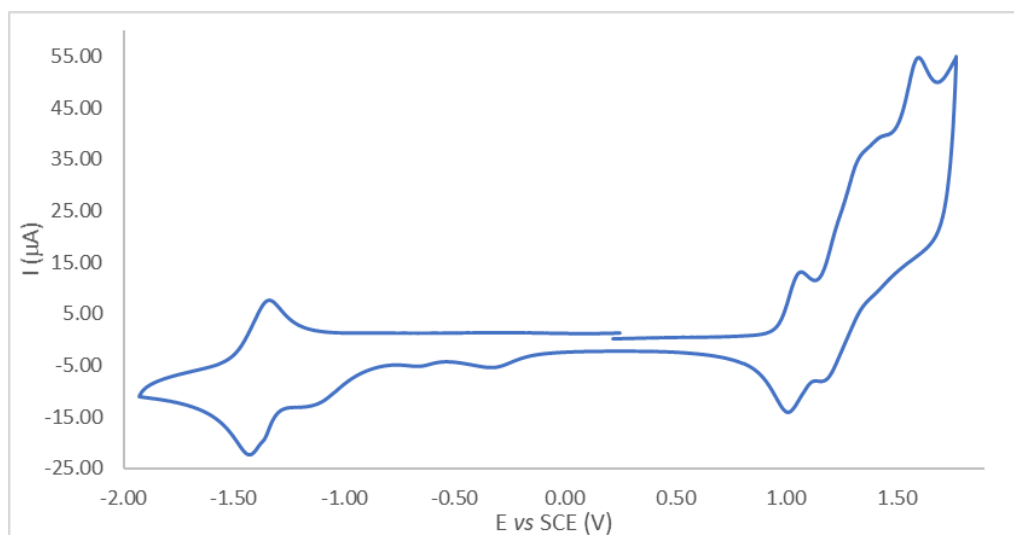


Figure 51: Cyclic voltammetry of 4OMeCZIPN (**5.28**) in acetonitrile 0.1 V/S

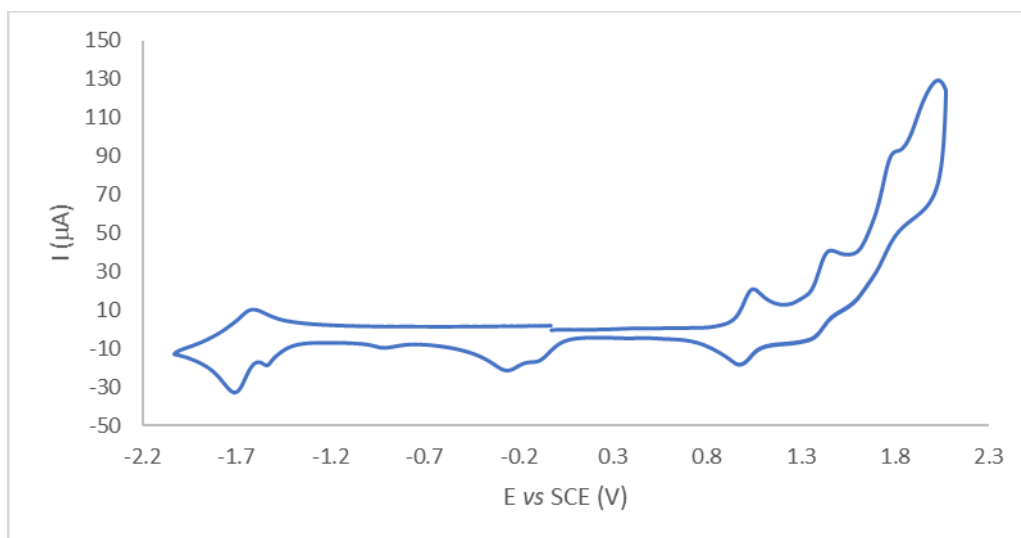


Figure 52: Cyclic voltammetry of 4DPAIPN (**2.22**) in acetonitrile 0.1 V/S

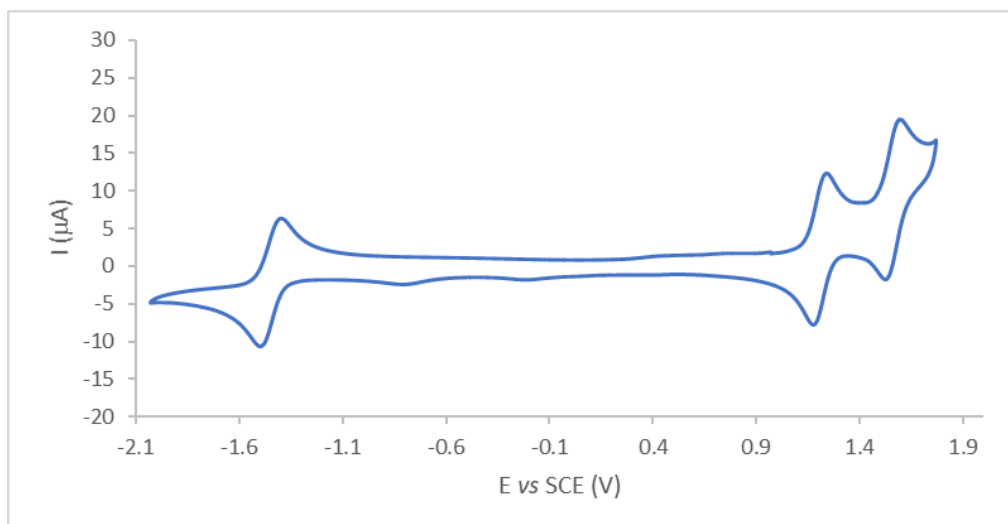


Figure 53: Cyclic voltammetry of 4CIDPAIPN (**5.25**) in acetonitrile 0.1 V/S

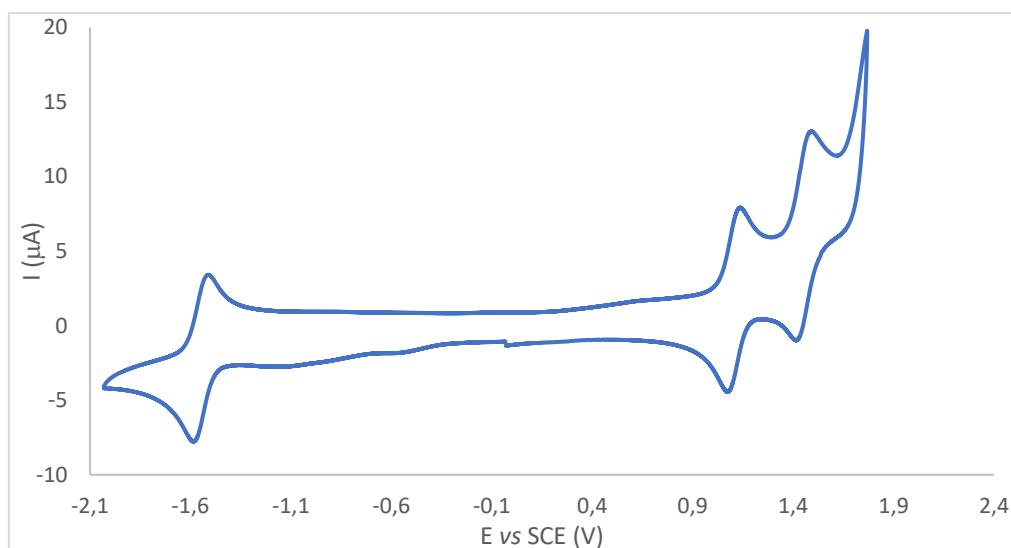


Figure 54 : Cyclic voltammetry of 4BrDPAIPN (**5.26**) in acetonitrile 0.1 V/S

Graphs for reversibility determination.

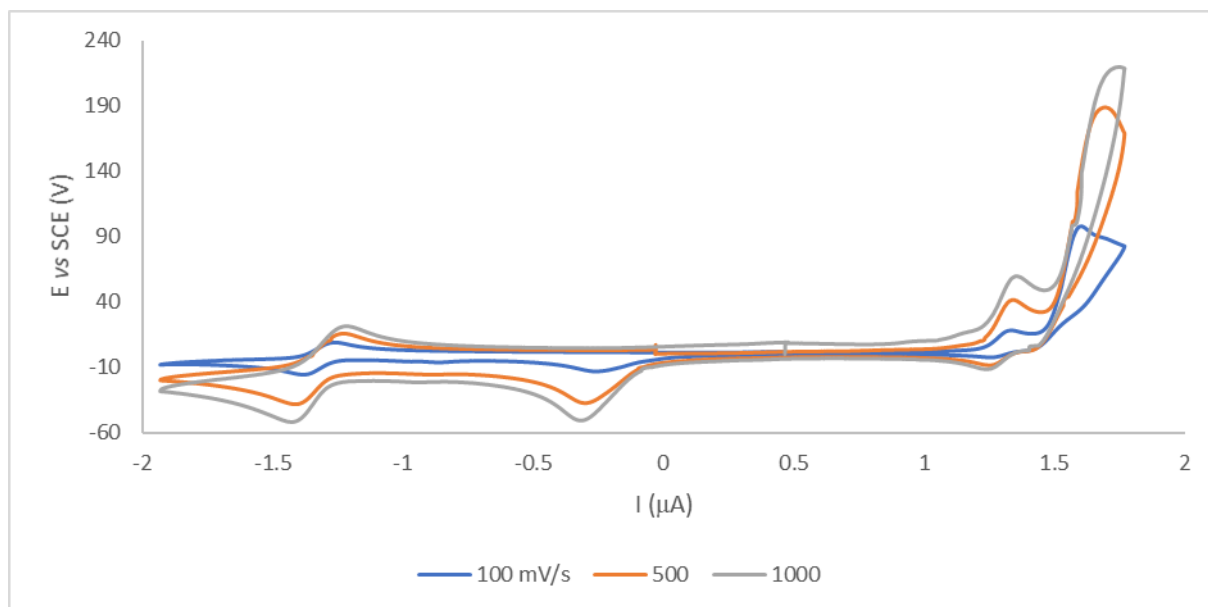


Figure 55: Cyclic voltammetry of 4tBuCzIPN (5.27)

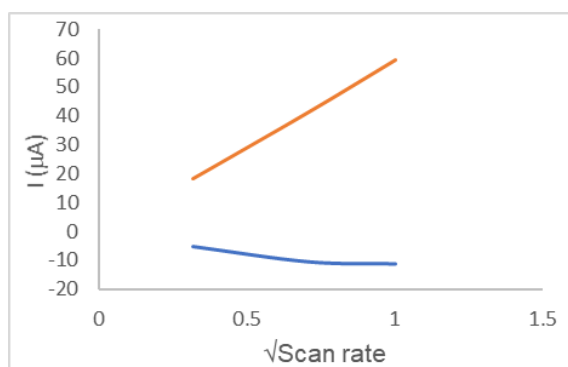


Figure 56: Intensity vs $\sqrt{\text{scan rate}}$, 4tBuCzIPN-Red

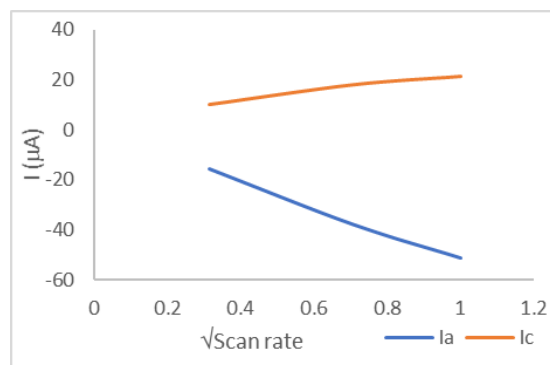


Figure 57: Intensity vs $\sqrt{\text{scan rate}}$, 4tBuCzIPN-Ox

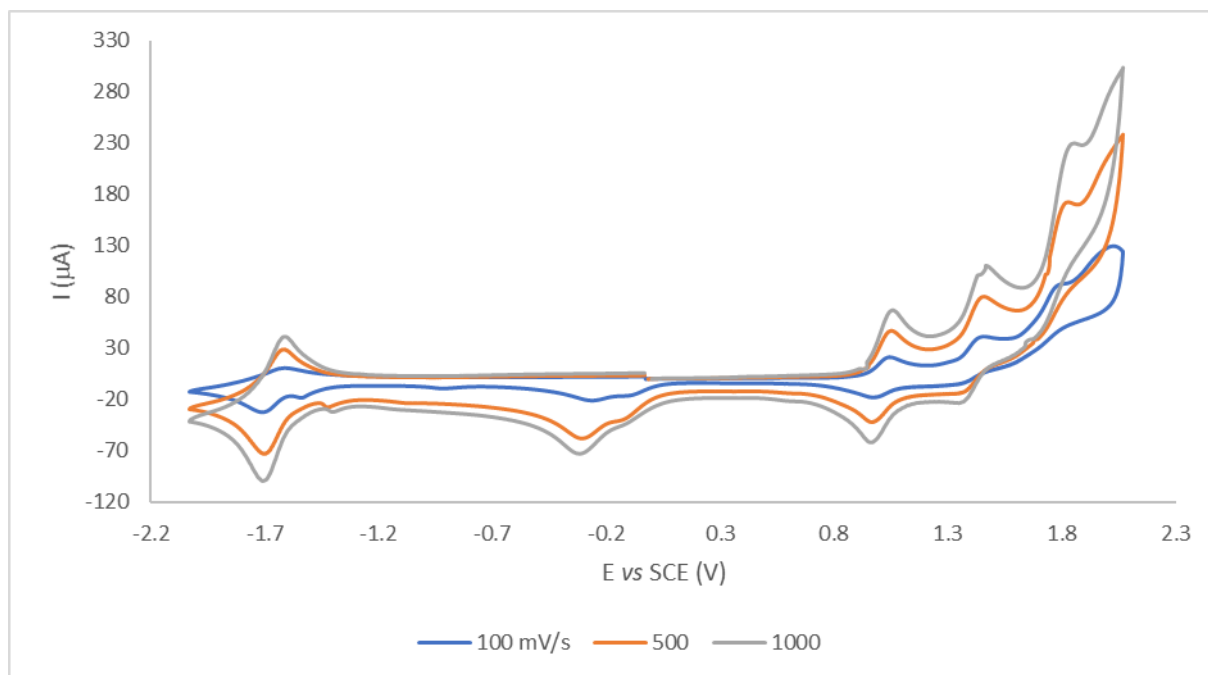


Figure 58: Cyclic voltammetry of 4DPAIPN (2.22)

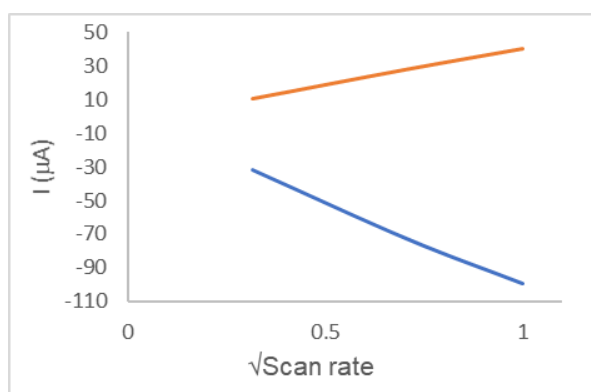


Figure 59: Intensity vs $\sqrt{\text{scan rate}}$, 4DPAIPN-Red

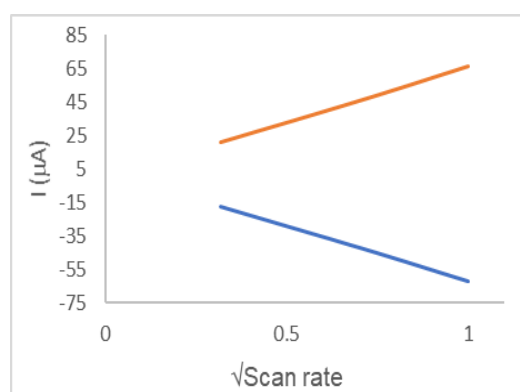


Figure 60: Intensity vs $\sqrt{\text{scan rate}}$, 4DPAIPN-Ox

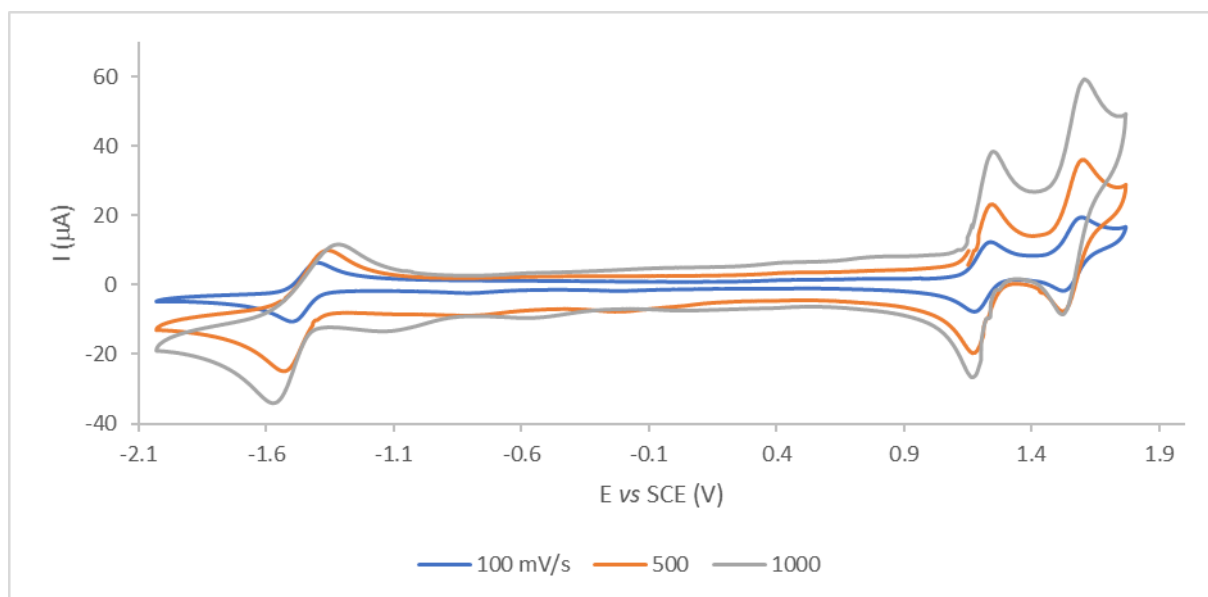


Figure 61: Cyclic voltammetry of 4CIDPAIPN (5.25)

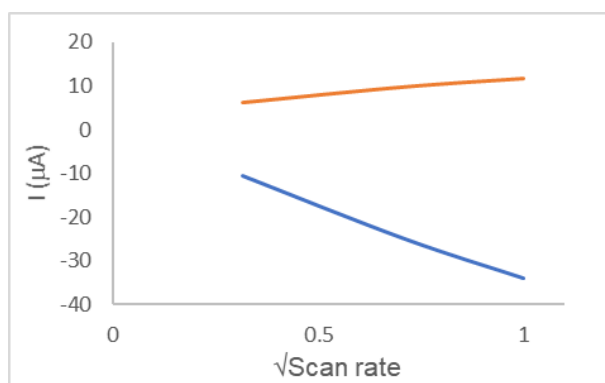


Figure 62: Intensity vs $\sqrt{\text{scan rate}}$, 4CIDPAIPN-Red

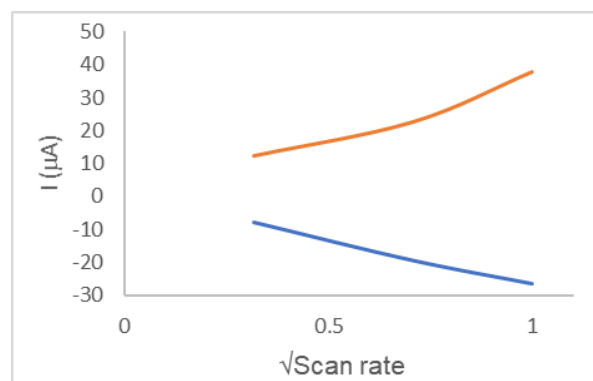


Figure 63: Intensity vs $\sqrt{\text{scan rate}}$, 4CIDPAIPN-Ox

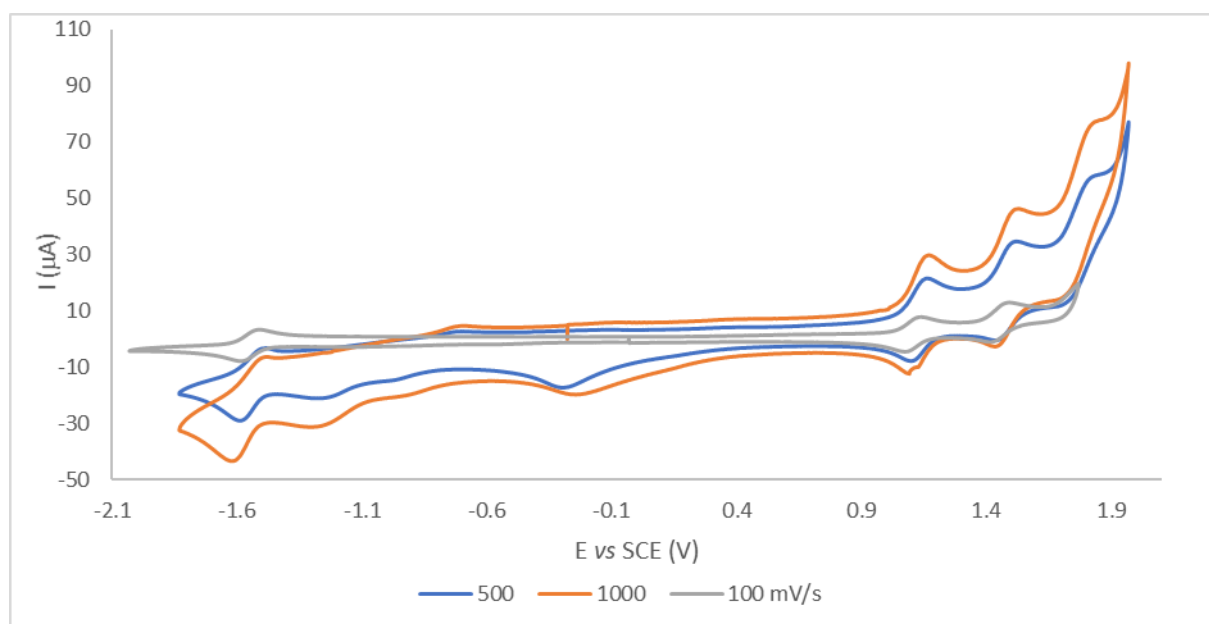


Figure 64: Cyclic voltammetry of 4BrDPAIPN (5.26)

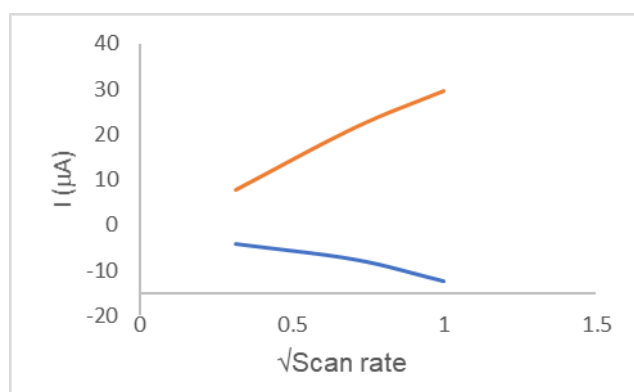
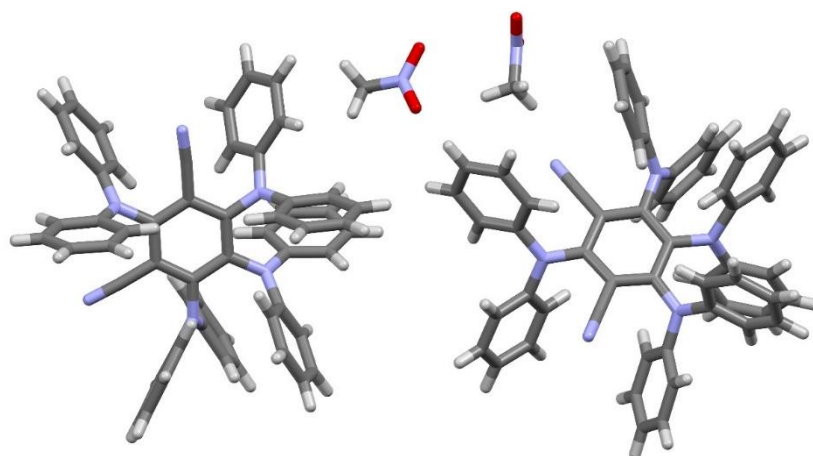
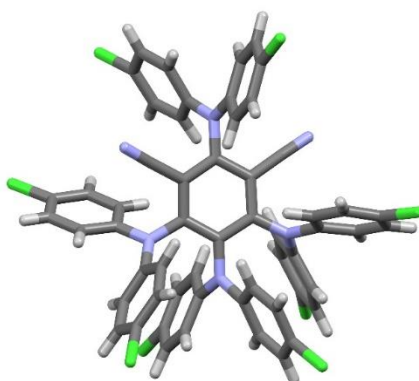


Figure 65: Intensity vs $\sqrt{\text{scan rate}}$, 4BrDPAIPN-Ox

12.3.4 Crystal structures



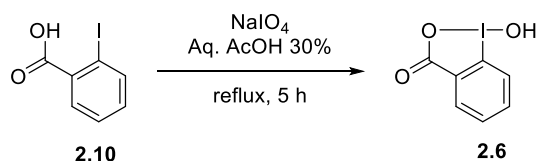
A single crystal was grown by slow diffusion of a solution of **2.22** in nitromethane. Supplementary crystallographic data for this compound have been deposited at Cambridge Crystallographic Data Centre (**CCDC 1879098**) and can be obtained free of charge via www.ccdc.cam.ac.uk/data_request/cif.



A single crystal was grown by slow diffusion of a solution of **5.25** in CDCl_3 . Supplementary crystallographic data for this compound have been deposited at Cambridge Crystallographic Data Centre (**CCDC 1879097**) and can be obtained free of charge via www.ccdc.cam.ac.uk/data_request/cif.

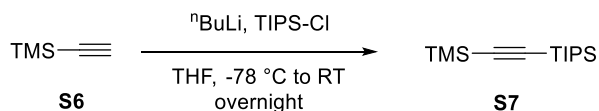
12.4 Decarboxylative alkynylation of peptides

12.4.1 Preparation of reagents

1-Hydroxy-1,2-benziodoxol-3-(1*H*)-one (**2.6**)

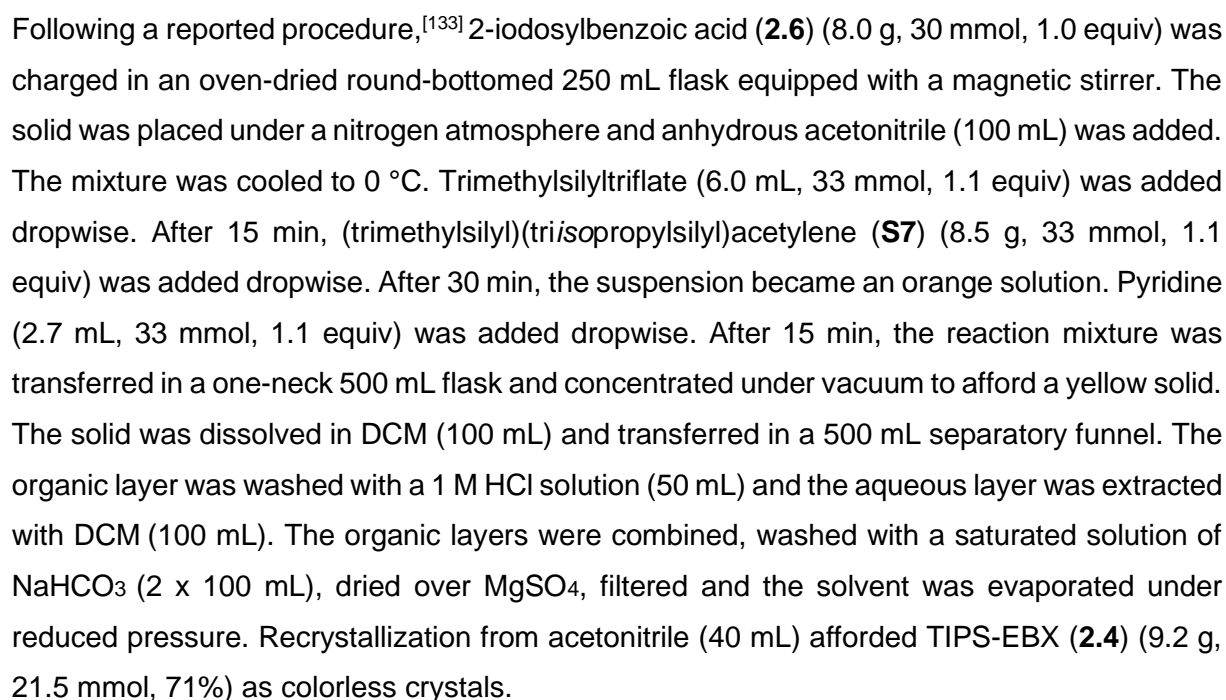
Following a reported procedure,^[339] NaIO₄ (40.5 g, 189 mmol, 1.05 equiv) and 2-iodobenzoic acid (**2.10**) (44.8 g, 180 mmol, 1.0 equiv) were suspended in 30% (v:v) aq. AcOH (350 mL). The mixture was vigorously stirred and refluxed for 5 h. The reaction mixture was then diluted with cold water (250 mL) and allowed to cool to rt, protecting it from light. After 1 h, the crude product was collected by filtration, washed on the filter with ice water (3 x 150 mL) and acetone (3 x 150 mL), and air-dried in the dark overnight to afford 1-Hydroxy-1,2-benziodoxol-3-(1*H*)-one (**2.6**) (44.3 g, 168 mmol, 93%) as a white solid.

¹H NMR (400 MHz, DMSO-*d*₆) δ 8.02 (dd, *J* = 7.7, 1.4 Hz, 1H, Ar*H*), 7.97 (m, 1H, Ar*H*), 7.85 (dd, *J* = 8.2, 0.7 Hz, 1H, Ar*H*), 7.71 (td, *J* = 7.6, 1.2 Hz, 1H, Ar*H*). ¹³C NMR (100 MHz, DMSO-*d*₆) δ 167.7, 134.5, 131.5, 131.1, 130.4, 126.3, 120.4. Consistent with reported data.^[339]

Triisopropylsilyl trimethylsilylacetylene (**S7**)

Following a reported procedure,^[340] *n*-butyllithium (2.5 M in hexanes, 28 mL, 70 mmol, 0.98 equiv) was added dropwise to a stirred solution of ethynyltrimethylsilane (**S6**) (7.0 g, 71 mmol, 1.0 equiv) in THF (100 mL) at -78 °C. The mixture was warmed to 0 °C and stirred for 5 min. The mixture was then cooled back to -78 °C and chlorotriisopropylsilane (15 mL, 71 mmol, 1.0 equiv) was added dropwise. The mixture was then allowed to warm to room temperature and

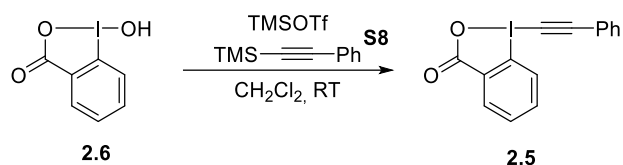
1-[(Triisopropylsilyl)ethynyl]-1,2-benziodoxol-3(1*H*)-one (TIPS-EBX, 2.4)



263

(m), 1140 (m), 1016 (m), 999 (m), 883 (m), 833 (m), 742 (m), 702 (s), 636 (m). Consistent with reported data.^[133]

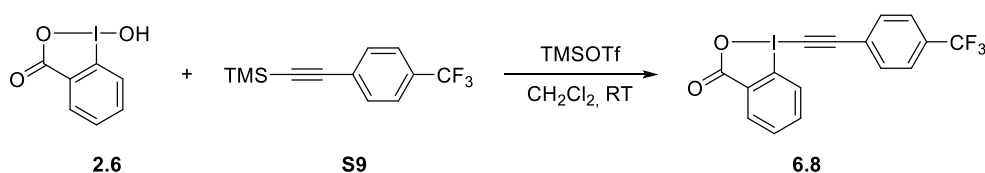
1-[Phenylethynyl]-1,2-benziodoxol-3(1*H*)-one (Ph-EBX, **2.5**)



Following a reported procedure,^[339] trimethylsilyltriflate (7.5 mL, 42 mmol, 1.1 equiv) was added dropwise to a suspension of 2-iodosylbenzoic acid (**2.6**) (10 g, 38 mmol, 1.0 equiv) in CH_2Cl_2 (100 mL) at 0 °C. The mixture was stirred for 1 h, followed by the dropwise addition of trimethyl(phenylethynyl)silane (**S8**) (8.2 mL, 42 mmol, 1.1 equiv) (slightly exothermic). The resulting suspension was stirred for 6 h at RT, during this time a white solid was formed. A saturated solution of NaHCO_3 (100 mL) was added and the mixture was stirred vigorously for 5 min. The resulting suspension was filtered on a glass filter. The two layers of the mother liquors were separated and the organic layer was washed with sat. NaHCO_3 (100 mL), dried over MgSO_4 , filtered and evaporated under reduced pressure. The resulting mixture was combined with the solid obtained by filtration and boiled in CH_3CN (150 mL). The mixture was cooled down, filtered and dried under high vacuum to afford Ph-EBX (**2.5**) (8.6 g, 25 mmol, 65%) as a colorless solid.

Mp (Dec.) 155 – 160 °C. ^1H NMR (400 MHz, Chloroform-*d*) δ 8.46 (m, 1H, Ar*H*), 8.28 (m, 1H, Ar*H*), 7.80 (m, 2H, Ar*H*), 7.63 (m, 2H, Ar*H*), 7.48 (m, 3H, Ar*H*). ^{13}C NMR (101 MHz, Chloroform-*d*) δ 163.9, 134.9, 132.9, 132.5, 131.6, 131.3, 130.8, 128.8, 126.2, 120.5, 116.2, 106.6, 50.2. Consistent with reported data.^[339]

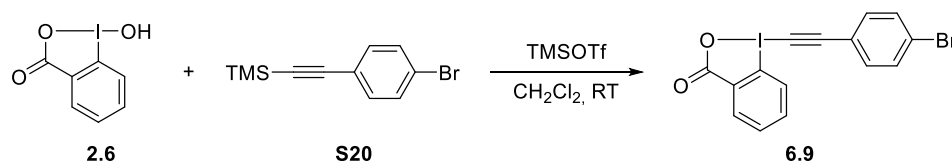
1-[4-Trifluoromethylphenylethynyl]-1,2-benziodoxol-3(1*H*)-one (**1c**)



Following a reported procedure,^[341] trimethylsilyl triflate (1.0 mL, 5.5 mmol, 1.1 equiv) was added to a suspension of 2-iodosylbenzoic acid (**2.6**) (1.3 g, 5.0 mmol, 1.0 equiv) in CH₂Cl₂ (15 mL) at RT. The resulting suspension was stirred for 1 h, followed by the dropwise addition of trimethyl((4-(trifluoromethyl)phenyl)ethynyl)silane (**S9**) (1.3 mL, 5.5 mmol, 1.1 equiv), which was dissolved in CH₂Cl₂ (1 mL). The resulting suspension was stirred for 6 h at RT. A saturated solution of NaHCO₃ (20 mL) was then added and the mixture was stirred vigorously for 30 min, the two layers were separated and the organic layer was washed with sat. NaHCO₃ (20 mL), dried over MgSO₄, filtered and evaporated under reduced pressure. The resulting solid was boiled in CH₃CN (20 mL). The mixture was cooled down, filtered and dried under high vacuum to afford **6.8** (1.3 g, 3.2 mmol, 64%) as a pale yellow solid.

¹H NMR (400 MHz, Chloroform-*d*) δ 8.46 – 8.38 (m, 1H, *ArH*), 8.28 – 8.19 (m, 1H, *ArH*), 7.84 – 7.74 (m, 2H, *ArH*), 7.74 – 7.65 (m, 4H, *ArH*). ¹³C NMR (101 MHz, Chloroform-*d*) δ 166.6, 135.0, 133.0, 132.6, 132.2 (q, *J*_{C-F} = 33.0 Hz), 131.7, 131.2, 126.3, 125.7 (q, *J*_{C-F} = 3.6 Hz), 124.4, 123.4 (q, *J*_{C-F} = 272.6 Hz), 116.1, 104.2, 53.7. Consistent with reported data.^[341]

1-[4-Bromophenylethynyl]-1,2-benziodoxol-3(1*H*)-one (**1d**)



Following a reported procedure,^[342] trimethylsilyl triflate (1.0 mL, 5.5 mmol, 1.1 equiv) was added to a suspension of 2-iodosylbenzoic acid (**2.6**) (1.3 g, 5.0 mmol, 1.0 equiv) in CH₂Cl₂ (15 mL) at RT. The resulting suspension was stirred for 1 h, followed by the dropwise addition of ((4-bromophenyl)ethynyl)trimethylsilane (**S20**) (1.2 g, 5.5 mmol, 1.1 equiv), which was dissolved in CH₂Cl₂ (1 mL). The resulting suspension was stirred for 6 h at RT. A saturated solution of NaHCO₃ (20 mL) was then added and the mixture was stirred vigorously for 30 min, the two layers were separated and the organic layer was washed with sat. NaHCO₃ (20 mL), dried over MgSO₄, filtered and evaporated under reduced pressure. The resulting solid was boiled in CH₃CN (20 mL). The mixture was cooled down, filtered and dried under high vacuum to afford **6.9** (1.4 g, 3.3 mmol, 66%) as a pale yellow solid.

Mp 158-163 °C (decomposition). ¹H NMR (400 MHz, Chloroform-*d*) δ 8.51 – 8.30 (m, 1H, *ArH*), 8.30 – 8.13 (m, 1H, *ArH*), 7.84 – 7.72 (m, 2H, *ArH*), 7.58 (d, 2H, *J* = 8.5 Hz, *ArH*), 7.46 (d, 2H,

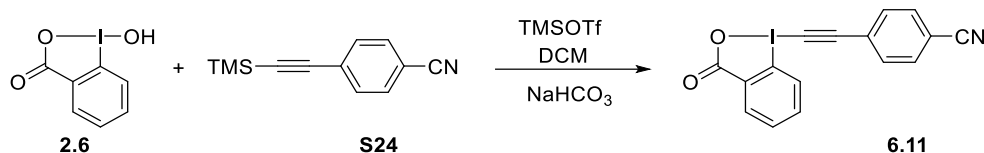
¹H NMR (400 MHz, DMSO-*d*₆) δ 10.08 (s, 1H, CHO), 8.35 (d, *J* = 9.1 Hz, 1H, ArH), 8.14 (dd, *J* = 7.4, 1.7 Hz, 1H, ArH), 8.02 (d, *J* = 8.5 Hz, 2H, ArH), 7.96 – 7.88 (m, 3H, ArH), 7.82 (t, *J* = 7.3 Hz, 1H, ArH). ¹³C NMR (101 MHz, DMSO-*d*₆) δ 192.6, 166.3, 136.7, 135.3, 133.2, 131.9, 131.4, 129.8, 127.7, 126.1, 116.4, 102.9, 56.6. Consistent with reported data.^[215]

266

(**S23**) (1.2 mL, 8.7 mmol, 2.0 equiv) the green suspension was stirred at RT for 3 h. The reaction mixture was concentrated under vacuum, dissolved in CH₂Cl₂ (30 mL), washed with a saturated ammonium chloride solution (30 mL) and water (30 mL). The organic layers were then dried over MgSO₄, filtered and concentrated under vacuum. The resulting oil was purified by column chromatography (pentane/ethyl acetate 25:1) to afford 4-((trimethylsilyl)ethynyl)benzonitrile (**S24**) (847 mg, 4.25 mmol, 97%) as a white solid.

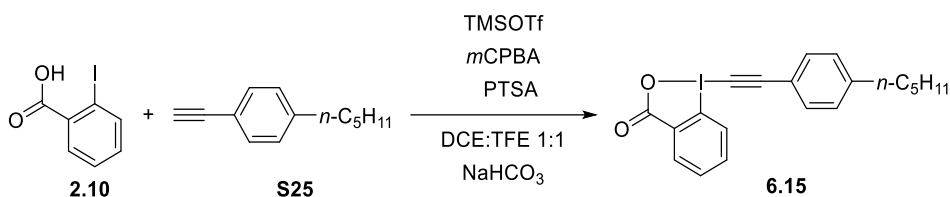
¹H NMR (400 MHz, Chloroform-*d*) δ 7.59 (d, *J* = 8.7 Hz, 2H, *ArH*), 7.53 (d, *J* = 8.8 Hz, 2H, *ArH*), 0.26 (s, 9H, SiCH₃). ¹³C NMR (101 MHz, Chloroform-*d*) δ 132.6, 132.1, 128.1, 118.6, 111.9, 103.1, 99.7, -0.12. Consistent with reported data.^[343]

1-[4-Cyanophenylethynyl]-1,2-benziodoxol-3(1*H*)-one (**6.11**)



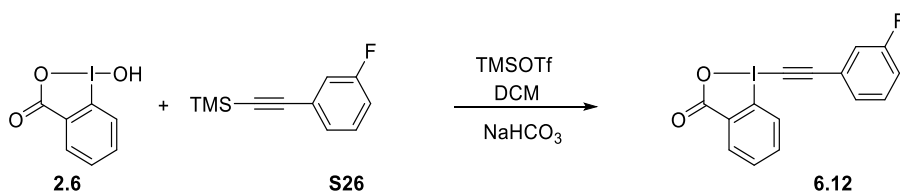
Following a reported procedure,^[342] trimethylsilyl triflate (0.73 mL, 4.0 mmol, 1.1 equiv) was added to a suspension of 2-iodosylbenzoic acid (**2.6**) (963 mg, 3.65 mmol, 1.00 equiv) in CH₂Cl₂ (12 mL) at RT. The resulting suspension was stirred for 1 h, followed by the drop wise addition of ((4-cyanophenyl)ethynyl)trimethylsilane (**S24**) (800 mg, 4.01 mmol, 1.10 equiv), which was dissolved in CH₂Cl₂ (1 mL). The resulting suspension was stirred for 6 h at RT. A saturated solution of NaHCO₃ (20 mL) was then added and the mixture was stirred vigorously for 30 minutes, the two layers were separated and the organic layer was washed with sat. NaHCO₃ (20 mL), dried over MgSO₄, filtered and evaporated under reduced pressure. The resulting solid was boiled in CH₃CN (20 mL). The mixture was cooled down, filtered and dried under high vacuum to afford **6.11** (865 mg, 2.32 mmol, 64%) as a pale brown solid.

¹H NMR (400 MHz, DMSO-*d*₆) δ 8.34 (d, *J* = 8.2 Hz, 1H, *ArH*), 8.13 (dd, *J* = 7.4, 1.7 Hz, 1H, *ArH*), 7.99 (d, *J* = 8.6 Hz, 2H, *ArH*), 7.90 (d, *J* = 8.6 Hz, 3H, *ArH*), 7.81 (t, *J* = 7.3 Hz, 1H, *ArH*). ¹³C NMR (101 MHz, DMSO-*d*₆) δ 166.3, 135.3, 133.3, 132.8, 131.9, 131.4, 131.4, 127.8, 125.3, 118.2, 116.4, 112.7, 102.0, 57.4. Consistent with reported data.^[342]

1-((4-Pentylphenyl)ethynyl)-1,2-benziodoxol-3(1*H*)-one (6.15)

Following a reported procedure,^[260] in a sealed tube, 2-iodobenzoic acid (**2.10**) (1.00 g, 4.03 mmol, 1.00 equiv), 4-methylbenzenesulfonic acid (775 mg, 4.03 mmol, 1.00 equiv) and *m*CPBA (994 mg, 4.44 mmol, 1.10 equiv) were suspended in DCE:TFE 1:1 (12 mL) and stirred for 1 h at 55 °C. After 1 h, 1-ethynyl-4-pentylbenzene (**S25**) (1.1 mL, 5.6 mmol, 1.4 equiv) was added and the reaction was stirred at 55 °C for 24 h. After 24 h, the solvent was evaporated and the residue was redissolved in CH₂Cl₂ (20 mL) and stirred vigorously with NaHCO₃ sat. (30 mL). After 1 h, the reaction mixture was transferred into a separating funnel and the layers were separated. The aqueous layer was extracted with CH₂Cl₂ (2x50 mL). The combined organic layers were washed with sat. NaHCO₃, dried over MgSO₄, filtered and concentrated under vacuum. The resulting solid was boiled in MeCN (20 mL), then filtered and the collected solid was further purified by column chromatography using pure ethyl acetate. Trituration in pentane afforded **6.15** (191 mg, 0.457 mmol, 11%) as a pale yellow solid.

¹H NMR (400 MHz, Chloroform-*d*) δ 8.45 – 8.40 (m, 1H, Ar*H*), 8.28 – 8.21 (m, 1H, Ar*H*), 7.79 – 7.74 (m, 2H, Ar*H*), 7.56 – 7.48 (m, 2H, Ar*H*), 7.26 – 7.23 (m, 2H, Ar*H*), 2.71 – 2.60 (m, 2H, ArCH₂), 1.69 – 1.54 (m, 2H, ArCH₂CH₂), 1.40 – 1.27 (m, 4H, CH₂CH₂CH₃), 0.90 (t, *J* = 6.8 Hz, 3H, CH₂CH₃). ¹³C NMR (101 MHz, Chloroform-*d*) δ 166.6, 146.7, 135.0, 133.0, 132.6, 131.7, 131.5, 129.0, 126.3, 117.7, 116.4, 107.4, 49.4, 36.2, 31.5, 31.0, 22.6, 14.1. Consistent with reported data.^[260]

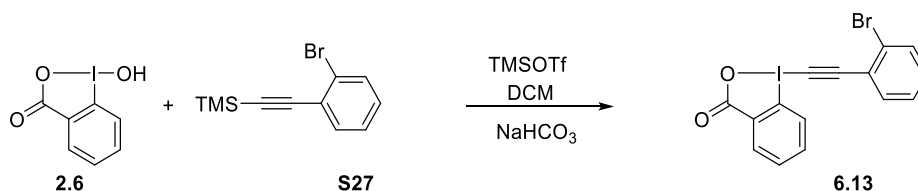
1-[3-Fluorophenylethynyl]-1,2-benziodoxol-3(1*H*)-one (1h)

Following a reported procedure,^[260] trimethylsilyl triflate (1.0 mL, 5.5 mmol, 1.1 equiv) was added to a suspension of 2-iodosylbenzoic acid (**2.6**) (1.32 g, 5.00 mmol, 1.00 equiv) in CH₂Cl₂

(15 mL) at RT. The resulting suspension was stirred for 1 h, followed by the drop wise addition of ((3-fluorophenyl)ethynyl)trimethylsilane (**S26**) (1.1 mL, 5.5 mmol, 1.1 equiv). The resulting suspension was stirred for 6 h at RT. A saturated solution of NaHCO₃ (20 mL) was then added and the mixture was stirred vigorously for 30 minutes, the two layers were separated and the organic layer was washed with sat. NaHCO₃ (20 mL), dried over MgSO₄, filtered and evaporated under reduced pressure. The resulting solid was boiled in CH₃CN (20 mL). The mixture was cooled down, filtered and the collected solid was dried under high vacuum to afford **6.12** (787 mg, 2.15 mmol, 43%) as a colorless solid.

¹H NMR (400 MHz, DMSO-*d*₆) δ 8.33 (dd, *J* = 8.2, 0.8 Hz, 1H, Ar*H*), 8.13 (dd, *J* = 7.4, 1.7 Hz, 1H, Ar*H*), 7.91 (ddd, *J* = 8.2, 7.2, 1.7 Hz, 1H, Ar*H*), 7.81 (td, *J* = 7.3, 0.9 Hz, 1H, Ar*H*), 7.64 – 7.59 (m, 1H, Ar*H*), 7.58 – 7.53 (m, 2H, Ar*H*), 7.47 – 7.37 (m, 1H, Ar*H*). ¹³C NMR (101 MHz, DMSO-*d*₆)²³ 166.3, 161.8 (d, *J* = 245.6 Hz), 135.3, 131.9, 131.3, 131.2 (d, *J* = 8.7 Hz), 129.0 (d, *J* = 2.9 Hz), 127.7, 122.4 (d, *J* = 9.6 Hz), 119.2 (d, *J* = 23.4 Hz), 118.1 (d, *J* = 21.1 Hz), 116.4, 102.5 (d, *J* = 3.3 Hz), 53.8. ¹⁹F NMR (376 MHz, DMSO-*d*₆) δ -111.7. Consistent with reported data.^[260]

1-[2-Bromophenylethynyl]-1,2-benziodoxol-3(1*H*)-one (**6.13**)

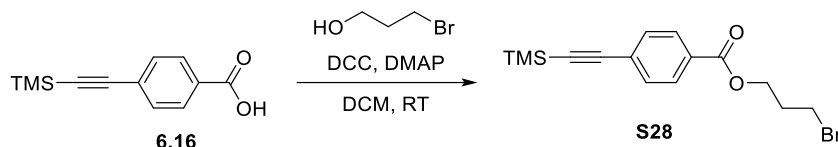


Following a reported procedure,^[13] trimethylsilyl triflate (1.0 mL, 5.5 mmol, 1.1 equiv) was added to a suspension of 2-iodosylbenzoic acid (**2.6**) (1.32 g, 5.00 mmol, 1.00 equiv) in CH₂Cl₂ (15 mL) at RT. The resulting suspension was stirred for 3 h, followed by the drop wise addition of ((2-bromophenyl)ethynyl)trimethylsilane (**S27**) (1.17 g, 5.50 mmol, 1.10 equiv). The resulting suspension was stirred for 6 h at RT. A saturated solution of NaHCO₃ (20 mL) was then added and the mixture was stirred vigorously for 30 minutes, the two layers were separated and the organic layer was washed with sat. NaHCO₃ (20 mL), dried over MgSO₄, filtered and evaporated under reduced pressure. The resulting solid was boiled in CH₃CN (20 mL). The mixture was cooled down, filtered and the collected solid was dried under high vacuum to afford **6.13** (1.50 g, 3.51 mmol, 70%) as a colorless solid.

²³ One carbon is not resolved.

^1H NMR (400 MHz, Chloroform-*d*) δ 8.44 (td, $J = 7.3, 2.1$ Hz, 2 H, ArH), 7.84 – 7.74 (m, 2 H, ArH), 7.68 (d, $J = 1.1$ Hz, 1 H, ArH), 7.61 (dd, $J = 7.6, 1.7$ Hz, 1 H, ArH), 7.36 (m, 2 H, ArH). ^{13}C NMR (101 MHz, Chloroform-*d*)²³ δ 166.6, 135.2, 134.7, 133.0, 132.7, 131.8, 131.3, 127.6, 126.8, 126.4, 123.2, 116.5, 104.3, 55.4. Consistent with reported data.^[13]

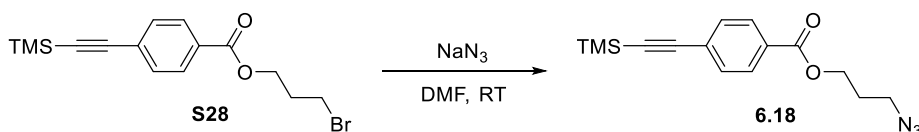
3-Bromopropyl 4-((trimethylsilyl)ethynyl)benzoate (**S28**)



4-(Dimethylamino)-pyridine (67 mg, 0.55 mmol, 12 mol%) was added to a stirred reaction mixture of 4-((trimethylsilyl)ethynyl)benzoic acid (**6.16**) (1.0 g, 4.6 mmol, 1.0 equiv), dicyclohexylcarbodiimide (1.0 g, 5.0 mmol, 1.1 equiv), 3-bromopropan-1-ol (0.62 mL, 6.9 mmol, 1.5 equiv) in dry CH_2Cl_2 (15 mL) at room temperature. The reaction mixture was filtered after 15 h and the solid was rinsed with dichloromethane (2 x 10 mL). The combined filtrates were concentrated under vacuum. Purification by column chromatography pentane/ethyl acetate 9:1 afforded 3-bromopropyl 4-((trimethylsilyl)ethynyl)benzoate (**S28**) (1.3 g, 3.8 mmol, 82 %) as a white solid.

Mp 37.2 – 39.3 °C. R_f (pentane/ethyl acetate 9:1): 0.8. ^1H NMR (400 MHz, Chloroform-*d*) δ 7.96 (d, $J = 8.6$ Hz, 2H, ArH), 7.52 (d, $J = 8.7$ Hz, 2H, ArH), 4.46 (t, $J = 6.0$ Hz, 2H, OCH_2), 3.54 (t, $J = 6.6$ Hz, 2H, BrCH_2), 2.32 (p, $J = 6.4$ Hz, 2H, CH_2CH_2), 0.26 (s, 9H, TMS). ^{13}C NMR (101 MHz, Chloroform-*d*) δ 165.8, 131.9, 129.5, 129.4, 127.9, 104.0, 97.9, 62.9, 31.8, 29.4, -0.2. IR (ν_{max} , cm^{-1}) 2957 (w), 2926 (w), 2353 (w), 2162 (w), 1725 (s), 1608 (w), 1410 (w), 1269 (s), 1176 (m), 1108 (m), 1016 (w), 868 (s), 769 (m). HRMS (ESI/QTOF) m/z : $[\text{M} + \text{Na}]^+$ Calcd for $\text{C}_{15}\text{H}_{19}^{79}\text{BrNaO}_2\text{Si}^+$ 361.0230, 363.0209; Found 361.0235, 363.0216.

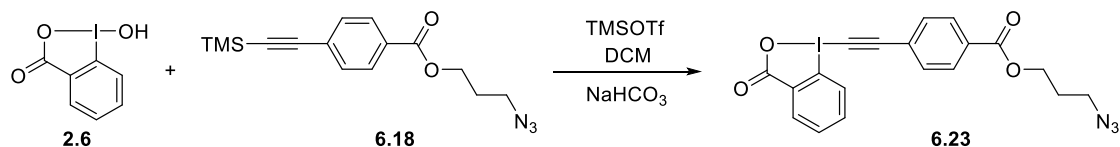
3-Azidopropyl 4-((trimethylsilyl)ethynyl)benzoate (**6.18**)



NaN₃ (0.25 g, 3.9 mmol, 1.2 equiv) was added to a solution of 3-bromopropyl 4-((trimethylsilyl)ethynyl)benzoate (**S28**) (1.1 g, 3.2 mmol, 1.0 equiv) in dry DMF (16 mL) at RT. The mixture was heated at 50 °C overnight. Ice water was added and the aqueous layer was extracted with diethyl ether (3x). The combined organic layers were washed with brine (3x), dried over MgSO₄ and concentrated under vacuum. The crude was purified by column chromatography pentane to pentane/ethyl acetate 95:5 to afford 3-azidopropyl 4-((trimethylsilyl)ethynyl)benzoate (**6.18**) (0.60 g, 2.0 mmol, 61 % yield) as a pale yellow oil.

Rf: 0.7 (pentane/ethyl acetate 9:1). ¹H NMR (400 MHz, Chloroform-*d*) δ 7.96 (d, *J* = 8.7 Hz, 2H, Ar*H*), 7.52 (d, *J* = 8.7 Hz, 2H, Ar*H*), 4.41 (t, *J* = 6.2 Hz, 2H, OCH₂), 3.48 (t, *J* = 6.7 Hz, 2H, N₃CH₂), 2.05 (p, *J* = 6.5 Hz, 2H, CH₂CH₂), 0.26 (s, 9H, TMS). ¹³C NMR (101 MHz, Chloroform-*d*) δ 165.8, 131.9, 129.5, 129.4, 128.0, 104.0, 97.9, 62.0, 48.3, 28.2, -0.2. IR (ν_{max}, cm⁻¹) 3666 (w), 2970 (m), 2902 (m), 2101 (s), 1725 (s), 1608 (m), 1472 (w), 1410 (w), 1281 (s), 1115 (m), 1065 (m), 868 (s), 856 (s), 769 (m). HRMS (ESI/QTOF) *m/z*: [M + Na]⁺ Calcd for C₁₅H₁₉N₃NaO₂Si⁺ 324.1139; Found 324.1137.

1-((4-(Prop-2-yn-1-yl-benzoate)ethynyl)-1,2-benziodoxol-3(1*H*)-one (**6.23**)

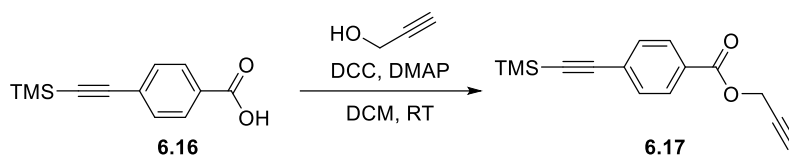


Trimethylsilyl triflate (0.34 mL, 1.9 mmol, 1.1 equiv) was added to a suspension of 2-iodosylbenzoic acid (**2.6**) (454 mg, 1.72 mmol, 1.00 equiv) in CH₂Cl₂ (5 mL) at RT. The resulting suspension was stirred for 1 h, followed by the drop wise addition of 3-azidopropyl 4-((trimethylsilyl)ethynyl)benzoate (**6.18**) (570 mg, 1.89 mmol, 1.10 equiv), which was dissolved in CH₂Cl₂ (0.5 mL). The resulting suspension was stirred for 4 h at RT. A saturated solution of NaHCO₃ (10 mL) was then added and the mixture was stirred vigorously for 30 minutes, the two layers were separated and the organic layer was washed with sat. NaHCO₃ (10 mL), dried over MgSO₄, filtered and evaporated under reduced pressure. The resulting solid was boiled in CH₃CN (10 mL). The mixture was cooled down, filtered and dried under high vacuum to afford **6.23** (431 mg, 0.907 mmol, 53%) as a pale brown solid.

Mp (Dec.) 106.4 – 109.3 °C. ¹H NMR (400 MHz, Chloroform-*d*) δ 8.47 – 8.41 (m, 1H, Ar*H*), 8.34 – 8.20 (m, 1H, Ar*H*), 8.10 (d, *J* = 8.7 Hz, 2H, Ar*H*), 7.87 – 7.76 (m, 2H, Ar*H*), 7.67 (d, *J* =

8.6 Hz, 2H, ArH), 4.46 (t, $J = 6.2$ Hz, 2H, OCH₂), 3.50 (t, $J = 6.6$ Hz, 2H, N₃CH₂), 2.08 (p, $J = 6.4$ Hz, 2H, CH₂CH₂). ¹³C NMR (101 MHz, Chloroform-*d*) δ 166.4, 165.3, 135.1, 132.7, 132.6, 131.8, 131.6, 131.2, 129.8, 126.2, 125.1, 116.1, 105.0, 62.4, 54.1, 48.2, 28.2. IR (ν_{\max} , cm⁻¹) 3678 (w), 3389 (w), 2988 (s), 2908 (s), 2366 (w), 2101 (m), 1774 (w), 1719 (m), 1638 (m), 1454 (w), 1398 (m), 1281 (m), 1071 (s), 868 (m), 769 (m). HRMS (ESI/QTOF) m/z : [M + H]⁺ Calcd for C₁₉H₁₅IN₃O₄⁺ 476.0102; Found 476.0112.

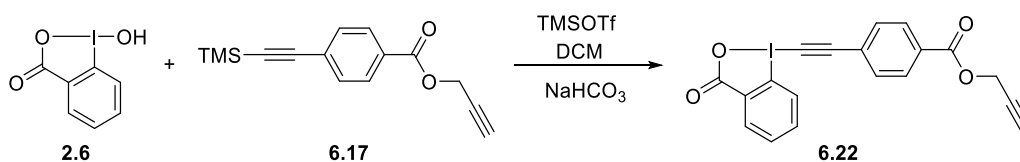
Prop-2-yn-1-yl 4-((trimethylsilyl)ethynyl)benzoate (**6.17**)



4-(Dimethylamino)-pyridine (27 mg, 0.22 mmol, 12 mol%) was added to a stirred reaction mixture of 4-((trimethylsilyl)ethynyl)benzoic acid (**6.16**) (0.40 g, 1.8 mmol, 1.0 equiv), dicyclohexylcarbodiimide (0.42 g, 2.0 mmol, 1.1 equiv) and 2-propynol (0.16 mL, 2.8 mmol, 1.5 equiv) in dry CH₂Cl₂ (7 mL) at RT. The reaction mixture was filtered after 15 h and the solid was rinsed with dichloromethane (2 x 5 mL). The combined filtrates were concentrated under vacuum. Purification by column chromatography pentane/ethyl acetate 9:1 afforded prop-2-yn-1-yl 4-((trimethylsilyl)ethynyl)benzoate (**6.17**) (375 mg, 1.46 mmol, 80 %) as a white solid.

Mp 58 – 60 °C. R_f (pentane/ethyl acetate 9:1): 0.8. ¹H NMR (400 MHz, Chloroform-*d*) δ 8.00 (d, $J = 8.7$ Hz, 2H, ArH), 7.52 (d, $J = 8.7$ Hz, 2H, ArH), 4.92 (d, $J = 2.5$ Hz, 2H, OCH₂), 2.52 (t, $J = 2.5$ Hz, 1H, CH), 0.26 (s, 9H, TMS). ¹³C NMR (101 MHz, Chloroform-*d*) δ 165.2, 131.9, 129.6, 128.9, 128.2, 103.9, 98.1, 77.5, 75.1, 52.6, -0.2. IR (ν_{\max} , cm⁻¹) 3678 (w), 3296 (w), 2963 (m), 2902 (m), 2359 (w), 2162 (w), 2125 (w), 1725 (s), 1608 (m), 1410 (m), 1373 (m), 1262 (s), 1176 (m), 1102 (s), 868 (s), 763 (m). HRMS (APCI/QTOF) m/z : [M + H]⁺ Calcd for C₁₅H₁₇O₂Si⁺ 257.0992; Found 257.0995.

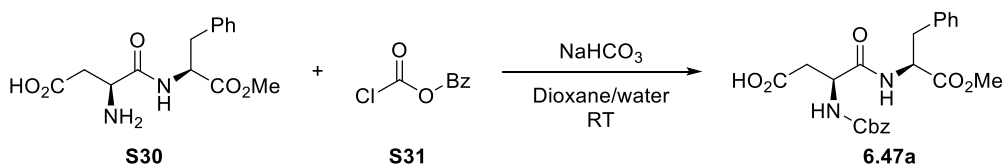
1-((4-(Prop-2-yn-1-yl-benzoate)ethynyl)-1,2-benziodoxol-3(1H)-one (**6.22**)



H₂O (25 mL) and the layers were separated. The aqueous layer was extracted with CH₂Cl₂ (3 x 50 mL) and the combined organic layers were washed with brine, dried (Mg₂SO₄) and filtered. The solvent was removed under reduced pressure. The crude mixture contained a lot of impurities, so purification by column chromatography over silica gel (DCM with 2 to 10% Acetone) afforded 500 mg of pure Ph-VBX **6.34a** as off white crystalline solid (29%).

¹H NMR (400 MHz, Methanol-*d*₄) δ 8.28 (dd, *J* = 5.8, 3.4 Hz, 1H, *ArH*), 7.96 (d, *J* = 15.4 Hz, 1H, *ArH*), 7.74 (dd, *J* = 5.9, 3.5 Hz, 1H, *ArH*), 7.70 (dd, *J* = 7.5, 3.5 Hz, 4H, *ArH*), 7.66 (d, *J* = 8.7 Hz, 1H, *ArH*), 7.49 (dd, *J* = 5.1, 2.0 Hz, 3H, *ArH*). The NMR shifts match the literature data.^[266]

(S)-3-(((benzyloxy)carbonyl)amino)-4-(((S)-1-methoxy-1-oxo-3-phenylpropan-2-yl)amino)-4-oxobutanoic acid (6.47a)

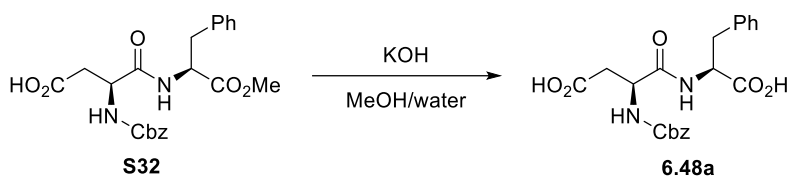


The synthesis was carried out adapting a reported procedure.^[268]

To a solution of (S)-3-amino-4-(((S)-1-methoxy-1-oxo-3-phenylpropan-2-yl)amino)-4-oxobutanoic acid (**S30**) (0.60 g, 2.0 mmol, 1 equiv) and sodium bicarbonate (0.51 g, 6.1 mmol, 3 equiv) in water/dioxane (2/1) (4.5 mL) was added dropwise a solution of benzyl chloroformate (0.41 mL, 2.9 mmol, 1.4 equiv) in dioxane (1 mL). The mixture was stirred overnight at RT and extracted with ethyl acetate (3 x 10 mL). The pH was brought to 2 with 1M HCl and the aqueous phase was extracted with ethyl acetate (3 x 10 mL). Organic layers were combined dried over magnesium sulfate and concentrated under vacuum to afford (S)-3-(((benzyloxy)carbonyl)amino)-4-(((S)-1-methoxy-1-oxo-3-phenylpropan-2-yl)amino)-4-oxobutanoic acid (**6.47a**) (0.49 g, 1.1 mmol, 56 % yield) as a white solid.

¹H NMR (400 MHz, CDCl₃) δ 7.33 (m, 11H, *ArH* and *NH*), 5.89 (d, *J* = 8.8 Hz, 1H, *NH*), 5.09 (s, 2H, OCH₂Ph), 4.79 (dt, *J* = 8.0, 6.1 Hz, 1H, CHNHCbz), 4.58 (bs, 1H, NCHCO₂Me), 3.67 (s, 3H, CO₂Me), 3.03 – 2.70 (m, 4H, CH₂CO₂H non resolved with CH₂Ph). ¹³C NMR (101 MHz, CDCl₃) δ 175.3, 171.7, 170.4, 156.2, 136.0, 135.7, 129.4, 128.7, 128.7, 128.5, 128.3, 127.3, 67.6, 53.7, 52.6, 50.9, 37.8, 35.9. Consistent with reported data.^[269]

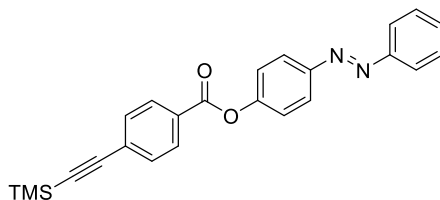
(S)-3-(((benzyloxy)carbonyl)amino)-4-(((S)-1-carboxy-2-phenylethyl)amino)-4-oxobutanoic acid (6.48a**)**



In a single necked 25 mL round bottomed flask, (S)-3-(((benzyloxy)carbonyl)amino)-4-(((S)-1-methoxy-1-oxo-3-phenylpropan-2-yl)amino)-4-oxobutanoic acid (**S32**) (0.25 g, 0.58 mmol) was dissolved in MeOH (3 mL). The solution was cooled to 0°C and a solution of potassium hydroxide (0.13 mg, 2.3 mmol) in water (1.5 mL) was slowly added. The cooling bath was removed and stirring was continued at room temperature for 2 hours. During this time, the initial suspension converted into a pale yellow clear solution. Most of MeOH was then removed under reduced pressure. The resulting aqueous mixture was diluted with aq. NaOH (1.0 M) and extracted with ether (3 x). It was then acidified with concentrated aq. HCl until pH < 3 and extracted with DCM (3 x). The combined organic extracts were washed with brine, dried MgSO₄, concentrated under vacuum to provide **6.48a** as a white solid (0.20 g, 0.48 mmol, 82%).

¹H NMR (400 MHz, MeOD) δ 7.43 – 7.10 (m, 12H, ArH and NH), 5.08 (s, 2H, OCH₂Ph), 4.63 (dd, *J* = 7.5, 5.2 Hz, 1H, CHNHCBz), 4.52 (dd, *J* = 8.1, 5.4 Hz, 1H, NCHCO₂Me), 3.09 (ddd, *J* = 61.0, 13.9, 6.4 Hz, 2H, CH₂Ph), 2.83 – 2.50 (m, 2H, CH₂CO₂H). ¹³C NMR (101 MHz, MeOD) δ 173.1, 158.3, 138.1, 138.0, 130.5, 129.5, 129.4, 129.0, 128.8, 127.8, 67.8, 55.1, 52.9, 50.4, 38.3, 36.9. In accordance with literature data.^[344]

(E)-4-(phenyldiazenyl)phenyl 4-((trimethylsilyl)ethynyl)benzoate (6.19**)**



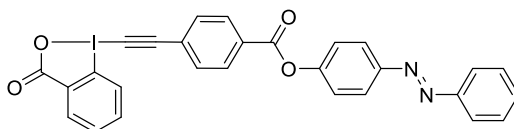
DMAP (54 mg, 0.44 mmol, 12 mol%) was added to a stirred reaction mixture of 4-((trimethylsilyl)ethynyl)benzoic acid (800 mg, 3.66 mmol, 1 equiv), DCC (832 mg, 4.03 mmol, 1.1 equiv) and (E)-4-(phenyldiazenyl)phenol (1.09 g, 5.50 mmol, 1.5 equiv) in dry

dichloromethane (10 mL) at room temperature. The reaction mixture was filtered after 15 h and the solid was rinsed with dichloromethane (2 x 10 mL). The combined filtrates were concentrated under vacuum. Purification by column chromatography pentane/ethyl acetate 9:1 afforded (E)-4-(phenyldiazenyl)phenyl 4-((trimethylsilyl)ethynyl)benzoate (635 mg, 1.59 mmol, 43.5 % yield) as an orange solid.

^1H NMR (400 MHz, Chloroform-*d*) δ 8.21 – 8.14 (m, 2H, *ArH*), 8.07 – 8.00 (m, 2H, *ArH*), 7.98 – 7.87 (m, 2H, *ArH*), 7.67 – 7.59 (m, 2H, *ArH*), 7.58 – 7.45 (m, 3H, *ArH*), 7.44 – 7.33 (m, 2H, *ArH*), 0.29 (s, 9H, TMS). ^{13}C NMR (101 MHz, Chloroform-*d*, two carbons are not resolved) δ 164.3, 152.8, 152.6, 150.4, 132.1, 131.1, 130.0, 129.1, 128.7, 124.1, 122.9, 122.3, 103.9, 98.5, -0.2. HRMS (ESI/QTOF) m/z : $[\text{M} + \text{H}]^+$ Calcd for $\text{C}_{24}\text{H}_{23}\text{N}_2\text{O}_2\text{Si}^+$ 399.1523; Found 399.1522.

**(E)-4-(phenyldiazenyl)phenyl
yl)ethynyl)benzoate (6.24)**

4-((3-oxo-1*λ*3-benzo[d][1,2]iodaoxol-1(3H)-

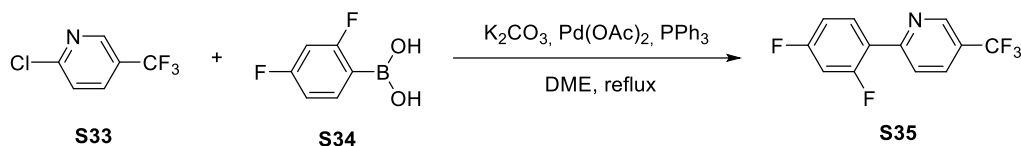


Trimethylsilyl triflate (0.27 mL, 1.5 mmol, 1.1 equiv) was added to a suspension of 2-iodosylbenzoic acid (**2.6**) (361 mg, 1.37 mmol, 1.00 equiv) in CH_2Cl_2 (5 mL) at RT. The resulting suspension was stirred for 1 h, followed by the drop wise addition of (E)-4-(phenyldiazenyl)phenyl 4-((trimethylsilyl)ethynyl)benzoate (**30**) (600 mg, 1.51 mmol, 1.10 equiv) which was dissolved in CH_2Cl_2 (1 mL). The resulting suspension was stirred for 4 h at RT. A saturated solution of NaHCO_3 (10 mL) was then added and the mixture was stirred vigorously for 30 minutes, the precipitate was filtered. The resulting solid was boiled in CH_3CN (10 mL). The mixture was cooled down, filtered and dried under high vacuum to afford **6.24** (568 mg, 0.992 mmol, 72.5 % yield) as an orange solid.

^1H NMR (400 MHz, Chloroform-*d*) δ 8.49 – 8.43 (m, 1H, *ArH*), 8.33 – 8.24 (m, 3H, *ArH*), 8.07 – 8.01 (m, 2H, *ArH*), 7.97 – 7.90 (m, 2H, *ArH*), 7.88 – 7.78 (m, 2H, *ArH*), 7.78 – 7.73 (m, 2H, *ArH*), 7.58 – 7.47 (m, 3H, *ArH*), 7.44 – 7.37 (m, 2H, *ArH*). ^{13}C NMR (101 MHz, Chloroform-*d*, all the carbons are not resolved) δ 163.8, 152.6, 150.5, 135.1, 132.9, 132.7, 131.8, 131.2, 130.9, 130.4, 129.1, 126.2, 125.8, 124.2, 122.9, 122.2, 116.1, 104.8, 54.7. HRMS (ESI/QTOF) m/z : $[\text{M} + \text{Na}]^+$ Calcd for $\text{C}_{28}\text{H}_{17}\text{IN}_2\text{NaO}_4^+$ 595.0125; Found 595.0137.

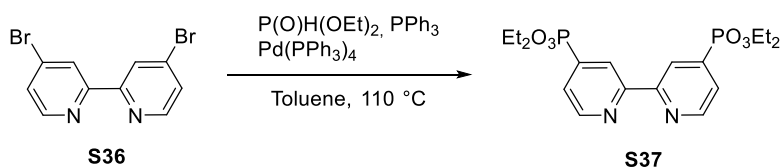
12.4.2 Preparation of water-soluble iridium catalysts

Preparation of ligands

2-(2,4-Difluorophenyl)-5-(trifluoromethyl)pyridine (**S35**)

In a 100 mL round-bottomed flask were added 2-chloro-5-(trifluoromethyl)pyridine (**S33**) (2.0 g, 11 mmol, 1 equiv), (2,4-difluorophenyl)boronic acid (**S34**) (2.1 g, 13 mmol, 1.2 equiv), and triphenylphosphine (0.29 g, 1.1 mmol, 10 mol%) and potassium carbonate (4.1 g, 30 mmol, 2.7 equiv) in DME (20 mL) to give a white suspension. The mixture was degassed by argon bubbling for 15 min and palladium acetate (0.062 mg, 0.28 mmol, 2.5 mol%) was added. The mixture was degassed for 15 min more before being heated at reflux overnight. The reaction mixture was cooled to RT and extracted with DCM (3 x 20 mL). The combined organic layers were washed with water (3 x 20 mL) and brine (20 mL), dried over MgSO_4 and concentrated under vacuum. The crude material was filtered on a silica pad, eluting with DCM to afford **S35** (2.8 g, 11 mmol, 96%) as yellow/orange solid which was used in the following step without further purification.

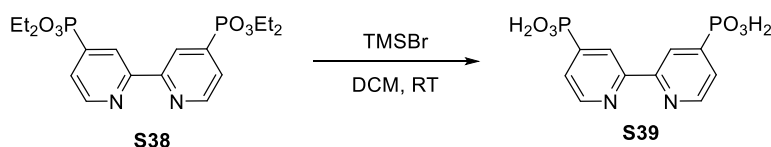
^1H NMR (CDCl_3 , 400 MHz) δ 9.01 – 8.92 (m, 1H, ArH), 8.10 (td, J = 8.8, 6.6 Hz, 1H, ArH), 8.00 (dd, J = 8.4, 2.3 Hz, 1H, ArH), 7.91 (d, J = 8.4 Hz, 1H, ArH), 7.05 (td, J = 8.4, 2.5 Hz, 1H, ArH), 6.95 (ddd, J = 11.3, 8.6, 2.5 Hz, 1H, ArH). Consistent with reported data.^[156]

Tetraethyl [2,2'-bipyridine]-4,4'-diylbis(phosphonate) (**S37**)

4,4'-dibromo-2,2'-bipyridine (**S36**) (0.30 mg, 0.95 mmol, 1.0 equiv), diethyl phosphite (0.28 mL, 2.2 mmol, 2.3 equiv), triphenylphosphine (2.5 g, 9.5 mmol, 10 equiv), triethylamine (0.31 mL, 2.2 mmol, 2.3 equiv) and tetrakis(triphenylphosphine)palladium (0.11 g, 0.095 mmol, 10 mol%) in toluene (10 mL) were heated at 110 °C under an argon atmosphere for 6 h. The reaction mixture was washed with an ammonium hydroxide solution, water, dried over MgSO₄ and concentrated under vacuum. The crude oil was purified by column chromatography (DCM/MeOH 10:0 to 99:1) to afford **S37** as a pale yellow solid (0.31 g, 0.72 mmol, 76%).

¹H NMR (400 MHz, CDCl₃): δ 8.78 (t, *J* = 5.1 Hz, 2H, Ar*H*), 8.71 (d, *J* = 14.0 Hz, 2H, Ar*H*), 7.66 (dd, *J* = 13.1, 4.9 Hz, 2H, Ar*H*), 4.26 – 4.01 (m, 8H, PCH₂CH₃), 1.30 (t, *J* = 7.1 Hz, 12H, PCH₂CH₃). ¹H NMR consistent with reported data.^[172]

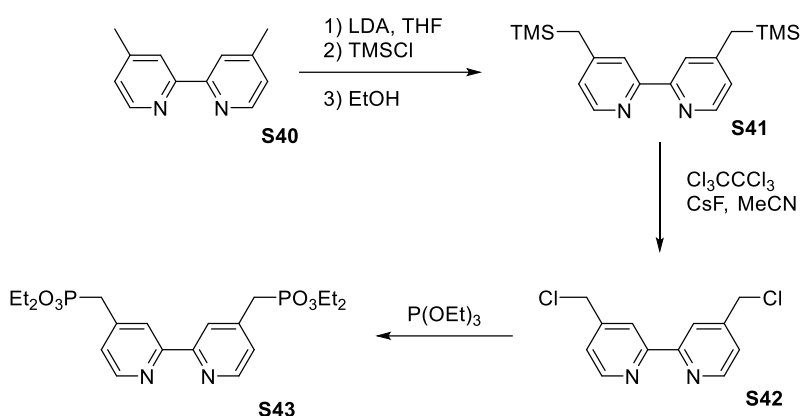
[2,2'-bipyridine]-4,4'-diylbisphosphonic acid (**S39**)



In a 10 mL microwave flask was tetraethyl [2,2'-bipyridine]-4,4'-diylbis(phosphonate) (**S38**) (0.10 g, 0.23 mmol, 1.0 equiv) dissolved in dry DCM (5 mL) under an atmosphere of argon to give a pale yellow solution. Bromotrimethylsilane (0.15 mL, 1.2 mmol, 5.0 equiv) was added and the reaction was stirred at RT for 3 days. The solvent was removed under vacuum, anhydrous MeOH (3 mL) was added and the mixture stirred 30 min at RT. A pale pink solid precipitated. The mixture was concentrated under vacuum and diethyl ether (6 mL) was added. The mixture was stirred for 2 h at RT and filtered to obtain **S39** as a pale pink solid (66 mg, 0.21 mmol, 89%). The compound was used without further purification.

¹H NMR (400 MHz, DMSO-*d*₆) δ 8.83 (t, *J* = 4.8 Hz, 2H, Ar*H*), 8.67 (d, *J* = 13.6 Hz, 2H, Ar*H*), 7.68 (dd, *J* = 12.5, 4.8 Hz, 2H, Ar*H*). ¹³C NMR (101 MHz, DMSO-*d*₆) δ 154.4, 154.2, 149.6, 149.5, 145.2, 143.5, 125.3, 125.2, 121.6, 121.5, 39.1. ¹H NMR consistent with reported data.^[173]

Tetraethyl ([2,2'-bipyridine]-4,4'-diylbis(methylene))bis(phosphonate) (bpy-MePO₃Et₂ – **S43**)



The following sequence was carried out following reported procedures.^[239,240]

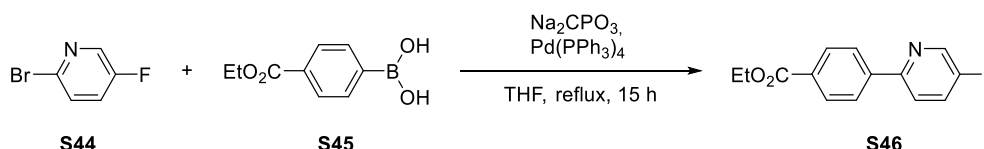
A 1.7 M solution of n-BuLi (3.1 mL, 5.2 mmol, 2.4 equiv) was added dropwise to a solution of diisopropylamine (0.84 mL, 5.9 mmol, 2.7 equiv) in anhydrous THF (8 mL) at -78 °C under nitrogen. The solution was stirred for 10 min, warmed at 0 °C and stirred for 10 min before being cooled back to -78 °C. A solution of 4,4'-dimethyl-2,2'-bipyridine (**S40**) (0.40 g, 2.2 mmol, 1.0 equiv) in anhydrous THF (10 mL) was added dropwise and the mixture stirred for 1 h to become dark purple. Trimethylchlorosilane (0.75 mL, 5.9 mmol, 2.7 equiv) was fastly added and the mixture became green. 15 sec later the reaction was quenched by rapid addition of absolute ethanol (0.8 mL). (the reaction has to be quenched very rapidly in order to prevent over silylation). The cold reaction mixture was poured into a separatory funnel containing an aqueous saturated solution of sodium bicarbonate (20 mL) and allowed to warm up to RT. The layers were separated and the aqueous layer was extracted with DCM (3 x 30 mL). The combined organic layers were washed with brine (20 mL), dried over MgSO₄ and filtered and concentrated under vacuum to afford **S41** (0.63 g, 1.9 mmol, 88%) as a yellow solid.

In a 100 mL round-bottomed flask were charged 4,4'-bis((trimethylsilyl)methyl)-2,2'-bipyridine (**S41**) (0.60 g, 1.8 mmol, 1.0 equiv), perchloroethane (1.70 g, 7.30 mmol, 4.0 equiv), and cesium fluoride (1.1 g, 7.3 mmol, 4.0 equiv) in anhydrous acetonitrile (30 mL) under an argon atmosphere to give a yellow solution. The mixture was stirred at 60 °C for 5 h. Distilled water (10 mL) and ethyl acetate (10 mL) were added to the cold mixture. The layers were separated and the aqueous layer was extracted with ethyl acetate (2 x 30 mL). The combined organic layers were washed with brine (10 mL), dried over MgSO₄ and concentrated under vacuum to afford 1.1 g of a slightly brown solid. The crude product was purified by flash chromatography on deactivated silica (washed with pentane, 10% of Et₃N then pentane), pentane/ethyl acetate 4:6 to afford **S42** (0.22 g, 0.87 mmol, 48%) as a pale yellow solid. Loss of product during drying process.

A 25-mL three-neck round bottom flask containing 4,4'-bis(chloromethyl)-2,2'-bipyridine (**S42**) (0.20 g, 0.79 mmol, 1.0 equiv) was placed under an argon atmosphere, and triethyl phosphite (1.4 mL, 7.9 mmol, 10 equiv) was added. The solution was refluxed overnight and cooled to room temperature. After removal of volatile materials under reduced pressure, the residue was purified by column chromatography on silica gel using a 4:4:1 toluene:hexanes:triethylamine eluent to yield **S43** (0.27 g, 0.59 mmol, 75%) as a white solid.

^1H NMR (400 MHz, CDCl_3) δ 8.64 – 8.55 (m, 2H, ArH), 8.37 – 8.27 (m, 2H, ArH), 7.32 (m, 2H, ArH), 4.15 – 3.95 (m, 8H, PCH_2CH_3), 3.25 (s, 2H, ArCH_2P), 3.20 (s, 2H, ArCH_2P), 1.26 (t, J = 7.1 Hz, 12H, PCH_2CH_3). Consistent with reported data.^[240]

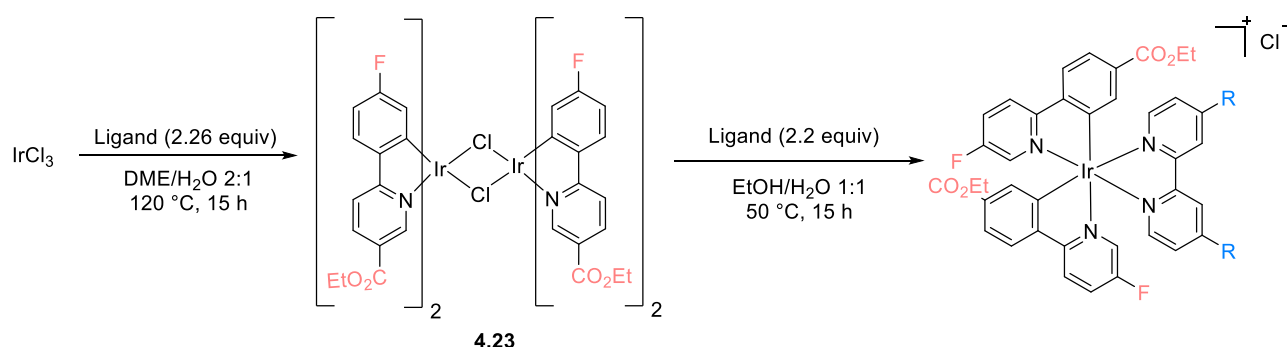
Ethyl 4-(5-fluoropyridin-2-yl)benzoate (**S46**)^[177]



In a 25 mL tube were added 2-bromo-5-fluoropyridine (**S44**) (0.50 g, 2.8 mmol, 1 equiv), (4-(ethoxycarbonyl)phenyl)boronic acid (**S45**) (0.77 g, 4.0 mmol, 1.4 equiv), and sodium carbonate (0.90 g, 8.5 mmol, 3 equiv) in a 2:1 v:v mixture of THF/water (6 mL) to give a yellow suspension. The mixture was degassed by argon bubbling for 15 min and palladium tetrakis (0.13 g, 0.11 mmol, 4 mol%) was added. The mixture was degassed for 15 min more before being heated at reflux overnight to afford a yellow suspension. The reaction mixture was cooled to RT and extracted with DCM (3x). The combined organic layers were washed with water, dried over MgSO_4 and concentrated under vacuum to afford a yellow solid. The crude material was purified by column chromatography pentane/DCM 1:1 then a gradient DCM/MeOH until 10% of MeOH to afford **S46** (0.54 g, 2.2 mmol, 77%) as a pale yellow solid.

^1H NMR (400 MHz, DMSO-d_6) 8.71 (d, J = 2.9 Hz, 1H, ArH), 8.19 (t, J = 8.7 Hz, 2H, ArH), 8.15 (dd, J = 8.9 Hz, 4.3 Hz, 1H, ArH), 8.06 (dd, J = 8.5 Hz, 2.0 Hz, 2H, ArH), 7.88 (td, J = 8.6 Hz, 2.7 Hz, 1H, ArH), 4.34 (q, J = 7.1 Hz, 2H, CH_2CH_3), 1.34 (t, J = 7.1 Hz, 3H, CH_2CH_3). Consistent with reported data.^[177]

Synthesis of ester-substituted bis-cyclometalated Ir bridge dimer (4.23)

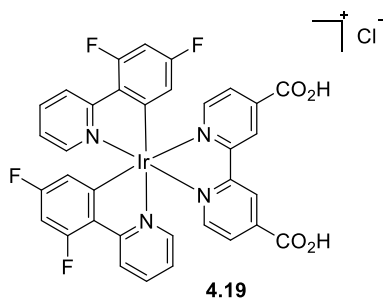


A slightly modified procedure was used.^[177]

In a 25 mL microwave tube were placed IrCl_3 (142 mg, 0.449 mmol, 1.00 equiv) and ethyl 4-(5-fluoropyridin-2-yl)benzoate (**S46**) (249 mg, 1.01 mmol, 2.26 equiv) in a 2:1 v:v mixture of 2-methoxyethanol/water (12 mL) to give a dark purple solution. The mixture was degassed with Ar (Ar bubbling for 10 min) and heated under reflux overnight to afford a yellow/orange suspension. The reaction mixture was cooled down and filtered to afford **4.23** (136 mg, 0.0950 mmol, 42%) as an orange solid, which was used in the following step without further purification.

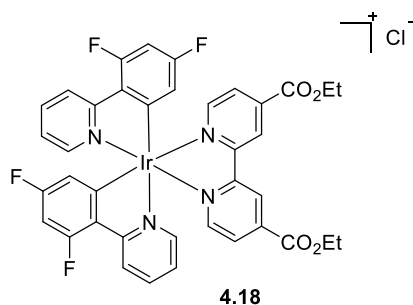
General procedure for the synthesis of water-soluble iridium catalysts

In a 25 mL microwave tube were added the Ir bridged dimer (20 mg, 0.016 mmol, 1.0 equiv) and the ligand (2.1 equiv) in a 1:1 v:v mixture of ethanol/water (8 mL) to give a yellow suspension. The mixture was degassed by argon bubbling for 15 min and heated in a microwave at 160 °C for 20 min to afford a yellow solution. The crude mixture was concentrated under vacuum and the resulting yellow solid was recrystallized in acetone/diethyl ether to afford a yellow solid. The catalysts were not soluble enough to afford an exploitable ^{13}C NMR spectra.

[Ir(dFppy)₂(bpy-CO₂H)]Cl (4.19)

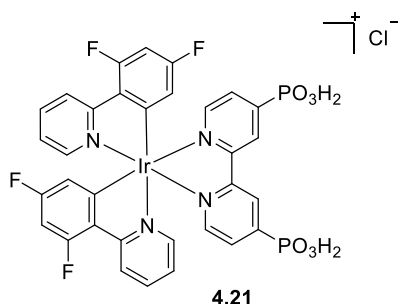
Starting from **4.16** (30 mg, 0.025 mmol), **4.19** was obtained directly from filtration of the final yellow suspension as a yellow solid (30 mg, 0.035 mmol, 71%).

¹H NMR (400 MHz, DMSO-*d*⁶) δ 9.18 (s, 2H, *ArH*), 8.92 (dd, *J* = 4.9, 0.8 Hz, 1H, *ArH*), 8.87 – 8.84 (m, 1H, *ArH*), 8.30 (d, *J* = 8.4 Hz, 1H, *ArH*), 8.03 (td, *J* = 8.0, 1.6 Hz, 2H, *ArH*), 7.99 (d, *J* = 1.5 Hz, 2H, *ArH*), 7.92 (dd, *J* = 5.0, 1.6 Hz, 1H, *ArH*), 7.73 (dd, *J* = 5.9, 1.5 Hz, 2H, *ArH*), 7.22 (ddd, *J* = 7.4, 5.8, 1.4 Hz, 2H, *ArH*), 6.99 (ddd, *J* = 12.2, 9.5, 2.4 Hz, 2H, *ArH*), 5.61 (dd, *J* = 8.3, 2.4 Hz, 2H, *ArH*). HRMS (ESI) calcd for C₃₄H₂₀F₄IrN₄O₄ [*M*⁺] 817.1044; found 817.1053.

[Ir(dFppy)₂(deeb)]Cl (4.18)

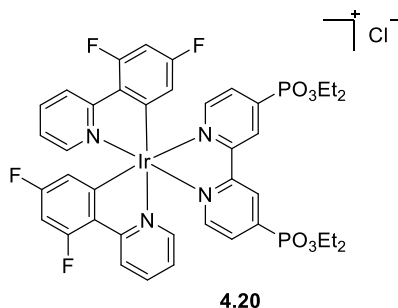
Starting from **4.16** (30 mg, 0.025 mmol), heating at 150 °C for 40 min afforded **4.18** as an orange solid (25 mg, 0.028 mmol, 56%).

¹H NMR (400 MHz, DMSO-*d*⁶) δ 9.35 (t, *J* = 1.2 Hz, 2H, *ArH*), 8.30 (d, *J* = 8.5 Hz, 2H, *ArH*), 8.15 – 8.10 (m, 3H, *ArH*), 8.10 – 8.02 (m, 3H, *ArH*), 7.76 (dd, *J* = 6.1, 1.4 Hz, 2H, *ArH*), 7.21 (ddd, *J* = 7.4, 5.8, 1.4 Hz, 2H, *ArH*), 7.02 (ddd, *J* = 12.2, 9.4, 2.4 Hz, 2H, *ArH*), 5.59 (dd, *J* = 8.4, 2.4 Hz, 2H, *ArH*), 4.45 (q, *J* = 7.1 Hz, 4H, CO₂CH₂CH₃), 1.37 (t, *J* = 7.1 Hz, 6H, CO₂CH₂CH₃). HRMS (ESI) calcd for C₃₈H₂₈F₄IrN₄O₄ [*M*⁺] 873.1670; found 873.1671. Consistent with reported data for the same catalyst with PF₆⁻ as counter-ion.^[345]

[Ir(dFppy)₂(bpy-PO₃H₂)]Cl (4.21)

Starting from **4.16** (40 mg, 0.033 mmol), heating at 160 °C for 20 min afforded **4.21** as a yellow solid (47 mg, 0.051 mmol, 77%).

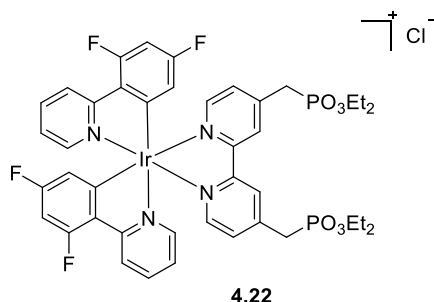
¹H NMR (400 MHz, DMSO-*d*₆) δ 9.25 (s, 2H, *ArH*), 8.29 (d, *J* = 8.8 Hz, 2H, *ArH*), 8.14 – 7.93 (m, 4H, *ArH*), 7.89 – 7.71 (m, 4H, *ArH*), 7.22 (t, *J* = 6.8 Hz, 2H, *ArH*), 6.98 (ddd, *J* = 12.1, 9.4, 2.4 Hz, 2H, *ArH*), 5.61 (dd, *J* = 8.3, 2.4 Hz, 2H, *ArH*). HRMS (ESI) calcd for C₃₂H₂₂F₄IrN₄O₆P₂ [*M*⁺] 889.0574; found 889.0589.

[Ir(dFppy)₂(bpy-PO₃Et₂)]Cl (4.20)

Starting from **4.16** (40 mg, 0.033 mmol), heating at 160 °C for 20 min afforded **4.20** as an unpure yellow solid (47 mg, 0.051 mmol, 77%).

¹H NMR (400 MHz, acetone-*d*₆) δ 9.69 (d, *J* = 13.2 Hz, 1H, *ArH*), 8.42 – 8.18 (m, 4H, *ArH*), 8.11 – 7.83 (m, 6H, *ArH*), 7.78 – 7.46 (m, 1H, *ArH*), 7.33 – 7.12 (m, 2H, *ArH*), 6.87 – 6.62 (m, 2H, *ArH*), 5.78 (dt, *J* = 8.5, 2.9 Hz, 2H, *ArH*), 3.99 (d, *J* = 7.3 Hz, 8H, POCH₂CH₃), 1.10 (t, *J* = 7.0 Hz, 12H, POCH₂CH₃). HRMS (ESI) calcd for C₄₀H₃₈F₄IrN₄O₆P₂ [*M*⁺] 1001.1826; found 1001.1827.

[Ir(dFppy)₂(bpy-MePO₃Et₂)]Cl (4.22)

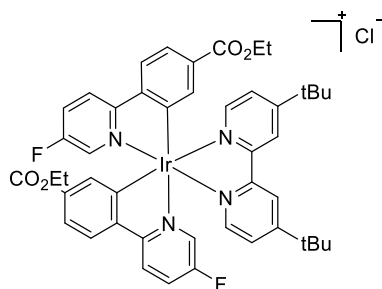


Starting from **4.16** (20 mg, 0.016 mmol), heating at 160 °C for 20 min afforded **4.22** as a yellow solid (23 mg, 0.022 mmol, 66%).

The compound was not pure enough for characterization.

HRMS (ESI) calcd for C₄₂H₄₂F₄IrN₄O₆P₂ [M⁺] 1029.2139; found 1029.2132.

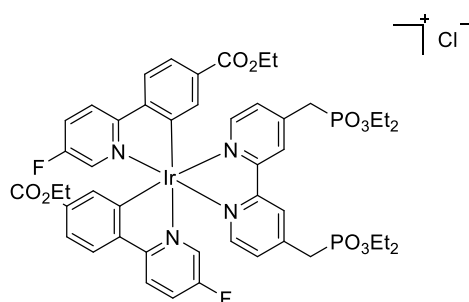
[Ir(F(CO₂Et)ppy)₂(dtbpy)]Cl (4.24)



Starting from **4.23** (20 mg, 0.016 mmol), heating at 50 °C overnight afforded after recrystallization in acetone/hexane **4.24** as a yellow solid (28 mg, 0.028 mmol, 99%).

¹H NMR (400 MHz, DMSO-d₆) δ 8.87 (s, 1H), 8.53 (dd, *J* = 9.3, 5.4 Hz, 2H), 8.17 (ddd, *J* = 9.2, 7.8, 2.7 Hz, 2H), 8.05 (d, *J* = 8.3 Hz, 2H), 7.74 (t, *J* = 2.7 Hz, 2H), 7.73 – 7.61 (m, 3H), 7.59 (dd, *J* = 8.2, 1.7 Hz, 2H), 6.74 (d, *J* = 1.7 Hz, 2H), 4.14 (q, *J* = 7.1 Hz, 4H), 1.40 (s, 18H), 1.18 (t, *J* = 7.1 Hz, 6H).

HRMS (ESI) calcd for C₄₆H₄₆F₂IrN₄O₄ [M⁺] 949.3111; found 949.3099.

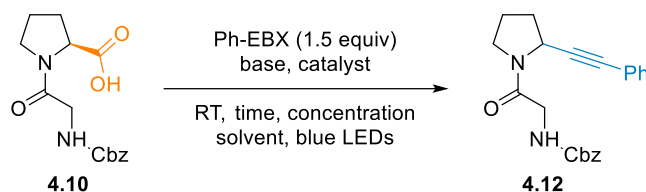
[Ir(F(CO₂Et)ppy)₂(bpy-MePO₃Et₂)]Cl (4.25)

Starting from **4.23** (20 mg, 0.014 mmol), heating at 50 °C overnight afforded **4.25** as an unpure yellow solid (30 mg, 0.026 mmol, 92%).

¹H NMR (400 MHz, DMSO-*d*₆) δ 8.83 – 8.65 (m, 2H, *ArH*), 8.54 (dt, *J* = 9.5, 4.8 Hz, 2H, *ArH*), 8.18 (dddd, *J* = 9.2, 6.9, 4.1, 2.7 Hz, 2H, *ArH*), 8.07 (dd, *J* = 8.3, 3.2 Hz, 2H, *ArH*), 7.85 – 7.65 (m, 3H, *ArH*), 7.65 – 7.52 (m, 4H, *ArH*), 6.74 (dd, *J* = 5.3, 1.8 Hz, 2H, *ArH*), 4.14 (q, *J* = 7.1 Hz, 4H, *CH*₂P), 3.96 (dq, *J* = 8.9, 7.0 Hz, 8H, POCH₂CH₃), 3.65 – 3.52 (m, 4H, CO₂CH₂CH₃), 1.18 (t, *J* = 7.1 Hz, 6H, CO₂CH₂CH₃), 1.06 (tt, *J* = 7.0, 1.3 Hz, 12H, POCH₂CH₃).

HRMS (ESI) calcd for C₄₈H₅₂F₂IrN₄O₁₀P₂ [M⁺] 1137.2750; found 1137.2762.

12.4.3 Optimization



Degassed solvent (10 mL) was added in a 10 mL test tube containing a teflon coated stirring bar, Z-Gly-Pro (**4.10**) (31 mg, 0.10 mmol, 1.0 equiv), Ph-EBX (**2.5**) (52 mg, 0.15 mmol, 1.5 equiv), the base and the catalyst under a nitrogen atmosphere. The reaction mixture was irradiated using blue light LEDs at RT.

Procedure for HPLC yields:

0.5 mL of the reaction mixture was diluted with acetonitrile (3 x volume). In the case of metal based catalysts, a filtration over reverse phase silica was performed. The yield was determined using a calibration curve based on absorbance at 214 nm after a linear regression with Excel. The calibration curve was obtained with samples between 0.25 to 1.25 mg/mL using the method A described in the general methods.

Procedure for isolated yields:

The crude mixture was diluted with 10 mL of brine and extracted with diethyl ether (3 x 50 mL). The combined organic layers were washed with brine (3 x 20 mL), dried over MgSO₄, filtered and concentrated under vacuum. The crude product was purified by preparative TLC (pentane/ethyl acetate 1:1 or DCM/ethyl acetate 8:2).

Table 24. Optimization of the decarboxylative alkynylation on dipeptides

Entry	Peptide	Solvent	Concentration (mM)	Catalyst (mol%)	Base (equiv)	Time	Ratio SM/P ^[a]	HPLC yield (%)
1 ^[b]	Z-Gly-Pro	DCE ^[c]	200	Ir cat (2.15) (1)	CsOBz (3)	22 h	-	mixture
2	Z-Gly-Pro	THF ^[c]	10	Ir cat (2.15) (2)	Cs ₂ CO ₃ (1)	15 h	>5:95	66 ^[d]
3	Z-Gly-Pro	MeCN ^[c]	10	Ir cat (2.15) (2)	Cs ₂ CO ₃ (1)	15 h	>5:95	55 ^[d]
4	Z-Gly-Pro	DMF ^[c,e]	5	Ir cat (2.15) (6)	K ₂ HPO ₄ (2)	15 h	>5:95	86

5	Z-Gly-Pro	DMF ^[c,e]	5	4CzIPN (2.23) (6)	K ₂ HPO ₄ (2)	15 h	>5:95	86
6	Z-Gly-Pro	DMF ^[c]	5	4CzIPN (2.23) (6)	K ₂ HPO ₄ (2)	15 h	>5:95	>95
7	Z-Gly-Pro	DMF ^[c,e]	5	DCA (6)	K ₂ HPO ₄ (2)	15 h	24:76	33
8	Z-Ala-Ala	DMF ^[c,e]	5	4CzIPN (2.23) (6)	K ₂ HPO ₄ (2)	2 h	>5:95	83
9 ^[f]	Z-Ala-Ala	DMF ^[c,e]	5	4CzIPN (2.23) (6)	K ₂ HPO ₄ (2)	2 h	25:74	27
10	Z-Ala-Ala	DMF ^[c,g]	10	4CzIPN (2.23) (3)	K ₂ HPO ₄ (2)	1 h	>5:95	77-90
11	Z-Ala-Ala	DMF ^[c,g]	10	4CzIPN (2.23) (0.5-6)	K ₂ HPO ₄ (2)	30 min	>5:95	65-72
12 ^[h]	Z-Ala-Ala	DMF ^[g]	10	4CzIPN (2.23) (3)	K ₂ HPO ₄ (2)	30 min	>5:95	86
13 ^[i]	Z-Ala-Ala	DMF ^[g]	10	4CzIPN (2.23) (3)	K ₂ HPO ₄ (2)	30 min	>5:95	71

^[a] Ratio of integration at 214 nm by RP-HPLC, ^[b] using TIPS-EBX^[13], ^[c] degassed by nitrogen bubbling, ^[d] isolated yield, ^[e] DMF/H₂O 99:1, ^[f] 40 W CFL household bulb, ^[g] DMF/H₂O 98:2, ^[h] freeze-pump-throw degassing, ^[i] non-degassed solvents.

With the optimized conditions (Table 17, entry 12), a catalyst screening of the novel organic dyes was performed (Table 25). Degassed (by freeze-pump-throw cycles) DMF (10 mL) and degassed water (0.20 mL) were added in a 15 mL microwave tube containing a teflon coated stirring bar, Cbz-Gly-Pro (**4.10**) (15.3 mg, 0.0500 mmol, 1.0 equiv), Ph-EBX (**2.5**) (26.1 mg, 0.0750 mmol, 1.5 equiv), K₂HPO₄ (17.4 mg, 0.100 mmol, 2.0 equiv) and the organic dye (3 mol%) under a nitrogen atmosphere. The reaction mixture was irradiated using blue light LEDs at RT for 30 min.

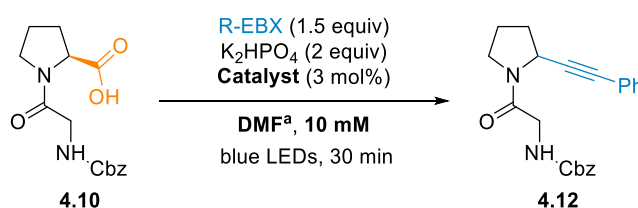


Table 25: Catalyst screening on Z-Gly-Pro

Entry	Catalyst	HPLC yield (%)
1	4CzIPN (2.23)	99
2	4ClCzIPN (5.4)	89
3	4DPAIPN (2.22)	43
4	4BrDPAIPN (5.26)	50
5	4CIDPAIPN (5.25)	65

6	4tBuCzIPN (5.27)	44
7	4MeOCzIPN (5.28)	<5
8	4tBuCzIPN (5.27) ^[b]	57
9	Ir cat (2.15)	99
10 ^[c]	4CzIPN (2.23)	87

^[a] with 111 equivalents of water, ^[a] 5 mol%, ^[b] non-degassed solvents.

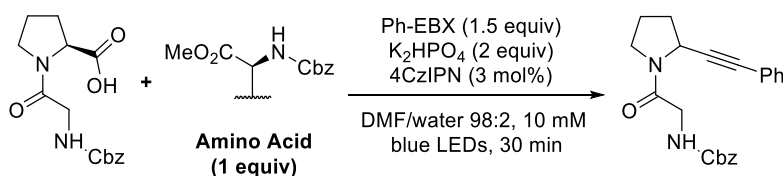
Control experiments were carried out and only traces of the desired product were observed in the absence of light or catalyst. Interestingly, the presence of a base is not required for the transformation as 24% yield was still obtained without addition of base.

12.4.4 Robustness experiments

Degassed DMF (10 mL) and degassed water (0.20 mL) were added in a 15 mL microwave tube containing a teflon coated stirring bar, Cbz-Gly-Pro (**4.10**) (31 mg, 0.10 mmol, 1.0 equiv), the protected amino acid (0.10 mmol, 1.0 equiv), Ph-EBX (**2.5**) (52 mg, 0.15 mmol, 1.5 equiv), K₂HPO₄ (35 mg, 0.20 mmol, 2.0 equiv) and 4CzIPN (**2.23**) (2.4 mg, 3.0 μmol, 3 mol%) under a nitrogen atmosphere. The reaction mixture was irradiated using blue light LEDs at RT for 30 min.

0.5 mL of the crude was filtered under an inverse phase silica pad and eluted with 1.5 mL of acetonitrile. 1 mL was injected into HPLC. The yield was determined using a calibration curve based on absorbance at 214 nm after a linear regression with Excel.

Table 26. Robustness experiments



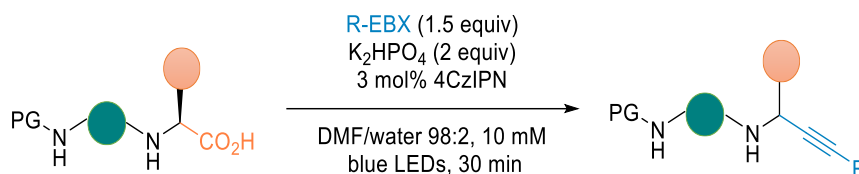
Entry	Amino acid (1 equiv)	Ratio SM/P ^a	HPLC yield (%)
1	Cbz-Met-OMe	>5:95	117
2	Cbz-Ser-OMe	5:95	108
3	Cbz-His-OMe	6:94	81
4	Cbz-Arg-OMe	19:81	79
5	Cbz-Tyr-OMe	43:57	43

6	Cbz-Val-Trp-OMe	65:35	35
7	Cbz-Gln-OMe	55:44	60
8	Cbz-Lys-OMe	42:58	58
9	(Cbz-Cys-OMe) ₂	43:57	50
		2h: 29:71	2h: 71
10	Cbz-Cys-OMe	25:75	62

^a Ratio of product compared to remaining starting material by HPLC analysis.

In all cases the reactions were clean, with no byproducts. Unreacted starting material was detected when the yield were low.

12.4.5 Reagents and dipeptide scope

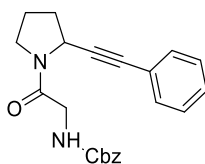


General procedure 3 for the decarboxylative alkynylation of dipeptides

Degassed DMF and water (30 mL, 98:2) were added in a 50 mL schlenk flask containing a teflon coated stirring bar, Cbz-Gly-Pro (**4.10**) (92 mg, 0.10 mmol, 1.0 equiv), Ph-EBX (**2.5**) (0.16 g, 0.45 mmol, 1.5 equiv), K₂HPO₄ (0.11 g, 0.60 mmol, 2.0 equiv) and 4CzIPN (**2.23**) (7.1 mg, 9.0 μmol, 3 mol%) under a nitrogen atmosphere. The reaction mixture was irradiated using blue light LEDs for 30 min at RT.

0.5 mL of the crude was filtered under an inverse phase silica pad and eluted with 1.5 mL of acetonitrile. 1 mL was injected into HPLC to determine the conversion.

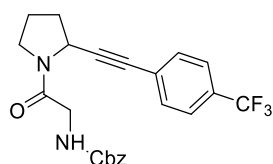
The crude mixture was diluted with 30 mL of brine and extracted with diethyl ether (3 x 150 mL). The combined organic layers were washed with brine (3 x 50 mL), dried over MgSO₄, filtered and concentrated under vacuum. The crude product was purified by column chromatography DCM to DCM/ethyl acetate 8:2. In some cases a preparative TLC DCM/ethyl acetate 9:1 was performed for characterization.

Benzyl (2-oxo-2-(2-(phenylethynyl)pyrrolidin-1-yl)ethyl)carbamate (**4.12**)

Starting with Cbz-Gly-Pro (**4.10**) (92 mg, 0.30 mmol, 1.0 equiv), **4.12** was obtained after column chromatography DCM to DCM/ethyl acetate 8:2 as a pale yellow oil (100 mg, 0.276 mmol, 92%).

Rf (DCM/ethyl acetate 95:5): 0.3. ^1H NMR (400 MHz, Chloroform-*d*, 6:4 mixture of rotamers (major/minor))²⁴ δ 7.47 – 7.28 (m, 10H, ArH, (major+minor)), 5.84 – 5.55 (m, 1H, NH (major+minor)), 5.13 (s, 2H, OCH₂Ph (major+minor)), 5.01 (dd, J = 7.4, 2.3 Hz, 0.4H, NCHC \equiv C (minor)), 4.69 (t, J = 4.9 Hz, 0.6H, NCHC \equiv C (major)), 4.31 (dd, J = 17.2, 3.8 Hz, 0.6H, NC(O)CH₂NHCbz (major)), 4.18 (dd, J = 17.2, 5.1 Hz, 0.6H, NC(O)CH₂NHCbz (major)), 4.06 – 3.90 (m, 0.8H, NC(O)CH₂NHCbz (minor)), 3.70 (ddd, J = 11.4, 8.0, 3.3 Hz, 0.6H, NCH₂(CH₂)₂CHC \equiv C (major)), 3.63 – 3.47 (m, 1H, NCH₂(CH₂)₂CHC \equiv C (major+minor)), 3.44 – 3.31 (m, 0.4H, NCH₂(CH₂)₂CHC \equiv C (minor)), 2.38 – 1.91 (m, 4H, NCH₂(CH₂)₂CHC \equiv C (major+minor)). ^{13}C NMR (101 MHz, Chloroform-*d*, mixture of rotamers, signals not fully resolved) δ 167.1, 166.3, 156.2, 136.4, 131.8, 131.7, 128.7, 128.4, 128.3, 128.2, 128.1, 128.0, 128.0, 127.9, 122.7, 121.9, 88.0, 86.8, 84.4, 82.3, 66.8, 48.7, 48.3, 46.1, 45.2, 43.5, 34.5, 32.4, 24.7, 22.9. IR 3293 (w), 2986 (w), 2880 (w), 2362 (w), 2341 (w), 1718 (s), 1648 (s), 1542 (m), 1445 (m), 1263 (m), 1057 (w). HRMS (ESI) calcd for C₂₂H₂₃N₂O₃⁺ [M+H]⁺ 363.1703; found 363.1702.

Benzyl (2-oxo-2-(2-((4-(trifluoromethyl)phenyl)ethynyl)pyrrolidin-1-yl)ethyl)carbamate (6.27)



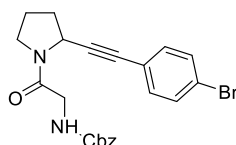
Starting with Cbz-Gly-Pro (**4.10**) (92 mg, 0.30 mmol, 1.0 equiv) and *p*CF₃-Ph-EBX (**6.8**) (187 mg, 0.450 mmol, 1.50 equiv), **6.27** was obtained after column chromatography DCM to DCM/ethyl acetate 8:2 as a yellow oil (124 mg at 95% purity, 0.274 mmol, 91%).

Rf (DCM/ethyl acetate 9:1): 0.3. ^1H NMR (400 MHz, Chloroform-*d*, 1:1 mixture of rotamers (R¹/R²)) δ 7.59 – 7.47 (m, 4H, ArH, (R¹+R²)), 7.45 – 7.27 (m, 5H, ArH, (R¹+R²)), 5.76 (bs, 1H, NH (R¹+R²)), 5.12 (s, 2H, OCH₂Ph, (R¹+R²)), 5.01 (dd, J = 7.3, 2.7 Hz, 0.5H, NCHC \equiv C (R¹)), 4.71 (t, J = 4.9 Hz, 0.5H, NCHC \equiv C (R²)), 4.31 (dd, J = 17.1, 3.9 Hz, 0.5H, NC(O)CH₂NHCbz (R²)), 4.15 (dd, J = 17.1, 4.7 Hz, 0.5H, NC(O)CH₂NHCbz (R²)), 3.99 (d, J = 4.3 Hz, 1H, NC(O)CH₂NHCbz (R¹)), 3.75 – 3.66 (m, 0.5H, NCH₂(CH₂)₂CHC \equiv C (R²)), 3.64 – 3.46 (m, 1H

²⁴ The signals of each rotamer were assigned by 2D NMR (see section 7). For clarity, only the spectra of **6a** are presented. Following products were assigned by analogy when a 1:1 ratio was measured.

$\text{NCH}_2(\text{CH}_2)_2\text{CHC}\equiv\text{C}$ (R^1+R^2), 3.46 – 3.33 (m, 0.5H, $\text{NCH}_2(\text{CH}_2)_2\text{CHC}\equiv\text{C}$ (R^1)), 2.39 – 1.93 (m, 4H, $\text{NCH}_2(\text{CH}_2)_2\text{CHC}\equiv\text{C}$, (R^1+R^2)). ^{13}C NMR (101 MHz, Chloroform-*d*, mixture of rotamers, signals not fully resolved)²⁵ δ 167.1, 166.4, 162.0, 156.2, 136.4, 132.0 (d, J = 3.8 Hz), 130.4 (d, J = 33.1 Hz), 129.9 (d, J = 32.7 Hz), 128.5, 128.0 (d, J = 8.8 Hz), 126.1 (d, J = 79.2 Hz), 125.3 (q, J = 4.0 Hz), 125.0 (q, J = 3.5 Hz), 122.5 (d, J = 9.4 Hz), 90.6, 89.2, 83.1, 81.0, 66.9, 48.5, 48.2, 46.2, 45.2, 43.5, 34.4, 32.3, 24.8, 22.9. ^{19}F NMR (376 MHz, Chloroform-*d*) δ -62.8, -62.9. IR 3290 (w), 2986 (w), 2881 (w), 2831 (w), 2362 (m), 2343 (w), 2122 (w), 1717 (m), 1653 (s), 1542 (m), 1457 (w), 1437 (w), 1326 (s), 1263 (w), 1170 (m), 1129 (m), 1068 (m), 845 (w). HRMS (ESI) calcd for $\text{C}_{23}\text{H}_{21}\text{F}_3\text{N}_2\text{NaO}_3^+$ [$\text{M}+\text{Na}$] $^+$ 453.1396; found 453.1395.

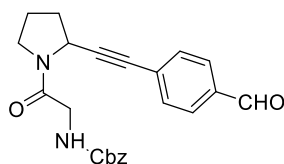
Benzyl (2-(2-((4-bromophenyl)ethynyl)pyrrolidin-1-yl)-2-oxoethyl)carbamate (**6.28**)



Starting with Cbz-Gly-Pro (**4.10**) (92 mg, 0.30 mmol, 1.0 equiv) and *p*Br-Ph-EBX (**6.9**) (192 mg, 0.450 mmol, 1.50 equiv), **6.28** was obtained after column chromatography DCM to DCM/ethyl acetate 8:2 as a yellow oil (122 mg, 0.276 mmol, 92%).

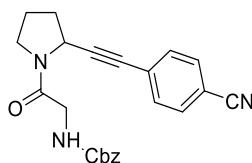
R_f (DCM/ethyl acetate 9:1): 0.3. ^1H NMR (400 MHz, Chloroform-*d*, 1:1 mixture of rotamers (R^1/R^2)) δ 7.46 – 7.28 (m, 9H, ArH (R^1+R^2)), 5.78 (s, 1H, NH, (R^1+R^2)), 5.12 (s, 2H, OCH_2Ph , (R^1+R^2)), 4.98 (dd, J = 7.2, 2.5 Hz, 0.5H, $\text{NCHC}\equiv\text{C}$ (R^1)), 4.67 (t, J = 5.0 Hz, 0.5H, $\text{NCHC}\equiv\text{C}$ (R^2)), 4.29 (dd, J = 17.1, 4.0 Hz, 0.5H, $\text{NC}(\text{O})\text{CH}_2\text{NHCbz}$ (R^2)), 4.14 (dd, J = 18.1, 4.2 Hz, 0.5H, $\text{NC}(\text{O})\text{CH}_2\text{NHCbz}$ (R^2)), 4.06 – 3.89 (m, 1H, $\text{NC}(\text{O})\text{CH}_2\text{NHCbz}$ (R^1)), 3.74 – 3.63 (m, 0.5H, $\text{NCH}_2(\text{CH}_2)_2\text{CHC}\equiv\text{C}$ (R^2)), 3.61 – 3.46 (m, 1H, $\text{NCH}_2(\text{CH}_2)_2\text{CHC}\equiv\text{C}$ (R^1+R^2)), 3.44 – 3.27 (m, 0.5H, $\text{NCH}_2(\text{CH}_2)_2\text{CHC}\equiv\text{C}$ (R^1)), 2.38 – 1.90 (m, 4H, $\text{NCH}_2(\text{CH}_2)_2\text{CHC}\equiv\text{C}$ (R^1+R^2)). ^{13}C NMR (101 MHz, Chloroform-*d*, mixture of rotamers, signals not fully resolved) δ 167.0, 166.3, 156.2, 136.4, 133.2, 133.1, 131.6, 131.4, 128.4, 128.0, 128.0, 123.0, 122.4, 121.6, 120.9, 89.3, 88.0, 83.4, 81.2, 66.8, 48.5, 48.2, 46.1, 45.2, 43.5, 34.4, 32.3, 24.7, 22.8. IR 3285 (w), 2976 (w), 2880 (w), 2361 (w), 2343 (w), 1718 (s), 1654 (s), 1542 (m), 1437 (m), 1436 (m), 1339 (w), 1260 (m), 1176 (w), 1070 (w), 1011 (w), 830 (w). HRMS (ESI) calcd for $\text{C}_{22}\text{H}_{21}\text{BrN}_2\text{NaO}_3^+$ [$\text{M}+\text{Na}$] $^+$ 463.0628; found 463.0612.

²⁵ The quadruplets corresponding to the CF_3 couplings were not resolved and appeared as doublets.

Benzyl (2-(2-((4-formylphenyl)ethynyl)pyrrolidin-1-yl)-2-oxoethyl)carbamate (6.29)

Starting with Cbz-Gly-Pro (**4.10**) (92 mg, 0.30 mmol, 1.0 equiv) and *p*CHO-Ph-EBX (**6.10**) (169 mg, 0.450 mmol, 1.50 equiv), **6.29** was obtained after column chromatography DCM to DCM/ethyl acetate 8:2 as a yellow oil (105 mg, 0.269 mmol, 90%).

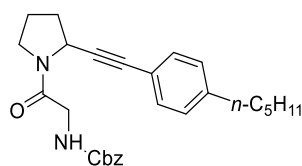
R_f (DCM/ethyl acetate 9:1): 0.33. ¹H NMR (400 MHz, Chloroform-*d*, 1:1 mixture of rotamers (R¹/R²)) δ 9.98 (s, 0.5H, CHO (R¹)), 9.96 (s, 0.5H, CHO (R²)), 7.78 (dd, *J* = 14.0, 8.0 Hz, 2H, ArH (R¹+R²)), 7.53 (t, *J* = 7.6 Hz, 2H, ArH (R¹+R²)), 7.35 – 7.26 (m, 5H, ArH (R¹+R²)), 5.81 (s, 1H, NH (R¹+R²)), 5.11 (s, 2H, OCH₂Ph (R¹+R²)), 5.00 (d, *J* = 4.5 Hz, 0.5H, NCHC≡C (R¹)), 4.72 (t, *J* = 5.0 Hz, 0.5H, NCHC≡C (R²)), 4.29 (d, *J* = 17.1 Hz, 0.5H, NC(O)CH₂NHCbz (R²)), 4.15 (d, *J* = 17.2 Hz, 0.5H, NC(O)CH₂NHCbz (R²)), 4.05 – 3.91 (m, 1H, NC(O)CH₂NHCbz (R¹)), 3.76 – 3.63 (m, 0.5H, NCH₂(CH₂)₂CHC≡C (R²)), 3.63 – 3.29 (m, 1.5H, NCH₂(CH₂)₂CHC≡C (R¹+R²)), 2.35 – 1.93 (m, 4H, NCH₂(CH₂)₂CHC≡C (R¹+R²)). ¹³C NMR (101 MHz, Chloroform-*d*, mixture of rotamers, signals not fully resolved) δ 191.4, 191.3, 167.1, 166.4, 156.2, 136.3, 135.7, 135.3, 132.3, 132.2, 129.4, 129.3, 128.9, 128.4, 128.0, 128.0, 127.9, 92.2, 90.7, 83.5, 81.4, 66.8, 65.7, 48.5, 48.2, 46.1, 45.2, 43.4, 34.3, 32.2, 24.8, 22.8, 15.2. IR (ν_{max}, cm⁻¹) 3654 (w), 3401 (w), 3321 (w), 2982 (w), 2883 (w), 2729 (w), 2347 (w), 2230 (w), 1700 (s), 1657 (s), 1601 (m), 1515 (m), 1435 (s), 1336 (w), 1262 (m), 1213 (m), 1170 (m), 1053 (m), 985 (w), 911 (w), 825 (m), 733 (s). HRMS (ESI/QTOF) *m/z*: [M + Na]⁺ Calcd for C₂₃H₂₂N₂NaO₄⁺ 413.1472; Found 413.1478.

Benzyl (2-(2-((4-cyanophenyl)ethynyl)pyrrolidin-1-yl)-2-oxoethyl)carbamate (6.30)

Starting with Cbz-Gly-Pro (**4.10**) (92 mg, 0.30 mmol, 1.0 equiv) and *p*CN-Ph-EBX (**6.11**) (168 mg, 0.450 mmol, 1.50 equiv), **6.30** was obtained after column chromatography DCM to DCM/ethyl acetate 8:2 as an amorphous solid (108 mg, 0.279 mmol, 93%).

R_f (DCM/ethyl acetate 9:1): 0.33. ¹H NMR (400 MHz, Acetonitrile-*d*₃, 55:45 mixture of rotamers (R¹/R²)) δ 7.51 – 7.41 (m, 2H, ArH (R¹+R²)), 7.35 (d, *J* = 8.0 Hz, 1H, ArH (R¹+R²)), 7.28 (d, *J* = 8.1 Hz, 1H, ArH (R¹+R²)), 7.17 – 7.02 (m, 5H, ArH (R¹+R²)), 5.76 – 5.54 (bs, 1H, NH (R¹+R²)), 4.86 (s, 2H, OCH₂Ph (R¹+R²)), 4.70 – 4.64 (m, 0.55H, NCHC≡C (R¹)), 4.59 (dd, *J* = 7.6, 2.4 Hz, 0.45H, NCHC≡C (R²)), 4.01 (dd, *J* = 17.0, 5.8 Hz, 0.5H, NC(O)CH₂NHCbz (R²)), 3.78 (dd, *J* = 17.0, 5.5 Hz, 0.5H, NC(O)CH₂NHCbz (R²)), 3.74 – 3.56 (m, 1.1H, NC(O)CH₂NHCbz (R¹)), 3.65 (dd, *J* = 5.5, 1.5 Hz, 1.1H, NC(O)CH₂NHCbz (R¹)), 3.41 – 3.26 (m, 1H, NCH₂(CH₂)₂CHC≡C (R¹+R²)), 3.24 – 3.11 (m, 1H, NCH₂(CH₂)₂CHC≡C (R¹+R²)), 2.14 – 1.66 (m, 4H, NCH₂(CH₂)₂CHC≡C (R¹+R²)). ¹³C NMR (101 MHz, Acetonitrile-*d*₃, mixture of rotamers, signals not fully resolved) δ 168.3, 167.9, 157.5, 157.4, 138.2, 133.3, 133.3, 133.1, 133.0, 129.4, 128.8, 128.7, 128.6, 128.1, 119.3, 119.2, 112.7, 112.3, 94.9, 93.2, 82.9, 80.8, 67.1, 49.2, 48.8, 46.8, 46.1, 44.0, 34.8, 32.9, 25.6, 23.5. IR (ν_{max}, cm⁻¹) 3616 (m), 3398 (w), 2918 (w), 2613 (w), 2370 (m), 2264 (s), 1728 (s), 1659 (s), 1510 (m), 1453 (m), 1348 (w), 1254 (m), 1048 (m), 843 (m), 749 (w). HRMS (ESI/QTOF) *m/z*: [M + Na]⁺ Calcd for C₂₃H₂₁N₃NaO₃⁺ 410.1475; Found 410.1482.

Benzyl (2-oxo-2-(2-((4-pentylphenyl)ethynyl)pyrrolidin-1-yl)ethyl)carbamate (**6.31**)

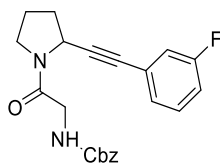


Starting with Cbz-Gly-Pro (**4.10**) (92 mg, 0.30 mmol, 1.0 equiv) and *p*C₅H₁₁-Ph-EBX (**6.12**) (168 mg, 0.450 mmol, 1.50 equiv), **6.31** was obtained after column chromatography DCM to DCM/ethyl acetate 8:2 as a yellow oil (119 mg, 0.275 mmol, 92%).

R_f (DCM/ethyl acetate 9:1): 0.36. ¹H NMR (400 MHz, Chloroform-*d*, 6:4 mixture of rotamers (major/minor)) δ 7.40 – 7.27 (m, 7H, ArH (major + minor)), 7.09 (dd, *J* = 13.5, 8.0 Hz, 2H, ArH (major + minor)), 5.93 – 5.72 (m, 1H, NH (major + minor)), 5.13 (s, 2H, OCH₂Ph (major+minor)), 5.06 – 4.96 (m, 0.4H, NCHC≡C (minor)), 4.68 (t, *J* = 4.9 Hz, 0.6H, NCHC≡C (major)), 4.31 (dd, *J* = 17.1, 2.6 Hz, 0.6H, NC(O)CH₂NHCbz (major)), 4.18 (dd, *J* = 17.1, 4.0 Hz, 0.6H,

NC(O)CH₂NHCbz (major)), 4.07 – 3.87 (m, 0.5H, NC(O)CH₂NHCbz (minor)), 3.74 – 3.61 (m, 0.6H, NCH₂(CH₂)₂CHC≡C (major)), 3.63 – 3.43 (m, 1H, NCH₂(CH₂)₂CHC≡C (major+minor)), 3.44 – 3.24 (m, 0.4H, NCH₂(CH₂)₂CHC≡C (minor)), 2.57 (q, *J* = 7.9 Hz, 2H, ArCH₂ (major+minor)), 2.40 – 1.86 (m, 4H, NCH₂(CH₂)₂CHC≡C (major+minor)), 1.70 – 1.49 (m, 2H, ArCH₂CH₂ (major+minor)), 1.44 – 1.20 (m, 4H, CH₂CH₂CH₃ (major+minor)), 0.97 – 0.76 (m, 3H, CH₂CH₃ (major+minor)). ¹³C NMR (101 MHz, Chloroform-*d*, mixture of rotamers, signals not fully resolved) δ 167.1, 166.2, 156.2, 143.8, 143.2, 136.4, 131.6, 131.5, 128.4, 128.2, 127.9, 127.9, 127.9, 119.7, 119.0, 87.3, 86.1, 84.5, 82.3, 66.7, 48.5, 48.3, 46.0, 45.1, 43.4, 35.7, 35.7, 34.4, 32.4, 31.3, 30.8, 24.6, 22.8, 22.4, 13.9. IR (ν_{max}, cm⁻¹) 3654 (w), 3407 (m), 3333 (w), 2982 (s), 2926 (s), 2224 (w), 1725 (s), 1657 (s), 1509 (m), 1435 (s), 1336 (w), 1250 (s), 1164 (m), 1059 (s), 917 (w), 837 (m), 745 (m). HRMS (ESI/QTOF) *m/z*: [M + Na]⁺ Calcd for C₂₇H₃₂N₂NaO₃⁺ 455.2305; Found 455.2310.

Benzyl (2-(2-((3-fluorophenyl)ethynyl)pyrrolidin-1-yl)-2-oxoethyl)carbamate (**6.32**)

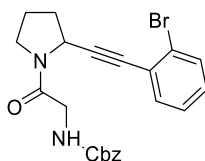


Starting with Cbz-Gly-Pro (**4.10**) (92 mg, 0.30 mmol, 1.0 equiv) and *m*F-Ph-EBX (**6.13**) (165 mg, 0.450 mmol, 1.50 equiv), **6.32** was obtained after column chromatography DCM to DCM/ethyl acetate 8:2 as a yellow oil (101 mg, 0.266 mmol, 89%).

R_f (DCM/ethyl acetate 9:1): 0.25. ¹H NMR (400 MHz, Chloroform-*d*, 1:1 mixture of rotamers (R¹/R²)) δ 7.24 – 6.83 (m, 9H, ArH (R¹+R²)), 5.74 – 5.60 (m, 1H, NH (R¹+R²)), 5.02 (s, 2H, OCH₂Ph (R¹+R²)), 4.89 (dd, *J* = 7.3, 2.5 Hz, 0.5H, NCHC≡C (R¹)), 4.58 (t, *J* = 4.9 Hz, 0.5H, NCHC≡C (R²)), 4.19 (dd, *J* = 17.1, 4.0 Hz, 0.5H, NC(O)CH₂NHCbz (R²)), 4.06 (dd, *J* = 17.1, 5.1 Hz, 0.5H, NC(O)CH₂NHCbz (R²)), 3.96 – 3.80 (m, 1H, NC(O)CH₂NHCbz (R¹)), 3.66 – 3.54 (m, 0.5H, NCH₂(CH₂)₂CHC≡C (R²)), 3.53 – 3.35 (m, 1H, NCH₂(CH₂)₂CHC≡C (R¹+R²)), 3.34 – 3.20 (m, 0.5H, NCH₂(CH₂)₂CHC≡C (R¹+R²)), 2.27 – 1.78 (m, 4H, NCH₂(CH₂)₂CHC≡C (R¹+R²)). ¹³C NMR (101 MHz, Chloroform-*d*, mixture of rotamers, signals not fully resolved) δ 167.01, 166.3, 162.2 (d, *J* = 246.9 Hz), 162.2 (d, *J* = 246.2 Hz), 156.2, 136.4, 129.9 (d, *J* = 8.6 Hz), 129.7 (d, *J* = 8.7 Hz), 128.4, 128.0, 128.0, 127.9, 127.7 (d, *J* = 3.0 Hz), 127.6 (d, *J* = 3.0 Hz), 124.5 (d, *J* = 9.5 Hz), 123.7 (d, *J* = 9.3 Hz), 118.7 (d, *J* = 6.1 Hz), 118.4 (d, *J* = 6.3 Hz), 116.1

(d, $J = 21.1$ Hz), 115.5 (d, $J = 21.1$ Hz), 89.1, 87.7, 83.2 (d, $J = 3.5$ Hz), 81.1 (d, $J = 3.1$ Hz), 66.8, 48.5, 48.2, 46.1, 45.2, 43.5, 34.4, 32.3, 24.8, 22.8. ^{19}F NMR (376 MHz, Chloroform- d) δ -112.6, -113.2. IR (ν_{max} , cm^{-1}) 3426 (m), 3308 (m), 3068 (w), 2976 (m), 2889 (m), 2359 (w), 2329 (w), 1719 (s), 1657 (s), 1583 (m), 1527 (w), 1435 (s), 1343 (m), 1262 (s), 1158 (m), 1059 (s), 991 (m), 868 (m), 794 (m), 739 (m). HRMS (ESI/QTOF) m/z : $[\text{M} + \text{Na}]^+$ Calcd for $\text{C}_{22}\text{H}_{21}\text{FN}_2\text{NaO}_3^+$ 403.1428; Found 403.1437.

Benzyl (2-(2-((2-bromophenyl)ethynyl)pyrrolidin-1-yl)-2-oxoethyl)carbamate (**6.33**)

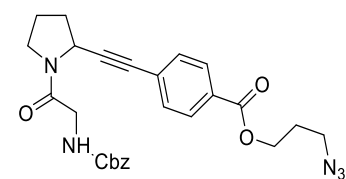


Starting with Cbz-Gly-Pro (**4.10**) (92 mg, 0.30 mmol, 1.0 equiv) and *o*-Br-Ph-EBX (**6.14**) (194 mg, 0.450 mmol, 1.50 equiv), **6.33** was obtained after column chromatography DCM to DCM/ethyl acetate 8:2 as a yellow oil (127 mg, 0.290 mmol, 95%).

R_f (DCM/ethyl acetate 9:1): 0.34. ^1H NMR (400 MHz, Chloroform- d , 6:4 mixture of rotamers (major/minor)) δ 7.45 (ddd, $J = 9.1, 7.9, 1.3$ Hz, 1H, ArH (major+minor)), 7.33 (dd, $J = 7.7, 1.8$ Hz, 1H, ArH (major+minor)), 7.29 – 6.95 (m, 7H, ArH (major+minor)), 5.70 (d, $J = 14.9$ Hz, 1H, NH (major+minor)), 5.03 (s, 2H, OCH_2Ph (major+minor)), 4.94 (d, $J = 6.1$ Hz, 0.4H, $\text{NCHC}\equiv\text{C}$ (minor)), 4.63 (dd, $J = 6.6, 2.7$ Hz, 0.6H, $\text{NCHC}\equiv\text{C}$ (major)), 4.27 (dd, $J = 17.2, 3.9$ Hz, 0.6H, $\text{NC(O)CH}_2\text{NHCbz}$ (major)), 4.10 (dd, $J = 17.2, 5.2$ Hz, 0.6H, $\text{NC(O)CH}_2\text{NHCbz}$ (major)), 3.95 – 3.80 (m, 0.8H, $\text{NC(O)CH}_2\text{NHCbz}$ (minor)), 3.67 – 3.56 (m, 0.6H, $\text{NCH}_2(\text{CH}_2)_2\text{CHC}\equiv\text{C}$ (major)), 3.55 – 3.34 (m, 1H, $\text{NCH}_2(\text{CH}_2)_2\text{CHC}\equiv\text{C}$ (minor+major)), 3.35 – 3.24 (m, 0.4H, $\text{NCH}_2(\text{CH}_2)_2\text{CHC}\equiv\text{C}$ (minor)), 2.39 – 1.78 (m, 4H, $\text{NCH}_2(\text{CH}_2)_2\text{CHC}\equiv\text{C}$ (major+minor)). ^{13}C NMR (101 MHz, Chloroform- d , mixture of rotamers, signals not fully resolved) δ 167.1, 166.3, 156.2, 136.4, 136.4, 133.4, 133.3, 132.3, 132.2, 129.8, 129.4, 128.4, 128.0, 127.9, 127.0, 126.9, 125.8, 125.8, 124.7, 124.1, 92.9, 91.4, 83.0, 80.9, 66.8, 48.6, 48.3, 46.1, 45.1, 43.5, 43.5, 34.3, 32.3, 29.6, 24.7, 22.8. IR 3411 (w), 3316 (w), 2953 (w), 2880 (w), 2249 (w), 1717 (m), 1651 (s), 1511 (w), 1435 (s), 1341 (w), 1250 (m), 1175 (w), 1052 (m), 1027 (w), 908 (s). HRMS (ESI) calcd for $\text{C}_{22}\text{H}_{22}\text{BrN}_2\text{O}_3^+$ $[\text{M}+\text{H}]^+$ 441.0808; found 441.0803.

3-Azidopropyl

4-((1-(2-(((benzyloxy)carbonyl)amino)acetyl)pyrrolidin-2-yl)ethynyl)benzoate (6.35)

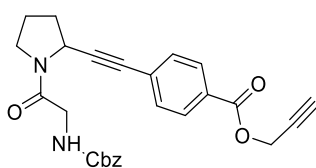


Starting with Cbz-Gly-Pro (**4.10**) (15.3 mg, 0.0500 mmol, 1.00 equiv) and **6.23** (35.6 mg, 0.0750 mmol, 1.50 equiv), **6.35** was obtained after preparative TLC DCM/ethyl acetate 9:1 as a yellow oil (16.3 mg, 0.0330 mmol, 67%).

R_f (DCM/ethyl acetate 9:1): 0.2. ¹H NMR (400 MHz, Chloroform-*d*, 1:1 mixture of rotamers (R¹/R²)) δ 8.02 – 7.91 (m, 2H, ArH (R¹+R²)), 7.50 – 7.44 (m, 2H, ArH (R¹+R²)), 7.40 – 7.28 (m, 5H, ArH (R¹+R²)), 5.75 (bs, 1H, NH (R¹+R²)), 5.13 (s, 2H, OCH₂Ph (R¹+R²)), 5.02 (dd, *J* = 7.3, 2.6 Hz, 0.5H, NCHC≡C (R¹)), 4.72 (t, *J* = 5.0 Hz, 0.5H, NCHC≡C (R²)), 4.41 (q, *J* = 6.1 Hz, 2H, OCH₂ (R¹+R²)), 4.30 (dd, *J* = 17.1, 4.0 Hz, 0.5H, NC(O)CH₂NHCbz (R²)), 4.17 (dd, *J* = 17.1, 5.0 Hz, 0.5H, NC(O)CH₂NHCbz (R²)), 4.05 – 3.93 (m, 1H, NC(O)CH₂NHCbz (R¹)), 3.71 (ddd, *J* = 11.5, 8.0, 3.2 Hz, 0.5H, NCH₂(CH₂)₂CHC≡C (R²)), 3.61 (t, *J* = 9.0 Hz, 0.5H, NCH₂(CH₂)₂CHC≡C (R¹)), 3.57 – 3.35 (m, 1H, NCH₂(CH₂)₂CHC≡C (R¹+R²)), 3.48 (td, *J* = 6.7, 2.9 Hz, 2H, N₃CH₂ (R¹+R²)), 2.39 – 1.92 (m, 4H, NCH₂(CH₂)₂CHC≡C (R¹+R²)), 2.05 (td, *J* = 6.4, 3.8 Hz, 2H, CH₂CH₂ (R¹+R²)). ¹³C NMR (101 MHz, Chloroform-*d*, mixture of rotamers, signals not fully resolved) δ 167.1, 166.4, 166.4, 165.8, 165.7, 156.2, 136.4, 131.8, 131.7, 129.8, 129.5, 129.3, 129.3, 128.5, 128.1, 128.0, 127.6, 126.8, 91.3, 89.9, 83.7, 81.6, 66.9, 62.1, 62.0, 48.6, 48.3, 46.2, 45.3, 43.5, 34.4, 32.3, 29.7, 28.2, 24.8, 22.9. IR (ν_{max}, cm⁻¹) 3407 (w), 3333 (w), 2951 (w), 2107 (m), 1719 (s), 1657 (s), 1534 (w), 1447 (m), 1275 (s), 1182 (w), 1102 (m), 1053 (m), 862 (w), 776 (m). HRMS (ESI/QTOF) *m/z*: [M + Na]⁺ Calcd for C₂₆H₂₇N₅NaO₅⁺ 512.1904; Found 512.1912.

Prop-2-yn-1-yl

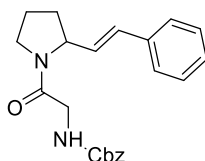
4-((1-(2-(((benzyloxy)carbonyl)amino)acetyl)pyrrolidin-2-yl)ethynyl)benzoate (6.36)



Starting with Cbz-Gly-Pro (**4.10**) (30.6 mg, 0.100 mmol, 1.00 equiv) and **6.22** (64.5 mg, 0.150 mmol, 1.50 equiv), **6.36** was obtained after preparative TLC DCM/ethyl acetate 8:2 as a yellow oil (31.1 mg pure at 95%, 0.066 mmol, 67%). The isolated product contained traces of alkynylated DMF, a sample for was purified by a second preparative TLC DCM/ethyl acetate 9:1 for characterization.

R_f (DCM/ethyl acetate 9:1): 0.2. ¹H NMR (400 MHz, Chloroform-*d*, 1:1 mixture of rotamers (R¹/R²)) δ 7.99 (dd, *J* = 13.1, 8.1 Hz, 2H, ArH (R¹+R²)), 7.60 – 7.28 (m, 7H, ArH (R¹+R²)), 5.88 – 5.64 (m, 1H, NH (R¹+R²)), 5.12 (s, 2H, OCH₂Ph (R¹+R²)), 5.02 (d, *J* = 4.6 Hz, 0.5H, NCHC≡C (R¹)), 4.92 (dd, *J* = 5.6, 2.4 Hz, 2H, CH₂C≡C (R¹+R²)), 4.72 (t, *J* = 4.8 Hz, 0.5H, NCHC≡C (R²)), 4.29 (d, *J* = 18.3 Hz, 0.5H, NC(O)CH₂NHCbz (R²)), 4.16 (dd, *J* = 17.5, 3.7 Hz, 0.5H, NC(O)CH₂NHCbz (R²)), 4.12 – 3.92 (m, 1H, NC(O)CH₂NHCbz (R¹)), 3.78 – 3.65 (m, 0.5H, NCH₂(CH₂)₂CHC≡C (R²)), 3.66 – 3.46 (m, 1H, NCH₂(CH₂)₂CHC≡C (R¹+R²)), 3.41 (q, *J* = 9.4 Hz, 0.5H, NCH₂(CH₂)₂CHC≡C (R¹)), 2.52 (dt, *J* = 4.7, 2.6 Hz, 1H, HC≡C (R¹+R²)), 2.42 – 1.90 (m, 4H, NCH₂(CH₂)₂CHC≡C (R¹+R²)). ¹³C NMR (101 MHz, Chloroform-*d*, mixture of rotamers, signals not fully resolved) δ 167.1, 166.4, 165.2, 165.1, 156.2, 136.4, 131.8, 131.7, 129.7, 129.5, 129.2, 128.7, 128.5, 128.1, 128.0, 128.0, 127.9, 127.0, 91.5, 90.0, 83.6, 81.5, 75.2, 75.1, 66.9, 52.6, 52.6, 48.6, 48.3, 46.2, 45.3, 43.5, 34.4, 32.3, 24.8, 22.9. IR (ν_{max}, cm⁻¹) 3660 (w), 3407 (w), 3271 (w), 2982 (m), 1725 (s), 1651 (m), 1515 (w), 1429 (m), 1256 (s), 1102 (s), 1059 (s), 1010 (m), 862 (m), 751 (m), 745 (m). HRMS (ESI/QTOF) *m/z*: [M + Na]⁺ Calcd for C₂₆H₂₄N₂NaO₅⁺ 467.1577; Found 467.1569.

(E)-Benzyl (2-oxo-2-(2-styrylpyrrolidin-1-yl)ethyl)carbamate (**6.34**)

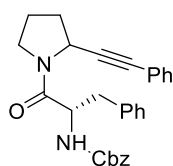


Starting with Cbz-Gly-Pro (**4.10**) (92 mg, 0.30 mmol, 1.0 equiv) and Ph-VBX (**6.34a**) (158 mg, 0.450 mmol, 1.50 equiv), **6.34** was obtained after column chromatography DCM to DCM/ethyl acetate 8:2 as a yellow oil (89.5 mg, 0.246 mmol, 82%).

R_f (DCM/ethyl acetate 9:1): 0.17. ¹H NMR (400 MHz, Chloroform-*d*, 6:4 mixture of rotamers (major/minor)) δ 7.44 – 7.23 (m, 10H, ArH (major+minor)), 6.42 (dd, *J* = 15.8, 7.7 Hz, 1H,

=CHPh (major+minor)), 6.10 (dd, J = 15.9, 6.1 Hz, 1H, NCHCH= (major+minor)), 5.79 (s, 0.4H, NH (minor), 5.73 (s, 0.6H, NH (major), 5.12 (s, 0.8H, OCH₂Ph (minor)), 5.09 (s, 1.2H, OCH₂Ph (major)), 4.83 (t, J = 6.3 Hz, 0.4H, NCHC≡C (minor)), 4.50 (t, J = 7.0 Hz, 0.6H, NCHC≡C (major)), 4.17 – 3.84 (m, 2H, NC(O)CH₂NHCbz (major+minor)), 3.71 – 3.36 (m, 2H, NCH₂(CH₂)₂ (major+minor)), 2.27 – 1.83 (m, 4H, NCH₂(CH₂)₂CHC≡C). ¹³C NMR (101 MHz, Chloroform-*d*, mixture of rotamers, signals not fully resolved) δ 167.3, 166.5, 156.2, 156.1, 136.5, 136.4, 135.8, 133.6, 130.6, 130.2, 128.7, 128.7, 128.6, 128.4, 128.3, 128.1, 128.0, 128.0, 127.9, 127.5, 126.5, 126.4, 126.4, 123.9, 123.2, 66.8, 58.8, 46.5, 45.7, 43.5, 43.4, 33.2, 30.7, 23.8, 21.6. IR (ν_{max}, cm⁻¹) 3666 (w), 3401 (w), 3308 (w), 2982 (s), 2902 (m), 2341 (w), 2187 (w), 1731 (s), 1657 (s), 1509 (m), 1441 (m), 1262 (m), 1164 (w), 1065 (s), 905 (w), 751 (m). HRMS (ESI/QTOF) m/z : [M + Na]⁺ Calcd for C₂₂H₂₄N₂NaO₃⁺ 387.1679; Found 387.1684.

Benzyl ((2S)-1-oxo-3-phenyl-1-(2-(phenylethynyl)pyrrolidin-1-yl)propan-2-yl)carbamate (6.46)



Starting with Cbz-Phe-Pro (**6.46a**) (119 mg, 0.300 mmol), the crude product was purified by column chromatography DCM to DCM/ethyl acetate 8:2 to afford **6.46** as two separable diastereoisomers (ratio 2:1 by RP-HPLC analysis and NMR of the crude mixture): a pale yellow oil (59.7 mg, 0.132 mmol, 44%, major) as fraction 1 and an amorphous solid (47.0 mg, 0.104 mmol, 35%, minor) as fraction 2.

R_f (DCM/ethyl acetate 9:1): 0.44 (fraction 1); 0.32 (fraction 2).

Fraction 1 (major):

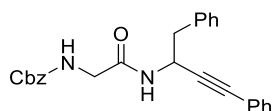
¹H NMR (400 MHz, Chloroform-*d*, 6:4 mixture of rotamers (major/minor)) δ 7.52 – 7.02 (m, 15H, ArH (major+minor)), 5.81 – 5.62 (m, 1H, NH (major+minor)), 5.13 – 5.03 (m, 2.4H, OCH₂Ph (major+minor) and NC(O)CHN (minor)), 4.98 (dd, J = 6.0, 4.0 Hz, 0.6H, NCHC≡C (major)), 4.62 (td, J = 8.5, 5.5 Hz, 0.6H, NC(O)CHN (major)), 3.77 – 3.68 (m, 0.4H, NCHC≡C (minor)), 3.67 – 3.57 (m, 0.6H, NCH₂ (major)), 3.43 – 3.22 (m, 1H, NCH₂ (major+minor)), 3.20 (dd, J = 12.7, 4.9 Hz, 0.4H, CH₂Ph (minor)), 3.13 – 3.01 (m, 1.2H, CH₂Ph (major+minor)), 2.95 (dd, J = 12.7, 10.0 Hz, 0.4H, CH₂Ph (minor)), 2.80 – 2.69 (m, 0.4H, NCH₂ (minor)), 2.06 – 1.51 (m, 4H, NCH₂(CH₂)₂CHC≡C (major+minor)). ¹³C NMR (101 MHz, Chloroform-*d*, mixture of rotamers, signals not fully resolved) δ 169.9, 169.5, 155.6, 155.1, 136.4, 136.4, 135.8, 131.9,

131.7, 129.8, 129.5, 128.5, 128.5, 128.4, 128.4, 128.2, 128.2, 128.1, 128.0, 127.9, 127.0, 126.9, 123.0, 122.2, 88.2, 87.0, 84.2, 82.3, 66.8, 66.6, 54.4, 53.8, 48.7, 48.3, 46.0, 45.6, 41.1, 40.0, 33.8, 32.2, 24.8, 22.7. IR (ν_{\max} , cm^{-1}) 3284 (m), 3031 (w), 2963 (w), 2359 (w), 2335 (w), 1712 (s), 1632 (s), 1534 (m), 1435 (s), 1336 (m), 1262 (s), 1041 (m), 763 (m). HRMS (ESI/QTOF) m/z : $[M + Na]^+$ Calcd for $C_{29}H_{28}N_2NaO_3^+$ 475.1992; Found 475.2008.

Fraction 2 (minor):

^1H NMR (400 MHz, Chloroform- d , 6:4 mixture of rotamers (major/minor)) δ 7.45 – 7.09 (m, 15H, ArH (major+minor)), 5.83 – 5.71 (m, 0.4H, NH (minor)), 5.46 (bs, 0.6H, NH (major)), 5.25 (dd, J = 5.9, 3.7 Hz, 0.6H, NCHC \equiv C (major)), 5.15 – 4.95 (m, 2.4H, OCH $_2$ Ph (major+minor) + NC(O)CHN (major)), 4.82 (dd, J = 7.8, 2.0 Hz, 0.4H, NCHC \equiv C (minor)), 4.67 (td, J = 9.0, 5.7 Hz, 0.4H, NC(O)CHN (major)), 3.72 – 3.47 (m, 1.6H, NCH $_2$ (major+minor)), 3.32 (dd, J = 14.1, 4.1 Hz, 0.6H, CH $_2$ Ph (major)), 3.13 – 2.91 (m, 1.4H, CH $_2$ Ph (major+minor)), 2.54 (td, J = 9.2, 6.9 Hz, 0.4H, NCH $_2$ (minor)), 2.36 – 1.89 (m, 3.6H, NCH $_2$ (CH $_2$) $_2$), 1.63 (dtd, J = 9.7, 6.7, 3.5 Hz, 0.4H, NCH $_2$ (CH $_2$) $_2$). ^{13}C NMR (101 MHz, Chloroform- d , mixture of rotamers, signals not fully resolved) δ 171.0, 169.3, 156.0, 155.5, 136.6, 136.3, 136.2, 131.8, 131.6, 129.5, 129.3, 128.6, 128.4, 128.4, 128.3, 128.0, 128.0, 128.0, 127.9, 127.8, 127.0, 126.6, 122.8, 122.1, 88.4, 88.2, 84.2, 82.1, 66.7, 54.1, 53.7, 49.3, 48.5, 46.1, 45.9, 40.3, 38.3, 34.5, 32.3, 24.3, 23.1. HRMS (ESI/QTOF) m/z : $[M + Na]^+$ Calcd for $C_{29}H_{28}N_2NaO_3^+$ 475.1992; Found 475.1994.

Benzyl (2-((1,4-diphenylbut-3-yn-2-yl)amino)-2-oxoethyl)carbamate (**4.13**)



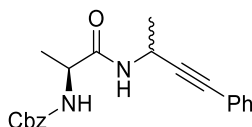
Starting with Cbz-Gly-Phe (**4.13a**) (107 mg, 0.300 mmol), the crude product was purified by column chromatography DCM to DCM/ethyl acetate 9:1 to afford **4.13** as a pale yellow solid (93 mg, 0.23 mmol, 68%).

R_f (DCM/ethyl acetate 9:1): 0.36. Mp 128.9 – 130.8 °C. ^1H NMR (400 MHz, Chloroform- d)²⁶ δ 7.33 (m, 15H, ArH), 6.15 (d, J = 8.4 Hz, 1H, NH), 5.36 (bs, 1H, NH), 5.29 – 5.20 (m, 1H, NCHC \equiv C), 5.13 (s, 2H, OCH $_2$ Ph), 3.95 – 3.77 (m, 2H, NC(O)CH $_2$ NHCbz), 3.07 (m, 2H, Ph-CH $_2$). ^{13}C NMR (101 MHz, Chloroform- d)⁶ δ 168.7, 167.7, 136.1, 136.1, 131.7, 130.0, 128.6, 128.6, 128.4, 128.3, 128.2, 127.1, 122.3, 87.2, 84.7, 67.4, 43.1, 41.5, 29.7. IR 3316 (w), 2988

²⁶ One carbon is not resolved.

(w), 2881 (w), 2361 (s), 2342 (s), 2125 (w), 2086 (w), 1772 (w), 1683 (s), 1542 (s), 1397 (w), 1267 (m), 1138 (w). HRMS (ESI) calcd for $C_{26}H_{24}N_2NaO_3^+$ $[M+Na]^+$ 435.1679; found 435.1682.

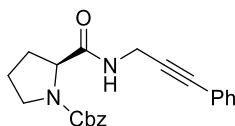
Benzyl (1-oxo-1-((4-phenylbut-3-yn-2-yl)amino)propan-2-yl)carbamate (**6.7**)



Starting with Cbz-Ala-Ala (**6.7a**) (88 mg, 0.30 mmol, 1.0 equiv), **6.7** was obtained after column chromatography DCM to DCM/ethyl acetate 8:2 as a white solid (83 mg, 0.24 mmol, 79%) and as a mixture of unresolved diastereoisomers.

R_f (DCM/ethyl acetate 95:5): 0.28. Mp 171 – 172 °C. ¹H NMR (400 MHz, Chloroform-*d*) δ 7.45 – 7.28 (m, 10H, *ArH*), 6.32 (bs, 1H, *NH*), 5.30 (bs, 1H, *NH*), 5.12 (s, 2H, *OCH*₂Ph), 5.07 – 4.94 (m, 1H, *NCHC*≡C), 4.24 (m, 1H, *CCHNHCbz*), 1.46 (d, *J* = 6.9 Hz, 3H, *CH*₃*CHC*≡C), 1.40 (d, *J* = 7.0 Hz, 3H, *CH*₃*CHNHCbz*). ¹³C NMR (101 MHz, Chloroform-*d*) δ 170.9, 156.0, 136.0, 131.7, 128.6, 128.4, 128.3, 128.1, 128.1, 122.5, 88.9, 82.5, 67.1, 50.5, 37.8, 37.8, 22.4. IR 3294 (m), 3067 (w), 3035 (w), 2984 (w), 2361 (w), 1708 (s), 1656 (s), 1540 (s), 1456 (m), 1330 (w), 1257 (m), 1241 (m), 1135 (w), 1071 (m), 1029 (w), 956 (w), 915 (w). HRMS (ESI) calcd for $C_{21}H_{23}N_2O_3^+$ $[M+H]^+$ 351.1703; found 351.1697.

(S)-Benzyl 2-((3-phenylprop-2-yn-1-yl)carbamoyl)pyrrolidine-1-carboxylate (**6.45**)



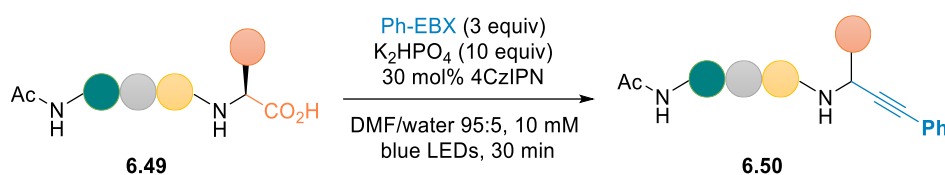
Starting with Cbz-Pro-Gly (**6.45a**) (92 mg, 0.30 mmol), and using 4ClCzIPN (9.58 mg, 900 μmol, 3.00 mol%) as catalyst, the crude product was purified by column chromatography DCM to DCM/ethyl acetate 85:15 to afford **6.45** as a pale yellow solid (63.4 mg, 0.175 mmol, 58%).

R_f (DCM/ethyl acetate 9:1): 0.36. Mp 124.7 – 126.1 °C. ¹H NMR (400 MHz, Acetonitrile-*d*₃, mixture of rotamers, signals not fully resolved) δ 7.18 – 6.88 (m, 10H, *ArH*), 6.79 (d, *J* = 18.0 Hz, 1H, *NH*), 4.83 – 4.65 (m, 2H, *OCH*₂Ph), 3.88 (dd, *J* = 8.8, 3.5 Hz, 1H, *NCH*), 3.79 (dd, *J* =

14.1, 5.7 Hz, 2H, $\text{CH}_2\text{C}\equiv\text{C}$), 3.26 – 3.04 (m, 2H, NCH_2), 1.61 (p, $J = 2.5$ Hz, 2H, NCH_2CH_2), 1.53 (q, $J = 6.9$ Hz, 2H, NCHCH_2). ^{13}C NMR (101 MHz, Acetonitrile- d_3 , mixture of rotamers, signals not fully resolved) δ 173.4, 173.0, 138.1, 132.4, 129.4, 129.4, 129.3, 128.8, 128.6, 128.3, 123.6, 86.8, 82.6, 67.5, 67.4, 61.8, 61.5, 48.1, 47.7, 32.0, 30.6, 29.8, 25.0, 24.2.

IR (ν_{max} , cm^{-1}) 3678 (w), 3302 (w), 2982 (s), 2889 (m), 2359 (w), 1700 (s), 1534 (m), 1417 (s), 1349 (m), 1244 (m), 1195 (w), 1115 (m), 1090 (m), 924 (w), 757 (s). HRMS (ESI/QTOF) m/z : $[\text{M} + \text{Na}]^+$ Calcd for $\text{C}_{22}\text{H}_{22}\text{N}_2\text{NaO}_3^+$ 385.1523; Found 385.1519.

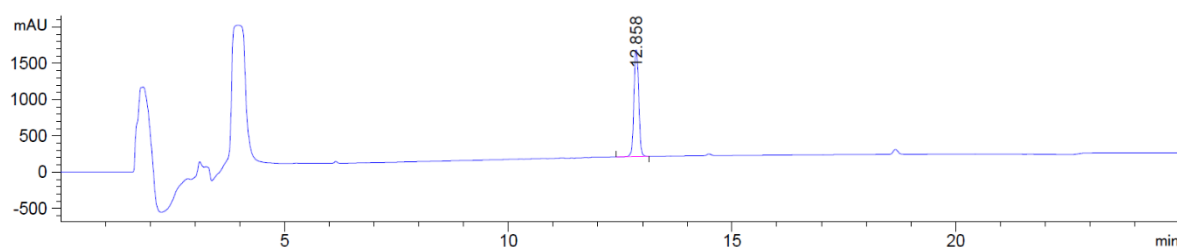
12.4.6 Peptide tetramers scope

**General procedure 4 for the decarboxylative alkylation of tetramers**

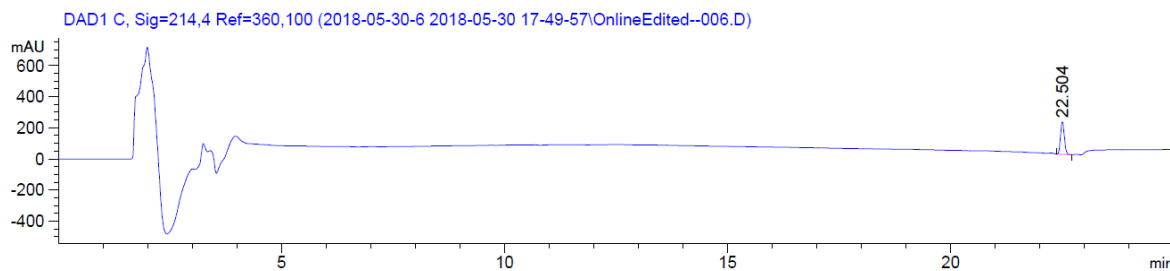
A 20 mM solution of the tetramer in non-degassed DMF (50 μ L, 1.0 μ mol), a 60 μ M solution of Ph-EBX (**2.5**) in DMF (25 μ L, 3.0 μ mol, 3.0 equiv), a 15 μ M solution of 4CzIPN (**2.23**) in DMF (20 μ L, 0.30 μ mol, 30 mol%) and a 2 M solution of K_2HPO_4 in milli-Q purified water (5 μ L, 10 μ mol, 10 equiv) were placed into a vial. The vial was then capped and degassed by bubbling with argon for 1-2 min and the mixture was irradiated using blue light LEDs for 30 min at RT.

Intermediate samples were prepared by dilution of 10 μ L of the reaction mixture with 30 μ L of MeOH. At the end of the reaction, the crude was diluted with 3x the volume of MeCN/water 1:1 or with 3x the volume of MeCN/water 3:1 and injected in RP-HPLC (volume of injection adapted to the dilution). The yields were determined as the ratio of $A_{\text{prod}}/A_{\text{total}}$ where A_{prod} = area in mAU of the product peak and A_{total} = area in mAU of all peptides products (product, starting material, and side-products if present).

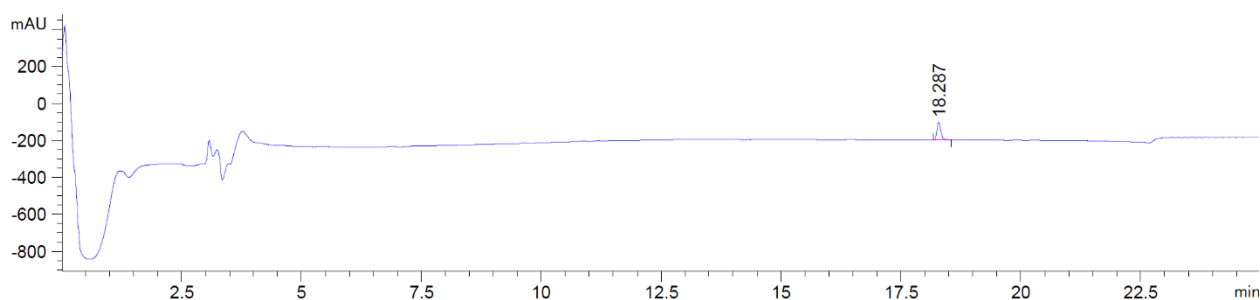
Reported results are an average of a minimum of 3 independent trials. The products are described as peptide-AH.

Reference HPLC-UV chromatograms of reagents at 214 nm**PhEBX (2.5)**

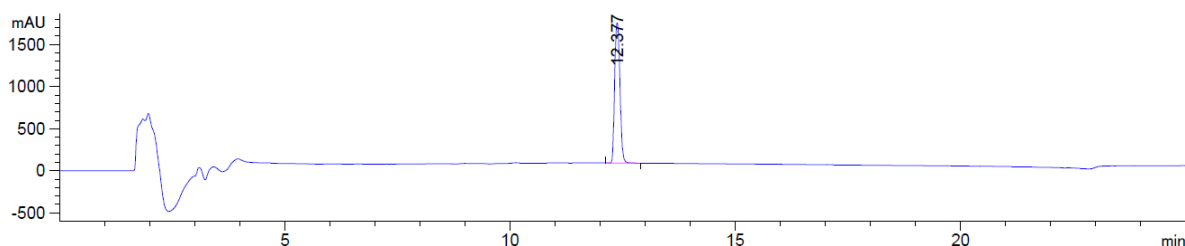
4CzIPN (2.23)



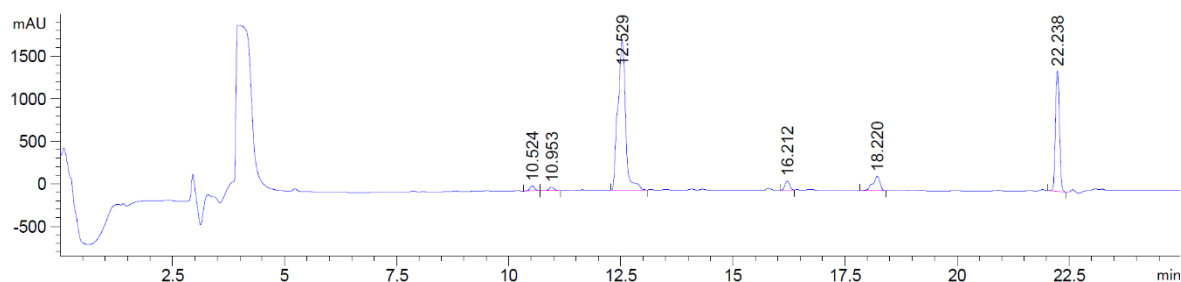
{Ir[dF(CF₃)ppy]₂dtbbpy}PF₆ (2.15)



Iodobenzoic acid (2.10)

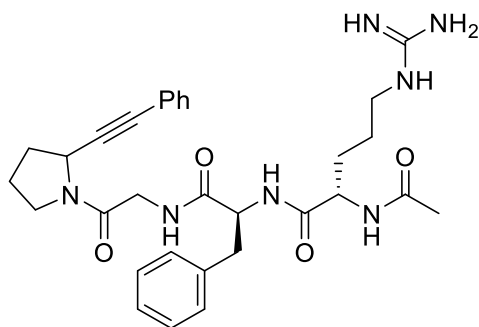


Control experiment without peptide



For clarity in the reaction chromatograms, the peaks of peptide-based products are indicated by an arrow. In all reactions, iodobenzoic acid, Ph-EBX and the catalyst were present, together with side products at 10.524, 16.212 and 18.220 min. The alkyne dimer and alkynylated DMF were identified by NMR but low ionization did not allow confirmation of their retention time.

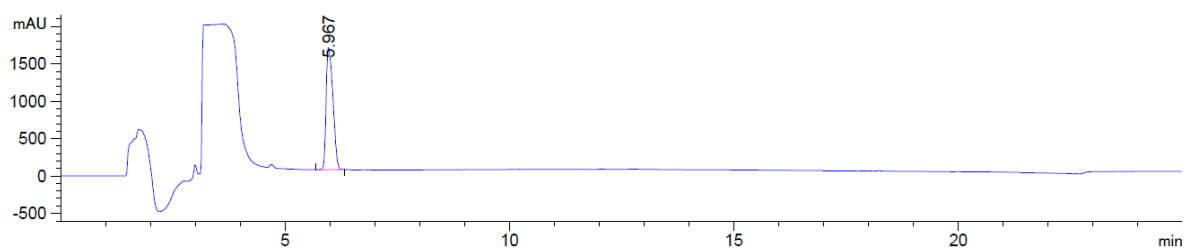
Ac-Arg-Phe-Gly-Pro-AH (6.50b)



Following the general procedure, Ac-Arg-Phe-Gly-Pro-OH (**6.49b**) afforded **6.50b** in more than 95% yield (retention time 10.573).

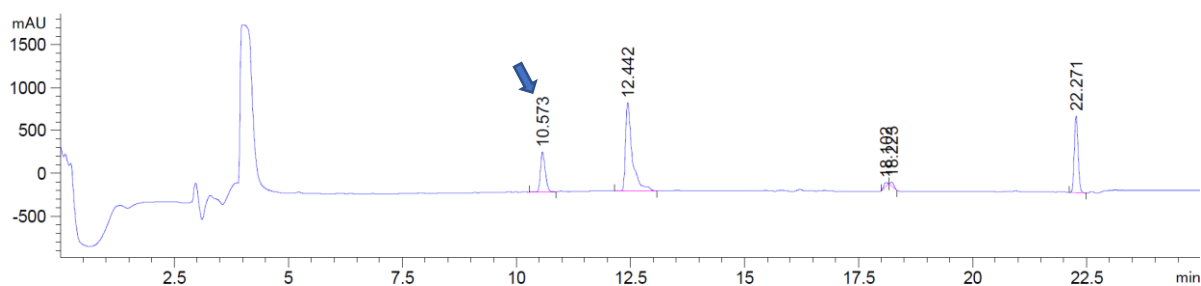
HRMS (ESI/QTOF) m/z : $[M]^+$ Calcd for $C_{31}H_{40}N_7O_4^+$ 574.3136; Found 574.3151.

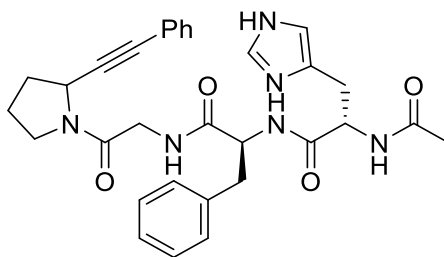
Ac-Arg-Phe-Gly-Pro-OH (6.49b)



HRMS of **6.49b** (ESI/QTOF) m/z : $[M + H_1]^-$ Calcd for $C_{24}H_{34}N_7O_6^-$ 516.2576; Found 516.2579.

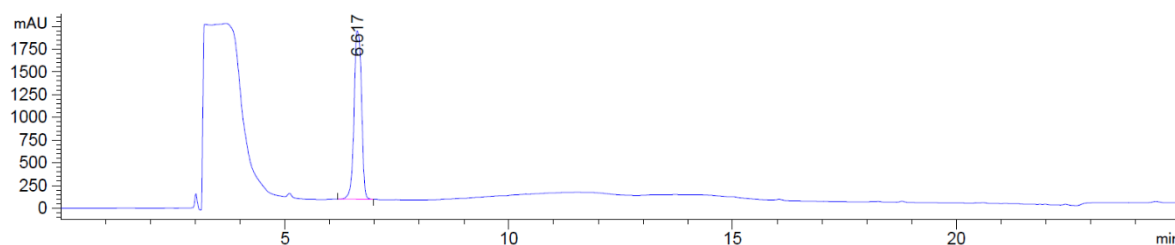
HPLC-UV chromatogram at 214 nm of the crude reaction mixture



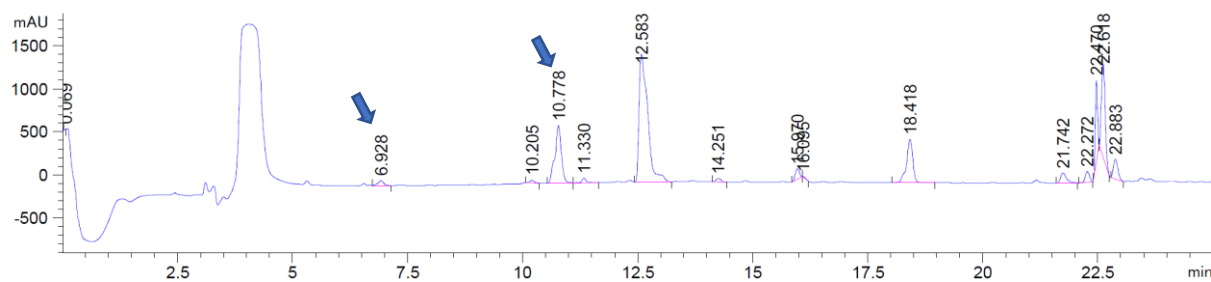
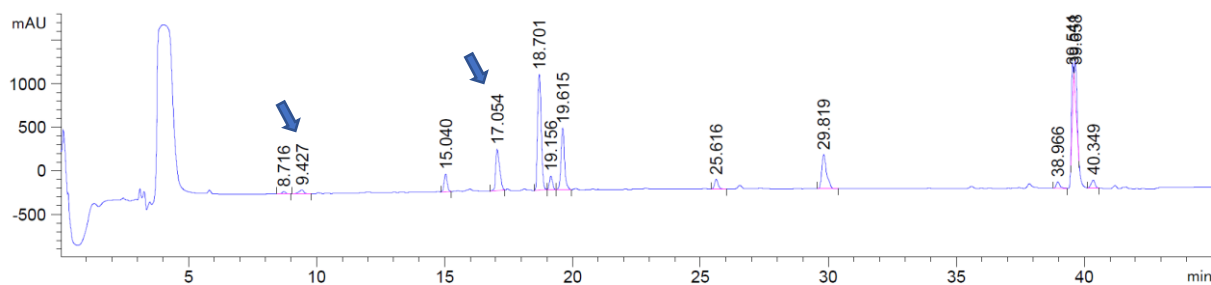
Ac-His-Phe-Gly-Pro-AH (6.50g)

Following the general procedure, Ac-His-Phe-Gly-Pro-OH (**6.49g**) afforded **6.50g** in 84% yield (retention time 10.778 with method A, 17.054 with method B for a better separation).

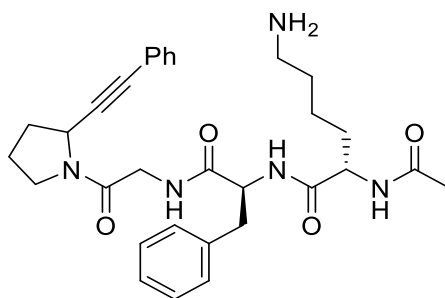
HRMS (ESI/QTOF) m/z : $[M + H]^+$ Calcd for $C_{31}H_{35}N_6O_4^+$ 555.2714; Found 555.2722.

Ac-His-Phe-Gly-Pro-OH (6.49g)

HRMS of **6.49g** (ESI/QTOF) m/z : $[M + H_1]^-$ Calcd for $C_{24}H_{29}N_6O_6^-$ 497.2154; Found 497.2147.

HPLC-UV chromatogram at 214 nm of the crude reaction mixture (method A)**HPLC-UV chromatogram at 214 nm of the crude reaction mixture (method B)**

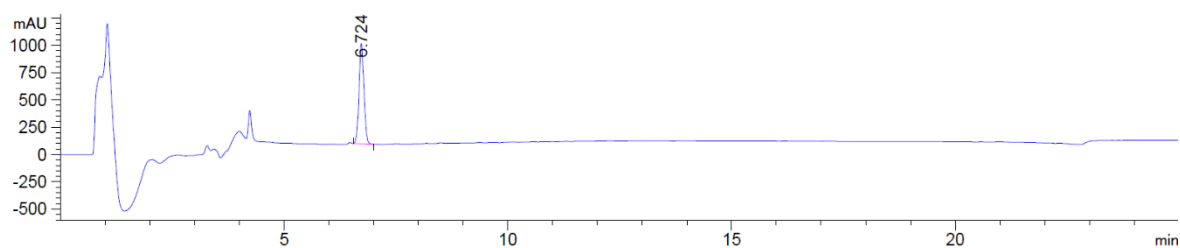
Ac-Lys-Phe-Gly-Pro-AH (6.50f)



Following the general procedure, Ac-Lys-Phe-Gly-Pro-OH (**6.49f**) afforded **6.50f** in 47% yield (retention time 10.670).

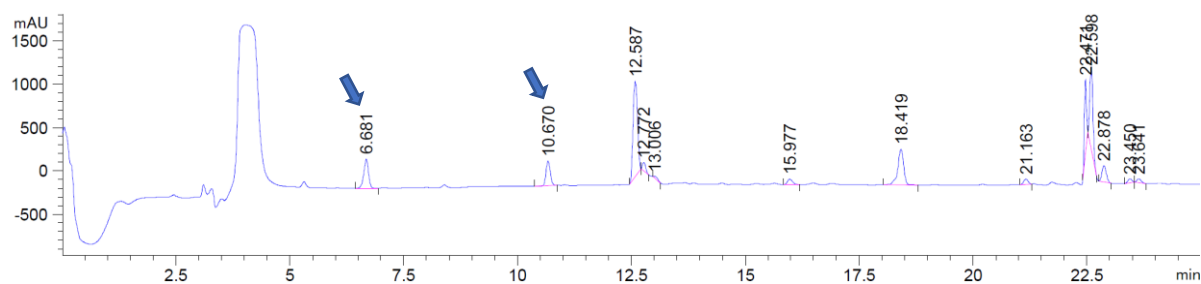
HRMS (ESI/QTOF) m/z : $[M]^+$ Calcd for $C_{31}H_{40}N_5O_4^+$ 546.3075; Found 546.3071.

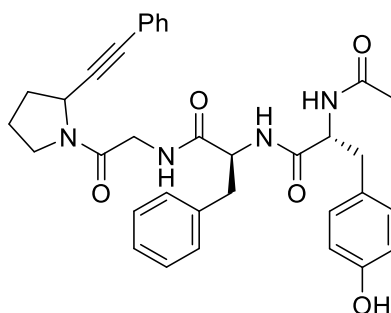
Ac-Lys-Phe-Gly-Pro-OH (6.49f)



HRMS of **6.49f** (ESI/QTOF) m/z : $[M + H-1]^-$ Calcd for $C_{24}H_{34}N_5O_6^-$ 488.2515; Found 488.2518.

HPLC-UV chromatogram at 214 nm of the crude reaction mixture

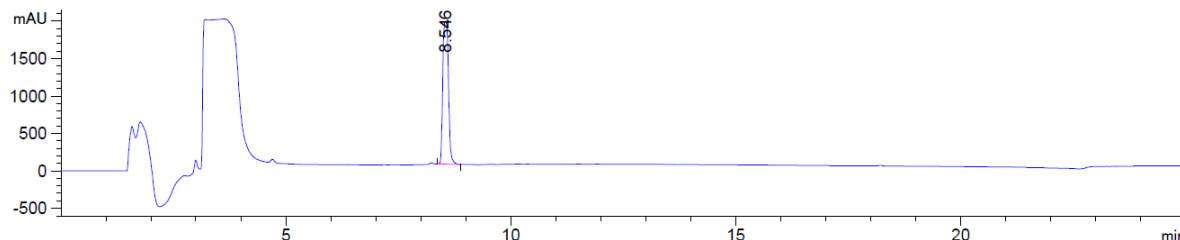


Ac-Tyr-Phe-Gly-Pro-AH (6.50h)

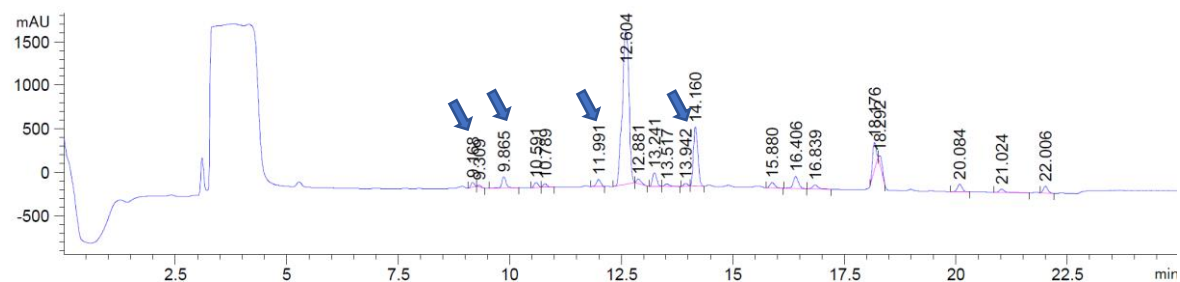
Following the general procedure and using 4*t*BuCzIPN (**5.27**) as catalyst, Ac-Tyr-Phe-Gly-Pro-OH (**6.49h**) afforded **6.50h** in 20% yield (retention time 13.942).

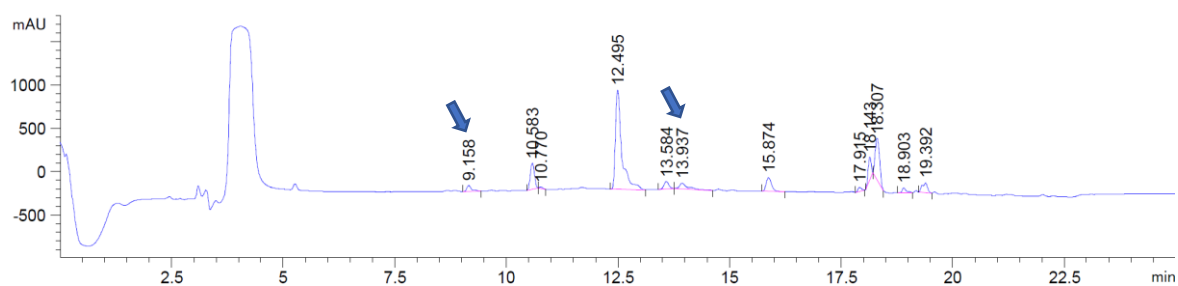
Following the general procedure and using Ir (**2.15**) as catalyst, Ac-Tyr-Phe-Gly-Pro-OH (**6.49h**) afforded **6.50h** in 54% yield (retention time 13.937).

HRMS (ESI/QTOF) *m/z*: [M + Na]⁺ Calcd for C₃₄H₃₆N₄NaO₅⁺ 603.2578; Found 603.2580.

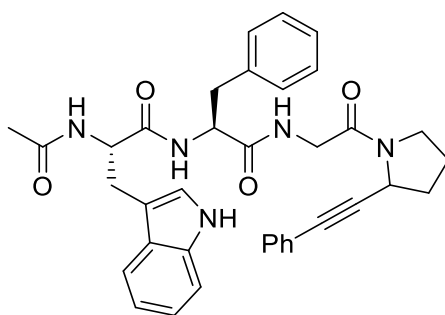
Ac-Tyr-Phe-Gly-Pro-OH (6.50h)

HRMS of **6.49h** (ESI/QTOF) *m/z*: [M + H]⁺ Calcd for C₂₇H₃₁N₄O₇⁺ 523.2198; Found 523.2205.

4*t*BuCzIPN (2.27) as the catalyst**{Ir[dF(CF₃)ppy]₂dtbbpy}PF₆ (2.15) as the catalyst**

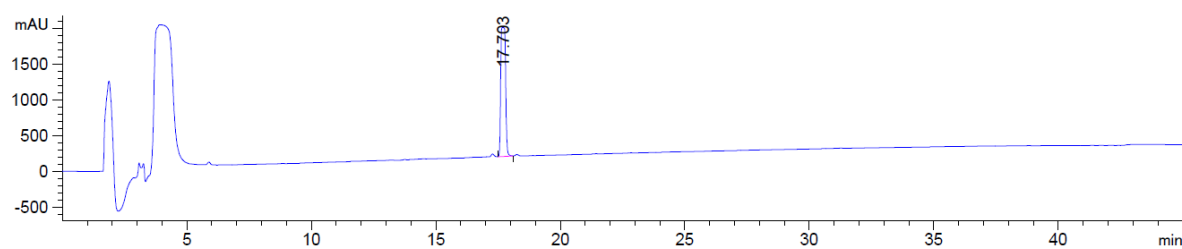


Ac-Trp-Phe-Gly-Pro-AH (6.50i)

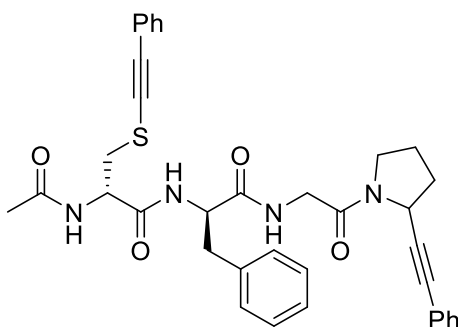


Following the general procedure, no desired product was detected from Ac-Trp-Phe-Gly-Pro-OH (**6.49i**) neither with 4CzIPN (**2.23**) nor 4*t*BuCzIPN (**5.27**).

Ac-Trp-Phe-Gly-Pro-OH (**6.49i**)

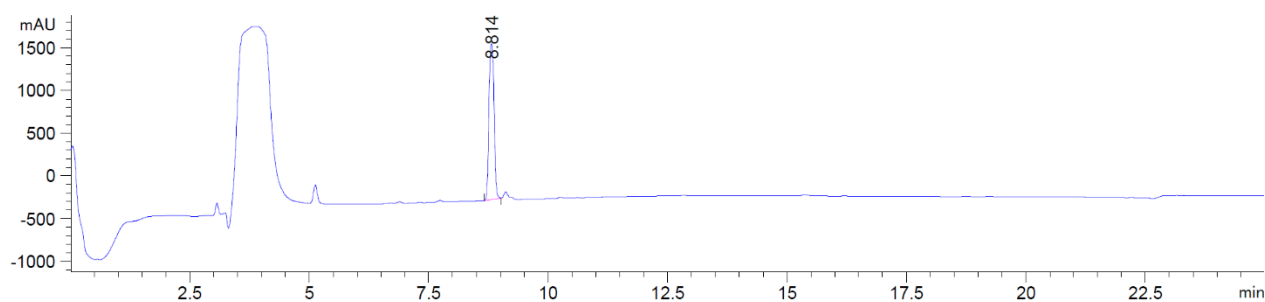


HRMS of **6.49i** (ESI/QTOF) m/z : $[M + H-1]^-$ Calcd for $C_{29}H_{32}N_5O_6^-$ 546.2358; Found 546.2357.

Ac-Cys-Phe-Gly-Pro-AH (6.50j)

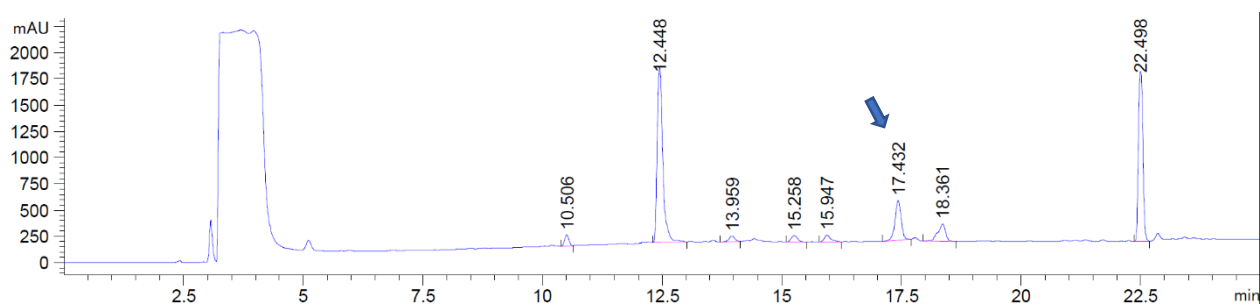
Following the general procedure, Ac-Cys-Phe-Gly-Pro-OH (**6.49j**) afforded **6.50j** in more than 95% yield (retention time 17.432).

HRMS (QTOF) m/z : $[M + K]^+$ Calcd for $C_{36}H_{36}KN_4O_4S^+$ 659.2089; Found 659.2091.

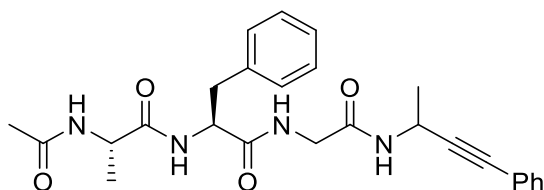
Ac-Cys-Phe-Gly-Pro-OH (6.49j)

HRMS of **6.49j** (ESI/QTOF) m/z : $[M + Na]^+$ Calcd for $C_{21}H_{28}N_4NaO_6S^+$ 487.1622; Found 487.1632.

HPLC-UV chromatogram at 214 nm of the crude reaction mixture



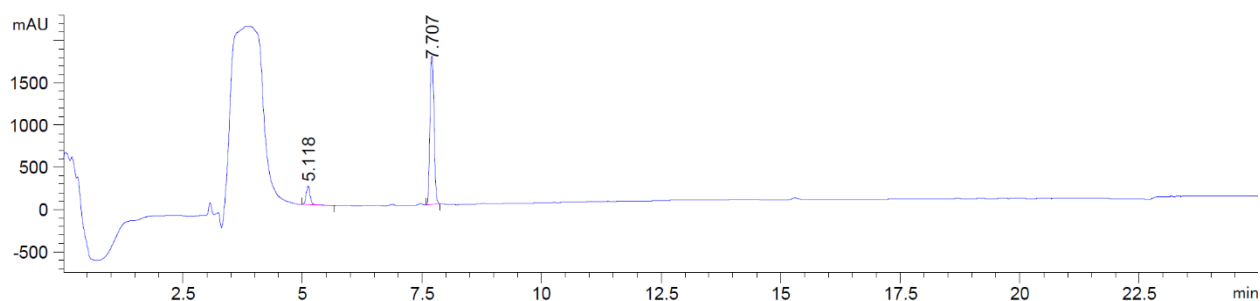
Ac-Ala-Phe-Gly-Ala-AH (6.50a)



Following the general procedure, Ac-Ala-Phe-Gly-Ala-OH (**6.49a**) afforded **6.50a** in more than 95% yield (retention time 12.755).

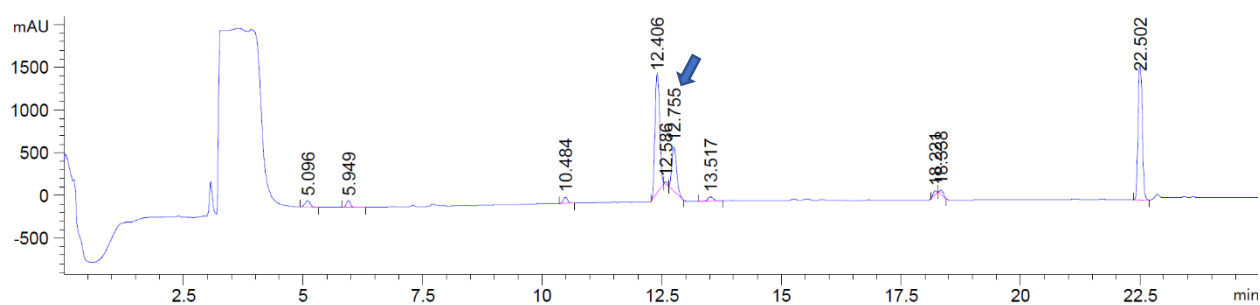
HRMS (ESI/QTOF) m/z : $[M + K]^+$ Calcd for $C_{26}H_{30}KN_4O_4^+$ 501.1899; Found 501.1908.

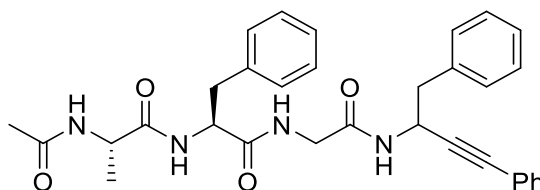
Ac-Ala-Phe-Gly-Ala-OH (6.49a)



HRMS of **6.49a** (ESI/QTOF) m/z : $[M + Na]^+$ Calcd for $C_{19}H_{26}N_4NaO_6^+$ 429.1745; Found 429.1736.

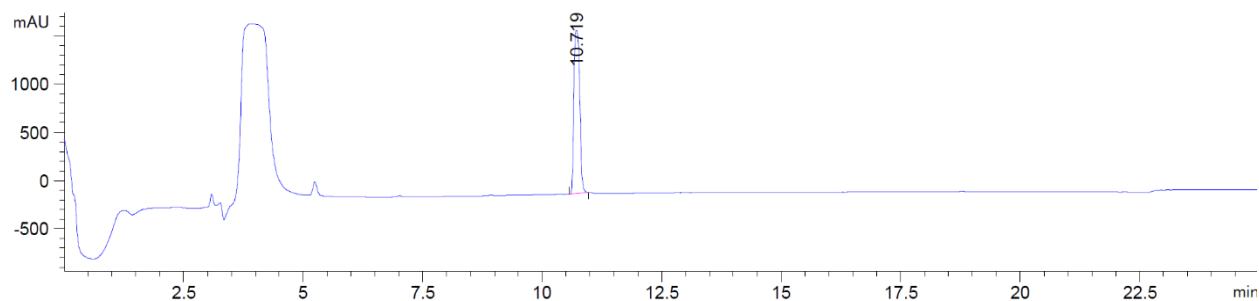
HPLC-UV chromatogram at 214 nm of the crude reaction mixture



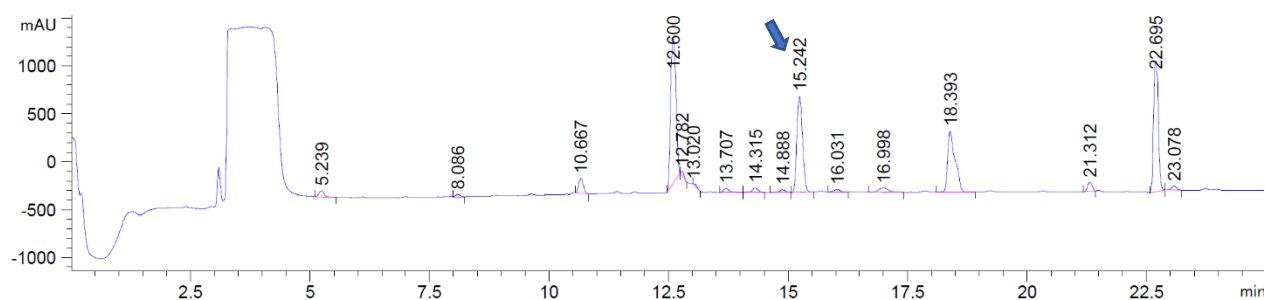
Ac-Ala-Phe-Gly-Phe-AH (6.50I)

Following the general procedure, Ac-Ala-Phe-Gly-Phe-OH (**6.49I**) afforded **6.50I** in more than 95% yield (retention time 15.242).

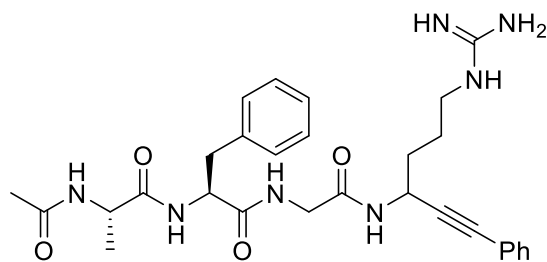
HRMS (QTOF) m/z : $[M + K]^+$ Calcd for $C_{32}H_{34}KN_4O_4^+$ 577.2212; Found 577.2225.

Ac-Ala-Phe-Gly-Phe-OH (6.49I)

HRMS of **6.49I** (ESI/QTOF) m/z : $[M + Na]^+$ Calcd for $C_{25}H_{30}N_4NaO_6^+$ 505.2058; Found 505.2069.

HPLC-UV chromatogram at 214 nm of the crude reaction mixture

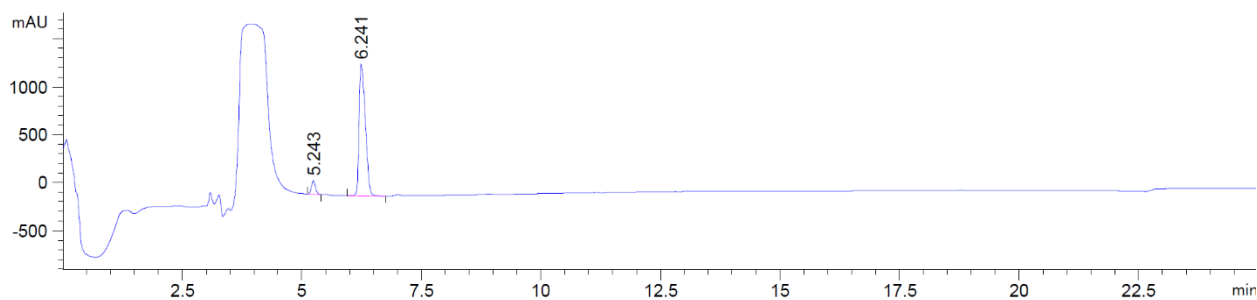
Ac-Ala-Phe-Gly-Arg-AH (6.50m)



Following the general procedure, Ac-Ala-Phe-Gly-Arg-OH (**6.49m**) afforded **6.50m** in more than 95% yield (retention time 9.735).

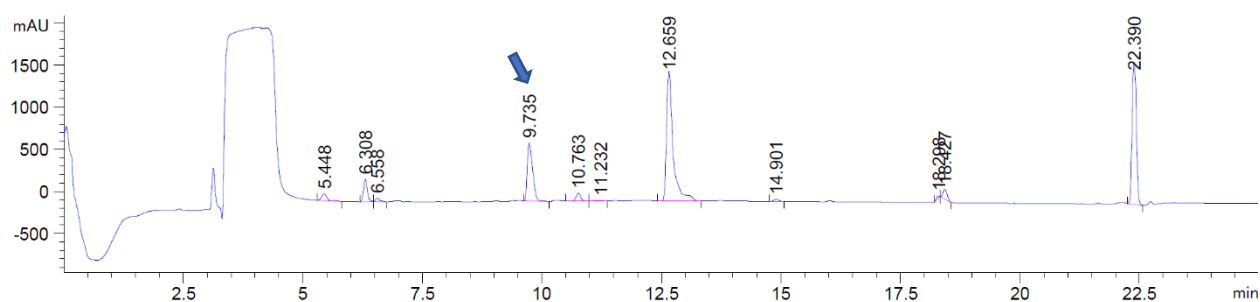
HRMS (ESI/QTOF) m/z : $[M + H]^+$ Calcd for $C_{29}H_{38}N_7O_4^+$ 548.2980; Found 548.2988.

Ac-Ala-Phe-Gly-Arg-OH (6.49m)

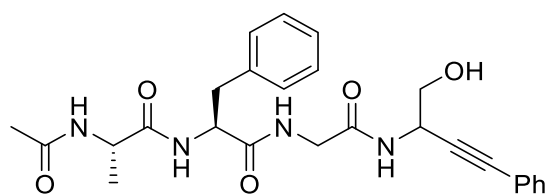


HRMS of **6.49m** (ESI/QTOF) m/z : $[M + H]^+$ Calcd for $C_{22}H_{34}N_7O_6^+$ 492.2565; Found 492.2576.

HPLC-UV chromatogram at 214 nm of the crude reaction mixture



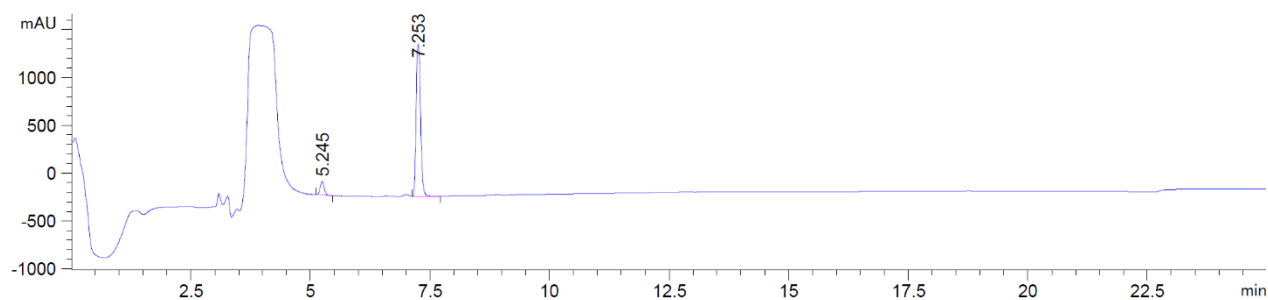
Ac-Ala-Phe-Gly-Ser-AH (6.50n)



Following the general procedure, Ac-Ala-Phe-Gly-Ser-OH (**6.49n**) afforded **6.50n** in more than 95% yield (retention time 11.436).

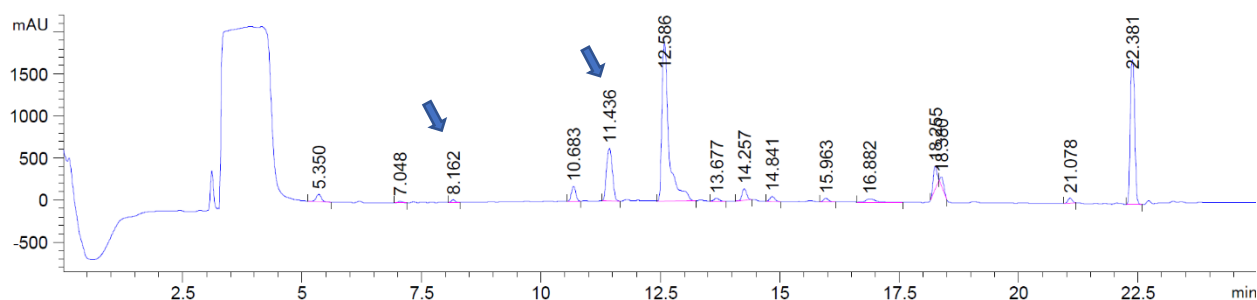
HRMS (ESI/QTOF) m/z : $[M + Na]^+$ Calcd for $C_{26}H_{30}N_4NaO_5^+$ 501.2108; Found 501.2107.

Ac-Ala-Phe-Gly-Ser-OH (**6.49n**)

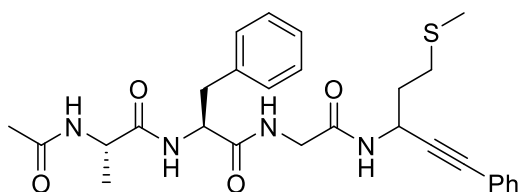


HRMS of **6.49n** (ESI/QTOF) m/z : $[M + Na]^+$ Calcd for $C_{19}H_{26}N_4NaO_7^+$ 445.1694; Found 445.1688

HPLC-UV chromatogram at 214 nm of the crude reaction mixture



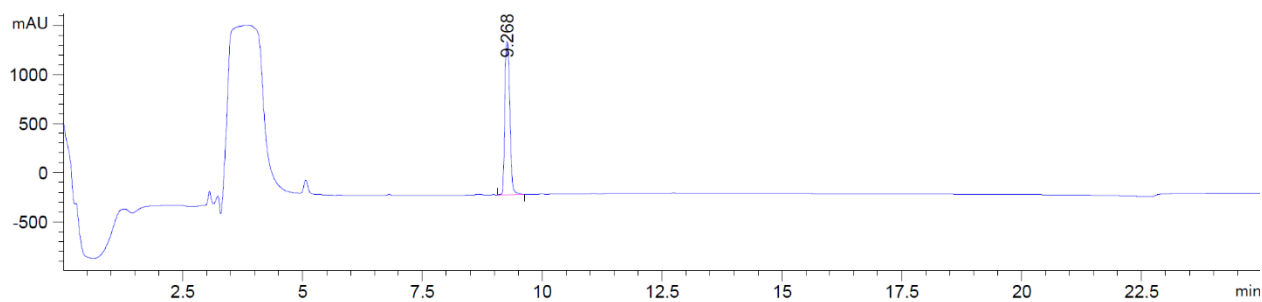
Ac-Ala-Phe-Gly-Met-AH (**6.50o**)



Following the general procedure, Ac-Ala-Phe-Gly-Met-OH (**6.49o**) afforded **6.50o** in more than 95% yield (retention time 12.124).

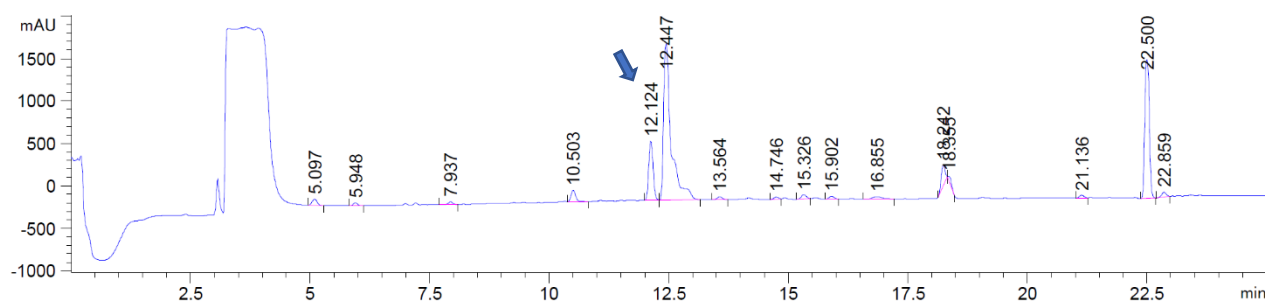
HRMS (ESI/QTOF) m/z : $[M + H]^+$ Calcd for $C_{28}H_{35}N_4O_4S^+$ 523.2374; Found 523.2375

Ac-Ala-Phe-Gly-Met-OH (**6.49o**)

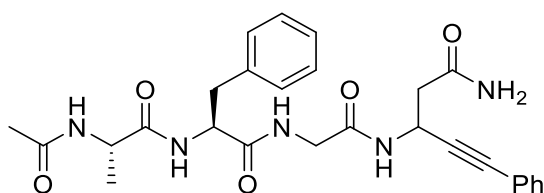


HRMS of **6.49o** (ESI/QTOF) m/z : $[M + Na]^+$ Calcd for $C_{21}H_{30}N_4NaO_6S^+$ 489.1778; Found 489.1774.

HPLC-UV chromatogram at 214 nm of the crude reaction mixture



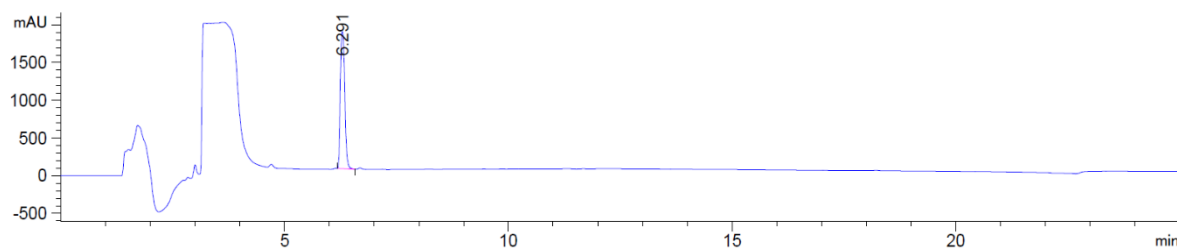
Ac-Ala-Phe-Gly-Asn-AH (**6.50p**)



Following the general procedure, Ac-Ala-Phe-Gly-Asn-OH (**6.49p**) afforded **6.50p** in more than 95% yield (retention time 10.724).

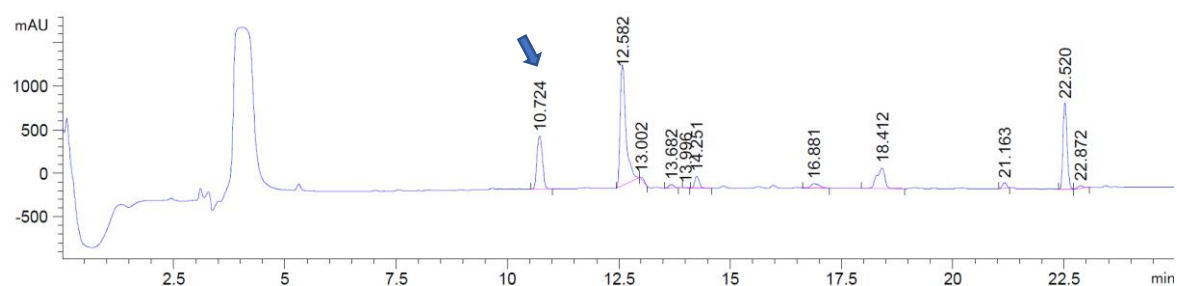
HRMS (ESI/QTOF) m/z : $[M + Na]^+$ Calcd for $C_{27}H_{31}N_5NaO_5^+$ 528.2217; Found 528.2223.

Ac-Ala-Phe-Gly-Asn-OH (**6.49p**)

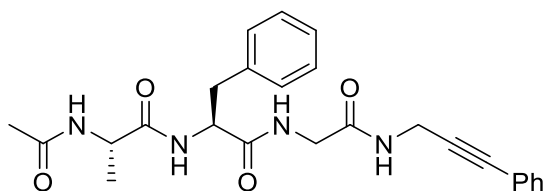


HRMS of **6.49p** (ESI/QTOF) m/z : $[M + H_1]^-$ Calcd for $C_{20}H_{26}N_5O_7^-$ 448.1838; Found 448.1830.

HPLC-UV chromatogram at 214 nm of the crude reaction mixture



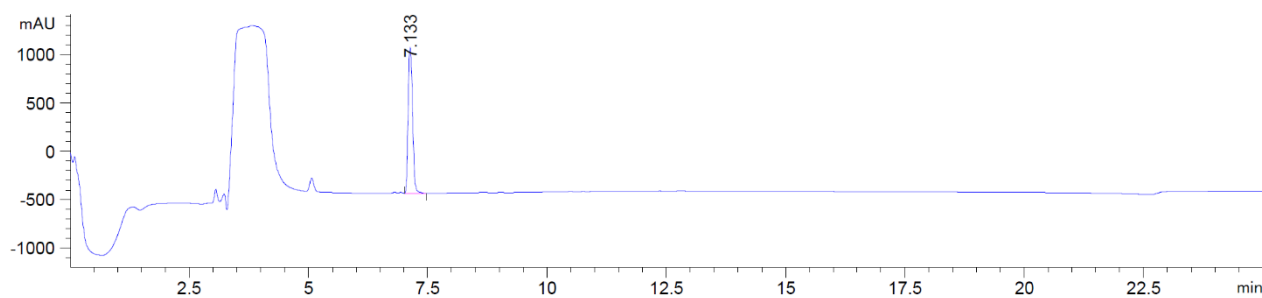
Ac-Ala-Phe-Gly-Gly-AH (**6.50d**)



Following the general procedure, Ac-Ala-Phe-Gly-Gly-OH (**6.49d**) afforded **6.50d** in more than 95% yield (retention time 11.995).

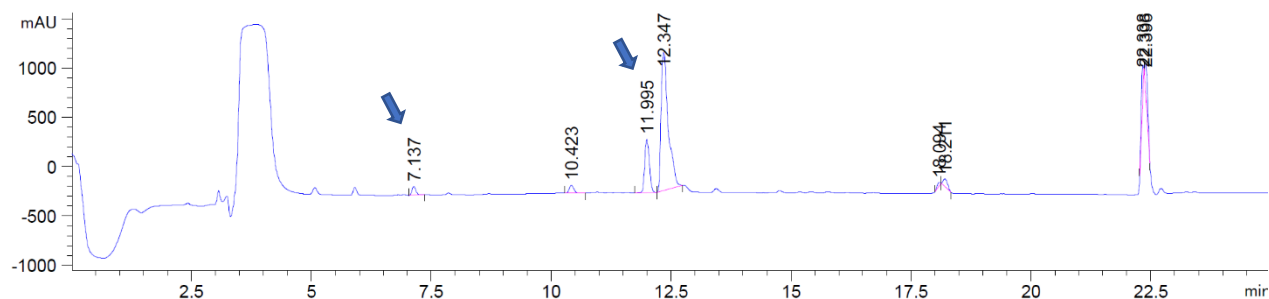
HRMS (ESI/QTOF) m/z : $[M + K]^+$ Calcd for $C_{25}H_{28}KN_4O_4^+$ 487.1742; Found 487.1757.

Ac-Ala-Phe-Gly-Gly-OH (**6.49d**)

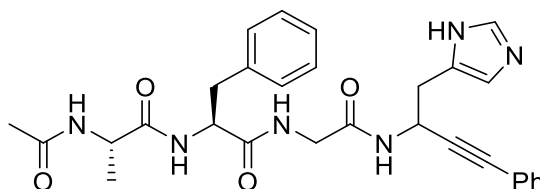


HRMS of **6.49d** (ESI/QTOF) m/z : $[M + Na]^+$ Calcd for $C_{18}H_{24}N_4NaO_6^+$ 415.1588; Found 415.1585.

HPLC-UV chromatogram at 214 nm of the crude reaction mixture



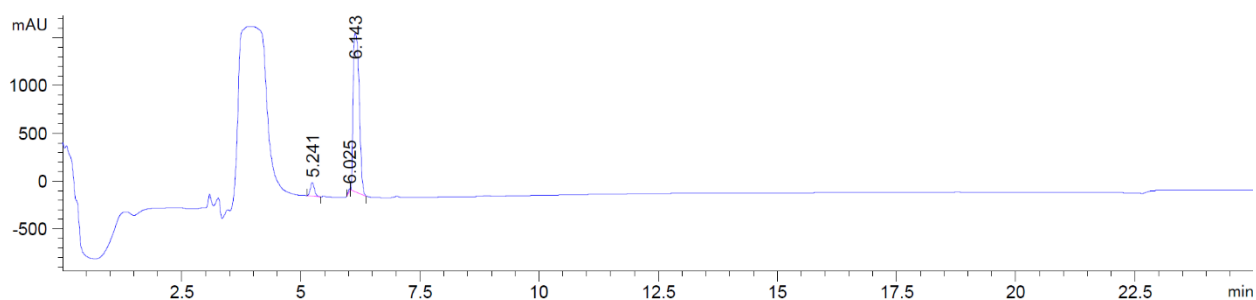
Ac-Ala-Phe-Gly-His-AH (**6.50q**)



Following the general procedure, Ac-Ala-Phe-Gly-His-OH (**6.49q**) afforded **6.50q** in an average of 76% yield (retention time 9.386).

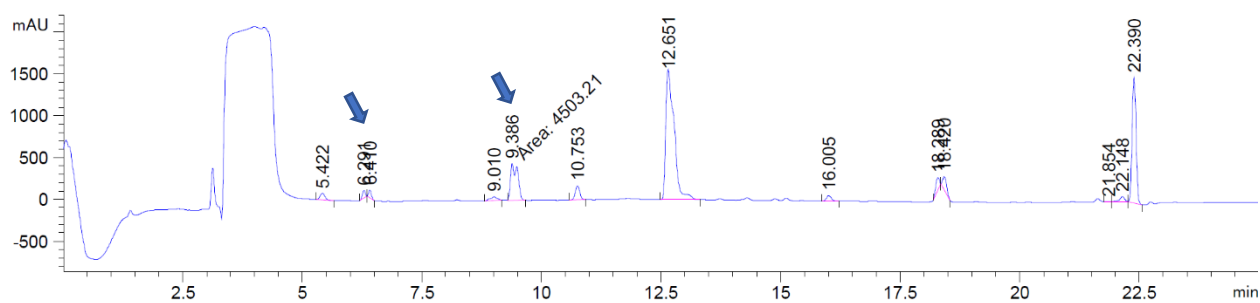
HRMS (ESI/QTOF) m/z : $[M + H]^+$ Calcd for $C_{29}H_{33}N_6O_4^+$ 529.2558; Found 529.2566.

Ac-Ala-Phe-Gly-His-OH (**6.49q**)

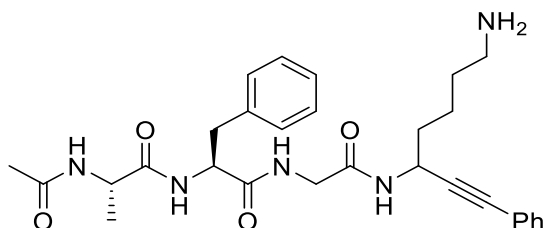


HRMS of **6.49q** (ESI/QTOF) m/z : $[M + H]^+$ Calcd for $C_{22}H_{29}N_6O_6^+$ 473.2143; Found 473.2148.

HPLC-UV chromatogram at 214 nm of the crude reaction mixture



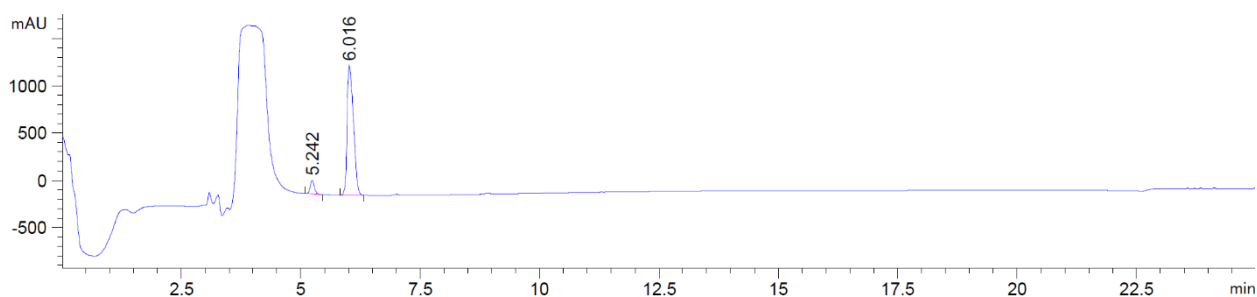
Ac-Ala-Phe-Gly-Lys-AH (6.50r)



Following the general procedure, Ac-Ala-Phe-Gly-Lys-OH (**6.49r**) afforded **6.50r** in an average of 17% yield (retention time 9.432).

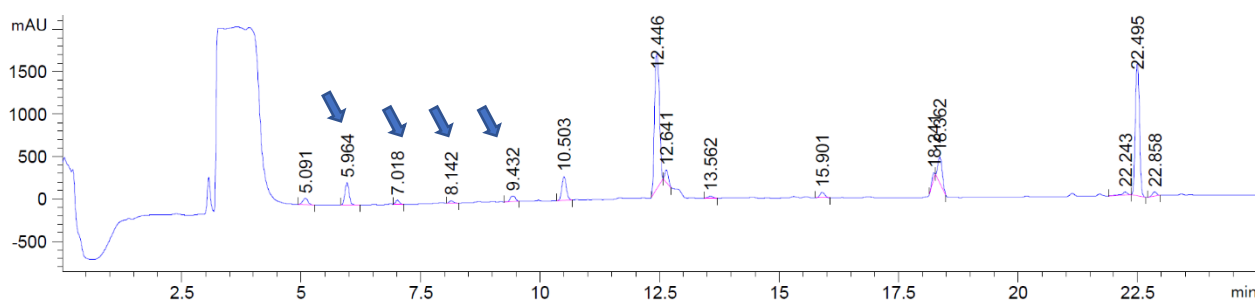
HRMS (ESI/QTOF) m/z : $[M + H]^+$ Calcd for $C_{29}H_{38}N_5O_4^+$ 520.2918; Found 520.2922.

Ac-Ala-Phe-Gly-Lys-OH (6.49r)

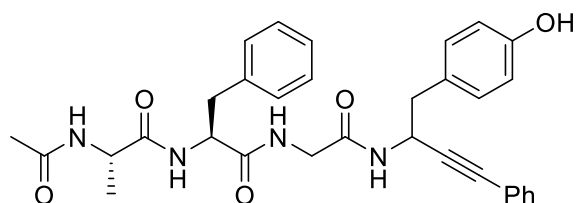


HRMS of **6.49r** (ESI/QTOF) m/z : $[M + H]^+$ Calcd for $C_{22}H_{34}N_5O_6^+$ 464.2504; Found 464.2514.

HPLC-UV chromatogram at 214 nm of the crude reaction mixture



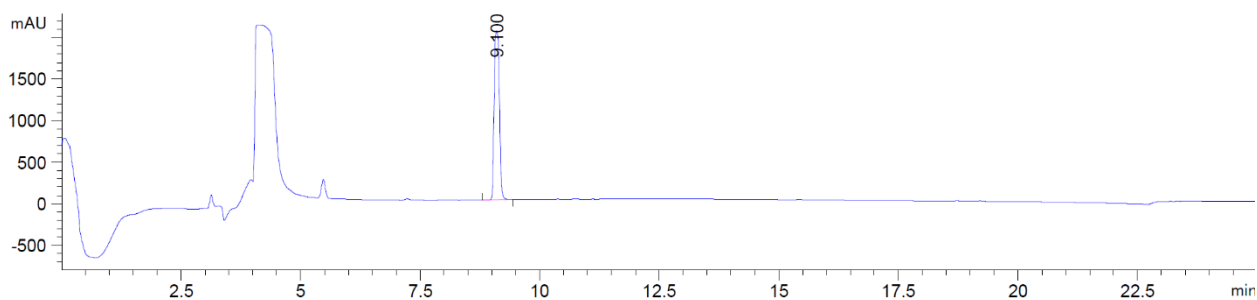
Ac-Ala-Phe-Gly-Tyr-AH (6.50s)



Following the general procedure and using Ir (**2.15**) as catalyst, Ac-Ala-Phe-Gly-Tyr-OH (**6.49s**) afforded **6.50s** in an average of 29% yield (retention time 13.243).

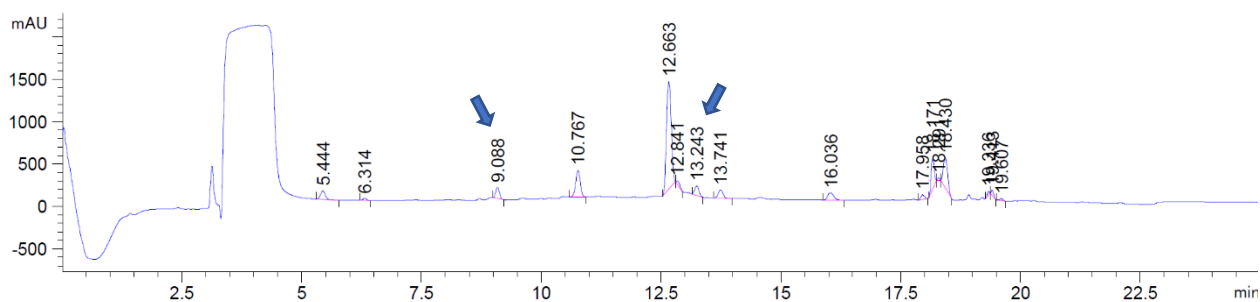
HRMS (ESI/QTOF) m/z : $[M + K]^+$ Calcd for $C_{32}H_{34}KN_4O_5^+$ 593.2161; Found 593.2172.

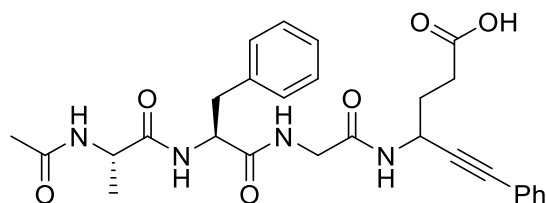
Ac-Ala-Phe-Gly-Tyr-OH (6.49s)



HRMS of **6.49s** (ESI/QTOF) m/z : $[M + H]^+$ Calcd for $C_{25}H_{31}N_4O_7^+$ 499.2187; Found 499.2187.

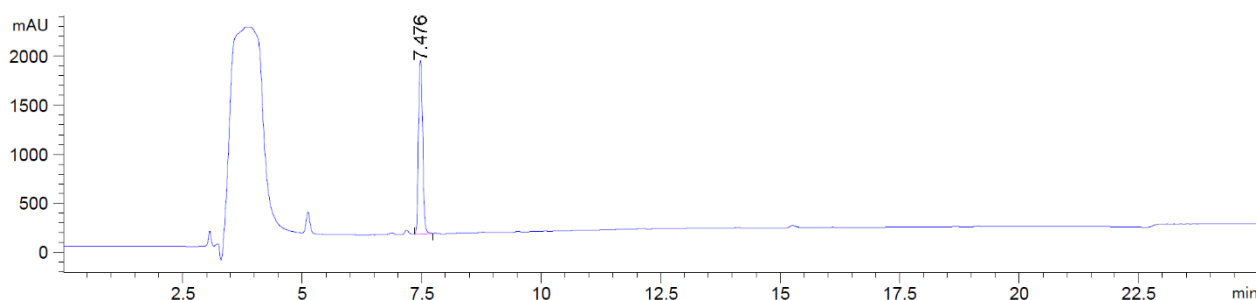
HPLC-UV chromatogram at 214 nm of the crude reaction mixture



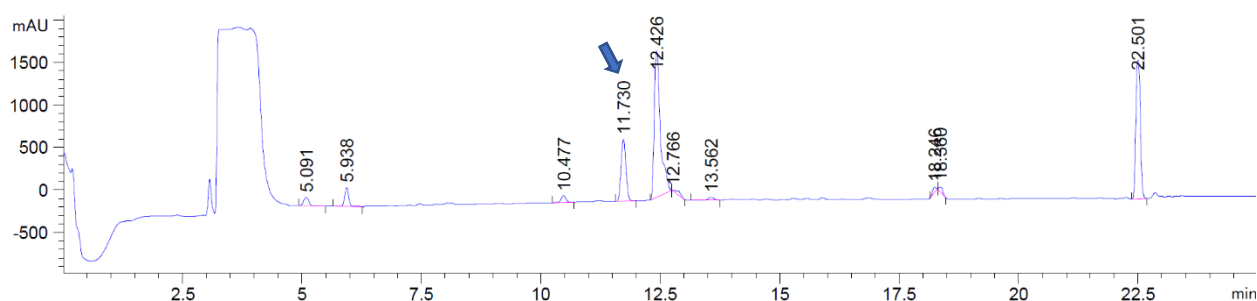
Ac-Ala-Phe-Gly-Glu-AH (6.50x)

Following the general procedure, Ac-Ala-Phe-Gly-Glu-OH (**6.49x**) afforded **6.50x** in more than 95% yield (retention time 11.730). The product with double alkynylation was detected at a retention time of 16.9 as less than 5% as the single alkynylation at the C-terminal position.

HRMS (ESI/QTOF) m/z : $[M + K]^+$ Calcd for $C_{28}H_{32}KN_4O_6^+$ 559.1953; Found 559.1962.

Ac-Ala-Phe-Gly-Glu-OH (6.49x)

HRMS of **6.49x** (ESI/QTOF) m/z : $[M + Na]^+$ Calcd for $C_{21}H_{28}N_4NaO_8^+$ 487.1799; Found 487.1807.

HPLC-UV chromatogram at 214 nm of the crude reaction mixture

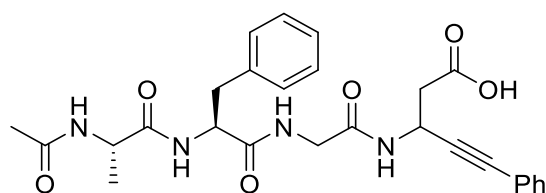
The 3 independent trials were gathered and purified by preparative HPLC using a gradient of 100% A to 100% B in 20 minutes (see general methods). The desired peptide was obtained

as a mixture at 40% pure together with iodobenzoic acid. The site of decarboxylative alkynylation was assigned by NMR. The signal in α position of the alkyne was attributed with the ^1H and the HMBC NMR. As an integration of 1 was measured, selective alkynylation at the C-terminal position was achieved. The signals are reported bellow, with signals of iodobenzoic acid in italics in brackets.

^1H NMR (800 MHz, $\text{DMF}-d_7$, 1:1 mixture of diastereoisomers, signals only partially resolved, only relevant protons were attributed) δ 8.29 – 8.10 (m, 4H, ArH), (8.07 (dd, $J = 7.9, 1.1$ Hz, 2H), 8.03 (s, 4H), 7.85 (dd, $J = 7.7, 1.7$ Hz, 2H), 7.55 (td, $J = 7.5, 1.2$ Hz, 2H),) 7.46 (tdd, $J = 4.8, 3.1, 1.9$ Hz, 2H, ArH), 7.42 – 7.37 (m, 3H, ArH), (7.32 – 7.27 (m, 6H),) 7.24 – 7.18 (m, 1H, ArH), 5.08 – 4.97 (m, 1H, $\text{NCHC}\equiv\text{C}$), 4.56 (ddd, $J = 9.5, 7.5, 4.8$ Hz, 0.5H, $\text{NC(O)CH}_2\text{NH}$), 4.52 (ddd, $J = 9.6, 7.4, 4.8$ Hz, 0.5H, $\text{NC(O)CH}_2\text{NH}$), 4.32 – 4.24 (m, 1H, $\text{NC(O)CHCH}_3\text{NH}$), 3.97 (dd, $J = 6.3, 1.6$ Hz, 1H), 3.95 (dd, $J = 6.3, 1.5$ Hz, 1H), 3.82 (dd, $J = 16.7, 5.6$ Hz, 0.5H), 3.79 (dd, $J = 16.7, 5.6$ Hz, 0.5H), 3.25 (ddd, $J = 14.0, 6.8, 4.8$ Hz, 1H), 3.06 – 2.97 (m, 1H), 2.59 – 2.48 (m, 2H, CHCH_2CH_3), 2.12 – 2.02 (m, 2H, NHCHCH_2), 1.90 (d, $J = 3.4$ Hz, 3H, Ac-NH), 1.22 (t, $J = 6.8$ Hz, 3H, $\text{NC(O)CHCH}_3\text{NH}$).

^{13}C NMR (201 MHz, $\text{DMF}-d_7$) δ 174.3, 174.2, 173.6, 173.5, 171.8, 170.6, 170.5, 168.7, (168.3, 141.4), 138.6, 138.6, (137.4, 132.8), 132.6, 131.9, 131.9, (130.8), 129.6, 129.3, 128.9, 128.9, 128.9, 128.6, (128.5), 126.6, 123.0, (93.9), 89.5, 89.5, 82.6, 82.6, 55.4, 55.3, 49.7, 42.8, 40.9, 40.9, 37.2, 31.2, 22.4, 17.3, 17.3.

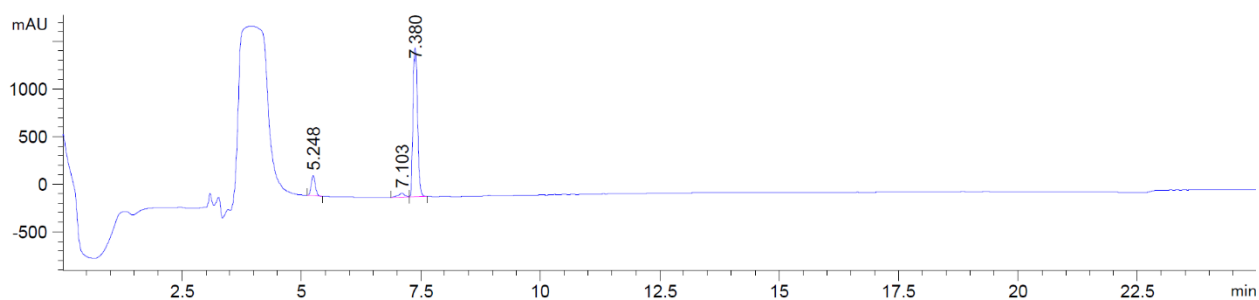
Ac-Ala-Phe-Gly-Asp-AH (6.50y)



Following the general procedure, Ac-Ala-Phe-Gly-Asp-OH (**6.49y**) afforded **6.50y** in an average of 37% yield (retention time 11.684). The product with double alkynylation was not detected in the HPLC chromatogram.

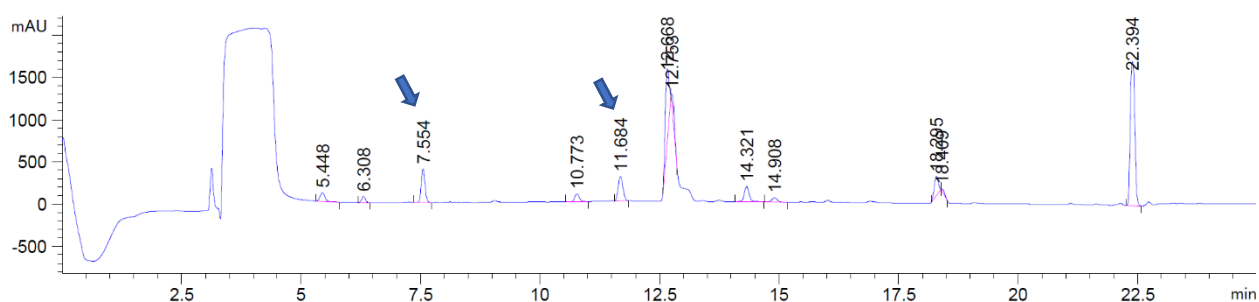
HRMS (nanochip-ESI/LTQ-Orbitrap) m/z : $[\text{M}]^-$ Calcd for $\text{C}_{27}\text{H}_{29}\text{N}_4\text{O}_6^-$ 505.2093; Found 505.2077.

Ac-Ala-Phe-Gly-Asp-OH (6.49y)



HRMS of **6.49y** (ESI/QTOF) m/z : $[M + Na]^+$ Calcd for $C_{20}H_{26}N_4NaO_8^+$ 473.1643; Found 473.1646.

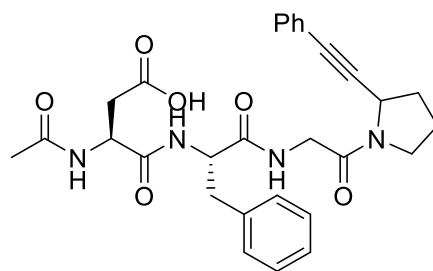
HPLC-UV chromatogram at 214 nm of the crude reaction mixture



The 3 independent trials were gathered and purified by preparative HPLC using a gradient of 100% A to 100% B in 20 minutes (see general methods). The desired peptide was obtained as a mixture at 75% pure together with iodobenzoic acid. The site of decarboxylative alkynylation was assigned by NMR by analogy to Ac-Ala-Phe-Gly-Glu-AH (**11r**) as not enough material was obtained to record an interpretable ^{13}C or HMBC NMR. The signal in α position of the alkyne was attributed with the 1H NMR. As an integration of 1 was measured, selective alkynylation at the C-terminal position was achieved. The signals are reported below, with signals of iodobenzoic acid in *italics* in brackets.

1H NMR (800 MHz, $DMF-d_7$, 1:1 mixture of diastereoisomers, signals only partially resolved, only relevant protons were attributed) δ 8.32 – 8.18 (m, 2H, ArH), (7.81 (d, $J = 7.5$ Hz, 0.3H), 7.54 – 7.49 (m, 0.3H)), 7.46 – 7.38 (m, 5H, ArH), 7.33 – 7.26 (m, 2H, ArH (and 2H)), 7.24 – 7.19 (m, 1H, ArH), 5.33 – 5.23 (m, 1H, $NCHC\equiv C$), 4.58 (ddd, $J = 9.2, 7.6, 4.7$ Hz, 1H, $NC(O)CH_2NH$), 4.31 – 4.21 (m, 1H, $NC(O)CH_2NH$), 4.00 – 3.97 (m, 0.5H), 3.97 – 3.95 (m, 0.5H), 3.81 (dd, $J = 16.7, 5.5$ Hz, 0.5H), 3.77 (dd, $J = 16.7, 5.2$ Hz, 0.5H), 3.27 (dt, $J = 14.0, 4.6$ Hz, 1H), 3.06 – 2.99 (m, 2H), 1.93 (d, $J = 14.2$ Hz, 3H, Ac-NH), 1.22 (t, $J = 7.5$ Hz, 3H, $NC(O)CHCH_3NH$).

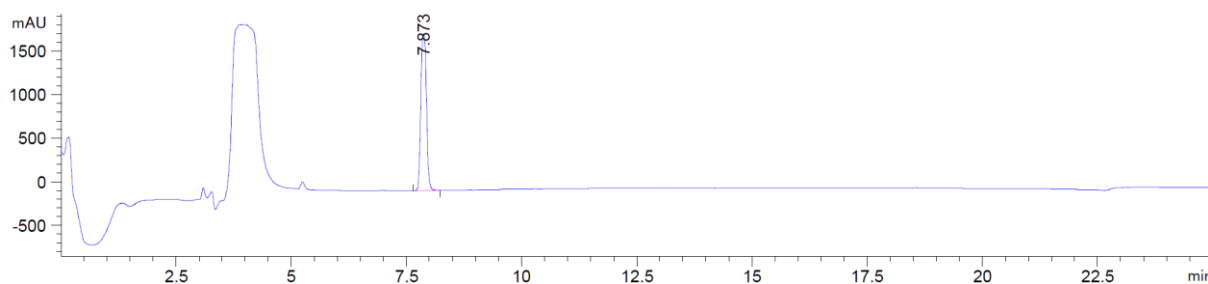
Ac-Asp-Phe-Gly-Pro-AH (6.50e)



Following the general procedure, Ac-Asp-Phe-Gly-Pro-OH (**6.49e**) afforded **6.50e** in more than 95% yield (retention time 13.020).

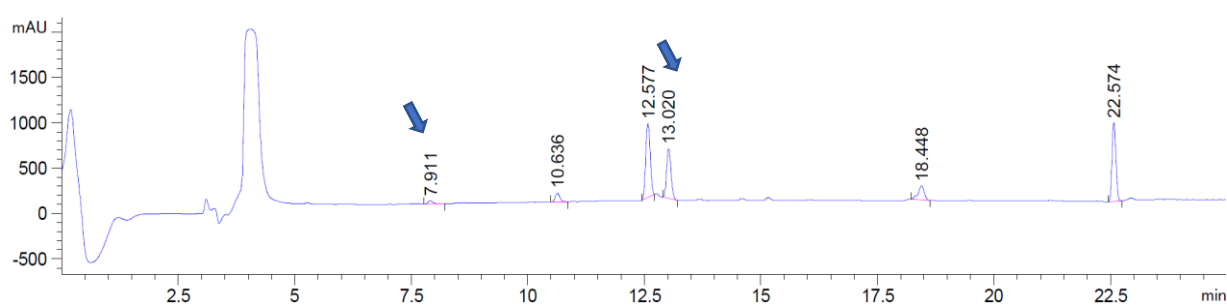
HRMS (ESI/QTOF) m/z : $[M + Na]^+$ Calcd for $C_{22}H_{27}N_4O_8^-$ 555.2214; Found 555.2218.

Ac-Asp-Phe-Gly-Pro-OH (6.49e)



HRMS of **6.49e** (ESI/QTOF) m/z : $[M + H_1]^-$ Calcd for $C_{24}H_{34}N_7O_6^-$ 475.1834; Found 475.1832.

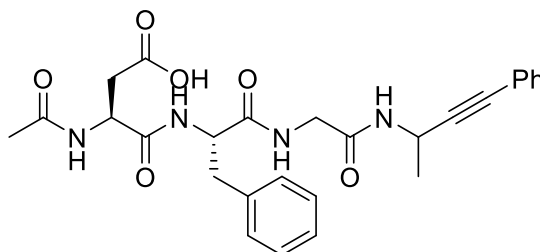
HPLC-UV chromatogram at 214 nm of the crude reaction mixture



MSMS (nanochip-ESI/LTQ-Orbitrap): selected ion 533.2399. Measured **b** and **y** ions are reported in the table below.

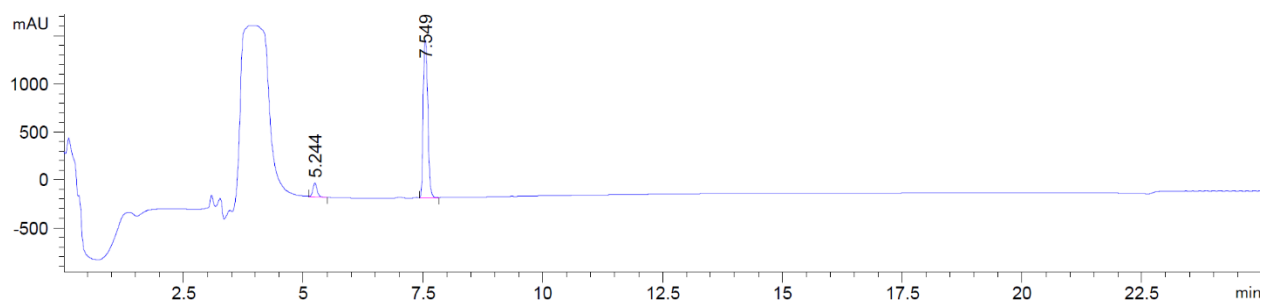
	D	F	G	P*
N-terminal	1	2	3	4
b	-	305.11	362.13	-

C-terminal	4	3	2	1
y	-	-	376.20	229.13

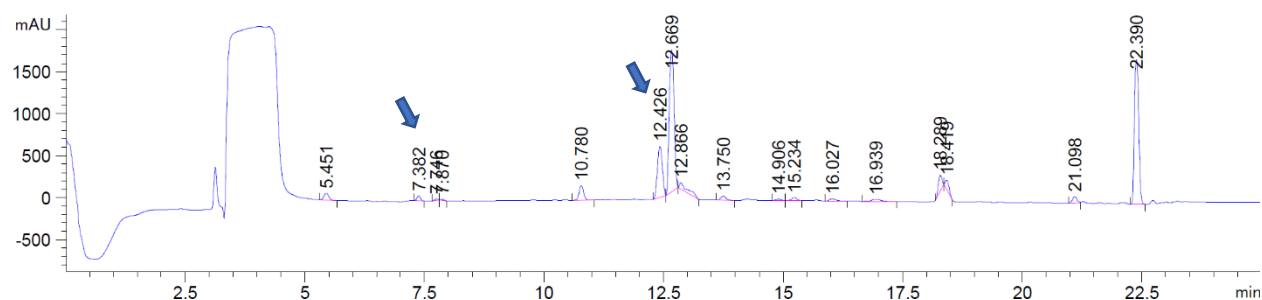
Ac-Asp-Phe-Gly-Ala-AH (6.49t)

Following the general procedure, Ac-Asp-Phe-Gly-Ala-OH (**6.49t**) afforded **6.50t** in more than 95% yield (retention time 12.426). The product with double alkynylation was detected at a retention time of 15.88 as less than 5% as the single alkynylation at the C-terminal position.

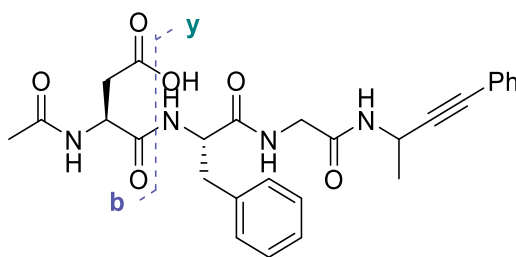
HRMS (nanochip-ESI/LTQ-Orbitrap) m/z: $[M + H]^+$ Calcd for $C_{27}H_{31}N_4O_6^+$ 507.2238; Found 507.2235.

Ac-Asp-Phe-Gly-Ala-OH (6.49t)

HRMS of **6.49t** (ESI/QTOF) m/z: $[M + Na]^+$ Calcd for $C_{20}H_{26}N_4NaO_8^+$ 473.1643; Found 473.1646.

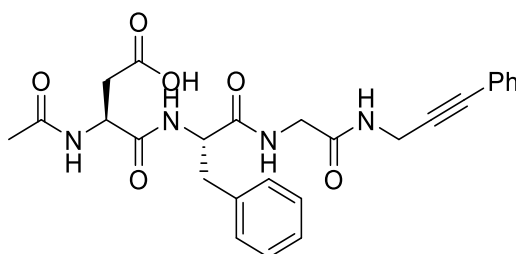
HPLC-UV chromatogram at 214 nm of the crude reaction mixture

MSMS (nanochip-ESI/LTQ-Orbitrap): selected ion 507.2235. Measured **b** and **y** ions are reported in the table below.



	D	F	G	A*
N-terminal	1	2	3	4
b	158.0448	305.1134	362.1348	-
C-terminal	4	3	2	1
y	-	350.1863	203.1178	-

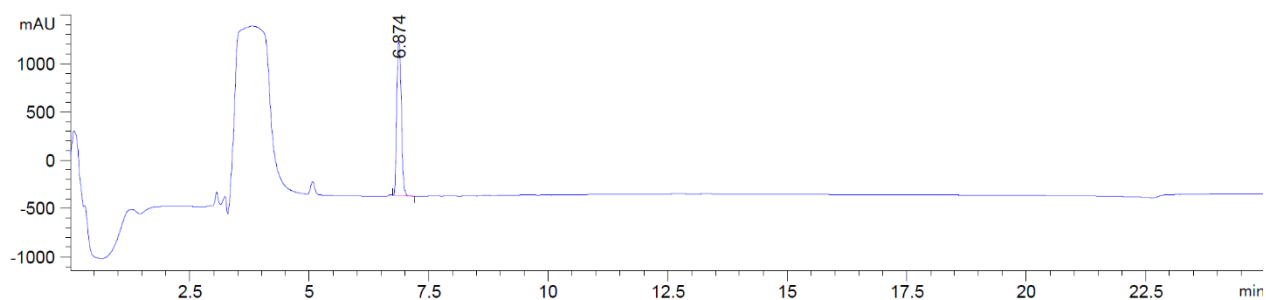
Ac-Asp-Phe-Gly-Gly-AH (6.50u)



Following the general procedure, Ac-Asp-Phe-Gly-Gly-OH (**6.49u**) afforded **6.50u** in an average of 48% yield (retention time 11.503). The product with double alkynylation was detected at a retention time of 15.38 as less than 5% as the single alkynylation at the C-terminal position.

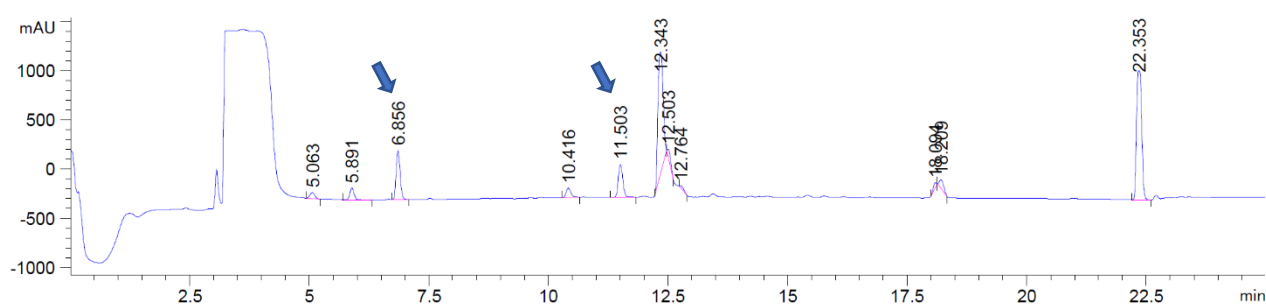
HRMS (ESI/QTOF) m/z: $[M + Na]^+$ Calcd for $C_{26}H_{28}N_4NaO_6^+$ 515.1901; Found 515.1896.

Ac-Asp-Phe-Gly-Gly-OH (6.49u)

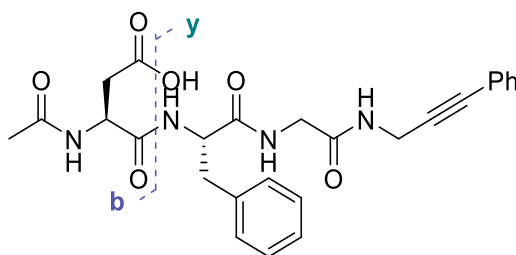


HRMS of **6.49u** (ESI/QTOF) m/z : $[M + Na]^+$ Calcd for $C_{19}H_{24}N_4NaO_8^+$ 459.1486; Found 459.1481.

HPLC-UV chromatogram at 214 nm of the crude reaction mixture

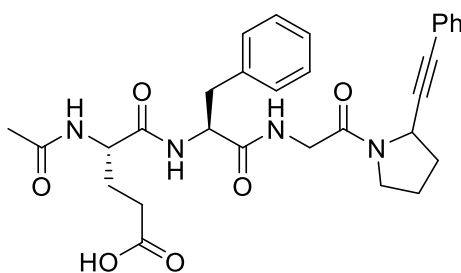


MSMS (nanochip-ESI/LTQ-Orbitrap): selected ion 493.2085. Measured **b** and **y** ions are reported in the table below.



	D	F	G	G*
N-terminal	1	2	3	4
b	-	305.1134	362.1347	-
C-terminal	4	3	2	1
y	-	336.1708	189.1022	-

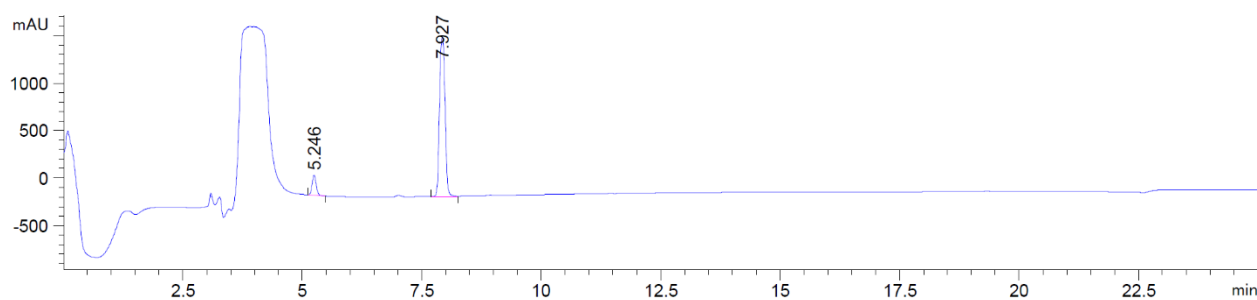
Ac-Glu-Phe-Gly-Pro-AH (6.50v)



Following the general procedure, Ac-Glu-Phe-Gly-Pro-OH (**6.49v**) afforded **6.50v** in more than 95% yield (retention time 13.017). The product with double alkylation was not detected.

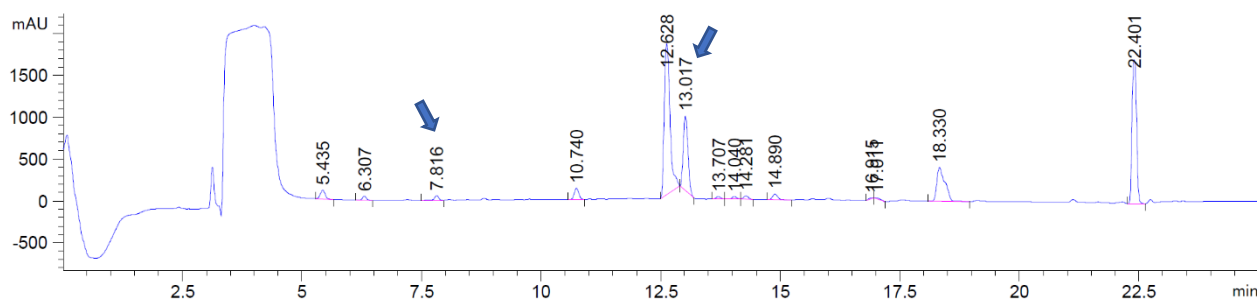
HRMS (nanochip-ESI/LTQ-Orbitrap) m/z : $[M + H]^+$ Calcd for $C_{30}H_{35}N_4O_6^+$ 547.2551; Found 547.2547.

Ac-Glu-Phe-Gly-Pro-OH (6.49v)

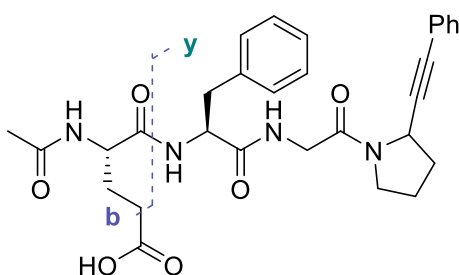


HRMS of **6.49v** (ESI/QTOF) m/z : $[M + Na]^+$ Calcd for $C_{23}H_{30}N_4NaO_8^+$ 513.1956; Found 513.1958.

HPLC-UV chromatogram at 214 nm of the crude reaction mixture

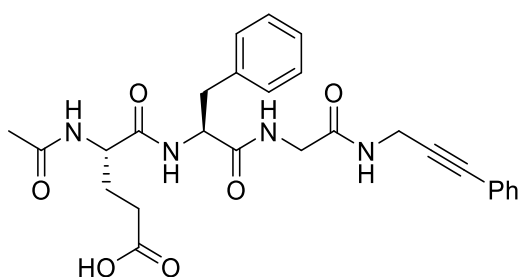


MSMS (nanochip-ESI/LTQ-Orbitrap): selected ion 547.3604. Measured **b** and **y** ions are reported in the table below.



	E	F	G	P*
N-terminal	1	2	3	4
b	172.0606	319.1288	376.1500	-
C-terminal	4	3	2	1
y	-	376.2023	229.1334	-

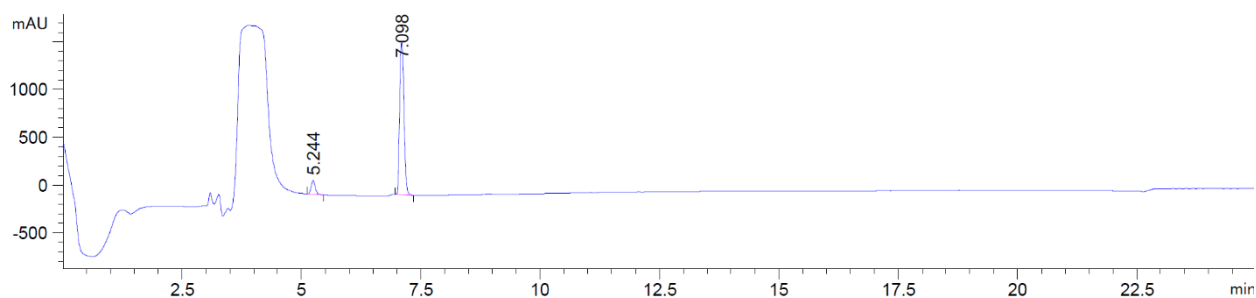
Ac-Glu-Phe-Gly-Gly-AH (6.50w)



Following the general procedure, Ac-Glu-Phe-Gly-Gly-OH (**6.49w**) afforded **6.50w** in an average of 75% yield (retention time 11.738). The product with double alkylation was only detected in HRMS of the crude, not in the HPLC chromatogram.

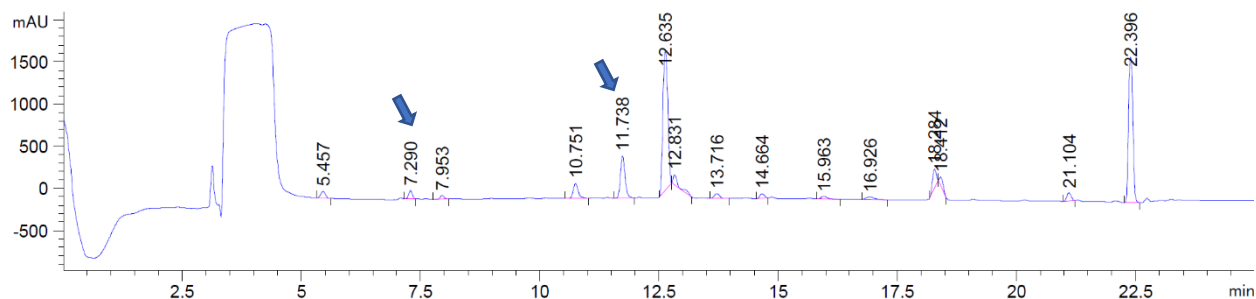
HRMS (ESI/QTOF) m/z : $[M + Na]^+$ Calcd for $C_{27}H_{30}N_4NaO_6^+$ 529.2058; Found 529.2059.

Ac-Glu-Phe-Gly-Gly-OH (6.49w)

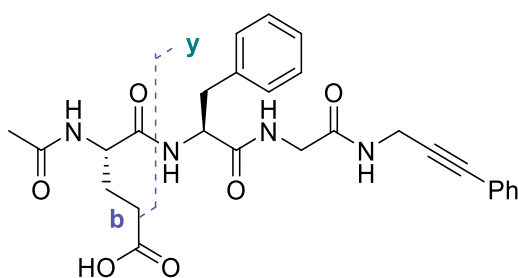


HRMS of **6.49w** (ESI/QTOF) m/z : $[M + Na]^+$ Calcd for $C_{20}H_{26}N_4NaO_8^+$ 473.1643; Found 473.1648.

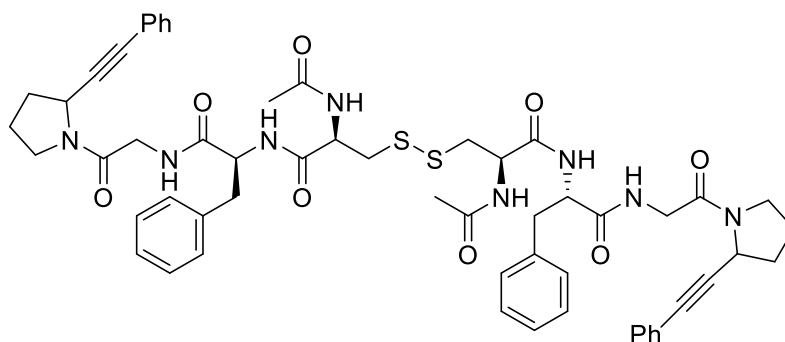
HPLC-UV chromatogram at 214 nm of the crude reaction mixture



MSMS (nanochip-ESI/LTQ-Orbitrap): selected ion 507.2235. Measured **b** and **y** ions are reported in the table below.

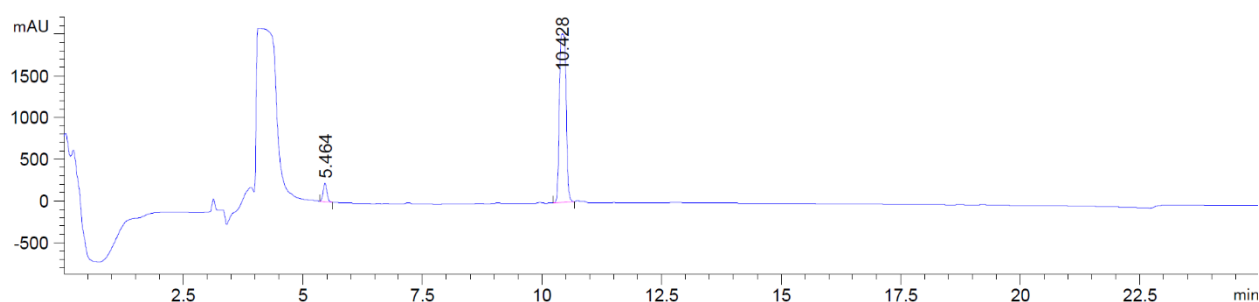


	E	F	G	G*
N-terminal	1	2	3	4
b	172.0605	319.1289	376.1503	-
C-terminal	4	3	2	1
y	-	336.1708	189.1023	-

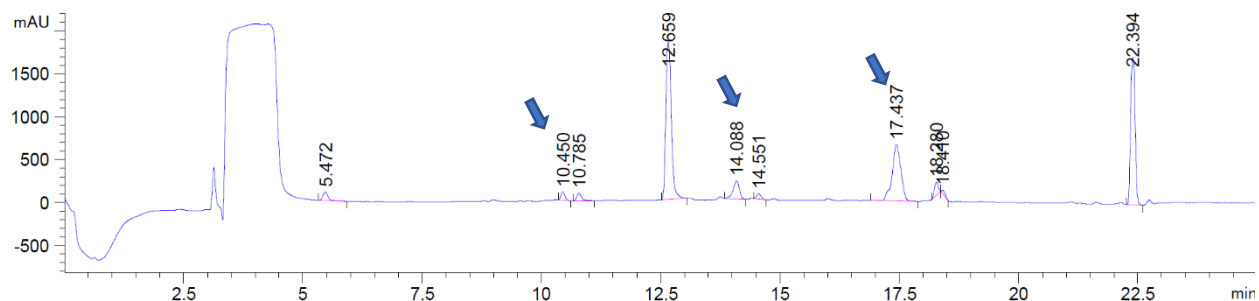
(Ac-Cys-Phe-Gly-Pro-AH)SS(Ac-Cys-Phe-Gly-Pro-AH) (6.50k)

Following the general procedure, (Ac-Cys-Phe-Gly-Pro-OH)SS(Ac-Cys-Phe-Gly-Pro-OH) (**6.49k**) afforded **6.50k** in good conversion, however overlap with **6.50j** prevented any yield determination (retention time 17.437).

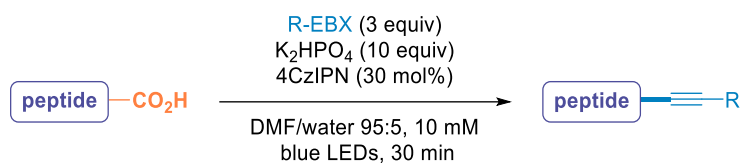
HRMS (ESI/QTOF) m/z : $[M + K]^+$ Calcd for $C_{56}H_{62}KN_8O_8S_2^+$ 1077.3764; Found 1077.3797.

(Ac-Cys-Phe-Gly-Pro-OH)SS(Ac-Cys-Phe-Gly-Pro-OH) (6.49k)

HRMS of **6.49k** (ESI/QTOF) m/z : $[M + H]^+$ Calcd for $C_{42}H_{55}N_8O_{12}S_2^+$ 927.3375; Found 927.3381.

HPLC-UV chromatogram at 214 nm of the crude reaction mixture

12.4.7 Scope on Gly-Arg-Gly-Asp-Asn-Pro-OH

**General procedure for the decarboxylative alkynylation of Gly-Arg-Gly-Asp-Asn-Pro-OH**

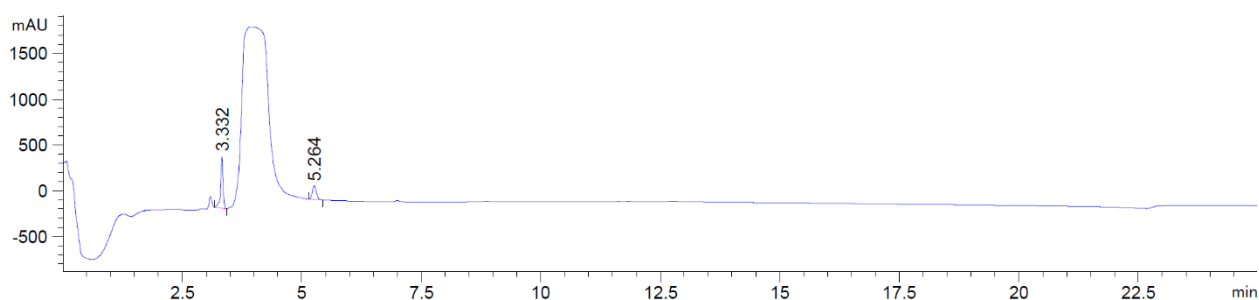
A 20 mM solution of the peptide in non-degassed DMF (50 μ L, 1.0 μ mol), a 60 μ M solution of R-EBX in DMF (25 μ L, 3.0 μ mol, 3.0 equiv), a 15 μ M solution of 4CzIPN (**2.23**) in DMF (20 μ L, 0.30 μ mol, 30 mol%) and a 2 M solution of K₂HPO₄ in milli-Q purified water (5 μ L, 10 μ mol, 10 equiv) were placed into a vial. The vial was then capped and degassed by bubbling with argon for 1-2 min and the mixture was irradiated using blue light LEDs for 30 min at RT.

At the end of the reaction, the crude was diluted with 3x the volume of MeCN/water 1:1 and injected in RP-HPLC. The yields were determined as the ratio of $A_{\text{prod}}/A_{\text{total}}$ where A_{prod} = area in mAU of the product peak and A_{total} = area in mAU of all peptides products (product, starting material, and side-products if present).

Reported results are an average of 3 independent trials.

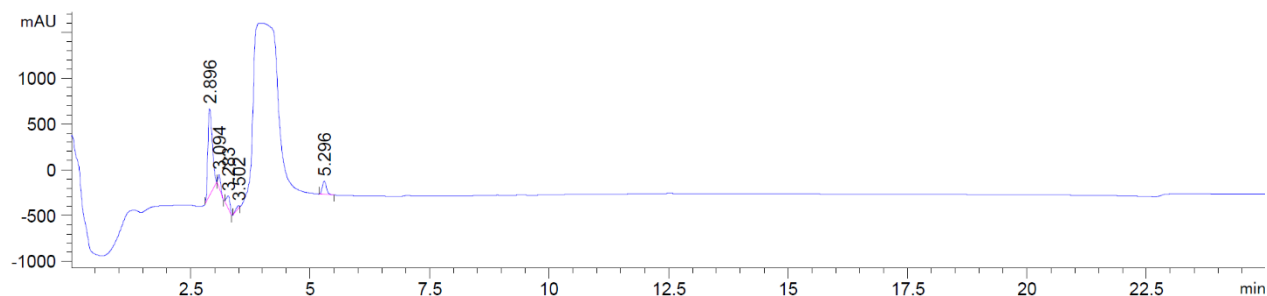
The products are described as peptide-AR with R standing for the substitution on the aryl ring.

Reference HPLC-UV chromatograms of reagents at 214 nm (Iodobenzoic acid, and 4CzIPN in section 12.4.6)

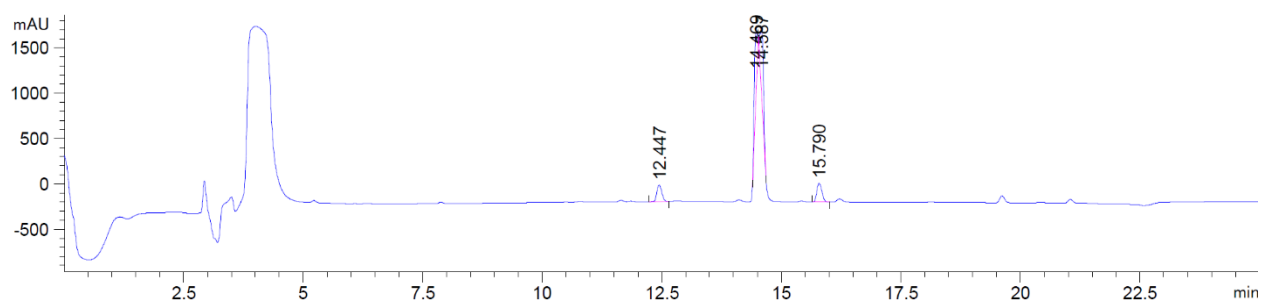
Ac-Gly-Arg-Gly-Asp-Asn-Pro-OH (6.51a)

HRMS (ESI/QTOF) m/z : $[M + H_1]^-$ Calcd for $C_{25}H_{39}N_{10}O_{11}^-$ 655.2805; Found 655.2802.

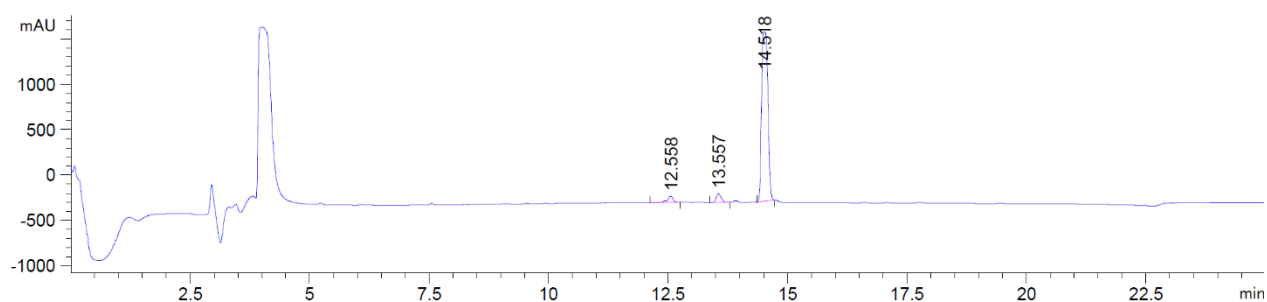
H-Gly-Arg-Gly-Asp-Asn-Pro-OH (6.51b)



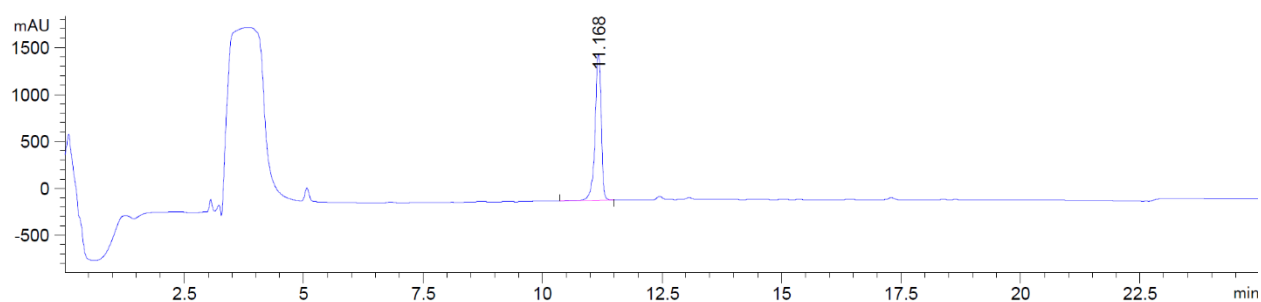
1-[4-Bromophenylethynyl]-1,2-benziodoxol-3(1H)-one (pBr-Ph-EBX, 6.9)



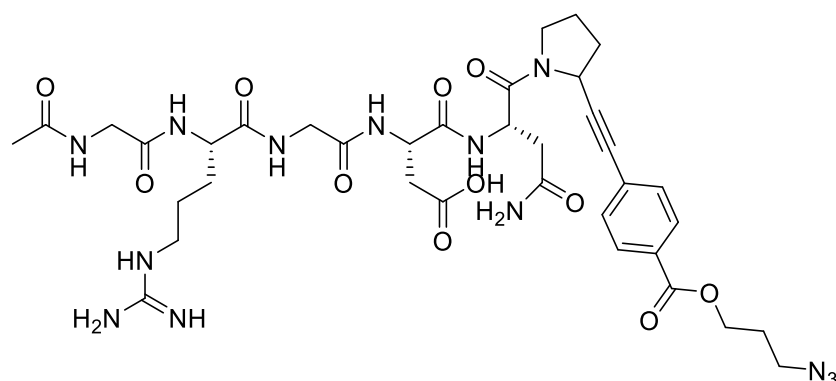
1-((4-(Prop-2-yn-1-yl)benzoate)ethynyl)-1,2-benziodoxol-3(1H)-one (N₃-Ar-EBX, 6.23)



1-((4-Formylphenyl)ethynyl)-1,2-benziodoxol-3(1H)-one (CHO-Ph-EBX, 6.10)



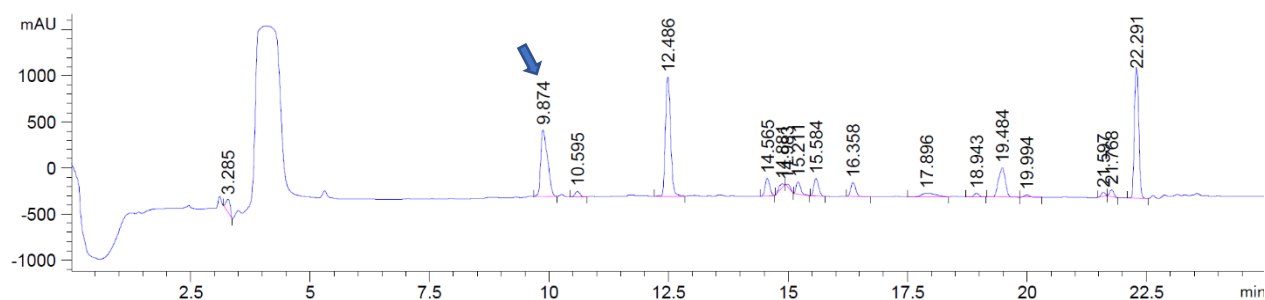
Ac-Gly-Arg-Gly-Asp-Asn-Pro-AN₃ (**6.52a**)



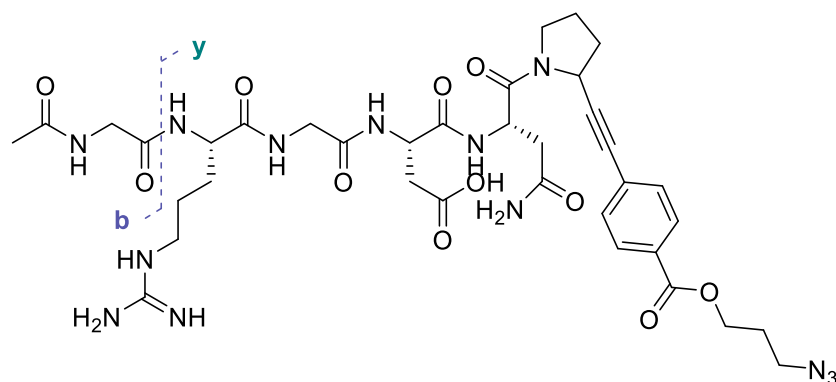
Following the general procedure, Ac-Gly-Arg-Gly-Asp-Asn-Pro-OH (**6.51a**) afforded **6.52a** in quantitative yield (retention time 9.874).

HRMS (nanochip-ESI/LTQ-Orbitrap) m/z : $[M + H]^+$ Calcd for $C_{36}H_{50}N_{13}O_{11}^+$ 840.3747; Found 840.3739.

HPLC-UV chromatogram at 214 nm:



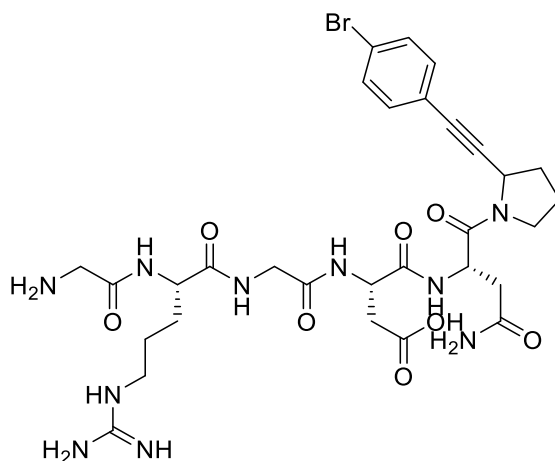
MSMS (nanochip-ESI/LTQ-Orbitrap): selected ion 840.3739. Identified **b** ions are reported in the table below. **y** ions could not be identified due to non-controlled fragmentation.



	G	R	G	D	N	P*
N-terminal	1	2	3	4	5	6
b	100.03	256.14	313.16	428.19	542.23	-

C-terminal	6	5	4	3	2	1
y	-	642.30	486.20	429.18	314.15	-

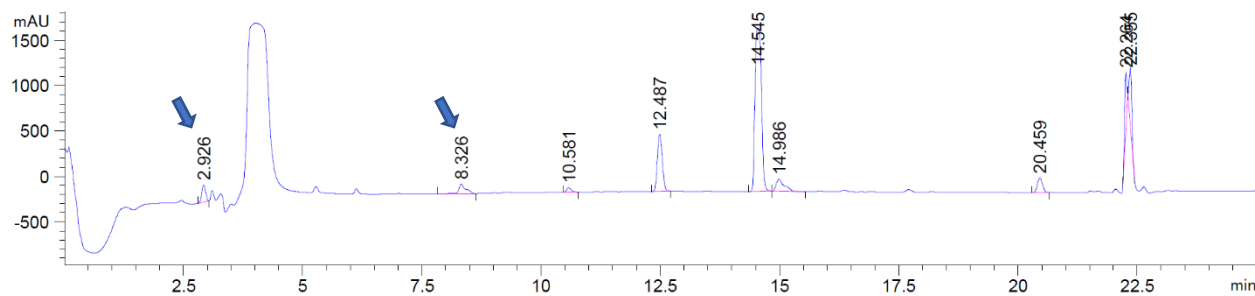
H-Gly-Arg-Gly-Asp-Asn-Pro-ABr (6.52c)



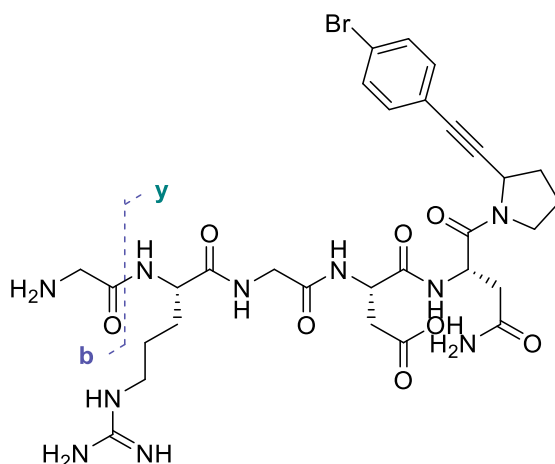
Following the general procedure, H-Gly-Arg-Gly-Asp-Asn-Pro-OH (**6.51b**) afforded **6.52c** in 52% yield (retention time 8.326).

HRMS (ESI/QTOF) m/z : $[M + H]^+$ Calcd for $C_{30}H_{42}^{79}BrN_{10}O_8^+$ 749.2365, 751.2345; Found 749.2350, 751.2342.

HPLC-UV chromatogram at 214 nm:

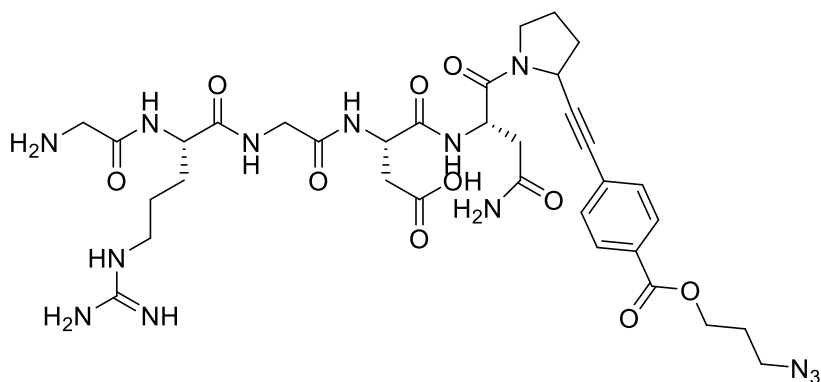


MSMS (nanochip-ESI/LTQ-Orbitrap): selected ion 749.2350. Identified **b** and **y** ions are reported in the table below.



	G	R	G	D	N	P*
N-terminal	1	2	3	4	5	6
b	-	214.13	271.15	386.18	500.22	-
C-terminal	6	5	4	3	2	1
y	-	692.21	536.11	479.09	364.07	250.02

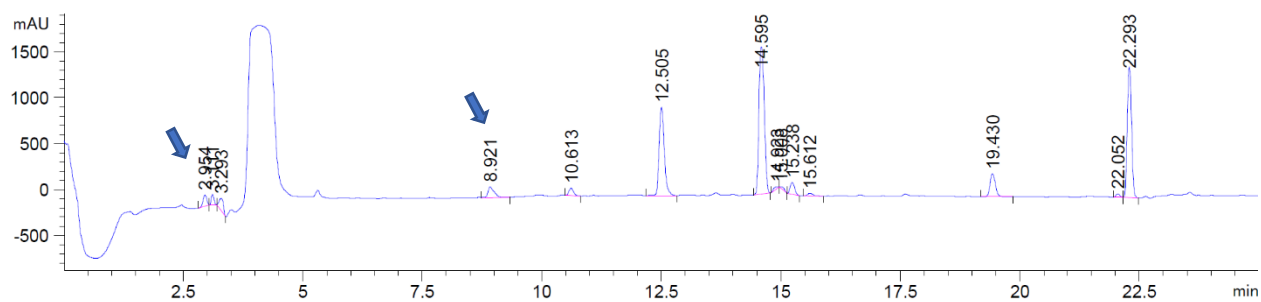
H-Gly-Arg-Gly-Asp-Asn-Pro-AN₃ (**6.52d**)



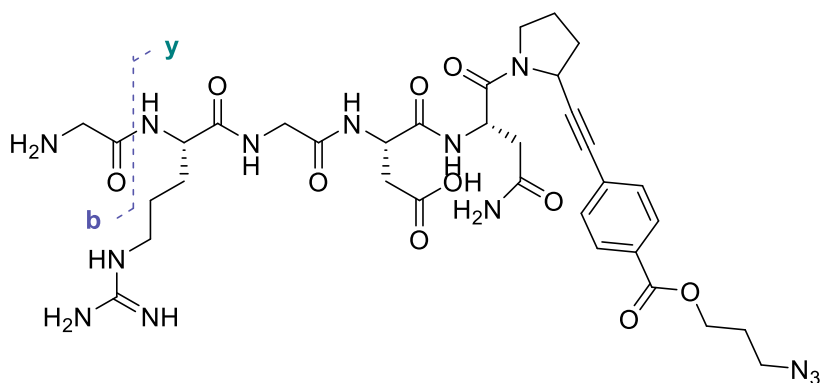
Following the general procedure, H-Gly-Arg-Gly-Asp-Asn-Pro-OH (**6.51b**) afforded **6.52d** in 57% yield (retention time 8.921).

HRMS (QTOF) m/z : $[M + H]^+$ Calcd for $C_{34}H_{48}N_{13}O_{10}^+$ 798.3642; Found 798.3640.

HPLC-UV chromatogram at 214 nm:



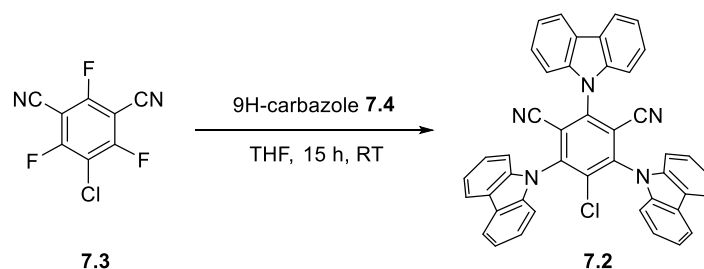
MSMS (nanochip-ESI/LTQ-Orbitrap): selected ion 798.3640. Identified **b** ions are reported in the table below. **y** ions could not be identified due to non-controlled fragmentation.



	G	R	G	D	N	P*
N-terminal	1	2	3	4	5	6
b	-	214.12	271.15	386.17	500.22	-

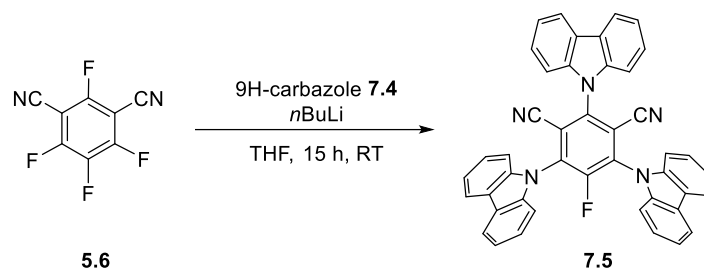
12.5 Towards a proximity-induced proteins C-terminal decarboxylative alkylation

12.5.1 Preparation of catalysts

(2*r*,4*r*)-2,4,6-Tri(9*H*-carbazol-9-yl)-5-chloroisophthalonitrile (7.2**)**

Following a reported procedure,^[346] sodium hydride (60% suspension in mineral oil, 451 mg, 11.3 mmol, 5.64 equiv) was added slowly to a stirred solution of 9*H*-carbazole **7.3** (1.25 g, 7.50 mmol, 3.75 equiv) in dry THF (40 mL) under a nitrogen atmosphere at RT. After 30 min, 5-chloro-2,4,6-trifluoroisophthalonitrile **36** (0.433 g, 2.00 mmol, 1 equiv) was added. After stirring at RT for 15 h, water (2 mL) was added to the reaction mixture to quench the excess of NaH. The resulting mixture was then concentrated under reduced pressure. The crude product was diluted in DCM, washed with water, dried over MgSO₄, filtered and concentrated under vacuum. The crude product was purified by column chromatography pentane/DCM 9:1 to 7:3 to afford **7.2** as a yellow/orange solid (943 mg, 1.43 mmol, 72%).

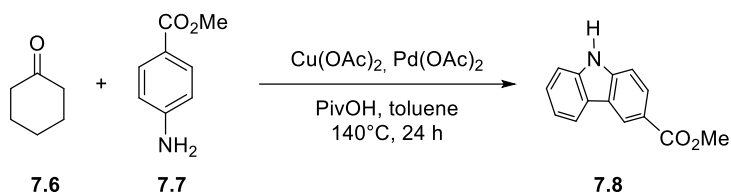
R_f (DCM/MeOH 95:5) = 0.32. (yellow spot on TLC). ¹H NMR (400 MHz, Chloroform-*d*) δ 8.18 (d, *J* = 7.8 Hz, 6H, *ArH*), 7.64 – 7.54 (m, 6H, *ArH*), 7.48 – 7.41 (m, 6H, *ArH*), 7.40 – 7.35 (m, 2H, *ArH*), 7.27 (d, *J* = 8.1 Hz, 4H, *ArH*). ¹³C NMR (101 MHz, Chloroform-*d*) δ 145.1, 144.2, 139.7, 139.2, 137.0, 126.9, 126.9, 124.8, 124.6, 122.4, 122.2, 121.3, 121.2, 117.6, 110.7, 109.5, 109.3. Consistent with reported data.^[346]

(2r,4r)-2,4,6-Tri(9*H*-carbazol-9-yl)-5-fluoroisophthalonitrile (7.5)

Following a reported procedure,^[285] a 2.5 M solution of *n*BuLi in hexanes (2.52 mL, 6.30 mmol, 3.15 equiv) was added dropwise to a stirred solution of 9*H*-carbazole (1.0 g, 6.0 mmol, 3 equiv) in dry THF (33 mL) under a nitrogen atmosphere at 0 °C. The reaction was warmed to RT and after 10 min, 2,4,5,6-tetrafluoroisophthalonitrile **5.6** (0.40 g, 2.0 mmol, 1 equiv) was added. After stirring at RT for 15 h, water was added to the reaction mixture to quench the excess of NaH. The resulting mixture was then concentrated under reduced pressure. The crude product was diluted in ethyl acetate, washed with water, dried over MgSO₄, filtered and concentrated under vacuum. The crude product was purified by column chromatography pentane/DCM 7:3 to 1:1 to afford **7.5** as a yellow/orange solid (597 mg, 0.930 mmol, 47%). Due to the very close polarity of **7.5** and 4CzIPN (**2.23**) (*R_f* (DCM/MeOH 95:5) = 0.3), a second fraction was obtained as a mixture and could be used in the following steps without purification (not accounted for yield determination). This reaction was repeated on scales from 2 to 4 mmol with a range of 44-47 % yield.

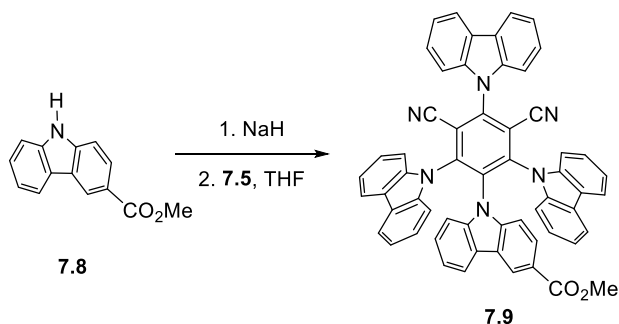
R_f (DCM/MeOH 95:5) = 0.32. (yellow spot on TLC). ¹H NMR (400 MHz, Chloroform-*d*) δ 8.21 (dt, *J* = 7.8, 1.0 Hz, 2H, Ar*H*), 8.16 (dt, *J* = 7.7, 1.0 Hz, 4H, Ar*H*), 7.63 (ddd, *J* = 8.4, 7.3, 1.2 Hz, 2H, Ar*H*), 7.57 (ddd, *J* = 8.3, 7.3, 1.3 Hz, 4H, Ar*H*), 7.49 – 7.39 (m, 8H, Ar*H*), 7.37 (d, *J* = 8.1 Hz, 2H, Ar*H*). ¹³C NMR (101 MHz, Chloroform-*d*) δ 140.0, 139.2, 135.2 (d, *J* = 14.6 Hz), 127.0, 126.9, 124.9, 124.7, 122.5, 122.3, 121.3, 121.1, 115.3 (d, *J* = 2.4 Hz), 110.9 (d, *J* = 2.7 Hz), 109.8, 109.1.²⁷ Consistent with reported data.^[285]

²⁷ Two carbons are not resolved

Methyl-9*H*-carbazole-3-carboxylate (7.8)

Following a reported procedure,^[286] a schlenk tube (10 mL) was charged with methyl 4-aminobenzoate (106 mg, 0.700 mmol, 1.4 equiv), palladium acetate (22 mg, 0.10 mmol, 20 mol%), copper acetate (0.55 g, 3.0 mmol, 6 equiv) and cyclohexanone (52 μ L, 0.50 mmol, 1 equiv) in pivalic acid (2 mL) and toluene (2 mL). The resulting mixture was degazed by freeze-pump throw (3 cycles) and placed under an argon atmosphere. The reaction was heated at 140 $^\circ$ C for 24 h. Two different vials on 0.5 mmol scale were gathered for workup and purification. After cooling to RT, a saturated solution of K_2CO_3 (5 mL) was added and the mixture extracted with ethyl acetate (3* 20 mL). The combined organic layers were washed with brine (10 mL), dried over MgSO_4 , filtered and concentrated under vacuum. The crude product was purified by column chromatography pentane/ethyl acetate 9:1 to 7:3 to afford **7.8** as a pale brown solid (59 mg, 0.26 mmol, 26%), together with a yellow oil which was characterized as the non-oxidized intermediate (44 mg, 0.20 mmol, 19%).

^1H NMR (400 MHz, Chloroform- d) δ 8.63 (dd, J = 1.7, 0.8 Hz, 1H, Ar*H*), 7.98 – 7.91 (m, 2H, Ar*H*), 7.28 – 7.21 (m, 3H, Ar*H*), 7.13 – 7.06 (m, 1H, Ar*H*), 3.80 (d, J = 2.9 Hz, 3H, Me). ^1H NMR consistent with reported data.^[286]

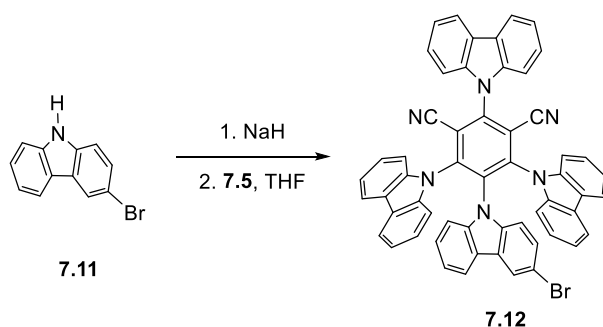
Methyl 9-((1*s*,2*s*,4*r*)-2,4,6-tri(9*H*-carbazol-9-yl)-3,5-dicyanophenyl)-9*H*-carbazole-3-carboxylate (7.9)

Sodium hydride (60% suspension in mineral oil, 6.0 mg, 0.15 mmol, 1.5 equiv) was added slowly to a stirred solution of **7.5** (27 mg, 0.12 mmol, 1.2 equiv) in dry THF (2 mL) under a nitrogen atmosphere at RT. After 30 min, **7.8** (64 mg, 0.10 mmol, 1 equiv) was added. After

stirring at RT for 15 h, water was added to the reaction mixture to quench the excess of NaH. The resulting mixture was then concentrated under reduced pressure. The crude product was diluted in DCM, washed with water, dried over MgSO₄, filtered and concentrated under vacuum. The crude product was purified by column chromatography pentane/DCM 7:3 to afford **7.9** as a yellow solid (48 mg, 0.056 mmol, 56%).

R_f (DCM/MeOH 8:2) = 0.3. (yellow spot on TLC). ¹H NMR (400 MHz, Chloroform-*d*) δ 8.26 – 8.19 (m, 2H, ArH), 8.07 (s, 1H, ArH), 7.77 – 7.63 (m, 8H, ArH), 7.56 – 7.45 (m, 2H, ArH), 7.41 – 7.30 (m, 2H, ArH), 7.24 – 7.16 (m, 4H, ArH), 7.15 – 7.04 (m, 8H, ArH), 6.93 – 6.81 (m, 3H, ArH), 6.72 – 6.63 (m, 1H, ArH), 3.87 (s, 3H, Me). ¹³C NMR (101 MHz, Chloroform-*d*) δ 167.1, 145.2, 139.9, 138.0, 138.0, 137.6, 133.8, 127.0, 126.3, 125.9, 125.8, 125.4, 125.0, 124.5, 123.7, 123.4, 122.9, 122.5, 122.2, 122.1, 122.0, 121.7, 121.4, 120.6, 120.0, 116.4, 111.5, 109.8, 109.8, 109.5, 109.5, 109.0, 52.0. HRMS (ESI/QTOF) *m/z*: [M + Na]⁺ Calcd for C₅₈H₃₄N₆NaO₂⁺ 869.2635; Found 869.2648.

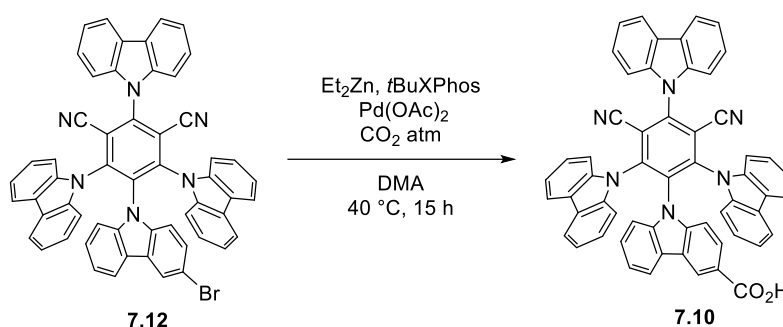
(2*r*,4*s*,5*s*)-5-(3-Bromo-9*H*-carbazol-9-yl)-2,4,6-tri(9*H*-carbazol-9-yl)isophthalonitrile (7.12)



Following a reported procedure,^[285] sodium hydride (60% suspension in mineral oil, 27 mg, 0.66 mmol, 1.5 equiv) was added slowly to a stirred solution of 3-bromo-9*H*-carbazole **7.11** (130 mg, 0.53 mmol, 1.2 equiv) in dry THF (15 mL) under a nitrogen atmosphere at RT. After 30 min, **7.5** (283 mg, 0.441 mmol, 1 equiv) was added. After stirring at RT for 15 h, water was added to the reaction mixture to quench the excess of NaH. The resulting mixture was then concentrated under reduced pressure. The crude product was diluted in DCM, washed with water, dried over MgSO₄, filtered and concentrated under vacuum. The crude product was purified by column chromatography pentane/DCM 7:3 to 1:1 to afford **7.12** as an orange solid (208 mg, 0.240 mmol, 54%). This reaction was repeated on scales from 0.3 to 1.6 mmol with a range of 54-59 % yield.

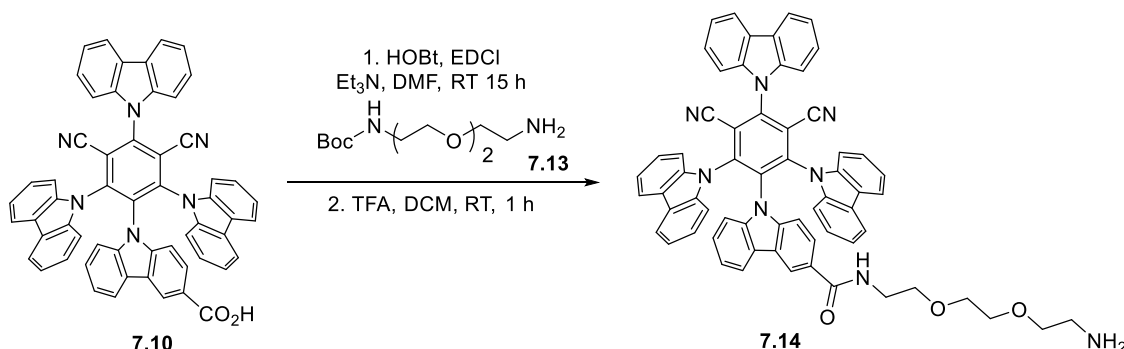
R_f (DCM/MeOH 95:5) = 0.3. (yellow spot on TLC). ¹H NMR (400 MHz, Chloroform-*d*) δ 8.27 – 8.20 (m, 2H, Ar*H*), 7.77 – 7.65 (m, 8H, Ar*H*), 7.52 – 7.44 (m, 3H, Ar*H*), 7.22 – 7.15 (m, 4H, Ar*H*), 7.14 – 7.03 (m, 8H, Ar*H*), 6.88 – 6.78 (m, 2H, Ar*H*), 6.74 – 6.69 (m, 2H, Ar*H*), 6.69 – 6.60 (m, 1H, Ar*H*). ¹³C NMR (101 MHz, Chloroform-*d*) δ 145.2, 144.9, 139.9, 139.8, 138.1, 138.1, 137.4, 135.8, 134.1, 127.3, 127.0, 126.7, 125.9, 125.8, 125.6, 125.5, 125.0, 124.6, 124.5, 122.6, 122.6, 122.5, 122.2, 122.1, 121.9, 121.4, 121.4, 120.9, 120.6, 119.8, 116.4, 113.8, 111.5, 110.7, 109.9, 109.9, 109.7, 109.6, 109.5.²⁸ Consistent with reported data.^[285]

9-((1*s*,2*s*,4*r*)-2,4,6-Tri(9*H*-carbazol-9-yl)-3,5-dicyanophenyl)-9*H*-carbazole-3-carboxylic acid (7.10**)**



R_f (DCM/MeOH 95:5) = 0.5. (yellow spot on TLC). ¹H NMR (400 MHz, Chloroform-*d*) δ 8.24 (d, *J* = 7.7 Hz, 2H, Ar*H*), 8.12 (d, *J* = 1.7 Hz, 1H, Ar*H*), 7.71 (dq, *J* = 7.0, 2.3 Hz, 8H, Ar*H*), 7.55 – 7.47 (m, 2H, Ar*H*), 7.47 – 7.36 (m, 2H, Ar*H*), 7.24 – 7.16 (m, 4H, Ar*H*), 7.16 – 6.97 (m, 7H, Ar*H*), 6.96 – 6.82 (m, 3H, Ar*H*), 6.73 – 6.65 (m, 1H, Ar*H*).²⁹ ¹³C NMR (151 MHz, Chloroform-*d*) δ 170.4, 145.3, 140.5, 139.8, 138.0, 138.0, 137.6, 133.6, 127.0, 126.8, 126.0, 125.9, 125.6, 125.0, 124.5, 123.8, 123.3, 122.7, 122.5, 122.3, 122.1, 121.9, 121.6, 121.5, 120.6, 120.1, 116.4, 111.5, 109.8, 109.7, 109.5, 109.2. HRMS (ESI/QTOF) *m/z*: [M + Na]⁺ Calcd for C₅₇H₃₂N₆NaO₂⁺ 855.2479; Found 855.2475.

N-(2-(2-(2-aminoethoxy)ethoxy)ethyl)-9-((1*s*,2*s*,4*r*)-2,4,6-tri(9*H*-carbazol-9-yl)-3,5-dicyanophenyl)-9*H*-carbazole-3-carboxamide (7.14)



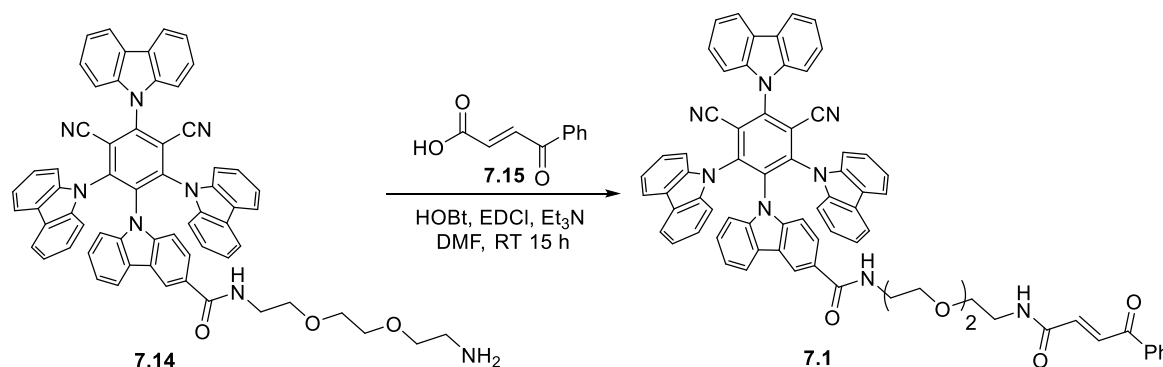
Following an adapted procedure,^[76] 9-((1*s*,2*s*,4*r*)-2,4,6-tri(9*H*-carbazol-9-yl)-3,5-dicyanophenyl)-9*H*-carbazole-3-carboxylic acid **7.10** (0.25 g, 0.30 mmol, 1 equiv), HOBT (69 mg, 0.45 mmol, 1.5 equiv), EDCI (86 mg, 0.45 mmol, 1.5 equiv) and *tert*-butyl (2-(2-(2-aminoethoxy)ethoxy)ethyl)carbamate **7.13** (0.30 g, 1.2 mmol, 4 equiv) were dissolved in anhydrous DMF (23 mL) under nitrogen. Triethylamine (84 μL, 0.60 mmol, 2 equiv) was added and the resulting mixture stirred overnight at RT, protected from the light. The reaction was quenched by addition of a 1 M solution of HCl (20 mL). The mixture was extracted with ethyl acetate (3* 100 mL). The combined organic layers were washed with a saturated solution of NaHCO₃ (50 mL), brine (3* 50 mL), dried over MgSO₄, filtered and concentrated under vacuum. The crude product was dissolved in DCM (25 mL) and TFA (2.3 mL, 30 mmol, 100 equiv) was added dropwise. The mixture was stirred for 1 h at RT, protected from the light. The reaction was quenched by addition of a saturated solution of NaHCO₃ and extracted with DCM. The combined organic layers were washed with brine, dried over MgSO₄, filtered and

²⁹ The carboxylic acid proton is not resolved

concentrated under vacuum. The crude product was purified by column chromatography DCM to DCM/methanol 75:25 to afford **7.14** as a yellow solid (94 mg, 0.097 mmol, 33%).

R_f (DCM/MeOH 9:1) = 0.1. (yellow spot on TLC). ¹H NMR (400 MHz, Chloroform-*d*) δ 8.25 – 8.16 (m, 2H, ArH), 7.91 (s, 1H, ArH), 7.75 – 7.64 (m, 8H, ArH), 7.53 – 7.44 (m, 2H, ArH), 7.38 (d, *J* = 7.7 Hz, 1H, ArH), 7.25 – 7.16 (m, 5H, ArH), 7.15 – 7.02 (m, 8H, ArH), 6.97 – 6.80 (m, 4H, ArH), 6.70 – 6.61 (m, 1H, ArH), 3.71 – 3.37 (m, 12H, CH₂), 2.76 (t, *J* = 5.2 Hz, 2H, NH₂).³⁰ ¹³C NMR (151 MHz, Chloroform-*d*) δ 167.4, 145.3, 145.2, 139.9, 139.8, 139.1, 138.1, 137.6, 134.2, 126.9, 125.9, 125.9, 125.4, 125.0, 124.9, 124.5, 124.4, 124.1, 123.8, 123.4, 122.5, 122.1, 122.0, 121.6, 121.4, 121.3, 120.6, 120.5, 120.1, 119.5, 116.4, 111.6, 110.0, 109.8, 109.7, 109.4, 109.4, 69.9, 69.9, 40.4, 39.7.³¹ HRMS (ESI/QTOF) *m/z*: [M + H]⁺ Calcd for C₆₃H₄₇N₈O₃⁺ 963.3766; Found 963.3767.

N-(2-(2-(2-((*E*)-4-oxo-4-phenylbut-2-enamido)ethoxy)ethoxy)ethyl)-9-((1*s*,2*s*,4*r*)-2,4,6-tri(9*H*-carbazol-9-yl)-3,5-dicyanophenyl)-9*H*-carbazole-3-carboxamide (7.1)



To a solution of **7.14** (25 mg, 0.026 mmol, 1 equiv), HOBT (6.0 mg, 0.039 mmol, 1.5 equiv), EDCI (7.5 mg, 0.039 mmol, 1.5 equiv) and (*E*)-4-oxo-4-phenylbut-2-enoic acid **7.15** (4.6 mg, 0.026 mmol, 1 equiv) in anhydrous DMF (2.0 mL) under nitrogen, was added triethylamine (18 μL, 0.13 mmol, 5 equiv) and the resulting mixture stirred overnight at RT, protected from the light. The reaction was quenched by addition of a 1 M solution of HCl (2 mL). The mixture was extracted with ethyl acetate (3* 10 mL). The combined organic layers were washed with a saturated solution of NaHCO₃ (10 mL), brine (3* 10 mL), dried over MgSO₄, filtered and concentrated under vacuum. The crude product was purified by preparative TLC

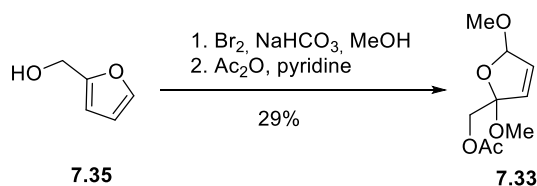
³⁰ The NH proton could not be assigned among ArH

³¹ One carbon is not resolved

DCM/methanol 9:1 to afford **7.1** as a yellow solid (19.7 mg, 0.0180 mmol, 68%). Degradation in acidic media was observed during purification.

R_f (DCM/MeOH 9:1) = 0.5. (yellow spot on TLC). ¹H NMR (400 MHz, Chloroform-*d*) δ 8.25 – 8.17 (m, 2H, ArH), 8.01 (s, 2H, ArH), 7.95 – 7.89 (m, 2H, ArH), 7.89 – 7.81 (m, 1H, ArH), 7.77 (dd, *J* = 7.1, 2.0 Hz, 1H, ArH), 7.74 – 7.62 (m, 8H, ArH), 7.56 – 7.43 (m, 3H, ArH), 7.42 – 7.30 (m, 5H, ArH), 7.26 – 7.18 (m, 3H, ArH), 7.13 – 6.91 (m, 9H, ArH), 6.90 – 6.80 (m, 2H, ArH), 6.70 – 6.59 (m, 2H, NH), 3.77 – 3.45 (m, 12H, PEG).³² ¹³C NMR (101 MHz, Chloroform-*d*) δ 189.4, 167.9, 164.6, 162.8, 144.9, 141.0, 139.9, 138.1, 137.7, 136.6, 135.1, 133.8, 133.3, 128.8, 128.4, 127.0, 126.5, 126.2, 125.9, 125.2, 124.5, 123.7, 122.4, 122.0, 121.6, 121.4, 121.4, 120.5, 120.1, 119.5, 117.1, 116.5, 111.5, 111.2, 109.9, 109.4, 70.5, 70.1, 70.0, 69.4, 39.8, 36.6, 31.5.³³ IR (ν_{max}, cm⁻¹) 2959 (s), 2920 (s), 2360 (w), 1649 (m), 1544 (m), 1457 (s), 1334 (m), 1226 (m), 1078 (m), 1069 (m), 970 (w), 909 (w), 748 (s), 613 (m). HRMS (ESI/QTOF) *m/z*: [M + Na]⁺ Calcd for C₇₃H₅₂N₈NaO₅⁺ 1143.3953; Found 1143.3950.

(2,5-Dimethoxy-2,5-dihydrofuran-2-yl)methyl acetate (**7.33**)



Following a reported procedure,^[291] to a solution of furfuryl alcohol (1.00 g, 10.2 mmol, 1 equiv) in dry MeOH (10 mL), was added NaHCO₃ (1.29 g, 15.3 mmol, 1.5 equiv). The mixture was cooled to -40 °C and a solution of bromine (0.551 mL, 10.7 mmol, 1.05 equiv) in dry MeOH (4 mL) was added dropwise. The mixture was stirred for 2 h at -40 °C before being warmed to RT. A saturated solution of NaHCO₃ was added until a pH around 8 was obtained and the methanol was concentrated. The residue was extracted with ethyl acetate. The combined organic layers were washed with brine, dried over MgSO₄, filtered and concentrated under vacuum. The crude mixture was diluted in dry pyridine (20 mL) and acetic anhydride (1.44 mL, 15.3 mmol, 1.5 equiv) was added dropwise. After stirring for 30 min at RT, water (1 mL) was added and the mixture was concentrated under vacuum. The residue was diluted in NaHCO₃ sat (20 mL) and extracted with DCM (50 mL). The combined organic layers were washed with water (10 mL), dried over MgSO₄, filtered and concentrated under vacuum. The crude product

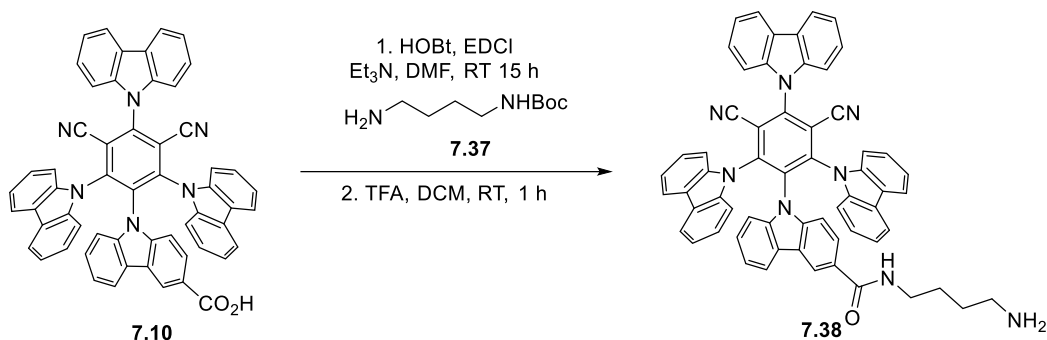
³² One NH and the alkene protons could not be distinguished within the aromatic region

³³ Several carbons are not resolved

was purified by column chromatography DCM to DCM/ethyl acetate 95:5 to afford **7.33** as a pale yellow oil and a mixture of diastereoisomers (597 mg, 2.95 mmol, 29%).

R_f (DCM/MeOH 20:1): 0.35. ¹H NMR (400 MHz, Chloroform-*d*) δ 6.16 – 6.07 (m, 2H), 5.96 (dd, *J* = 5.9, 1.3 Hz, 2H), 5.92 (dd, *J* = 5.9, 1.3 Hz, 1H), 5.77 (s, 1H), 5.77 (s, 1H), 5.51 (d, *J* = 1.3 Hz, 1H), 4.33 (d, *J* = 11.4 Hz, 1H), 4.24 (d, *J* = 4.6 Hz, 1H), 4.06 (d, *J* = 11.3 Hz, 1H), 3.52 (s, 3H), 3.44 (s, 3H), 3.24 (s, 3H), 3.17 (s, 3H), 2.05 (s, 6H). ¹³C NMR (101 MHz, Chloroform-*d*) δ 170.5, 132.7, 132.5, 131.5, 131.0, 112.5, 111.5, 108.4, 107.3, 66.6, 66.5, 56.4, 56.4, 55.5, 50.4, 49.9, 20.8.³⁴ Consistent with reported data.^[291]

N-(4-aminobutyl)-9-((1*s*,2*s*,4*r*)-2,4,6-tri(9*H*-carbazol-9-yl)-3,5-dicyanophenyl)-9*H*-carbazole-3-carboxamide (7.39**)**



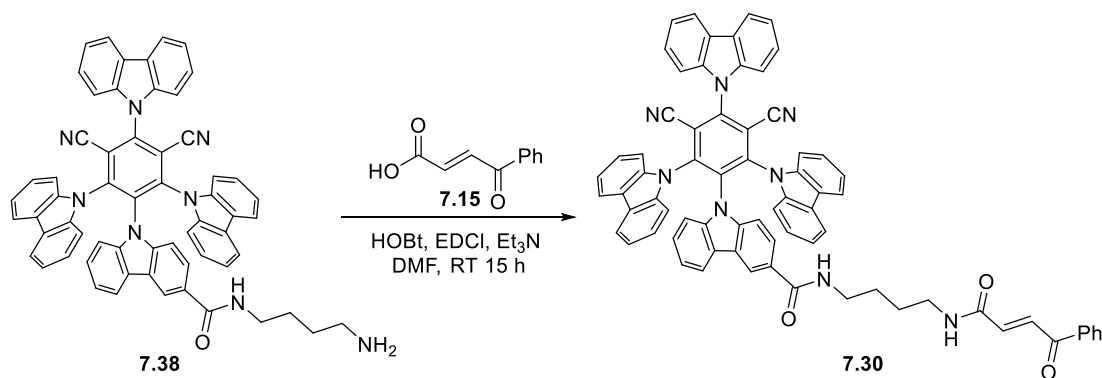
Following an adapted procedure,^[76] 9-((1*S*,2*s*,4*r*)-2,4,6-tri(9*H*-carbazol-9-yl)-3,5-dicyanophenyl)-9*H*-carbazole-3-carboxylic acid (**7.10**, 0.25 g, 0.30 mmol, 1 equiv), HOBT (69 mg, 0.45 mmol, 1.5 equiv), EDCI (86 mg, 0.45 mmol, 1.5 equiv) and *tert*-butyl (4-aminobutyl)carbamate (**7.37**, 0.23 g, 1.2 mmol, 4 equiv) were dissolved in anhydrous DMF (23 mL) under nitrogen. Triethylamine (84 μL, 0.60 mmol, 2 equiv) was added and the resulting mixture stirred overnight at RT, protected from the light. The reaction was quenched by addition of a 1M solution of HCl (20 mL). The mixture was extracted with ethyl acetate (3* 100 mL). The combined organic layers were washed with a saturated solution of NaHCO₃ (50 mL), brine (3* 50 mL), dried over MgSO₄, filtered and concentrated under vacuum. The crude product was dissolved in DCM (25 mL) and TFA (2.3 mL, 30 mmol, 100 equiv) was added dropwise. The mixture was stirred for 1 h at RT, protected from the light. The reaction was quenched by

³⁴ One carbon is not resolved

addition of a saturated solution of NaHCO_3 (10 mL) and extracted with DCM (20 mL). The combined organic layers were washed with brine, dried over MgSO_4 , filtered and concentrated under vacuum. The crude product was purified by column chromatography DCM to DCM/methanol 75:25 to afford **7.38** as a yellow solid (146 mg, 0.162 mmol, 54%).

Rf (DCM/MeOH 9:1) = 0.1. (yellow spot on TLC). The product was engaged in the next step without characterization.

N-(4-((*E*)-4-oxo-4-phenylbut-2-enamido)butyl)-9-((1*S*,2*s*,4*r*)-2,4,6-tri(9*H*-carbazol-9-yl)-3,5-dicyanophenyl)-9*H*-carbazole-3-carboxamide (7.30**)**

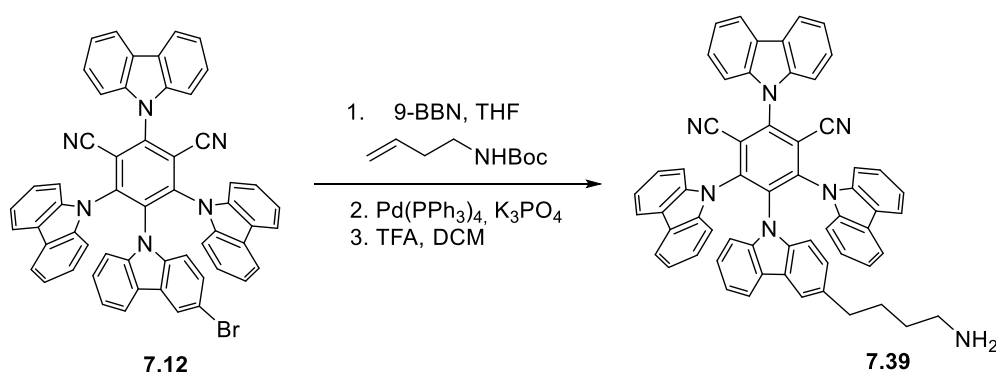


To a solution of **7.38** (17 mg, 0.019 mmol, 1 equiv), HOBt (4.3 mg, 0.028 mmol, 1.5 equiv), EDCI (5.4 mg, 0.028 mmol, 1.5 equiv) and (*E*)-4-oxo-4-phenylbut-2-enoic acid (**7.15**, 3.3 mg, 0.019 mmol, 1 equiv) in anhydrous DMF (1.5 mL) under nitrogen, was added triethylamine (5 μL , 0.04 mmol, 2 equiv) and the resulting mixture stirred overnight at RT, protected from the light. The reaction was quenched by addition of a 1 M solution of HCl (2 mL). The mixture was extracted with ethyl acetate (3* 10 mL). The combined organic layers were washed with a saturated solution of NaHCO_3 (10 mL), brine (3* 10 mL), dried over MgSO_4 , filtered and concentrated under vacuum. The crude product was purified by preparative TLC DCM/methanol 95:5 to afford **7.30** as a yellow solid (5.7 mg, 5.4 μmol , 29%). Degradation was observed during purification and no clean characterization could be obtained. NMR signals are hence given without assignment.

Rf (DCM/MeOH 95:5) = 0.3. (yellow spot on TLC). ^1H NMR (400 MHz, Chloroform-*d*) δ 8.29 – 8.16 (m, 2H), 8.07 – 7.90 (m, 1H), 7.82 (dd, J = 14.1, 1.7 Hz, 1H), 7.75 – 7.65 (m, 6H), 7.62 – 7.57 (m, 1H), 7.54 – 7.45 (m, 3H), 7.45 – 7.29 (m, 1H), 7.21 (q, J = 4.5, 4.0 Hz, 3H), 7.17 – 7.01 (m, 7H), 6.94 – 6.77 (m, 2H), 6.71 – 6.62 (m, 1H), 6.57 (s, 1H), 6.26 – 6.22 (m, 1H), 6.13

– 6.05 (m, 0H), 4.04 – 3.94 (m, 0H), 3.57 – 3.29 (m, 2H), 3.04 – 2.88 (m, 1H), 2.39 – 2.29 (m, 0H), 1.75 – 1.60 (m, 4H). ^{13}C NMR (101 MHz, Chloroform-*d*) δ 189.0, 167.0, 163.3, 145.2, 139.9, 138.1, 137.7, 136.5, 135.3, 133.8, 133.2, 128.8, 127.0, 126.0, 125.9, 125.0, 124.5, 123.6, 122.5, 122.2, 122.1, 121.4, 120.6, 120.3, 119.2, 116.4, 111.5, 109.8, 109.5, 39.5, 38.6, 30.2, 29.7, 27.1, 24.8. IR (ν_{max} , cm^{-1}) 2926 (m), 2017 (w), 1644 (s), 1547 (s), 1454 (s), 1311 (s), 1223 (m), 911 (m), 742 (s). HRMS (ESI/QTOF) m/z : $[\text{M} + \text{H}]^+$ Calcd for $\text{C}_{71}\text{H}_{49}\text{N}_8\text{O}_3^+$ 1061.3922; Found 1061.3944.

(2*r*,4*s*,5*s*)-5-(3-(4-aminobutyl)-9*H*-carbazol-9-yl)-2,4,6-tri(9*H*-carbazol-9-yl)isophthalonitrile (7.39**)**

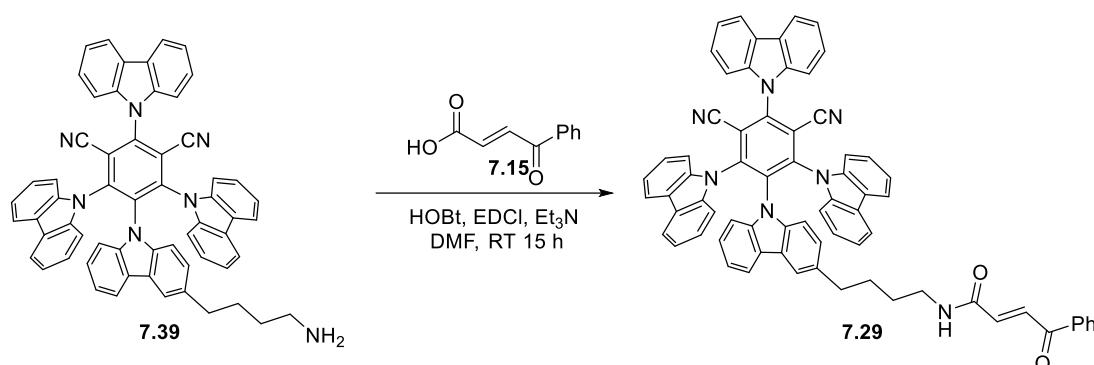


Following a modified procedure,^[293] a 0.5 M solution of 9-BBN in THF (0.25 μL , 0.13 mmol, 1.1 equiv) was added to a solution of *tert*-butyl pent-4-en-1-ylcarbamate (23 μL , 0.12 mmol, 1 equiv) in anhydrous THF (0.6 mL) in a microwave vial. The mixture was heated at 90 °C for 1 h and cooled to RT before being added to a second microwave tube containing **7.12** (100 mg, 0.115 mmol, 1 equiv), $\text{Pd}(\text{PPh}_3)_4$ (4.0 mg, 3.5 mmol, 3 mol%) and potassium phosphate (37 mg, 0.17 mmol, 1.5 equiv) in anhydrous DMF (0.6 mL). The resulting mixture was heated at 100 °C in the microwave for 3 h and then diluted in ethyl acetate, washed with brine (3*), dried over MgSO_4 , filtered and concentrated under vacuum. The crude product was dissolved in DCM (10 mL) and TFA (0.89 mL, 12 mmol, 100 equiv) was added dropwise. The mixture was stirred for 1 h at RT, protected from the light. The reaction was quenched by addition of a saturated solution of NaHCO_3 (10 mL) and extracted with DCM (20 mL). The combined organic layers were washed with brine (10 mL), dried over MgSO_4 , filtered and concentrated under vacuum. The crude product was purified by preparative TLC DCM/methanol 9:1 to afford **7.39** as a yellow solid (49 mg, 0.057 mmol, 49%).

Rf (DCM/MeOH 95:5) = 0.5. (yellow spot on TLC). ^1H NMR (400 MHz, Chloroform-*d*) δ 8.19 (dd, J = 7.8, 1.0 Hz, 2H, *ArH*), 7.75 – 7.63 (m, 4H, *ArH*), 7.63 – 7.55 (m, 4H, *ArH*), 7.51 – 7.38

(m, 2H, ArH), 7.23 – 7.17 (m, 5H, ArH), 7.14 – 6.97 (m, 9H, ArH), 6.81 (d, $J = 8.2$ Hz, 1H, ArH), 6.78 – 6.70 (m, 2H, ArH), 6.65 – 6.56 (m, 1H, ArH), 6.42 – 6.35 (m, 1H, ArH), 2.84 (bs, 2H NCH_2), 2.51 (bs, 2H, NH_2), 2.37 (t, $J = 7.3$ Hz, 2H, ArCH_2), 1.59 – 1.39 (m, 4H, CH_2CH_2). ^{13}C NMR (101 MHz, Chloroform- d) δ 145.1, 139.9, 138.2, 137.5, 135.1, 134.6, 133.6, 126.9, 125.8, 124.9, 124.5, 124.4, 123.7, 122.4, 121.9, 121.4, 120.4, 119.6, 119.1, 116.4, 111.6, 110.0, 109.4, 38.9, 34.4, 28.1, 26.8. HRMS (ESI/QTOF) m/z : $[\text{M} + \text{H}]^+$ Calcd for $\text{C}_{60}\text{H}_{42}\text{N}_7^+$ 860.3496; Found 860.3514.

(*E*)-4-oxo-4-phenyl-N-(4-(9-((1*s*,2*s*,4*r*)-2,4,6-tri(9*H*-carbazol-9-yl)-3,5-dicyanophenyl)-9*H*-carbazol-3-yl)butyl)but-2-enamide (7.29)

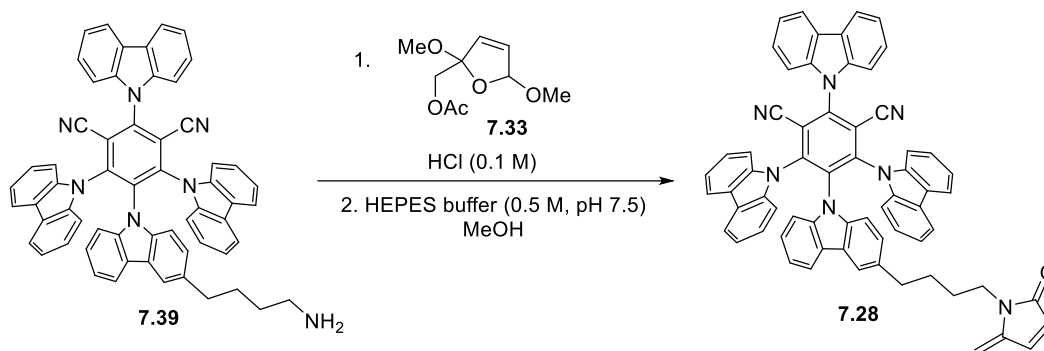


To a solution of **7.39** (30 mg, 0.035 mmol, 1 equiv), HOBt (8.0 mg, 0.052 mmol, 1.5 equiv), EDCI (10 mg, 0.052 mmol, 1.5 equiv) and (*E*)-4-oxo-4-phenylbut-2-enoic acid (**7.15**, 6.1 mg, 0.035 mmol, 1 equiv) in anhydrous DMF (2.6 mL) under nitrogen, was added triethylamine (10 μL , 0.070 mmol, 2 equiv) and the resulting mixture stirred overnight at RT, protected from the light. The reaction was quenched by addition of a 1 M solution of HCl (3 mL). The mixture was extracted with ethyl acetate (3* 10 mL). The combined organic layers were washed with a saturated solution of NaHCO_3 (10 mL), brine (3* 10 mL), dried over MgSO_4 , filtered and concentrated under vacuum. The crude product was purified by preparative TLC DCM/methanol 95:5 to afford **7.29** as a yellow solid (17 mg at 70% purity, 0.011 mmol, 33%). Larger scale synthesis should afford better purification. Characterization of the impure product with an unknown impurity is given for indication.

R_f (DCM/MeOH 95:5) = 0.9. (yellow spot on TLC). ^1H NMR (400 MHz, Dichloromethane- d) δ 8.28 (d, $J = 7.8$ Hz, 2H, ArH), 8.07 – 8.00 (m, 2H, ArH), 7.93 (d, $J = 15.0$ Hz, 1H, ArH), 7.82 – 7.69 (m, 9H, ArH), 7.67 – 7.58 (m, 1H, ArH), 7.57 – 7.43 (m, 4H, ArH), 7.42 – 7.31 (m, 2H, ArH), 7.33 – 7.21 (m, 3H, ArH), 7.19 – 7.06 (m, 8H, ArH), 6.90 – 6.75 (m, 2H, ArH), 6.68 (ddd, $J = 8.4, 7.2, 1.2$ Hz, 1H, ArH), 6.49 (dd, $J = 8.4, 1.7$ Hz, 1H, ArH), 5.87 (bs, 1H, NH), 3.37 (q,

$J = 6.6$ Hz, 2H, NCH_2), 2.51 (t, $J = 7.3$ Hz, 1H, ArCH_2), 1.67 – 1.60 (m, 1H, CH_2CH_2), 1.47 – 1.21 (m, 2H, CH_2CH_2). ^{13}C NMR (101 MHz, Dichloromethane- d_2) δ 164.0, 145.6, 140.3, 138.6, 137.8, 136.9, 136.0, 135.7, 135.6, 134.0, 133.4, 129.2, 129.1, 127.4, 126.2, 125.9, 125.2, 125.1, 124.8, 124.2, 122.8, 122.3, 121.7, 121.4, 120.8, 119.9, 119.5, 116.9, 112.2, 110.5, 110.0, 109.9, 40.1, 35.3, 29.4, 29.1. IR (ν_{max} , cm^{-1}) 2927 (m), 2142 (m), 1652 (m), 1548 (m), 1455 (s), 1309 (s), 1222 (s), 913 (m), 743 (s). HRMS (ESI/QTOF) m/z : $[\text{M} + \text{H}]^+$ Calcd for $\text{C}_{70}\text{H}_{48}\text{N}_7\text{O}_2^+$ 1018.3864; Found 1018.3866.

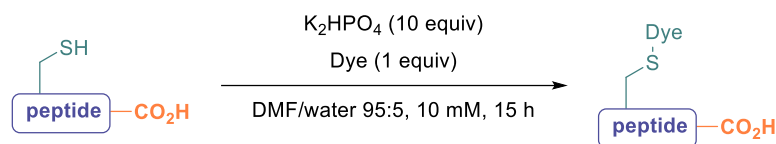
(2r,4s,5s)-2,4,6-Tri(9*H*-carbazol-9-yl)-5-(3-(5-(2-methylene-5-oxo-2,5-dihydro-1*H*-pyrrol-1-yl)pentyl)-9*H*-carbazol-9-yl)isophthalonitrile (7.28)



Following a modified reported procedure,^[291] **7.33** (9.3 mg, 0.046 mmol, 2 equiv) was stirred in HCl 0.1 M (0.2 mL) for 3 h at RT. NaHCO_3 was added until pH 7. HEPES buffer (0.5 M, pH 7.5, 0.2 mL) followed by a solution of **7.39** (20 mg, 0.023 mmol, 1 equiv) in MeOH (5 mL) were added and the mixture stirred for an hour at RT. The crude product was concentrated under vacuum and purified by preparative TLC DCM/methanol 9:1 to afford **7.28** as a yellow solid together with an unknown compound (2.6 mg, 0.0027 mmol, <12%). Larger scale synthesis should afford better purification. Characterization of the mixture of products is given for indication without assignment.

R_f (DCM/MeOH 95:5) = 0.9. (yellow spot on TLC). ^1H NMR (400 MHz, Chloroform- d) δ ^{13}C NMR (101 MHz, Chloroform- d) δ 8.22 (d, $J = 7.8$ Hz, 2H), 7.76 – 7.62 (m, 8H), 7.56 – 7.41 (m, 3H), 7.30 (d, $J = 3.6$ Hz, 1H), 7.20 (td, $J = 6.6, 2.2$ Hz, 4H), 7.13 – 7.04 (m, 9H), 6.98 (d, $J = 5.8$ Hz, 1H), 6.84 – 6.76 (m, 2H), 6.75 – 6.57 (m, 1H), 6.39 (dd, $J = 8.4, 1.7$ Hz, 1H), 6.23 (dd, $J = 5.7, 1.4$ Hz, 1H), 4.83 (d, $J = 12.4$ Hz, 1H), 4.06 – 3.92 (m, 2H), 3.67 – 3.55 (m, 2H), 2.50 – 2.46 (m, 2H), 2.37 – 2.29 (m, 2H), 1.70 – 1.62 (m, 2H), 1.50 – 1.43 (m, 4H). HRMS (ESI/QTOF) m/z : $[\text{M} + \text{Na}]^+$ Calcd for $\text{C}_{65}\text{H}_{43}\text{N}_7\text{NaO}^+$ 960.3421; Found 960.3418.

12.5.2 Scope on peptides



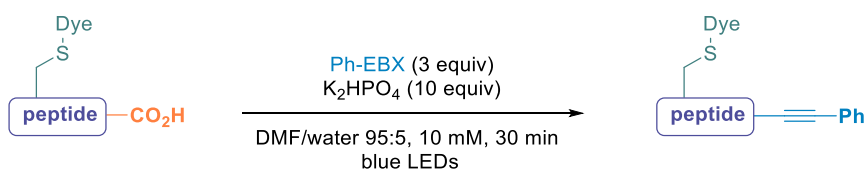
General procedure for the dye introduction

A 20 mM solution of the peptide in non-degassed DMF (150 μ L, 3.00 μ mol), a 22 μ M solution of dye in DMF (137 μ L, 3.0 μ mol, 1 equiv) and a 2 M solution of K₂HPO₄ in milli-Q purified water (15 μ L, 30 μ mol, 10 equiv) were placed into an Eppendorf and stirred at RT for 15 h, without protection from the light.

Intermediate samples were prepared by dilution of 10 μ L of the reaction mixture with 30 μ L of MeCN. At the end of the reaction, the crude was diluted with MeCN/water 1:1 (1 mL) and injected in RP-HPLC.

Isolation was performed by preparative RP-HPLC with injection of the diluted crude mixture, followed by lyophilisation.

The peptides are described as ODX-peptide-OH with X the number of the added dye.



General procedure for the proximity-induced decarboxylative alkynylation

A 20 mM solution of the intermediate peptide in non-degassed DMF (150 μ L, 3.00 μ mol), a 60 μ M solution of Ph-EBX (**2.5**) in DMF (75 μ L, 3.0 μ mol, 3.0 equiv), DMF (60 μ L) and a 2 M solution of K₂HPO₄ in milli-Q purified water (15 μ L, 30 μ mol, 10 equiv) were placed into a microwave vial. The vial was then capped and degassed by bubbling with argon for 1-2 min and the mixture was irradiated using blue light LEDs for 15 h at RT.

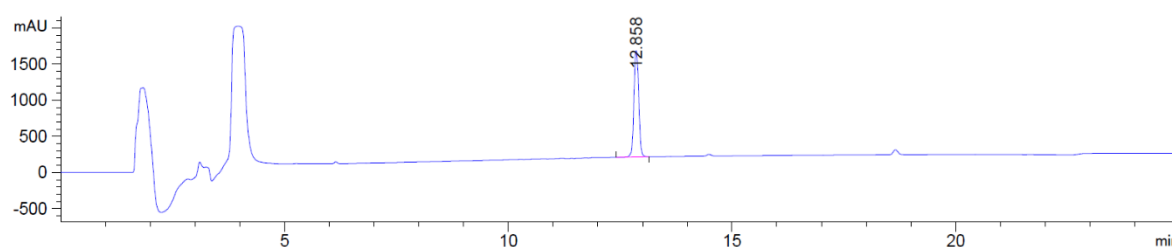
Intermediate samples were prepared by dilution of 10 μ L of the reaction mixture with 30 μ L of MeOH. At the end of the reaction, the crude was diluted with MeCN/water 1:1 (1 mL) and injected in RP-HPLC. The yields were determined as the ratio of $A_{\text{prod}}/A_{\text{total}}$ where A_{prod} = area in mAU of the product peak and A_{total} = area in mAU of all peptides products (product, starting material, and side-products if present).

Isolation was performed by preparative RP-HPLC with injection of the diluted crude mixture, followed by lyophilisation.

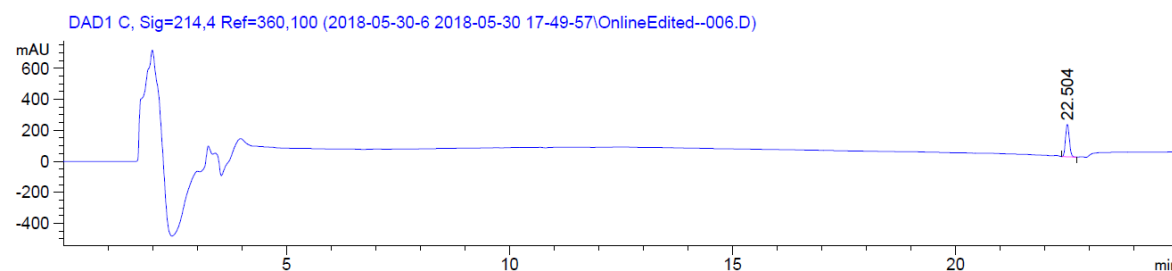
The peptides are described as as DX-peptide-AH with X the number of the added dye.

Reference HPLC-UV chromatograms of reagents at 214 nm

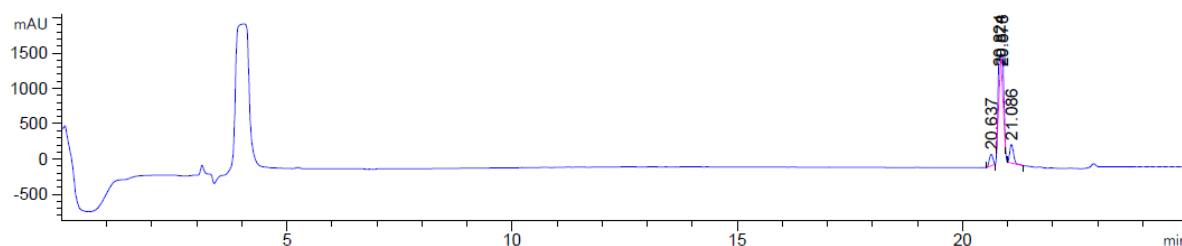
PhEBX (2.5)



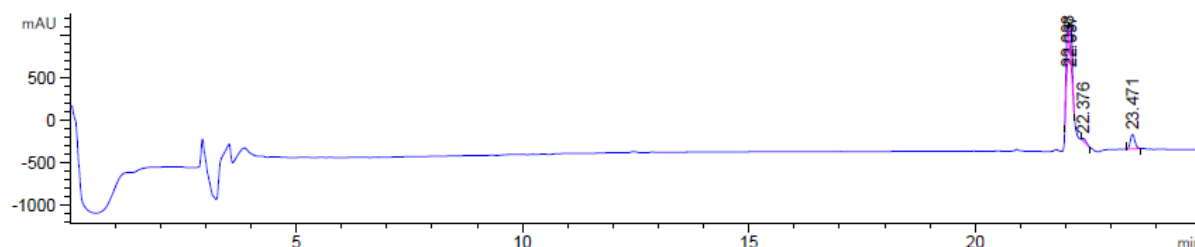
4CzIPN (2.23)



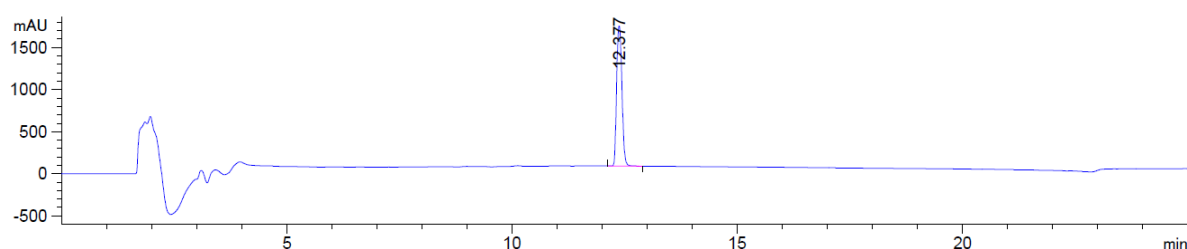
N-(2-(2-(2-((*E*)-4-oxo-4-phenylbut-2-enamido)ethoxy)ethoxy)ethyl)-9-((1*S*,2*s*,4*r*)-2,4,6-tri(9*H*-carbazol-9-yl)-3,5-dicyanophenyl)-9*H*-carbazole-3-carboxamide (**7.1**)



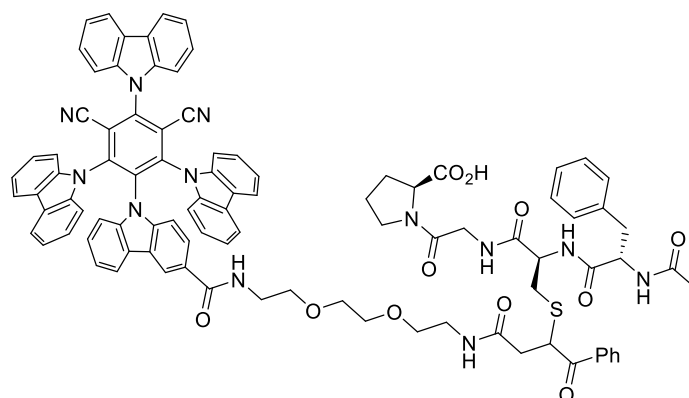
(*E*)-4-oxo-4-phenyl-N-(4-(9-((1*S*,2*S*,4*r*)-2,4,6-tri(9*H*-carbazol-9-yl)-3,5-dicyanophenyl)-9*H*-carbazol-3-yl)butyl)but-2-enamide (**7.29**)



Iodobenzoic acid (**2.10**)

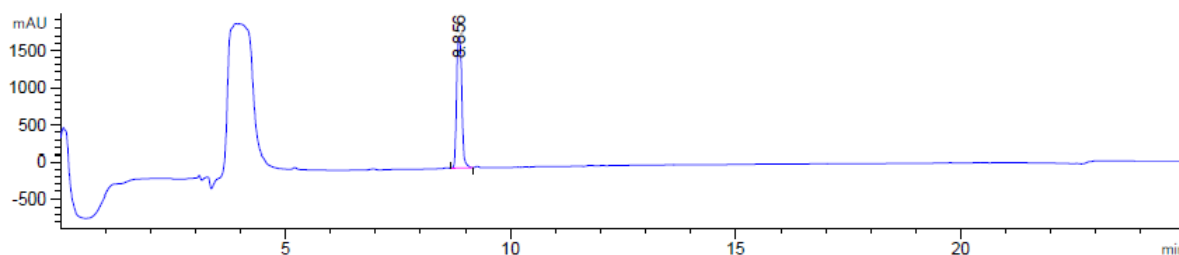


For clarity in the reaction chromatograms, the peaks of peptide-based products are indicated by an arrow. In all reactions, iodobenzoic acid, Ph-EBX and the catalyst were present, together with side products at 10.524, 16.212 and 18.220 min. The alkyne dimer and alkynylated DMF were identified by NMR but low ionization did not allow confirmation of their retention time.

DX-Ac-Phe-Cys-Gly-Pro-OH (7.17)

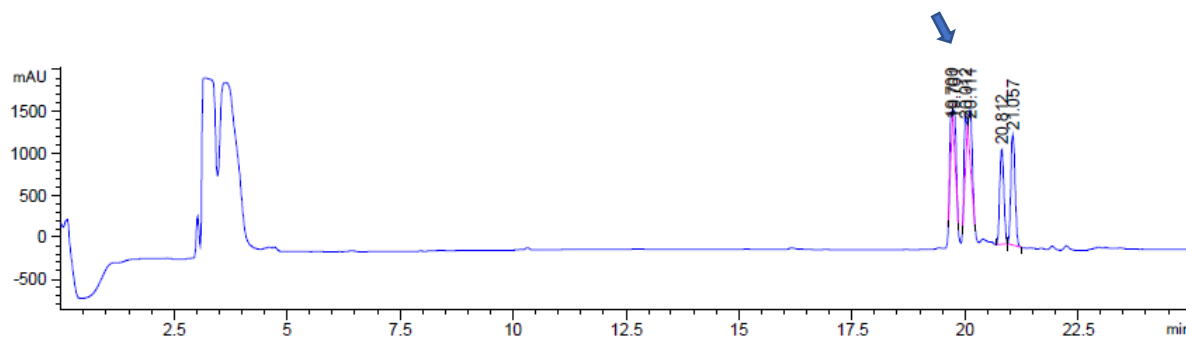
Following the general procedure, Ac-Phe-Cys-Gly-Pro-OH (**7.16**) afforded **7.17** in more than 95% yield as a mixture of diastereoisomers (retention time 19.728 and 20.053) in 3 h reaction time on 3 μ mol scale.

HRMS (nanochip-ESI/LTQ-Orbitrap) m/z : $[M + H_2]^{+2}$ Calcd for $C_{94}H_{82}N_{12}O_{11}S^{+2}$ 793.2968; Found 793.2954.

Ac-Phe-Cys-Gly-Pro-OH (7.16)

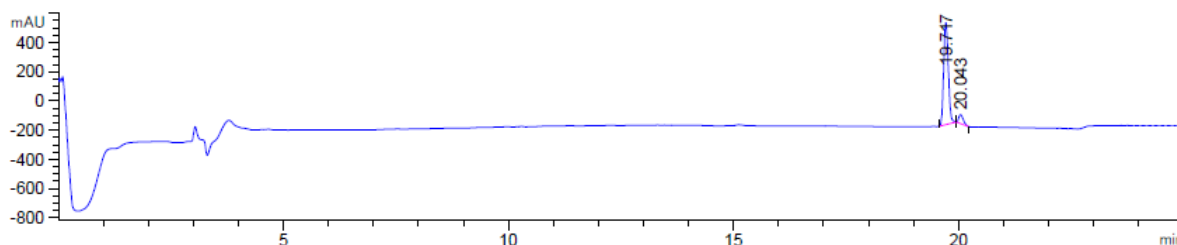
HRMS (ESI/QTOF) m/z : $[M + Na]^+$ Calcd for $C_{21}H_{28}N_4NaO_6S^+$ 487.1622; Found 487.1628.

HPLC-UV chromatogram at 214 nm of the crude reaction mixture

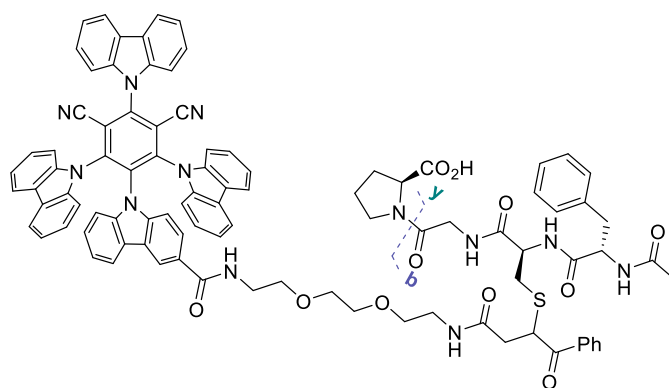


The crude was purified by preparative HPLC using a gradient of 100% A to 100% B in 20 minutes, followed by 10 min of B (see general methods) to afford **7.17** as a yellow solid (1.7 mg, 1.1 μ mol, 36%).

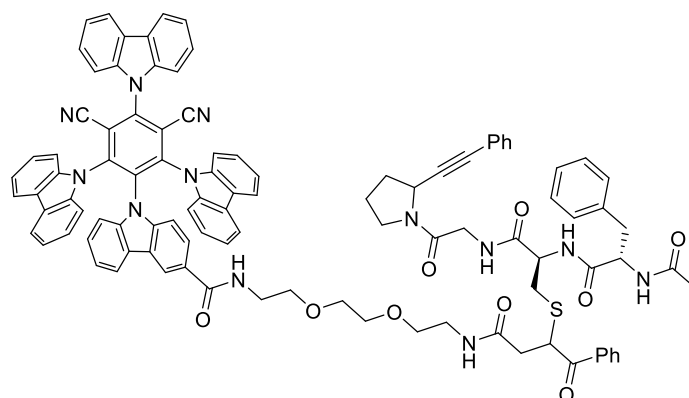
HPLC-UV chromatogram at 214 nm of **7.17**



MSMS (nanochip-ESI/LTQ-Orbitrap): selected ion 487.1628. Identified **b** and **y** ions are reported in the table below.



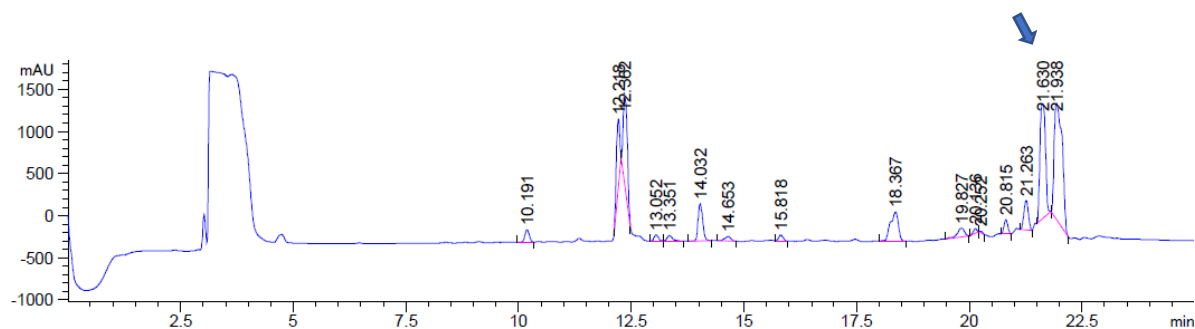
	F	C*	G	P
N-terminal	1	2	3	4
b	-	1413.50	1470.52	-
C-terminal	4	3	2	1
y	1543.58	1396.51	-	-

DX-Ac-Phe-Cys-Gly-Pro-AH (7.18)

Following the general procedure, DX-Ac-Phe-Cys-Gly-Pro-OH (**7.17**) afforded **7.18** in more than 95% yield as a mixture of diastereoisomers (retention time 21.630 and 21.938) with 30 min reaction time on 1 μ mol scale.

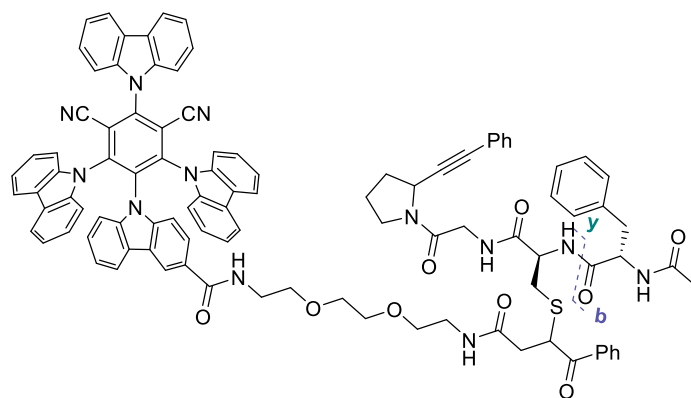
HRMS (ESI/QTOF) m/z : $[M + Na]^+$ Calcd for $C_{101}H_{84}N_{12}NaO_9S^+$ 1663.6097; Found 1663.6067.

HPLC-UV chromatogram at 214 nm of the crude reaction mixture

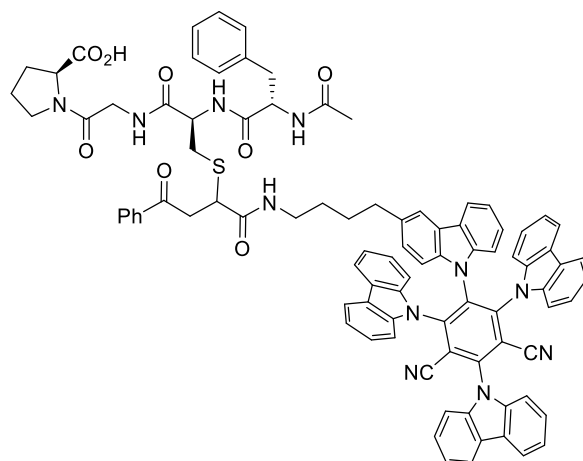


The crude was purified by preparative HPLC using a gradient of 100% A to 100% B in 20 minutes, followed by 10 min of B (see general methods).

MSMS (nanochip-ESI/LTQ-Orbitrap): selected ion 1663.6067. Identified **b** and **y** ions are reported in the table below.

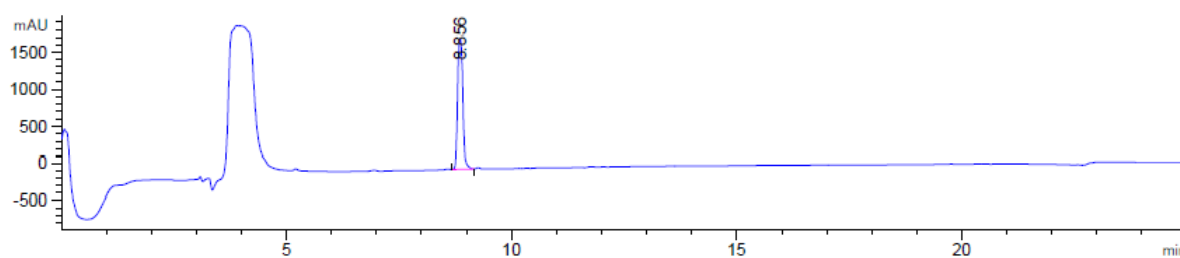


	F	C*	G	P*
N-terminal	1	2	3	4
b	-	1435.48	1492.50	-
C-terminal	4	3	2	1
y	1622.60	1474.53	-	-

DX-Ac-Phe-Cys-Gly-Pro-OH (7.41)

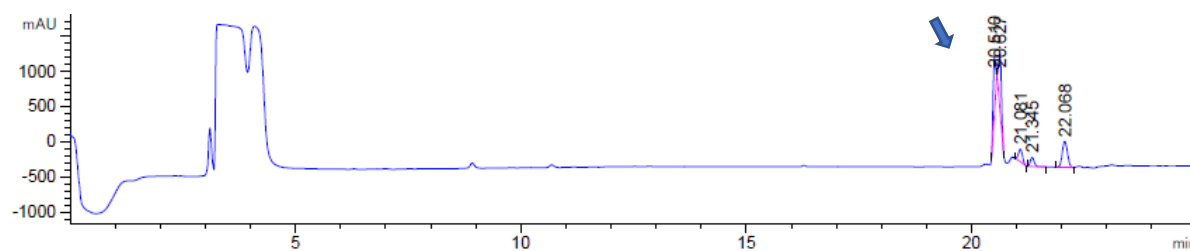
Following the general procedure, Ac-Phe-Cys-Gly-Pro-OH (**7.16**) afforded **7.41** in more than 95% yield as a mixture of diastereoisomers (retention time 19.728 and 20.053) in 15 h reaction time on 3 μ mol scale.

HRMS (nanochip-ESI/LTQ-Orbitrap) m/z : $[M + H]^+$ Calcd for $C_{91}H_{76}N_{11}O_8S^+$ 1482.5594; Found 1482.5649.

Ac-Phe-Cys-Gly-Pro-OH (7.16)

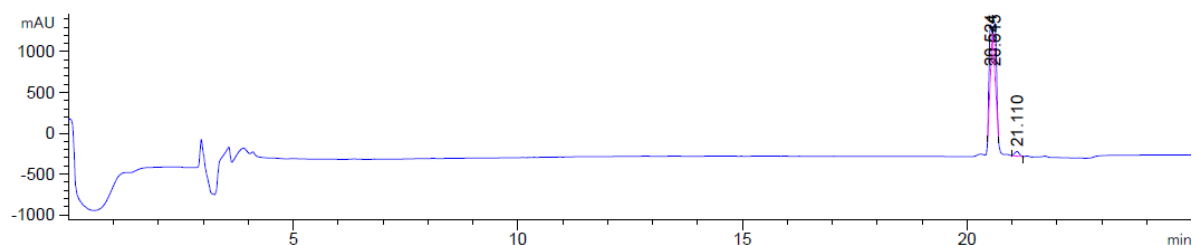
HRMS (ESI/QTOF) m/z : $[M + Na]^+$ Calcd for $C_{21}H_{28}N_4NaO_6S^+$ 487.1622; Found 487.1628.

HPLC-UV chromatogram at 214 nm of the crude reaction mixture

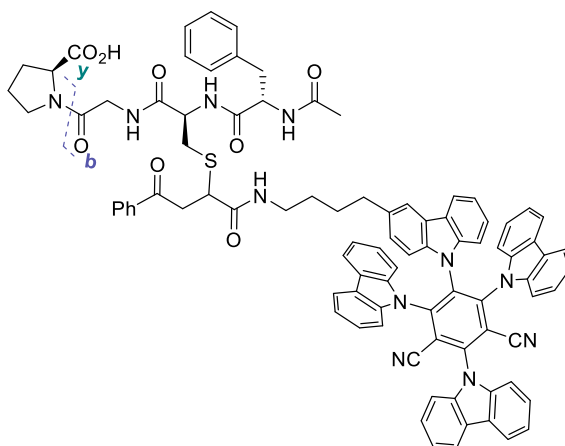


The crude was purified by preparative HPLC using a gradient of 100% A to 100% B in 20 minutes, followed by 10 min of B (see general methods). to afford **7.41** as a yellow solid (1.4 mg, 0.94 μ mol, 32%).

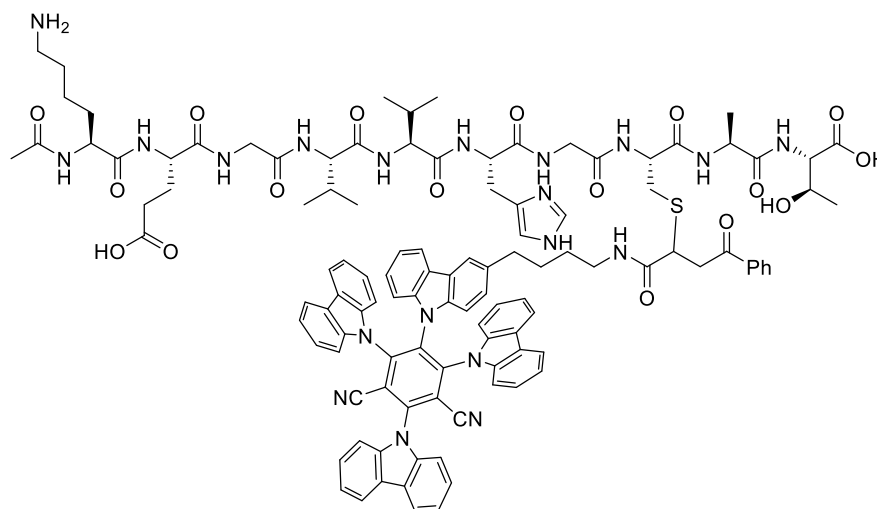
HPLC-UV chromatogram at 214 nm of **7.41**



MSMS (nanochip-ESI/LTQ-Orbitrap): selected ion 1482.5649. Identified **b** and **y** ions are reported in the table below.

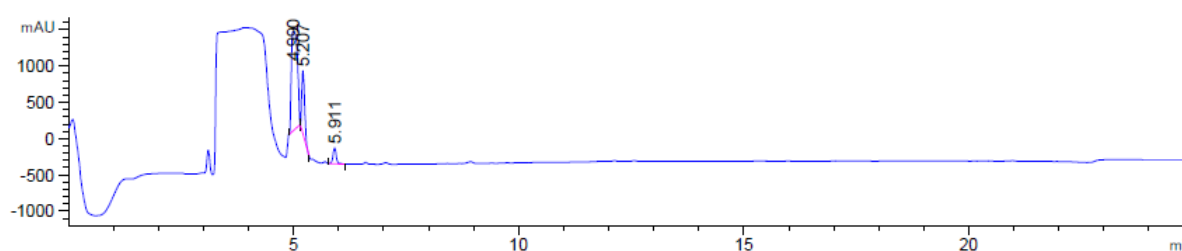


	F	C*	G	P
N-terminal	1	2	3	4
b	-	1310.47	1367.50	-
C-terminal	4	3	2	1
y	1440.55	1293.48	-	-

DX-Ac-Lys-Glu-Gly-Val-Val-His-Gly-Cys-Ala-Thr-OH (7.43)

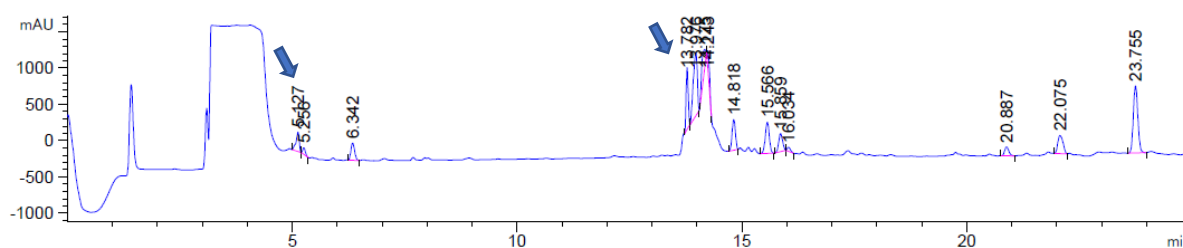
Following the general procedure, Ac-Lys-Glu-Gly-Val-Val-His-Gly-Cys-Ala-Thr-OH (**7.42a**) afforded **7.43** in more than 95% yield as a mixture of diastereoisomers (retention time 13.782 to 14.249) on 7.9 μ mol scale. Due to the impure batch of organic dye **7.29**, side-products of similar retention time were detected.

HRMS (nanochip-ESI/LTQ-Orbitrap) m/z : $[M + H]^{+2}$ Calcd for $C_{113}H_{120}N_{20}O_{17}S^{+2}$ 1030.4425; Found 1030.4470.

Ac-Lys-Glu-Gly-Val-Val-His-Gly-Cys-Ala-Thr-OH (7.42a)

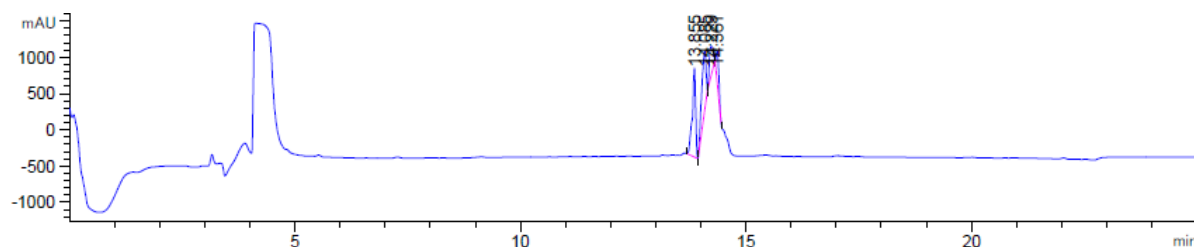
HRMS (ESI/QTOF) m/z : $[M + H]^+$ Calcd for $C_{43}H_{72}N_{13}O_{15}S^+$ 1042.4986; Found 1042.5001.

HPLC-UV chromatogram at 214 nm of the crude reaction mixture

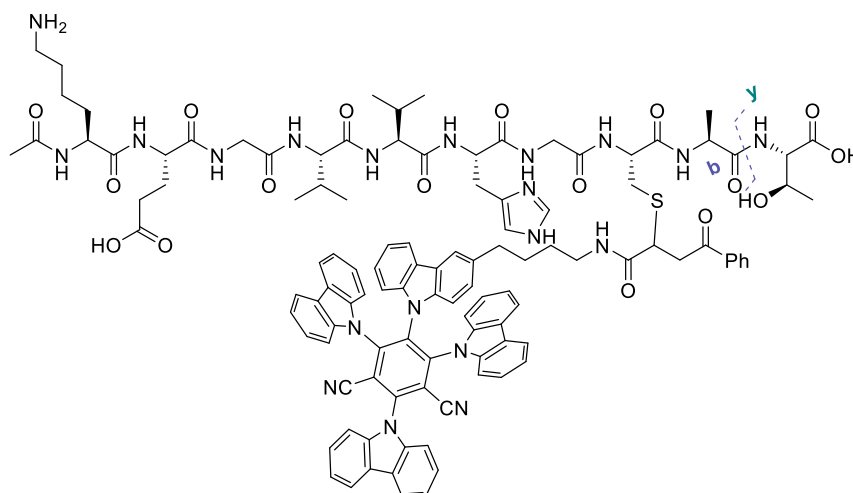


The crude was purified by preparative HPLC using a gradient of 100% A to 100% B in 20 minutes, followed by 10 min of B (see general methods) to afford **7.43** as a yellow solid (7.6 mg, 3.3 μ mol, 42%).

HPLC-UV chromatogram at 214 nm of **7.43**

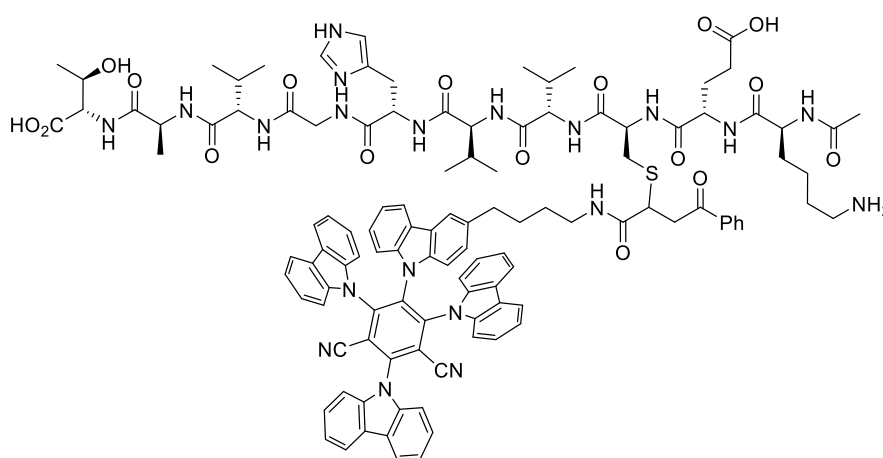


MSMS (nanochip-ESI/LTQ-Orbitrap): selected ion 1030.4470. Identified **b** and **y** ions are reported in the table below.



	K	E	G	V	V	H	G	C*	A	T
N-terminal	1	2	3	4	5	6	7	8	9	10
b	-	300.16	357.18	456.25	555.31	692.37	749.39	1870.79	1941.82	-
C-terminal	10	9	8	7	6	5	4	3	2	1
y	-	1890.78	1761.73	1704.71	1605.64	1505.57	1368.51	1311.49	-	-

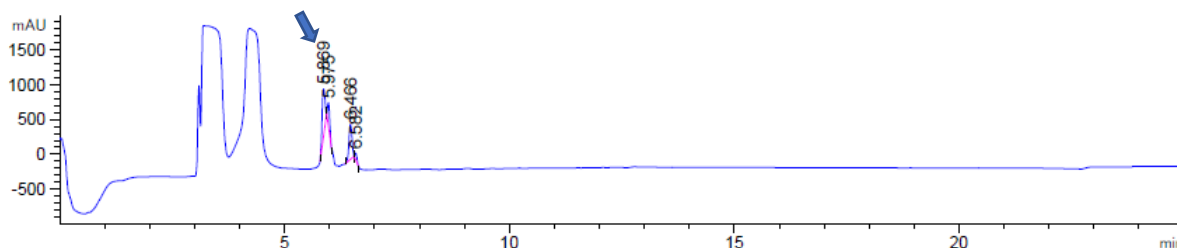
DX-Ac-Lys-Glu-Cys-Val-Val-His-Gly-Val-Ala-Thr-OH (7.44)



Following the general procedure, Ac-Lys-Glu-Cys-Val-Val-His-Gly-Val-Ala-Thr-OH (**7.42b**) afforded **7.44** in more than 95% yield as a mixture of diastereoisomers (retention time 13.827 to 14.482) on 6.1 μ mol scale. Due to the impure batch of organic dye **7.29**, side-products of similar retention time were detected.

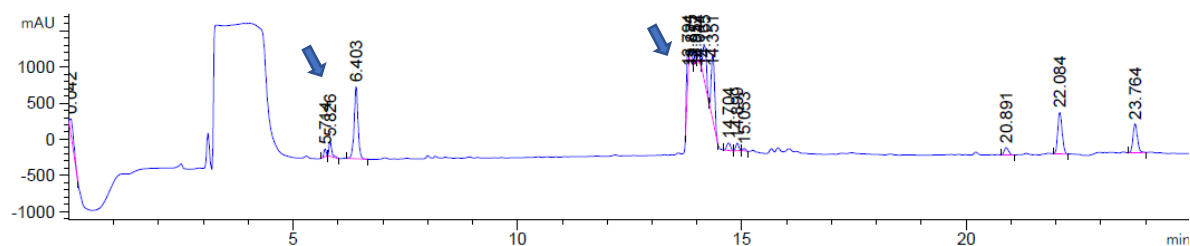
HRMS (ESI/QTOF) m/z : $[M + H_2]^{+2}$ Calcd for $C_{116}H_{126}N_{20}O_{17}S^{+2}$ 1051.4660; Found 1051.4664.

Ac-Lys-Glu-Cys-Val-Val-His-Gly-Val-Ala-Thr-OH (7.42b)



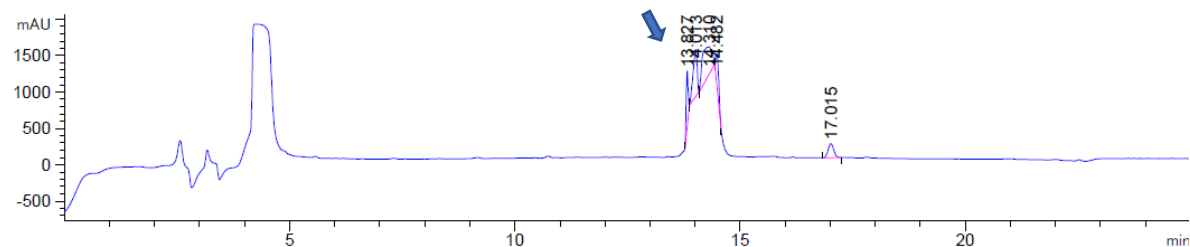
HRMS (ESI/QTOF) m/z : $[M + H]^+$ Calcd for $C_{46}H_{78}N_{13}O_{15}S^+$ 1084.5456; Found 1084.5463.

HPLC-UV chromatogram at 214 nm of the crude reaction mixture



The crude was purified by preparative HPLC using a gradient of 100% A to 100% B in 20 minutes, followed by 10 min of B (see general methods) to afford **7.44** as a yellow solid (6.3 mg, 2.7 μ mol, 44%).

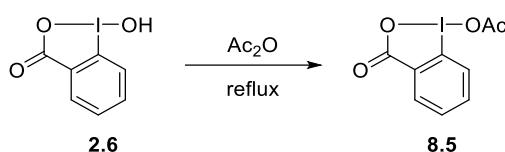
HPLC-UV chromatogram at 214 nm of **7.44**



12.6 Photoredox-catalyzed sequential decarboxylative-oxidation-arylation of peptides C-terminus

12.6.1 Preparation of reagents and catalysts

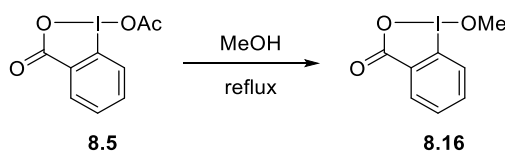
1-Acetoxy-1,2-benziodoxol-3-(1H)-one (**BI-OAc**, **8.5**)



Following a reported procedure,^[184] 1-hydroxy-1,2-benziodoxol-3-(1H)-one (**2.6**, 10.3 g, 39.1 mmol, 1.00 equiv) was suspended in acetic anhydride (35 mL) and heated to reflux for 30 minutes. The resulting clear, slightly yellow solution was slowly let to warm up to room temperature and then cooled to 0 °C for 30 minutes. The white suspension was filtered and the filtrate was again cooled to 0 °C for 30 minutes. The suspension was once again filtered and the combined two batches of solid product were washed with hexane (2 x 20 mL) and dried in vacuo affording **8.5** (10.8 g, 35.3 mmol, 90%) as a white solid.

¹H NMR (400 MHz, Chloroform-*d*) δ 8.24 (dd, 1H, $J = 7.6, 1.6$ Hz, ArH), 8.00 (dd, 1H, $J = 8.3, 1.0$ Hz, ArH), 7.92 (ddd, 1H, $J = 8.4, 7.2, 1.6$ Hz, ArH), 7.71 (td, 1H, $J = 7.3, 1.1$ Hz, ArH), 2.25 (s, 3H, COCH₃). ¹³C NMR (100 MHz, Chloroform-*d*) δ 176.5, 168.2, 136.2, 133.3, 131.4, 129.4, 129.1, 118.4, 20.4. The values of the NMR spectra are in accordance with reported literature data.^[184]

1-Methoxy-1,2-benziodoxol-3-(1H)-one (**BI-OMe**, **8.16**)



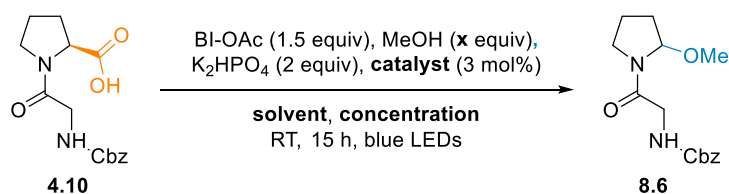
Following a reported procedure,^[318] BI-OAc (**8.5**, 1.0 g, 3.3 mmol, 1.0 equiv) was refluxed in MeOH (10 mL) for 15 min until a clear, colorless solution was obtained. The mixture was cooled to room temperature and then to -20°C. The precipitate was filtered, washed with a minimal

amount of MeOH, and dried under vacuum. BI-OMe (0.69 g, 2.5 mmol, 76%) was obtained as white crystals.

^1H NMR (400 MHz, Chloroform-*d*) δ 8.27 (dd, J = 7.6, 1.6 Hz, 1H, Ar*H*), 7.90 (ddd, J = 8.5, 7.2, 1.6 Hz, 1H, Ar*H*), 7.76 (dd, J = 8.3, 1.0 Hz, 1H, Ar*H*), 7.69 (td, J = 7.4, 1.0 Hz, 1H, Ar*H*), 4.27 (s, 3H, OMe). ^{13}C NMR (101 MHz, Chloroform-*d*) δ 168.1, 135.2, 133.0, 131.1, 130.7, 126.0, 118.6, 62.4. Consistent with reported data.^[318]

12.6.2 Optimization

Optimization of the oxidative decarboxylation



Degassed solvent was added in a 10 mL test tube containing a teflon coated stirring bar, Cbz-Gly-Pro (**4.10**) (31 mg, 0.10 mmol, 1.0 equiv), R-EBX (0.15 mmol, 1.5 equiv), the base and the catalyst under a nitrogen atmosphere. The reaction mixture was irradiated using blue light LEDs at RT.

Procedure for HPLC yields:

The reaction was monitored by dilution of 50 μL of the crude with 950 μL of acetonitrile. The yield was estimated by the absorbance of product in comparison to the overall absorbance of product, unreacted starting material and side-products if any.

Procedure for isolated yields:

The crude mixture was diluted with 10 mL of sat. NaHCO_3 and extracted with diethyl ether (3 x 50 mL). The combined organic layers were washed with brine (3 x 20 mL), dried over MgSO_4 , filtered and concentrated under vacuum. The crude product was purified by preparative TLC (DCM/ethyl acetate 8:2).

Table 27. Optimization of the oxidative decarboxylation on dipeptides

Entry	Solvent	Concentration (mM)	Catalyst	Base (equiv)	Alcohol (equiv)	HPLC yield (%) ^[a]
1	DMF	10	4CzIPN (2.23)	K ₂ HPO ₄ (2)	MeOH (50)	46
2	DMF	10	4CzIPN (2.23)	K ₂ HPO ₄ (2)	MeOH (50)	59
3	DMF	10	Ru(bpy) ₃ .Cl ₂ (2.14)	K ₂ HPO ₄ (2)	MeOH (10)	78
4	DMF	50	Ru(bpy) ₃ .Cl ₂ (2.14)	K ₂ HPO ₄ (2)	MeOH (10)	82
5	DMF	50	Ru(bpy) ₃ .Cl ₂ (2.14)	K ₂ HPO ₄ (2)	MeOH (5)	>95
6	DMF	50	Ru(bpy) ₃ .Cl ₂ (2.14)	K ₂ HPO ₄ (2)	MeOH (2)	>95
7	DMF	50	Ru(bpy) ₃ .Cl ₂ (2.14)	K ₂ HPO ₄ (2)	MeOH (5)	17
8 ^[b]	DMF	50	Eosin Y (2.17)	K ₂ HPO ₄ (2)	MeOH (5)	27
9 ^[b]	DMF	50	Rhodamine B (6.1)	K ₂ HPO ₄ (2)	MeOH (5)	35
10 ^[b]	DMF	50	Rose Bengal (8.7)	K ₂ HPO ₄ (2)	MeOH (5)	45
11	MeCN	50	4DPAIPN (2.22)	K ₂ HPO ₄ (2)	MeOH (5)	>95
12	MeCN	50	Ru(bpy) ₃ .Cl ₂ (2.14)	-	MeOH (5)	>95 (68) ^[c]
13	DCE	50	Ru(bpy) ₃ .Cl ₂ (2.14)	-	MeOH (5)	>95
15 ^[d]	MeCN	50	Ru(bpy) ₃ .Cl ₂ (2.14)	-	5	81

^[a] Ratio of integration at 214 nm by RP-HPLC, ^[b] green LEDs, ^[c] isolated yield, ^[d] no desassing.

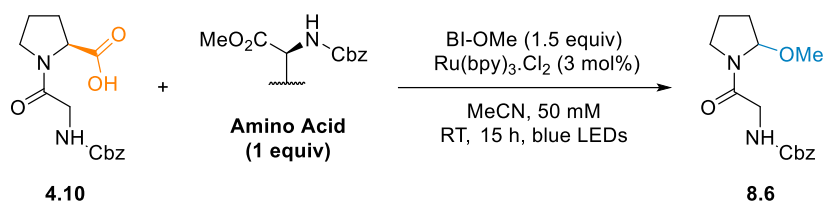
Control experiments were carried out and only traces of the desired product were observed in the absence of light or catalyst.

12.6.3 Robustness experiments

Degassed MeCN (2 mL) was added in a 5 mL test tube containing Cbz-Gly-Pro (**4.10**) (92 mg, 0.10 mmol, 1.0 equiv), the protected amino acid (0.1 mmol, 1 equiv), BI-OMe (**8.16**) (42 mg, 0.45 mmol, 1.5 equiv) and Ru(bpy)₃.Cl₂ (**2.14**) (2.2 mg, 3.00 μmol, 3 mol%) under a nitrogen atmosphere. The reaction mixture was irradiated using blue light LEDs for 15 h at RT.

The reaction was monitored by dilution of 50 μL of the crude with 950 μL of acetonitrile. The yield was estimated by the absorbance of product in comparison to the overall absorbance of product, unreacted starting material and side-products if any.

Table 28. Robustness experiments



Entry	Amino acid (1 equiv)	HPLC yield (%)
1	Cbz-Met-OMe	15
2	Cbz-Ser-OMe	90 ^a
3	Cbz-His-OMe	25
4	Cbz-Arg-OMe	>95
5	Cbz-Tyr-OMe	<5
6	Cbz-Trp-OMe	<5
7	Cbz-Gln-OMe	36
8	Cbz-Lys-OMe	<5
9	Cbz-Asp-OMe	>95
10	Cbz-Cys-OMe	62

^a + 10% of Serine addition on Z-Gly-Pro (x).

12.6.4 Scope on dipeptides

General procedure 1 for the oxidative decarboxylation of dipeptides

Degassed MeCN (6 mL) was added in a 10 mL test tube containing Cbz-Gly-Pro (**4.10**) (92 mg, 0.30 mmol, 1.0 equiv), BI-OMe (**8.16**) (125 mg, 0.450 mmol, 1.50 equiv) and Ru(bpy)₃.Cl₂ (**2.14**) (5.76 mg, 9.00 μmol, 3 mol%) under a nitrogen atmosphere. The reaction mixture was irradiated using blue light LEDs for 15 h at RT.

The reaction was monitored by dilution of 50 μL of the crude with 950 μL of acetonitrile.

The crude mixture was diluted with 10 mL of sat. NaHCO₃ and extracted with diethyl ether (3 x 30 mL). The combined organic layers were washed with brine (10 mL), dried over MgSO₄, filtered and concentrated under vacuum. The crude product was purified by column chromatography DCM to DCM/ethyl acetate on deactivated silica.

General procedure 2 for the oxidative decarboxylation of dipeptides

Degassed MeCN (6 mL) was added in a 10 mL test tube containing Cbz-Gly-Pro (**4.10**) (92 mg, 0.30 mmol, 1.0 equiv), BI-OAc (**8.5**) (138 mg, 0.450 mmol, 1.50 equiv), the alcohol (0.60 mmol, 2.0 equiv) and Ru(bpy)₃.Cl₂ (**2.14**) (5.76 mg, 9.00 μmol, 3 mol%) under a nitrogen atmosphere. The reaction mixture was irradiated using blue light LEDs for 15 h at RT.

The reaction was monitored by dilution of 50 μL of the crude with 950 μL of acetonitrile.

The crude mixture was diluted with 10 mL of sat. NaHCO₃ and extracted with diethyl ether (3 x 30 mL). The combined organic layers were washed with brine (10 mL), dried over MgSO₄, filtered and concentrated under vacuum. The crude product was purified by column chromatography DCM to DCM/ethyl acetate on deactivated silica.

General procedure 3 for the decarboxylative arylation of dipeptides with phenols

Degassed DCE (6 mL) was added in a 10 mL test tube containing Cbz-Gly-Pro (**4.10**) (92 mg, 0.30 mmol, 1.0 equiv), BI-OAc (**8.5**) (138 mg, 0.450 mmol, 1.50 equiv) and Ru(bpy)₃.Cl₂ (**2.14**) (5.76 mg, 9.00 μmol, 3 mol%) under a nitrogen atmosphere. The reaction mixture was irradiated using blue light LEDs for 15 h at RT.

The reaction was monitored by dilution of 50 μL of the crude with 950 μL of acetonitrile.

The phenol (0.45 mmol, 1.5 equiv) was added and the reaction mixture degassed by Ar bubbling before cooling at 0°C. $\text{BF}_3\cdot\text{OEt}_2$ (158 μL , 0.600 mmol, 2.00 equiv) was added dropwise and the mixture stirred for 2 h at 0 °C.

The crude mixture was diluted with 10 mL of sat. NaHCO_3 and extracted with diethyl ether (3 x 30 mL). The combined organic layers were washed with brine (10 mL), dried over MgSO_4 , filtered and concentrated under vacuum. The crude product was purified by column chromatography DCM to DCM/ethyl acetate.

General procedure 4 for the decarboxylative arylation of dipeptides with indoles

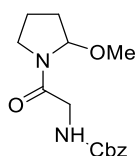
Degassed MeCN (6 mL) was added in a 10 mL test tube containing Cbz-Gly-Pro (**4.10**) (92 mg, 0.30 mmol, 1.0 equiv), AcOBX (**8.5**) (150 mg, 0.450 mmol, 1.50 equiv) and $\text{Ru}(\text{bpy})_3\cdot\text{Cl}_2$ (**2.14**) (5.76 mg, 9.00 μmol , 3 mol%) under a nitrogen atmosphere. The reaction mixture was irradiated using blue light LEDs for 15 h at RT.

The reaction was monitored by dilution of 50 μL of the crude with 950 μL of acetonitrile.

The indole (0.315 mmol, 1.05 equiv) was added and TFA (23 μL , 0.30 mmol, 1.0 equiv) was added dropwise and the mixture stirred for 1 h at RT.

The crude mixture was diluted with 10 mL of sat. NaHCO_3 and extracted with diethyl ether (3 x 30 mL). The combined organic layers were washed with brine (10 mL), dried over MgSO_4 , filtered and concentrated under vacuum. The crude product was purified by column chromatography DCM to DCM/ethyl acetate on deactivated silica.

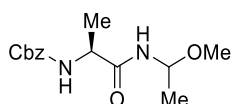
Benzyl (2-(2-methoxypyrrolidin-1-yl)-2-oxoethyl)carbamate (**8.6**)



Following General Procedure 1 and starting with Cbz-Gly-Pro (**4.10**) (92.0 mg, 0.300 mmol, 1.00 equiv), **8.6** was obtained after column chromatography DCM to DCM/ethyl acetate 8:2 as a pale yellow oil (65.8 mg, 0.225 mmol, 75%).

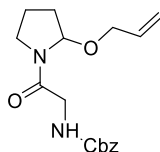
R_f (DCM/ethyl acetate 7:3): 0.3. ¹H NMR (400 MHz, Chloroform-*d*, 1:1 mixture of rotamers (R¹/R²)) δ 7.40 – 7.26 (m, 5H, ArH, (R¹+R²)), 5.70 (s, 1H, NH, (R¹+R²)), 5.43 (d, *J* = 4.9 Hz, 0.5H, NCHCOMe (R¹)), 5.12 (s, 2H, OCH₂Ph, (R¹+R²)), 4.96 (d, *J* = 4.5 Hz, 0.5H, NCHCOMe (R²)), 4.18 – 4.05 (m, 1H, NC(O)CH₂NHCbz (R¹)), 4.05 – 3.91 (m, 1H, NC(O)CH₂NHCbz (R²)), 3.67 (ddd, *J* = 11.3, 8.4, 2.3 Hz, 0.5H, NCH₂, (R¹)), 3.58 – 3.48 (m, 0.5H, NCH₂, (R²)), 3.38 (s, 1.5H, OCH₃, (R¹)), 3.43 – 3.32 (m, 1H, NCH₂, (R¹+R²)), 3.31 (s, 1.5H, OCH₃, (R²)), 2.24 – 1.66 (m, 4H, NCH₂(CH₂)₂CH, (R¹+R²)). ¹³C NMR (101 MHz, Chloroform-*d*, mixture of rotamers, signals not fully resolved) δ 168.3, 168.2, 156.2, 156.2, 136.4, 136.3, 128.4, 128.0, 127.9, 88.2, 87.5, 66.8, 66.8, 56.6, 54.2, 45.8, 44.8, 43.4, 42.9, 31.2, 30.7, 22.7, 20.7. IR (ν_{max}, cm⁻¹) 3324 (m), 2980 (m), 2886 (m), 2339 (w), 1718 (s), 1655 (s), 1520 (m), 1451 (m), 1246 (s), 1170 (m), 1055 (s), 914 (m), 826 (w), 741 (m), 699 (m). HRMS (ESI/QTOF) *m/z*: [M + Na]⁺ Calcd for C₁₅H₂₀N₂NaO₄⁺ 315.1315; Found 315.1315.

Benzyl ((2S)-1-((1-methoxyethyl)amino)-1-oxopropan-2-yl)carbamate (**8.25**)

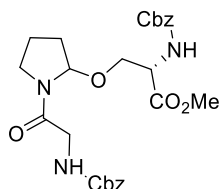


Following General Procedure 1 and starting with Cbz-Ala-Ala (**6.7a**) (88.0 mg, 0.300 mmol, 1.00 equiv), **8.25** was obtained after column chromatography DCM to DCM/ethyl acetate 8:2 as a white solid (56.7 mg, 0.203 mmol, 68%) and as a mixture of unresolved diastereoisomers.

R_f (DCM/ethyl acetate 7:3): 0.25. ¹H NMR (400 MHz, Chloroform-*d*, 6:4 mixture of rotamers (major/minor)) δ ¹H NMR (400 MHz, CDCl₃) δ 7.40 – 7.28 (m, 5H, ArH), 6.30 (bs, 1H, NH), 5.33 (s, 1H, NHCbz), 5.24 (dq, *J* = 9.2, 5.9, 3.3 Hz, 1H, NCHCOMe), 5.12 (s, 2H, OCH₂Ph), 4.22 (q, *J* = 6.8 Hz, 1H, NCHMe), 3.30 (s, 1H, OMe), 3.27 (s, 2H, OMe), 1.40 (t, *J* = 7.3 Hz, 3H, NCHMe), 1.30 (d, *J* = 5.9 Hz, 3H, CMeCOMe). δ ¹³C NMR (101 MHz, Chloroform-*d*) δ 172.3, 156.0, 136.0, 128.6, 128.3, 128.1, 78.4, 67.2, 55.6, 50.7, 28.9, 21.5, 18.7, 18.3. IR (ν_{max}, cm⁻¹) 3286 (m), 2981 (w), 1688 (s), 1651 (s), 1540 (s), 1453 (m), 1382 (w), 1324 (m), 1261 (s), 1135 (m), 1070 (m), 914 (m), 738 (s), 699 (s). HRMS (ESI/QTOF) *m/z*: [M + Na]⁺ Calcd for C₁₄H₂₀N₂NaO₄⁺ 303.1315; Found 303.1315.

Benzyl (2-(2-(allyloxy)pyrrolidin-1-yl)-2-oxoethyl)carbamate (8.19)

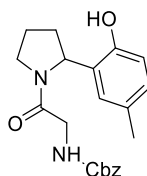
Following General Procedure 2 and starting with Cbz-Gly-Pro (**4.10**) (92.0 mg, 0.300 mmol, 1.00 equiv) and allyl alcohol (41 μ L, 0.60 mmol, 2.0 equiv), **8.19** was obtained after column chromatography DCM to DCM/ethyl acetate 9:1 as a pale yellow oil (73 mg, 0.229 mmol, 76%). R_f (DCM/ethyl acetate 7:3): 0.35. ^1H NMR (400 MHz, Chloroform- d , 55:45 mixture of rotamers (major/minor)) δ 7.42 – 7.27 (m, 5H, ArH (major+minor)), 5.97 – 5.81 (m, 1H, $\text{CH}_2\text{CH}=\text{CH}_2$ (major)), 5.72 (bs, 1H, NH (major+minor)), 5.56 (d, J = 4.9 Hz, 0.6H, NCHCOCH_2 (major)), 5.37 – 5.20 (m, 1.2H, $\text{CH}_2\text{CH}=\text{CH}_2$ (major)), 5.17 – 5.06 (m, 3.2H, $\text{CH}_2\text{CH}=\text{CH}_2$ (minor), OCH_2Ph (major+minor) and NCHCOCH_2 (minor)), 4.22 – 3.86 (m, 4H, $\text{CH}_2\text{CH}=\text{CH}_2$ and CH_2NHCbz (major+minor)), 3.68 (ddd, J = 11.3, 8.6, 2.0 Hz, 0.45H, NCH_2 (minor)), 3.57 – 3.48 (m, 0.55H, NCH_2 (major)), 3.44 – 3.25 (m, 1H, NCH_2 (major+minor)), 2.30 – 1.64 (m, 4H, $\text{NCH}_2(\text{CH}_2)_2\text{CH}$ (major+minor)). ^{13}C NMR (101 MHz, Chloroform- d , mixture of rotamers, signals not fully resolved) δ 168.2, 168.1, 156.2, 156.2, 136.4, 136.4, 136.3, 134.7, 133.5, 128.4, 128.0, 127.9, 117.9, 116.6, 86.8, 86.1, 70.2, 68.0, 66.9, 66.8, 66.8, 45.9, 44.9, 43.4, 43.1, 31.7, 31.5, 22.8, 20.7. IR (ν_{max} , cm^{-1}) 3331 (m), 2982 (m), 2898 (m), 1720 (s), 1657 (s), 1538 (m), 1451 (m), 1247 (s), 1171 (m), 1052 (s), 915 (m), 740 (m). HRMS (ESI/QTOF) m/z : $[\text{M} + \text{Na}]^+$ Calcd for $\text{C}_{17}\text{H}_{22}\text{N}_2\text{NaO}_4^+$ 341.1472; Found 341.1476.

(2S)-Methyl 2-(((benzyloxy)carbonyl)amino)-3-((1-(2-(((benzyloxy)carbonyl)amino)acetyl)pyrrolidin-2-yl)oxy)propanoate (8.21)

Following General Procedure 2 and starting with Cbz-Gly-Pro (**4.10**) (92.0 mg, 0.300 mmol, 1.00 equiv) and Cbz-Ser-OMe (114 mg, 0.450 mmol, 1.50 equiv), **8.21** was obtained after column chromatography DCM to DCM/ethyl acetate 1:1 as a pale yellow oil and a mixture of diastereoisomers (65.3 mg, 0.127 mmol, 42%).

R_f (DCM/ethyl acetate 7:3): 0.3. ¹H NMR (400 MHz, Chloroform-*d*, mixture of rotamers of diastereoisomers)³⁵ δ 7.40 – 7.25 (m, 10H, ArH), 6.05 (d, 0.3H, NH Ser), 5.93 (d, *J* = 8.4 Hz, 0.1H, NH Ser), 5.72 (bs, 1H, NH Gly), 5.65 (s, 0.4H, NH Ser), 5.47 (d, *J* = 4.8 Hz, 0.3H, NCHCOCH₂), 5.41 (d, *J* = 4.9 Hz, 0.4H, NCHCOCH₂), 5.12 (s, 4H, OCH₂ Gly+Ser), 5.09 – 5.05 (m, 0.3H, NCHCOCH₂), 4.59 – 4.49 (m, 0.3H, CHCO₂Me), 4.51 – 4.41 (m, 0.7H, CHCO₂Me), 4.12 – 3.78 (m, 4H, OCH₂ + CH₂NHCbz), 3.77 – 3.62 (m, 3H, CO₂Me), 3.59 – 3.19 (m, 2H, NCH₂(CH₂)₂CH), 2.19 – 1.61 (m, 4H, NCH₂(CH₂)₂CH). ¹³C NMR (101 MHz, Chloroform-*d*, mixture of rotamers of diastereoisomers, signals not fully resolved) δ 170.8, 170.7, 170.2, 168.5, 168.2, 156.2, 155.9, 136.3, 136.3, 136.2, 128.5, 128.4, 128.2, 128.1, 128.1, 128.0, 128.0, 127.9, 87.6, 87.2, 87.0, 86.7, 68.9, 68.6, 67.1, 67.0, 66.9, 66.3, 66.2, 54.6, 54.4, 54.3, 54.0, 52.8, 52.7, 52.5, 52.4, 45.9, 45.1, 44.9, 43.4, 43.4, 42.9, 42.8, 33.7, 31.5, 31.4, 31.1, 31.1, 22.7, 22.7, 20.7, 20.6, 20.4. IR (ν_{max}, cm⁻¹) 3324 (m), 2979 (m), 2885 (w), 1718 (s), 1658 (s), 1518 (m), 1436 (m), 1242 (m), 1054 (s), 914 (m), 738 (s), 699 (m). HRMS (ESI/QTOF) *m/z*: [M + Na]⁺ Calcd for C₂₆H₃₁N₃NaO₈⁺ 536.2003; Found 536.2014.

Benzyl (2-(2-(2-hydroxy-5-methylphenyl)pyrrolidin-1-yl)-2-oxoethyl)carbamate (**8.17**)



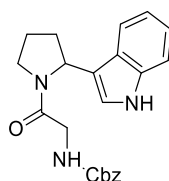
Following General Procedure X and starting with Cbz-Gly-Pro (**4.10**) (92.0 mg, 0.300 mmol, 1.00 equiv) and *p*-cresol (**x**) (49.0 mg, 0.450 mmol, 1.50 equiv), **8.17** was obtained after column chromatography DCM to DCM/ethyl acetate 7:3 as a pale yellow amorphous solid (68.0 mg, 0.185 mmol, 62%).

R_f (DCM/ethyl acetate 7:3): 0.4. ¹H NMR (400 MHz, Chloroform-*d*, 7:3 mixture of rotamers (R¹/R²)) δ 8.94 (s, 1H, OH, R¹+R²), 7.33 (dt, *J* = 9.12, 4.58 Hz, 5H, ArH, R¹+R²), 6.94 (d, *J* = 8.14 Hz, 0.7H, ArH, R¹), 6.89 (s, 0.7H, ArH, R¹), 6.82 (d, *J* = 7.62 Hz, 0.3H, ArH, R²), 6.76 (d, *J* = 8.14 Hz, 0.7H, ArH, R¹), 6.66 (s, 0.3H, ArH, R²), 6.51 (d, *J* = 7.98 Hz, 0.3H, ArH, R²), 5.79 (br s, 0.3H, NH, R²), 5.67 (br s, 0.7H, NH, R¹), 5.39 (dd, *J* = 7.52, 2.97 Hz, 0.7H, NCHCCOH, R¹), 5.17 (d, *J* = 7.67 Hz, 0.3H, NCHCCOH, R²), 5.11 (s, 1.4H, OCH₂Ph, R¹), 5.07 (s, 0.6H,

³⁵ Due to the complexity of the mixture, signals were not attributed to each rotamer and diastereoisomer.

OCH₂Ph, R²), 4.07 (td, J = 20.31, 18.91, 4.57 Hz, 1H, NC(O)CH₂NHCbz, R¹+R²), 3.92 (dd, J = 17.40, 4.01 Hz, 0.7H, NC(O)CH₂NHCbz, R¹), 3.79 (d, J = 6.02 Hz, 0.3H, NCH₂(CH₂)₂CHCCOH, R²), 3.73 (d, J = 8.14 Hz, 0.3H, NCH₂(CH₂)₂CHCCOH, R²), 3.67-3.51 (m, 1.4H, NCH₂(CH₂)₂CHCCOH, R¹), 3.43 (dd, J = 17.18, 3.29 Hz, 0.3H, NC(O)CH₂NHCbz, R²), 2.43-2.14 (m, 6H, NCH₂(CH₂)₂CH and CH₃, R¹+R²), 1.98-1.82 (m, 1H, NCH₂(CH₂)₂CH, R¹+R²). ¹³C NMR (101 MHz, Chloroform-*d*, mixture of rotamers, signals not fully resolved) δ 167.4, 156.6, 156.4, 153.1, 150.7, 136.4, 129.9, 129.6, 129.0, 128.6, 128.3, 128.1, 127.8, 127.4, 126.5, 125.9, 118.4, 115.6, 67.1, 55.9, 55.2, 47.5, 46.2, 43.6, 43.3, 34.4, 31.2, 30.5, 25.2, 21.8, 21.0, 20.9. IR (ν_{\max} , cm⁻¹) 3313 (w), 2978 (m), 2899 (w), 2360 (w), 1714 (s), 1640 (s), 1510 (m), 1436 (m), 1269 (m), 1055 (m), 738 (m), 699 (m). HRMS (ESI/QTOF) m/z : [M + Na]⁺ Calcd for C₂₁H₂₂N₂NaO₄⁺ 389.1472; Found 389.1472.

Benzyl (2-(2-(1H-indol-3-yl)pyrrolidin-1-yl)-2-oxoethyl)carbamate (8.10)



Following General Procedure X and starting with Cbz-Gly-Pro (**4.10**) (92.0 mg, 0.300 mmol, 1.00 equiv) and 1H-indole (**x**) (36.0 mg, 0.306 mmol, 1.02 equiv), **8.10** was obtained after column chromatography DCM to DCM/ethyl acetate 10:1 as a pale yellow amorphous solid (75.0 mg, 0.199 mmol, 66%).

R_f (DCM/ethyl acetate 7:3): 0.25. ¹H NMR (400 MHz, Chloroform-*d*, 7:3 mixture of rotamers(R¹/R²)) δ 8.42 (s, 0.3H, NH, R²), 8.35 (s, 0.7H, NH, R¹), 7.58 (d, J = 7.85 Hz, 0.3H, ArH, R²), 7.50 (d, J = 7.88 Hz, 0.7H, ArH, R¹), 7.39-7.27 (m, 6H, ArH, R¹+R²), 7.24-7.17 (m, 1H, ArH, R¹+R²), 7.17-7.09 (m, 1H, ArH, R¹+R²), 6.88-6.80 (m, 1H, ArH, R¹+R²), 5.80 (s, 0.3H, NH, R²), 5.66 (s, 0.7H, NH, R¹), 5.59 (dd, J = 7.12, 2.74 Hz, 0.3H, C(O)NCH, R²), 5.23-5.14 (m, 0.7H, C(O)NCH, R¹), 5.11 (s, 0.6H, OCH₂Ph, R²), 5.04 (s, 1.4H, OCH₂Ph, R¹), 4.04 (dd, J = 15.76, 4.59 Hz, 1.3H, NC(O)CH₂NHCbz, R¹+R²), 3.81 (dt, J = 11.96, 5.79 Hz, 0.7H, C(O)NCH₂, R¹), 3.69 (ddd, J = 21.33, 16.67, 6.03 Hz, 1.7H, NC(O)CH₂NHCbz, R¹ and C(O)NCH₂, R¹+R²), 3.53 (q, J = 8.08 Hz, 0.3H, C(O)NCH₂, R²), 2.36-1.85 (m, 4H, NCH₂CH₂CH₂CH, R¹+R²). ¹³C NMR (101 MHz, Chloroform-*d*, mixture of rotamers, signals not fully resolved) δ 167.7, 166.7, 156.5, 156.3, 137.0, 136.6, 128.6, 128.2, 128.1, 125.3, 124.8, 122.7, 122.2, 121.4, 121.3, 120.0, 119.6, 119.0, 118.7, 116.8, 116.7, 111.8, 111.6, 67.0, 66.9,

55.0, 54.9, 46.9, 46.0, 45.9, 43.7, 43.4, 34.5, 32.1, 24.2, 22.2. IR (ν_{max} , cm^{-1}) 3311 (m), 3046 (w), 2977 (m), 2876 (w), 1710 (s), 1638 (s), 1521 (m), 1455 (s), 1252 (s), 1165 (m), 1055 (m), 910 (m), 737 (s) HRMS (ESI/QTOF) m/z : $[\text{M} + \text{Na}]^+$ Calcd for $\text{C}_{22}\text{H}_{23}\text{N}_3\text{NaO}_3^+$ 400.1632; Found 400.1629.

13 Annexes

13.1 NMR spectra

See UBS stick.

13.2 List of publications

Research articles

E. Le Du,¹ M. Garreau,¹ J. Waser. Peptide Diversification through Photoredox-Catalyzed Oxidative C-Terminal Modification. *Manuscript submitted*.

E. Voutyritsa, M. Garreau, M. G. Kokotou, I. Triandallidi, J. Waser, C. Kokotos. Photochemical Functionalization of Heterocycles with EBX Reagents; C-H Alkynylation versus Deconstructive Ring Cleavage. *Chem. Eur. J.* *Just accepted*.

G. Barzanò, R. Mao, M. Garreau, J. Waser, X. Hu. Tandem photoredox and copper-catalyzed decarboxylative C(sp³)-N coupling of anilines and imines using an organic photocatalyst. *Org. Lett.* **2020**, 22, 5412-5416.

M. Garreau, F. Le Vaillant, J. Waser. C-Terminal Bioconjugation of Peptides through Photoredox-Catalyzed Decarboxylative Alkynylation. *Angew. Chem. Int. Ed.* **2019**, 58, 8182-8186.

F. Le Vaillant, M. Garreau, S. Nicolai, G. Gryn'ova, C. Corminboeuf, J. Waser. Fine-Tuned Organic Photoredox Catalysts for Fragmentation-Alkynylation Cascades of Cyclic Oxime Ethers. *Chem. Sci.* **2018**, 9, 5883-5889.

B. Riss, M. Garreau, P. Fricero, P. Podsiadly, N. Berton, S. Buchter. Total synthesis of TMS-*ent*-bisabolangelone. *Tetrahedron* **2017**, 73, 3202-3212.

H. Wachenfeldt, A. V. Polukeev, N. Loganathan, F. Paulsen, P. Röse, M. Garreau, O. F. Wendt, D. Strand. Cyclometallated Gold(III) Aryl-Pyridine Complexes as Efficient Catalysts for Three-Component Synthesis of Substituted Oxazoles. *Dalton Trans.* **2015**, 44, 5347-5353.

Preview

J. Ceballos,¹ M. Garreau,¹ J. Waser. An Alternative One-Electron Oxidation Strategy to Access Hypervalent Iodine Reagents. *Chem* **2019**, 5, 2287-2289.

Review

S. G. Amos,¹ M. Garreau,¹ L. Buzzetti,¹ J. Waser. Photocatalysis with Organic Dyes: Facile Access to Reactive Intermediates for Synthesis. *Beilstein J. Org. Chem.* **2020**, 16, 1163-1187.

¹: These authors contributed equally.



Address: Chemin des Deux-Ponts, 7 1007 Lausanne, Switzerland **Date of Birth:** 24 September 1993
Nationality: French **Email:** marion.ma.garreau@gmail.com **Mobile:** +41 (0) 765778920

EDUCATION

Ecole Polytechnique Fédérale de Lausanne (EPFL), Switzerland, Oct. 2016 - Nov. 2020.

PhD student in the Laboratory of Catalysis and Organic Synthesis (LCSO). Adviser: Prof. Jérôme Waser. Peptide functionalisation using photoredox catalysis and hypervalent iodine reagents. Design and characterisation of photoredox catalysts. Scholarship from the NCCR Chemical Biology.

University of Cambridge, UK, Jan.-Apr. 2020.

Exchange PhD student in the GBernardes lab for 3 months. Adviser: Prof. Gonalo Bernardes. Photoredox catalysed bioconjugation on proteins. Mobility grant awarded by the SNF.

Ecole Nationale Supérieure de Chimie de Montpellier (ENSCM), France, 2012 - 2016.

French “Diplôme d’ingénieur chimiste”. Major: Organic Chemistry.

Lund University, Sweden, Spring 2014.

Erasmus exchange student. Half Semester project in the Strand Group. Adviser: Prof. Daniel Strand. Gold-catalysed A³-coupling to form propargylamines. Major in Organometallic Chemistry. Beginner Swedish course.

“Classes préparatoires” at Lycée Saint-Louis, Paris, 2010 - 2012.

High-level intensive university level preparation in Physics, Mathematics, Chemistry and Humanities for the competitive exam to French “Grandes Ecoles”.

WORK EXPERIENCE

- Research and development

Novartis, Basel, Switzerland, Mar. - Aug. 2016.

Master Thesis in the Chemical and Analytic Development unit (CHAD). Adviser: Dr. Bernard Riss. Total synthesis of Bisabolangelone.

Firmenich SA, Geneva, Switzerland, Oct. 2014 - Aug. 2015.

Gap year in a discovery group. Adviser: Dr. Alec Birkbeck. Design and synthesis of novel molecules for perfumery. Olfactory panels.

Givaudan, Argenteuil, France, Jul. - Aug. 2014.

Internship. Pilot Laboratory of the European Creation Center. Applications for consumer tests including fine fragrances and cosmetics.

Givaudan, Argenteuil, France, Aug. 2013.

Internship. Perfumer’s assistant in Personal Care. Weighings of raw fragrances ingredients.

Institut de Chimie des Substances Naturelles (ICSN), Gif-sur-Yvette, France, Jun. - Jul. 2013.

Internship. Group leader: Prof. Max Malacria. Adviser: Dr. Giovanni Maestri. Organic synthesis.

- Additional experiences

Ecole de ski suisse (ESS) de Lausanne, Switzerland, Winter 2015.

Part-time assistant ski instructor for children (6-11 years old), diploma in Vaud Canton 2015-2017.

Osmothèque, Versailles, France, Sept. 2014. The unique international conservatory of perfumes.

Full-time assistant, one month. Planning and communicating about an event for the European Heritage Days.

SCIENTIFIC CONTRIBUTIONS

- Publications

Research articles

E. Voutyritsa, M. Garreau, M. G. Kokotou, I. Triandafillidi, J. Waser, C. Kokotos. Photochemical Functionalization of Heterocycles with EBX Reagents; C-H Alkynylation versus Deconstructive Ring Cleavage. *Chem. Eur. J.* Just accepted.

G. Barzanò, R. Mao, M. Garreau, J. Waser, X. Hu. Tandem photoredox and copper-catalyzed decarboxylative C(sp³)-N coupling of anilines and imines using an organic photocatalyst. *Org. Lett.* **2020**, *22*, 5412–5416.

M. Garreau, F. Le Vaillant, J. Waser. C-Terminal Bioconjugation of Peptides through Photoredox Catalyzed Decarboxylative Alkynylation. *Angew. Chem. Int. Ed.* **2019**, *58*, 8182–8186.

Highlighted in Chimia within the “Swiss Science Concentrated” of June 2019 and as the Synfact of the month in July 2019. Among the among the top 10% most downloaded within one year after publishing.

F. Le Vaillant, M. Garreau, S. Nicolai, G. Gryn'ova, C. Corminboeuf, J. Waser. Fine-Tuned Organic Photoredox Catalysts for Fragmentation-Alkynylation Cascades of Cyclic Oxime Ethers. *Chem. Sci.* **2018**, *9*, 5883–5889. *Selected for the “2018 Chemical Science HOT article collection” and for the “Functional Organic Materials Symposium Collection”.*

B. Riss, M. Garreau, P. Fricero, P. Podsiadly, N. Berton, S. Buchter. Total synthesis of TMS-ent-bisabolangelone. *Tetrahedron* **2017**, *73*, 3202–3212.

H. v. Wachenfeldt, A. V. Polukeev, N. Loganathan, F. Paulsen, P. Röse, M. Garreau, O. F. Wendt, D. Strand. Cyclometallated Gold(III) Aryl-Pyridine Complexes as Efficient Catalysts for Three-Component Synthesis of Substituted Oxazoles. *Dalton Trans.* **2015**, *44*, 5347–5353.

Preview

J. Ceballos,¹ M. Garreau,¹ J. Waser. An Alternative One-Electron Oxidation Strategy to Access Hypervalent Iodine Reagents. *Chem* **2019**, *5*, 2287–2289.

Review

S. G. Amos,¹ M. Garreau,¹ L. Buzzetti,¹ J. Waser. Photocatalysis with Organic Dyes: Facile Access to Reactive Intermediates for Synthesis. *Beilstein J. Org. Chem.* **2020**, *16*, 1163–1187.

¹: These authors contributed equally.

- Oral presentations in conferences

SCS (Swiss Chemical Society) Annual Meeting, Zürich, Sept. 2019. “C-terminal bioconjugation through photoredox catalyzed decarboxylative alkynylation”

NCCR Chemical Biology Annual Retreat, Villars-sur-Ollon, Jun. 2019. “C-Terminal Bioconjugation of Peptides through Photoredox Catalyzed Decarboxylative Alkynylation”

Swiss Summer School in Chemical Biology, Villars-sur-Ollon, Aug. 2018. “Decarboxylative alkynylation of peptides using hypervalent iodine and photoredox catalysis”

NCCR Chemical Biology Annual Retreat, Villars-sur-Ollon, Jun. 2017. “Decarboxylative alkynylation of amino acids using photoredox catalysis”

- Poster presentations

NCCR Chemical Biology, Switzerland, Fall Meeting 2018 and Annual Retreat 2019, “C-Terminal Bioconjugation of Peptides through Photoredox Catalyzed Decarboxylative Alkynylation”, Fall meeting 2017 and Annual Retreat 2018, “Decarboxylative Alkynylation of Peptides C-terminal Using Photoredox Catalysis”

PSL Chemical Biology Symposium, Paris, Jan. 2019. “C-Terminal Bioconjugation of Peptides through Photoredox Catalyzed Decarboxylative Alkynylation”

SCS (Swiss Chemical Society) Annual Meeting, Lausanne, Sept. 2018. “Decarboxylative Alkynylation of Peptides C-terminal Using Photoredox Catalysis”

Swiss Summer School in Chemical Biology, Villars-sur-Ollon, Aug. 2018. “Decarboxylative Alkynylation of Peptides C-terminal Using Photoredox Catalysis”

Photoredox Catalysis for Novel Organic Reactions, Postdam, Germany, Apr. 2018. “Decarboxylative alkynylation of carboxylic acids using hypervalent iodine and photoredox catalysis”

- Attended conferences without presentation

Swiss Summer School in Organic Chemistry, Villars-sur-Ollon, Aug. 2017.

International Symposium on Chemical Biology, Geneva, Jan. 2018.

TEACHING

Practical sessions of Organic Chemistry for second year Bachelor students. EPFL, 2017-2018. In charge of 6 students during one semester. One day per week dedicated to lab work followed by report corrections, 64 h.

Supervision of a master student one day per week during half a semester, EPFL, Fall 2018, 80 h.

Exercices sessions and exam corrections of Bachelor courses “Atoms, ions, molecules and functions”, “Organic Chemistry”, “Organic functions and reactions I”. EPFL, 2017-2019.

SKILLS

Languages: French (native speaker), English (fluent, TOEFL 102/120 in 2020) and German (intermediate).

Computing: Microsoft Office, L^AT_EX. **Scientific softwares:** SciFinder, Chemdraw, MestReNova.

Laboratory techniques: organic and peptides synthesis and purification techniques, photoredox catalysis, protein expression, usage of analytical instruments and data interpretation (NMR, IR, Mass spectrometry and MS/MS, GC, RP-LCMS and preparative HPLC, absorbance and fluorescence measurements, cyclic-voltammetry).

Additional responsibilities: In charge of several common instruments during the PhD and of the relation with the mechanical and electronic workshops (maintenance and ordering of equipments).

GRANTS AND AWARDS

Mobility Travel grant from the SNF (Swiss National Foundation), 10 000 CHF, Sept. 2019.

Runners up (Second) price for the Best Poster Presentation Awards in Organic Chemistry, SCS (Swiss Chemical Society) Annual Meeting, 200 CHF, Sept. 2018.

OTHER ACTIVITIES

Sports: alpinism (leading experience in AD and volunteering for the beginners training from the Club Alpin Suisse in Lausanne), ski touring (leading experience in AD+), cross-country skiing (skating) and dinghy sailing on Laser. **Art:** wood ship modelling and photography.

REFERENCES

Prof. Jérôme Waser: EPFL, LCSO, jerome.waser@epfl.ch, +41 (0) 216939388.

Dr. Bernard Riss: Novartis, CHAD, bernard.riss@novartis.com.

Dr. Alec Birkbeck: Firmenich SA, Product and Process research, keb@firmenich.com, +41 (0) 227803605.